



HAL
open science

Role de GRPR dans la formation des métastases de mélanome

Jérémy Raymond

► **To cite this version:**

Jérémy Raymond. Role de GRPR dans la formation des métastases de mélanome. Biologie moléculaire. Université Paris sciences et lettres, 2021. Français. NNT : 2021UPSL071 . tel-04368452

HAL Id: tel-04368452

<https://pastel.hal.science/tel-04368452>

Submitted on 1 Jan 2024

HAL is a multi-disciplinary open access archive for the deposit and dissemination of scientific research documents, whether they are published or not. The documents may come from teaching and research institutions in France or abroad, or from public or private research centers.

L'archive ouverte pluridisciplinaire **HAL**, est destinée au dépôt et à la diffusion de documents scientifiques de niveau recherche, publiés ou non, émanant des établissements d'enseignement et de recherche français ou étrangers, des laboratoires publics ou privés.



THÈSE DE DOCTORAT
DE L'UNIVERSITÉ PSL

Préparée à l'Institut Curie

**Rôle de GRPR dans la formation
des métastases de mélanome**

Soutenue par

Jérémy RAYMOND

Le 14 décembre 2021

École doctorale n° 582

**CANCEROLOGIE, BIOLOGIE,
MEDECINE, SANTE**

Spécialité

Biologie Cellulaire

Composition du jury :

Marie-Dominique GALIBERT PU-PH, IGDR	<i>Présidente</i>
Sophie, TARTARE-DECKERT DR, C3M	<i>Rapporteuse</i>
Nicolas, DUMAZ DR, INSERM UMRS97	<i>Rapporteur</i>
Séverine, MORISSET-LOPEZ CR, CBM	<i>Examinatrice</i>
Gabriel, MALOUF PU-PH, IGBMC-CHU Strasbourg	<i>Examineur</i>
Medhi, KHALED CR, IGR	<i>Examineur</i>
Lionel, LARUE DR, Institut Curie	<i>Examineur</i>
Véronique, DELMAS DR, Institut Curie	<i>Directrice de thèse</i>

Remerciements

Je souhaite remercier vivement tous les membres du jury d'avoir accepté de juger ce travail. J'adresse un franc merci au Dr. Nicolas DUMAZ et au Dr. Sophie TARTARE-DECKERT d'avoir accepté d'évaluer mes travaux en tant que rapporteurs et pour les commentaires et corrections que vous avez pu apporter à ce manuscrit. J'ai eu beaucoup de plaisir à échanger avec vous lors des congrès ou cours où j'ai pu vous rencontrer et j'espère avoir la joie de pouvoir vous présenter de nouveaux travaux scientifiques dans le futur. Je tiens également à remercier la Professeure Marie-Dominique GALIBERT d'avoir accepté de présider ce jury. Merci à mes examinateurs. Je remercie le Pr. Gabriel MALOUF et la Dr. Séverine MORISSET-LOPEZ d'avoir accepté sans hésitation de participer à ce jury de thèse. Merci à Mehdi KHALED de participer à ce jury. J'ai vraiment apprécié échanger avec toi lors de mes comités de thèse ou des quelques fois où l'on s'est rencontré.

Je remercie sincèrement le Dr. Véronique DELMAS de m'avoir encadré au cours de ces 4 dernières années. Ça a été un vrai plaisir de travailler avec vous et je pense que l'on a su bien se compléter pour réussir à obtenir ces beaux résultats. Je vous dois beaucoup pour tout le soutien que vous m'avez apporté des candidatures pour obtenir les bourses de thèse jusqu'à la rédaction de ce manuscrit et pour le scientifique que je suis et que vous avez avec certitudes participé à façonner. J'ai vraiment pu apprécier avoir loisir d'être actif et assez libre dans le projet aussi bien sur la réflexion que sur l'organisation et la réalisation des manip'.

Je remercie le Dr. Lionel LARUE pour m'avoir accueilli dans son laboratoire. Merci également pour toute la rigueur que tu as pu m'apporter sur la réflexion scientifique ou sur la façon de partager ses résultats. Merci également de nous avoir laissé expérimenter avec Marie pour créer cette « boîte » pour imager au mieux nos souris ou imaginer d'autres objets pour faciliter notre vie au labo.

Je remercie également les membres de mes comités de thèse : le Dr. Isabelle JANOUEIX-LEROSEY, le Dr. Guillaume LEBON, le Dr. Mehdi KHALED et le Dr. Marie-Christine MULTON. Vos conseils ont été réellement précieux pour l'orientation du projet en nous confortant dans la voie que nous avons choisi de suivre.

Je remercie vivement Marie et Valérie, nos deux « mamans » de l'équipe sans qui le laboratoire et ce projet n'aurait pas aussi bien tourné. Merci Marie, pour toute l'aide que tu as apporté au projet notamment sur la partie *in vivo*. Malgré l'heure précoce de la journée, j'ai vraiment apprécié ces moments passés à injecter nos souris qui sont finalement les moments où j'ai pu vraiment te découvrir. J'espère avoir suivi le protocole et avoir été suffisamment sage dans l'animalerie ! Merci également Valérie pour toute l'aide que tu as pu m'apporter. Je sais que tu as tendance à minimiser ton impact tant que tu n'as pas mis directement les mains dans le cambouis, mais tu es d'une façon ou d'une autre derrière tous les résultats présentés dans ce manuscrit, que ce soit par un conseil, une astuce, un coup de main ... et surtout cette rigueur à la paillasse qui te caractérise si bien. Je vous remercie également toutes les deux pour tous ces moments passés hors du labo qui font tellement de bien.

Je souhaite également remercier les autres membres ou ex-membres de « l'équipe développement normal et pathologique du mélanocyte » grâce à qui les dernières années se sont passées si vite. Je remercie tous les amis que j'ai pu y rencontrer. Merci à mon p'tit loup de Dr Zackie AKTARY qui a été la première personne à venir me parler alors que je n'étais même pas encore dans l'équipe. Avoir quelqu'un comme toi dans une équipe permet très vite de s'y sentir à l'aise et même malgré tes questions métaphysiques sur la reine d'Angleterre. Je remercie également le Pierre. Merci de m'avoir initié à R et à la bio-informatique, tout ce que j'ai appris à faire je le dois à cette initiation qui m'a appris à ne pas avoir peur de ce langage étrange que je croyais réservé à d'obscurs mathématiciens. Merci également pour toutes nos discussions sur des sujets scientifiques ou non. J'espère bientôt pouvoir lire tes bananes dans le journal de Mickey ou surtout ailleurs. Vielen Dank Mike. Merci pour m'avoir intégré à toutes tes aventures à Curie même si désormais je passe pour l'annuaire de Curie-Orsay auprès des autres ! Tu as été d'une très grande aide pour mon intégration dans le site particulièrement auprès des autres équipes. Je vous souhaite avec Britta le meilleur pour la suite. Je remercie ma presque jumelle, Anne-Cécile, même si l'on s'est plus rapproché après ton départ du labo. C'est toujours un vrai plaisir de passer du temps avec toi. J'espère qu'on arrivera au bout de cette liste (oui, oui, je te le rappelle jusqu'ici !). J'espère que tu réussiras à venir me voir dans mes pérégrinations futures en tous cas je ne manquerai pas de faire un saut à Sceaux ! Je remercie également Ha-Yeon pour tous ces moments au laboratoire et hors du laboratoire malgré ces lâches tentatives d'assassinat. Étant, comme toi, dans la team du soir au laboratoire ça a toujours été plaisant de pouvoir compter sur

toi dans ces moments-là, j'ai vraiment passé de bons moments avec toi même si tu écoutes de la « musique sale » ! Merci encore Marie et Valérie car une fois ne suffisait pas ! Merci Juliette, j'ai toujours apprécié discuter avec toi tout comme ces visites de musée (trop) tôt le dimanche matin. Je te souhaite le meilleur pour ta vie désormais marseillaise. Thank you Nisa even though I think you've clogged all my arteries with the cholesterol your sweets have brought me. I'm still looking out for your "baby" who's really picking up steam! Je remercie aussi Madeleine ma plus longue voisine de bureau, j'espère que tu t'éclates dans ta vie japonaise que tu avais si longtemps rêvée. Merci à Henri que je n'espère pas avoir trop embêté avec ses qPCRs ou ses courbes de survies ! Merci également à Evelyne pour sa joie de vivre communicative. Tes passages au laboratoire m'ont toujours fait chaud au cœur. Merci pour finir à tous ceux qui ont été au passage au laboratoire, avec qui j'ai partagé mon bureau, Franck, Nour, Camille, Bilén, Christine, Pawen. Merci à Victoire que j'ai pu encadrer quelques mois. Cette expérience d'encadrement a vraiment été enrichissante et tu as vraiment été à la hauteur du projet que l'on t'avait confié.

Je remercie tout le personnel des plateformes pour leur aides, leurs formations qu'ils ont pu m'apporter. Merci Charlène pour son aide en cytométrie, Sophie pour toute l'aide en histologie et merci Laetitia et Claire pour leur aide en microscopie. Merci à Elodie, Cedric, Christophe et Pauline pour s'être occupés de nos souris.

Merci à nos collaborateurs, à Curie, Dr. Florence MAHUTEAU-BETZER et Dr. Marie AUVRAY pour tout leur travail, malheureusement pas toujours fructueux, sur les ligands de GRPR. Merci au Dr. Guillaume LEBON et à Ludovic BERTO pour leur aide sur la pharmacologie notamment. Merci au Pr. Béatrice VERGIER pour son aide quant à l'obtention et l'analyse des échantillons de patients. Votre aide à tous a réellement permis de faire avancer ce projet.

Merci à nos deux superwomen à l'administration, Sandrine et Véronique, qui font des merveilles et nous facilitent tellement la vie

Je remercie tous les copains que j'ai pu rencontrer à travers les années sur Orsay, les résistantes Floriane et Julie, et les anciens Anne, Benedetta, Charlène, Hugo, Laurent, Mansour, Méghane, Puja, Satish, Sofia. J'aimerais remercier tous les membres de ReSiPi, des différentes équipes

Happy Friday ou des deux Curieous at Christmas, on a fait de jolies choses en répondant notamment à la question « est-ce que les chats sont liquides ».

Je remercie tous les membres de l'U1021, du site d'Orsay de Curie, et les personnes que j'ai pu croiser au cours de ma thèse pour leurs discussions, leurs sourires qui ont rendu ces 4 années meilleures. Merci particulièrement à Laurence pour tes sourires et ta douceur, j'ai hâte qu'il fasse meilleur pour aller faire les 50 bosses avec toi ! Merci également à Christophe pour « le bazar » en pièce ES, jamais la culture n'a été si sympa à faire. Merci à Cédric pour toutes ces discussions.

Merci à mes amis, les copains de Pharma, les p'tits Lus, Alice, Manu aka trop de pseudos pour les citer, Valentin, Hélène, Lolo, Maëlys et les nombreuses personnes hors de ce milieu avec qui j'ai pu passer du temps, prendre un verre, discuter, ...

Merci à toute ma famille pour son soutien depuis tant d'années.

Listes des principales abréviations

ADN	Acide désoxyribonucléique
AMPc	Adénosine monophosphate cyclique
ARN	Acide ribonucléique
BRAF	B-Raf proto-oncogene, serine/threonine kinas
<i>CDH1/Cdh1</i>	Cadhérine-1
CDKN2A/Cdkn2a	Cyclin dependent kinase inhibitor 2A
Cre	Cre-recombinase
CREB	cAMP-responsive element-binding protein
DAG	Diacyl-glycérol
DCT	Dopachrome tautomerase
Ecad	E-cadhérine
ERK	Extra-cellular signal regulated kinase
FZD	Frizzled receptors
$G\alpha_{q/11/s/i}$	Sous unité alpha q/11/s/i du complexe des protéines-G hétérotrimériques
GPCR	G-Protein-coupled receptor (voir RCPG)
GRP	Gastrin-releasing peptide
GRPR/Grpr	Gastrin-releasing peptide receptor
IP1	Inositol Monophosphate
IVIS	<i>In vivo</i> imaging system
MAPK	Mitogen-activated protein kinase
MC1R	Melanocortin Receptor type 1
MITF	Melanocyte inducing transcription factor
mGluR	Metabotropic glutamate receptor
NRAS	Proto-oncogene, GTPase
RCPG	Récepteur couplé aux protéines-G
TCGA	The cancer genome atlas
TPM	Transcrits par million
Tyr	Tyrosinase
YAP1	Yes-associated protein-1

Table des matières

REMERCIEMENTS	3
LISTES DES PRINCIPALES ABREVIATIONS	7
TABLE DES MATIERES	8
TABLES DES ILLUSTRATIONS	11
RESUME	12
ABSTRACT	13
INTRODUCTION	14
A. LE MELANOCYTE DANS LA PEAU	14
I. <i>Composition de la peau</i>	14
1. Structure de la peau	14
2. Cohésion des cellules dans l'épiderme.....	15
a. Kératinocytes	16
b. Cellules minoritaires de l'épiderme	16
c. Mélanocytes	16
II. <i>Tumeurs des cellules de la peau</i>	19
1. Carcinomes	19
2. Tumeurs des cellules de Merkel et de Langerhans.....	20
3. Tumeurs des cellules mélanocytaires.....	20
a. Lésions bénignes causées par les mélanocytes : les nævus.....	20
b. Mélanomes	21
i. Classifications.....	21
ii. Épidémiologie.....	22
iii. Facteurs de risques.....	23
iv. Diagnostics.....	24
v. Voie MAPK/ERK.....	25
vi. Mélanomagenèse.....	29
vii. Modèles précliniques du mélanome.....	31
viii. Traitements du mélanome.....	34
B. E-CADHERINE	43
I. <i>Structure et interactions cellulaires</i>	43
II. <i>Rôle dans le développement de l'oncogenèse</i>	44
1. Rôle dans le développement et l'homéostasie	44
2. Rôle dans l'oncogenèse.....	46
a. Cancer du sein.....	46
b. Cancer gastrique.....	46
c. Mélanome.....	47
3. Signalisation d'E-cadhérine et impact sur des processus cellulaires de l'oncogenèse.....	49
a. Prolifération.....	49
b. Mort cellulaire	50
c. Effet sur la clonogénicité.....	51
d. Transition épithélio-mésenchymateuse	51
e. Migration et invasion	51
f. Résumé des fonctions cellulaires d'E-cadhérine	52

C.	LES RECEPTEURS COUPLES AUX PROTEINES-G (RCPG).....	53
I.	<i>Présentation des RCPGs</i>	53
1.	Description et organisation.....	53
a.	Structure.....	53
b.	Classification.....	54
c.	Mécanismes d'activation.....	55
2.	Fonctions physiologiques des RCPGs.....	56
a.	La prolifération cellulaire.....	57
b.	L'échappement à l'inhibition de la croissance.....	58
c.	L'immortalisation.....	58
d.	La résistance à la mort cellulaire.....	58
e.	La production énergétique.....	59
f.	L'inflammation.....	59
g.	L'échappement immunitaire.....	59
h.	Induction de l'angiogenèse.....	60
i.	La réparation de l'ADN.....	60
j.	L'invasion cellulaire.....	60
k.	Résumé et complexité du rôle des RCPGs.....	61
II.	<i>Rôle des RCPGs et de leur signalisation dans le lignage mélanocytaire</i>	62
1.	Les RCPGs dans le lignage mélanocytaire.....	62
a.	Récepteur à l'endothéline de type B.....	63
b.	Récepteur à la mélanocortine de type 1.....	65
c.	Récepteur au glutamate.....	67
d.	Récepteurs Frizzled à Wnt.....	69
e.	Autres RCPGs.....	72
2.	La signalisation associée aux RCPGs dans le lignage mélanocytaire.....	73
a.	Signalisation via l'AMPC.....	74
b.	Signalisation par l'Inositol tri-phosphate et le Diacyl-Glycérol.....	81
c.	Signalisation via $G\alpha_{12/13}$	87
d.	Signalisation Wnt/ β -caténine.....	88
e.	Signalisation par le complexe $G\beta/G\gamma$	91
f.	Signalisation biaisée.....	91
III.	<i>Le récepteur au peptide relarguant la gastrine (GRPR)</i>	95
1.	Découverte.....	95
2.	Structure.....	95
3.	Expression de GRPR et de son ligand.....	96
4.	Signalisation de GRPR.....	100
5.	Fonctions physiologiques.....	101
a.	Sécrétions hormonales et enzymatiques.....	101
b.	Régulation de l'appétit.....	102
c.	Immunologie et inflammation.....	102
d.	Reproduction.....	102
e.	Démangeaison et le prurit.....	103
6.	Rôle de GRPR dans le cancer.....	103
a.	Cancer du poumon.....	103
b.	Cancer du sein.....	104
c.	Cancer de la prostate.....	104
d.	Mélanome.....	105
	OBJECTIF DE LA THESE	106
	RESULTATS	108
	DISCUSSION	145

A.	IMPORTANCE DE LA E-CADHERINE DANS LE MELANOME	145
B.	ROLE DE GRPR DANS LA PROGRESSION DU MELANOME	147
C.	IMPORTANCE DE L'INHIBITION DE GRPR DANS LA PROGRESSION DU MELANOME.....	150
D.	MECANISMES MOLECULAIRES CONDUISANT A L'EXPRESSION DE GRPR.....	152
CONCLUSION.....		154
BIBLIOGRAPHIE.....		155
ANNEXES.....		193
A.	PARTICIPATION A D'AUTRES PROJETS	193
I.	<i>C57BL/6 congenic mouse NRAS Q61K melanoma cell lines are highly sensitive to the combination of Mek and Akt inhibitors in vitro and in vivo.....</i>	193
II.	<i>BRN2 is a non-canonical melanoma tumor-suppressor.....</i>	207
III.	<i>Efficacy of Targeted Radionuclide Therapy Using [131 I]ICF01012 in 3D Pigmented BRAF- and NRAS-Mutant Melanoma Models and In Vivo NRAS-Mutant Melanoma.....</i>	224
IV.	<i>CLEC12B Decreases Melanoma Proliferation by Repressing Signal Transducer and Activator of Transcription 3.....</i>	245
B.	REVUE : TARGETING GPCRS & THEIR SIGNALING AS A THERAPEUTIC OPTION IN MELANOMA	256
C.	SCRIPTS R.....	311
I.	<i>Analyse différentielle de donnée transcriptomiques.....</i>	311
II.	<i>Visualisation par volcano plot.....</i>	313
III.	<i>Téléchargement des données du TCGA.....</i>	314
I.	<i>Analyse des scores des signatures phénotypiques et de YAP1</i>	315
D.	CURRICULUM VITAE	317

Tables des illustrations

Figure 1: Représentation de la peau (gauche) et de l'épiderme (droite).	14
Figure 2: Voies de synthèses de l'eumélanine et de la pheomélanine	17
Figure 3: Migration des mélanocytes depuis le tube neural et dans l'épiderme	19
Figure 4: Estimation de l'incidence du mélanome à travers le monde en 2020.	22
Figure 5: Estimation de la mortalité du mélanome à travers le monde en 2020.	22
Figure 6: Mortalité brute et standardisée (ASR world) du mélanome en France et aux USA.	23
Figure 7: Site d'implantation des métastases de mélanome et survie associée	25
Figure 8: Liste des MAPKs et de leurs MAP2Ks et MAP3Ks associées.	26
Figure 9: Voie MAPK/ERK.	29
Figure 10: La Mélanomagenèse.	30
Figure 11: Système d'épuisement lymphocytaire T.	36
Figure 12: Kaplan Meiers de l'essai clinique évaluant la combinaison nivolumab, ipilimumab.	37
Figure 13: Courbe de survie des différentes thérapies utilisées dans le mélanome.	39
Figure 14: Arbre décisionnel de prise en charge du mélanome métastatique en France	42
Figure 15: Structure des jonctions E-cadhérine/E-cadhérine	43
Figure 16: Photos représentatives des souris E-cad WT et Δ E-cad montrant les défauts de pigmentation des zones glabre.	45
Figure 17: Kaplan Meier de l'OS et de la PFS selon le niveau d'expression d'E-cad	47
Figure 18: Mécanismes d'expression de CDH1	48
Figure 19: Résumé des fonctions cellulaires d'E-cadherine	52
Figure 20: Exemple de structure de RCPG, le récepteur de classe A CCR5.	53
Figure 21: Modes de fixation des ligands selon la classe des RCPGs.	55
Figure 22: Mécanismes d'activation des RCPGs.	56
Figure 23: RCPGs impliqués dans les processus des Hallmarks of cancer.	61
Figure 24: Voies de signalisation de l'AMPC et conséquences cellulaires.	80
Figure 25: Voies de signalisation du Diacyl-glycérol et de l'IP3 et conséquences cellulaires.	86
Figure 26: Voie de signalisation des récepteurs couplés $G\alpha_{12/13}$ et conséquences cellulaires.	88
Figure 27: Voie de signalisation β -caténine et conséquences cellulaires	90
Figure 28: Signalisation via $G\beta/\gamma$ et conséquences cellulaires.	91
Figure 29: Signalisation biaisée via les arrestines et conséquences cellulaires.	92
Figure 30: Voies de signalisation des RCPG selon la protéine-G hétérotrimérique couplée.	94
Figure 31: Structure de GRPR humain.	96
Figure 32: Expression de GRPR dans le corps humain	98
Figure 33: Expression du ligand endogène de GRPR, la GRP chez l'Homme et la souris	99
Figure 34: Schéma de la production de GRP à partir de la pré-pro GRP	99
Figure 35: Valeur du couplage de GRPR avec les différentes familles de protéines-G.	100
Figure 36: Signalisations potentielles de GRPR.	101
Figure 37: Croissance des cellules de mélanome GRPR pos 1057 stimulées par la GRP et traitées par la binimétinib	152
Figure 38: Expression de Grpr et d'Esr1 dans les lignées cellulaires de mélanomes murins établies au laboratoire.	153
Tableau 1: Rôle de RCPGs dans la mélanomagenèse.....	62

Résumé

Des progrès considérables ont été réalisés dans la compréhension des mécanismes conduisant aux cancers, malheureusement ceux responsables de l'évolution métastatique reste mal connus. La E-cadhérine (Ecad) est une protéine d'adhésion cellulaire essentielle à l'homéostasie des cellules épithéliales et des mélanocytes dans la peau. De nombreuses études ont montré que le gène codant pour la E-cadhérine, *CDH1*, est un gène suppresseur de tumeurs dans de nombreux carcinomes. Le rôle de CDH1 dans la mélanomagenèse n'a jamais été formellement établi, seules des corrélations entre la diminution de son expression et un potentiel métastatique accru ont été mises en évidence. Lors de cette thèse, nous avons adressé les conséquences de la perte de *Cdh1* dans la mélanomagenèse à l'aide de souris génétiquement recombinaées exprimant une forme oncogénique de NRAS^{Q61K} dans les mélanocytes. Nous avons montré que la délétion conditionnelle de *Cdh1* n'influence pas l'initiation du mélanome, mais favorise efficacement le développement des métastases. De manière intéressante, la perte de *Cdh1* induit fortement l'expression du récepteur au peptide relarguant la gastrine (*Grpr*). GRPR, qui appartient à la famille des récepteurs couplés aux protéines G, est surexprimé dans plusieurs types de cancers, dont les carcinomes. Chez l'homme, nous avons montré une anti-corrélation de l'expression entre CDH1 et GRPR dans plusieurs carcinomes et dans les mélanomes. D'un point de vue fonctionnel, nous avons montré *in vitro* que l'expression de *Grpr* favorise les processus cellulaires essentiels pour le processus métastatique, tels que la croissance cellulaire, la clonogénicité, la migration et l'invasion. *In vivo*, la surexpression de *Grpr* dans des cellules de mélanome humain ou de souris induit de la formation de foyers métastatiques après allogreffe et xélogreffe, respectivement. Les métastases des cellules surexprimant GRPR sont fortement réduites en présence de l'antagoniste du GRPR, RC-3095. Le GRPR signale via Gαq conduisant à l'activation de la signalisation YAP1, expliquant les caractéristiques moléculaires et cellulaires induits lors de la cascade métastatique. Cette étude souligne l'importance de l'axe Ecad-GRPR dans les métastases de mélanome et apporte la preuve de concept que le GRPR est une cible thérapeutique pour le mélanome métastatique.

Abstract

While tremendous progress has been made in the understanding of the mechanisms leading to cancers, the understanding of the mechanisms governing the formation of metastases remains poorly understood. E-cadherin (Ecad) is a cell-cell adhesion molecule essential for the homeostasis of epithelial cells and melanocytes in the skin. A large number of studies have established that *CDH1* (encoding for Ecad) is a tumor suppressor gene in carcinomas. However in melanoma, only correlative studies link its reduced expression to metastatic potential. In this thesis, we addressed the consequences of *Cdh1* loss in melanomagenesis using genetically recombinant mice expressing an oncogenic form of NRAS^{Q61K} in melanocytes. We showed that the conditional deletion of *Cdh1* does not influence melanoma initiation but dramatically promotes metastasis. Interestingly, loss of *Cdh1* intensely induces the expression of the Gastrin-releasing peptide receptor (Grpr). GRPR, which belongs to the G protein-coupled receptor family, is overexpressed in several types of cancers, including carcinomas. In humans, we have shown anti-correlation of expression between CDH1 and GRPR in several carcinomas and in melanomas. From a functional point of view, we have shown *in vitro* that *Grpr* expression promotes crucial cellular processes required for metastasis, such as cell growth, clonogenicity, migration and invasion. *In vivo*, overexpression of GRPR in mouse or human melanoma cells induces metastasis after allograft and xenograft, respectively. Metastasis of cells overexpressing GRPR is strongly affected in the presence of the GRPR antagonist RC-3095. GRPR signals through G α_q leading to activation of YAP1 signaling, which explains the molecular and cellular characteristics induced during the metastatic cascade. This study highlights the importance of the Ecad-GRPR axis in melanoma metastases and provides proof-of-concept that GRPR is a therapeutic target for metastatic melanoma.

Introduction

A. Le mélanocyte dans la peau

I. Composition de la peau

1. Structure de la peau

La peau est le plus grand organe corps humain, par sa taille, sa superficie (~1.8m²), mais aussi, malgré sa finesse d'en moyenne 2mm (1 à 4 mm d'épaisseur selon la localisation) l'un des plus volumineux. La peau est un organe complexe dont la fonction principale est la protection de l'organisme contre les agressions extérieures. Sa position à l'interface entre milieu interne de l'individu et l'environnement en fait une barrière entre ces deux milieux, mais aussi une zone d'échange. Le rôle de barrière physique s'effectue dans les deux sens. De l'extérieur vers intérieur la peau assure la protection physique contre les agressions extérieures qu'elles soient physiques, chimiques ou microbiennes. Dans le sens inverse, elle joue un rôle de barrière limitant notamment les pertes en eau. Le rôle d'échange se fait à plusieurs niveaux. La peau participe à la thermorégulation, à la transmission de signaux vers le reste de l'organisme via la nociception et la somesthésie, mais aussi à l'éducation de cellules immunitaires T aux antigènes cutanés.

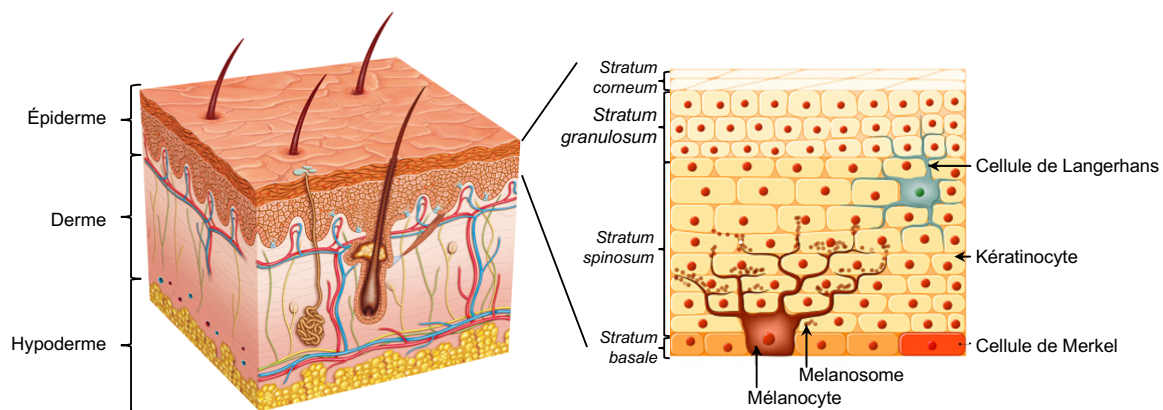


Figure 1: Représentation de la peau (gauche) et de l'épiderme (droite).

La peau est composée de 3 couches superposées de l'intérieur vers l'extérieur l'hypoderme, le derme et l'épiderme. Cette structure est décrite dans la .Figure 1.

- La couche la plus interne est l'hypoderme. Il est majoritairement composé de tissu adipeux spécialisés dans le stockage des graisses. Il a un rôle mécanique, de stockage d'énergie et d'isolant par la graisse et régule la température du corps (Zouboulis, 2000).

- La couche intermédiaire est le derme. Il est composé de tissu conjonctif lâche et de fibres conjonctives constituées de collagène et d'élastine. La synthèse de la matrice et de ces fibres est assurée par les fibroblastes. C'est aussi dans cette couche que l'on retrouve vaisseaux et nerfs. Le derme est un tissu vascularisé et innervé et contenant des annexes cutanées : pilaires, sébacées et sudorales.
- La couche superficielle est l'épiderme qui joue le rôle d'une vraie barrière physique. L'épiderme est un épithélium stratifié, pavimenteux, non vascularisé, mais innervé. L'épiderme et le derme sont séparés par lame basale composée de protéoglycane, de laminine, de collagène et de fibronectine. La densité cellulaire est importante sur la lame basale et les cellules sont très fortement associées entre elles.

2. Cohésion des cellules dans l'épiderme

L'épiderme comme tout tissu épithélial a une cohésion tissulaire forte maintenue par de nombreuses jonctions cellules-cellules assurées par 4 types de jonctions, les jonctions communicantes, adhérentes, desmosomes et jonctions serrées. Ces différents types de jonctions assurent non seulement l'adhésion cellulaire, mais interviennent dans la signalisation, la différenciation, la prolifération et la perméabilité. Les jonctions communicantes sont constituées des canaux formés par la jonction de 2 héli-canaux avec 6 connexines et créer un pore entre les deux cellules. Les jonctions serrées composées de claudines et d'occludines qui vont sceller l'épithélium et participer à la polarisation des kératinocytes. Les deux dernières jonctions, les jonctions adhérentes et desmosomes sont composées de protéines de la superfamille des cadhérines. Les desmosomes sont constitués par les desmocollines et les desmogléines. Les jonctions adhérentes (Zonula adherens) sont constituées de cadhérine et particulièrement de la E-cadhérine (E-cad), prototype épithélial. La E-cad établit une adhésion homotypique avec d'autres molécules d' E-cad présentes dans différents types cellulaires, les kératinocytes, les cellules de Langherans (Tang et al., 1993; Udey, 1997; Mayumi et al., 2013), les cellules de Merkel (Tanaka et al., 2004) et les mélanocytes. E-cad est essentielle à l'établissement des tissus épithéliaux dont l'épiderme, mais également à la formation des jonctions serrées et la perméabilité de la peau (Larue et al., 1994; Niessen, 2007; Tunggal et al., 2005). Il est intéressant de noter que les mélanocytes ne sont capables d'établir que des jonctions adhérentes et des jonctions communicantes.

a. Kératinocytes

Les kératinocytes sont les cellules les plus abondantes dans la peau, représentant plus de 90% des cellules qui la compose. Ce sont ces cellules qui assurent principalement la fonction barrière de la peau. Les kératinocytes sont responsables de la sécrétion d'hormones (alpha-MSH) et de vitamine D. Les kératinocytes se différencient au cours de leur maturation pour former les différentes couches de l'épiderme. Dans la couche la plus interne, le *stratum basale*, les kératinocytes prolifèrent et se détachent de la lame basale pour former le *stratum spinosum*. Sous la pression induite par la prolifération des cellules des couches internes, les cellules vont migrer vers les couches plus externes et accumuler des grains de kératohyaline pour former le *stratum granulosum* puis perdre leurs noyaux pour former le *stratum corneum* qui finira par desquamer. A noter que des zones palmaires il existe une cinquième couche entre *stratum granulosum* et *corneum*, le *stratum lucidum*. Ce phénomène de maturation des kératinocytes est rapide et continu, l'épiderme se renouvelle complètement en environ 6 semaines.

b. Cellules minoritaires de l'épiderme

Dans l'épiderme sain, on retrouve aussi deux types de cellules plus faiblement représentées. Les cellules de Langerhans sont des cellules dendritiques, elles ont un rôle de sentinelle du système immunitaire, captant les agents exogènes se trouvant dans l'épiderme et allant les présenter dans les ganglions. Les cellules de Merkel sont des mécanorécepteurs présents aux jonctions dans la couche basale de l'épiderme et du derme et groupées en clusters (Halata et al., 2008).

c. Mélanocytes

Le dernier type cellulaire présent dans l'épiderme est le mélanocyte dont le rôle principal est de produire la mélanine responsable de la pigmentation de la peau, les poils et les cheveux.

Les mélanocytes cutanés sont situés dans le *stratum basal* et dans le follicule pileux. La localisation de ceux-ci va permettre de distinguer deux sous-types de mélanocytes : les mélanocytes inter-folliculaires situés dans l'épiderme et les mélanocytes folliculaires dans le follicule pileux. Chez l'Homme, les mélanocytes inter-folliculaires sont majoritaires alors que chez les rongeurs, et autres animaux à fourrures, on retrouve majoritairement des mélanocytes folliculaires, les mélanocytes inter-folliculaires étant limités aux régions glabres comme la queue, les oreilles et les pattes par exemple chez la souris. Cette différence de localisation implique des différences au niveau moléculaires qui seront discutées plus loin.

Dans l'épiderme, les mélanocytes émettent des dendrites jusque dans le *stratum spinosum* pour interagir avec environ 36 kératinocytes et forment ainsi une unité de mélanisation. Les

mélanocytes vont transférer aux kératinocytes leurs pigments. La production de ces pigments se fait lors de la mélanogénèse dans les mélanosomes présents dans les mélanocytes et va aboutir à la production de deux types de pigments : l'eumélanine (de couleur brune) et la phéomélanine (rouge-orange).

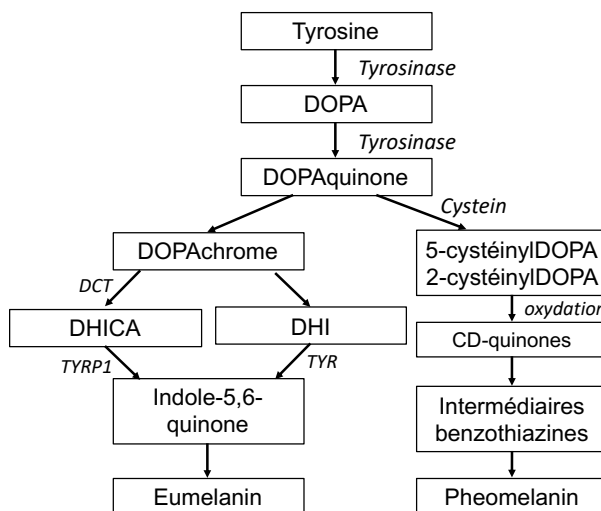


Figure 2: Voies de synthèses de l'eumélanine et de la phéomélanine

Les premières voies de la synthèse de la mélanine sont communes aux deux types de mélanines via l'action de l'enzyme Tyrosinase qui catalyse la conversion de la tyrosine en DOPA puis DOPAquinone. Ensuite les voies de synthèse divergent, l'eumélanine est produite par la cyclisation de la DOPAquinone en Dopachrome puis par la réduction en acide 5,6-dihydroxy-1H-indole-2-carboxylique (DHICA) par la dopachrome tautomérase (DCT) suivi d'une oxydation par la Tyrosinase-related protein (TYRP1) pour former des intermédiaires quinones. Une autre voie existe via la tyrosinase et la production de 5,6Dihydroxyindole (DHI). L'oligopolymérisation des quinones produira l'eumélanine. La phéomélanine est produite par la réaction de la DOPAquinone avec des cystéines produisant la 2- cystéinylDOPA et 5-cystéinylDOPA. Celles-ci seront ensuite oxydées puis polymérisées en pheomélanine. Ces voies de synthèses sont résumées dans la Figure 2. Cette production se fait au sein des mélanosomes qui vont mûrir et se charger en mélanine tout en migrant vers la périphérie des mélanocytes et l'extrémité de leurs dendrites. Le transfert de mélanine des mélanocytes vers les kératinocytes s'effectue par un(des) mécanisme(s) qui reste(nt) controversé(s) (exocytose-endocytose, cytophagocytose, délivrance par vésicule ou par nanotubes). Ces mécanismes ont été observés dans différents systèmes pigmentaires provenant d'espèces différentes. Il n'est pas exclu que plusieurs modèles coexistent ensemble en fonction du phototype, de la localisation dans la peau ou du rayonnement solaire.

La pigmentation de la peau est principalement déterminée par le type de mélanine produit, le ratio phéomélanine et eumélanine et non pas par le nombre de mélanocytes présents qui varie très peu en fonction de la localisation et du phototype. La pigmentation de la peau et la capacité de la peau à se pigmenter vont permettre de déterminer les différents phototypes :

- Phototype I : peau très claire et taches de rousseur. Les cheveux sont blonds ou roux. Les individus ne bronzent pas et prennent systématiquement des coups de soleil.
- Phototype II : peau très claire et les cheveux sont blonds ou châtain. Des taches de rousseur apparaissent au soleil. Les individus ont les yeux clairs, bronzent difficilement et prennent fréquemment des coups de soleil.
- Phototype III : peau claire et les cheveux blonds ou châtain. Les individus bronzent progressivement et avec parfois des coups de soleil.
- Phototype IV : peau mate et cheveux châtain, bruns ou noirs. Les yeux sont foncés. Les individus attrapent peu de coups de soleil et bronze rapidement.
- Phototype V : peau foncée, yeux foncés et cheveux foncés. Les individus ont rarement des coups de soleil et bronzent rapidement.
- Phototype VI : peau noire et cheveux noirs. Les individus n'ont jamais de coups de soleil.

Quelle que soit leur localisation dans le corps, les mélanocytes dérivent tous des cellules des crêtes neurales (CCN). Les CCN sont issues des plaques neurales, un épaissement du neurectoderme, qui délimite le neurectoderme de l'ectoderme non neural lors de la neurulation. Après l'invagination du neurectoderme les cellules du toit du tube neural vont délaminer, proliférer et migrer. Cette étape est particulièrement liée à la transition épithélio-mésenchymateuse (TEM) des CCN. Cette transition est contrôlée spatio-temporellement par différents facteurs de transcription comme SNAI et SLUG dont l'expression est induite par des facteurs paracrines WNT, BMP et NOTCH (Artinger and Monsoro-Burq, 2021; Pla and Monsoro-Burq, 2018; Prasad et al., 2019). L'émergence des CCN du tube neural se fait par vagues successives et génère différents lignages cellulaires. La spécification en différents types cellulaires dépend de la position des CCN lors de leur sortie du tube neural (Gandhi and Bronner, 2021; York and McCauley, 2020). Par exemple, la signalisation β -caténine activée par des ligands comme Wnt3a induit la spécification des cellules en mélanoblastes via l'activation du récepteur couplé aux protéines G (RCPG) frizzled-3 (Chang et al., 2014).

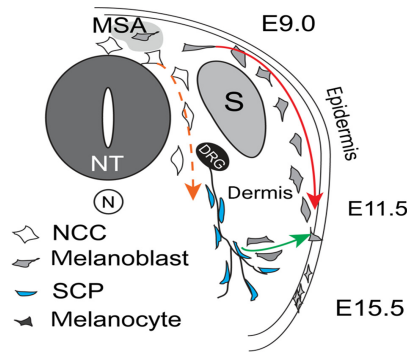


Figure 3: Migration des mélanocytes depuis le tube neural et dans l'épiderme

(A) voies de migration des précurseurs des mélanocytes depuis le tube neural. Voie dorso-latérale en rouge et voie ventro-latérale en vert. D'après Petit et Larue, 2016.

Les CCN prolifèrent de façon extensive et suivent deux voies majeures de migration, la voie dorso-latérale et la voie dorso-ventrale. La première ne produit que des précurseurs de mélanocytes, les mélanoblastes, et suit une orientation dorso-latérale entre l'ectoderme et les somites. Cette voie est à l'origine de la majorité des mélanocytes produits. La deuxième voie est dorso-ventrale, entre le tube neural et les somites, elle va donner naissance à différents types cellulaires neurones, cellules de Schwann, cellules chromaffines de la glande médullosurrénale, cellules musculaires lisses. Il est à noter que les mélanoblastes peuvent également dériver de précurseurs bipotents Schwann/Mélanocytes migrant dorso-ventralement. Ces deux voies de migrations sont décrites dans la Figure 3. L'exacte contribution de cette voie dans la genèse de l'ensemble des mélanocytes n'est pas encore définie (Bonaventure et al., 2013; Petit and Larue, 2016). Les principales voies de signalisation essentielle dans la mise en place du lignage mélanocytaire sont les voies de signalisation EDN3/ EDNRB (endothéline), WNT/ β -caténine et SCF/KIT (Larue et al., 2013).

II. Tumeurs des cellules de la peau

Toutes les cellules de l'épiderme sont susceptibles de subir une transformation maligne, les cellules étant exposées régulièrement aux radiations, aux substances chimiques et pathogènes.

1. Carcinomes

La majorité des cancers de la peau (>90%) sont des carcinomes, ces cancers sont peu métastatiques et donc peu létaux. Ils sont fortement associés avec l'exposition aux UVs. On retrouve deux grands types de carcinomes :

- Les carcinomes baso-cellulaires formant des petits nodules rosés, légèrement brillants non métastatiques, mais capables de détruire la peau voir les tissus sous-jacents s'ils ne sont pas traités. Ils proviennent des kératinocytes du *stratum basal*.
- Les carcinomes épidermoïdes se présentent sous la forme de tumeurs crouteuses, bourgeonnantes pouvant saigner. Leur évolution est potentiellement plus maligne, car on retrouve occasionnellement des métastases ganglionnaires. L'origine se trouve cette fois-ci dans les kératinocytes du *stratum spinosum*.

2. Tumeurs des cellules de Merkel et de Langerhans

Les cellules de Merkel sont susceptibles de subir une évolution maligne et de donner naissance à un carcinome à cellules de Merkel. C'est un cancer rare, l'incidence est environ 30 fois moindre que celle du mélanome, mais il est très invasif et agressif, aboutissant au décès d'un malade sur trois. Il est lui aussi associé aux UVs (Ramahi et al., 2013).

Les cellules de Langerhans sont susceptibles d'avoir une évolution tumorale appelée l'histiocytose à cellules de Langerhans. Son incidence est très faible (5-8 cas par millions), mais elle est très difficilement curable et laisse de lourdes séquelles cliniques. C'est une pathologie pédiatrique se révélant très tôt. L'histiocytose à cellules de Langerhans est liée à des activations de la voie de signalisation MAPK, plus de 60% des patients étant mutés BRAF^{V600E} et environ 10% des patients étant mutés pour MEK1 (Allen et al., 2018).

3. Tumeurs des cellules mélanocytaires

a. Lésions bénignes causées par les mélanocytes : les nævus

L'expression d'oncogènes activant la voie des MAPK, principalement la mutation BRAF^{V600E}, dans les mélanocytes va conduire à la formation de nævus (Roh et al., 2015). La plupart des individus ont des nævus, mais leur nombre est très variable. Ceux-ci sont globalement bénins, évoluant rarement en mélanomes. Cet aspect globalement bénin est lié à l'entrée en sénescence des cellules en réponse à la suractivation de la voie MAPK. La sénescence est contrôlée par la surexpression de gènes suppresseurs de tumeurs comme *CDKN1A* et *CDKN2A* (Damsky and Bosenberg, 2017). Les nævus bleus ont une génétique très particulière, car elle implique la présence de mutations activatrices de *GNAQ* et *GNA11* induisant une signalisation de RCPG de type G α_q (Van Raamsdonk et al., 2009).

b. Mélanomes

i. Classifications

La classification des mélanomes repose sur des critères de localisation anatomique et de morphologie. On différencie les zones selon l'exposition aux UVs entre exposées chroniquement (visage, extrémités des membres), exposées de façon intermittente (tronc, racine des membres) et non-exposées (paumes, plantes de pied, muqueuses). Cinq types de mélanomes cutanés principaux sont identifiés, le mélanome superficiel extensif, le mélanome de Dubreuilh, le mélanome des muqueuses, mélanome acro-lentigineux et le mélanome nodulaire. D'autres mélanomes plus rares existent aussi comme le mélanome desmoplastique ou le mélanome sur nævus bleu. Cette catégorisation n'impacte que peu la prise en charge du patient.

L'activation de la prolifération du mélanome est associée avec l'activation de la voie MAPK. Le type de mutations permet de classer les mélanomes. L'étude menée par le consortium TCGA a identifié 4 grandes catégories : les mutations activant BRAF, celles activant NRAS, les mutations inactivatrices de NF1 et autres cas dits triple-WT (respectivement 50%, 20-25% et 10 à 15% des mélanomes). Il est intéressant de noter que parmi les cas triple-WT on retrouve environ 1% de mutations GNAQ/GNA11 capable d'activer la signalisation $G\alpha_q$ (The Cancer Genome Atlas Network, 2015). Cette classification est valable pour les types de mélanomes nodulaires, superficiels extensifs et de Dubreuilh, mais ne l'est pas pour les autres types de mélanomes. Par exemple, les mélanomes acro-lentigineux sont plus rarement mutés pour les trois gènes déterminant la classification issue du TCGA (seulement un cas sur deux), mais présentent plutôt de nombreuses amplifications de *KIT* (10-35%) (Tod et al., 2020). Les mélanomes sur nævus bleu présentent de nombreuses activations de *GNAQ* (50 et 85% des cas) et de *GNA11* (7% des patients) (Van Raamsdonk et al., 2009).

Un autre type de mélanome existe, mais n'est pas issu de la peau, mais des tissus de l'uvée, le mélanome uvéal. Il représente autour de 5% des mélanomes totaux. Le mélanome uvéal est induit par l'activation de mutations de *GNAQ* et de *GNA11* qui a elles deux totalisent environ 90% des cas. Il est également intéressant de noter que parmi les 10% restants on retrouve des mutations qui affectent elles aussi la signalisation $G\alpha_q$ telle que des mutations activatrices de *CYTRL2*, un récepteur couplé $G\alpha_q$, et des mutations de *PLCB4* que l'on suppose activatrices elles aussi (Johansson et al., 2016; Nell et al., 2021; Robertson et al., 2017).

ii. Épidémiologie

Pour l'année 2020, les estimations prédisent qu'en France il y a eu 16449 nouveaux cas de mélanome et 2125 décès ce qui représente une incidence et une mortalité normalisée de respectivement 15,2 et 1.5 pour 100 000 (ASR monde). Dans le monde on retrouve 324 635 nouveaux cas et 57 045 décès. Ce qui en fait le 6^e cancer ayant l'incidence la plus élevée. Les taux normalisés (ASR monde) pour la population mondiale sont plus faibles que pour la population française – incidence de 3,4 pour 100 000 et une mortalité de 0,56 pour 100 000. Ces plus faibles valeurs s'expliquent par la grande disparité d'incidence du mélanome à travers le monde, des pays très peuplés comme la Chine ou l'Inde n'étant que peu sujets aux mélanomes (Sung et al., 2021, Figure 4-5).

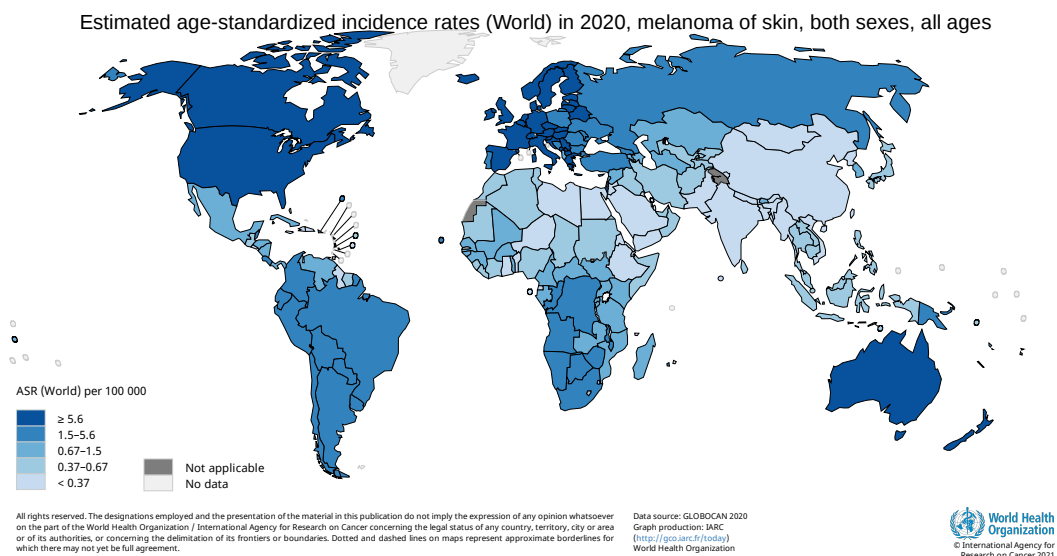


Figure 4: Estimation de l'incidence du mélanome à travers le monde en 2020.

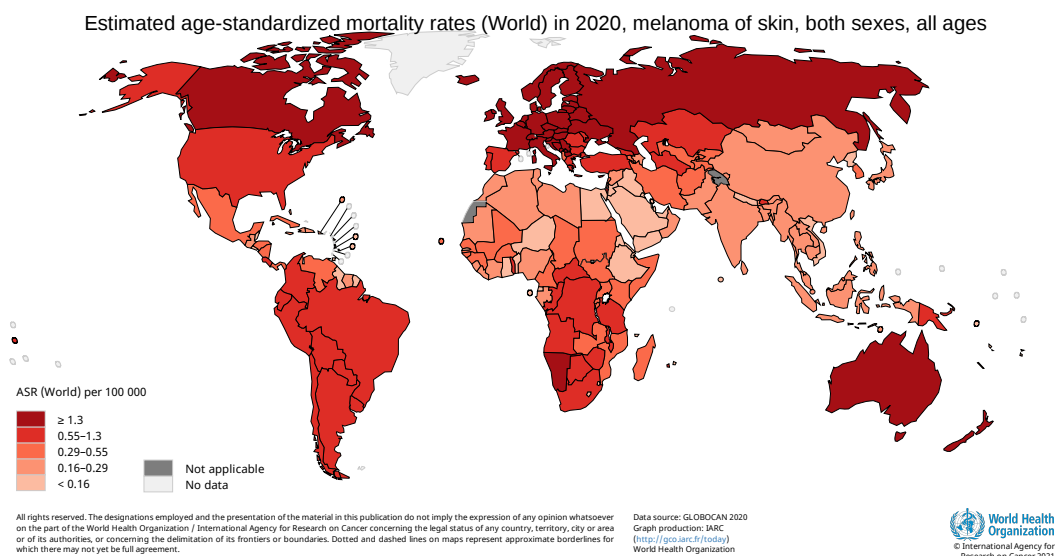


Figure 5: Estimation de la mortalité du mélanome à travers le monde en 2020.

L'évolution de l'incidence du mélanome sur les dernières décennies est à la hausse constante (autour de 4% par an). Cette hausse est particulièrement liée à la surexposition aux UVs qu'ils soient naturels ou artificiels (IARC, 2006). Les estimations prédisent une augmentation de la mortalité du mélanome d'ici 2040, avec par exemple une augmentation d'environ 30% pour la France (versus une augmentation de population de seulement 5%) (Sung et al., 2021). Mais cette donnée est à relativiser, car les recensements, sur lesquels les estimations se basent datent de 2016 au plus récent, l'impact des thérapies arrivées au milieu des années 2010s n'étant pas visible ni pris en compte par les estimations. Les données de recensement américaines suggèrent même une nette diminution à partir de 2014 non visible encore en France en 2015 (Figure 6). Il faut toutefois probablement nuancer ces valeurs à la hausse à cause des conséquences de la pandémie de maladie à coronavirus où les premières études rapportent une diminution franche des diagnostics de cancer corrélés avec une diminution des consultations d'oncologie (Coma et al., 2021; Erdmann et al., 2021; Rashid and Tsao, 2021).

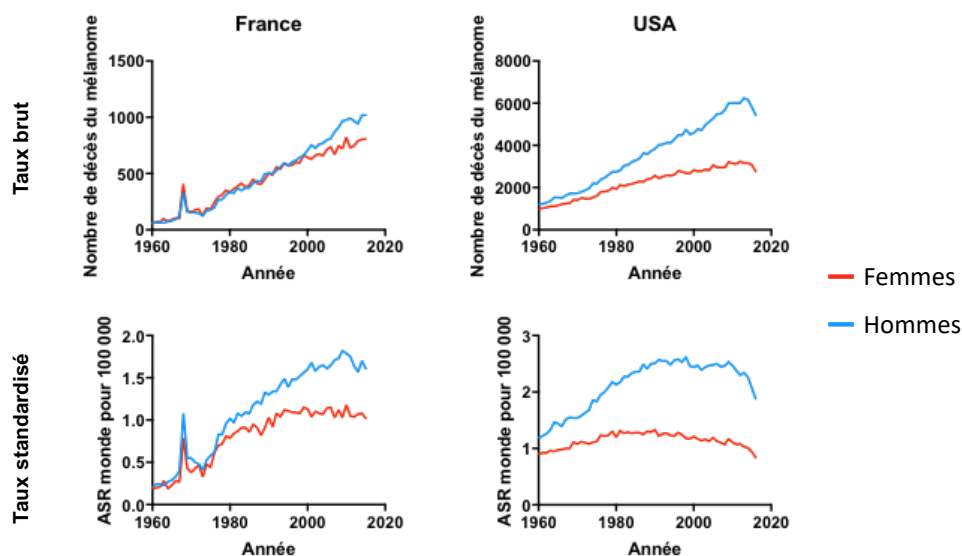


Figure 6: Mortalité brute et standardisée (ASR world) du mélanome en France et aux USA.

iii. Facteurs de risques

Différents facteurs de risques ont été mis en évidence pour le mélanome. La présence d'un phototype clair conjoint avec une exposition abondante aux rayonnements UVs, particulièrement durant l'enfance et une forte fréquence de brûlures solaires est des facteurs favorisant le mélanome. Ces facteurs de risques sont nettement observés dans les populations où l'incidence du mélanome est la plus élevée : Australie, Nouvelle-Zélande, pays scandinaves et anglo-saxons. Le nombre de nævus du patient est aussi corrélé avec le risque de mélanome. Les patients immunodéprimés sont aussi plus susceptibles de produire des mélanomes.

On retrouve également des prédispositions familiales au mélanome. Celles-ci sont classées selon l'importance du risque. Un risque fort de mélanome est apporté par des mutations dans de nombreux gènes suppresseurs de tumeurs (*ACD, BAP1, CDKN2A, CDK4, POT1, RAD51B, TERF2IP, TERT* (Aoude et al., 2015; Horn et al., 2013; Hussussian et al., 1994; Kamb et al., 1994; Molven et al., 2005; Robles-Espinoza et al., 2014; Wadt et al., 2015; Wiesner et al., 2011)). La présence de variants spécifiques induit un risque intermédiaire de développer un mélanome. Le variant *MITF^{E318K}* ainsi que de nombreux variants de *MC1R* comme les variants *R151C, R160W, and D294H*, qui augmentent le risque de développer un mélanome d'environ 60% sont dans cette catégorie (Bonet et al., 2017, 2017; Tagliabue et al., 2018). Enfin, des études GWAS ont également associé un risque faible de développer des mélanomes avec la présence de polymorphisme, particulièrement sur des gènes de la pigmentation comme *ASIP, KIT, OCA2, MTAP, SCLC45A2, TYR* ou *TYRP1* ou d'autres variants de *MC1R* (Bourillon et al., 2013; Chatzinasiou et al., 2011; Liu et al., 2015; Marasigan et al., 2019)

iv. Diagnostics

Le mélanome primaire est établi le plus souvent lors de l'examen clinique du patient par l'analyse de la lésion superficielle. La règle ABCDE classifie la lésion selon 5 critères : son asymétrie, la régularité de ses bordures, l'homogénéité de sa couleur, son diamètre et son évolution. La lésion suspecte est retirée et analysée pour examen cyto-pathologique qui va confirmer ou non le diagnostic du dermatologue. Cette deuxième analyse va s'accompagner d'une analyse de facteurs pronostiques comme l'indice de Breslow, l'ulcération de la tumeur ou son indice mitotique. En fonction du bilan histologique, un bilan complémentaire de recherches de métastases pourra être entrepris. Le mélanome sera classé en 4 stades selon les résultats des différents bilans :

- Le stade I : tumeurs locales < 1mm ou < 2mm non-ulcérées
- Le stade II : tumeurs locales >2mm ou < 2mm ulcérées
- Le stade III : marqué par un envahissement loco-régional et une invasion ganglionnaire locale.
- Le stade IV : marqué par la présence de métastases dans des organes à distance.

	Site de métastases				
	Os	Foie	Cerveau	poumons	Peau/ganglions
Cas avec métastases (à l'autopsie)	11-17%	10-20%	12-20%	36%	59%
	23-49%	54-77%	36-54%	85%	?%
Survie médiane (mois)	4-6	2.4-6.5	5-8	8-14	12-20

Figure 7: Site d'implantation des métastases de mélanome et survie associée

Le mélanome est capable de coloniser de nombreux organes à distance. Le site métastatique le plus fréquent est la peau et les ganglions avec plus d'un patient sur deux qui présente des métastases loco-régionales visibles en clinique. Ces métastases cutanées et ganglionnaires sont en elle-même non létales et la survie médiane des patients non traités est de 12 à 20 mois. Le deuxième site métastatique le plus retrouvé est le poumon, un patient atteint de mélanome métastatique sur 3 présente des métastases pulmonaires. A l'autopsie ce chiffre augmente nettement pour atteindre 85% des patients. La présence de métastases pulmonaires corrèle avec une diminution de la survie des patients à 8-14 mois. L'atteinte du cerveau, du foie et des os vus en clinique se fait à la même fréquence, de l'ordre de 10 à 20% bien qu'à l'autopsie on détecte plus de métastases hépatiques (54-77%) que dans le cerveau (36-54%) ou que dans les os (23-49%). La présence de métastases dans ces organes corrèle avec une diminution nette de la survie avec une médiane autour de 5 mois dans les trois cas précédents (Damsky and Bosenberg, 2017; McDermott et al., 2014; Tas, 2012; Zekri et al., 2017). Ces données sont résumées dans la Figure 7.

v. Voie MAPK/ERK

La classification du mélanome repose sur la présence de mutations dans des gènes de la voie MAPK/ERK ou dans des facteurs la régulant. Cette voie MAPK/ERK est une voie très fréquemment activée dans le cancer et particulièrement dans le mélanome où elle joue un rôle majeur. Elle est l'une des voies de la famille des MAPK.

Les voies de signalisation des MAPK sont des voies de signalisation majeure de la cellule qui vont réguler de nombreux processus cellulaires comme la prolifération, l'apoptose et la réponse aux

signaux de stress. Comme leur nom l'indique, les MAPK sont activées par des stimuli extérieurs. Historiquement ces voies de signalisation étaient décrites comme reposant sur l'activation en cascade de 3 kinases successives : une MAPK kinase kinase (MAP3K), une MAPK kinase (MAP2K) et pour finir une MAPK qui donnera la spécificité de la voie. Quatre principales familles de MAPK différentes ont été à ce jour caractérisées : la famille des extracellular signal-regulated kinase (ERK1 et ERK2), la famille des p38 MAPKs (*MAPK 11-14*), la famille des c-Jun N-terminal kinase (JNK, codées par *MAPK9-10*) et la famille de ERK5 (Coulombe and Meloche, 2007). Elles sont appelées les MAPK conventionnelles et partagent toutes la présence d'un motif Thr-Xaa-Tyr dans leur boucle d'activation. Des MAPKs, dites atypiques, existent également et diffèrent par l'absence de ce motif Thr-Xaa-Tyr et par leur mécanisme d'activation – encore méconnu – qui ne semblent pas reposer sur cette cascade, ces protéines n'étant pas activées par la phosphorylation exercée par une MAP2K. Seule NLK semble échapper à cette dernière règle, car les kinases TAK1 et HIPK2 pourraient respectivement agir comme MAP3K et MAP2K sur l'activation de cette MAPK. Les différentes voies de signalisation des MAPKs sont détaillées dans la Figure 8.

	Classical MAPK				Atypical MAPK		
MAP3K	RAF-1 ; BRAF ; ARAF c-MOST	MLK1/2/3/7 ; LZK TAK1 ; TPL2 MEKK1-4 ; DLK ASK1/2 ; MLTK	TAO1/2 ; ASK1 ; TAK1 MEKK1-4	MEKK2/3 ; TPL2	-	TAK1	-
MAP2K	MEK1/2	MKK4/7	MKK3/6	MEK5	ERK3/4 ?	HIPK2	-
MAPK	ERK1/2	JNK1/2/3	p38 $\alpha/\beta/\gamma/\delta$	ERK5	ERK3/4	NLK	ERK7

Modifié d'après Coulombe et Meloche 2007.

Figure 8: Liste des MAPKs et de leurs MAP2Ks et MAP3Ks associées.

Pour la suite de ce manuscrit, la voie MAPK/ERK sera appelée voie MAPK sauf mention contraire.

La voie MAPK est la cascade de signalisation qui conduit de l'activation des protéines MAP3K RAF (ARAF, BRAF et RAF-1), à l'activation des MAPKs ERK 1 et d'ERK2 via l'activation des MAP2K MEK1 et 2. Physiologiquement, l'activation de la voie MAPK est principalement connue pour être médiée par l'activation de récepteurs tyrosine kinase (RTK), mais d'autres récepteurs tels que les RCPGs peuvent activer cette voie tout comme différents stress cellulaires (Cargnello and Roux, 2011). La fixation des ligands sur les RTKs induit la dimérisation de ces récepteurs accompagnée de l'autophosphorylation croisée de tyrosines situées dans la partie

cytoplasmique des récepteurs. Ces tyrosines phosphorylées vont servir de substrat pour la fixation d'enzymes telles que la phosphatase SHP2 ou la kinase SRC mais aussi pour des protéines adaptatrices – comme Growth factor receptor-bound protein 2 (GRB2) ou SHC adaptor protein 1 (SHC)- et des protéines d'ancrage – comme les GRB2-associated binding protein 1-3 (GAB1-3).

Ces protéines adaptatrices vont fixer et activer des protéines d'échange de nucléotide guanidique (GEF) tel que Son of sevenless (SOS). Cette protéine va permettre l'échange du GDP fixé aux protéines RAS par un GTP induisant l'activation de la protéine RAS. L'inactivation des RAS se fait par hydrolyse du GTP en GDP due à l'activité GTPase des protéines RAS. Cette activité enzymatique est relativement lente, mais est catalysée par la fixation de GTPase-activating protein (GAP) tel que la neurofibromine 1 (NF1). La famille des protéines RAS est composée de 3 membres NRAS, KRAS et HRAS. Ces protéines localisées à la membrane sont des carrefours de signalisation étant à l'interface de la voie MAPK, de la voie PI3K/AKT, mais aussi des signalisations moins décrites via les protéines RAL ou PLC ϵ (Bunney and Katan, 2006; Kashatus, 2013; Petit et al., 2019). La protéine RAS activée va se fixer sur les MAP3K (ARAF, BRAF et RAF1). Cette fixation permet le recrutement des RAF à la membrane, leur dimérisation en homo- ou hétéro-dimères et finalement leur activation. Les RAF sont des sérines/thréonines kinases qui vont phosphoryler deux résidus sérines dans le segment d'activation du domaine kinase des MAP2K (MEK1 et MEK2) induisant l'activité catalytique des kinases MEKs. La MAP2K MEK est une sérine/thréonine et tyrosine kinase qui va activer les MAPK (ERK1 et ERK2) en phosphorylant à la fois un résidu tyrosine et un résidu thréonine. Les kinases ERK1/2 une fois phosphorylées vont avoir de nombreuses cibles différentes à la fois dans le noyau ou dans le cytoplasme. Dans le noyau, les kinases ERK1/2 vont phosphoryler des facteurs de transcriptions comme c-Fos, c-Myc, particulièrement impliqués dans la prolifération cellulaire. Dans le cytoplasme, ERK1/2 vont phosphoryler de nombreuses cibles comme les 90 kDa ribosomal S6 kinase (RSK), des kinases impliquées dans la régulation de la prolifération ainsi que d'autres protéines impliquées dans la migration comme WASP and verprolin homologous protein 2 (WAVE2), un membre du WAVE2 regulatory complex (WRC) régulant l'activité du complexe Arp2/3, ou les focal adhesion kinases (FAK) (Danson et al., 2007; Hunger-Glaser et al., 2003; Mendoza et al., 2011). Cette cascade de phosphorylation est décrite dans la Figure 9.

L'activation de la voie MAPK induit la prolifération cellulaire en régulant la transition G1-S du cycle cellulaire (Meloche and Pouyssegur, 2007). Cet effet se fait notamment via l'induction de

l'expression de facteurs de transcriptions comme c-Fos, qui via son association avec c-Jun va former le complexe AP1. Ce complexe va permettre l'expression de la cyclin-D1 nécessaire à la transition G1-S (Meloche and Pouyssegur, 2007). L'activation de la voie MAPK va aussi induire la migration cellulaire en favorisant la polymérisation de l'actine permettant la formation des protrusions cellulaires nécessaires à la motilité (Tanimura and Takeda, 2017). L'effet sur la migration est également dû à l'activation des FAK qui permettent l'établissement de points de contacts focaux avec la matrice extracellulaire (Hunger-Glaser et al., 2003).

Le mélanome est un cancer où la voie MAPK est particulièrement activée. Cette activation est principalement due à la présence de mutation de membres de la voie ou de ses régulateurs. En effet, environ 1 mélanome cutané sur deux est muté pour BRAF, principalement BRAFV600E (75-90% des cas mutés BRAF). Concernant les autres mutations de membres de la voie MAPK, dans 5% des cas sont retrouvées des mutations oncogéniques de MEK1. Deux autres facteurs – RAF1 et MEK2 – sont bien plus rarement mutés dans approximativement 1% des cas. Les autres membres de la voie MAPK ne sont pas ou exceptionnellement muté dans le mélanome (<0.3%). Toutes ces mutations sont mutuellement exclusives dans le mélanome non traité. Des facteurs régulateurs de la voie MAPK sont également mutés dans le mélanome, 25% des patients sont mutés pour NRAS (90% touchant la glutamine 61). Les mutations activatrices de KRAS et de HRAS sont retrouvées dans 1% des cas de mélanome. Toutes ces mutations sont exclusives entre elles et exclusives avec les mutations activatrices des membres de la voie MAPK. Des pertes de NF1 sont également retrouvées dans environ 15% des cas. D'autres mécanismes d'activation plus mineurs sont également décrits comme la survenue de mutations activatrice de $G\alpha_{q/11}$, ou des récepteurs tyrosine kinase c-KIT et VEGFR (2% chacun) (Catalanotti et al., 2017; Hodis et al., 2012; Krauthammer et al., 2012; Shi et al., 2014; Snyder et al., 2014; The Cancer Genome Atlas Network, 2015; Van Allen et al., 2015; Zehir et al., 2017). Les protéines mutées et régulant la voie MAPK sont annotées dans la Figure 9.

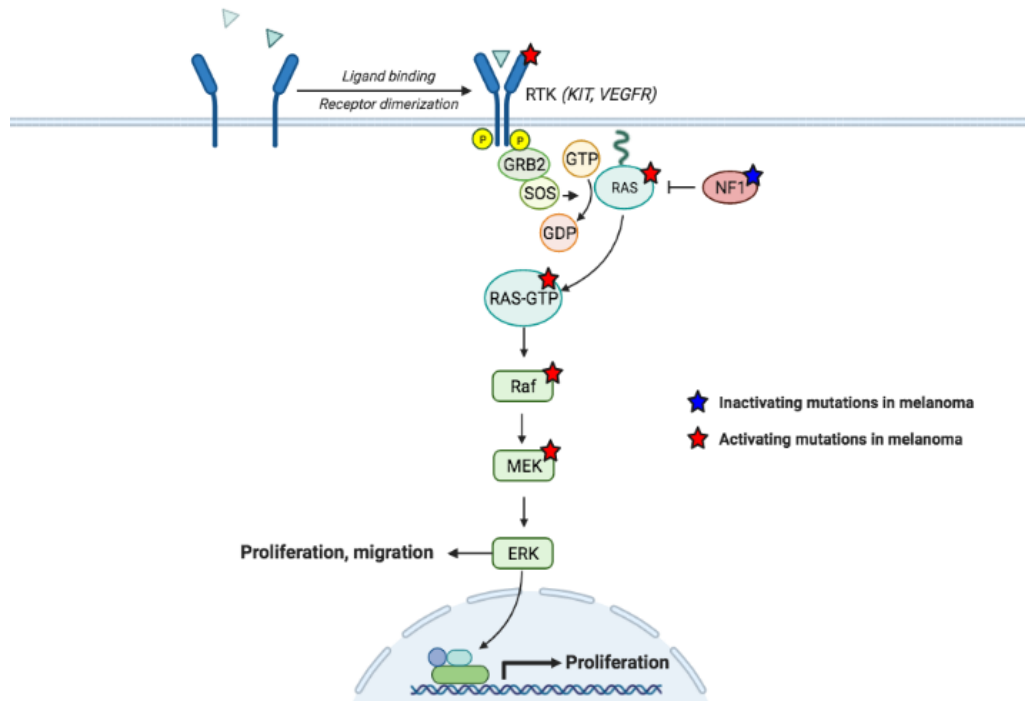
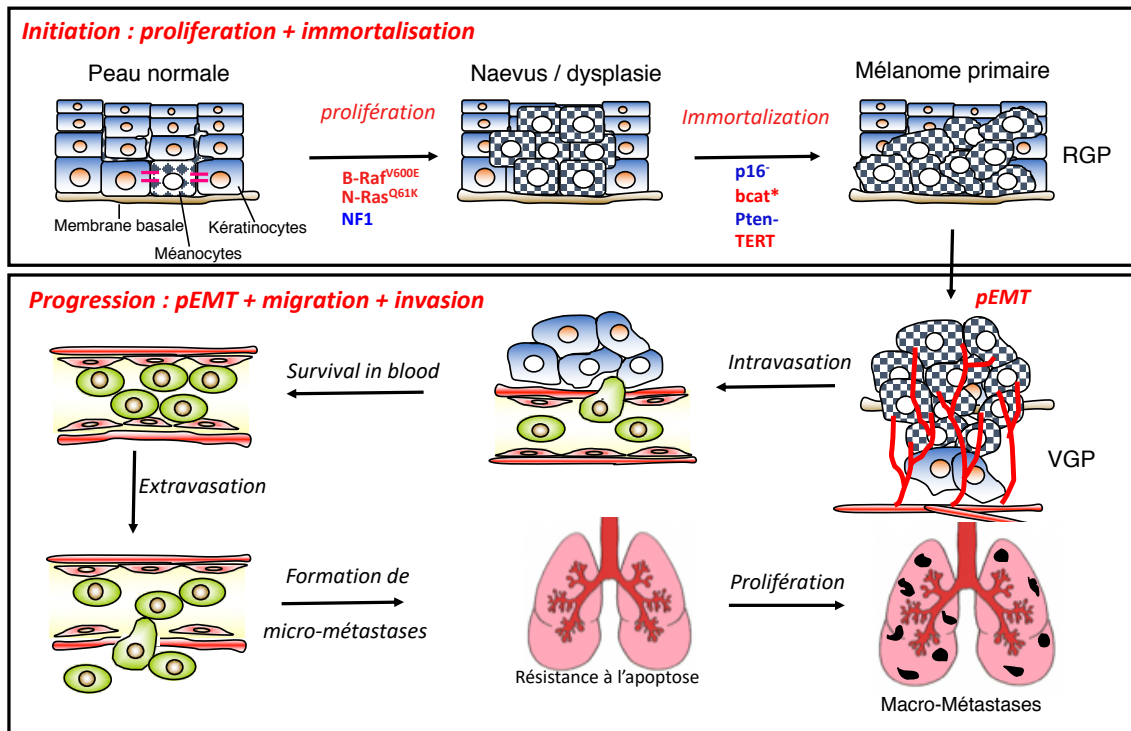


Figure 9: Voie MAPK/ERK.

L'activation de RTK va induire l'activation de RAS grâce à la fixation sur RAS de GTP grâce à la protéine SOS. RAS va se lier aux protéines RAF pour induire leur activation. L'activation de RAF va activer la phosphorylation en cascade des membres de la voie MAPK ce qui aboutit à l'activation de ERK. ERK va interagir avec des cibles nucléaires et cytoplasmiques pour induire l'activation de différents processus cellulaires comme la prolifération ou la migration. Les protéines marquées d'une étoile rouge sont fréquemment porteuses de mutations activatrices dans le mélanome. L'étoile bleue marque NF1, régulièrement inactivée dans le mélanome. Créé avec BioRender.com.

vi. Mélanomagenèse

L'ensemble des processus conduisant au mélanome métastatique s'appelle la mélanomagenèse. Elle est composée de plusieurs étapes et de deux grandes phases : l'initiation et la progression. Au cours de l'initiation, un mélanome primaire est formé et pendant la phase de progression le mélanome sort de l'environnement épidermique pour former de façon ultime des métastases dans des organes distants. La connaissance des événements moléculaires de la mélanomagenèse est principalement due à la mise en place de modèle in vivo, murin et poisson-zèbre principalement.



D'après (Larue and Beermann, 2007)

Figure 10: La Mélanomagenèse.

La description des évènements est très linéaire sur ce schéma (Figure 10), mais il faut garder à l'esprit qu'en réalité, ceux-ci peuvent avoir lieu simultanément. La première étape va reposer sur deux principes : 1) l'induction de la prolifération des mélanocytes par l'activation de la voie MAPK. Cette activation se fait principalement par le biais de l'acquisition de mutation de BRAF, de NRAS ou des pertes de fonctions de NF1. D'autres mutations ont été identifiées comme capables d'engendrer des mélanomes, avec de très faibles fréquences. On peut notamment citer la mutation GNAQ^{Q209L} 2) le passage de la sénescence. Pour contourner la sénescence induite par les oncogènes liés à la suractivation de la voie MAPK, des mutations induisant l'immortalisation vont avoir lieu. Sans ces deuxièmes mutations, le stade nævus n'est pas dépassé. Parmi les gènes susceptibles d'être mutés, on retrouve des mutations perte de fonction et des pertes d'hétérozygotie de *CDKN2A* (60%) et *PTEN* (12%) ainsi que des mutations activatrices de *CTNNB1* (2.7%) et *CDK4* et l'activation de la transcription de *TERT* (66%) (Bertrand et al., 2020). Ces évènements immortalisant ne sont pas mutuellement exclusifs et sont fréquemment associés dans le mélanome. Sans que l'on ne sache exactement pourquoi, les pertes de fonction de *PTEN* sont majoritairement associées aux mélanomes BRAF – 17% des mélanomes BRAF sont inactivés pour *PTEN* vs 7-8% dans les autres sous-types – et les mutations de *CDKN2A* sont plus associées aux mélanomes NRAS et NF1 – 58% des mélanomes BRAF portes des invalidations de

CDKN2A contre 72% et 71% pour les mélanomes *NRAS* et *NF1* respectivement. Il faut noter qu'il y a d'autres facteurs ou étapes encore non identifiés pour former un mélanome primaire, car par exemple, une souris *Tyr::NRAS^{Q61K}; Cdkn2a^{-/-}* dans laquelle tous les mélanocytes expriment la forme activée de *NRAS* associée à l'inactivation *Cdkn2a* ne va développer que peu de mélanomes durant sa vie. Cela suggère un contrôle important sur la prolifération induite et que d'autres événements sont nécessaires pour transformer le mélanocyte en mélanome.

La deuxième étape est dite de progression et conduit à la formation du mélanome métastatique. Elle commence par une modification du phénotype lors de la transition pseudo-épithélio-mésenchymateuse (pEMT) des cellules qui confère aux cellules la capacité d'envahir les tissus sous-jacents à commencer par le derme. Cette étape est encore peu étudiée sur des modèles de mélanomagenèse *in vivo*, la souris et le poisson-zèbre n'étant pas adaptés. Les cellules vont ensuite pénétrer dans la circulation lymphatique ou sanguine et rejoindre des organes distants pour potentiellement former de nouveaux foyers tumoraux. Ces étapes requièrent de nombreux mécanismes cellulaires comme l'intravasation, l'extravasation et l'envahissement des tissus cibles, les cellules doivent acquérir des capacités migratoires et invasives. Les cellules devront également être capables de résister à l'apoptose et à l'anoïkis dans la circulation et les organes cibles puis de proliférer. Cette étape est régulièrement évaluée par l'injection de cellules dans la veine de la queue des souris et leur capacité à envahir les poumons, mais pas à l'aide de modèle retraçant toute la complexité de la cascade métastatique (Aktary et al., 2017).

vii. Modèles précliniques du mélanome

Les connaissances sur la mélanomagenèse ont été établies à partir des données épidémiologiques, cellulaires et moléculaires et également à l'aide de différents modèles précliniques. La qualité de ces modèles est essentielle pour le développement ultérieur d'essais cliniques pertinents.

- *Xénogreffes de cellules*

Cette technique est le plus couramment utilisée par sa simplicité d'accès et la relative aisance pour modifier génétiquement les cellules. Ces cellules ont été pour la plupart déjà préalablement établies et sont largement utilisées pour des essais *in vitro*. Elles sont injectées sous la peau de souris immunodéficientes (SCID/NSG). Ces modèles sont très utiles pour évaluer l'effet d'un gène sur la croissance tumorale ou d'autres processus comme l'angiogenèse. D'autres types d'injections sont possibles pour tester la capacité des cellules à croître dans d'autres organes

comme les injections dans la veine de la queue pour évaluer la capacité à coloniser le poumon ou des stéréotaxies cérébrales pour tester la croissance dans le cerveau. Ces modèles sont aussi bien adaptés pour réaliser des tests de molécules pharmacologiques. Il y a néanmoins des limites franches à ces modèles à savoir que les cellules utilisées sont passées par des étapes de cultures en 2D, régulièrement clonées et sélectionnées sur leur capacité à proliférer rapidement et à survivre. De ce fait, les lignées établies en culture ne sont plus forcément représentatives du mélanome initial. De plus, les cellules sont injectées dans des souris immunodéficientes donc le rôle du système immunitaire dans les processus observés ne sera pas évalué.

- *Xénogreffes de tumeurs de patients*

Lors de la biopsie ou la résection de tumeurs de patients, des morceaux sont prélevés et implantés directement sous la peau de souris sans passer par des étapes de culture *in vitro*. Ainsi les caractéristiques du mélanome initial et notamment l'hétérogénéité cellulaire du mélanome est conservée, au moins lors des premiers passages *in vivo*. Ainsi, lors de tests d'efficacité de molécules, l'effet sur plusieurs sous-types cellulaires est en réalité observé, ce qui est intéressant, notamment pour étudier la présence de sous-population plus résistante/plus sensible aux traitements. L'emploi de méthode pour modifier génétiquement les xénogreffes est possible, mais plus compliqué, car de nombreux protocoles classiques sont inopérants. Les limitations sont similaires à celles décrites pour les xénogreffes de cellules, la greffe se faisant dans un environnement immunodéficient.

- *Modèles murins génétiquement modifiés*

Les modèles précédents permettent d'évaluer l'effet de gènes ou de drogues sur des phases limitées de la mélanomagenèse et n'adressent principalement que le rôle de ces gènes ou molécules dans des processus cellulaires de survie et de croissance. Par conséquent, le développement de modèles murins développant de manière spontanée ou non des mélanomes permet d'évaluer toutes les étapes de la mélanomagenèse. Des modèles murins ont été développés avec des mutations découvertes lors des études cliniques de patients atteints de mélanomes. Deux méthodes ont été appliquées pour créer ces modèles : l'ajout de transgènes codant pour des protéines mutées ou non exprimées dans la cellule originale ou la modification de gènes par recombinaison homologue. Cette dernière méthode étant utilisée pour invalider un gène ou ses transcrits, créer des mutations du gène ou insérer/remplacer des séquences du gène par des séquences LoxP pour induire la mutation conditionnelle du gène *in vivo*. On peut citer

parmi les modèles très utilisés, le modèle *Braf^{CA/WT}* – dans lequel a été inséré dans le gène de *Braf* une cassette flanquée de LoxP codant pour BRAFV600E – et le modèle transgénique *Tyr::NRAS^{Q61K}* – où le transgène codant pour la forme mutée de NRAS humain sous contrôle du promoteur tyrosinase a été inséré dans le génome de souris. Ces modèles reprenant les mutations activatrices bien connues, activant la prolifération du mélanome, sont régulièrement couplés avec des modèles régulant l’immortalisation. On peut citer notamment les souris *Cdkn2a^{-/-}*, les souris *Pten^{F/F}*, ou *Tyr::bcat**. De nombreux modèles de mélanomes sont établis grâce à l’utilisation de promoteur spécifique du mélanocyte (*Tyr*, *Dct*, *Mitf*). Par exemple, dans les souris *Tyr::NRAS^{Q61K}* et *Tyr::bcat**, les transgènes sont exprimés sous contrôle du promoteur tyrosinase à partir du jour embryonnaire E10.5 *in vivo* dans les mélanoblastes puis dans les mélanocytes. Le modèle *Braf^{CA/WT}* nécessite l’activation d’une recombinaise (CRE) pour exprimer la mutation *Braf^{V600E}*. Deux grands types de construction transgénique exprimant la recombinaise CRE ont été établis dans le mélanome. Le premier, *Tyr::CreA* (Tg(Tyr-cre)#Lru) permet un contrôle spatial de Cre sous le contrôle du promoteur de la tyrosinase (Delmas et al., 2003). Le deuxième, permet un contrôle spatial et temporel en utilisant des recombinaises fusionnées avec le récepteur aux œstrogènes modifié (ERT2). Celui-ci ne reconnaît que le tamoxifène et la liaison de ce dernier sur le récepteur ERT2 induit la translocation nucléaire du complexe Cre-ERT2 et permet l’action de la recombinaise sur l’ADN. Le contrôle est spatial, car la Cre-ERT2 est sous contrôle d’un promoteur spécifique, mais aussi temporel, car son activation est dépendante du traitement des souris par le tamoxifène. On peut citer dans ce cas le modèle Tg(Tyr-cre/ERT2)1Lru/J établi au laboratoire ou celui établi dans le laboratoire de L. Chin Tg(Tyr-cre/ERT2)13Bos/J (Bosenberg et al., 2006; Yajima et al., 2006). En fonction des modifications génétiques introduites, les souris vont produire spontanément des mélanomes. Ainsi toutes les étapes de la mélanomagenèse peuvent être étudiées que ce soit l’initiation ou les différents processus de la progression tumorale

Ces modèles murins sont généralement dans un fond génétique C57BL/6 et permettent d’évaluer la mélanomagenèse dans un fond génétiquement pur et dans un environnement immunocompétent. A partir de ces modèles, des lignées de cellules de mélanomes en culture peuvent être établies, elles pourront ensuite être réinjectées dans des souris C57BL/6 et garder cet environnement immunocompétent. Les limites sont le temps (temps de génération du modèle + temps de génération des croisements adéquats en nombre suffisant + temps de développement des mélanomes *in vivo*) et le coût très élevé. Une autre limitation est le caractère murin et non-humain, certains gènes exprimés n’étant pas tous homologues.

- *Modèles non murins*

D'autres modèles ont été également générés et sont toujours utilisés activement. Le poisson-zèbre est le deuxième modèle le plus utilisé dans la recherche contre le mélanome. C'est notamment dans ce modèle qu'a été établi le premier modèle de mélanome BRAF muté par Elizabeth Patton en 2005 (Patton et al., 2005). Ces modèles, bien que plus éloignés génétiquement que les modèles murins pour l'homme restent très intéressants pour leur facilité et rapidité de production. Ils sont particulièrement adaptés pour la réalisation de cribles génétiques ou thérapeutiques. Leur aspect transparent est également une aide précieuse pour l'observation des tumeurs et de leur vascularisation.

Des modèles, plus historiques utilisant le chien, le cochon ou le cheval ont aussi été établis profitant de la prédisposition de certaines races à produire des mélanomes. Le chien est un modèle particulièrement intéressant pour les mélanomes muqueux.

viii. Traitements du mélanome

La connaissance de la mélanomagenèse et la création des modèles précliniques mis en place ont permis de tester différents traitements. La thérapeutique du patient va dépendre du diagnostic et de la génétique de la tumeur.

- *Chirurgie*

La résection de la tumeur primaire est le traitement de première ligne pour les mélanomes résécables (Garbe et al., 2020). Elle est suffisante si la tumeur n'a pas envahi les tissus environnants, ce qui met l'accent sur le diagnostic précoce. Un curage ganglionnaire peut être fait en complément. Le curage apporte plus de bénéfice sur les patients présentant des macro-métastases que sur les patients avec des micro-métastases. La surveillance médicale renforcée est favorisée pour les mélanomes métastatiques (Leiter et al., 2019). La chirurgie dans les organes distants est elle aussi réalisable, mais nécessite un nombre de foyers métastatiques faible et les conséquences sur la survie ne sont malheureusement pas si importantes (Deutsch et al., 2017; Okereke, 2015).

- *Radiothérapies*

La radiothérapie a été testée dans le traitement du mélanome avant l'arrivée des nouvelles thérapies. Elle présentait l'avantage de cibler précisément les zones à traiter à l'inverse des thérapies médicamenteuses. Dans le cadre du mélanome primaire, cette thérapie n'a pas montré

de résultats probants sauf dans le cas de mélanome primaire non résecable (Farshad et al., 2002). Cette technique a toutefois montré un intérêt dans le traitement de métastases cérébrales en particulier en combinaison avec l'emploi d'immunothérapies ou de thérapies ciblées (Grimaldi et al., 2014; Lehrer et al., 2019). Le traitement de l'entièreté du cerveau peut également être une solution de dernier recours malgré les effets secondaires importants qu'il induit (Mahajan et al., 2017). Le traitement de métastases osseuses par radiothérapie était parfois effectué en particulier dans un cadre palliatif, lorsque ces métastases dégradent la qualité de vie du patient (Kirova et al., 1999; Rate et al., 1988).

- *Chimiothérapies classiques*

Les premières thérapies médicamenteuses mises en place ont été des molécules de chimiothérapie classique. Beaucoup ont été testées, mais seule la dacarbazine, une pro-drogue dont le produit déméthylé, le 5-amino-imidazole-4-carboxamide, exerce une action alkylante sur l'ADN empêchant sa réplication combinée à un effet inhibiteur indépendant du cycle cellulaire. La dacarbazine a été utilisée largement depuis sa mise sur le marché en 1975 malgré son absence flagrante d'efficacité à cause de l'absence d'alternative thérapeutique. En effet, peu de patients répondaient (de l'ordre de 10 à 20%) et la survie médiane ne dépassait pas 9 mois (Luke et al., 2017).

- *Immunothérapies*

Les premières immunothérapies sont arrivées sur le marché du médicament à la fin des années 1990s. Le but des immunothérapies est de stimuler le système immunitaire du patient pour l'élimination de la tumeur. Les premières testées étaient des protéines recombinantes injectées chez le patient, l'interféron α et IL-2. Les gains de survie étaient faibles (12 mois versus les 9 mois pour la dacarbazine) et des effets secondaire très sévère, notamment marqués par de fortes dépressions accompagnées d'envies suicidaires (Atkins et al., 2000; Kirkwood et al., 2001)

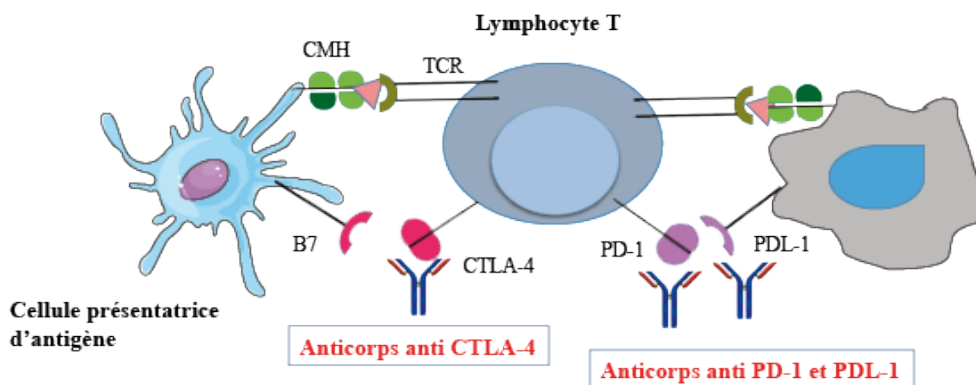


Figure 11: Système d'épuisement lymphocytaire T.

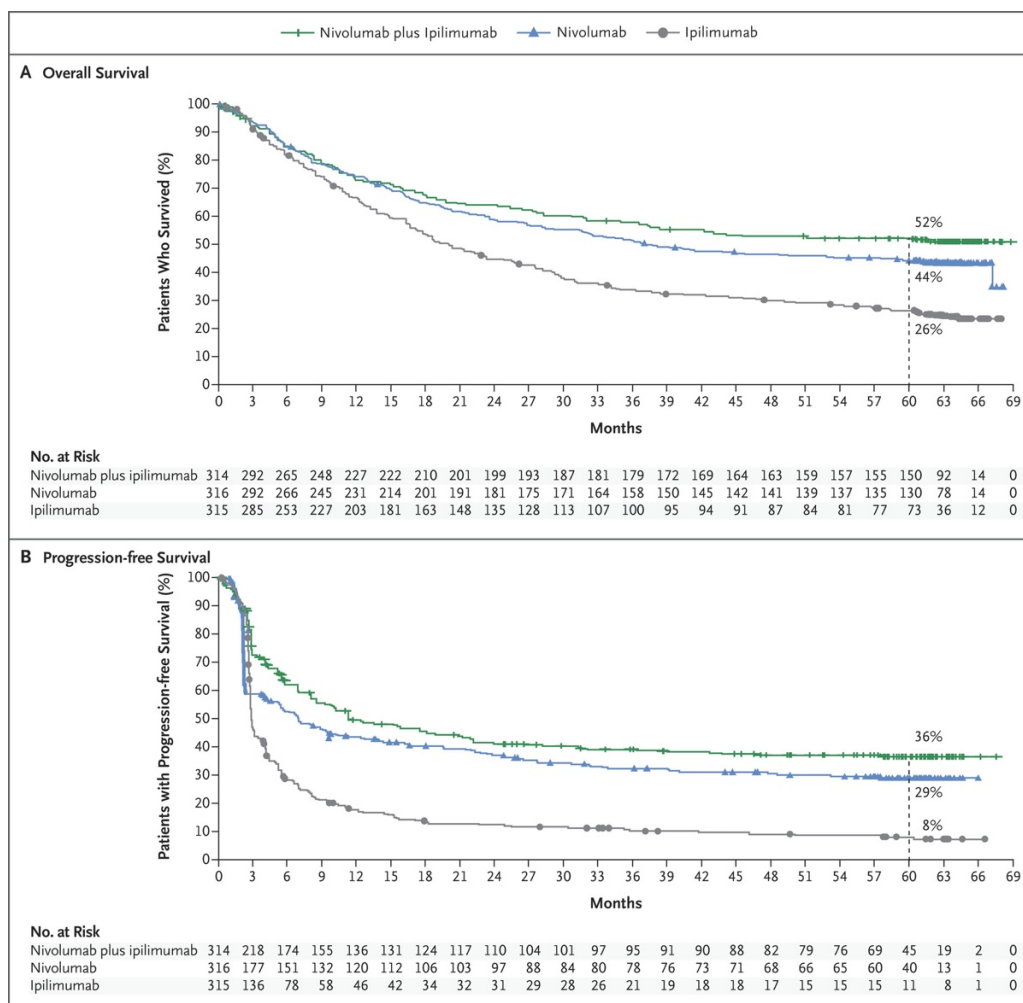
A gauche entre la cellule présentatrice d'antigènes et le lymphocyte T et à droite entre lymphocyte T et tumeur. A noter que ces deux effets ne s'exercent pas aux mêmes localisations anatomiques : l'implication de CTLA4 a lieu dans les ganglions lymphatiques alors que l'interaction PD1-PDL-1 a lieu sur le site tumoral. Adapté de Aparicio et al, POSTU' 2018.

Ce n'est que dans le courant des années 2010s qu'ont été mis sur le marché les premiers traitements efficaces du mélanome, des anticorps ciblant le système d'épuisement des lymphocytes, responsables de l'inactivation des lymphocytes T après leur premier contact. En effet, dans le ganglion lymphatique, l'activation du lymphocyte T par la reconnaissance par son TCR d'un peptide présenté par le CMH d'une cellule présentatrice d'antigène (CPA) va induire l'expression de CTLA4 à sa surface. Ce récepteur va se lier avec ses ligands CD80 and CD86 (aussi appelés B7.1 et B7.2) exprimés à la surface des CPA de façon constitutive. Cette liaison va induire une signalisation dans le lymphocyte T qui va réduire l'activité de celui-ci (Figure 11). A l'opposé à l'interface entre Lymphocyte T et cellule tumorale, une autre interaction va aussi engendrer une activation du système d'épuisement des lymphocytes. Là encore, l'activation du lymphocyte va conduire à l'expression du récepteur PD1 qui se liera à son ligand PDL-1 pour engendrer la perte d'activation du lymphocyte (Figure 11). L'idée a été d'empêcher cet épuisement en inhibant la fixation des récepteurs CTLA4 puis PD1 avec leurs ligands.

Des anticorps thérapeutiques ont été développés dans ce but.

Le premier mis sur le marché, ciblant CTLA4, est l'ipillimumab. Il a obtenu son AMM en 2011. Son taux de réponse objective est de l'ordre de 40% et il a montré une légère augmentation de la survie des patients en monothérapie (10 à 20 mois de survie médiane et une survie à 5 ans de 26%). La progression tumorale reste très importante, car 8% des patients seulement n'ont pas subi de progression tumorale après 5 ans et la survie sans progression est de l'ordre de 3 mois (Larkin et al., 2019; Luke et al., 2017).

Le deuxième mis sur le marché est l'anticorps ciblant PD1, nivolumab. Ciblant directement l'activation des lymphocytes T au niveau des tumeurs il a montré un effet thérapeutique plus important. En effet la survie à 5 ans des patients traités par nivolumab est de 44% (médiane de survie à 37 mois). Il y a quand même toujours une progression du mélanome importante avec une médiane de survie sans progression de 7 mois, seulement 29 % des patients n'avaient pas rechuté à 5 ans. La combinaison du nivolumab avec l'ipilimumab a également été testée en clinique et a montré une additivité d'effet (Figure 12). En effet, après 5 ans 52% des patients sont toujours en vie (la médiane de survie n'étant pas atteinte encore). Il y a néanmoins 36% des patients seulement sans progression tumorale (Larkin et al., 2019; Luke et al., 2017).



Larkin et al, 2019

Figure 12: Kaplan Meier de l'essai clinique évaluant la combinaison nivolumab, ipilimumab.

Survie globale (A) et sans progression (B) des patients traités par nivolumab, ipilimumab ou la combinaison des deux traitements.

Le troisième anticorps utilisé en clinique est le pembrolizumab développé en 2015. Cet anticorps montre un profil similaire à celui du nivolumab. La survie médiane est de 33 mois avec un taux

de survie à 5 ans de 42%. Le taux de patients sans progression à 5 ans est de 26% avec une médiane de survenue de la progression de 8.5 mois (Robert et al., 2019a). La combinaison du pembrozilumab avec l'ipilimumab a aussi été testée, mais n'a pas encore l'ancienneté pour présenter des résultats à 5 ans. A 3 ans, les premiers résultats suggèrent de meilleurs résultats que pour la combinaison nivolumab/ipilimumab avec une survie sans progression chez 59% des patients et 71% toujours en vie (Carlino et al., 2020).

- *Thérapies ciblées visant la voie MAPK*

La connaissance de la mélanomagenèse et l'importance démontrée par les modèles animaux de la voie MAPK dans la prolifération cellulaire du mélanome ont conduit à l'élaboration de thérapies visant son inhibition pour traiter le mélanome. Le ciblage de BRAF a été fait pour la première fois à l'aide du sorafenib, un inhibiteur pan-RAF. Mais malgré de bons résultats précliniques, les essais cliniques n'ont pas réussi à montrer un effet thérapeutique (Dal Lago et al., 2008; Sharma et al., 2005). La thérapeutique est devenue ensuite plus ciblée et dépendante des mutations du patient.

L'intérêt s'est ensuite porté sur le design de molécules spécifiques de BRAF^{V600E} dans le but de traiter les patients portant ces mutations. Ce but a été atteint par drug-screening et aboutit à la synthèse du Vémurafénib (PLX4032) (Kim and Cohen, 2016). Celui-ci a rapidement montré de bons résultats précliniques poussant son développement en essais cliniques. Les essais cliniques des inhibiteurs de BRAF^{V600E} ont montré un gain de 4 mois de survie globale et de survie sans progression tout en ayant une réponse objective élevée par rapport aux autres traitements (50%). Ces résultats prometteurs ont conduit à sa mise sur le marché en 2012. En revanche, il a été rapidement mis en évidence que si le patient répondait bien et que la survie sur des temps précoces était grandement améliorée, les patients traités par inhibiteurs de BRAF rechutaient rapidement, le taux de patients en vie après 4 ans était similaire entre dacarbazine et vémurafénib, le vémurafénib seul ne permettant qu'un décalage des courbes de survies de quelques mois (Chapman et al., 2017). Par la suite d'autres inhibiteurs de BRAF^{V600E} ont été produits et mis sur le marché : le dabrafénib en 2013 et l'encorafénib en 2018. Le dabrafénib présente un profil clinique similaire (Hauschild et al., 2012). Le traitement par monothérapie avec l'encorafénib a un taux de patients répondeurs de 51%. 40% des patients sont toujours en vie après 5 ans de traitements et 81% des patients ont vu leur mélanome progresser dans ce laps de temps (Dummer et al., 2021).

Rapidement, il a été suggéré que pour pallier aux déficits d'efficacité à long terme, la combinaison de l'inhibition de BRAF^{V600E} et de MEK serait utile. De plus, l'inhibition de BRAF^{V600E} étant inutile dans les mélanomes non BRAF^{V600E}, des monothérapies MEK pourraient être bénéfiques dans ce cadre. 3 molécules ont été successivement mises sur le marché : le tramétinib en 2014, le cobimétinib en 2015 et la binimétinib en 2018. La bi-thérapie a obtenu de meilleurs résultats cliniques que la monothérapie avec un taux de réponse objective de 68% et un gain de survie sans progression de 6 mois. 5 ans après l'établissement du traitement, 31% des patients traités par dabrafénib et tramétinib étaient encore en vie (Long et al., 2017; Robert et al., 2019b). La combinaison entre vémurafénib et cobimétinib a des résultats similaires (réponse objective de 60%, survie à 5 ans de 31%) (Ascierto et al., 2021). De façon plus intrigante, la combinaison entre encorafénib et binimétinib, même si elle augmente le nombre de patients répondeurs à 64% et la durée de cette réponse, n'améliore pas le nombre de décès comparé à la monothérapie seule par encorafénib avec 68% de décès (Dummer et al., 2021). Les résultats des essais cliniques sont synthétisés dans la Figure 13.

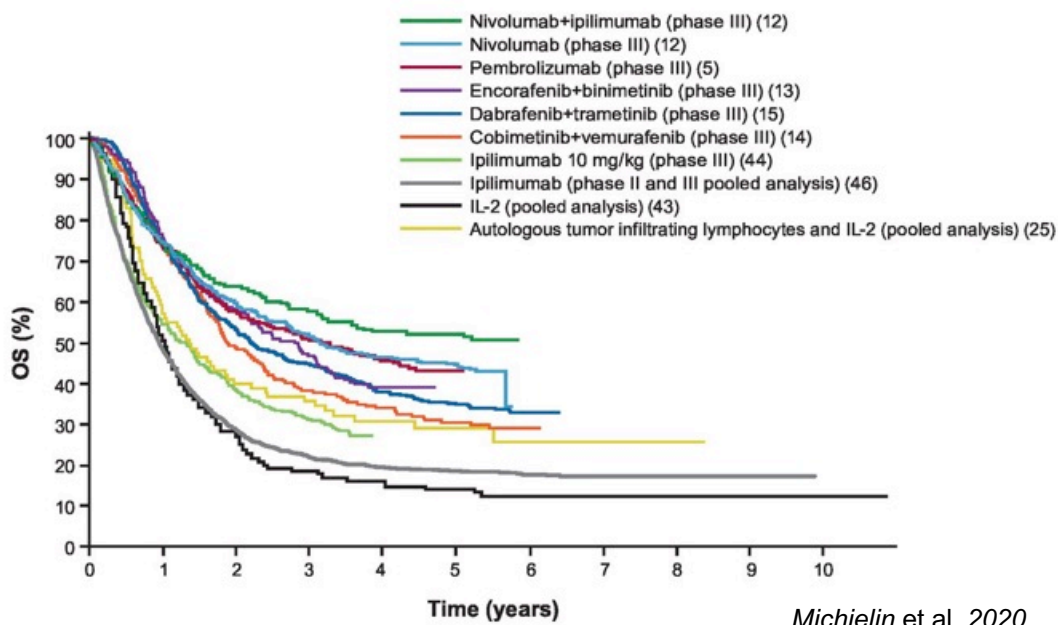


Figure 13: Courbe de survie des différentes thérapies utilisées dans le mélanome.

Dans le cadre des patients portant des mutations NRAS, les choix de traitements ciblant la voie MAPK sont nettement plus limités, l'utilisation des inhibiteurs spécifiques de BRAF^{V600E} étant bien évidemment impossible. L'utilisation d'inhibiteurs de MEK a été testée en clinique, mais n'a montré que des résultats décevants. La cobimétinib a été testée sur des patients dont les

mélanomes présentait des mutations NRAS, mais l'effet a été faible, de l'ordre d'un à deux mois de gain de survie sans progression (Dummer et al., 2017). NRAS étant connu pour également activer AKT (Davies, 2012; Petit et al., 2019) un essai clinique a été entrepris pour évaluer l'effet d'une bithérapie ciblant AKT et MEK, mais aucun effet probant n'a été observé (Algazi et al., 2018),

Le principal écueil avec les thérapies ciblant la voie MAPK vient des rapides résistances acquises qui rendent les traitements très vite inopérants. De nombreux mécanismes moléculaires, qui peuvent être acquis et/ou induits/sélectionnés par le traitement, inhérents à la cellule de mélanome sont mis en jeu au sein desquels :

- Des amplifications de BRAF ou des variants d'épissage qui vont conduire à une réactivation de la voie MAPK et donc à la prolifération des cellules de mélanome (Long et al., 2014; Poulikakos et al., 2011).
- Une réactivation d'AKT via la perte de PTEN ce qui favorise la survie cellulaire (Catalanotti et al., 2017; Paraiso et al., 2011)
- Des amplifications de CCND1 (codant la Cyclin-D1) qui favorisent la prolifération cellulaire (Nathanson et al., 2013).
- Des mutations de RAC1, notamment la mutation RAC1^{P29S}, qui vont favoriser la prolifération cellulaire (Van Allen et al., 2014; Watson et al., 2014).
- Des mutations constitutives de MEK réactivant de ce fait, la signalisation MAPK (Carlino et al., 2015).
- L'activation de récepteurs tyrosine kinase comme AXL ou EGFR, dont l'activation va favoriser la survie et la prolifération cellulaire via l'activation de la voie AKT et une réactivation de la signalisation MAPK (Müller et al., 2014; Shaffer et al., 2017).
- L'activation de RCPG comme le récepteur à l'endothéline A (EDNRA) et B (EDNRB). Le traitement par les inhibiteurs de MAPK va engendrer la production d'endothéline-1 par les cellules de mélanomes qui par des mécanismes paracrines et autocrines vont activer EDNRB et EDNRA. Cette activation va provoquer l'activation d'une signalisation $G\alpha_q$ et réactivation de la croissance cellulaire en présence d'inhibiteurs de MAPK (Smith et al., 2017a).

- *Prise en charge actuelle, en France*

La prise en charge suit un arbre décisionnel en fonction de la situation du patient vis-à-vis de certains facteurs clefs comme le stade de la tumeur, l'indice de breslow de la tumeur primaire ou le statut BRAF. L'arbre de décision est détaillé ci-dessous (Figure 14). Le suivi des patients est régulier et dépend du stade auquel le mélanome est détecté ainsi que du traitement.

Le dernier élément n'est pas une prise en charge du malade, mais est l'importance de la prévention auprès de la population pour diminuer l'incidence de mélanome en insistant sur les dangers du soleil et des UVs artificiels. La sensibilisation du grand public à l'auto-dépistage, à réaliser régulièrement, tous les 6 mois / un an est aussi importante pour découvrir précocement les lésions. Celui-ci est relativement aisé à l'aide de la règle ABCDE. La prise en photo régulière de son corps pour suivre l'évolution et voir l'apparition de grains de beauté ou de mélanomes primaires est très utile particulièrement pour les zones difficiles d'accès aux regards (dos, fesses, cuisses par exemple).



Figure 14: Arbre décisionnel de prise en charge du mélanome métastatique en France

B. E-cadhérine

I. Structure et interactions cellulaires

La E-cadhérine (E-cad) fait partie de la superfamille des cadhérines. Cette superfamille de plus de 350 membres dans 30 espèces différentes est divisée en différentes sous-familles : les cadhérines, les proto-cadhérines et les cadhérines desmosomales. Ces protéines partagent une structure similaire basée sur la présence de domaines cadhérines extracellulaires même si leur nombre est variable. La partie extracellulaire des protéines de la superfamille des cadhérines est rigidifiée par la fixation de 3 ions Ca^{++} entre les domaines cadhérines (Kemler, 1992; Shapiro and Weis, 2009). E-cad est une cadhérine dite « classique » de type 1 au même titre que N-cadhérine et P-cadhérine. La structure de ces cadhérines classiques de type 1 est basée sur la répétition de 5 domaines cadhérine (EC1-EC5), où EC1 est le domaine N-terminal, le plus éloigné de la membrane plasmique. Les cadhérines exercent leur action d'adhésion par le biais de jonctions homophiliques, une cadhérine ne va établir de liaison qu'avec une autre cadhérine identique et non pas avec d'autres cadhérines. Ces jonctions vont permettre la formation des jonctions adhérentes et sont dépendantes du calcium. L'interaction entre les 2 molécules d'E-cad se fait au niveau du domaine EC1 chacune d'entre elles, comme schématisé ci-dessous (Figure 15A). La spécificité de l'interaction des cadhérines provient de la variation de quelques acides aminés du domaine EC1 situé sur une région dite « brin A » qui est un feuillet beta N-terminal. Lorsque les cadhérines sont non-liées le brin A est lié au domaine EC1. Lors de la liaison homophile entre deux cadhérines, les domaines EC1 vont s'échanger leurs brins A et stabiliser ainsi la jonction (Chen et al., 2005, Figure 15B).

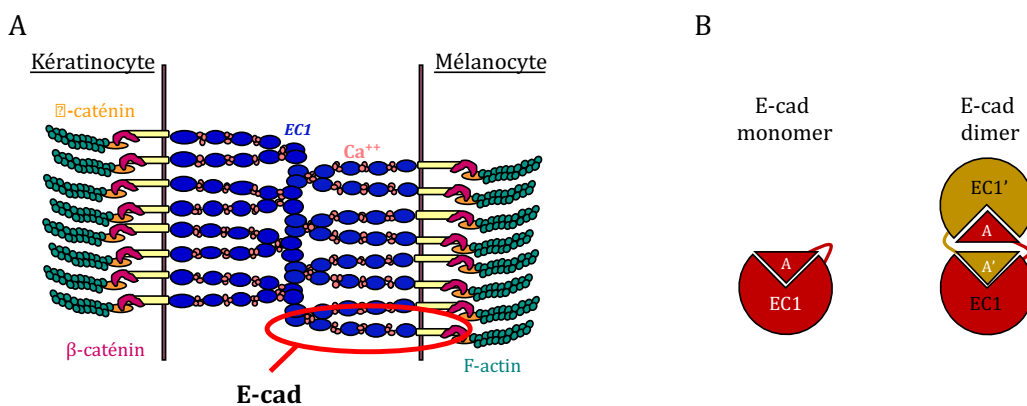


Figure 15: Structure des jonctions E-cadhérine/E-cadhérine
(A) schéma des liaisons homophiliques engendrée par E-cad au niveau de la jonction entre kératinocyte et mélanocyte. (B) schéma de l'échange de brin lors de l'interaction E-cad - E-cad.

Le reste de la structure d'E-cad est composé d'une hélice alpha transmembranaire et d'un domaine intracellulaire. Ce domaine intracellulaire est important, car il est le site de fixation des protéines qui vont permettre les fonctions de la E-cad. Deux protéines se fixent sur E-cad : p120-caténine et β -caténine. La p120-caténine stabilise l'expression d'E-cad à la surface cellulaire favorisant ainsi l'adhésion cellulaire (Kourtidis et al., 2013; Oas et al., 2013). β -caténine, au niveau du complexe E-cad/ β -caténine joue le rôle de support pour la fixation d'autres protéines. β -caténine fixe l' α -caténine qui établit la jonction entre le complexe E-cad/ β -caténine et le cytosquelette d'actine (Tian et al., 2011). D'autres protéines peuvent se fixer sur le complexe E-cad/ β -caténine et moduler sa cohésion. Parmi elles, on peut citer la Préséniline 1 qui est capable de cliver E-cadhérine libérant ainsi tous les composants du complexe dans le cytoplasme (Marambaud et al., 2002; Parisiadou et al., 2004), Hakai qui régule l'endocytose du complexe et Src qui phosphoryle le complexe induisant sa dissociation (Avizienyte et al., 2002; Nam et al., 2002; Niessen et al., 2011).

II. Rôle dans le développement de l'oncogénèse

1. Rôle dans le développement et l'homéostasie

La E-cadhérine joue un rôle fondamental dans un certain nombre d'événements se déroulant au cours du développement. Les souris invalidées pour *Cdh1* meurent au stade de l'implantation, les embryons réussissent à franchir l'étape de la compaction de la morula, largement due à la présence résiduelle de E-cadhérine maternelle, mais ne forme pas de trophoctoderme, le premier tissu épithélial du développement (Larue et al., 1994, 1996). Cette importance est retrouvée au niveau de la formation d'autres structures épithéliales, notamment lors de la formation du tissu mammaire. E-cad est nécessaire à l'établissement de l'épithélium luminal (Chanson et al., 2011; Daniel et al., 1995). La surexpression du domaine cytoplasmique de la E-cadhérine induit une morphogénèse trop précoce (Delmas et al., 1999) alors que la perte d'expression induit des défauts d'adhésion, de différenciation et de survie des cellules épithéliales en période de fin de gestation (Boussadia et al., 2002).

Au cours du développement mélanocytaire, la E- et P-cadhérine sont faiblement exprimées dans les mélanoblastes dermiques, mais l'expression de la E-cadhérine est fortement induite lorsque les cellules pénètrent dans l'épiderme où elles établissent des contacts avec les kératinocytes exprimant le E-cadhérine. La faible expression de la E-cadhérine dans les mélanoblastes du derme peut empêcher l'autoagrégation et la colonisation prématurée dans l'épiderme. L'entrée

des mélanoblastes dans les follicules pileux entraîne une réduction du niveau de la E-cadhérine et une augmentation de celui de la P-cadhérine. Les mélanocytes dermiques expriment la N-cadhérine comme les fibroblastes environnants, ce qui permet peut-être leur interaction cellule-cellule (Pla et al., 2001). Les changements dynamiques dans l'expression des cadhérines pourraient favoriser les mélanoblastes à s'adapter à leur environnement local dans la peau. Chez la souris, l'inactivation de *Cdh1* dans les mélanoblastes entraîne une réduction du nombre de mélanoblastes épidermiques inter-folliculaires due à un défaut de prolifération de ces cellules et une hypopigmentation est observée dans les zones glabres contenant des mélanocytes épidermiques. Aucun phénotype n'est observé au niveau de la coloration de la robe, les mélanocytes du follicule pileux exprimant majoritairement la P-cadhérine. En conclusion, l'expression de la E-cadhérine dans les mélanoblastes est requise spécifiquement pour l'établissement d'un nombre adéquat de mélanocytes épidermiques (Wagner et al., 2015, Figure 16).

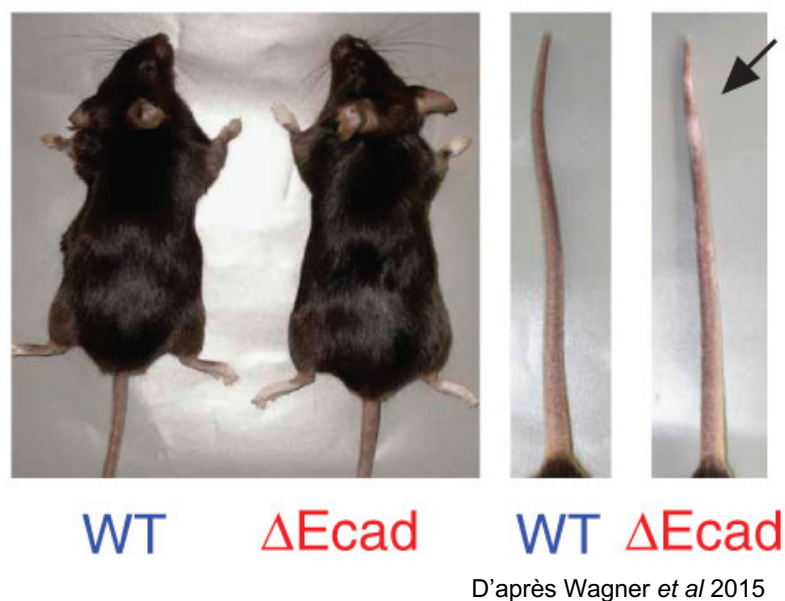


Figure 16: Photos représentatives des souris *E-cad* WT et $\Delta E-cad$ montrant les défauts de pigmentation des zones glabre.

La présence de la E-cadhérine est majeure dans l'homéostasie des mélanocytes épidermique et dans l'intégrité de l'unité épidermique de mélanisation (Delmas et Larue 2019). Ainsi, le rôle d'E-cadhérine a été montré dans une pathologie pigmentaire, le vitiligo. Cette pathologie bénigne est liée à une disparition des mélanocytes de l'épiderme. Elle est souvent associée à des processus auto-immuns – on en retrouve par exemple régulièrement secondairement à des traitements par immunothérapies de patients atteints par un mélanome (Boniface et al., 2018; Samson, 2015). La perte d'E-cad précède les manifestations cliniques du vitiligo, les mélanocytes déficients en

E-cad se détachent de l'épiderme dans les couches supra-basales. Tant que le renouvellement des mélanocytes dans l'épiderme a lieu, la peau est normalement pigmentée. En revanche, lors de stress physique ou chimique, le processus de détachement des mélanocytes est accéléré et aboutit à l'épuisement des cellules souches et au non-renouvellement des mélanocytes épidermiques, la peau présente alors une hypopigmentation (Boukhedouni et al.; Grill et al., 2018; Seneschal et al., 2021; Wagner et al., 2015). Les mélanocytes présentant un défaut d'adhésion dans les couches supra-basales sont en majorité apoptotiques (Wagner et al., 2015). Par ailleurs un polymorphisme de *CDH1* a été associé avec la susceptibilité au vitiligo (Tarlé et al., 2015).

2. Rôle dans l'oncogenèse

a. Cancer du sein

CDH1 est particulièrement mutée dans le cancer du sein et plus particulièrement dans les cancers lobulaires. En effet 56% des cancers lobulaires ont perdu E-cadhérine par mutation combinée à une perte du deuxième allèle ou par perte des deux allèles contre seulement 3% dans les cancers canaux (Koboldt et al., 2012). *CDH1* est considéré comme un gène suppresseur de tumeur (Corso et al., 2018) et son inactivation corrélée avec une plus forte invasion métastatique et une diminution de la survie des patients (Hunt et al., 1997; Li et al., 2016b; Onder et al., 2008). Ces résultats suggéraient même l'intérêt d'utiliser E-cad comme facteur de pronostic. Des résultats récents ont montré l'importance de E-cad dans l'établissement de métastases pulmonaire de carcinome canalaire. Dans ce modèle, la perte d'expression d'E-cad induit une diminution de la formation des métastases liée à une augmentation de l'apoptose (Padmanaban et al., 2019). En fonction du type cellulaire, canalaire ou lobulaire, la perte de la E-cadhérine a des effets opposés sur la formation des métastases (Corso et al., 2018). Ces résultats sont à mettre en relation avec la découverte de cluster de cellules E-cad positive dans les tumeurs du seins corrélant avec une survie diminuée (Yamashita et al., 2018)

b. Cancer gastrique

La majorité des cas de cancer gastrique diffus héréditaire sont dus à des mutations germinales inactivatrices de *CDH1*. De nombreuses études ont montré que l'initiation et les métastases du cancer gastrique sont largement liées à la perte d'expression de la E-cadhérine. *CDH1* présente des anomalies génétiques et épigénétiques dans les cancers gastriques germinaux et

sporadiques conduisant à une expression anormale. La perte d'E-cadhérine corrèle avec un mauvais pronostic et une formation accrue de métastases (Corso et al., 2013).

c. Mélanome

Dans le mélanome, peu d'études ont adressé l'importance de la E-cadhérine dans le processus tumoral. Seules des études corrélatives ont été menées. Celles-ci ont montré que la perte ou la diminution d'expression d'E-cad était fréquente dans les mélanomes primaires de l'ordre de 40% (Danen et al., 1996; Pećina-Slaus et al., 2007; Venza et al., 2016). Cette perte d'expression corrèle avec une formation accrue de métastases (Danen et al., 1996; Tucci et al., 2007; Venza et al., 2016). Cette formation de métastases induit une diminution de la survie des patients (Figure 17). A l'inverse des carcinomes précédemment cités, dans le mélanome la régulation de l'expression est liée à la perte d'expression par méthylation des régions régulatrices de *CDH1* (The Cancer Genome Atlas Network, 2015; Venza et al., 2016, Figure 18). L'usage d'agent déméthylant de l'ADN a permis d'induire à nouveau l'expression de *CDH1* (Venza et al., 2016). Les expériences de CHIP menée avec une réduction ou non de MITF ont montré que MITF régule l'expression de *CDH1* dans le mélanome (Laurette et al., 2015). Cette donnée est consolidée par le fait que l'expression de *CDH1* corrèle avec l'expression des gènes cibles de MITF dans le TCGA (The Cancer Genome Atlas Network, 2015). La régulation négative de *CDH1* est reliée à l'expression de facteur de transcription comme SNAI1 ou ZEB1 particulièrement important dans l'EMT (Perrot et al., 2013; Poser et al., 2001; Veloso et al., 2020).

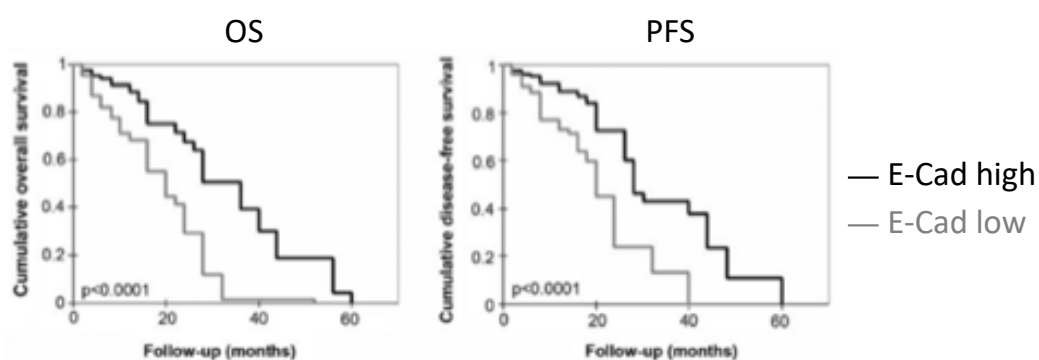


Figure 17: Kaplan Meier de l'OS et de la PFS selon le niveau d'expression d'E-cad

OS = survie globale et PFS = survie sans progression de la perte d'expression de *CDH1*. L'expression d'E-cadhérine est associée à une meilleure survie globale et à une progression retardée. D'après Venza, 2016.

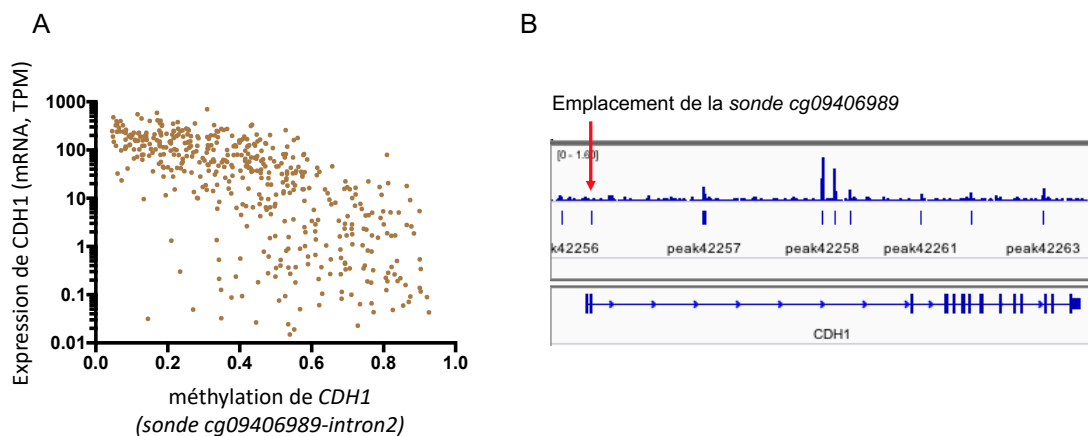


Figure 18: Mécanismes d'expression de CDH1

(A) corrélation entre l'expression de CDH1 et la méthylation de la sonde cg09406989. le coefficient de pearson est de 0.7. (B) ChIP-seq MITF montrant la présence de pic dans le deuxième intron de CDH1.

Au niveau fonctionnel, la réexpression d'E-cad dans des cellules de mélanome ne l'exprimant plus induit la perte de prolifération par le rétablissement des liaisons avec les kératinocytes (Hsu et al., 2000). La surexpression d'E-cad dans des modèles cellulaire *in vitro* a montré une diminution de l'invasion et de la migration cellulaire (Molina-Ortiz et al., 2009). Cet effet a également été observé dans des modèles de peau reconstituée où l'expression d'E-cad diminue l'invasion (Hsu et al., 2000). L'effet sur l'invasion et la migration de nombreuses protéines été observé via des études corrélatives reliant des systèmes où la perte d'E-cadhérine était induite chimiquement ou via l'action d'autres protéines avec pour conséquence un gain de motilité (Kreiseder et al., 2013; Sun et al., 2018; Wu et al., 2008). Mais ces modèles indirects ne permettent pas de formellement de mettre en évidence un rôle réel d'E-cadhérine dans ces processus de migration ou d'invasion. L'injection en sous cutanée de cellules de mélanome B16 dans lesquelles l'expression de d'E-cad a été induite a montré que l'expression d'E-cad induit une diminution de la prolifération tumorale *in vivo* ainsi qu'une légère diminution du nombre de métastases dans les poumons (Shields et al., 2019). La perte de l'expression d'E-cad est également associée avec la diminution de la réponse aux traitements par inhibiteur des checkpoint immunitaires. L'expression de E-cad dans la tumeur facilite la réponse immunitaire de manière additive avec le traitement par inhibiteur de checkpoint immunitaire anti-CTLA4 et anti PD1 (Shields et al., 2019).

E-cad intervient également dans la signalisation cellulaire. E-cad est un répresseur de la signalisation p38 et NFκB, via la stabilisation de β-caténine à la membrane (Kuphal et al., 2004). Le maintien de l'expression d'E-cad réduit l'expression de métalloprotéases via l'inhibition de

l'activation de c-Jun (Spangler et al., 2011). E-cadhérine contrôle l'activité de RhoA en séquestrant à la membrane p120-caténine qui ne peut donc pas interagir et activer RhoA (Molina-Ortiz et al., 2009). Il est à noter que ces effets ont été observés *in vitro* et n'ont pas été reliés à des évènements précis dans la mélanomagenèse.

3. Signalisation d'E-cadhérine et impact sur des processus cellulaires de l'oncogenèse

a. Prolifération

L'expression et la stabilisation d'E-cadhérine à la membrane a des conséquences sur la signalisation intracellulaire, comme par exemple la séquestration de β -caténine à la membrane empêchant la translocation nucléaire de cette dernière et son rôle dans la régulation transcriptionnelle. Ainsi, E-cadhérine est un régulateur négatif de la signalisation Wnt/ β -caténine (Hernández-Martínez et al., 2019; Heuberger and Birchmeier, 2010). La conséquence de manque de signalisation active de β -caténine est souvent reliée à une inhibition de la prolifération cellulaire. Cependant, dans les mélanocytes/mélanomes la situation est plus complexe. MITF interagit avec la β -caténine et redirige l'activité transcriptionnelle médiée par la β -caténine de ses gènes cibles vers des gènes cibles spécifiques de MITF pour activer leur transcription (Luciani et al., 2011; Schepsky et al., 2006). D'autres niveaux de signalisation croisée entre la voie β -caténine et MITF ont été décrits et l'effet de β -caténine sur la prolifération cellulaire dépend de la quantité de β -caténine/MITF et de LEF1.

E-cadhérine est également un régulateur négatif de la signalisation YAP1. Cette régulation est dépendante de β -caténine et va engendrer l'activation de la voie Hippo, les kinases LATS1/2 vont phosphoryler YAP1 sur la sérine 127. Cette phosphorylation séquestre YAP1 dans le cytoplasme, l'empêchant de se lier à ses gènes cibles. Ceci aura pour conséquence une diminution de la croissance cellulaire (Benham-Pyle et al., 2015; Kim et al., 2011).

E-Cadhérine va également négativement réguler la signalisation de p120-caténine en la séquestrant à la membrane. En effet, le clivage de E-cad par des γ -sécrétases va induire la libération dans le cytoplasme du fragment cytoplasmique d'E-cad toujours complexé avec la p120-caténine (Ferber et al., 2008). Ce complexe va interagir avec Kaiso pour se lier à l'ADN et réguler des gènes cibles (Ferber et al., 2008). Kaiso est un répresseur de transcription connu pour activer la prolifération et l'invasion cellulaire (Wang et al., 2016).

L'effet antiprolifératif de la E-cadhérine est observé sur des lignées de cellules cultivées à forte confluence principalement. Par ailleurs, lorsque les confluences cellulaires sont trop faibles pour

induire des contacts cellules-cellules, la prolifération diminue. L'induction d'un engagement des liaisons E-cadhérine avec un substrat recouvert de fragments extracellulaires de E-cadhérine réactive la prolifération cellulaire à densité cellulaire intermédiaire. Ce mécanisme passe par l'activation de Rac1 via p120-caténine (Liu et al., 2006). A la membrane, les cadhérines peuvent s'associer à certains récepteurs de facteur de croissance comme IGF1R (Insulin Growth Factor Receptor) ou EGFR (Epidermal Growth Factor Receptor) IGF1R. Cette association module à la fois la signalisation intracellulaire liée à ces récepteurs, mais aussi l'activité adhésive et signalétique. En présence de E-cadhérine, la signalisation des récepteurs IGF1R et EGFR est inhibée. En présence de ligand comme IGF, l'adhésion cellule-cellule disparaît, le complexe E-cadhérine/ β -caténine associé à IGF-1R est internalisé dans la cellule, IGF1R est recircularisé, puis E-cadhérine est dégradée dans les endosomes tardifs (Morali et al., 2001). La perte de la E-cadhérine facilite l'activité mitotique de ces récepteurs et l'induction par les facteurs de croissance diminue l'adhésion cellulaire. Au cours de l'oncogenèse, ces deux mécanismes sont essentiels à la prolifération des cellules tumorales et à leurs capacités invasives. E-cadhérine peut également participer à l'activation de la voie PI3K/AKT via sa liaison au récepteur EGFR (De Santis et al., 2009).

b. Mort cellulaire

Dans le cancer du sein, l'établissement des liaisons homophiliques E-cad/E-cad a été associé avec l'augmentation de la signalisation STAT3 via l'activation de Rac1. Cette activation de STAT3 a été associée avec la résistance à l'apoptose (Arulanandam et al., 2009). Cet effet inhibiteur de l'apoptose a également été confirmé dans des cellules MDCK montrant l'importance de l'engagement des liaisons cadhérine-cadhérine (Capra and Eskelinen, 2017). De plus, l'élimination de la partie intracellulaire de E-cadhérine est nécessaire pour induire l'apoptose lors des processus d'involution de la glande mammaire et de la prostate (Vallorosi et al., 2000). Ces résultats ont été confirmés *in vivo* où des cellules injectées invalidées pour *Cdh1* mourraient par l'apoptose dans les poumons (Padmanaban et al., 2019). Ces résultats suggèrent que E-cad a un rôle protecteur de l'apoptose lorsqu'elle est engagée dans des liaisons d'adhésion cellulaire. Un autre mécanisme de mort cellulaire est important dans la progression tumorale : l'anoïkis, c'est-à-dire la capacité des cellules à survivre sans attache à un substrat. Il a été montré que E-cadhérine a un rôle de sensibilisateur à l'anoïkis et que sa perte d'expression induit une résistance à l'anoïkis (Derksen et al., 2006; Onder et al., 2008). Cet effet passe par la séquestration à la membrane du facteur NRAGE. Ce facteur est un inhibiteur de l'activité du

facteur de transcription TBX2 régulant la transcription de gène tel que p14^{ARF} impliqué dans la sensibilité à l'anoïkis. L'inhibition de TBX2 par NRAGE en absence d'E-cad induit l'anoïkis par absence d'expression de p14^{ARF} (Kumar et al., 2011). La réexpression d'E-cad dans les cellules rétablit la sensibilité à l'anoïkis (Huang et al., 2013).

c. Effet sur la clonogénicité

La clonogénicité est la capacité des cellules à croître, lorsqu'elles sont ensemencées en cellule unique. La perte de E-cadhérine diminue la capacité à croître en cellules isolées dans des modèles de cancer du sein (Padmanaban et al., 2019). Ce résultat est cohérent avec ceux trouvés avec des cellules embryonnaires humaines où la réexpression d'E-cad induit la clonogénicité des cellules en régulant leur survie (Li et al., 2010a).

d. Transition épithélio-mésenchymateuse

E-cadhérine via sa perte d'expression est un marqueur de la transition épithélio-mésenchymateuse (EMT) (Loh et al., 2019; Mikesch et al., 2010; Zhu et al., 2018b). Mais son rôle en tant que régulateur négatif dans le déclenchement de l'EMT a également été montré. La perte d'E-cad dans des cellules pluripotentes induit une EMT partielle incluant l'expression de *SNAI1* (Aban et al., 2021). Dans des cellules épithéliales de sein, la perte d'expression d'E-cad induite par l'utilisation de shRNA induit l'expression d'une signature d'EMT avec une expression marquante de TWIST (Onder et al., 2008). L'EMT est particulièrement essentiel dans de nombreux processus de migration et d'invasion (Larue and Bellacosa, 2005).

e. Migration et invasion

Dans le cancer du sein de nombreuses études ont montré que la perte d'E-cad est associée avec un potentiel invasif plus important (Frixen et al., 1991; van Roy and Berx, 2008; Vleminckx et al., 1991). Ces observations étaient aussi confirmées dans des modèles d'invasion cellulaire en 3D dans du collagène de type I (Padmanaban et al., 2019). L'effet sur la migration est plus controversé. La perte d'expression d'E-cad induit une diminution de la migration dans des modèles de carcinomes (Haraguchi et al., 2019). Ceci peut s'expliquer par son rôle dans le maintien de la directionnalité des protrusions des cellules en mouvement (Cai et al., 2014; Grimaldi et al., 2020). La E-cad est importante dans les phénomènes de migration collective où elle va participer au maintien de la cohésion du groupe de cellules en migration. Cette migration collective a été observée dans des carcinomes ainsi que dans la migration des cellules de crêtes neurale (Cousin, 2017; Gupta and Yap, 2021; Hwang et al., 2012; Janiszewska et al., 2020). Dans

le mélanome, un nouvel axe impliquant TBX3-ID1-MITF-E-cadherin dans la migration cellulaire a été mis en évidence et le maintien du phénotype migratoire (Peres et al., 2021).

f. Résumé des fonctions cellulaires d'E-cadhérine

L'ensemble des fonctions cellulaires de le E-cadhérine est résumé dans le schéma suivant (Figure 19).

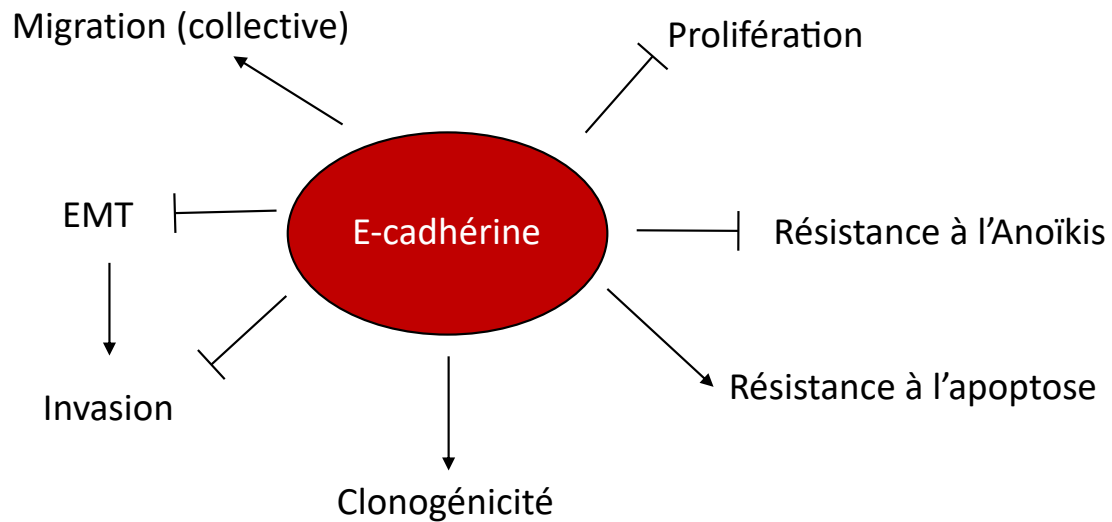


Figure 19: Résumé des fonctions cellulaires d'E-cadherine

C. Les récepteurs couplés aux protéines-G (RCPG)

I. Présentation des RCPGs

1. Description et organisation

a. Structure

Les récepteurs couplés aux protéines-G (RCPG) composent la plus grande superfamille de récepteur membranaire chez les mammifères. Les caractéristiques clefs de la structure des RCPG sont la présence de 7 domaines transmembranaires (7TM) liés par 3 domaines intracellulaires et 3 domaines extracellulaires. Les RCPG sont également caractérisés par un couplage avec des protéines G hétérotrimériques dans la partie intracellulaire (Figure 20). Leur présence est une caractéristique des eucaryotes. On retrouve néanmoins des molécules membranaires de structures similaires – présentant ces 7 domaines transmembranaires – chez les procaryotes (Rozenberg et al., 2021). On peut notamment citer les protéo-, bactério- et halorhodopsines sensibles à la lumière retrouvée chez certaines archées et bactéries. Mais il est important de noter que leur signalisation est indépendante des protéines-G hétérotrimériques, celle-ci s'établissant sur la mise en place de gradients ioniques qui activent des ATPases membranaires (Hasegawa et al., 2020). Il faut aussi noter que la relation phylogénétique entre ces protéines procaryotiques et les RCPGs n'est pas encore claire même les dernières études suggèrent une relation évolutive (Shalaeva et al., 2015; Zabelskii et al., 2021).

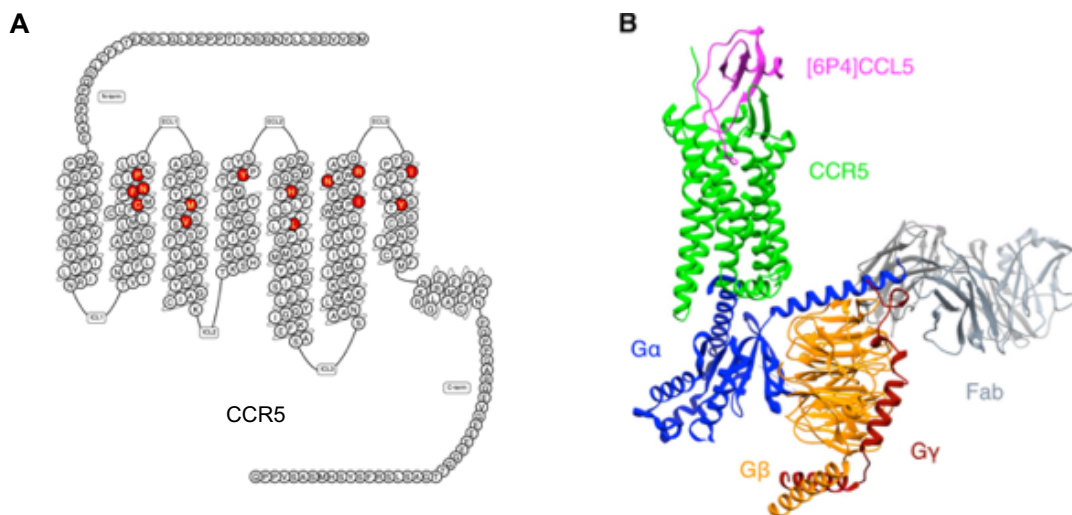


Figure 20: Exemple de structure de RCPG, le récepteur de classe A CCR5.

(A) Séquence et identifications des différents domaines de CCR5. Les acides aminés surlignés en rouge correspondent aux sites d'interaction avec le ligand CCL5. (B) Structure en 3D du récepteur complexé avec son ligand et les sous-unités $G\alpha$, $G\beta$ et $G\gamma$ des protéines G hétérotrimériques. Le Fab est un fragment d'immunoglobuline utilisé pour stabiliser le complexe lors de la cristallographie.

b. Classification

La superfamille des RCPGs se compose de plus de 800 membres chez l'humain. Ils ont été classés en fonction de leurs séquences, de leurs fonctions et de leur mode d'activation (Alexander et al., 2019; Attwood and Findlay, 1994; Basith et al., 2018). Ceux-ci sont catégorisés en 6 classes principales :

- La classe A dite des « Rhodopsin-like » composée de 290 membres. L'activation des récepteurs de la classe A se fait par reconnaissance du ligand dans la région des 7TM.
- La classe B dite famille des sécrétines regroupant 15 RCPGs la reconnaissance des ligands activateurs se fait par les régions extracellulaires et les 7TM.
- La classe C dite classe de récepteur métabotropique du glutamate, composée de 22 récepteurs. L'activation des récepteurs au glutamate se fait par reconnaissance du glutamate par une poche dans le domaine extracellulaire qui contient un domaine Venus Flytrap.
- La classe F dite classe des récepteurs Frizzled et Smoothened avec 11 membres. L'activation se fait par la fixation du ligand – WNT (le ligand de SMO n'est toujours pas identifié) – sur un domaine CRD extracellulaire.

Les mécanismes d'activation de ces deux 4 classes sont décrits dans la (Figure 21). On peut noter que chez d'autres espèces eucaryotes comme les mycètes on retrouve d'autres classes : la classe D dite classe des récepteurs aux phéromones pour la reproduction fongique et la classe E dite classe des récepteurs à l'AMP cyclique. Nombre de ces récepteurs sont toujours orphelins de ligand (Alexander et al., 2019).

Il existe deux classes supplémentaires chez l'Homme (Alexander et al., 2019; Basith et al., 2018) :

- Les récepteurs adhésifs au nombre de 33 chez l'Homme. Ces récepteurs vont partager des homologies de séquences avec des molécules d'adhésions comme les cadhérines ou les intégrines et permettre l'interaction de la cellule hôte avec d'autres cellules ou matrices portant ces molécules d'adhésion.
- Les récepteurs sensoriels. Ils représentent la grande majorité des récepteurs et participent à des fonctions sensorielles comme l'olfaction (environ 400 récepteurs impliqués), le goût (33), la perception de la lumière (10) de phéromones (5).

Il existe également 5 récepteurs non classés : GPR107, GPR137, TPRA1, GPR143 et GPR157.

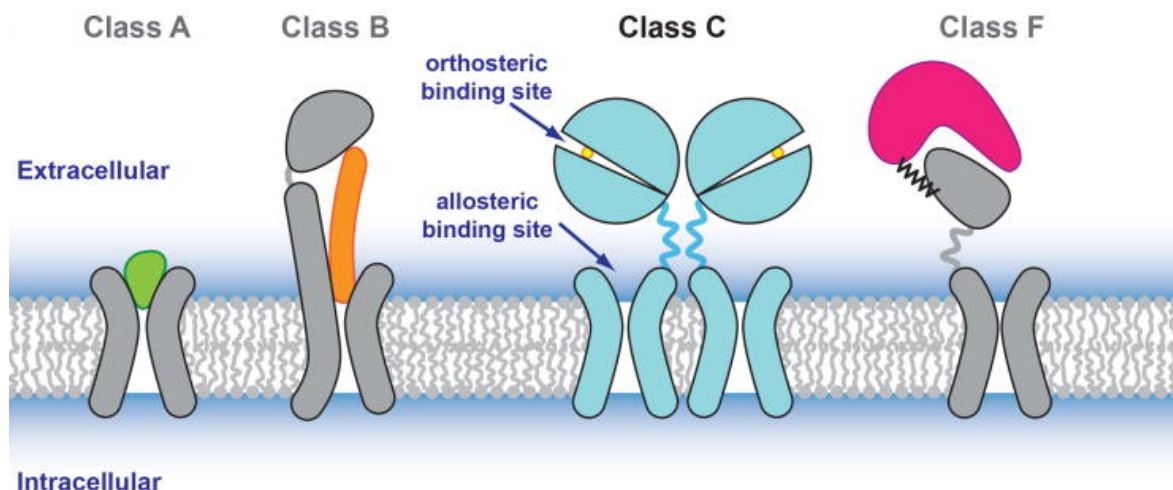


Figure 21: Modes de fixation des ligands selon la classe des RCPGs.

Le ligand des récepteurs de classe A se lie au niveau des domaines transmembranaires, celui des récepteurs de classe B à cheval sur les domaines TM et le domaine extracellulaire. Les récepteurs de classe C sont activés par la fixation du glutamate sur des sites de liaison orthostérique (et non allostérique comme les récepteurs de classe A) et les récepteurs de classe F sont activés par la fixation du ligand sur le domaine extracellulaire. D'après Wu et al. 2014.

Au cours des 20 dernières années, de nombreuses connaissances au niveau de la structure ont été apportées. Néanmoins il est difficile de prédire les structures des RCPGs non-cristallisés à partir des structures déjà déterminées, car, si les domaines TM restent assez conservés entre les espèces, les domaines non membranaires sont très différents et très mobiles. De plus, la différence au niveau des sites de fixation tient, en particulier pour la classe A, de légères variations de séquence qui font la spécificité de la liaison RCPG-ligand.

c. Mécanismes d'activation

L'activation des RCPGs se fait, physiologiquement, par la fixation du ligand dans sa poche. Cette fixation va induire de légers mouvements des domaines transmembranaires qui révèlent un site de fixation pour le complexe des protéines-G avec le GTP. La fixation de ce complexe sur le RCPG va entraîner la libération du GDP et son remplacement par une molécule de GTP. La fixation du GTP sur la protéine $G\alpha$ va provoquer sa dissociation du récepteur et la dissociation du complexe en séparant la sous-unité $G\alpha$ des sous-unités $G\beta$ et $G\gamma$ qui restent liées (Figure 22). Les protéines $G\alpha$ et $G\beta/G\gamma$ vont ensuite exercer leur action de signalisation propre (Weis and Kobilka, 2018). Des motifs communs à nombreux RCPGs ont été retrouvés par analyse des séquences telles que les motifs CWxP, DRY, la poche Na^+ , NPxxY et PIF. Ils sont associés à la fixation de la protéine G et donc à l'activation de la signalisation du récepteur (Zhou et al., 2019). Les mutations des motifs DRY et NPxxY peuvent induire une augmentation de l'activité constitutive du récepteur (Alewijns et al., 2000; Ragnarsson et al., 2019; Rovati et al., 2007). La stimulation des récepteurs

peut également activer des kinases, les GRKs qui vont se lier sur le récepteur actif et le phosphoryler la queue C-terminale. Cette phosphorylation va permettre la fixation des arrestines. Les arrestines vont servir de protéines d'échafaudages pour la formation des puits de clathrines et l'internalisation du récepteur. Cette internalisation induit la désensibilisation de la cellule et la diminution de la réponse à un stimuli identique (Figure 22). Les récepteurs sont ensuite recyclés ou dégradés. Les arrestines peuvent aussi être en complexe avec des éléments de signalisation comme des membres de la voie MAPK et induire leur activation. Ce deuxième phénomène induit la signalisation arrestine des RCPGs (Weis and Kobilka, 2018).

Les mécanismes à l'échelle moléculaire permettant de cibler la signalisation vers la voie des arrestines ou vers la voie des protéines-G sont encore peu décrits. De premiers résultats suggèrent que l'activation tiendrait de conformation particulière de la structure des TM6 et TM7 pour activer respectivement la signalisation des protéines-G et celle des arrestines (Suomivuori et al., 2020; Wingler and Lefkowitz, 2020).

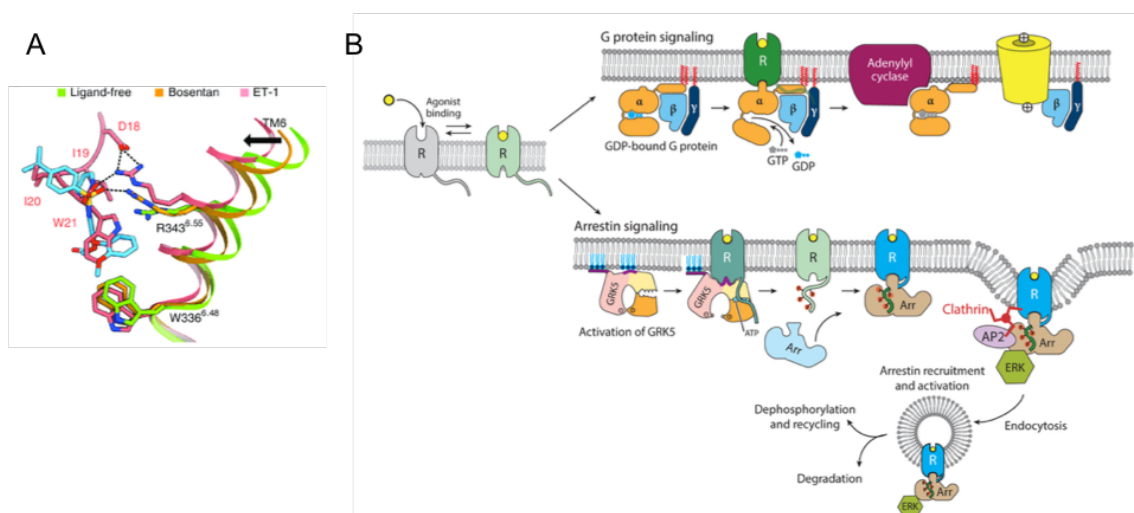


Figure 22: Mécanismes d'activation des RCPGs. (A) exemple du récepteur à l'endothéline de type B montrant la finesse des mouvements des hélices transmembranaires en réponse à la fixation de ligand agoniste (ET1) ou antagoniste (Bosentan). D'après Shihoya et al. 2017. (B) mécanismes intracellulaires induits par l'activation des RCPGs. Voie "classique" des protéines G en haut et voie "biaisée" et de désensibilisation par les arrestines en bas. D'après Weis & Kobilka, 2019.

2. Fonctions physiologiques des RCPGs

Les RCPGs sont capables d'exercer de nombreuses fonctions physiologiques qui vont différer selon les cellules, tissus ou organes dans lesquels le récepteur est exprimé ou activé. Les fonctions sont très diverses, on peut notamment citer :

- Le comportement : la peur est notamment régulée par PAR1, et les récepteurs à la somatostatine sont impliqués dans la prise de nourriture (Bourgognon et al., 2013; Kumar and Singh, 2020).
- La pression sanguine qui est régulée notamment par les récepteurs à l'angiotensine (Zhang et al., 2021)
- Les propriétés cognitives : la maladie d'Alzheimer est associée au récepteur au glutamate (mGluR5) et les récepteurs sérotoninergique 5-HT2A et 5HT4 à l'apprentissage (Azam et al., 2020).
- La réponse immunitaire, dans l'attraction cellulaire (récepteurs aux chimiokines) ou dans l'activation des cellules immunitaires (récepteurs au succinate, au formyl-peptides) (Lämmermann and Kastenmüller, 2019).
- L'humeur : les récepteurs sérotoninergiques sont impliqués dans la dépression (Senese et al., 2018).
- La perception sensitive, l'odorat est régulé par la perception de molécules odorantes par des RCPGs au niveau du bulbe olfactif (Block, 2018).

La première preuve de l'implication de RCPGs dans le cancer est venue des travaux de Young et de ses collègues qui ont mis évidence le rôle oncogénique de Mas1 dans la souris (Young et al., 1986).

La formation et la progression cancéreuse sont liées à l'activation de nombreux processus cellulaires qui ont été rassemblés sous l'appellation de « hallmark of cancer », un concept proposé par Hanahan et Weinberg en 2000 (Hanahan and Weinberg, 2000, 2011). Initialement composé de 6 processus, on retrouve désormais plutôt 10 mécanismes cellulaires impliqués dans les processus oncogéniques (Arang and Gutkind, 2020). Des RCPGs ou des éléments de leurs signalisations ont été montrés comme impliqués dans chacun des processus cellulaires importants de l'oncogenèse (Arang and Gutkind, 2020). Des exemples d'implication de RCPGs dans chacun des processus cellulaires des « hallmarks of cancer » seront détaillés ci-dessous.

a. La prolifération cellulaire

Des mutations activatrices du récepteur à l'hormone stimulant la thyroïde (*TSHR*) ont été identifiées dans 60 à 80% des cas d'adénomes toxiques de la thyroïde (Rodien et al., 2003). L'activation de ce récepteur induit la croissance cellulaire des cellules via l'activation de la signalisation $G\alpha_s$ (Huang et al., 2016; Kleinau et al., 2013). Ces mutations activatrices sont

également retrouvées, tout comme des mutations du gène qui code pour $G\alpha_s$ (*GNAS*) dans des carcinomes thyroïdiens (Tong et al., 2015). Par ailleurs on retrouve à faible fréquence, mais à des pourcentages restants significatifs, des mutations des protéines G – premier élément en aval de RCPGs. Par exemple, les gènes codants pour les protéines-G de la famille $G\alpha_{q/11}$ sont mutés dans 2,9% des cancers. En dehors des cancers associés aux mélanocytes, ces mutations sont retrouvées à des fréquences importantes dans les carcinomes du corps de l'utérus (8,12%) ou dans les adénocarcinomes du colon (5.06%) (Arang and Gutkind, 2020).

b. L'échappement à l'inhibition de la croissance

Des récepteurs peuvent perdre leurs fonctions régulatrices de la croissance par mutation. C'est probablement le cas d'ADGRB1 à qui l'on prête des fonctions anti-tumorogéniques dans les cancers cérébraux (Zhu et al., 2011). La perte d'activité de ce récepteur a été associée avec une diminution de l'expression de p53, l'un des suppresseurs de tumeurs les mieux caractérisés (Zhu et al., 2018a).

c. L'immortalisation

Les ligands des récepteurs de la classe F, FZD1-10, sont particulièrement exprimés dans les cancers colorectaux (Nie et al., 2020). L'activation de ces récepteurs va induire l'activation de β -caténine en empêchant sa dégradation. L'activation de β -caténine dans le cancer colorectal a été associée avec l'immortalisation des cellules cancéreuses (Wagenaar et al., 2001). A noter que β -caténine et son régulateur APC sont fréquemment mutés dans les cancers colorectaux (Morin et al., 1997; Sparks et al., 1998).

d. La résistance à la mort cellulaire

Le sarcome de Kaposi est une tumeur endothéliale induite par une infection par le virus de l'herpès associé au syndrome de Kaposi (KSHV) (Mesri et al., 2010). Ce virus code notamment pour un GPCR, le v GPCR. Ce GPCR, outre une action en faveur de la prolifération va avoir également une action en faveur de la résistance à l'anoïkis. Les cellules tumorales exprimant le récepteur seront donc plus résistantes à la mort cellulaire une fois détachées de leur matrice (He et al., 2012). Ce récepteur est également capable d'induire la résistance à l'apoptose des cellules infectées (Montaner et al., 2013).

Cette action anti-apoptotique est également retrouvée avec des récepteurs «nativement humain ». Par exemple, dans le cancer du sein, le récepteur à la bradykinine induit la résistance à l'apoptose des cellules cancéreuses (Dubuc et al., 2018).

e. La production énergétique

Cet aspect est encore peu étudié, mais par exemple, le récepteur α 2a-adrénergique est capable de modifier le métabolisme cellulaire. Son activation va induire la formation de purinosome et la synthèse de purines qui en découle (Verrier et al., 2011). Ces purines sont des éléments de base de la synthèse d'ADN et donc des éléments importants de la prolifération. Le mécanisme peut être inversé et des métabolismes énergétiques dérégulés peuvent induire l'activation de RCPGs. Les cellules cancéreuses subissent régulièrement l'effet Warburg qui, notamment via des inhibitions de la succinate déshydrogénase, va perturber le bon fonctionnement du cycle de Krebs (Pascale et al., 2020). Cette perturbation du métabolisme vers un mode de production énergétique anaérobie va entraîner l'accumulation de succinate et de lactate (Bouillaud et al., 2021; Brault et al., 2018). Ces deux métabolites, possèdent leur propre RCPGs. Le récepteur au succinate, SUCNR1 est notamment associé à la formation de métastases dans le cancer du poumon (Zhang et al., 2020b). Le récepteur au lactate, HCAR1, a lui aussi des fonctions pro-tumorales par des fonctions pro-angiogéniques et immunosuppressives (Wagner et al., 2017).

f. L'inflammation

Le cancer peut être lié à une inflammation chronique. Cette inflammation est particulièrement liée à la production de prostaglandine. La fixation de la prostaglandine E2 sur ses récepteurs EP1-4 induit une réponse inflammatoire. Cette inflammation favorise l'oncogenèse, en particulier dans le contexte du cancer gastro-intestinal (Chang et al., 2005). Cette inflammation induite par les prostaglandines E2 est également capable de favoriser l'initiation de cancers colorectaux (Brown and DuBois, 2005).

g. L'échappement immunitaire

Le système immunitaire a un rôle de sentinelle dans lutte contre l'apparition et la prolifération de cellules tumorales. Pour échapper à cette destruction immunitaire, les cellules immunitaires ont mis en place plusieurs mécanismes. L'un d'entre eux est la sécrétion de chimiokines qui vont attirer préférentiellement des cellules immunosuppressives. On peut notamment citer la sécrétion de CCL17 et CCL22 qui vont attirer les lymphocytes T régulateurs via l'activation de CCR4, un RCPG, sur ces dernières (Nagarsheth et al., 2017). Les lymphocytes T vont ensuite

inhiber l'action des lymphocytes T cytotoxiques dans la tumeur et des cellules de l'immunité innée comme les macrophages .

h. Induction de l'angiogénèse

Les tumeurs vont sécréter des facteurs angiogéniques qui vont être reconnus par des RCPGs comme S1PR ou PAR1. L'activation de ces récepteurs va induire la sécrétion de facteurs comme le VEGF qui vont permettre une néo-vascularisation irriguant la tumeur (Balaji Raguathrao et al., 2020; Tsopanoglou and Maragoudakis, 2004). La sécrétion d'interleukine 8 par la tumeur, le stroma et même les cellules immunitaires va induire l'angiogénèse par sa fixation au RCPGs CXCR1 et CXCR2 (Waugh and Wilson, 2008).

i. La réparation de l'ADN

L'acide lysophosphatidique se lie aux récepteurs LPA₁ et LPA₂. La fixation de celui-ci à ses récepteurs a été associée avec une augmentation de la survie de cellules soumises aux dommages de l'ADN par chimiothérapies ou rayonnement ionisant (Deng et al., 2002). Cette augmentation de la survie est due à l'induction des mécanismes de réparation cellulaire (Deng et al., 2007). Le blocage du récepteur CXCR4 a également un effet sur la réponse cellulaire au dommage de l'ADN en réduisant l'activité des points de contrôle (checkpoints) lors du cycle cellulaire. Son blocage induit la mort cellulaire par catastrophe mitotique : l'ADN étant trop endommagé pour poursuivre la mitose, la cellule rentre en apoptose (Kwong et al., 2009).

j. L'invasion cellulaire

Les ligands des récepteurs aux chimiokines sont parfois produits au niveau des organes où vont s'établir les métastases. Leur présence via la fixation aux récepteurs cibles va permettre d'attirer les cellules tumorales en migrations vers ces sites métastatiques (Zlotnik et al., 2011). Les chimiokines vont donc diriger le tropisme métastatique de certains cancers (Zlotnik et al., 2011). Cette interaction a particulièrement été mise en évidence dans le cancer du sein. Les cellules tumorales expriment fortement CXCR4 et CCR7 (Rizeq and Malki, 2020; Xu et al., 2015). Leurs ligands sont eux fortement exprimés dans les sites métastatiques comme le poumon. Cette interaction est suggérée comme mécanisme pour diriger les cellules de cancer du sein vers ces sites métastatiques (Burger and Kipps, 2006; Dillenburg-Pilla et al., 2015).

k. Résumé et complexité du rôle des RCPGs

Comme décrit dans les paragraphes précédents, seuls quelques RCPGs ont été décrits comme ayant une implication dans les processus cellulaires de l'oncogenèse résumés dans la Figure 23.

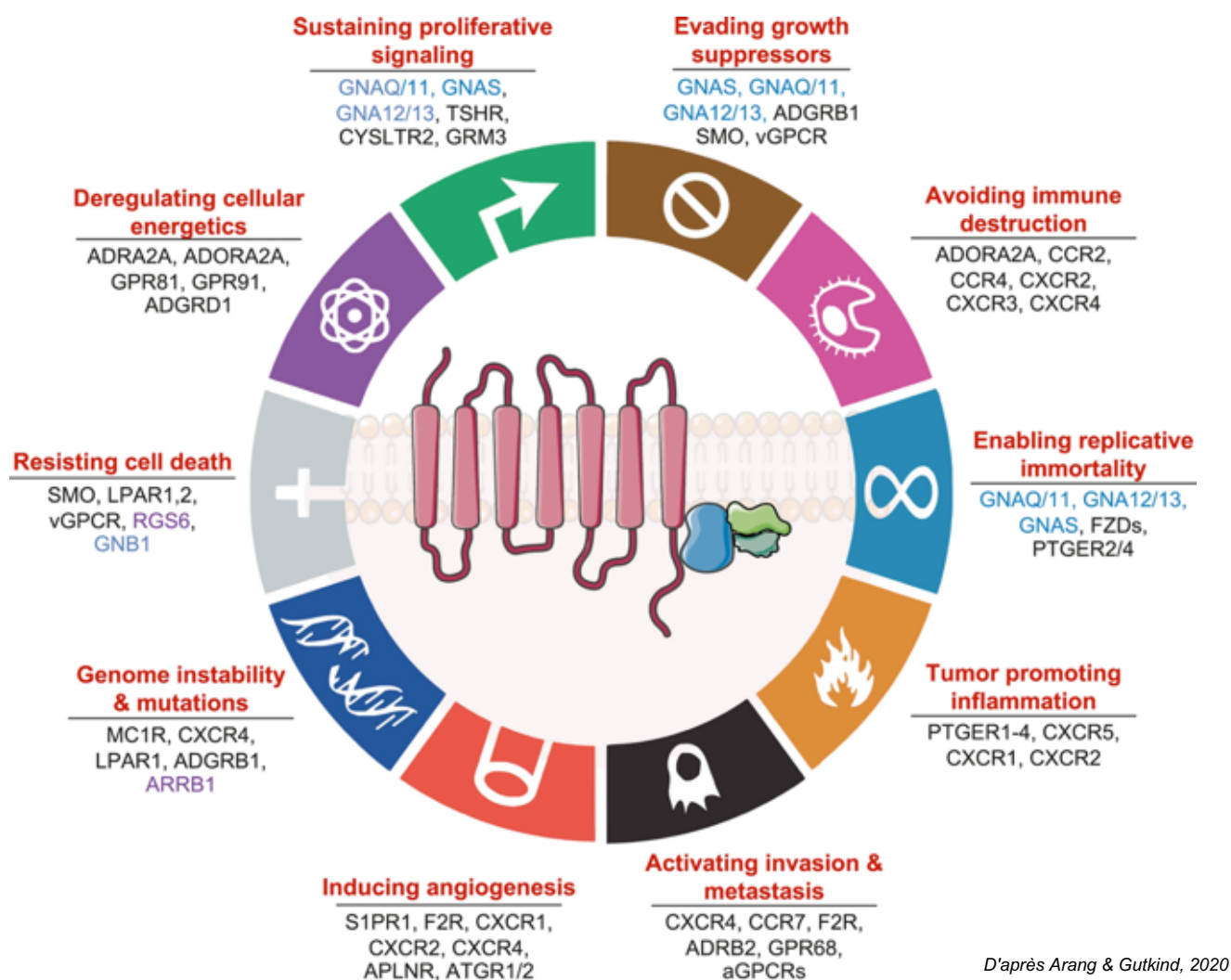


Figure 23: RCPGs impliqués dans les processus des Hallmarks of cancer.

Néanmoins de nombreux récepteurs sont exprimés dans les cellules tumorales, mais leur potentiel oncogénique n'a pas encore été évalué. Cette évaluation est rendue compliquée par le fait que l'activation des RCPGs passe rarement par l'acquisition de mutation, mais plus par la liaison de leurs ligands ce qui leur donne un rôle d'oncogène agoniste-dépendant (Gutkind et al., 1991). Cette activation dépend souvent de la présence du ligand dans le milieu ou l'organe étudié. Ceci complexifie également les études, car l'action devient organe-dépendante.

II. Rôle des RCPGs et de leur signalisation dans le lignage mélanocytaire

Cette partie a été le sujet de l'écriture d'une revue encore en cours de préparation. La version actuelle de celle-ci se trouve en annexe B du manuscrit.

1. Les RCPGs dans le lignage mélanocytaire

Les RCPG régulent de nombreuses fonctions biologiques clés, telles que la différenciation, la prolifération, la migration et l'activité métabolique des cellules. Il n'est donc pas surprenant qu'ils jouent un rôle dans l'oncogenèse, y compris la mélanomagenèse (Lee et Chen, 2008). Il existe quatre mécanismes principaux par lesquels les RCPG peuvent stimuler l'oncogenèse : (i) une disponibilité excessive du ligand, (ii) une expression excessive des RCPG, (iii) des mutations activatrices des RCPG et (iv) des mutations activatrices des protéines $G\alpha$.

Le rôle de certains RCPG au cours de la mélanomagenèse a été étudié à l'aide de mutants de souris naturels (ou induits chimiquement) de gènes d'intérêt ou de nouveaux mutants à gain et perte de fonction. Une liste de mutants de souris présentant des phénotypes de pigmentation est disponible et régulièrement mise à jour (<http://www.ifpcs.org/colorgenes>) (Baxter et al., 2019). Les RCPGs connus impliqués dans la mélanomagenèse sont présentés dans la section suivante. Le rôle de certains RCPG dans la transformation des mélanocytes était prévisible, étant donné leur fonction clé dans le développement et l'homéostasie des mélanocytes (ET/EDNRB, MSH/MC1R, WNT/FZD), alors que l'implication d'autres dans la mélanomagenèse était moins attendue (GLU).

Les effets des récepteurs dont l'action a été validées par des modèles murins génétiquement modifiés sont détaillés ci-dessous (Tableau 1). Leurs rôles et fonctions seront détaillés plus en détails dans les paragraphes suivant.

Gene	Nom	Signalisation	Souris	Fonctions
EDNRB	Récepteur à l'endothéline B	$G\alpha_q$	Initiation (<i>Mitf-cre/+</i> ; <i>Rosa-fs-GNAQ^{Q209L/+}</i> ; <i>Ednrb^{F/F}</i>)	Prolifération, Migration, Invasion
MC1R	Récepteur de la mélanocortine de type 1	$G\alpha_s$	Initiation (<i>Braf^{V600E}</i> ; <i>MC1R^{e/e}</i>)	Prolifération, survie Réparation de l'ADN
GRM1	Récepteur métabotrope du glutamate 1	$G\alpha_q$	Initiation, progression (<i>Dct::Grm1</i>)	Prolifération, Survie
GRM5	Récepteur métabotrope du glutamate 5	$G\alpha_q$	Initiation, progression (<i>Tyrp1::Grm5</i>)	Prolifération

Tableau 1: Rôle de RCPGs dans la mélanomagenèse.

a. Récepteur à l'endothéline de type B

Le système de l'endothéline (ET) est constitué de deux récepteurs couplés aux protéines G de classe A, les récepteurs de l'endothéline de type A et B (EDNRA et EDNRB, respectivement) et de leurs trois ligands peptidiques similaires, l'endothéline-1, -2 et -3 (ET1,2,3). L'EDNRB est le récepteur prédominant exprimé par les mélanocytes/mélanomes et se lie à tous les ET avec la même affinité. On a dans un premier temps découvert que Edn3 et Ednrb jouent un rôle majeur au cours du développement des mélanocytes à partir des NCC en utilisant des modèles génétiques de souris knock-out puis, par analogie, des mutants classiques de la souris, « piebald » et « lethal spotting » (Baynash et al., 1994; Hosoda et al., 1994). En effet, les souris génétiquement modifiées (GEM) Ednrb et Edn3 sont toutes deux alléliques aux mutations spontanées de la souris qui se produisent sur les loci piebald et lethal spotting. Les mutants récessifs de l'un ou l'autre de ces loci donnent lieu à des phénotypes similaires consistants en différents degrés d'hypo-pigmentation et en un mégacôlon a-ganglionnaire dû à l'absence de ganglions entériques, qui ont la même origine embryonnaire, les crêtes neurales, que les mélanocytes. Réciproquement, l'expression accrue d'Edn3 dans l'épiderme entraîne une augmentation du nombre de mélanocytes et une hyperpigmentation (Garcia et al., 2008). La délétion germinale d'Ednrb ne conduit pas à une oncogenèse mais à l'absence de mélanocytes, principalement dans le derme. Le rôle d'Ednrb dans la mélanomagenèse a été évalué dans le contexte de la signalisation oncogène GNAQ^{Q209L} (voir paragraphe suivant). L'expression de GNAQ^{Q209L} (codant pour G α_q) n'est pas suffisante pour remplacer la signalisation d'EDNRB pendant le développement embryonnaire, ce qui suggère que G α_q n'est peut-être pas la seule protéine G activée en aval d'EDNRB (ou d'autres voies de signalisation). En utilisant une approche de knock-out conditionnel, la mélanomagenèse induite par GNAQ^{Q209L} est inhibée en l'absence d'Ednrb, y compris les métastases pulmonaires (Mitf-cre/+ ; Rosa-fs-GNAQ^{Q209L/+} ; fond génétique Ednrb^{F/F}). De manière intrigante, l'haploinsuffisance germinale pour Ednrb a l'effet inverse dans le modèle de mélanome de souris RET (Metallothionein-1/RFP-RET ; souris Ednrb (+/-)), dans lequel elle accélère la tumorigenèse, avec une augmentation des métastases pulmonaires (Kumasaka et al., 2010). Ces deux modèles murins sont intéressants et montrent clairement que l'expression d'Ednrb affecte la mélanomagenèse, mais ont l'inconvénient de représenter une situation oncogénique peu commune dans le mélanome cutané, consistant en une haploinsuffisance ou en un manque d'Ednrb combinée à une mutation driver GNAQ^{Q209L} ou à une augmentation de la signalisation RET, ce qui n'est pas observé dans le mélanome humain, réduisant la pertinence clinique de ce modèle.

L'intérêt pour d'EDNRB dans le mélanome provient principalement des premières observations chez l'homme montrant que l'expression de l'EDNRB était positivement associée à la progression du mélanome cutané ; on a constaté que les niveaux d'ARNm et de protéine de l'EDNRB augmentaient des nævus communs aux nævus dysplasiques et du mélanome primaire au métastatique (Demunter et al., 2001). Conformément à cette observation, des expériences *in vitro* ont montré que l'ET favorisait la prolifération, la migration et l'invasion des cellules de mélanome et que les inhibiteurs d'EDNRB réduisaient la croissance et la survie des cellules de mélanome en culture et en xénogreffes (Asundi et al., 2014; Lahav et al., 1999, 2004). Cependant, la surexpression d'EdnrB, seule ou combinée à des mutations driver, n'a pas été réalisée chez la souris pour aborder génétiquement son rôle dans l'oncogénèse

Un autre aspect de la signalisation ET dans le mélanome est son activité dans la réparation de l'ADN, qui a un rôle dans la réduction de l'effet génotoxique induit par les UVR (Swope et al., 2020). En effet, la signalisation ET augmente la mobilisation intracellulaire du Ca^{++} , et l'activation en aval des MAP kinases JNK et p38 induites par le stress, ce qui améliore la réparation des cyclobutanes pyrimidines (CPD), la forme majeure des photo-produits de l'ADN, dans les mélanocytes humains irradiés par les UV (von Koschembahr et al., 2015). Enfin, une étude récente a suggéré que la signalisation ET a un rôle multifonctionnel dans le mélanome, agissant à la fois sur les cellules tumorales et stromales, et module l'immunosuppression (Freitas et al., 2021). Ainsi, bien que le rôle de la signalisation EDNRB soit relativement bien compris pendant le développement des mélanocytes, son rôle dans la transformation maligne est beaucoup moins clair, car il agit dans de multiples voies de signalisation et dépend du contexte. Il n'est donc pas surprenant que les thérapies qui ciblent l'EDNRB n'aient pas eu beaucoup de succès jusqu'à présent. Il a été démontré que les petites molécules inhibitrices de EDNRB, A-192621 et BQ788, inhibent la croissance et la survie des cellules de mélanome en culture et dans les xénogreffes *in vivo* (Bagnato and Natali, 2004; Lahav et al., 1999, 2004). Cependant, le Bosentan, antagoniste double EDNRA/EDNRB, a été testé dans des essais cliniques de phase II et n'a pas réussi à produire une réponse robuste chez les patients atteints de mélanome cutané en clinique, que ce soit seul ou en combinaison avec la dacarbazine (Kefford et al., 2007, 2010). De même, le traitement à l'A-192621 de souris exprimant l'EDNRB dans le contexte de l'oncogène GNAQ^{Q209L} n'a montré aucun effet sur la tumorigénèse, alors que l'haploinsuffisance pour l'Ednrb l'inhibe. Le ciblage d'EDNRB avec un conjugué anticorps-médicament (DEDN6526A) est actuellement testé en phase I (Sandhu et al., 2020). Il serait très intéressant de générer un modèle murin qui reflète la situation de l'EDNRB humain dans le mélanome cutané : surexpression de l'EDNRB

(humain et murin) dans les mélanocytes/mélanomes combinée avec les mutations oncogènes BRAF^{V600E} ou NRAS^{Q61K/R}, les principales mutations driver du mélanome cutané humain. De tels modèles permettraient de mieux comprendre l'effet de la surexpression d'EDNRB sur la mélanomagenèse, d'étudier sa signalisation en aval et de tester des inhibiteurs dans un modèle de souris préclinique pertinent pour l'homme préalablement aux essais cliniques.

b. Récepteur à la mélanocortine de type 1

Les mélanocytes présentent un récepteur (MC1R) qui contrôle la mélanogenèse. Le MC1R appartient à une petite sous-famille de RCPGs, classée en cinq sous-types (MCR1-5) qui contribuent à d'importants processus physiologiques. Le MC1R est le seul récepteur de la mélanocortine exprimé dans les mélanocytes. Le MC1R est un récepteur de classe A et est couplé à la protéine G α_s . Le MC1R se lie au peptide dérivé de la pro-opiomélanocortine, l'hormone α -mélanocytaire stimulante (α -MSH), ce qui entraîne l'activation de cascades de signalisation en aval, de manière dépendante de l'AMP-PKA (García-Borrón et al., 2014). Lors de l'exposition aux UV, l' α -MSH est libérée par les kératinocytes, ce qui entraîne la stimulation de MC1R au niveau de la membrane des mélanocytes, et induit consécutivement une augmentation des niveaux d'AMPc et l'activation de la protéine kinase A (PKA). Une cible importante de la PKA est le facteur de transcription CREB (cAMP-Responsive Element-Binding Protein), qui devient phosphorylé et active ensuite le promoteur de *MITF*, qui à son tour active la transcription des gènes *Tyr*, *Tyrp1* et *Dct*, l'enzyme de la mélanogenèse, ainsi que ceux qui régulent d'autres processus cellulaires, notamment la prolifération, l'invasion et le métabolisme (Bertolotto et al., 1998; Goding and Arnheiter, 2019). L'activation de la signalisation de MC1R est inhibée par la fixation de la neurofibromine 1 (NF1) (Deraredj Nadim et al., 2021). MC1R est le produit du gène situé au locus extension et stimule la synthèse du pigment, l'eumélanine (noir, brun). La mutation de perte de fonction dans ce locus, « *recessive yellow (e/e)* », entraîne la production de phéomélanine (jaune, rouge) au lieu de l'eumélanine (Tamate and Takeuchi, 1984). Il existe un antagoniste naturel de MC1R, la protéine de signalisation Agouti (ASP). Les mutations du gène Agouti dans la souris qui provoquent une expression accrue et ectopique de l'ASIP (« *viable yellow* », *A^v*) entraînent une couleur de pelage jaune, similaire au phénotype des souris *e/e*, ainsi qu'une obésité due à la liaison de l'ASIP au MC4R. Chez l'homme, plus de 200 variants de MC1R ont été identifiés dont un nombre élevé de variants fortement associés à des phénotypes pigmentaires, ce qui prouve que MC1R est le principal déterminant de la pigmentation humaine et qu'il joue un rôle central dans la régulation de l'eu- et du phéomélanine (García-Borrón et al., 2014). De la même manière

que chez la souris, les variants de MC1R chez l'homme peuvent entraîner une réduction de l'activité du récepteur et un déplacement de la synthèse de mélanine de l'eumélanine vers la phéomélanine. Le récepteur MC1R est inactivé par la présence de mutations chez les personnes rousses, ces mutations rendant les individus prédisposés au mélanome. Par exemple, il a été démontré les variants R151C, R160W et D294H, sont associés à une peau claire et peu pigmentée (Smith et al., 1998), alors que la forme WT est associée à une peau foncée et très pigmentée (Harding et al., 2000; Scott et al., 2002). Ces variants diminuent la sensibilité du récepteur et la liaison de l'hormone α -MSH, produite par les kératinocytes en réponse aux UV. Les études épidémiologiques ont fortement établi que le MC1R fonctionne comme un gène de prédisposition au mélanome. Cependant, on ne savait toujours pas si cela est dû à l'absence d'eumélanine, aux activités photoprotectrices et antioxydantes, ou à l'expression de phéomélanine, connue pour amplifier les espèces réactives de l'oxygène (ROS) induites par les UVA, ou à d'autres fonctions non liées à la pigmentation. L'équipe de D. Fisher a montré que la phéomélanine favorisait la mélanomagenèse via l'induction de dommages oxydatifs à l'ADN, sans exposition à aucun agent cancérigène, tel que les UV, chez des souris portant la mutation activatrice $Braf^{V600E}$ combinée à $MC1R^{e/e}$ (Mitra et al., 2012). Ainsi, la perte de fonction de MC1R favorise l'initiation du mélanome de manière indépendante des UV, démontrant son activité de suppresseur de tumeur. En dehors de son rôle central dans le changement du type de pigment, il MC1R a des rôles non pigmentaires dans les défenses antioxydantes et les mécanismes de réparation de l'ADN (Swope and Abdel-Malek, 2016). La voie de l'AMPc renforce l'activité de réparation par excision des nucléotides (NER) des mélanocytes, qui fonctionne par un mécanisme de "cut and patch", pour éliminer les lésions dues aux UV. L'activation du MC1R par sa liaison de l' α -MSH entraîne la phosphorylation des capteurs de dommages à l'ADN ataxia telangiectasia mutated (ATM) et Rad3 related (ATR), ainsi que le recrutement des protéines de complémentation du xeroderma pigmentosum XPC (groupe C) et XPA (groupe A) (Swope et al., 2020). En accord avec le fait que le MC1R favorise la réparation des lésions de l'ADN, une déficience de la voie NER chez les sujets porteurs d'une mutation perte de fonction du MC1R a été observée. D'autres effets de MC1R non liés à la pigmentation peuvent être attribués à l'activation de l'expression de MITF, qui contrôle les gènes impliqués dans la réparation des dommages à l'ADN, la stabilité des chromosomes et l'intégrité des centromères (Guida et al., 2021).

Les thérapies impliquant une signalisation défectueuse de MC1R visent à restaurer son activité. Des mutants de souris de MC1R sont caractérisés depuis des années et peuvent être utilisés pour

évaluer des thérapies visant à améliorer la protection contre les UV. L'application topique de forskoline, un inducteur de la production d'AMPc, sur des souris porteuses de mutations de perte de fonction ou d'haplo-insuffisance de $Mc1r^{e/e}$ peut stimuler l'eumélanogenèse et induire une résistance aux UV (Bautista et al., 2020; D'Orazio et al., 2006). Ces études ont confirmé les études épidémiologiques suggérant que l'haploinsuffisance en MC1R augmente la susceptibilité mutagène aux UV et le risque de mélanome. Une autre approche thérapeutique consiste à utiliser des agonistes de MC1R pour augmenter la pigmentation, et la réparation de l'ADN. L'analogue le plus connu est la NDP-MSH, qui est 100 fois plus puissante que l' α -MSH et actuellement utilisée pour traiter les maladies de photosensibilité, comme la protoporphyrie érythropoïétique (PPE). Un analogue très prometteur est le tripeptide (LK-514), qui est > 105 fois plus sélectif pour le MC1R que pour les autres récepteurs à la mélanocortine (Koikov et al., 2021). Le défi des thérapies basées sur le MC1R est d'utiliser un analogue hautement spécifique du MC1R pour éviter les effets toxiques dus à l'activation d'autres récepteurs.

c. Récepteur au glutamate

Le glutamate est le neurotransmetteur excitateur le plus abondant dans le système nerveux central humain, où il joue un rôle essentiel dans la communication intercellulaire au niveau des connexions synaptiques. Les récepteurs du glutamate sont également exprimés dans les tissus en dehors du système nerveux et sont impliqués dans la modulation de divers processus normaux et pathologiques. La famille des récepteurs du glutamate est divisée en deux groupes principaux : les récepteurs ionotropiques du glutamate (iGluRs) et les récepteurs métabotropiques du glutamate (mGluRs). Les mGluRs appartiennent à la famille des RCPGs de classe C, caractérisée par un grand domaine globulaire orthostérique extracellulaire de liaison au ligand. La famille des mGluRs comprend huit membres (mGluR1-8), qui sont organisés en 3 groupes en fonction de l'homologie de séquence, de leurs effecteurs de signalisation et de leur localisation générale. Les mGluRs du groupe I, composés de mGluR1 et mGluR5, sont des récepteurs à couplage multiple pouvant signaler à la fois par les voies $G\alpha_{q/11}$ et $G\alpha_{i/o}$. Les mGluRs du groupe II sont constitués de mGluR2 et de mGluR3 et se couplent à la voie $G\alpha_{i/o}$. Les mGluRs du groupe III sont constitués de mGluR4, mGluR6, mGluR7 et mGluR8 et sont couplés aux voies de signalisation $G\alpha_{i/o}$. Trois membres des récepteurs métabotropiques du glutamate (mGluR1, mGluR5, mGluR3) ont été clairement identifiés comme régulateurs de la mélanomagenèse (voir pour revue (Eddy and Chen, 2021)).

L'implication des récepteurs métabotropiques du glutamate dans la mélanomagenèse a été initialement révélée par hasard dans une étude complexe utilisant la mutagenèse insertionnelle, qui a conduit à une expression aberrante de mGluR1. De façon surprenante, la souris a développé des mélanomes métastatiques, alors que mGluR1 n'est pas détecté dans les mélanocytes normaux de la souris (Chen et al., 1996). Confirmant cette première observation, des souris transgéniques contenant mGluR1 sous le contrôle du promoteur *Dct* (*Dct::Grm1*) ont développé un mélanome avec une pénétrance de 100% (Pollock et al., 2003). Initialement, aucune métastase dans un organe distant n'a été observée, mais des cellules disséminées ont ensuite été détectées dans des organes distants, tels que le poumon et le foie (Schiffner et al., 2012). Un modèle transgénique conditionnel utilisant le système régulé par la tétracycline pour exprimer le mGluR1 à l'âge adulte a démontré que l'expression du mGluR1 est requise non seulement pour l'initiation du mélanome, mais aussi pour sa progression *in vivo* (Ohtani et al., 2008). Le gène codant pour le récepteur humain (GRM1) est altéré dans le mélanome par des mutations ponctuelles, une amplification et/ou des délétions. Chez l'homme, l'expression de GRM1 n'est pas détectée dans les mélanocytes normaux, mais dans 80% des mélanomes métastatiques ou des lignées cellulaires. Les travaux menés par l'équipe de Suzie Chen ont montré que l'expression de mGluR1 et GRM1 résulte de l'activation des voies MAPK et PI3K/AKT, les principales voies activées dans le mélanome (Eddy and Chen, 2021). Les mélanomes exprimant mGluR1 présentent des niveaux élevés de glutamate dans le microenvironnement tumoral, contribuant à l'hyperactivation du récepteur et de ses effecteurs en aval. L'identification de cette boucle autocrine entre l'expression de mGluR1 et la sécrétion de glutamate a conduit à des essais cliniques pour tester le riluzole, connu pour réduire la libération de glutamate et donc l'activation du récepteur. Aucune réponse objective n'a toutefois été observée. Cependant, le riluzole en monothérapie a montré un plus grand nombre d'infiltrats de cellules immunitaires chez les patients dont la maladie est stable comparé à ceux avec une maladie est progressive, ce qui suggère que l'association du riluzole à un traitement l'immunothérapie pourrait avoir un effet additif ou synergique. Cependant, cette hypothèse n'a pas encore été testée.

Contrairement au mGluR1, le mGluR5 est normalement exprimé à la fois dans les mélanocytes normaux et dans les mélanomes. Des souris transgéniques surexprimant mGluR5 (*Tyrp1 ::Grm5*) présentent de multiples mélanomes localisés sur la queue, avec une pénétrance de 100% et la présence de métastases, démontrant que mGluR5 dirige l'initiation et la progression du mélanome (Choi et al., 2011). Il convient de noter que les souris atteintes de mélanome mGluR1 ou mGluR5 présentent toutes deux des mélanomes sur la peau glabre plutôt

que sur les zones du tronc, comme cela a été observé pour les mélanomes induits par BRAF^{V600E} et NRAS^{Q61K}, ce qui suggère que l'origine de la cellule transformée peut n'est probablement pas être identique (épidermique vs follicule pileux). Aucune information concernant GRM5 chez l'homme n'est disponible.

Le séquençage par capture d'exons de 734 RCPG dans des mélanomes malins a montré qu'un troisième récepteur au glutamate, GRM3 est fréquemment muté dans les mélanomes humains. L'identification de la même mutation G18E/R ou M518I chez plusieurs individus suggère que ces mutations peuvent être « driver » du processus oncogénique (The Cancer Genome Atlas Network, 2015). Le mutant GRM3 régule la phosphorylation de MEK, ce qui entraîne une augmentation de la croissance et de la migration indépendante de l'ancrage (Prickett et al., 2011). Les cellules portant la mutation de GRM3 sont plus sensibles aux inhibiteurs de MEK. À ce jour, aucun modèle transgénique avec des mutants GRM3 n'a été développé pour étudier son effet dans la transformation cellulaire et la sensibilité aux inhibiteurs de MEK. Les mutants GRM3 peuvent contribuer à la mélanomagenèse par le biais d'un dialogue croisé entre les voies de signalisation AMPc et MAPK (Neto and Ceol, 2018). L'expression de deux autres récepteurs du glutamate, mGluR4 et mGluR8, a été détectée dans les mélanomes, mais leur rôle précis n'a pas encore été clairement démontré (Eddy and Chen, 2021). Plus de 60% des mélanomes humains expriment des mGluRs, ce qui corrobore l'importance des signaux glutamatergiques dans ce type de tumeur. Il semble que les récepteurs du glutamate soient non seulement impliqués dans la signalisation neuronale et les troubles neurologiques, mais aussi dans la transformation des cellules originaires de la crête neurale, les mélanocytes en mélanome.

d. Récepteurs Frizzled à Wnt

La voie Wnt (fusion des mots wingless et integrated) est l'une des voies de signalisation les plus importantes au cours du développement embryonnaire et de l'homéostasie de l'adulte et sa dérégulation a souvent été associée au cancer. Les protéines Wnt activent au moins trois voies de signalisation intracellulaire différentes : les voies Wnt/ β -caténine (dite canonique), Wnt/ Ca^{++} et Wnt/polarité planaire. Le type de protéine Wnt sécrétée détermine laquelle de ces trois cascades de signalisation est activée. La famille Wnt contient au moins 19 glycoprotéines sécrétées et riches en cystéine chez l'homme. Les protéines Wnt se lient aux cellules cibles par l'intermédiaire de deux familles de récepteurs : les sept récepteurs transmembranaires Frizzled (FZD) et les ses corécepteurs LRP5/6. Les récepteurs Frizzled (FZDs) sont composés de dix membres (FZD1-FZD10), dont la plupart sont couplés à la voie de signalisation canonique de la

β -caténine. Les récepteurs FZD sont fréquemment surexprimés dans les tissus tumoraux par rapport aux tissus normaux et sont potentiellement associés à un mauvais pronostic. Aucune surexpression de FZD n'a été directement liée au mélanome, mais sa signalisation associée à la β -caténine joue clairement un rôle central dans la mélanomagenèse. Nous pouvons néanmoins citer le récepteur FZD7 impliqué dans la formation de métastases pulmonaires après injection intraveineuses de cellules dans la veine de la queue dans des souris NSG (Tiwary and Xu, 2016). Par ailleurs, l'inactivation du récepteur FZD4 chez la souris génère une dépigmentation de la robe (Wang et al., 2001).

La voie Wnt a été largement étudiée et revue. Nous présentons ici les connaissances actuelles sur la signalisation Wnt/FZD dans le mélanome, notamment à travers l'activité de β -caténine, codée par *Ctnnb1* (Larue and Delmas, 2006; Zhan et al., 2017).

La voie Wnt/ β cat est essentielle au développement des mélanocytes à partir des CCN (Dorsky et al., 1998). Aucun mutant naturel impliquant des membres de la voie WNT/ β -caténine n'a été trouvé. Ainsi, les preuves de l'implication de cette voie dans le développement des mélanocytes proviennent d'études utilisant des souris nouvellement modifiées. WNT1 et WNT3a sont exprimés dans la partie dorsale du tube neural et β cat dans les mélanoblastes à tous les stades du développement. En particulier, les ligands WNT1 et WNT3a sont nécessaires à la spécification, l'expansion et la différenciation des mélanoblastes à partir des CCN (Dunn et al., 2000; Ikeya et al., 1997). β -caténine régule directement la détermination des mélanoblastes dans plusieurs modèles, avec des effets variables selon la temporalité de son activation (Dorsky et al., 2000; Hari et al., 2002). Chez la souris, la perte de β -caténine dans les CCN pré-migratoires (modèle *Wnt1::Cre ; Ctnnb1ex2-6^{F/F}*) ou dans les mélanoblastes (*Tyr::Cre ; Ctnnb1ex2-6^{F/F}*) induit la disparition des mélanoblastes (Hari et al., 2002; Luciani et al., 2011). L'activation précoce de la signalisation β -caténine dans les CCN pré-migratoires via l'utilisation l'expression d'une forme stabilisée de β -caténine (*Wnt1::Cre ; Ctnnb1 Δ ex3*) favorise le lignage neuronal sensoriel au détriment du lignage mélanocytaire (Hari et al., 2002; Lee et al., 2004). Au contraire, l'activation dans les CCN en migration(*Sox10::Cre ; Ctnnb1ex3^{F/+}*) favorise le lignage mélanocytaire, avec l'apparition de mélanocytes ectopiques dans les organes cibles d'autres lignages (Hari et al., 2012). L'expression d'une forme stabilisée de β cat (*Tyr::bcat-mut-nls-egfp*) conduit à des souris présentant un ventre blanc associé à un défaut de migration des mélanoblastes (Gallagher et al., 2013). Il a été démontré que plusieurs cibles de β -caténine sont impliquées dans la prolifération cellulaire, notamment les gènes ubiquitaires *Myc* et *CyclinD1* et

le gène *Mitf* spécifique des mélanocytes. Les protéines CMYC et Cyclin D1 induisent la prolifération cellulaire. MITF peut exercer un effet antiprolifératif ou prolifératif, selon le contexte cellulaire. Dans les mélanoblastes exprimant la β -caténine stabilisée, le niveau de MITF augmente, β -caténine interagit avec MITF ce qui interfère avec l'activité transcriptionnelle de β -caténine, inhibant l'activation de *cMyc* et de CyclinD1 et réduisant ainsi la prolifération. Les niveaux de β -caténine et de MITF sont probablement maintenus dans une fourchette très étroite au cours du développement des mélanoblastes, toute réduction ou augmentation, comme celles observées dans les mutants β -caténine, altère la prolifération des mélanoblastes. La multiplicité des rôles de β -caténine soulève des questions sur la nature des mécanismes qui permettent à une seule voie de signalisation de contrôler autant de processus différents au cours du développement et de l'homéostasie tissulaire. La β -caténine a la capacité de réguler la transcription de nombreux gènes pour exercer ses divers rôles. Cependant, les réponses transcriptionnelles de la signalisation Wnt/ β -caténine sont souvent très spécifiques à un stade de développement, un tissu ou une lignée cellulaire donnés.

Le mélanome a été l'un des premiers cancers dans lesquels des mutations de *CTNNB1* ont été identifiées. Dans les modèles murins, l'activation de la signalisation WNT/ β -caténine, mais n'est pas suffisante pour induire l'initiation. L'expression d'un mutant stabilisé de β -caténine dans les mélanocytes doit être associé à un oncogène activant de façon constitutive la voie MAPK (Tyr::*NRAS*^{Q61K}/^o ; Tyr::*bcat*-mut/^o) pour générer des mélanomes (Delmas et al., 2007). Cette propriété a été relié à l'immortalisation accrue des mélanocytes par la répression de l'expression de p16. Dans un modèle de souris *Braf*^{V600E} ; *Pten*^{-/-} ; *bcat*-KO (Tyr::*CreERT2*-Bos ; *Braf*^{CA} ; *Pten*^{F/F} ; *Ctnnb1ex2-6*^{F/F}), dans lequel la β -caténine est inactivée, l'apparition du mélanome est fortement retardée par rapport à celle d'un modèle *Braf*^{V600E} ; *Pten*^{-/-} (Damsky et al., 2011). Dans un modèle de souris *Braf*^{V600E} ; *Pten*^{-/-} ; *bcat** (Tyr::*CreERT2*-Bos ; *Braf*^{CA} ; *Pten*^{F/F} ; *Ctnnb1ex3*^{F/F}), dans lequel β -caténine est activée, l'apparition du mélanome est accélérée (Damsky et al., 2011). Dans les modèles murins de mélanome *Braf*^{V600E}, *Pten*^{-/-} et *NRAS*^{Q61R}, l'activation de *bcat* augmente le nombre de métastases pulmonaires, alors que l'inactivation de β -caténine diminue le nombre de métastases ganglionnaires et pulmonaires (Damsky et al., 2011; Gallagher et al., 2013). En conclusion, l'activation de *bcat* augmente à la fois l'initiation et la progression du mélanome dans les modèles murins. À noter que chez l'homme, plusieurs études ont lié la voie Wnt/ β -caténine à la réponse immunitaire antitumorale dans le mélanome (Nsengimana et al., 2018; Shah et al., 2008; Spranger et al., 2015).

e. Autres RCPGs

D'autres RCPG ont été impliqués dans la mélanomagenèse, mais leur rôle n'a pas été évalué de manière approfondie, en particulier *in vivo* en utilisant des modèles de souris génétiquement modifiées.

- Les récepteurs activés par la protéase (PAR) sont une famille de RCPG composée de quatre membres (PAR1-4) impliqués dans la régulation de divers processus cellulaires, notamment l'inflammation et la coagulation. Le clivage de PAR1 (également connu sous le nom de récepteur de la thrombine) par la thrombine active le récepteur et la signalisation en aval par le biais de multiples protéines G hétérotrimériques telles que $G\alpha_{q/11}$, $G\alpha_{i/0}$ et $G\alpha_{12/13}$. À leur tour, les voies de signalisation MAPK, de la phosphatidylinositol 3-kinase (PI3-K) et de la phospholipase C- β (PLC- β) sont activées. Il a été suggéré que l'expression élevée de PAR-1 pendant la progression du mélanome favorise les processus clés qui contribuent aux métastases du mélanome. Le ciblage de PAR-1 réduit la croissance tumorale et les métastases des cellules de mélanome dans les expériences de xénogreffe (Villares et al., 2008). La surexpression de PAR-1, ainsi que l'activation continue de la thrombine, favorise l'expression des gènes impliqués dans l'adhésion, l'invasion, l'angiogenèse et les métastases (Zigler et al., 2011). Comme la signalisation PAR-1 affecte à la fois les cellules de mélanome et leur microenvironnement, elle a été considérée comme une cible thérapeutique attractive pour le traitement des patients atteints de mélanome. Cependant, les essais thérapeutiques n'ont pas été poursuivis dans le mélanome en raison de l'activité de PAR1 dans la coagulation.
- Les récepteurs des chimiokines appartiennent à la famille des RCPG et sont classés en quatre groupes : CXCR, CCR, XCR et CX3CR. Chaque récepteur peut se lier à plusieurs chimiokines. Divers récepteurs de chimiokines sont exprimés à la surface des cellules immunitaires et tumorales. L'expression de CXCR4, CCR7 et CCR10 à la surface des cellules de mélanome est associée à un mauvais pronostic (Jacquelot et al., 2018). En dehors de leur rôle critique dans la réponse immunitaire, les chimiokines et leurs récepteurs ont été étudiés pour leur capacité à guider les cellules cancéreuses vers des organes spécifiques. Les chimiokines ont des propriétés chimiotactiques et peuvent attirer les cellules de mélanome exprimant les récepteurs correspondants. De fortes concentrations de CXCL12, le ligand de CXCR4, est produit dans les poumons ce qui attire les cellules de mélanome B16 exprimant. Cette colonisation est réduite en présence de

T22, un inhibiteur spécifique de CXCR4 (Drury et al., 2011). En outre, un gel à base d'acide hyaluronique (HA), chargé de CXCL12 a été capable de recruter et de piéger les cellules de mélanome B16 exprimant CXCR4 injectées à des souris, entraînant par conséquent une réduction des métastases pulmonaires (Ieranò et al., 2019). Cent trente-huit (138) essais cliniques avec des inhibiteurs de CXCR4 sont en cours/ont été réalisés, mais aucun n'inclut le mélanome. Chez la souris, il a été montré que la surexpression de CCR7 ou CCR10 dans les cellules de mélanome B16 augmentait les métastases vers les ganglions lymphatiques, phénomène bloqué en neutralisant son ligand, CCL21, à l'aide d'un anticorps spécifique (Jacquelot et al., 2018). Cependant, la plupart de ces expériences ont utilisé des cellules de mélanome B16 de souris, qui ne sont pas nécessairement les meilleures représentantes du mélanome humain. L'effet des différentes chimiokines sur la réponse immunitaire n'est pas discuté ici.

2. La signalisation associée aux RCPGs dans le lignage mélanocytaire

L'activation des RCPG entraîne une modulation de l'activité des voies de signalisation cellulaire, marquée par la production de seconds messagers. Le premier élément de cette signalisation est constitué par les protéines-G hétérotrimériques auxquelles ces récepteurs sont couplés par leur domaine intracellulaire. Ces protéines G sont constituées de trois sous-unités, $G\alpha$, $G\beta$, et $G\gamma$ (Hamm, 1998). La sous-unité C-terminale des protéines-G est responsable de la sélectivité de la liaison récepteur/protéine G (Hamm, 1998; Martin et al., 1996). La sous-unité $G\alpha$ est responsable de la sélectivité des voies de signalisation en aval (Wettschureck and Offermanns, 2005). Il existe un total de 21 sous-unités des protéines-G regroupées en quatre sous-familles : $G\alpha_s$, $G\alpha_{i/0}$, $G\alpha_{q/11}$, et $G\alpha_{12/13}$.

Les RCPGs se couplent généralement à une protéine-G spécifique, mais peuvent interagir avec plusieurs protéines-G différentes (Harding et al., 2000; Inoue et al., 2019). Le couplage semble dépendre de la cellule. Ainsi, une analyse minutieuse de la signalisation en aval est nécessaire pour chaque type de cellule. La liaison d'un ligand à son RCPG va entraîner un changement de conformation du RCPG qui permet la fixation de la protéine G liée à son GDP. Cette fixation va induire le relargage du GDP et son remplacement par le GTP. Cette fixation du GTP sépare la protéine de son récepteur et disloque le complexe en deux parties : la sous-unité $G\alpha$ d'un côté et les sous-unités $G\beta$ - $G\gamma$ de l'autre. Ce dimère module ensuite l'activité d'autres protéines intracellulaires (Hamm, 1998). Les complexes $G\alpha$ GTP et $G\beta$ / $G\gamma$ génèrent ensuite différents

signaux intracellulaires comprenant l'AMPc, l'inositol-triphosphate, le diacyl-glycérol ou encore les protéines Rho.

Les différentes voies de signalisations sont résumées dans la Figure 30.

a. Signalisation via l'AMPc

L'AMPc a été le premier second messager à être découvert et régule de nombreux processus cellulaires en aval (Sutherland and Rall, 1958, Sassone-Corsi 2012). Deux classes de sous-unités $G\alpha$ modulent les niveaux intracellulaires d'AMPc, $G\alpha_s$ et $G\alpha_{i/0}$, avec des effets diamétralement opposés (Wettschureck and Offermanns, 2005; Zaccolo et al., 2021). L'enzyme responsable de la production d'AMPc, l'adénylate cyclase (ADCY), est une enzyme associée à la membrane qui convertit l'ATP en AMPc (Hanoune and Defer, 2001; Zaccolo et al., 2021). La différence entre $G\alpha_s$ and $G\alpha_{i/0}$ est due à la différence du domaine de liaison sur l'adénylate cyclase : les membres de la famille $G\alpha_s$ se lient au domaine intracellulaire C2 de l'adénylate cyclase, qui stimule son activité enzymatique, conduisant *in fine* à une augmentation des niveaux d'AMPc intracellulaire (Dessauer et al., 1997). Inversement, les membres de la famille $G\alpha_{i/0}$ se lient au domaine intracellulaire C1 de l'adénylate cyclase, inhibant ainsi son activité.

La sous-famille des protéines G hétérotrimériques $G\alpha_s$ est composée de trois membres : $G\alpha_s$ et $G\alpha_{sxl}$ deux variants d'épissage du gène *GNAS*, et $G\alpha_{olf}$, codé par le gène *GNAL* (Wettschureck and Offermanns, 2005). Seul $G\alpha_s$ est exprimé dans les mélanocytes et les mélanomes (Plagge et al., 2008) et activé par un récepteur associé, tel que le MC1R (Sánchez-Más et al., 2005). Les mutations par gain de fonction de *GNAS* sont regroupées au niveau des acides aminés R201 et Q227, situées dans la poche où se trouve l'activité GTPase, et induisent la perte de cette activité GTPase intrinsèque. Elles maintiennent la protéine $G\alpha_s$ dans un état activé. Les mutations de *GNAS* sont fréquemment retrouvées dans diverses tumeurs du pancréas, du rein et de l'estomac, mais sont plus anecdotiques dans le mélanome, touchant moins de 1% des cas (Innamorati et al. 2018, The Cancer Genome Atlas Network, 2015). De manière plus frappante, le polymorphisme SNP *GNAS T393C* est associé à la progression tumorale dans le mélanome métastatique (Frey et al., 2010), ainsi que dans d'autres cancers, comme le cancer colorectal ou le cancer de la vessie (Frey et al., 2005a, 2005b). L'effet de ce polymorphisme sur l'activité de $G\alpha_s$ n'a pas été évalué sur le processus oncogénétique. Cependant, cette observation suggère que l'activation de $G\alpha_s$ favorise la progression du mélanome.

La sous-famille des protéines G hétérotrimériques $G_{i/0}$ est composée de huit membres : $G\alpha_{i1}$, $G\alpha_{i2}$, $G\alpha_{i3}$, $G\alpha_0$, $G\alpha_z$, $G\alpha_{t-r}$, $G\alpha_{t-c}$, et $G\alpha_{gust}$. Cependant, seuls $G\alpha_{i1}$, $G\alpha_{i2}$, and $G\alpha_{i3}$ sont exprimés

dans les mélanocytes et les mélanomes, et codés respectivement par *GNAI1-3* (The Cancer Genome Atlas Network, 2015; Thul et al., 2017; Uhlen et al., 2017; Wettschureck and Offermanns, 2005). Les mutations par gain de fonction de *GNAI2* sont regroupées au niveau des acides aminés R179 et T182 et conduisent à une activation constitutive de la sous-unité $G\alpha_{i2}$ en augmentant la capacité de liaison au GTP (Nishina et al., 1995; Pace et al., 1991). *GNAI2* est principalement impliqué dans les dommages cellulaires et les réponses inflammatoires, mais ces mutations activatrices peuvent conduire à des tumeurs, selon le contexte cellulaire, en raison d'une activité de la de signalisation MAPK accrue. Les mutations $G\alpha_{i2}$ R179 et T182 sont retrouvées chez 1,4% des patients atteints de mélanome (The Cancer Genome Atlas Network, 2015), mais leur impact n'a pas encore été évalué.

$G\alpha_s$ and $G\alpha_{i/0}$ régulent directement l'activité de l'adénylate cyclase. Il existe dix enzymes codées par dix gènes *ADCY1-10* différents (Cooper, 2003 2017). Toutes sont liées à la membrane via leurs deux séries de six hélices transmembranaires (TM1 et TM2), suivies d'un domaine cytoplasmique (C1 et C2, respectivement). Seule ADCY10, qui est soluble, diffère des autres, car son activation est indépendante des RCPG, étant activée par le bicarbonate et le calcium (Kleinboelting et al., 2014). La plupart des adénylate cyclases sont exprimées dans les mélanomes, à l'exception d'ADCY5 et ADCY8 (The Cancer Genome Atlas Network, 2015; Uhlen et al., 2017). L'expression d'ADCY10 n'est pas claire, car, bien que des équipes aient trouvé la protéine par IHC, les bases de données suggèrent que l'ARNm est absent (Magro et al., 2012; The Cancer Genome Atlas Network, 2015). Il a été montré que les mélanomes métastatiques expriment davantage l'ARNm d'ADCY1 que les mélanomes primaires et qu'un niveau élevé d'expression d'ADCY1 est corrélé à un pronostic plus défavorable (Chen et al., 2019). Conformément à cette observation, l'extinction d'ADCY1 *in vitro* dans les lignées cellulaires de mélanome muqueux diminue la capacité des cellules à former des clones ainsi que leur capacités migratoire et invasive (Ma et al., 2019). Dans les expériences de xénogreffe, la diminution de l'expression d'ADCY1 diminue la croissance cellulaire sous-cutanée, ainsi que la colonisation du poumon après l'injection de cellules de mélanome dans la veine caudale de souris NOD/SCID (Ma et al., 2019). Plus généralement, la stimulation de l'activité de l'adénylate cyclase par la forskoline favorise la croissance tumorale dans le modèle de souris mélanome *Braf^{CA}/Pten^{-/-}*, tandis que son inhibition pharmacologique par le SQ22536 entraîne une diminution de la croissance tumorale de manière indépendante de la voie MAPK (Rodríguez et al., 2017, 2018). Cependant, le traitement de lignées cellulaires de mélanomes primaires et métastatiques humains par le SQ22536, même à des concentrations élevées, n'altère pas la croissance

cellulaire. Cela implique que le ciblage de l'adénylate cyclase transmembranaire n'est pas une stratégie thérapeutique réalisable en soi. L'activité de l'adénylate cyclase est également impliquée dans la résistance aux inhibiteurs de MAPK. En effet, traiter des cellules de mélanome BRAF^{V600E} avec de la forskoline augmente l'expression d'ADCY9 et la synthèse d'AMPc, ce qui conduit à une plus grande résistance à l'inhibition des MAPK (Johannessen et al., 2013).

La concentration intracellulaire d'AMPc est régulée négativement par les phosphodiésterases (PDE), qui hydrolysent l'AMPc en AMP, contrôlant ainsi l'amplitude et la durée du signal. Il existe 11 familles de PDE (PDE1-11) codées par un total de 21 gènes différents (Omori and Kotera, 2007). Des isoformes spécifiques de PDE sont localisées dans différents compartiments subcellulaires, où elles régulent les niveaux d'AMPc. En effet, l'AMPc ne diffuse pas librement dans la cellule, mais est plutôt produit dans des compartiments subcellulaires. Cette caractéristique a des conséquences importantes, car elle permet d'activer uniquement les cibles appropriées dans les microdomaines (Bang and Zippin, 2021).

Dans les mélanocytes, la phosphodiésterase 4 (PDE4), plus précisément son variant PD4ED3, est une cible directe de la signalisation MC1R-cAMP, constituant une boucle de contrôle négative (Khaled et al., 2010). Le blocage de l'activité de PDE4D3 en conjonction avec un traitement avec de la forskoline peut restaurer efficacement les niveaux d'AMPc et la pigmentation chez les souris MC1R^{e/e}. Dans le mélanome, l'expression de nombreuses PDEs a été rapportée et leur effet a été initialement montré sur la prolifération cellulaire (Dumaz et al., 2011; Lin et al., 2013). Leurs fonctions spécifiques dans les mélanomes mutés BRAF ou NRAS mettent en évidence la connexion entre les voies AMPc et MAPK (voir ci-dessous). La surexpression de la PDE4 et, par conséquent, l'inhibition de la signalisation AMPc est critique pour l'activation de la voie MAPK par l'oncogène RAS dans le mélanome (Dumaz et al., 2006; Marquette et al., 2011). Dans le mélanome muté BRAF, l'inhibition de l'activité de la PDE4 par des inhibiteurs pharmacologiques ou par interférence ARN diminue l'invasion des cellules de mélanome à travers la kinase d'adhésion focale FAK (Delyon et al., 2017). Globalement, 3,5 % des tumeurs solides (dont le mélanome) présentent des microdélétions homozygotes de PDE4D associées à une expression accrue et à un effet promoteur de tumeur (Lin et al., 2013). L'expression de PDE4D est élevée dans les mélanomes métastatiques et associée négativement à la survie. Plus généralement, l'inhibition de la signalisation de l'AMPc par l'expression des phosphodiésterases (PDE1, PDE2, PDE4 et PDE8) est associée à la progression du mélanome (Bang and Zippin, 2021). Il faudra évaluer à l'avenir si les inhibiteurs de la phosphodiésterase peuvent prévenir la prolifération, l'invasion ou la migration dans le mélanome.

La principale cible de l'AMPc est la protéine kinase A (PKA) (Walsh et al., 1968; Wettschureck and Offermanns, 2005). La PKA est une sérine/thréonine kinase composée de quatre sous-unités : deux régulatrices et deux catalytiques. Il existe quatre isoformes pour les sous-unités régulatrices (RI α , RI β , RII α , and RII β) et catalytiques (C α , C β et C γ), chaque isoforme présentant une localisation et une spécificité individuelle. Toutes sont exprimées dans les mélanocytes et les mélanomes (Skalhegg and Tasken, 2000). La liaison de l'AMPc aux sous-unités régulatrices induit leur dissociation des unités catalytiques qui deviennent actives et phosphorylent les cibles en aval (Taskén et al., 1997). Plus de 70% des patients atteints du complexe de Carney familial sont porteurs de trois mutations associées à des caractéristiques pathogènes (particulièrement c82C>T, c491_492delTG, c.709-2_709-7 delATTTTT) dans le gène *PRKAR1A*, qui code pour la sous-unité RI α (Liu et al., 2017). Cette mutation induit une action dominante-négative de la sous-unité régulatrice et en conséquence une activation constitutive de la sous-unité catalytique de la PKA. Ce syndrome néoplasique multiple autosomique dominant est marqué par une pigmentation mouchetée de la peau (Kirschner et al., 2000). Les mutations inactivatrices de *PRKAR1A* conduisent à une activation constitutive de la voie AMPc-PKA par perte de régulation des sous-unités catalytiques de la PKA. Dans le mélanome, des mutations sont retrouvées dans 1,4% des cas, ainsi qu'une perte d'hétérozygotie chez 11,8% des patients (The Cancer Genome Atlas Network, 2015). De plus, une perte de fonction de *PRKAR1A* est trouvée dans les mélanocytomes pigmentés épithélioïdes, une forme intermédiaire rare de mélanome (Cohen et al., 2020). En comparant l'activité de la PKA dans les cellules de mélanome primaire et métastatique, Beebe et ses collègues ont suggéré que l'activité de la PKA est plus élevée dans les métastases de mélanome (Beebe et al., 1993). L'inhibition pharmacologique de la PKA induit la croissance et l'invasion des cellules de mélanome (Hiramoto et al., 2014).

Un grand nombre de protéines cytosoliques et nucléaires ont été identifiées comme substrats de la PKA (Sassone-Corsi, 2012). Il est important de noter que la PKA est située au carrefour entre l'AMPc et MAPK/ERK. L'activation constitutive de l'AMPc conduit à la phosphorylation et à l'inactivation de CRAF par la PKA dans le mélanome (Marquette et al., 2011). CRAF est important pour maintenir l'activation de la voie MAPK dans les cancers mutés RAS car ERK1/2 exerce un action contrôle négatif par sur la phosphorylation de BRAF entraînant son inhibition (Dumaz et al., 2006; Lyons et al., 2013; Marquette et al., 2011). Par conséquent, l'activation des voies MAPK par le biais de CRAF nécessite que la voie de l'AMPc dans les cellules de mélanome soit inactivée pour lever l'inhibition de CRAF médiée par l'AMPc. La PKA peut également phosphoryler directement BRAF sur la sérine 365, disloquant le complexe RAS/BRAF/KSR et activant ainsi

BRAF (Takahashi et al., 2017). La sous-unité C α catalytique rend les cellules de mélanome BRAF^{V600E} résistantes aux inhibiteurs de MAPK (Johannessen et al., 2013). La protéine CRT3, un co-activateur de CREB qui est phosphorylé et activé par PKA et ERK (Ostojic et al., 2021), se situe à l'interface entre la signalisation par les voies AMPc et MAPK. Un modèle de souris knock-out pour *Crct3* a montré un grisonnement du pelage dû à des défauts de maturation des mélanocytes (Ostojic et al., 2021). Des mutations de *CRCT3* ont été identifiées dans 23% des mélanomes humains, la plupart conduisant à une augmentation de son expression et de son activité et à une réduction de la survie des patients (Ostojic et al., 2021). Ainsi, l'inhibition de CRT3 pourrait être bénéfique pour ces patients.

La régulation de la transcription par la PKA s'effectue principalement par la phosphorylation de CREB. La phosphorylation de CREB conduit à la dimérisation de ce facteur de transcription et à sa liaison ultérieure aux éléments de réponse à l'AMPc (CRE) dans les gènes cibles, ainsi qu'à son interaction avec les co-activateurs de transcription, tels que la protéine de liaison à CREB (CBP) et p300. Les sites de liaison CRE sont situés dans les régions promotrices de nombreux gènes, y compris dans le promoteur *MITF* (Bertolotto et al., 1998; Buscà and Ballotti, 2000). MITF est le facteur de transcription central du lignage mélanocytaire et régule de nombreux processus cellulaires majeurs, notamment la pigmentation, la croissance, la survie, la migration et l'invasion qui sont essentielles à la mélanogenèse comme à la mélanomagenèse (Goding and Arnheiter, 2019). Dans le mélanome, la surexpression de CREB est associée à la transition de la phase de croissance radiale à la phase de croissance verticale (Mobley et al., 2012).

Il a été démontré que l'inhibition de CREB dans les lignées cellulaires de mélanome diminuait la formation de métastases après injection dans les veines de la queue des souris (Xie et al., 1997; Dobroff et al., 2009). Cette perte du potentiel métastatique s'explique notamment par la perte d'expression de la métalloprotéinase MMP2 et de la molécule d'adhésion MCAM/MUC18. De manière surprenante, CREB, qui agit généralement comme un transactivateur, régule négativement le facteur de transcription AP2 et le gène codant la protéine 61 riche en cystéine (*CCN1/CYR61*). Dans les premières publications, ces deux gènes étaient considérés comme des gènes suppresseurs de tumeur dans le mélanome, mais des études plus récentes ont proposé que AP2 et CYR61 facilitent la progression du mélanome (Braeuer et al., 2011; Chen et al., 2020; White et al., 2021). L'enzyme d'édition de l'ARN adénosine désaminase agissant sur l'ARN1 (ADAR1) a été récemment identifiée comme une nouvelle cible de CREB. L'inhibition de l'expression d'ADAR1 augmente le pouvoir invasif des cellules de mélanome (Nemlich et al., 2018). CREB a été associé à la résistance aux inhibiteurs de la voie MAPK. La phosphorylation de

CREB est restaurée dans les récurrences de mélanomes précédemment traités par des inhibiteurs de MAPK, probablement par l'augmentation de AEBP1 (Hu et al., 2013; Johannessen et al., 2013). Une deuxième cible majeure de l'AMPC est la protéine d'échange activée par l'AMPC (EPAC) (Zhang et al., 2020a). EPAC est un facteur d'échange de nucléotides de guanine (GEF) pour les petites GTPases, comme par exemple RAP1 (Ras-related protein 1). L'activation de RAP1 se produit par l'échange de GDP pour GTP (Sassone-Corsi, 2012; Zhang et al., 2020a). Les conséquences de l'activation de l'EPAC sur la croissance du mélanome ne sont toujours pas claires et les données sont contradictoires. En effet, l'activation pharmacologique de l'EPAC à l'aide d'un analogue de l'AMPC spécifique de l'EPAC augmente la croissance des cellules HMG (Narita et al., 2007), mais n'a aucun effet sur le mélanome PMP (Hiramoto et al., 2014). L'utilisation de shRNA ciblant Rap1 augmente la croissance et la survie des cellules dérivées de mélanomes primaires, mais pas métastatiques (Rodríguez et al., 2017). L'hypothèse actuelle est que la voie EPAC-Rap1 est anti-proliférative dans le mélanome métastatique et pro-proliférative dans le mélanome primaire (Rodríguez and Setaluri, 2018).

Les derniers effecteurs majeurs de l'AMPC sont les canaux ioniques AMPC-dépendants : le canal ionique dépendant des nucléotides cycliques (CNG) et le canal dépendant des nucléotides cycliques activé par l'hyperpolarisation (HCN) (Fajardo et al., 2014; Zhang et al., 2020a). Ces canaux sont des canaux cationiques relativement non sélectifs et n'ont pas encore été étudiés dans le mélanome.

La signalisation de l'AMPC et les conséquences moléculaires et cellulaires dans le mélanome sont décrites dans la Figure 24.

cAMP signaling

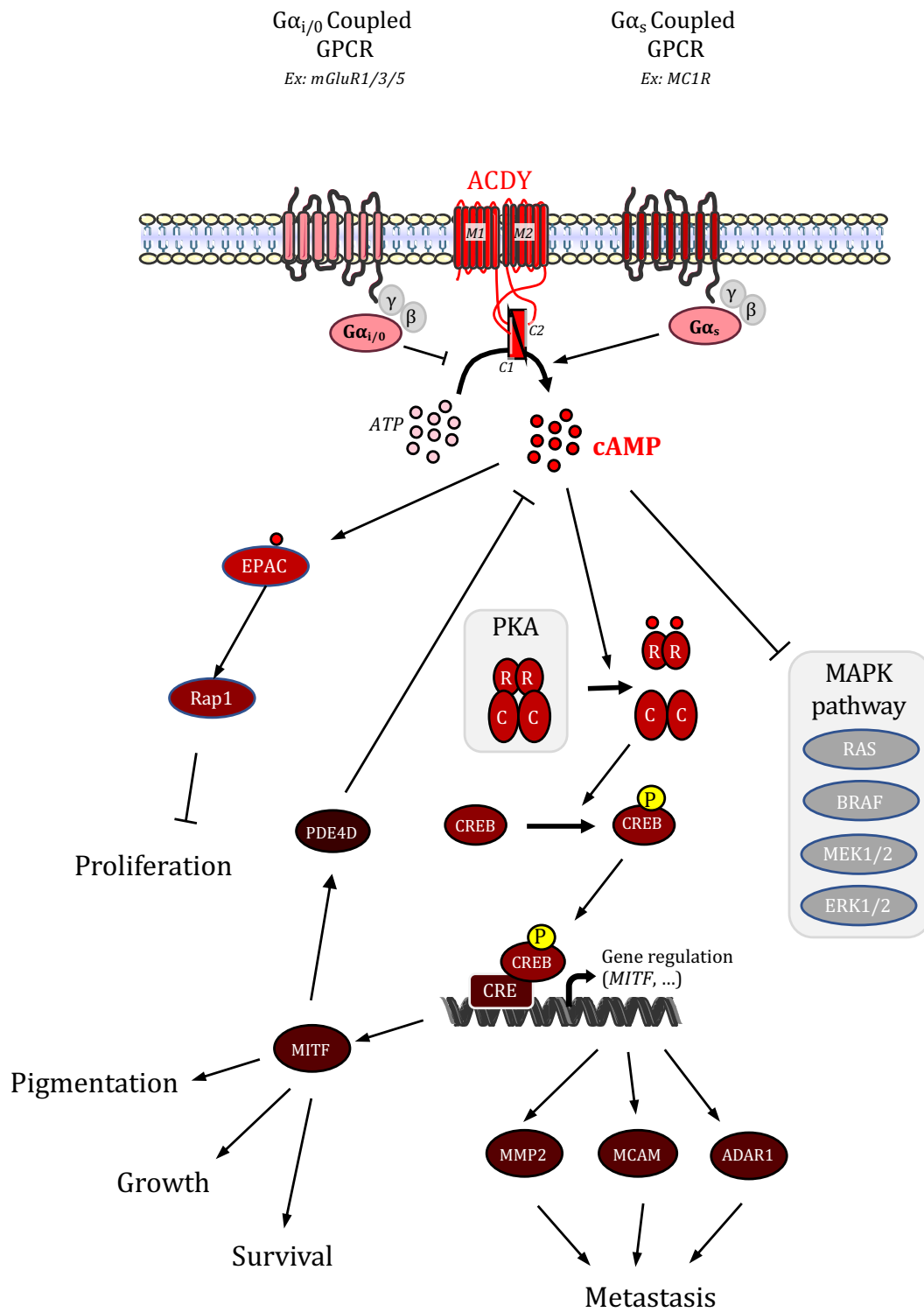


Figure 24: Voies de signalisation de l'AMPc et conséquences cellulaires.

b. Signalisation par l'Inositol tri-phosphate et le Diacyl-Glycérol

Les niveaux cellulaires d'inositol tri-phosphate (IP3) et de diacyl-glycérol sont fortement régulés par la stimulation des RCPGs de la classe $G\alpha_{q/11}$. Cette classe contient quatre membres : $G\alpha_q$, $G\alpha_{11}$, $G\alpha_{14}$, and $G\alpha_{16}$ (Wettschureck and Offermanns, 2005). Tous peuvent être exprimés dans les mélanocytes et les mélanomes, mais seuls $G\alpha_q$ et $G\alpha_{11}$ sont fortement exprimés dans ces cellules (The Cancer Genome Atlas Network, 2015; Uhlen et al., 2017). L'activation du récepteur induit l'échange du GDP lié à la sous-unité alpha contre du GTP, ce qui entraîne l'activation de cette sous-unité. Des mutations affectant les protéines-G de la classe $G\alpha_{q/11}$ sont presque systématiquement retrouvées dans les mélanomes uvéaux, dont environ 90% des mélanomes uvéaux métastatiques sont mutés pour $G\alpha_q$ ou $G\alpha_{11}$ affectant principalement la glutamine 209 dans les deux protéines, mais aussi, dans une moindre mesure, l'arginine 183 (Robertson et al., 2017; Van Raamsdonk et al., 2010). *GNAQ*, qui code pour $G\alpha_q$, est muté dans 50 à 85 % des lésions mélanocytaires non épithéliales, y compris les nævus bleus et les néoplasmes mélanocytaires leptoméningés, et les mutations de *GNA11*, qui code pour $G\alpha_{11}$, sont plus fréquentes dans les mélanomes uvéaux. (Urtatiz and Van Raamsdonk 2016). Ces mutations se retrouvent à des fréquences plus faibles (~1-6%) dans les autres types de mélanomes cutanés (O'Hayre et al., 2013; The Cancer Genome Atlas Network, 2015). Les mutations Q209L/P et R183C/Q dans *GNAQ* ou *GNA11* affectent le domaine GTPase (Maziarz et al., 2018), mais seules les mutations Q209L/P ont été réellement caractérisées. Ces mutations réduisent l'activité GTPase de la sous-unité $G\alpha_q$ et provoquent une signalisation hyperactive (Maziarz et al., 2018). Quel que soit le contexte tumoral, ces mutations sont mutuellement exclusives (Robertson et al., 2017) et le sont également avec les mutations BRAF et NRAS. À noter que dans le mélanome uvéal, les mutations de *CYSLTR2* (L129G), codant pour un RCPG couplé $G\alpha_{q/11}$, sont retrouvées de manière mutuellement exclusive avec les mutations $G\alpha_q$ et $G\alpha_{11}$ chez environ 3 % des patients. Cette mutation est également présente dans les nævus bleus (Möller et al., 2017; Robertson et al., 2017). La mutation *CYSLTR2*^{L129G} active de manière constitutive le récepteur et donc la signalisation en aval. Selon les modèles murins utilisés et les cellules ciblées (cellules de la crête neurale ou mélanoblastes), l'expression embryonnaire de $G\alpha_q$ ^{Q209L} est capable d'induire une gamme de lésions allant de l'hyperpigmentation dermique au mélanocytome leptoméningé, en passant par les nævus et le mélanome dermique, jusqu'aux mélanomes uvéaux malins avec invasion pulmonaire (Huang et al., 2015; Urtatiz et al., 2020). De même, l'expression postnatale de $G\alpha_{11}$ ^{Q209L} dans les mélanocytes induit des lésions mélanocytaires hyperpigmentées dans le tractus uvéal, la peau et les leptoméninges qui évoluent vers un

mélanome avec invasion pulmonaire (Moore et al., 2018). Les souris transplantées sous la peau avec des cellules de mélanome mutées $G\alpha_q$ montrent une inhibition de la signalisation MAPK et de la croissance tumorale après traitement par l'inhibiteur de $G\alpha_{q/11}$ FR900359 (Annala et al., 2019). À ce jour, l'inhibition du mélanome uvéal par FR900359 semble être plus puissante que l'inhibition avec YM254890, un autre inhibiteur $G\alpha_{q/11}$ (Kostenis et al., 2020). L'activation de $G\alpha_{q/11}$ est un mécanisme de résistance à l'inhibition de la voie MAPK par la surexpression de c-Jun (Ambrosini et al., 2012). Ces données sont cohérentes avec le gain de résistance aux inhibiteurs de MAPK montré par l'activation de EDNRB (Asundi et al., 2014). Inversement, l'inhibition de $G\alpha_{q/11}$ par l'YM-254890 a entraîné une inhibition de la signalisation MAPK, mais ne prévient pas la survenue d'un rebond après 24 heures dans des expériences de xéno greffe de mélanome uvéal. Le traitement combiné avec le YM-254890 et un inhibiteur de MEK a conduit à une inhibition soutenue de MAPK et à une réduction de la tumeur (Hitchman et al., 2021; Padmanaban et al., 2019). Une combinaison d'inhibiteurs de PKC et de MEK1 est actuellement en cours d'évaluation clinique pour les tumeurs solides porteuses de mutations *GNAQ/GNA11* ou des fusions PRKS. (Essais de phase I/II : NCT03947385).

La cible principale des sous-unités $G\alpha_{q/11}$ est la phospholipase C bêta (PLC β) (Smrcka et al., 1991; Taylor et al., 1991; Waldo et al., 1991). Cette sous-famille est codée par quatre gènes (*PLCB1-4*) codant pour sept protéines, qui ont toutes deux isoformes, sauf PLC β 3 (Lyon and Tesmer, 2013). Tous les PLC β sont probablement exprimés dans le mélanome cutané (The Cancer Genome Atlas Network, 2015), alors que seuls les gènes *PLCB2-4* sont exprimés dans le mélanome uvéal (Robertson et al., 2017). Les PLC β s fonctionnent en hydrolysant les phosphatidylinositol-4,5-biphosphates (PIP2) membranaires en inositol-1,4,5 trisphosphate (IP3) et en diacylglycérol (DAG) (Chua et al., 2017). Les mutations *PLCB4* se produisent dans environ 5 % des mélanomes uvéaux et sont mutuellement exclusives avec les mutations *GNAQ*, *GNA11* et *CYSLTR2* (Johansson et al., 2016). Les mutations PLC β 4^{D630Y} affectent le domaine Y du noyau catalytique de PLC β 4 (Johansson et al., 2016). Leur effet n'a pas été étudié précisément, mais leur exclusivité avec les mutations *GNAQ*, *GNA11* et *CYSLTR2* et le fait qu'elle se situe en aval de ces protéines suggèrent que les mutations PLC4 ont un effet similaire sur l'oncogénicité des mélanomes uvéaux (Johansson et al., 2016). En dehors du contexte du mélanome, il a souvent été démontré que les PLC β sont associés à la progression tumorale par l'activation de la prolifération et de la migration cellulaire (Li et al., 2016a; Sengelaub et al., 2016).

L'un des deux messagers secondaires produits par les PLC est le DAG, qui reste ancré dans la membrane. Les esters de phorbol, tels que le 12-O-tétradéconoyl phorbol-13-acétate (TPA) et le 12-myristate 13-acétate de phorbol (PMA), sont des analogues synthétiques du DAG. Le TPA est essentiel à la croissance des mélanocytes in vitro (Arita et al., 1992; Petit et al., 2019; Tamura et al., 1987). De manière intéressante, l'effet du TPA sur la prolifération des lignées cellulaires de mélanome semble dépendre du contexte cellulaire (Cooper, 2003; Iwasaki et al., 2017; Jørgensen et al., 2005; La Porta et al., 1998; Petit et al., 2019). Le PMA augmente la survie et l'invasion des cellules et la résistance à l'anoïkis (Dissanayake et al., 2007; Jørgensen et al., 2005; Zhao et al., 2000). Le TPA et le PMA activent les voies PKC et MAPK (Jørgensen et al., 2005). L'autre messenger secondaire produit par les PLC est l'IP3. La liaison de l'IP3 au récepteur de l'IP3 (IP3R) augmente les niveaux de Ca⁺⁺ intracellulaires (Foskett et al., 2007). La libération de calcium induite par IP3 favorise la migration et l'invasion des cellules de mélanome (Cox et al., 2002; Sun et al., 2014; Umemura et al., 2014).

Le DAG et le calcium activent la protéine kinase C en se liant aux domaines C1 et C2 de la PKC, respectivement (Denning, 2012). Il existe neuf gènes qui codent pour la PKC : PKC α , PKC β , PKC γ , PKC δ , PKC θ , PKC ϵ , PKC η , PKC ι et PKC ζ (Denning, 2012). Ils sont divisés en trois classes en fonction de leur mécanisme d'activation. Les PKC classiques (cPKCs) sont constitués de PKC α , PKC β et PKC γ et sont activés par le calcium et les DAGs. Les nouvelles PKC (nPKC) (PKC δ , PKC θ , PKC ϵ , PKC η) sont activées uniquement par les DAG. Les PKC atypiques (aPKCs) (PKC ι et PKC ζ) ne sont pas activés par le calcium ou les DAGs (Denning, 2012). Au moins une PKC de chaque classe est exprimée dans les cellules de mélanome, à l'exception de la PKC γ (Denning, 2012; The Cancer Genome Atlas Network, 2015). L'activité des PKC est régulée par la présence de leurs substrats et de cofacteurs et par leur recrutement par des protéines d'échafaudage, telles que le récepteur des kinases activées C (RACK) ou la protéine d'échafaudage 5 de la protéine kinase A (AKAP5) (Hoshi et al., 2010; Park et al., 2004; Schechtman and Mochly-Rosen, 2001; Voris et al., 2010). La PKC régule l'invasion des cellules de mélanome, mais les différents membres ont des effets différents : PKC α et PKC δ induisent la migration, l'invasion et la colonisation pulmonaire des mélanomes (Matsuoka et al., 2009). A l'inverse, PKC β diminue l'invasion et favorise la différenciation cellulaire et la pigmentation (Oka et al., 2008; Park et al., 1993). Il existe des mutations fréquentes de *PRKCB* et une perte d'expression dans le mélanome, mais leur impact sur l'activité de PKC β n'a pas été évalué (Voris et al., 2010; The Cancer Genome Atlas Network, 2015). De même, l'effet de la PKC sur la croissance cellulaire dépend de l'isotype (Lau et al., 2012; Chen et al., 2017; Mhaidat et al., 2017).

Parmi les cibles de la PKC figure la protéine 3 de libération de guanine de Ras (RASGRP3), un facteur d'échange de nucléotides guanine pour les protéines de la famille RAS (Chen et al., 2017; Moore et al., 2018). La PKC phosphoryle RASGRP3 sur la Thr133, contribuant à son activation conjointement avec la liaison du DAG (Aiba et al., 2004; Johnson et al., 2007; Teixeira et al., 2003). L'inhibition de RASGRP3 induit la perte de la liaison du GTP à RAS et donc de son activité (Chen et al., 2017; Moore et al., 2018). Cette diminution d'activité s'accompagne d'une diminution de l'activité de la voie MAPK associée à une diminution de la prolifération cellulaire (Moore et al., 2018). Ce mécanisme moléculaire peut expliquer l'activation de la voie MAPK observée après l'activation de PKC (Cozzi et al., 2006; Marín et al., 2006; Schönwasser et al., 1998; Tsubaki et al., 2007). PKC ϵ et PKC η sont capables de shunter l'inhibition pharmacologique de BRAF^{V600E}, rendant les cellules de mélanome résistantes à ces médicaments (Johannessen et al., 2010). En accord avec cette donnée, l'utilisation d'inhibiteurs de PKC inhibe la survie et la migration des cellules de mélanome résistantes au vémurafenib (Fu et al., 2020).

L'activité de la protéine 1 associée à Yes (YAP1) est régulée positivement par de nombreux RCPG, mais négativement par la voie de Hippo (Kwon et al., 2021; Yu et al., 2012a). Dans le mélanome uvéal, YAP1 est activé par G $\alpha_{q/11}$, induisant la croissance et la survie des cellules (Huang et al., 2015; Yu et al., 2014; Feng et al., 2014). L'inhibition de l'activité de YAP1 par la vertéporfine réduit la croissance tumorale (Feng et al., 2014; Yu et al., 2014). G $\alpha_{q/11}$ active le facteur d'échange de nucléotides guanine TRIO, qui active à son tour les petites GTPases RhoA et Rac1 (Feng et al., 2014; Vaqué et al., 2013). Cela a probablement une double action : (i) l'activation de FAK, qui à son tour inhibe la kinase LATS1/2 de la voie Hippo, inactivant l'action de YAP1, et (ii) l'activation directe de YAP1 en libérant le facteur de transcription angiomotine (AMOT) (Feng et al., 2014; Paradis et al., 2021). Dans le mélanome uvéal, l'activation de Rho et Rac est liée à l'activation des MAP kinases JNK et p38 (Vaqué et al., 2013). JNK et p38 phosphorylent c-Jun et induisent l'expression des cibles de AP-1 (Shaulian and Karin, 2001). La phosphorylation de c-Jun induit la prolifération cellulaire via des cibles AP1 qui régulent le cycle cellulaire, comme la cycline D1, p53, p21^{cip1}/Waf1, p19^{ARF} et p16^{INK4A} (Du et al., 2019; Estrada et al., 2009; Pathria et al., 2016; Shaulian and Karin, 2001). L'activation de p38 et JNK est susceptible d'être impliquée dans les mécanismes de résistance aux inhibiteurs de MAPK (Du et al., 2019; Estrada et al., 2009). Dans le mélanome cutané, l'activation de YAP1 est requise pour l'invasion cellulaire (Ma et al., 2021; Nallet-Staub et al., 2014; Zhang et al., 2020c; Zhao et al., 2021) ainsi que pour la viabilité et la résistance à l'anoikis (Ma et al., 2021; Nallet-Staub et al., 2014; Zhao et al., 2021). Bien que l'effet de YAP1 sur l'invasion soit clairement documenté, son effet sur la croissance des mélanomes est

encore débattu (Ma et al., 2021; Zhang et al., 2020c). Il a également été démontré que l'activité de YAP1 est associée à la migration cellulaire via la régulation du complexe 3 arp2/3 (Lui et al., 2021; Ma et al., 2021). Le phénotype invasif des cellules de mélanome a été corrélé avec la signature d'activation de YAP1 (Zhang et al., 2020c). *In vivo*, l'activation de YAP1 induit la formation d'un très grand nombre de métastases dans les poumons après l'injection de cellules portant les mutations activatrices de YAP1-5SA sous la peau de souris (Zhang et al., 2020c). La colonisation des poumons après l'injection de cellules dans la queue des souris diminue également lorsque les niveaux de YAP1 sont génétiquement diminués (Nallet-Staub et al., 2014; Zhao et al., 2021). Plus intéressant encore, l'inhibition de la voie Hippo reproduit cet effet, favorisant clairement la colonisation pulmonaire (Tan et al., 2021). L'action pro-invasive de YAP1 est médiée par la transcription d'un certain nombre de ses cibles, comme *CCN1*, *AXL* et *THBS1* (Zhang et al., 2020c). Ces cibles sont bien connues dans le mélanome. L'expression d'*AXL* est associée à la croissance tumorale, à l'invasion et à la migration des cellules, et à la résistance aux inhibiteurs de MAPK (Flem-Karlsen et al., 2020; Müller et al., 2014; Tizpa et al., 2020). Il a été démontré que *CCN1* est associé à un potentiel métastatique et à une angiogenèse accrue (Chen et al., 2020; Kunz et al., 2003). L'inhibition génétique de *THBS1* est associée à une diminution de l'invasion cellulaire (Jayachandran et al., 2014; Borsotti et al., 2015). YAP1 a besoin des cofacteurs transcriptionnels TEAD1-4 pour se lier à ses cibles. L'inhibition génétique de TEAD1-4 récapitule les effets *in vitro* de YAP1 sur l'invasion, avec une nette diminution de la capacité invasive des cellules de mélanome (Verfaillie et al., 2015). Les cofacteurs TEAD1-4 sont également impliqués dans la résistance aux inhibiteurs de MAPK. Ainsi l'inhibition des quatre membres de la famille TEAD sensibilise les cellules à ces inhibiteurs (Verfaillie et al., 2015). La signalisation cellulaire induite par l'activation de récepteurs couplés $G\alpha_{q/11}$ ainsi que les conséquences cellulaires induites sont décrites dans la Figure 25.

DAG/IP₃ signaling

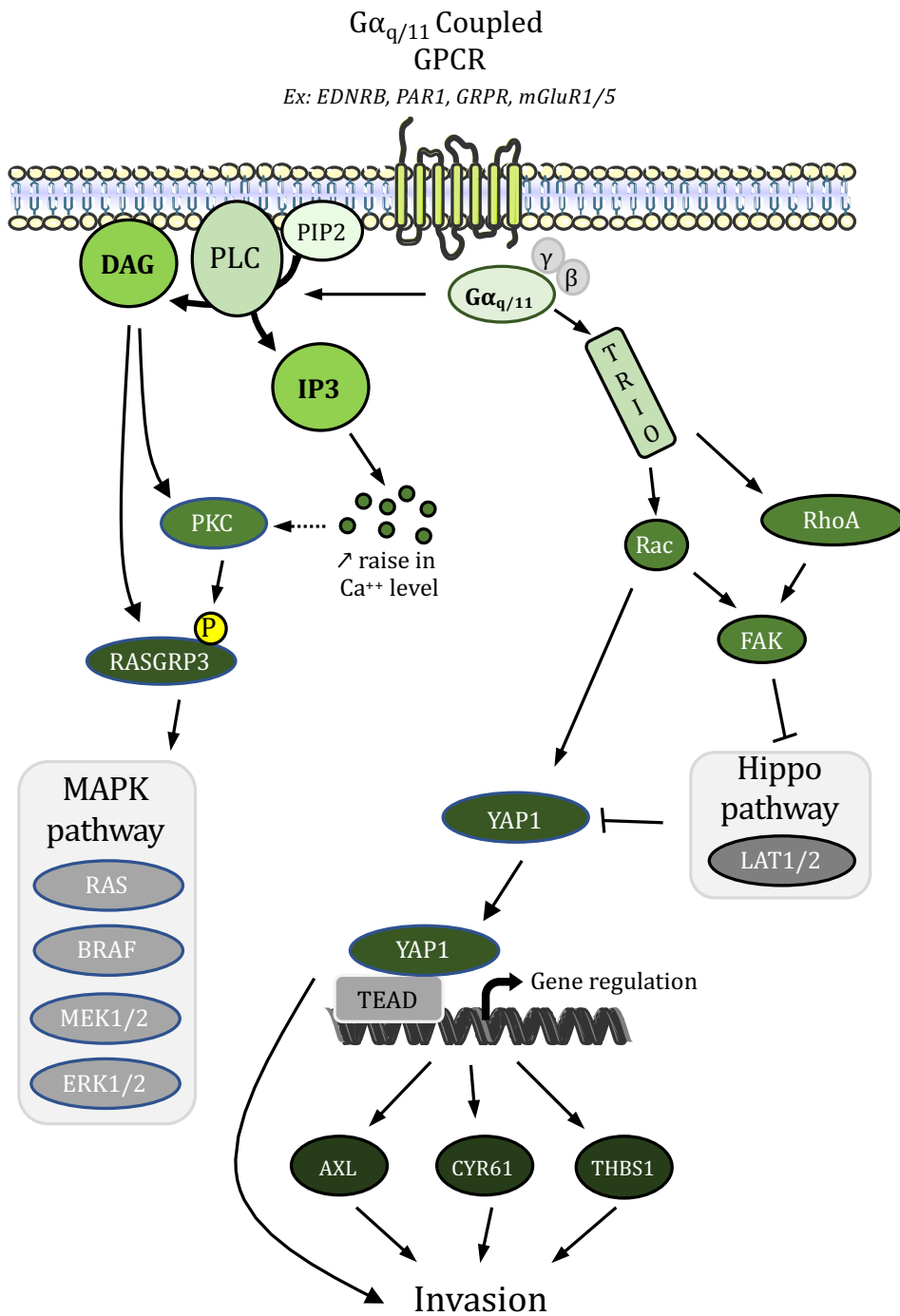


Figure 25: Voies de signalisation du Diacyl-glycérol et de l'IP₃ et conséquences cellulaires.

c. Signalisation via $G\alpha_{12/13}$

La troisième voie majeure de signalisation des RCPGs impliquée dans le mélanome est la voie impliquant $G\alpha_{12/13}$ (Wettschureck and Offermanns, 2005). Cette classe de sous-unités G compte deux membres, $G\alpha_{12}$ et $G\alpha_{13}$, codés respectivement par les gènes *GNA12* et *GNA13*. L'expression de ces gènes est ubiquitaire (The Cancer Genome Atlas Network, 2015; Uhlen et al., 2017; Wettschureck and Offermanns, 2005). L'activation de ces sous-unités active les Rho-GEF, comme le Rho-GEF associé à la leucémie (LARG) ou le Rho-GEF p115 (Hart et al., 1998; Suzuki et al., 2003). L'activation est réalisée par l'attachement de la sous-unité $G\alpha_{12}$ et $G\alpha_{13}$ au domaine RH des Rho-GEFs (Chen et al., 2005b). Une fois activés, les Rho-GEFs induisent l'activation de RhoA (Suzuki et al., 1996; Fukuhara et al., 1999; Wells et al., 2002; Vogt et al., 2003). Rho est un point de convergence pour la signalisation $G\alpha_{12/13}$ et $G\alpha_{q/11}$ (Vogt et al., 2003). La signalisation induite en aval se produit par l'activation de YAP1, comme décrit ci-dessus (Yu et al., 2012b). La signalisation $G\alpha_{12/13}$ a été peu analysée dans le contexte du mélanome. Les récepteurs PAR1 et 2, couplés aux protéines $G\alpha_{12/13}$ sont exprimés dans le mélanome (Elste and Petersen, 2010). L'activation des récepteurs PAR1 par son ligand TRAP6 induit l'activation de YAP1 dans un modèle cellulaire HEK293A (Mo et al., 2012). L'activation de YAP1 entraîne ensuite l'activation de RhoA et l'inhibition de LATS1 (Mo et al., 2012). De manière similaire à la signalisation $G\alpha_{q/11}$, la signalisation $G\alpha_{12/13}$ semble augmenter l'invasion et la migration tout en ne modifiant pas la croissance cellulaire (Kelly et al., 2006a, 2006b). Cependant, ces résultats ont été obtenus dans le cancer du sein et de la prostate et doivent être confirmés dans le mélanome. Il est à noter que l'activation des récepteurs LPA (LPA1-LPA6), couplée aux récepteurs $G\alpha_{12/13}$, est encore peu documentée dans le mélanome, bien qu'il ait été rapporté qu'elle améliore la chimiorésistance aux médicaments et augmente la survie des cellules de mélanome *in vitro* (Minami et al., 2020).

Cette signalisation est résumée dans la Figure 26.

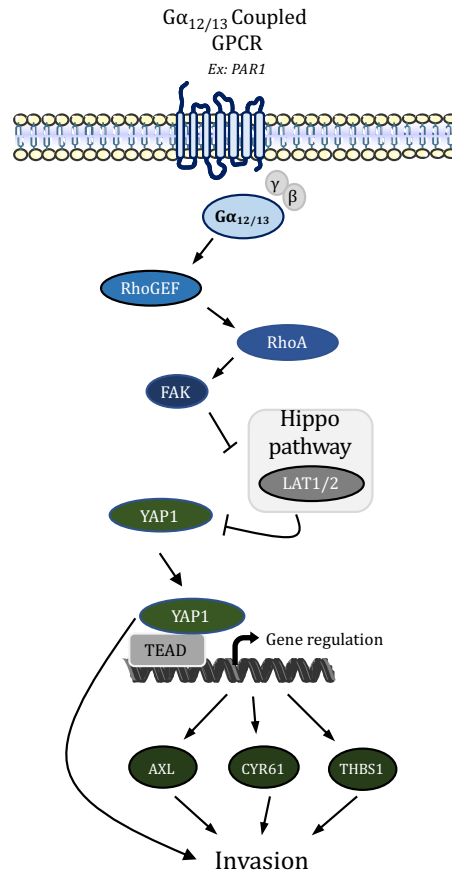


Figure 26: Voie de signalisation des récepteurs couplés $G\alpha_{12/13}$ et conséquences cellulaires.

d. Signalisation Wnt/ β -caténine

Les WNT activent 3 voies de signalisation WNT/ β -caténine, WNT/ Ca^{++} et WNT/polarité planaire. Dans ce chapitre seule la voie canonique WNT/ β -caténine est présentée, la voie WNT/ Ca^{++} correspond à la signalisation $G\alpha_q/11$ décrite en C.II.2.b et la signalisation WNT/polarité planaire est non détaillée car peu étudiée dans le mélanome. La voie canonique WNT est activée uniquement en réponse à la formation d'un complexe contenant WNT, FZD et LRP. Les protéines WNT sont difficiles à purifier sous une forme active et seuls quelques anticorps sont disponibles pour leur détection. Les protéines WNT les plus étudiées dans le contexte de l'activation de la β -caténine dans le mélanocyte/mélanome sont WNT1 et WNT3a. WNT5a a différents rôles et agit comme un antagoniste ou un agoniste de la voie canonique WNT/ β -caténine, en fonction du contexte cellulaire. Les protéines WNT sont soumises à des modifications post-traductionnelles, notamment la glycosylation et les modifications lipidiques. L'acylation sur les résidus conservés de sérine et de cystéine est nécessaire pour la sécrétion de WNT et la liaison efficace au récepteur Frizzled (Takada et al., 2006; Willert et al., 2003). À l'état basal, la protéine axine interagit par le biais de domaines distincts avec GSK-3, CK1 α , APC et β -

caténine. L'axine est considérée comme le composant limitant du complexe de destruction de la β -caténine (Lee et al., 2003; Salic et al., 2000). La modulation de ses niveaux serait donc un moyen efficace de réguler la destruction de la β -caténine. APC est une grande protéine qui interagit à la fois avec la β -caténine et l'axine. Elle contient trois domaines de liaison à l'axine, intercalés entre des domaines répétés armadillo (ARM), qui se lient à la β -caténine. La β -caténine est séquentiellement phosphorylée par CK1 α et GSK-3 sur des sérines (S) et des thréonines (T) (S45, T41, S37 et S33) dans la région N-terminale de la protéine. La β -caténine est ubiquitinée par β -TRCP1 avant d'être dégradée par le protéasome.

La liaison du ligand WNT conduit à la dimérisation de Frizzled avec le corécepteur LRP5/6. Cette dimérisation entraîne un changement de conformation des récepteurs, conduisant à la relocalisation du complexe de dégradation vers la membrane cellulaire sous la double interaction de l'axine avec DVL (lui-même associé à Frizzled) et avec l'extrémité cytoplasmique de LRP. Cette relocalisation membranaire diminue l'activité du complexe de dégradation, de sorte que la quantité de β -caténine cytoplasmique non phosphorylée augmente rapidement. La stabilisation de la β -caténine cytoplasmique entraîne une augmentation de la β -caténine nucléaire. L'équilibre entre la quantité de β -caténine cytoplasmique et nucléaire est dynamique, résultant de multiples mécanismes de transport et de rétention entre les deux compartiments. Dans le noyau, la β -caténine se lie à la famille des facteurs de transcription T-cell factor (TCF)/lymphoid enhancer-binding factor (LEF), qui reconnaissent des sites spécifiques dans l'ADN. En l'absence de β -caténine, les facteurs TCF interagissent avec les corépresseurs transcriptionnels de la famille Groucho/transducin-like enhancer of split (TLE) et répriment l'expression de leurs gènes cibles. L'accumulation nucléaire de β -caténine conduit à l'association de TCF avec la β -caténine, ce qui entraîne sa dissociation de Groucho/TLE1 et permet le recrutement d'autres coactivateurs pour l'activation transcriptionnelle par le biais de son domaine d'activation transcriptionnelle C-terminal. De nombreux facteurs de transcription n'appartenant pas à la famille des facteurs de transcription TCF/LEF ont été montrés comme capables de s'associer à la β -caténine pour activer ou réprimer la transcription. Aussi, dans les mélanocytes/mélanomes, MITF interagit avec la β -caténine et redirige l'activité transcriptionnelle médiée par la β -caténine des gènes cibles canoniques de Wnt/ β vers des gènes cibles spécifiques de MITF pour activer leur transcription. D'autres niveaux de signalisation croisée entre la voie WNT/ β -caténine et le MITF ont été décrits. Par exemple, il a été démontré que la β -caténine/TCF augmente la transcription de MITF (Dorsky et al., 2000). Il a également été démontré que MITF se lie à son propre promoteur et le régule par une

interaction directe avec LEF1 (Saito et al., 2002). Par conséquent, il semblerait difficile de cibler β -caténine dans le mélanome sans affecter l'expression et/ou l'activité de MITF. MITF pourrait potentiellement être une cible attrayante pour la thérapie du mélanome, mais le ciblage de MITF par des médicaments est très difficile. Comme déjà mentionné, MITF est considéré comme le "gène maître" de la différenciation des mélanocytes et joue un rôle essentiel dans la prolifération, la survie, la sénescence, la migration, l'invasion, la réparation de l'ADN et le métabolisme des cellules de mélanome (Goding and Arnheiter, 2019; Kawakami and Fisher, 2017). L'expression de *Mitf* est régulée par de multiples voies de signalisation en dehors de la voie canonique Wnt/ β -caténine, comme les voies AMPc/CREB, YAP1/PAX3, TGF β /GLI2, TNF/NFB, et des facteurs de transcription, comme SOX10 et BRN2, eux-mêmes régulés par de multiples voies dans le mélanome. Le concept de base dans le mélanome est que les états prolifératifs et invasifs sont définis, en partie, par le niveau/activité élevé de MITF et le niveau/activité faible de MITF, respectivement. Un niveau/activité élevé et faible de MITF coexiste dans les tumeurs de mélanome et le changement d'expression de MITF (élevé et faible) est réversible et responsable de l'hétérogénéité et de la plasticité du mélanome. MITF est également impliqué dans la résistance aux inhibiteurs de BRAF. Une vision actuelle de la stratégie thérapeutique consiste à augmenter les niveaux de MITF. La signalisation β -caténine est résumée dans la Figure 27.

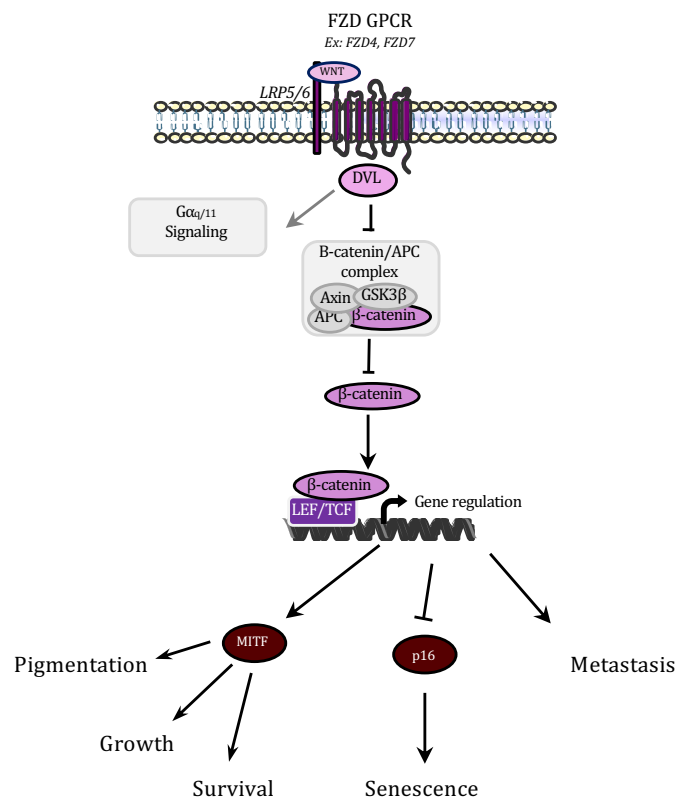


Figure 27: Voie de signalisation β -caténine et conséquences cellulaires

e. Signalisation par le complexe G β /G γ

L'activation des RCPGs induit principalement l'activation des sous-unités G α des protéines G, mais aussi celle du complexe G β /G γ . Il existe cinq sous-unités G β (G β ₁₋₅) chez l'homme, codées par les gènes *GNB1-5*. Tous, à l'exception de *GNB5*, sont exprimés dans le mélanome (Wettschureck and Offermanns, 2005). Il existe 16 sous-unités G γ codées par les gènes *GNG1-16*, dont seules les sous-unités G γ ₂, G γ ₄, G γ ₅, G γ ₆, G γ ₇, G γ ₁₀, G γ ₁₁, and G γ ₁₂ sont exprimées dans le mélanome (The Cancer Genome Atlas Network, 2015; Uhlen et al., 2017; Wettschureck and Offermanns, 2005). L'importance de la signalisation G β /G γ dans le mélanome n'a pas encore été complètement évaluée. Il existe deux mécanismes moléculaires majeurs induits par les sous-unités G β /G γ : la modulation des concentrations de calcium cytosolique et la signalisation par la phosphoinositide 3-kinase (PI3K) (Baljinnyam et al., 2011; Pfeil et al., 2020; New et al., 2007; Sellers et al., 2000). L'effet sur la concentration en calcium est lié à l'activation des PLC β (Bonacci et al., 2005). Concernant PI3K, les sous-unités G β /G γ se lient à p110, la sous-unité catalytique, et induisent son activation (Leopoldt et al., 1998). L'activation de PI3K induit l'activation de l'AKT et augmente la survie cellulaire (Sellers et al., 2000). Compte tenu de l'importance connue des voies PI3K/AKT dans le mélanome, sa régulation par les sous-unités G β /G γ doit être davantage analysée. La signalisation par les sous-unités G β /G γ et les conséquences cellulaires potentielles sont résumées dans la Figure 28.

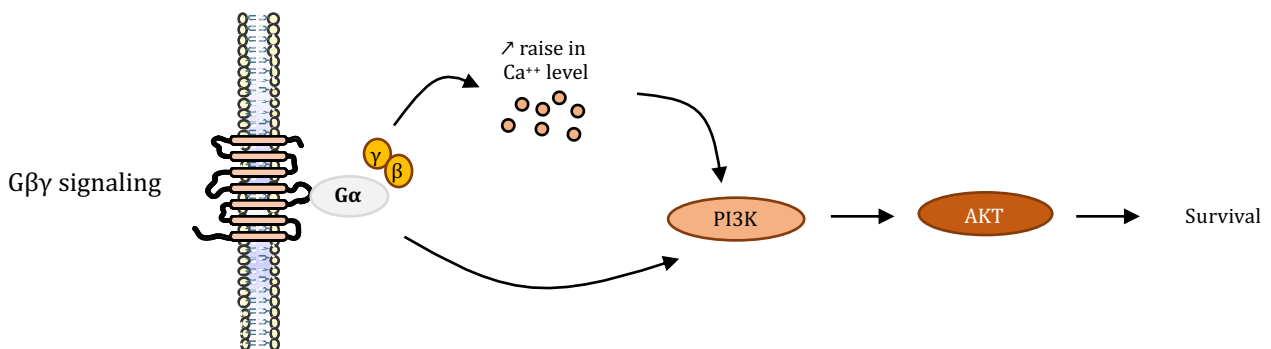


Figure 28: Signalisation via G β /G γ et conséquences cellulaires.

f. Signalisation biaisée

À la fin des années 1990, on a observé que les tyrosines kinases de la famille SRC sont recrutées par les β -arrestines (codées par les gènes *ARRB1-2*) sur le récepteur adrénergique 2a, membre de la famille des RCPGs (Luttrell et al., 1999). De manière surprenante, la liaison des protéines kinases n'induit l'activation de la voie MAPK/ERK que si le récepteur était internalisé (Luttrell et al., 1999; Miller et al., 2000). D'autres observations au milieu des années 2000 ont montré qu'une telle signalisation était non canonique et indépendante des protéines-G. En effet,

l'activation des RCPGs active trois types de protéines : les protéines-G, les protéines kinases des RCPGs (GRKs) et les arrestines. Les GRKs et les arrestines sont les éléments les plus importants impliqués dans la fin de l'activation des RCPGs. Les GRKs phosphorylent le récepteur sur ses résidus C-terminaux, ce qui empêche l'activation des protéines-G (Krupnick et al., 1997). Cette phosphorylation recrute les arrestines, β -arrestine 1 & 2, qui à leur tour recrutent la clathrine entraînant l'internalisation du récepteur par des puits de clathrine (Gurevich and Gurevich, 2015; Krupnick et al., 1997; Shenoy and Lefkowitz, 2003). Selon l'affinité du complexe RCPG/arrestine, les récepteurs peuvent être recyclés ou dégradés dans le protéasome (Oakley et al., 2000). Dans les endosomes précoces, le complexe RCPG/arrestine est capable de former un signalosome en recrutant des protéines de signalisation, comme les membres de la voie MAPK (Miller and Lefkowitz, 2001; Shenoy and Lefkowitz, 2003, 2005). Plusieurs voies peuvent être activées, telles que les voies MAPK/ERK et Src (Luttrell et al., 1999; Zhai et al., 2005), AKT (Beaulieu et al., 2005), MAPK/JNK (McDonald et al., 2000), MAPK/p38 (Luttrell et al., 2001), ou PDEs (Perry et al., 2002).

La signalisation GRK-arrestine a été peu étudiée dans le mélanome. La β -arrestin2 est capable de biaiser la signalisation du MC1R en favorisant l'activation de la voie MAPK vers celle de la signalisation dépendante de l'AMPc (Abrisqueta et al., 2013). Un transcrite du MC1R (MC1R-203) favorise naturellement une telle signalisation biaisée vers la voie de signalisation MAPK (Martínez-Vicente et al., 2020). Des mutants des récepteurs métaboliques du glutamate (mGluR3^{G848E}) peuvent favoriser une telle signalisation biaisée, caractérisée par une internalisation prolongée du récepteur (Abreu et al., 2021). Cette mutation est retrouvée dans de rares cas de mélanome cutané (< 1%) (The Cancer Genome Atlas Network, 2015). À l'inverse, dans le mélanome uvéal, la mutation CYSLTR2_{L129Q} force la signalisation via $G\alpha_{q/11}$ et inhibe la signalisation via les β -arrestins (Ceraudo et al., 2021). La signalisation des RCPG est certainement beaucoup plus complexe que celle présentée ici et résumée en Figure 29. Leurs interactions avec les GRK et les arrestines et la dynamique de leur désensibilisation ajoutent un autre niveau de complexité qui doit être étudié à l'avenir.

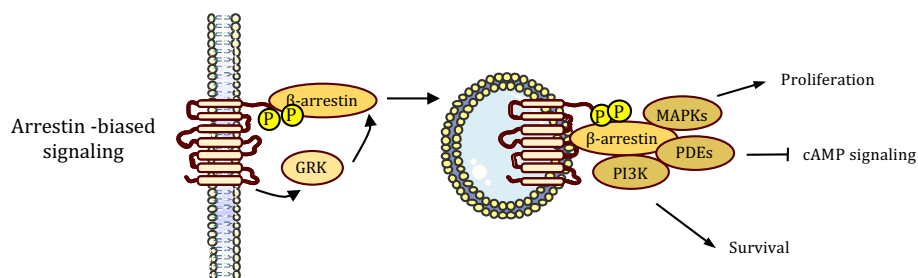


Figure 29: Signalisation biaisée via les arrestines et conséquences cellulaires.

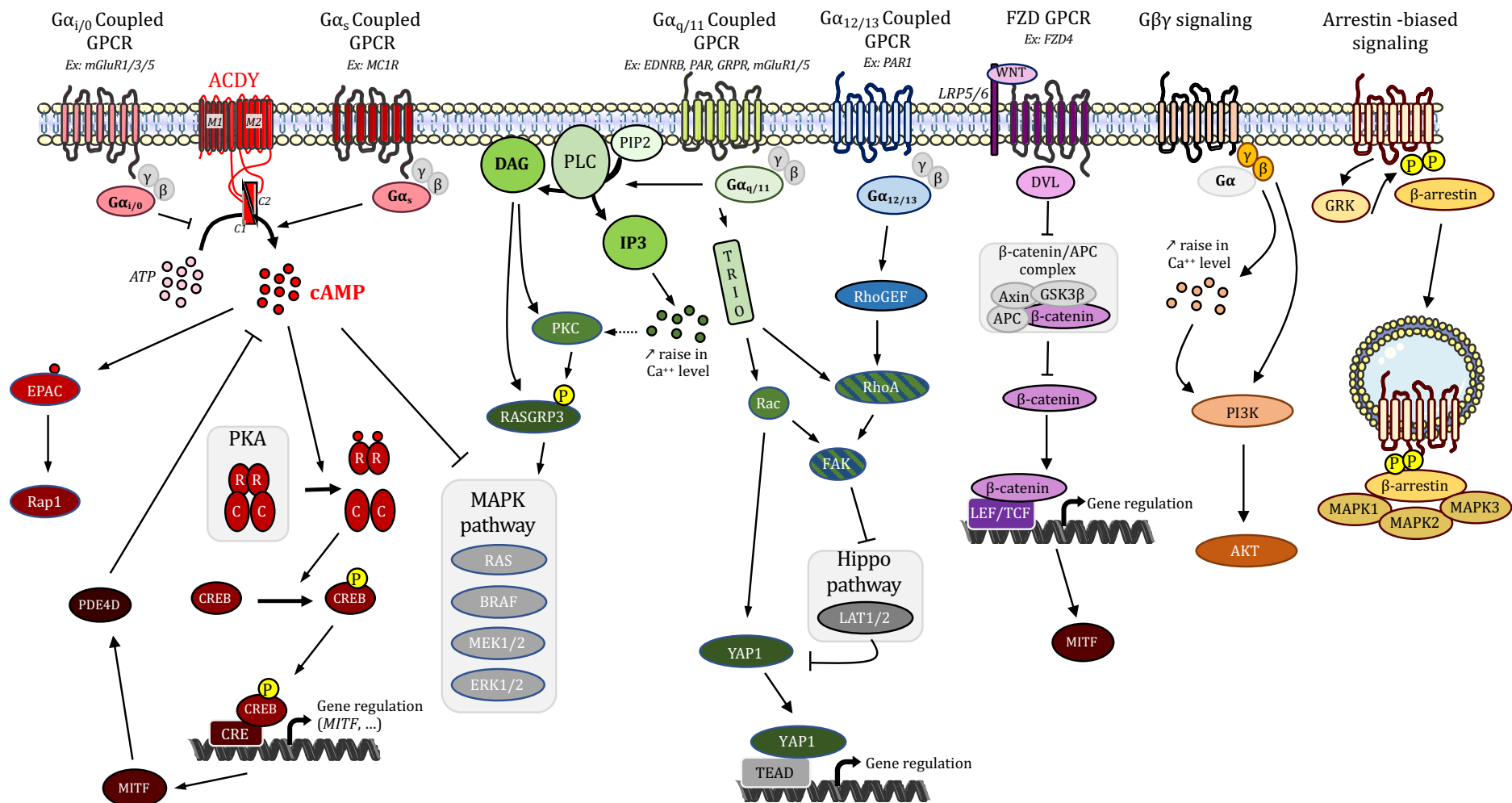


Figure 30: Voies de signalisation des RCPG selon la protéine-G hétérotrimérique couplée.

Chaque couleur correspond à une voie de signalisation, la voie $G\alpha_{12/13}$ reprend une grande partie de la signalisation de la voie $G\alpha_{12/13}$ à partir de l'activation de RhoA. Tous les récepteurs sont susceptibles d'activer les signalisation $G\beta/\gamma$ et biaisée-arrestine vers les arrestines.

III. Le récepteur au peptide relarguant la gastrine (GRPR)

1. Découverte

De la peau de batraciens du genre *Bombina bombina* a été identifié un peptide, nommé selon le genre des grenouilles, bombésine (Erspamer et al., 1970). 8 et 13 ans plus tard, en 1979 et 1983 deux ligands très similaires ont été successivement isolés respectivement le peptide relarguant la gastrine (GRP) dans l'estomac de porc, et la neuromédine B (NMB) dans la moelle épinière de porc (McDonald et al., 1979; Minamino et al., 1983). Le rapprochement entre la bombésine et les deux peptides a rapidement été fait, notamment par leur similarité de structures et d'effets biologiques (McDonald et al., 1979). Les tests réalisés sur des tissus stimulés avec ces peptides isolés et avec des antagonistes nouvellement synthétisés ont permis d'identifier deux classes de récepteurs répondant spécifiquement aux stimuli (Jensen and Gardner, 1981; Jensen et al., 1978; Moody et al., 1992). Ces récepteurs seront finalement isolés et clonés en 1990 et 1991 permettant d'identifier respectivement le récepteur au peptide relarguant la gastrine (GRPR) et le récepteur à la neuromédine (NMBR) (Spindel et al., 1990; Wada et al., 1991). Un troisième récepteur, orphelin a été identifié l'année suivante et nommé bombésine de sous-type 3 (BRS3) (Gorbulev et al., 1992). Un quatrième récepteur, BB4, a été identifié, mais sa présence n'est avérée que dans les grenouilles (Nagalla et al., 1995). Depuis GRPR a été identifié dans de nombreuses espèces de vertébrés. Sa présence est détectée chez tous les mammifères, mais également chez des poissons comme le poisson-zèbre, des reptiles comme le lézard des murailles des oiseaux comme le poulet. GRPR est plutôt conservé, car la séquence du récepteur humain possède respectivement 68%, 74%, 81% d'homologie avec les séquences du poisson zèbre, du lézard des murailles et du poulet. L'homologie monte à 90% entre Homme et souris. L'essentiel des régions conservées correspond aux domaines transmembranaires.

2. Structure

GRPR est un RCPG de classe A codé par le gène *GRPR* qui produit qu'un seul transcrit. La protéine est constituée de 384 acides aminés (Figure 31). Des études de fixation après mutagenèse ont identifié les acides aminés K101, Q121, F185, A198, P199, R288, S293, T297, A308 comme impliqués dans la liaison avec la GRP, car leur mutation diminuait l'affinité de cette dernière pour GRPR. L'acide Aspartique 98, toujours par la même méthode a été montré comme essentiel à l'expression de GRPR à la membrane (Akeson et al., 1997; Carroll et al., 2000; Donohue et al., 1999; Lin et al., 2000; Nakagawa et al., 2005).

principalement exprimé au niveau du cortex cérébral, dans les régions olfactives, dans l'hippocampe et dans l'amygdale. Dans les tissus sexués, GRPR est exprimé dans l'épididyme et dans le canal déférent chez l'homme et dans le sein et l'utérus chez la femme. Des cellules sanguines comme les monocytes expriment également GRPR (Fagerberg et al., 2014). Le niveau d'expression dans tous les tissus est résumé dans la Figure 32. Il est quand même intéressant de noter que GRPR est exprimé à faible niveau dans tous les tissus. La discrimination exacte des cellules exprimant le récepteur est dure à faire dû au manque de spécificité des anticorps. Les études d'expression d'ARN dans les cellules uniques (single-cell RNAseq) sont également incapables de déterminer l'expression de GRPR, car cette technique a du mal à capter les gènes peu exprimés et ne permet pas de voir tous les gènes exprimés dans la cellule, mais seulement les majoritaires. Néanmoins, des études menées notamment en utilisant la technique de RNAscope, laissent suggérer que cette faible expression tissulaire serait due à une expression dans des neurones. C'est notamment le cas dans la peau où GRPR n'est exprimé physiologiquement que dans les neurones (Barry et al., 2020).

Aussi, il ne faut pas nécessairement négliger les organes où l'expression est faible, car les RCPGs ne nécessitent pas une forte expression pour pouvoir exercer leurs actions. Les variations d'expression de GRPR au cours du développement sont peu connues, mais il a été montré que GRPR est significativement exprimé dans les poumons durant le développement de ceux-ci *in utero* (Emanuel et al., 1999; Shan et al., 2004). L'expression de GRPR est aussi dépendante du niveau d'inflammation. Par exemple la stimulation de kératinocytes avec de l'IL-22 induit l'expression de GRPR dans ces cellules (Lou et al., 2017).

Expression de GRPR

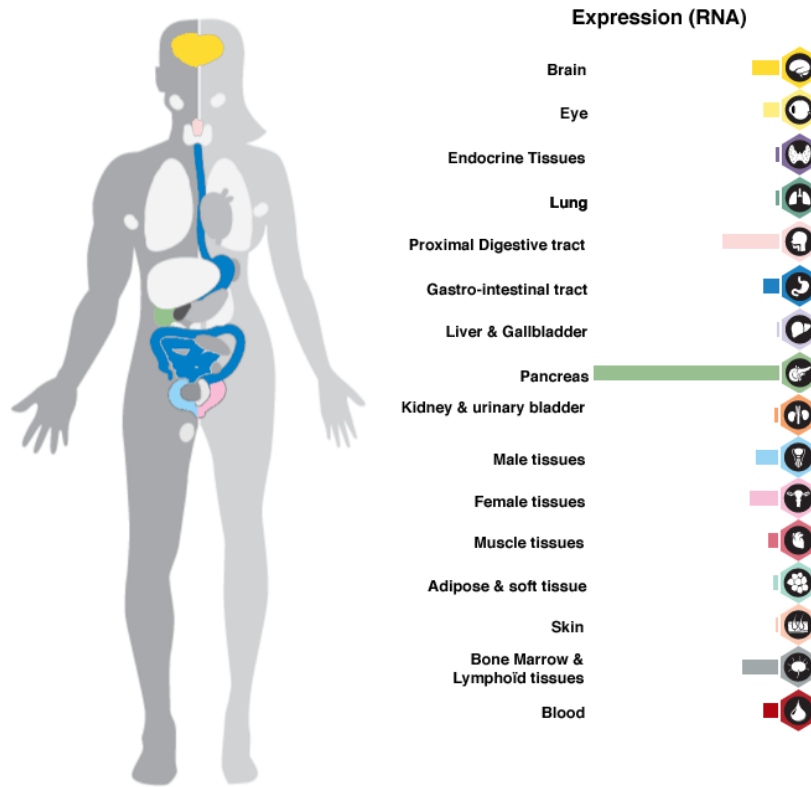


Figure 32: Expression de GRPR dans le corps humain

Le ligand de GRPR, la GRP est exprimée dans certains tissus spécifiques. La GRP est particulièrement exprimée dans les poumons et dans le thymus, à la fois chez l'Homme et chez la souris. Le cerveau est aussi un organe où la GRP est particulièrement exprimée avec une spécificité pour l'hippocampe, du pont et la médulla, et à un niveau un peu moindre du cortex, de l'hypothalamus et du mésencéphale. On le retrouve également exprimé dans l'estomac. Dans les tissus sexués, on retrouve dans la glande mammaire et dans les testicules une expression de GRP (Fagerberg et al., 2014, Figure 32). L'expression de GRP peut être induite par l'inflammation, par exemple via l'IL-22 ou via des signaux de dangers (LPA, Poly-IC) (Lou et al., 2017; Viegas et al., 2017).

Un point intéressant peut être fait sur les organes profonds où se trouvent les métastases de mélanomes, organes exprimant la GRP (poumons, cerveaux), ou des organes dont l'environnement proche l'exprime (la vésicule biliaire dans le cas des métastases hépatiques).

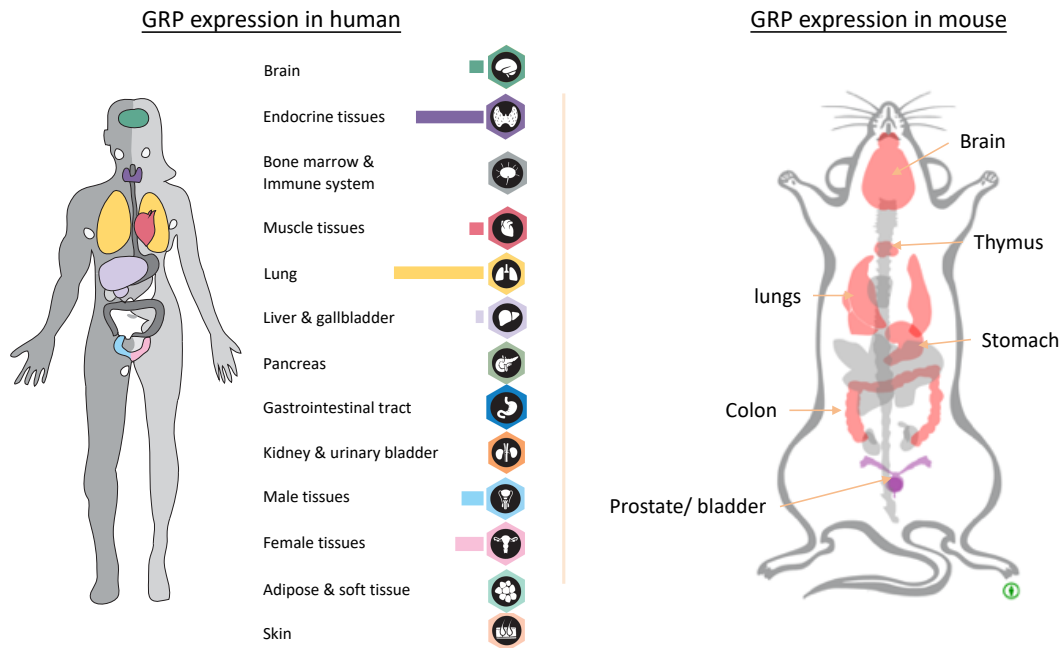


Figure 33: Expression du ligand endogène de GRPR, la GRP chez l'Homme et la souris

La GRP est synthétisée sous forme de prépropeptide, la PréPro-GRP va être successivement clivée en pro-GRP, après clivage du peptide signal, puis en GRP₁₋₂₇Gly une fois sécrétée. Cette dernière molécule est la première à montrer une activité vis-à-vis de GRPR. La glycine C-terminale va être perdue par réaction d'amidation pour produire la GRP₁₋₂₇. Cette dernière sera clivée une dernière fois pour donner la GRP₁₈₋₂₇, qui est la forme la plus affine pour GRPR (Figure 34). La GRP₁₈₋₂₇ a été isolée en 1984, nommée alors neuromédine C (Minamino et al., 1984). L'affinité de la GRP₁₈₋₂₇ pour GRPR est très bonne, de l'ordre de 0.5 à 1nM (Narayan et al., 1991). Il est intéressant de noter que malgré sa forme plus longue, la GRP₁₋₂₇ garde une bonne affinité pour GRPR, de l'ordre de 1nM (Jensen et al., 2008).

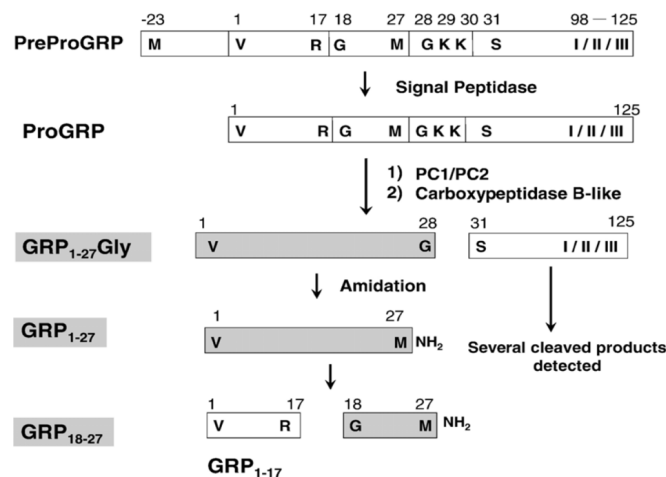


Figure 34: Schéma de la production de GRP à partir de la pré-pro GRP

4. Signalisation de GRPR

Le récepteur peut induire différentes signalisations, celles-ci dépendant du contexte cellulaire. Le récepteur a historiquement été défini comme couplé avec la famille $G\alpha_{q/11}$ (Rozengurt, 1998), mais plus récemment un couplage avec $G\alpha_{12/13}$ a également été démontré (Patel et al., 2014). Si l'on se réfère aux résultats plus récents de Inoue et de ses collègues qui ont testé le couplage de nombreux RCPGs avec les différentes familles de protéines-G, on ne peut seulement exclure un couplage $G\alpha_{15}$, tous les autres étant théoriquement possibles (Inoue et al., 2019, Figure 35). On peut néanmoins valider $G\alpha_{q/11}$ et peut être $G\alpha_{12/13}$ comme couplages principaux (Inoue et al., 2019). Cette donnée met en lumière l'importance de tester le couplage d'un RCPG dans son modèle avant de l'étudier.

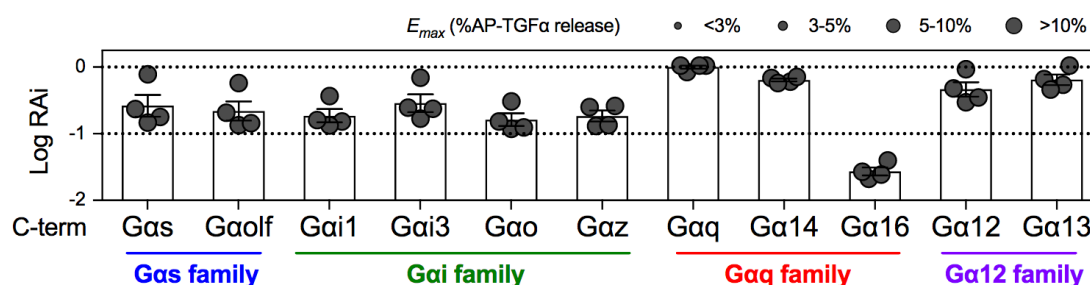


Figure 35: Valeur du couplage de GRPR avec les différentes familles de protéines-G. Mesuré par Inoue (Inoue et al. 2019 dans des cellules HEK. La valeur de logRAI de -1 est considérée comme seuil en dessous lequel le couplage est considéré comme improbable. Une valeur de 0 garantit un couplage certain.

L'analyse de la littérature permet également de suggérer que GRPR est capable d'induire un flux calcique (Squires et al., 1999), l'activation des MAPK/ ERK (Chen and Kroog, 2004; Li et al., 2010b; Thomas et al., 2005), MAPK/JNK (Chan and Wong, 2005) et MAPK/P38 (Czepielewski et al., 2012). L'activation de YAP1 a également été montrée liée à l'expression de GRPR (Yu et al., 2012a). Une activation de la voie PI3K/AKT est également possible (Clarimundo et al., 2017; Liu et al., 2007; Pereira et al., 2015). L'activation de la protéine G monomérique RhoA a également été suggérée (Patel et al., 2014). Les voies de signalisation susceptibles d'être activées par GRPR sont résumées en Figure 36. Ces données venant de la littérature ne sont pas forcément communes à tous les modèles cellulaires et devront donc être vérifiées. Il faut noter que le lien moléculaire entre la signalisation $G\alpha_{q/11}$ et YAP1 n'a pas été fait avec GRPR, mais à partir cas de mutations $G\alpha_{q}^{Q209L}$ dans le mélanome uvéal (Feng et al., 2014).

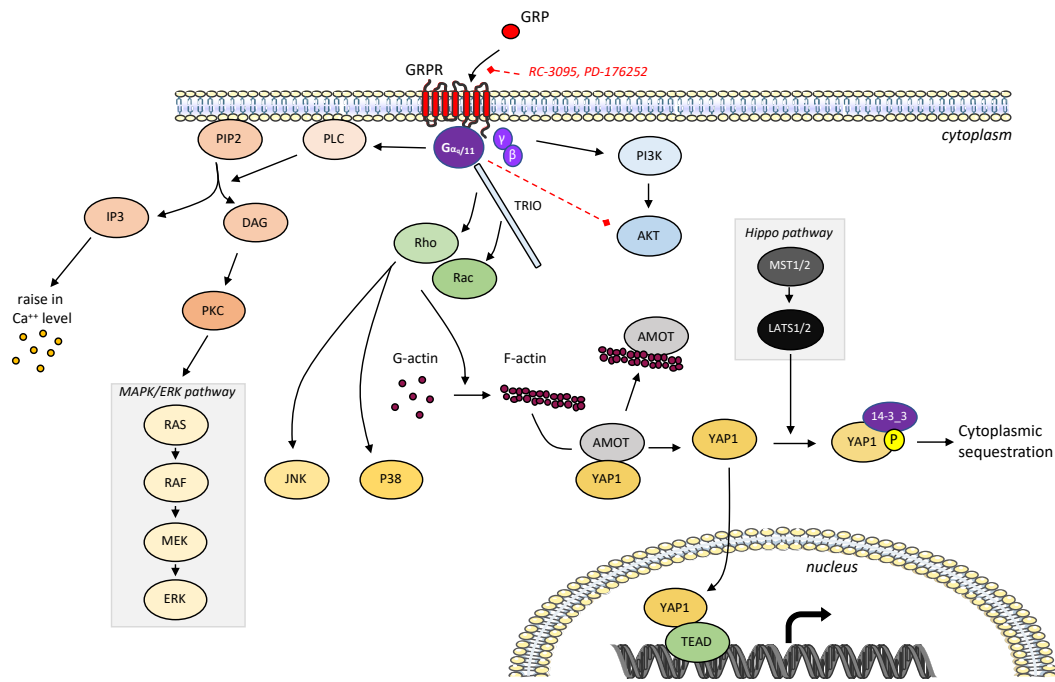


Figure 36: Signalisations potentielles de GRPR.

A noter que la signalisation $G\alpha_{12/13}$ -RhoA n'est dessinée sur ce schéma, mais elle reprend exactement la voie $G\alpha_q$ -Rho.

5. Fonctions physiologiques

Plusieurs fonctions physiologiques ont été identifiées pour GRPR.

a. Sécrétions hormonales et enzymatiques

Le premier rôle que l'on a attribué à GRPR est un rôle dans la sécrétion de la gastrine au niveau de l'estomac (McDonald et al., 1979). C'est ce rôle particulier qui a donné son nom au récepteur. La stimulation du récepteur se fait à la suite de la prise de nourriture. Elle va induire la sécrétion de la gastrine par les cellules G de l'antre gastrique qui va ensuite favoriser la sécrétion acide dans l'estomac (Hildebrand et al., 2001; Modlin et al., 1981; Schubert et al., 1991). Cet effet sur la sécrétion de la gastrine est également observé dans le cerveau (Taché et al., 1981). Au niveau de l'estomac, le récepteur a également été impliqué dans la sécrétion de somatostatine par les cellules D (Schubert et al., 1991).

Au niveau du pancréas, GRPR a un rôle dans la sécrétion exocrine des enzymes du pancréas en réponse au bol alimentaire (Niebergall-Roth and Singer, 2001). L'usage de modèle murin invalidé pour GRPR ont montré qu'il régulaient la sécrétion pancréatique d'insuline (Persson et al., 2002). Toujours dans le pancréas, l'activation de GRPR régule également la sécrétion de glucagon (Pettersson and Ahrén, 1987). Ces actions qui pourraient sembler antinomiques – le glucagon et

l'insuline ayant des rôles opposés sur l'absorption du glucose – sont en fait réalisées avec une cinétique différente. La sécrétion de glucagon étant rapide et intense alors que celle d'insuline est plus lente, mais soutenue (Pettersson and Ahrén, 1987).

Dans le reste du tractus digestif, GRPR a également été associé avec la sécrétion d'hormones (somatostatine, CCK, polypeptide pancréatique, entéroglucagon) (Guilloteau et al., 2006).

b. Régulation de l'appétit

Dans des modèles murins, l'invalidation de GRPR ou son inhibition a été associée avec une levée de la sensation de satiété (Ladenheim et al., 1996). Cette perte de satiété est associée sur des temps longs à une légère augmentation du poids de souris invalidées pour GRPR (Ladenheim et al., 2002). Néanmoins, la relative faiblesse de l'effet suggère que le rôle de GRPR n'est pas prépondérant dans la satiété.

c. Immunologie et inflammation

Le rôle de GRPR dans l'activation et la migration des cellules immunitaires n'a pas été largement étudié. On peut néanmoins citer d'anciennes études montrant que l'activation du récepteur attire les cellules immunitaires, principalement des monocytes/macrophages sur des sites d'expression, en l'occurrence tumoraux (Del Rio and De la Fuente, 1994; Ruff et al., 1985). GRPR a également été associé avec la prolifération de lymphocytes (Del Rio et al., 1994) et la stimulation de leucocytes cytotoxiques (De la Fuente et al., 1993).

L'activation de GRPR a également un rôle dans la pathogenèse de l'arthrose. La sécrétion de GRP peut attirer des neutrophiles sur les sites inflammatoires (Czepielewski et al., 2012). De plus, les synoviocytes – des cellules fibroblaste-like jouant un rôle délétère dans le développement de l'arthrose – sont activés par la fixation de GRP sur GRPR. Cette activation induit l'invasion de ces cellules dans l'articulation ce qui participe à la destruction de cette dernière (Clarimundo et al., 2017). L'inhibition de GRPR par un inhibiteur comme le RC-3095 réduit la progression de l'arthrose (Oliveira et al., 2011). L'usage d'antagoniste de GRPR réduit aussi l'inflammation et donc les conséquences délétères de l'ischémie hépatique dans des modèles murins (Guo et al., 2019).

d. Reproduction

GRPR a été associé à des fonctions reproductives chez les mâles. Un système vestigial présent chez les souris mâles et femelles au niveau de la moelle épinière lombaire supérieure contient des neurones qui projettent des axones sécrétant de la GRP vers les régions lombaires basses. La

stimulation pharmacologique de ces neurones induit l'érection du pénis des souris et l'éjaculation (Sakamoto et al., 2008). L'expression de GRP dans ces neurones est liée à la sécrétion d'androgènes, car la castration diminue l'expression de la GRP (Sakamoto et al., 2009a). Le stress semble aussi diminuer la sécrétion de GRP (Sakamoto et al., 2009b).

e. Démangeaison et le prurit

L'un des domaines dans lequel la recherche sur GRPR est la plus active actuellement est l'étude de son rôle dans la démangeaison. L'ablation des neurones exprimant GRPR de la moelle épinière induit la perte de démangeaison après la stimulation par des molécules pruritogènes (Sun et al., 2009). A l'inverse, l'inhibition optogénétique des neurones GABAergiques inhibiteurs de ces neurones GRPR positif induit la démangeaison des souris (Bardoni et al., 2019). Il a été montré que certains des neurones qui innervaient la peau étaient des neurones GRP positifs dont l'activation optogénétique induisait la démangeaison. Ces neurones vont stimuler les neurones GRPR positif de la moelle épinière. Cette activation de GRPR dans la moelle épinière, importante pour la démangeaison, a été validée par l'injection de GRP directement dans la thèque de souris. Il résultait de ces injections une intense démangeaison des souris. Les mécanismes cellulaires mis en jeu pour cette démangeaison impliquent la voie PI3K/AKT (Pereira et al., 2015). Ces mécanismes de démangeaison sont particulièrement mis en jeu dans le prurit de patients atteints de dermatite atopique (Lou et al., 2017).

6. Rôle de GRPR dans le cancer

L'étude de l'expression de GRPR dans de nombreux cancers a mis en évidence une surexpression dans de très nombreux cas tels que le neuroblastome, le cancer du poumon, le cancer du sein, le cancer du pancréas, le cancer colorectal ou par exemple le cancer de la prostate (Cornelio et al., 2007). L'étude du rôle de GRPR dans ces cancers a majoritairement été menée *in vitro* accompagnée d'études à partir de greffes de cellules dans des souris et montre un rôle en faveur de la croissance et de l'invasion cellulaires. GRPR n'a pas été étudié dans des modèles transgéniques en cancérologie. Les effets retrouvés dans les cancers les plus étudiés vont être détaillés ci-dessous.

a. Cancer du poumon

Des analyses de carcinomes ont montré une présence de GRPR dans 62,5% des cancers du poumon non à petites cellules et dans 52% des cas de cancer du poumon à petites cellules (Mattei et al., 2014). L'expression est augmentée dans les carcinomes non à petites cellules de stades

avancés (Mattei et al., 2014). *In vitro*, l'activation de GRPR induit la migration cellulaire (Jaeger et al., 2017). L'inhibition de GRPR induit une diminution de la croissance cellulaire. Cet effet est retrouvé *in vivo* dans des xénogreffes de cellules de cancer du poumon traitées par un antagoniste de GRPR (Moody et al., 2003). Une des hypothèses expliquant cet effet tiendrait de la transactivation du récepteur à l'EGFR et du récepteur HER2 (Moody et al., 2017). Des essais cliniques utilisant des anticorps ciblant GRPR ont été réalisés, mais n'ont pas montré d'effet sur la croissance tumorale (Kelley et al., 1997). En revanche, l'usage de GRPR pour rediriger le système immunitaire vers la tumeur a été fait à l'aide d'un antagoniste de GRPR couplé à un anticorps monoclonal liant le CD3. Une réduction de la croissance de l'ordre de 40% a été montrée *in vivo* (Zhou et al., 2006). De façon intéressante, l'expression de GRPR semble liée à l'historique du patient en matière de tabagisme (Shriver et al., 2000)

b. Cancer du sein

Dans le cancer du sein, GRPR a été retrouvé surexprimé dans 75% des cas (Morgat et al., 2017). Comme dans le cadre du cancer du poumon, l'activation de GRPR a été reliée à l'induction de la migration cellulaire (Chao et al., 2009). *In vivo* et *in vitro* le traitement de cellules de cancer du sein par des inhibiteurs de GRPR induit une diminution de la croissance (Yano et al., 1992, 1994). De façon intéressante, l'expression de GRPR a été liée à l'expression du récepteur aux estrogènes (ER) (Morgat et al., 2017). GRPR est fortement exprimé dans 83.2% des tumeurs ER positive mais seulement dans 12% des tumeurs ER-négatives (Morgat et al., 2017). L'expression élevée de GRPR est inversement corrélée avec la formation des métastases du cancer du sein (Morgat et al., 2017). Ce cancer est actuellement particulièrement étudié pour le développement d'approche théranostique – une approche qui permet de diagnostiquer et de soigner le patient en même temps – utilisant GRPR comme agent ciblant. La combinaison d'un ligand de GRPR avec un dérivé d'anthracycline a permis de réduire la croissance tumorale *in vivo* (Engel et al., 2005). D'autres approches utilisant des radionucléides ont permis de localiser les tumeurs et métastases de patients atteints de cancer du sein (Zhang et al., 2018).

c. Cancer de la prostate

GRPR est exprimé dans environ 3 cancers de la prostate sur 4 (Körner et al., 2014). Son activation a été associée à l'induction de l'EMT (Elshafae et al., 2016). GRPR induit également la croissance des cellules de carcinome et d'adénome de la prostate ainsi que l'invasion et la motilité cellulaire (Elshafae et al., 2016; Patel et al., 2007; Aprikian et al., 1997; Elshafae et al., 2016). L'activation de GRPR sur les cellules de carcinomes prostatiques va induire la sécrétion par celles-ci de

facteurs pro-angiogéniques (Levine et al., 2003). *In vivo*, l'inhibition de l'activité de GRPR dans des cellules de prostate PC-3 exprimant GRPR réduit la croissance tumorale (Pinski et al., 1993).

d. Mélanome

Une étude a montré l'expression de GRPR dans 82% des mélanomes (Marrone et al., 2013). Une équipe a également vacciné des souris contre la GRP par le biais d'un vaccin à ADN. Cette vaccination a réduit la croissance de cellules de mélanome B16F10 ainsi que l'angiogenèse au niveau du site tumoral (Fang et al., 2009). Ce vaccin a également réduit l'invasion des poumons après injection des cellules dans la veine de la queue de souris C57BL/6 (Fang et al., 2009).

Objectif de la thèse

Le mélanome est un cancer cutané agressif qui malgré une prévalence bien moindre que les carcinomes est responsable de la majorité des décès de cancers de la peau. Les nouvelles thérapies apportées dans le courant des années 2010 ont montré leurs limites, échouant à obtenir une réponse objective chez tous les patients et n'empêchant que partiellement la rechute chez les répondeurs. Pour ces nombreux patients en détresse thérapeutique, de nouvelles voies thérapeutiques doivent être développées. Elles passent par une meilleure caractérisation des processus cellulaires et moléculaires mis en jeu lors de la mélanomagenèse et notamment dans une meilleure connaissance de la cascade métastatique.

Au cours de ma thèse, je me suis intéressé principalement à évaluer le rôle d'une protéine d'adhérence cellulaire, la E-cadhérine dans la mélanomagenèse. La E-cadhérine régule l'homéostasie des mélanocytes dans la peau, elle est la molécule d'adhésion cellulaire principale contrôlant les interactions mélanocytes-kératinocytes. Le gène codant pour la E-cadhérine, *CDH1*, est considéré comme un gène suppresseur de tumeurs dans de nombreux carcinomes et sa perte favorise la progression tumorale. Dans le mélanome, très peu d'études ont évalué l'importance de la E-cadhérine dans l'initiation et la progression tumorale. Seules des analyses de corrélation proposent qu'une expression de la E-cadhérine est diminuée dans les mélanomes métastatiques. De par son rôle essentiel dans l'homéostasie du mélanocyte et dans la signature EMT liée à la progression tumorale, il nous a paru essentiel d'évaluer la fonction de la E-cadhérine, ou plus exactement de sa perte, dans le mélanome.

L'expression de la E-cadhérine est perdue au fur et à mesure des passages en culture des mélanocytes, l'étude de la perte de E-cadhérine ne nous semblait pas pertinente d'être réalisée *in vitro*, sachant que son expression pouvait être réprimée dans des lignées de mélanome uniquement par des conditions de culture et non par des processus oncogéniques. En conséquence, nous avons abordé cette problématique *in vivo* et avons généré un nouveau modèle murin génétiquement modifié pour évaluer l'importance de la E-cadhérine dans toutes les étapes de la mélanomagenèse. Au cours de cette étude, nous avons mis en évidence que la perte de la E-cadhérine n'influencait pas l'initiation du mélanome, mais favorisait de manière importante la formation des métastases.

Des analyses transcriptomiques ont montré qu'un récepteur couplé aux protéines-G, GRPR, montrait une expression très importante uniquement dans les mélanomes déficients en E-cadhérine. A partir de ces données, nos objectifs étaient doubles : 1- valider l'expression de GRPR dans les métastases de mélanomes chez l'humain et 2- établir une preuve de concept pour le ciblage de GRPR dans les métastases.

GRPR promotes the formation of lung metastasis

J.H. Raymond^{1,2,3}, M. Pouteaux^{1,2,3}, V. Petit^{1,2,3}, Z. Aktary^{1,2,3}, F. Luciani^{1,2,3}, M. Wehbe^{1,2,3},
F. Mahuteau-Betzer⁴, B. Vergier⁵, L. Larue^{1,2,3}, V. Delmas^{1,2,3}

(1) Institut Curie, PSL Research University, INSERM U1021, Normal and Pathological Development of Melanocytes, Orsay, France, (2) Univ Paris-Saclay, CNRS UMR 3347, Orsay, France, (3) Equipe Labellisée Ligue Contre le Cancer (4) UMR9187, CNRS, INSERM, Institut Curie, PSL Research University, Université Paris-Saclay, F-91405, Orsay, France. (5) Department of Pathology, University Hospital of Bordeaux, Pessac, France.

Abstract

While tremendous progress has been made in the understanding of the mechanisms leading to cancers, the understanding of the mechanisms governing the formation of metastases remains poorly understood. E-cadherin (Ecad) is a cell-cell adhesion molecule essential for the homeostasis of epithelial cells and melanocytes in the skin. A large number of studies have established that *CDH1* (encoding for Ecad) is a tumor suppressor gene in carcinomas. However, in melanoma, only correlative studies link its reduced expression to metastatic potential. Here, using a novel mouse model expressing the oncogenic form *NRAS*^{Q61K} in melanocyte, we show that the conditional deletion of *Cdh1* does not influence melanoma initiation but dramatically promotes metastases. Interestingly, loss of *Cdh1* induces intensely the expression of the Gastrin-releasing peptide receptor (Grpr). GRPR, which belongs to the G protein-coupled receptor family, is overexpressed in several types of cancers, including carcinomas. In humans, we have shown an anti-correlation of expression between *CDH1* and GRPR in several carcinomas and in melanomas. From a functional point of view, we have shown *in vitro* that *Grpr* expression promotes crucial cellular processes required for metastasis, such as cell growth, clonogenicity, migration and invasion. *In vivo*, overexpression of GRPR in mouse or human melanoma cells induces metastasis after allograft and xenograft, respectively. Metastasis of cells overexpressing GRPR is strongly affected in the presence of the GRPR antagonist RC-3095. GRPR signals through $G\alpha_q$ leading to activation of YAP1 signaling, which explains the molecular and cellular characteristics of melanoma expressing this receptor. This study highlights the importance of the Ecad-GRPR axis in melanoma metastases and provides proof-of-concept that GRPR is a therapeutic target for metastatic melanoma.

Introduction

Recent therapeutic advances have made it possible to combat metastases, but several major problems remain. In addition to non-responsive patients or innate/acquired resistance to therapies, prevention of metastasis is still very limited. The metastatic process is complex, requiring multiple steps such as escape of cells from the primary tumor, survival in the bloodstream or lymphatic circulation, proliferation, and adaptation of cells to new environments that are not always favorable. Unfortunately, the identification of the probably numerous drivers of the metastatic processes capable of orchestrating all the steps leading to the colonization of distant organs by tumor cells remains limited. Cutaneous melanoma is an aggressive cancer with high metastatic potential that results in the death of half of the patients despite new therapies (Carlino et al., 2021; Luke et al., 2017). Melanoma is very heterogeneous among patients and in the tumor itself, it develops through the acquisition of genetic and epigenetic changes of oncogenes and tumor suppressors, without forgetting the particular process of the phenotypic switch. However, the metastatic pathways are partially identified, as most mechanistic studies are performed with cell cultures (Rebecca et al., 2020). The incidence of metastatic melanoma continues to increase with each decade and new treatment options must be developed to combat the progression of the disease.

The first step in tumor progression is the loss of cell-cell interactions and matrix adhesion. The cell-cell adhesion molecule, E-cadherin (E-cad), regulates melanocyte homeostasis in the skin and is the primary adhesion molecule mediating melanocyte-keratinocyte interactions (Delmas and Larue, 2019; Wagner et al., 2015). Loss of Ecad is the key protein of epithelial mesenchymal transition (EMT) and loss or reduction of Ecad is a hallmark of carcinomas (Kaszak et al., 2020; Larue and Bellacosa, 2005; Mendonsa et al., 2018). E-cad is considered a suppressor gene in many carcinomas and its loss promotes carcinoma progression. In melanoma, the role of Ecad is not clearly proven in the metastatic process. However, its loss is observed in 40% of primary melanoma and is correlated with metastasis (Danen et al., 1996; Pećina-Slaus et al., 2007; Tucci et al., 2007; Venza et al., 2016). At this point, the function of Ecad during melanomagenesis relies on correlative studies. Surprisingly, how the loss of E-cad can affect the signaling network and cellular properties in melanoma has never really been addressed.

Here, we show that loss of Ecad in melanocytes does not impact tumor initiation

but promotes tumor progression, in particular metastases. We identified an increase in the level of the Gastrin releasing peptide receptor (*Grpr*) in melanoma lacking Ecad. This seven transmembrane receptor is coupled to $G\alpha_q$ and, upon ligand induction with GRP ligand, stimulation of YAP1 signaling is observed. GRPR acts as a driver of the metastatic process, being able to confer to melanoma cells a new capacity for growth, migration, invasion and colonization of organs, all of which are abolished in the presence of the RC3095 antagonist.

Results

Loss of E-cadherin does not affect melanoma initiation but increases metastatic potential.

To decipher the role of E-cadherin in melanomagenesis we established a mouse model with a conditional deletion of *Cdh1* in melanocytes (Tyr::*CreA*^o; *Cdh1*^{F/F}). Even after 2 years, no melanoma developed, showing that loss of *Cdh1* alone is insufficient to induce melanoma formation. Analysis of the TCGA database revealed that *CDH1* expression is lower when associated with an NRAS rather than BRAF mutation with a median of 17 TPM versus 46 TPM (p=0.0344). To initiate melanoma, we therefore crossed the Tyr::*CreA*^o; *Cdh1*^{F/F} mice to the well-characterized Tyr::*NRAS*^{Q61K}^o; *Cdkn2a*^{+/-} melanoma model (Ackermann et al., 2005). The Tyr::*NRAS*^{Q61K}^o; *Cdkn2a*^{+/-}; ^o/^o; *Cdh1*^{F/F} (called Ecad from hereon) and Tyr::*NRAS*^{Q61K}^o; *Cdkn2a*^{+/-}; Tyr::*CreA*^o; *Cdh1*^{F/F} (called ΔEcad from hereon) mice were followed for melanoma development. The loss of *Cdh1* did not modify the time of the apparition of the primary melanoma (Figure 1A). The median of onset (Supplementary Figure 1A) and the frequency of the apparition (Supplementary Figure 1B) are similar between Ecad and ΔEcad mice. No differences were observed when comparing mice by Ecad status and gender (Supplementary Figure 1C-F). However, the incidence of lung melanoma metastasis was significantly higher with loss of *Cdh1*, with 18% and 49% in Ecad and ΔEcad mice, respectively (Figure 1D). The number of metastases per lung was also approximately 7 times higher in the ΔEcad group compared with the Ecad group (Figure 1E). Analysis of metastasis occurrence by gender revealed that the frequency of lung metastasis was 32% and 62% for ΔEcad males and females, respectively (Figure 1F). In ΔEcad mice, the number of lung metastases was significantly higher in females than in males, 2401 and 579 respectively (Figure 1G). Both micrometastasis and macrometastasis were increased in female ΔEcad than in males (Figure 1H-I).

Loss of E-cadherin up-regulates GRPR expression

To characterize the consequences of Ecad loss, tumor RNA-seq was performed with eight samples per genotype and sex. The analysis revealed that the Gastrin releasing peptide receptor, *Grpr*, was dramatically up-regulated in the ΔEcad female melanoma compared to all other genotype including ΔEcad male (Figure 2A). No other striking difference (up

or down) with p-value < 0.05 was observed comparing male and female and Ecad versus Δ Ecad melanoma. These results were confirmed by quantitative PCR, *Grpr* being highly expressed only in Δ Ecad female tumors (Figure 2B). *Grpr* expression is not dependent of the Tyr::Cre line used since *Grpr* was expressed in the Tyr::NRAS^{Q61K}; *Cdkn2a*^{+/-}; Tyr::CreB; *Cdh1*^{F/F} female melanomas. In addition, Tyr::CreA expression did not induce *Grpr* expression in other genetically engineered mouse like the Tyr::NRAS^{Q61K}; Tyr::CreA; *Pten*^{F/F} mouse (Figure 2C).

We next analyzed the TCGA database and compared the overall survival and the progression-free survival of patients with a melanoma expressing *GRPR* (>1TPM) compared to melanoma not expressing *GRPR* (\leq 1TPM). Results showed that *GRPR* could impact women overall surviving (p=0.076) and particularly the progression-free survival (p=0.018) confirming a role of *Grpr* in disease progression in women (Figure 2E,G). No effect was observed when considering the whole population (Figure 2D,F). Moreover, the analysis of tumor transcriptomic data showed that *GRPR* expression correlated with an invasive phenotype (r=0.45) (Figure 2H-I) and *GRPR* expression was highly enriched in tumors with low *CDH1* expression (p=0.002) (Figure 2I). Out of the strong correlation with the invasive phenotype, *GRPR* expressing melanomas are clustered with the neuronal crest cells (NCSC) like phenotype (r=0.25) and inversely with the pigmentation phenotype (r= -0.21) (Figure 2I). The clustering in NCSC is not too surprising since *GRPR* is expressed in neurons where it regulates itch in the skin (Chen, 2021). This may reflect the common origin and plasticity of neural crest-derivatived cells, which is observed during embryonic development and may occur during oncogenesis.

GRPR expression was evaluated in lung melanoma metastasis from patients by immunohistochemistry (Figure 2J-K). 74% of the lung metastases were expressing *GRPR*, with the most frequent profile being Ecadneg / *GRPR*pos (Figure 2L). This indicates that mouse model developed here was pertinent and reflects the human pathology. The lung melanoma samples were from male or female patients with *NRAS* or *BRAF* mutations, suggesting that *GRPR* expression can be induced in the lung under different circumstances (Figure 2M).

The anticorrelation between *CDH1* and *GRPR* was assessed in carcinoma as well as melanoma using the TCGA database. Clear anticorrelation was visible in melanoma (SKCM) and in carcinoma as breast cancer (BRCA), kidney cancer (KIRC), lung cancer

(LUSC) and stomach cancer (STAD) indicating that the regulation of GRPR expression by Ecad could be common to many cancers (Figure 2N).

GRPR expression promotes cellular mechanisms essential for melanoma progression

To assess whether the mechanism leading to lung colonization by Δ Ecad melanoma cells was cell-autonomous or due to only cell adhesion defects related to Ecad loss, primary tumors were dissociated and cells were injected into the tail vein of C57BL/6/J mice. Δ Ecad female melanoma cells were able to colonize lungs within 30 days in contrast to Ecad melanoma cells (Supplementary Figure 3A). Thus, Δ Ecad melanoma cells expressing GRPR were able to colonize the lungs very efficiently and adapted immediately to the lung environment. We established melanoma cell lines in culture from the mouse primary melanoma tumors (described in Table 1). We noticed that tumor growth into C57BL/6J mouse was significantly more efficient for Δ Ecad female tumors compared to Ecad tumors (Supplementary Figure 3B). Thus, efficient lung colonization and rapid growth after grafting support the aggressiveness of Δ Ecad female melanomas. As the GRPR endogenous ligand, GRP, was particularly expressed in the lungs of humans and rodents, GRP could favor colonization of melanoma cells expressing GRPR in the lung. We next evaluated the effect of GRP stimulation on GRPR for fundamental cellular processes required for the metastatic pathway.

After the establishment in culture, only the Δ Ecad female melanoma cell lines expressed GRPR among all established melanoma cells, in agreement with gene expression observed in mouse primary melanomas (to show or to refer to table 1). GRP stimulation induced cell growth of mouse (1057) and human (MDA-MB-435S) melanoma cell lines expressing GRPR (GRPRpos) (Figure 3A,B). Co-treatment of these cells with the agonist GRP and antagonist RC-3095 (RC) blocked the GRP-induced growth (Figure 3A,B). Note that RC is a partial agonist acting as antagonist in presence of an agonist (GRP) and as a weak agonist without GRP, explaining the slight growth induction of cell treated with RC alone (Szepeshazi et al., 1997). Cellular growth regulation by GRP was confirmed with another cell line, 1064, expressing GRPR (Supplementary Figure 3D). As expected, GRP treatment had no effect on GRPR-negative (GRPRneg) mouse (1181 and 1014) and human(501mel) melanoma cell lines (Figure 3C,D; Supplementary Figure 3E). The specificity of GRPR induction by GRP was addressed by transfecting GRPR into GRPRneg

1181, 1014 and 501mel melanoma cells. Both murine and human melanoma cells transfected with Grpr responded to GRP induction and RC inhibition (Figure 3E,F; Supplementary Figure 3F). We have never been able to CRISPR-inactivate or reduce dramatically the expression of GRPR in GRPRpos cells in a constitutive or inducible manner. However, we could target one allele but never both. This may suggest that GRPR is required for survival/proliferation of the cells expressing it.

GRPRpos (1049, 1057, 1069, and 1064) mouse melanoma cells are able to grow at low concentration in culture while GRPRneg (1007, 1014, 1034, 1039, 1058, and 1181) cells do not (Figure 3G). GRPR ectopic expression in GRPRneg mouse (1181 and 1014) or human (501mel) melanoma cells was able to significantly promoted clonogenic growth (Figure 3H,I; Supplementary Figure 3C).

We next evaluated the resistance of the cells to anoikis, an important cellular mechanism required for efficient metastatic process. Cells were seeded on poly-HEMA-coated plates at low serum concentration and harvested after 48h. Resistance of anoikis was evaluated by the number of apoptotic (Annexin V positive) and necrotic (7-AAD positive) cells found in the various conditions. GRP induction promotes resistance to anoikis of murine and human GRPRpos cells (Figure 3J,N,L,P) but not to the GRPRneg melanoma cell lines (Figure 3K,O,M,Q). Upon RC inhibition, cells loose their resistance to anoikis (Figure 3J,N,L,P).

Bioinformatic analyses of TCGA database revealed that GRPR expression correlates with an invasive signature (Figure 2H,I). Thus, the invasion capacity of melanoma cells was evaluated on Matrigel®. GRP induction promoted GRPRpos mouse (1057) and human (MDA-MB-435S) melanoma cell invasion, an effect blocked by treating the cell with RC (Figure 3R,S). No effect was observed on mouse (1181) or human (501mel) GRPRneg melanoma cells unless ectopically transfected with Grpr (Figure 3T-W). All these results were confirmed using other melanoma GRPRpos (1064 and 1014+GRPR) and GRPRneg (1014) cell lines (Supplementary Figure 3G-I).

GRPR signals through G_q to activate YAP1 signaling

In other type of cells, mainly carcinoma, it was found that GRPR signals through the G_{αq} subunit. The most direct way to estimate the activity of the receptor and its coupling with G_{αq} is to measure the production of IP₃-IP₁ after GRP induction. GRPR activation by GRP induced production of IP₁ in GRPRneg (1057) melanoma cells revealing

an activation of $G\alpha_q$ and blocked by RC (Supplementary Figure 4A). No IP_1 production was observed in GRPRneg (1181) melanoma cells but was induced after GRPR expression (1181+GRPR) (Supplementary Figure 4A). In non-melanoma models, $G\alpha_q$ coupled-receptors have been associated with YAP1 activation (Fa-Xing Yu cell 2012). In cutaneous melanoma, analysis of the TCGA transcriptome revealed a correlation between GRPR expression and YAP1 activation score (Figure 4A $r=0.35$). Transcriptomic analysis of GRPRpos (1057 and 1181+GRPR) melanoma cell lines showed that YAP1 activation score is significantly increased upon GRPR activation (Figure 4C; Supplementary Figure 4D). The localization of YAP1 by immunofluorescence revealed that GRPR activation by GRP induced the nuclearization of YAP1 in GRPRpos cells, which was not the case in the presence of RC (Figure 4B). This nuclearization of YAP1 was also observed by overexpressing GRPR in the GRPRneg 1181 melanoma cell line. The activation of YAP1 was confirmed since CYR61, a YAP1 target, was induced after GRP stimulation and repressed in the presence of GRP and RC (Figure 4D, Supplementary Figure 4E).

GRPR expression promotes lung melanoma metastasis

The cellular processes regulated by GRPR are important for the colonization of distant organs by tumor cells. To assess the capacity of GRPR to promote metastasis, injection of mouse 1181-parental, 1181-Ctrl and 1181+Grpr melanoma cells were performed in the tail-vein of immunocompetent C57BL/6J mice. Only GRPR expressing cells (1181+Grpr) were able to lung colonized (Figure 5A). All mice injected with 1181+Grpr cell lines showed melanoma metastases in the lungs with approximately 50 visible foci (Figure 5B,C). The presence of 1181+Grpr metastatic cells in the lung was shown by RNAscope, using Dct as a marker. No Dct-positive cells were found in the lung after injection of 1181-Ctrl cells. Similarly, the human 501mel-parental, 501mel-Ctrl, and 501mel+GRPR cells were injected into the tail vein of immunodeficient (NSG) mice; only the 501mel+GRPR injected mice (6/6) presented lung metastasis (Figure 5D,E). Moreover, the only 501mel-Ctrl with metastasis in the lung, had only one metastatic spot compared to an average of 30 in the 501mel+GRPR injected mice (Figure 5F). All 501mel-injected mice (parental, Ctrl, and GRPR) showed liver and kidney metastases but only the GRPR expressing cells were able to colonize the lung efficiently. In addition, GRPR expression in 501mel decreased survival (20 days vs. 30 days) of mice compared to parental and control mice, likely due to overall more aggressive tumors.

GRPR-targeted drug reduces lung melanoma metastasis

GRPR belongs to the drug-targetable G protein-coupled receptor family. As a proof-of-concept, we followed the effect of the RC antagonist on lung colonization by GRPRpos 1057 *in vivo* by bioluminescent imaging (IVIS). First, in order to visualize lung colonization by melanoma cells, the GRPRpos 1057 was infected with a reporter CMV::firefly-luciferase to produce 1057Luc melanoma cell line. The 1057Luc cells are able to colonize the lungs of C57BL/6J mice; numerous macro- and micro-lung metastases were observed (Figure 6A). Lung melanoma foci are pigmented and expressed both Dct and Grpr as revealed by RNAscope experiments (Figure 6B). One day after tail-vein injection, mice were randomized in two groups (Supplementary Figure 6A,B) and treated with either vehicle or RC. Luminescence in the thorax was first detected around day 24 and expand exponentially (Supplementary Figure 6C). To avoid signals from other metastasis sites, mice were placed in a custom box with shutters blocking signals not originating from the thorax. Targeting GRPR with RC induced a strong inhibition of lung colonization (Figure 6C-F). At day 24 luminescence was detected at the thorax level only in vehicle-treated and not in RC-treated mice. The low level of lung colonization by 1057Luc cells was confirmed at sacrifice. Right after the sacrifice, *ex vivo* luminescence of the lungs was evaluated and results showed that the values were higher in vehicle-treated compared to RC-treated mice with a p-value of 0.0079 (Figure 6D-E and Supplementary 6D). Luminescence values were consistent with the number of visible lung metastasis found at sacrifice with a p-value of 0.0476 (Figure 6F). In conclusion, treatment of the mice by RC strongly limits colonization of the lungs by GRPR-expressing melanoma cells.

Discussion

Metastasis is the leading cause of cancer death and remains the major challenge in cancer treatment. Cutaneous malignant melanoma is one of the most devastating types of cancer (Sung et al., 2021). Melanoma is a highly heterogeneous tumor whose dynamic phenotypic changes are controlled by a network of factors regulating the invasive/proliferative state. Down regulation of E-cadherin (Ecad) expression is a hallmark of the EMT-phenotype change and is associated with restructuring of cell-cell interaction and metastasis. However, the consequences of the loss of Ecad in the metastatic cascade have never been characterized *in vivo*. Our result provides the first link between the loss of Ecad and the activation of the expression of a G-coupled receptor, GRPR, with aggressiveness properties.

GRPR has been identified as the G protein- coupled receptor most frequently ectopically expressed or overexpressed on an extremely large number of tumors, including carcinoma such as lung, prostate, and breast cancers (Patel et al., 2006). However, the molecular mechanisms underlying the high level of expression of GRPR remains totally unknown. Here, we connected that both loss of Ecad and female gender is required to GRPR expression in melanoma context. A very recent link between the presence of estrogen and the activation of GRP and GRPR transcription in the process of ichthyosis in women has been demonstrated (Takanami et al., 2021). This finding may explain why activation of GRPR transcription is observed only in females and not in males, but the requirement of E-cad loss for GRPR expression is not known. Consistent with our results, GRPR is often overexpressed in most carcinomas when Ecad is downregulated. The correlation between the loss of *Cdh1* and the upregulation of the *Grpr* that we established in our genetically well-defined Δ Ecad mouse model may represent a general mechanism and conserved during evolution. It should be pointed out that in non-tumoral context, during embryonic development, inactivation of E-cad leads to profound changes in gene expression (Larue et al., 1996). Preliminary experiments using the GRPR promoter placed upstream of the luciferase reporter gene revealed no difference in E-cad or Δ E-cad melanoma cells (data not shown). A full regulatory study is required to understand the regulation of *GRPR* since it is probably more complex than expected at the origin. Nevertheless, the anti-correlation between GRPR and E-cad that we observed in

melanoma is also present and other cancers like breast and gastric carcinoma.

In this study we highlighted a new axis for melanoma metastasis involving E-cad-GRPR-YAP1. Despite multiple studies suggesting the importance of YAP1 in cutaneous melanoma progression (Zhang et al., 2020; Zhao et al., 2021), our study provides the first molecular mechanism of YAP1 activation independent of mutation. It is more likely that much of metastatic behavior due to GRPR expression is driven by YAP1 transcription factor in particular anoikis resistance and invasion. The importance of YAP1 signaling in uveal melanoma was revealed by the presence of the $G\alpha_q$ mutation, which is also found in blue nevus melanoma (Van Raamsdonk et al., 2009). The YAP1 signaling may be particularly activated in metastases, especially in the lung, where GRP and endothelin (ET) ligands are produced and can activate $G\alpha_q$ -coupled receptor such as GRPR and EDNRB.

Currently melanoma metastases are treated by inhibitors of the MAPK pathway or by immune checkpoint inhibitors but the patient 5-year survival rate hardly exceeds 50% for the best therapies (Carlini et al., 2021). Metastasectomy can also be considered in patients on systemic therapies but the consequences on patient-survival is quite low (Okereke, 2015). Targeting metastatic drivers could constitute an interesting option. GRPR is over-expressed in a variety of cancers contrasting with its limited and only weak expression in normal human adult tissues. It is therefore a very attractive potential target. Targeting GRPR has the advantage also to inhibit the identified oncogenic downstream signaling and some resistance pathways. In a proof of concept experiment, we demonstrate that targeting of GRPR with the RC-3095 decreased lung metastasis in mice. However, GRPR antagonists have to be improved since injections of RC-3095 during phase I clinical trials induce side effects (Schwartzmann et al., 2006). Moreover, we evaluated the half-life of RC-3095. This compound has a very short half-life.

GRPR targeting can also be associated with theranostic approaches. These approaches combine the therapeutic effect of targeting GRPR with a diagnostic by detecting metastases and have been recently assessed in prostate and breast cancer in humans (Haendeler et al., 2021; Zang et al., 2018). This strategy using the [^{177}Lu]-NeoB antagonist has shown a good effect on tumor growth inhibition of gastrointestinal stromal tumors *in vivo* and is currently assessed in clinical trials (Advanced Accelerator

Applications, 2021; Montemagno et al., 2021). Finally, Targeted radiotherapy is highly relevant for the treatment of disseminated lesions and overcoming tumor heterogeneity through cross-fire irradiation with β -radionuclides characterized by a decay spectrum of between a few nanometers and 2 mm.

Material & Methods

Chemicals. GRP was purchased from Bachem (H-3120). RC-3095 was purchased from Sigma-Aldrich (#R9653). Blastocidin and geneticin were purchased respectively from Gibco (ant-bl-1) and (). Fetal bovine serum (FBS), Penicillin/streptomycin (100 U/ml penicillin and 100 µg/ml streptomycin (PS) and culture medium F-12 Ham and RPMI were purchased from GIBCO (respectively #10270106, #115140, #11765054, #11875101). Proteinase K originates from Roche (#11 243 233 001). Xenolight D-luciferin was purchased from Perkin-Elmer (#122799). Triton™ X-100 was purchased from Merck-Millipore (#1122981001). Paraformaldehyde (PFA) was ordered at VWR (#15714-S).

Mouse models. Mice were bred and maintained in the specific pathogen-free mouse colony of the Institut Curie, in accordance with the institute's regulations and French and European Union laws. The transgenic *Tyr::CreA* (B6.Cg-Tg(Tyr-cre)1Lru/J), *Tyr::NRAS^{Q61K}*, *Cdkn2a*^{-/+} and the *Cdh1^{F/F}* (B6.129-Cdh1tm2Kem/J) mice have been described and characterized previously in Larue laboratory and elsewhere (Ackermann et al., 2005; Boussadia et al., 2002; Delmas et al., 2003). The different mouse lines were backcrossed onto a C57BL/6J background for more than ten generations. Mice were crossed to obtain the desired genotypes. Mice were born with the expected ratio of Mendelian inheritance and no changes in gender ratios were observed. Mice were housed in a certified animal facility with a 12-hour light/dark cycle in a temperature-controlled room (22 ± 1 °C) with free access to water and food. Mice were checked weekly seeking for the appearance of new tumors. Tumors were let grown until reaching a volume of 2000mm³ and then autopsied to analyze the presence of metastasis in lymph nodes and distant organs.

Ethical rules. Animal care and all experimental procedures were conducted in accordance with recommendations of the European Community (86/609/EEC) and Union (2010/63/UE) and the French National Committee (87/848). Animal care and use were approved by the ethics committee of the Curie Institute in compliance with the institutional guidelines. Experimental procedures were carried out under the approval of ethics committee of the Institut Curie CEEA-IC #118 (CEEA-IC 2016-001) in compliance with the international guidelines.

Genotyping. Genomic DNA was extracted from melanoma cell and tumors and purified using the QIAamp Kit and protocol (Qiagen). Mice were genotyped from biopsies. Biopsies were digested overnight at 55°C using 200 ng proteinase K in 500 µL lysis buffer containing 16 mM [NH₄]₂ SO₄, 67 mM Tris-HCl [pH 8.8 at 25 °C], 0.01% [v/v] Tween-20, in deionized H₂O. Proteinase K was inactivated for 20 min at 95 °C. Primers and PCR conditions are described in Supplementary Tables 2 and 3. PCR products were separated by agarose (Invitrogen, #15510027) gel electrophoresis.

Establishment of melanoma cell lines Mouse melanoma cell lines were established from melanoma arising transgenic mice. Small pieces of tumors (2mm³) were washed in PBS, and re-implanted in the neck of C57BL/6J mice. Once the re-implanted tumors reached 1cm³, tumors were dissociated to single-cells and established as described (Gallagher et al., 2011). 1014 murine melanoma cell line was previously established in the laboratory (Petit et al., 2019). MDA-MB-435S and 501Mel human melanoma cell lines were previously established in other laboratories (Cailleau et al., 1978; Marincola et al., 1994). 1057-luciferase melanoma cell lines were generated by infecting the 1057 parental cells with the pLenti PGK Blast DEST V96_luc2 (LL#1231). Cell were selected with 4.5µg/mL Blasticidin for a week. 1014 and 1181 GRPR and corresponding Ctrl were obtained after transfection of the murine Grpr/tGFP plasmid (#MG224721, Origen) and tGFP plasmid. Cells were transfected with 2 µg of plamid and lipofectamine2000 following the manufacturer protocol. 1014 and 1181 transfected cells were selected by respectively 25 and 150µg/mL of geneticin.

Cell culture. Murine melanoma cell lines were cultured in Ham's F12 medium supplemented with 10% FBS and 1% PS. Human melanoma cell lines were cultivated in RPMI 1640 media supplemented with 10% FBS and 1% PS. All the cell lines were maintained at 37°C in a humidified atmosphere with 5% CO₂. The genetic status and the level of expression of key genes of these cell lines are given in Supplementary Table 1.

Cell growth and clonogenic assay. Six-well tissue culture plates were seeded with 3.10⁵ melanoma cells in complete medium. 24hours later, cells were incubated in low-serum conditions (0.5% for murine melanoma cell lines and 1% for human melanoma cells) for

18h and stimulated with 10nM GRP and/or 1 μ M RC-3095 for 48h. The plates were trypsinized right after stimulation or 48h later and cells were counted. All the experiments were made with 3 technical replicates and 3 biological replicates. For clonogenic assay six-well tissue culture plates were seeded with 500 cells in complete medium. After 10 days, colonies were fixed with 4% PFA (paraformaldehyde) for 15 minutes and stained with 10% Crystal violet in ethanol for 20 minutes and counted on images using ImageJ software.

Matrigel invasion assay. Matrigel invasion assays were performed on transwell with 8.0 μ m pore (Corning) coated with 100 μ L of 200 μ g/mL Matrigel. Cells were seeded in low serum – 0.5% FBS for murine cells and 1% for human cell lines with 10nM GRP and/or 1 μ M RC-3095 as attractant. Complete medium was used as positive control. 24h after stimulation, inserts were washed with PBS and cells that have not invaded were removed. Cells were fixed in methanol at -20°C overnight. Methanol was rinsed and the membrane was carefully removed from the insert with a sharp scalpel. Membrane was mounted in prolong glass DAPI (1.5 μ g/mL). The assays were performed in triplicate, the entire filter was counted using the Image J software.

Anoikis assay. Six-well plates were coated with poly-HEMA to avoid cell attachment to the well surface. Cells were seeded in low serum conditions treated with 10nM GRP and/or 1 μ M RC-3095. 48h after cell seeding, cells were harvested and washed with ice-cold PBS and resuspended in Annexin V binding buffer and incubated at R.T. in the dark with 7-AAD and Annexin-V FITC. FACS analysis determined the percentage of Annexin-V and/or 7-AAD positive cell using 488 and 675nm lasers.

RNA extraction and transcriptomic analysis. RNA was extracted from mouse melanoma cells lines and mouse tumors using the miRNeasy kit (Qiagen, #217004). RNA integrity (RIN) was measured using an Agilent Bioanalyser 2100 (Agilent Technologies). The minimum threshold for RNA integrity was assessed using an Agilent BioAnalyser 2100 (Agilent Technologies, Les Ulis, France), only RNA with a RNA integrity number (RIN) > 7 were kept for the analysis. This threshold led to the sequencing of 12 melanoma cell lines controls and 32 tumors. RNA concentrations were measured using a NanoDrop (NanoDrop Technologies, Wilmington, DA, USA). RNA sequencing libraries were prepared

from 1 µg of total RNA using the Illumina TruSeq Stranded mRNA Library preparation kit that allows to perform a strand specific sequencing. A first step of polyA selection using magnetic beads is done to focus sequencing on polyadenylated transcripts. After fragmentation, cDNA synthesis was performed and resulting fragments were used for dA-tailing followed by ligation of TruSeq indexed adapters. PCR amplification was finally achieved to generate the final barcoded cDNA libraries (12 amplification cycles). The 12 and 32 libraries were equimolarly pooled and subjected to qPCR quantification using the KAPA library quantification kit (Roche). Sequencing was carried out on the NovaSeq 6000 instrument from Illumina based on a 2×100 cycles mode (paired-end reads, 100 bases) using an S1 flow cell in order to obtain around 35 million clusters (70 million raw paired-end reads) per sample. Reads were mapped to the mouse reference genome mm10 (gencode m13 version-GRCm38.p5) using STAR (Dobin et al., 2013). STAR was also used to create the expression matrixes. Expressions were batch-corrected using combat (Johnson et al., 2007).

Differential gene expression was performed with R following the limma-voom pipeline using the limma package (Ritchie et al., 2015). edgeR and limma packages are both available from Bioconductor (<http://www.bioconductor.org>) (accessed on June 2020). The threshold for significantly differentially expressed genes was set as an absolute fold-change > two times the standard deviation of the fold-change and an adjusted p-value < 0.05. The volcano plot depicting the results was generated using the R package ggplot2 (Wickham, 2016). Gene-set enrichment analysis (GSEA) was performed using signatures from the literature described in Supplemental Table 4. One thousand permutations gene set-based were made per analysis. The enrichment score (ES) reflects the degree to which a given gene set is represented in a ranked list of genes. Calculation of the ES is based on walking down a ranked list of genes and adjusting a running-sum statistic based on the presence of absence of a gene in the gene set. The magnitude of the increment represents the correlation of the gene with the phenotype. p-values were estimated by gene-based permutation. GSEA normalizes the enrichment score for each gene set to account for the variation in set sizes, yielding a normalized enrichment score (NES). Only gene sets with an NES > 1.7 and an FDR < 0.01 were considered.

RNA quantification by RT-qPCR. RNA was extracted from melanoma cell lines and tumors using miRNeasy Kit. M-MLV reverse transcriptase (Invitrogen) was used

according to the manufacturer's protocol to synthesize cDNA from 2 µg total RNA in combination with random hexamers. The newly synthesized cDNA was used as template for the Real-time quantitative PCR (qPCR) which was performed using iTaq™ Universal SYBR Green Supermix. Each sample was run in technical triplicates and the quantified RNA normalized against *TBP* (human) or *Hprt* (mouse) as housekeeping transcripts (Supplementary Tables 2 and 3). Yap scoring was obtained by averaging the fold change of each Yap1 target.

Immunofluorescence. Cells were seeded on coverslip and cultivated until 100% confluence was achieved. After 24h starvation in 0.5% FCS for murine melanoma cell lines and 1% FBS for human melanoma, medium was complemented with 10nM GRP and/or 1µM RC-3095 for 1 hour. Cells were fixed with 4% PFA for 15 minutes, and non-specific antigen were blocked by incubating with a blocking solution composed of 5% normal goat serum and 0.3% Triton™ X-100 in PBS. Cells were incubated overnight at 4°C with the anti-YAP D8H1X antibody (#14074, cell signaling, 1/100 dilution) in 1% BSA and 0.3% Triton™ X-100 followed by incubation for 1.5 hours at R.T with goat anti-rabbit Alexa fluor 594 (#A-11012, Invitrogen, 1/500 dilution). Coverslip were mounted with Prolong® Gold with 1.5µg/mL DAPI. Image were acquired with an inverted SP8 Leica confocal microscope (Leica Microsystem). YAP1 localization was evaluated using ImageJ Software.

TCGA data mining. Transcriptome and corresponding clinical data of the TCGA-SKCM data sets (n = 473), were retrieved from the National Cancer Institute (NCI) Genomic Data Commons (GDC) repository using the TCGAbiolinks R package in august 2021 (Colaprico et al., 2016). mRNA levels were calculated from RNA sequencing read counts using RNA-Seq V2 RSEM and normalized to transcripts per million reads (TPM). Survival analyses were made by separating the cohort in two groups based on gene expression. The set threshold was 1 TPM, commonly admitted as limit to have a sufficient protein expression of the transcript. The negative group was set with expression <0.1 TPM to have a clear separation in term of expression (factor 10) from the positive group. YAP and melanoma phenotypic states scores were obtained by averaging the expression of marker genes detailed. Pigmentation states was defined by the expression of MITF, MLANA, TRPM1, DCT and TYR; SMC phenotype was defined by the expression of CD36, DLX5, IP6K3, PAX3 and TRIM67; the invasive state was based on the expression on AXL, CYR61, TCF4, LOXL2,

TNC and WNT5A and the NCSC like phenotypic state was based on the expression of AQP1, GFRA2, L1XAM, NGFR, SLC22A17 and TMEM176B. The scoring of YAP1 activation was made from the expression of CYR61, CTGF, TEAD4, LATS2 and CRIM1.

Tail vein injection. C57BL/6J mice were purchased from Charles River laboratories (France). NSG mice originated from our in-house breeding. All animals were housed under specific pathogen-free conditions in the animal facility and had access to food and water *ad libidum*. Animal care, use, and experimental procedures were conducted in accordance with recommendations of the European Community (86/609/EEC) and Union (2010/63/UE) and the French National Committee (87/848). The ethics committee of the Curie Institute in compliance with the institutional guidelines approved animal care and use. $5 \cdot 10^5$ of mouse and human melanoma cell lines were injected in 200 μ L PBS into the tail-vein of 8-week-old C57BL/6J mice and NSG respectively. For each experiment, 6 mice per group were injected per group. Mice were followed-up daily and weighted twice a week. Mice were euthanized and autopsied when mice had lost 20% of their maximal weight.

***In vivo* inhibition of GRPR activity.** Mice were shaved 3 days before cell injection and then every other week. $5 \cdot 10^5$ Grpr pos 1057 mouse melanoma cell lines were injected in 200 μ L PBS into the tail-vein of 8-week-old C57BL/6J mice. 5 mice per group were injected with cell lines and then treated. 10 minutes after cell-injection, mice were imaged by IVIS (IVIS spectrum, #124262, Perkin-Elmer). Briefly, mice were injected with 300 μ g of Xenolight D-luciferin and anesthetized immediately with isoflurane. 10 minutes after luciferin injection mice were placed in an opaque box with adaptable shutters to image only the thorax in the IVIS apparatus. Luminescence from the whole mouse and the mouse thorax was acquired successively for 2 minutes each. Luminescence was acquired at day 0, day 1 and then twice a week. The day after cell injection mice were randomized into two groups according to their weight and to the luminescence in the lung at Day 0. The treated-group were treated twice a day with 10 μ g RC-3095 and the mock group received only the vehicle (PBS/DMSO). Mice were treated for 1 month and were followed-up by both IVIS and weight twice a week. After sacrifice, lungs were carefully removed from mice thorax, quickly rinsed in R.T. PBS. Right lungs were separated from the left lobes and then incubated in a black opaque 12 well plate with 300 μ g/mL Xenolight D-luciferin

diluted in PBS for two minutes and luminescence was acquired for 1 minute. Left mouse lungs were washed in ice-cold PBS and then fixed for 48h in 4% PFA at 4°C and incubated in 30% sucrose and 30% sucrose/50% OCT solution for 48 hours each and embedded in OCT. OCT-embedded mouse lungs were sectioned into 7- μ m-thick coronal sections. Section were stained for Dct and Grpr mRNA and counterstained with using the RNAscope manufacturer protocol. RNAscope probes are listed in Supplementary Table 5. Image were acquired with an inverted SP8 Leica confocal microscope (Leica Microsystem).

Lung imaging. Right lungs were washed in PBS and both faces were imaged with a Leica MZFLIII binocular scope equipped with a Scion camera. Metastasis were enumerated using ImageJ. Macro-metastasis was defined by a diameter > 0.1 mm and micro-metastasis < 0.1 mm.

Software. GraphPad PRISM, R version 4.0.2 (R Foundation for Statistical Computing, Vienna, Austria), ImageJ, Adobe Illustrator and Adobe Photoshop software were used to analyze data and generate all graphs and figures.

Statistical analysis. Cell culture-based experiments were performed in at least biological triplicate and validated three times as technical triplicates. Significance of the effects were calculated using the Mann-Whitney test for the comparison of two groups or with Kruskal-Wallis when comparing 3 or more conditions. Comparison of categorical data were made using Fisher's exact test when 2 groups were compared or Chi² otherwise. Significance of difference of Kaplan–Meier curves were calculated using the log-rank test. All P values were reported as computed by Prism 6.

Acknowledgements,

We are grateful to Dr. Irwin Davidson for providing us the luciferase plasmid and the 501mel We thank the Institut Curie staff responsible for the animal colony (especially P. Dubreuil and C. Lantoine), and the histology (S. Leboucher), FACS (C. Lasgi), and PICT-IBiSA imaging (C. Lovo, L. Besse) facilities.

This work was supported by the Ligue nationale contre le cancer, INCa, ITMO Cancer, Fondation ARC (PGA), and is under the program «Investissements d’Avenir» launched by the French Government and implemented by ANR Labex CelTisPhyBio (ANR-11-LBX-0038 and ANR-10-IDEX-0001-02 PSL). J.H. Raymond had a fellowship from the Ligue nationale contre le cancer.

Ethical rules.

Animal care, use, and experimental procedures were conducted in accordance with recommendations of the European Community (86/609/EEC) and Union (2010/63/UE) and the French National Committee (87/848). Animal care and use were approved by the ethics committee of the Curie Institute in compliance with the institutional guidelines. Experimental procedures were specifically approved by the ethics committee of the Institut Curie CEEA-IC #118 (CEEA-IC 2016-001), and ministry of research (APAFIS#22000-2019091612246643v1) with an agreement for the establishment (D91471108) in compliance with the international guidelines.

References

- Ackermann, J., Frutschi, M., Kaloulis, K., McKee, T., Trumpp, A., and Beermann, F. (2005). Metastasizing melanoma formation caused by expression of activated N-RasQ61K on an INK4a-deficient background. *Cancer Res.* *65*, 4005–4011.
- Advanced Accelerator Applications (2021). A Phase I/IIa Open-label, Multi-center Study to Evaluate the Safety, Tolerability, Whole-body Distribution, Radiation Dosimetry and Anti-tumor Activity of [177Lu]-NeoB Administered in Patients With Advanced Solid Tumors Known to Overexpress Gastrin-releasing Peptide Receptor (GRPR) (clinicaltrials.gov).
- Boussadia, O., Kutsch, S., Hierholzer, A., Delmas, V., and Kemler, R. (2002). E-cadherin is a survival factor for the lactating mouse mammary gland. *Mech Dev* *115*, 53–62.
- Cailleau, R., Olivé, M., and Cruciger, Q.V. (1978). Long-term human breast carcinoma cell lines of metastatic origin: preliminary characterization. *In Vitro* *14*, 911–915.
- Carlino, M.S., Larkin, J., and Long, G.V. (2021). Immune checkpoint inhibitors in melanoma. *The Lancet* *398*, 1002–1014.
- Chen, Z.-F. (2021). A neuropeptide code for itch. *Nat Rev Neurosci* 1–19.
- Colaprico, A., Silva, T.C., Olsen, C., Garofano, L., Cava, C., Garolini, D., Sabedot, T.S., Malta, T.M., Pagnotta, S.M., Castiglioni, I., et al. (2016). TCGAAbiolinks: an R/Bioconductor package for integrative analysis of TCGA data. *Nucleic Acids Res* *44*, e71.
- Danen, E.H., de Vries, T.J., Morandini, R., Ghanem, G.G., Ruitter, D.J., and van Muijen, G.N. (1996). E-cadherin expression in human melanoma. *Melanoma Res* *6*, 127–131.
- Delmas, V., and Larue, L. (2019). Molecular and cellular basis of depigmentation in vitiligo patients. *Experimental Dermatology* *28*, 662–666.
- Delmas, V., Martinuzzi, S., Bourgeois, Y., Holzenberger, M., and Larue, L. (2003). Cre-mediated recombination in the skin melanocyte lineage. *Genesis* *36*, 73–80.
- Gallagher, S.J., Luciani, F., Berlin, I., Rambow, F., Gros, G., Champeval, D., Delmas, V., and Larue, L. (2011). General strategy to analyse melanoma in mice. *Pigment Cell Melanoma Res* *24*, 987–988.
- Haendeler, M., Khawar, A., Ahmadzadehfar, H., Kürpig, S., Meisenheimer, M., Essler, M., Gaertner, F.C., and Bundschuh, R.A. (2021). Biodistribution and Radiation Dosimetric Analysis of [68Ga]Ga-RM2: A Potent GRPR Antagonist in Prostate Carcinoma Patients. *Radiation* *1*, 33–44.
- Johnson, W.E., Li, C., and Rabinovic, A. (2007). Adjusting batch effects in microarray expression data using empirical Bayes methods. *Biostatistics* *8*, 118–127.
- Kaszak, I., Witkowska-Piłaszewicz, O., Niewiadomska, Z., Dworecka-Kaszak, B., Ngosa Toka, F., and Jurka, P. (2020). Role of Cadherins in Cancer-A Review. *Int J Mol Sci* *21*, E7624.
- Larue, L., and Bellacosa, A. (2005). Epithelial-mesenchymal transition in development and cancer: role of phosphatidylinositol 3' kinase/AKT pathways. *Oncogene* *24*, 7443–7454.
- Larue, L., Antos, C., Butz, S., Huber, O., Delmas, V., Dominis, M., and Kemler, R. (1996). A role for cadherins in tissue formation. *Development* *122*, 3185–3194.

- Luke, J.J., Flaherty, K.T., Ribas, A., and Long, G.V. (2017). Targeted agents and immunotherapies: optimizing outcomes in melanoma. *Nature Reviews Clinical Oncology* 14, 463–482.
- Marincola, F.M., Shamamian, P., Alexander, R.B., Gnarr, J.R., Turetskaya, R.L., Nedospasov, S.A., Simonis, T.B., Taubenberger, J.K., Yannelli, J., and Mixon, A. (1994). Loss of HLA haplotype and B locus down-regulation in melanoma cell lines. *J Immunol* 153, 1225–1237.
- Mendonsa, A.M., Na, T.-Y., and Gumbiner, B.M. (2018). E-cadherin in contact inhibition and cancer. *Oncogene* 37, 4769–4780.
- Montemagno, C., Raes, F., Ahmadi, M., Bacot, S., Debiossat, M., Leenhardt, J., Boutonnat, J., Orlandi, F., Barbato, D., Tedesco, M., et al. (2021). In Vivo Biodistribution and Efficacy Evaluation of NeOB, A Radiotracer Targeted to GRPR, in Mice Bearing Gastrointestinal Stromal Tumor. *Cancers (Basel)* 13, 1051.
- Okereke, I. (2015). Surgical management of malignant melanoma of the lung. *Melanoma Manag* 2, 301–303.
- Patel, O., Shulkes, A., and Baldwin, G.S. (2006). Gastrin-releasing peptide and cancer. *Biochimica et Biophysica Acta (BBA) - Reviews on Cancer* 1766, 23–41.
- Pećina-Slaus, N., Zigmund, M., Kusec, V., Martić, T.N., Cacić, M., and Slaus, M. (2007). E-cadherin and beta-catenin expression patterns in malignant melanoma assessed by image analysis. *J. Cutan. Pathol.* 34, 239–246.
- Petit, V., Raymond, J., Alberti, C., Pouteaux, M., Gallagher, S.J., Nguyen, M.Q., Aplin, A.E., Delmas, V., and Larue, L. (2019). C57BL/6 congenic mouse NRASQ61K melanoma cell lines are highly sensitive to the combination of Mek and Akt inhibitors in vitro and in vivo. *Pigment Cell & Melanoma Research* 32, 829–841.
- Rebecca, V.W., Somasundaram, R., and Herlyn, M. (2020). Pre-clinical modeling of cutaneous melanoma. *Nat Commun* 11, 2858.
- Ritchie, M.E., Phipson, B., Wu, D., Hu, Y., Law, C.W., Shi, W., and Smyth, G.K. (2015). limma powers differential expression analyses for RNA-sequencing and microarray studies. *Nucleic Acids Res* 43, e47.
- Sung, H., Ferlay, J., Siegel, R.L., Laversanne, M., Soerjomataram, I., Jemal, A., and Bray, F. (2021). Global Cancer Statistics 2020: GLOBOCAN Estimates of Incidence and Mortality Worldwide for 36 Cancers in 185 Countries. *CA: A Cancer Journal for Clinicians* 71, 209–249.
- Szepeshazi, K., Schally, A.V., Halmos, G., Lamharzi, N., Groot, K., and Horvath, J.E. (1997). A single in vivo administration of bombesin antagonist RC-3095 reduces the levels and mRNA expression of epidermal growth factor receptors in MXT mouse mammary cancers. *PNAS* 94, 10913–10918.
- Takanami, K., Uta, D., Matsuda, K.I., Kawata, M., Carstens, E., Sakamoto, T., and Sakamoto, H. (2021). Estrogens influence female itch sensitivity via the spinal gastrin-releasing peptide receptor neurons. *Proc Natl Acad Sci U S A* 118, e2103536118.
- Tucci, M. g., Lucarini, G., Brancorsini, D., Zizzi, A., Pugnali, A., Giacchetti, A., Ricotti, G., and Biagini, G. (2007). Involvement of E-cadherin, β -catenin, Cdc42 and CXCR4 in the progression and prognosis of cutaneous melanoma. *British Journal of Dermatology* 157, 1212–1216.

- Van Raamsdonk, C.D., Bezrookove, V., Green, G., Bauer, J., Gaugler, L., O'Brien, J.M., Simpson, E.M., Barsh, G.S., and Bastian, B.C. (2009). Frequent somatic mutations of GNAQ in uveal melanoma and blue naevi. *Nature* 457, 599–602.
- Venza, M., Visalli, M., Catalano, T., Biondo, C., Beninati, C., Teti, D., and Venza, I. (2016). DNA methylation-induced E-cadherin silencing is correlated with the clinicopathological features of melanoma. *Oncology Reports* 35, 2451–2460.
- Wagner, R.Y., Luciani, F., Cario-André, M., Rubod, A., Petit, V., Benzekri, L., Ezzedine, K., Lepreux, S., Steingrimsson, E., Taieb, A., et al. (2015). Altered E-Cadherin Levels and Distribution in Melanocytes Precede Clinical Manifestations of Vitiligo. *Journal of Investigative Dermatology* 135, 1810–1819.
- Wickham, H. (2016). *ggplot2: Elegant Graphics for Data Analysis* (New York: Springer-Verlag).
- Zang, J., Mao, F., Wang, H., Zhang, J., Liu, Q., Peng, L., Li, F., Lang, L., Chen, X., and Zhu, Z. (2018). 68Ga-NOTA-RM26 PET/CT in the Evaluation of Breast Cancer: A Pilot Prospective Study. *Clin Nucl Med* 43, 663–669.
- Zhang, X., Yang, L., Szeto, P., Abali, G.K., Zhang, Y., Kulkarni, A., Amarasinghe, K., Li, J., Vergara, I.A., Molania, R., et al. (2020). The Hippo pathway oncoprotein YAP promotes melanoma cell invasion and spontaneous metastasis. *Oncogene* 39, 5267–5281.
- Zhao, B., Xie, J., Zhou, X., Zhang, L., Cheng, X., and Liang, C. (2021). YAP activation in melanoma contributes to anoikis resistance and metastasis. *Exp Biol Med (Maywood)* 246, 888–896.

Figures

$\Delta Ecad = Tyr::NRAS Q61K^{o} ; Ink4a +/- ; Tyr::Cre^{o} ; Ecad F/F$

$Ecad = Tyr::NRAS Q61K^{o} ; Ink4a +/- ; \text{;}^{o} ; Ecad F/F$

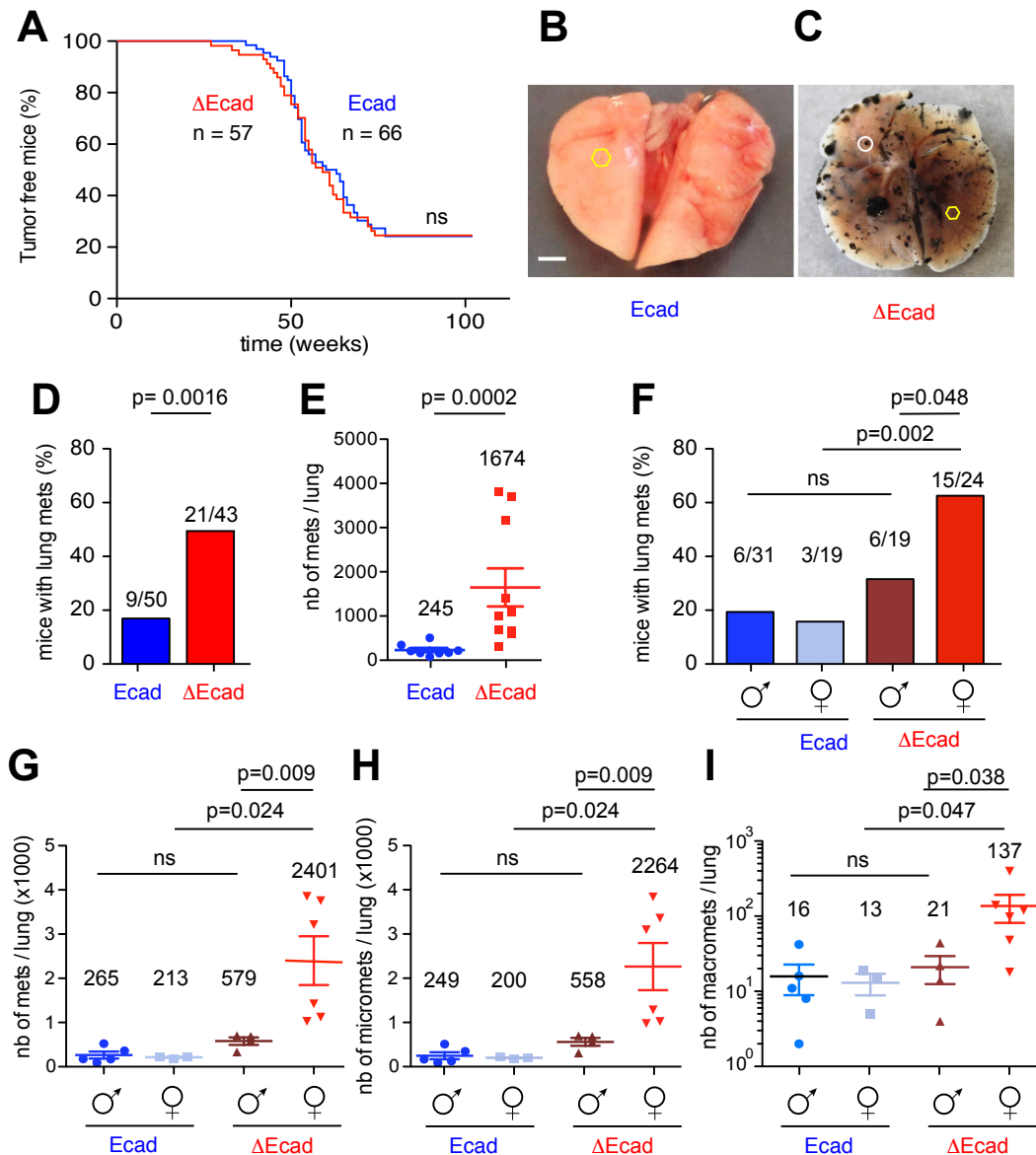


Figure 1: Ecad loss in primary melanoma promotes lung melanoma metastasis.

Appearance of the E-cad and ΔE -cad melanoma. The Kaplan-Meier curves between E-cad (66) and ΔE -cad (57) are not significantly different (A). Representative pictures of the lung of E-cad (B) and ΔE cad (C) mice with primary melanoma. Yellow hexagons show micrometastases ($30\mu\text{m}$ - $100\mu\text{m}$ size), white circles show macrometastases $>100\mu\text{m}$, scale bar $500\mu\text{m}$. Frequency of mice with lung metastasis (D) and mean number of lung melanoma metastases (E) in mice according to E-cad status. Frequency of mice with lung metastases (F) and mean number of lung melanoma metastases (G), micro- (H) and macro-metastases (I) in mice according to their E-cad status and gender. Macro and micro metastases are defined as metastases that can be seen with the naked eye and under the binocular, respectively.

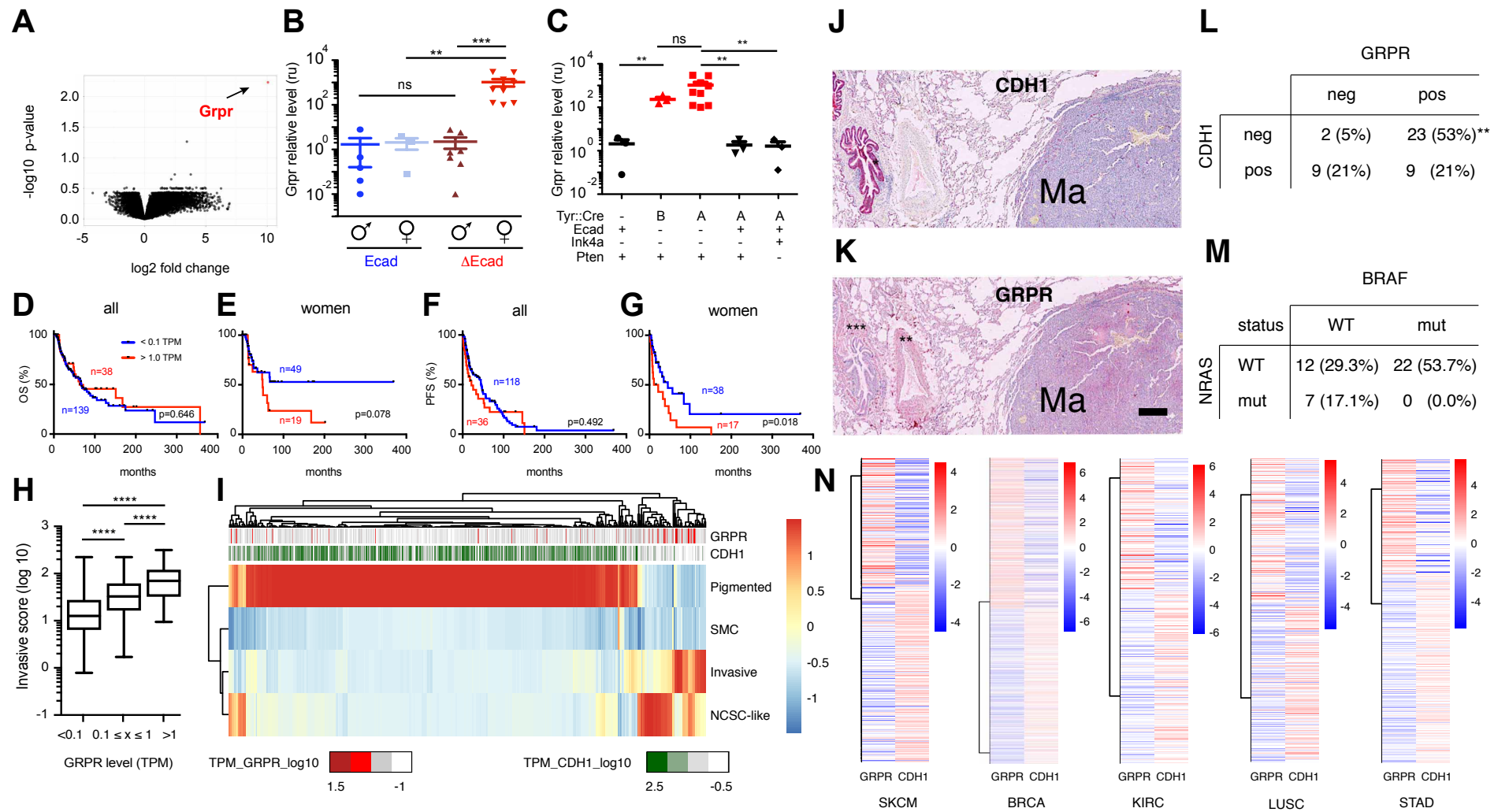


Figure 2: Loss of *Cdh1* induces *Grpr* expression.

Volcano plot depicting the differential expression between E-cad and Δ E-cad tumors with Grpr indicated in red (A). mRNA levels of Grpr as measured by quantitative reverse transcriptase-PCR (q-RT-PCR) in Δ E-cad and E-cad melanoma, in male and female (B) mRNA levels of Grpr as measured by q-RT-PCR in tumors expressing no recombinase (lane 1), Tyr::CreB transgene (lane 2), the Tyr::CreA transgene (lane 3-5), E-cad (lane 1, 4, 5), Ink4a (lane 5), Pten (lane 1-4) (C). Kaplan-Meier of the overall survival of all patients (D) and women only (E) according to GRPR expression (low/absent ≤ 0.1 TPM and expressed > 1 TPM). OS: overall survival. Kaplan-Meier of the progression-free survival of all patient (F) and (G) women patients according to GRPR expression (low/absent ≤ 0.1 TPM and expressed > 1 TPM). PFS: Progression-free survival. Invasive score according to GRPR expression level in the tumors from the TCGA-SKCM database. Spearman coefficient $r=0.35$ (H). Heatmap clustering TCGA-SKCM samples according to the main phenotype signatures expressed "Pigmented", "SMC" (starved-like melanoma cells), "Invasive", "NCSC-like" (neuronal crest cells-like). GRPR and CDH1 expression are indicated as color gradient from dark-colored (higher expression, red for GRPR and green for CDH1) to white (lower expression) (I). Immunohistochemistry staining for CDH1 (J) and GRPR (K) in human lung melanoma metastasis. Metastasis classification according to the CDH1 and GRPR expression status (L) and to the BRAF and NRAS status of the metastasis samples (M). *Bronchia as internal control for ECAD staining and **&*** smooth muscle for GRPR. Heatmap of CDH1 and GRPR expression extracted in the TCGA database in melanoma and in different carcinoma. SKCM means skin cutaneous melanoma, BRCA, breast invasive carcinoma, KIRC kidney renal clear cell carcinoma, LUSC lung squamous cell carcinoma & STAD stomach adenocarcinoma.

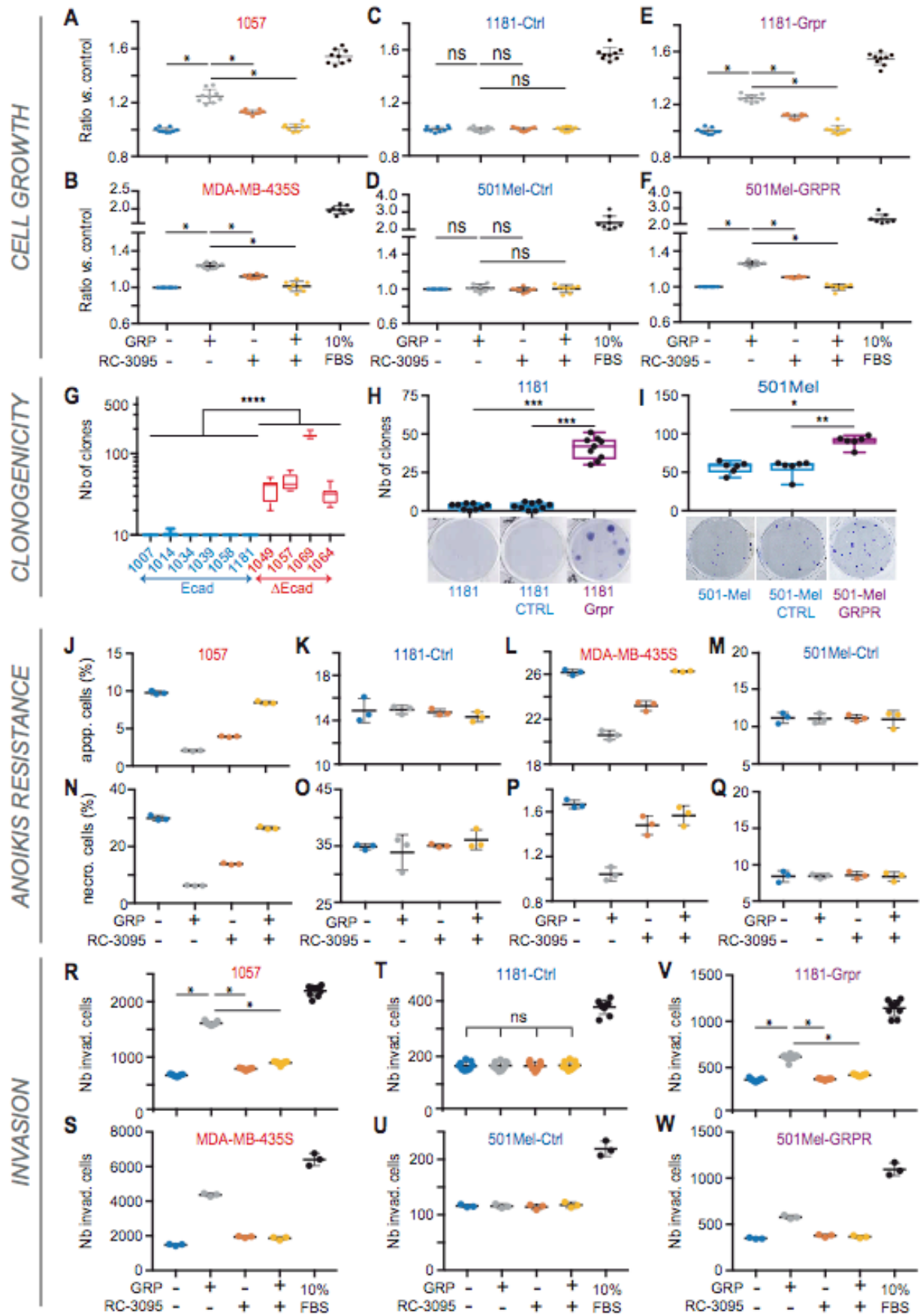


Figure 3: GRP promotes growth, survival and invasiveness of melanoma cells.

(A-F) GRPR activation promotes cell growth in vitro. 48h after the stimulation in low serum conditions – 0.5% FBS for murine and 1% for human cell lines (lane 1), 10 nM GRP (lane 2), 1 μ M RC-3095 (lane 3), both (lane 4) and 10% Serum (FBS, lane 5) were supplemented in the medium of mouse 1057 (A), 1181+GRPR (E) and human MDA-MB-435S (B) 501mel+GRPR (F) GRPRpos cells, and mouse 1181 (C) human 501mel (D) GRPRneg cells. (G-I) GRPR expression induces the clonogenic growth. Formation of colonies 20 days after seeding 500 melanoma cells in the presence of GRP. (G) Cells producing E-cadherin (Ecad) or not (Δ Ecad). Mouse (H, 1181) and human (I, 501mel) melanoma cells expressing (Grpr) or not (parental and Ctrl) GRPR. (J-Q) GRPR expression and GRP induction induce anoikis necrosis resistance. Percentage of apoptotic (J-M) and necrotic (N-Q) mouse (J,K,N,O) and human (L,M,P,Q) melanoma cells expressing (J,L,N,P) or not (K,M,O,Q) GRPR that were not treated (lane 1) or treated with 10 nM GRP (lane 2), 1 μ M RC-3095 (lane 3), both (lane 4). 1057 (J,N), 1181 (K,O), MDA-MB-435S (L,P), and 501mel (M,Q). (R,W) GRPR expression and GRP induction induce Matrigel invasion. Number (Nb) of invading (invad.) cells producing (R [1057], S [MDA-MB-435S], V [1181+GRPR], W [501mel+GRPR]) or not (T [1181], U [501mel]) that were not treated (lane 1), treated with 10 nM GRP (lane 2), 1 μ M RC-3095 (lane 3), both (lane 4), and 10% FBS. At least three independent biological experiments were performed for each test except for the Anoikis assay yet. Statistical analysis was performed using Kruskal wallis tests. Data are represented as mean \pm sd. * p < 0.05, ** p < 0.01, and *** p < 0.001. Data are presented as mean values \pm sd.

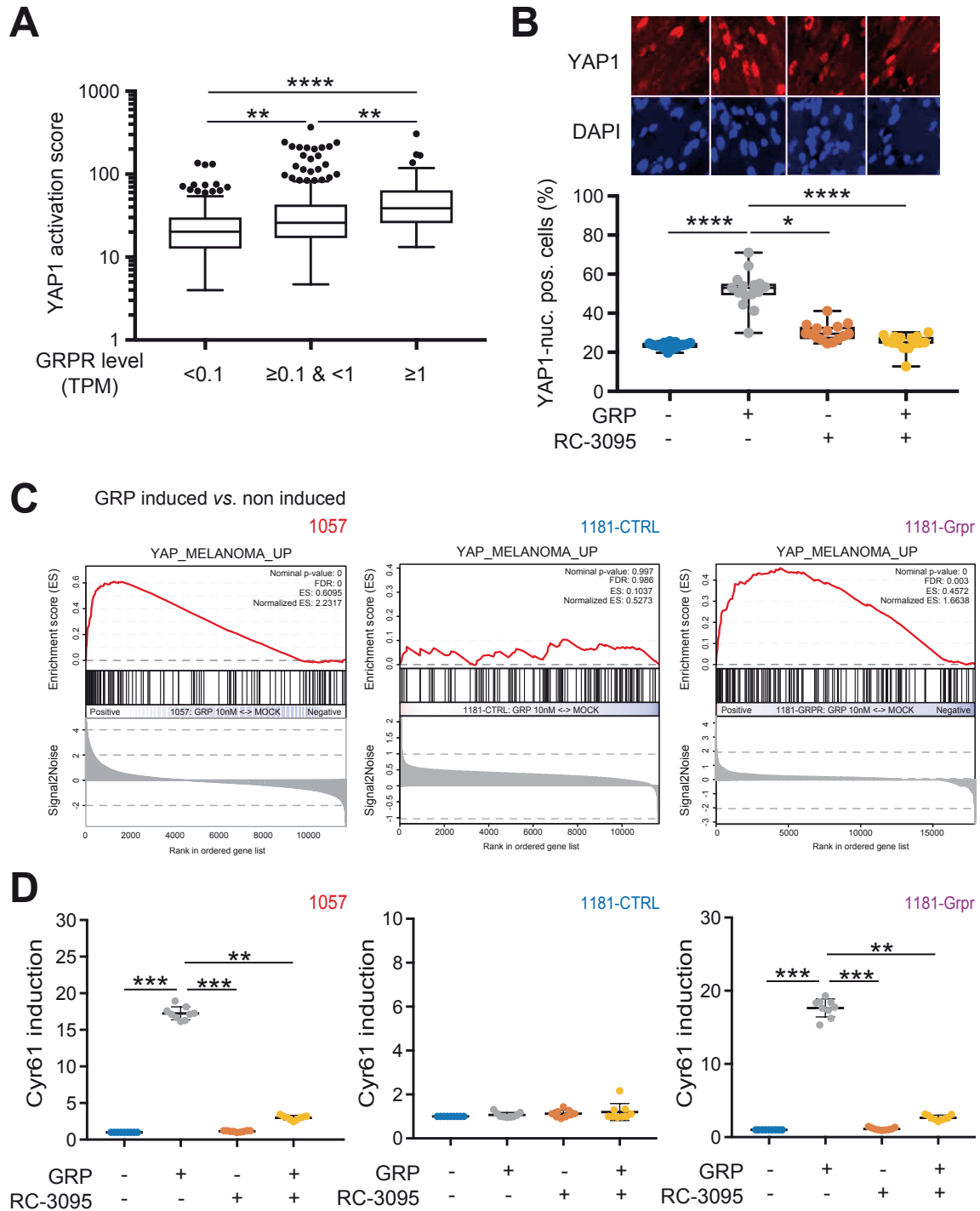


Figure 4: GRPR activation by GRP promotes YAP1 transcriptional program.

(A) YAP1 activation score according to GRPR expression level in the tumors from the TCGA-SKCM study. TPM means transcripts per million. (B) Percentage of cells with nuclear localization of YAP1 in GRPRpos mouse melanoma cell line (1057) after stimulation by 10 nM of GRP (lane 2,4) and treatment by 1 μ M of RC-3095 (lane 3,4). (C) Enrichment by GSEA of the YAP1 signature after GRP stimulation of 1057 (left), 1181-Ctrl (middle) and 1181+GRPR (right) murine melanoma cell lines. (D) Induction of YAP1 target Cyr61 in 1057 (left), 1181-Ctrl (middle) and 1181+GRPR (right) mouse melanoma cell lines.

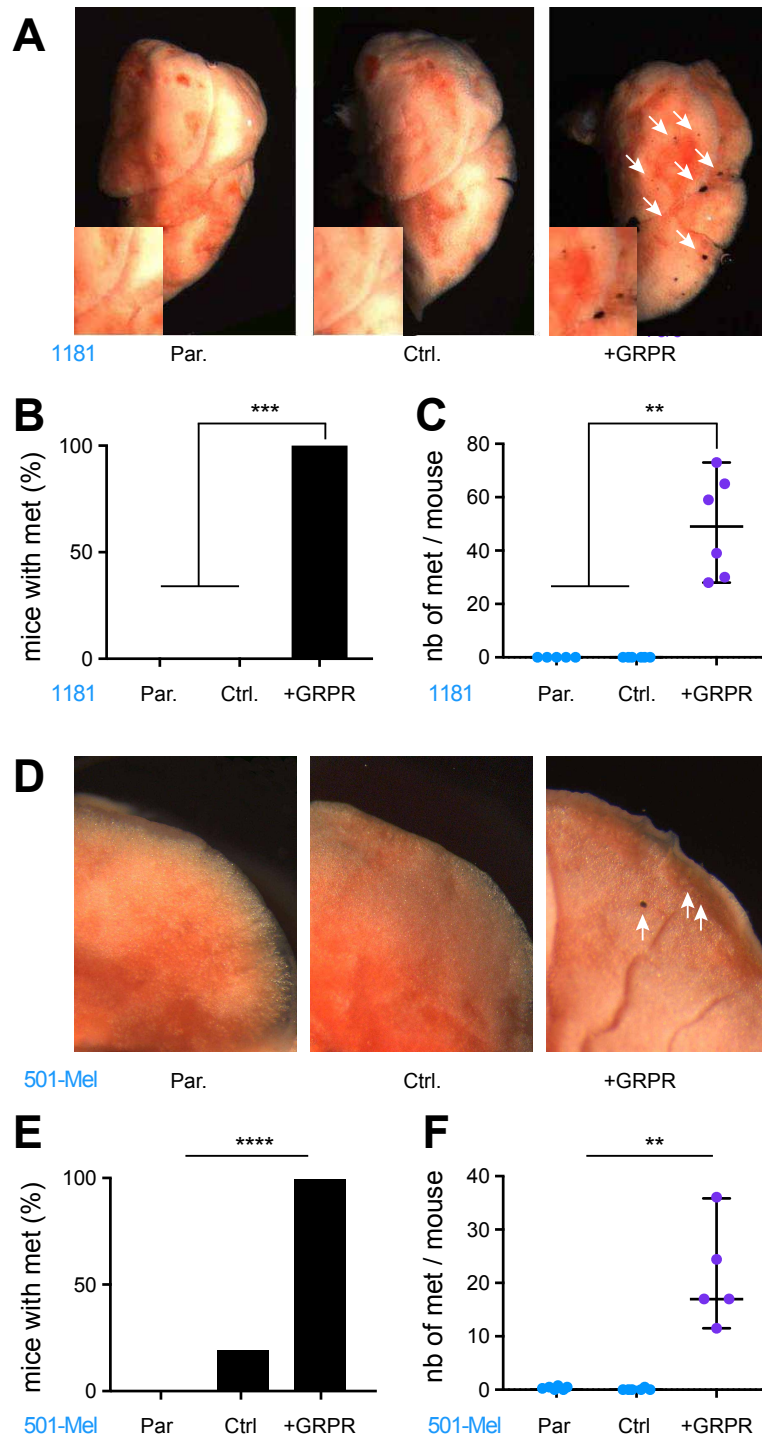


Figure 5: GRPR expression induces lung melanoma metastasis.

(A,D) Representative images of the lungs after tail-vein injection of mouse 1181-parental (Par.), 1181-Ctrl and 1181+GRPR, and human 501mel-Par., 501mel-Ctrl and 501mel+GRPR melanoma cells observed 35 and 20 days after injection, respectively. Arrows are pointing metastatic foci. Scale bar represents 200 μ m. In (A) Insets are enlargements. (B,E) Percentage of mice and (C,F) mean number of metastasis foci per mouse (n=6) presenting lung metastasis from mouse (B, [1181-Par., 1181-Ctrl and 1181+GRPR]) and human (E, [501mel-Par., 501mel-Ctrl and 501mel+GRPR]) melanoma cells. Data are represented as median \pm 95% CI. Statistical analysis for the percentage comparison was performed using the Chi-square test. Statistical analysis for the count comparison was performed using Kruskal Wallis tests.

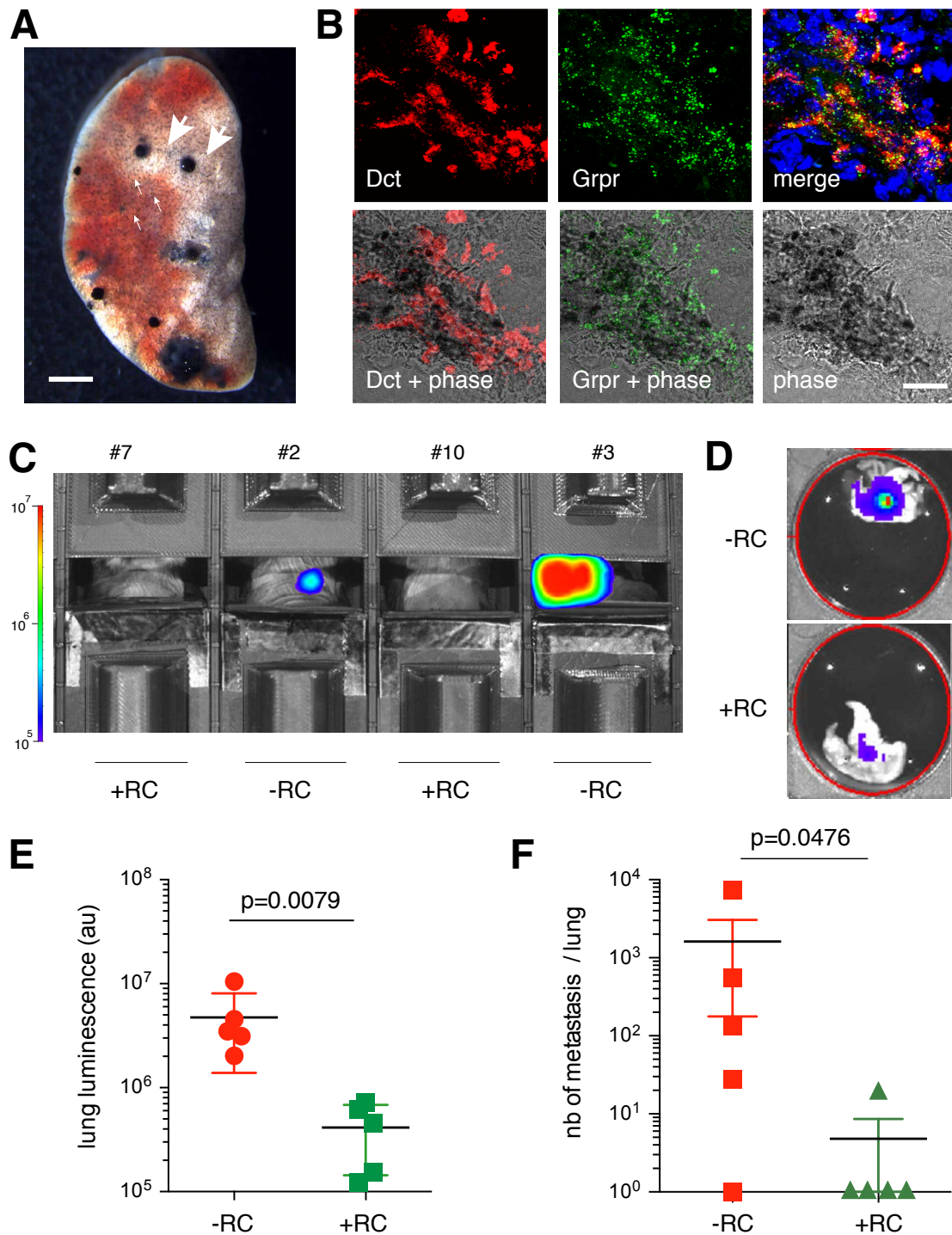


Figure 6: RC antagonist inhibits the growth and number of lung GRPR positive melanoma metastasis.

C57BL/6 female mice were intra-veinously injected with 5×10^5 1057Luc (GRPRpos) melanoma cells. (A) Melanoma metastasis present at the surface of the lung on day 28 Scale bar = 2mm. (B) RNA scope of 1057Luc injected-lung. GRPR (green) and Dct (red) mRNA colocalized in lung melanoma metastasis. Scale bar = 50µM. Luminescence of mice (C) and lungs after sacrifice and dissection (D) that were treated (+RC) or not (-RC) with RC-3095. (E) Evaluation of the luminescence and (F) estimation of the visible superficial metastasis from five isolated independent lungs treated or not with RC-3095. Note that four and one lung did not have any superficial met when they were treated or not with RC-3095, respectively. Statistical analysis was performed using the two-tailed Mann Whitney test. Data are presented as mean values +/- SD (E) and SEM (F).

Supplementary Figures

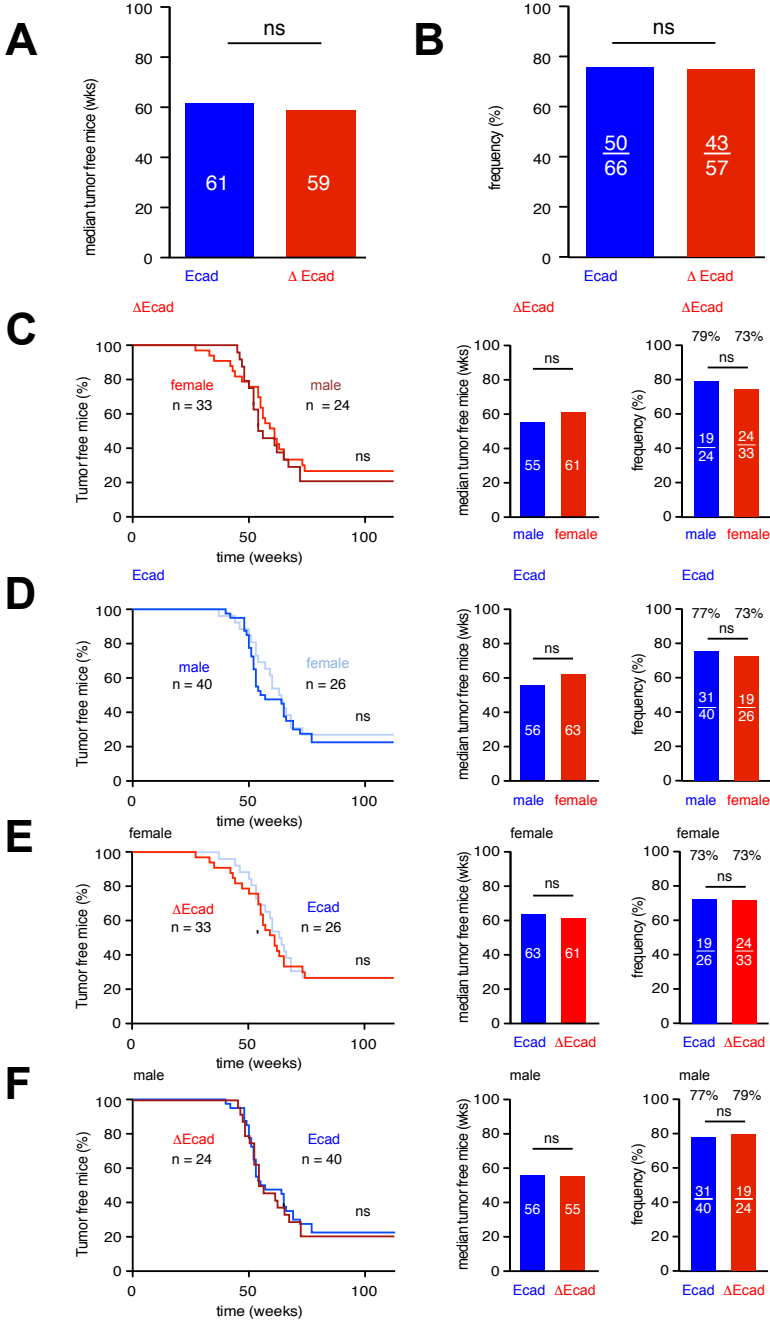


Figure 1S: Cdh1 inactivation has not effect on melanoma initiation in mice.

Median of the tumor-free (A) and percentage of mice with primary melanoma (B). Kaplan-Meier, median and frequency of tumor-free mice by genotype and sex. ΔEcad tumors male versus female (C), Ecad tumors male versus female (D), female tumors ΔEcad versus Ecad (E), male tumors ΔEcad versus Ecad (F).

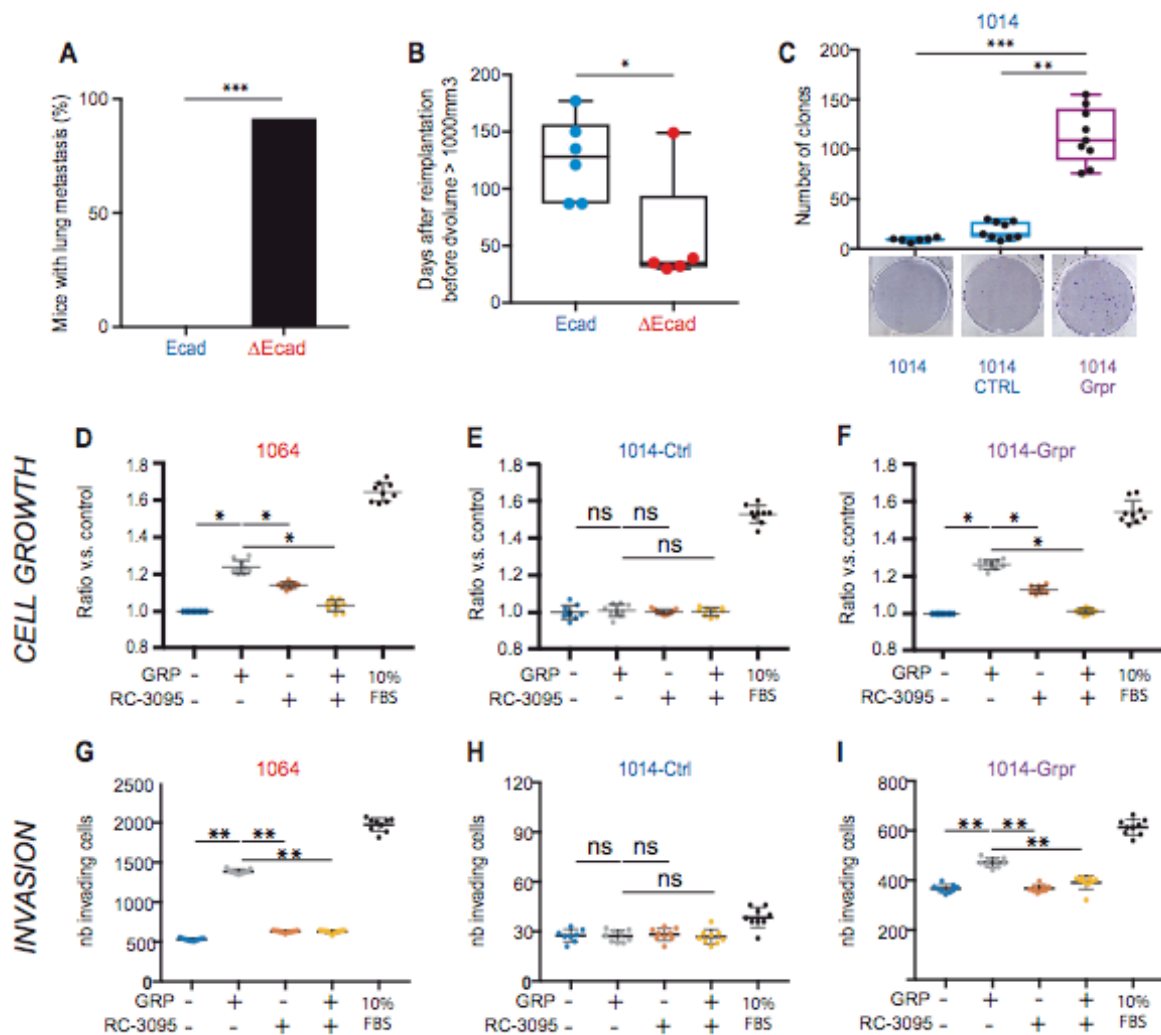


Figure 3S: GRPR promotes growth and invasiveness of melanoma cells

Tail-vein injection of melanoma cells after dissociation from 2 Ecad and 3 ΔEcad independent tumors (A). Lung mets were observed in 0/6 mice injected with Ecad cells and 12/13 mice injected with ΔEcad cells. Statistical analysis was performed using a two-sided Fisher's exact test. Time after melanoma neck-grafting to reach a volume of 1000mm³ with female Ecad and ΔEcad tumors (B) Statistical analysis was performed using a two-tailed Mann-Whitney test. Clonogenic growth of 1014 GRPRneg melanoma cell line, left parental cells, middle control cell line, right Grpr ectopic expression (C). Data are represented as mean±s.d. Effect of GRPR stimulation on GRPRpos 1064, 1014-Grpr (D, F, G, I) and GRPRneg 1014-Ctrl (E,H) melanoma cells on growth (D,E,F) and invasion (G,H,I). Cell number after starvation followed by 10nM GRP (lane 2,4), 1μM RC-3095 (3,4) and 10%SVF (lane 6) supplementation for 48h. Data are represented as mean±s.d. Number of invasive cells in presence of 200μg/mL Matrigel, with 10nM GRP (lane 2,4), 1μM RC-3095 (3,4) and 10%SVF (lane 6) supplementation for 48h. Data are represented as mean±s.d. Statistical analysis for C-I were performed using a two-tailed Kruskal-Wallis test.

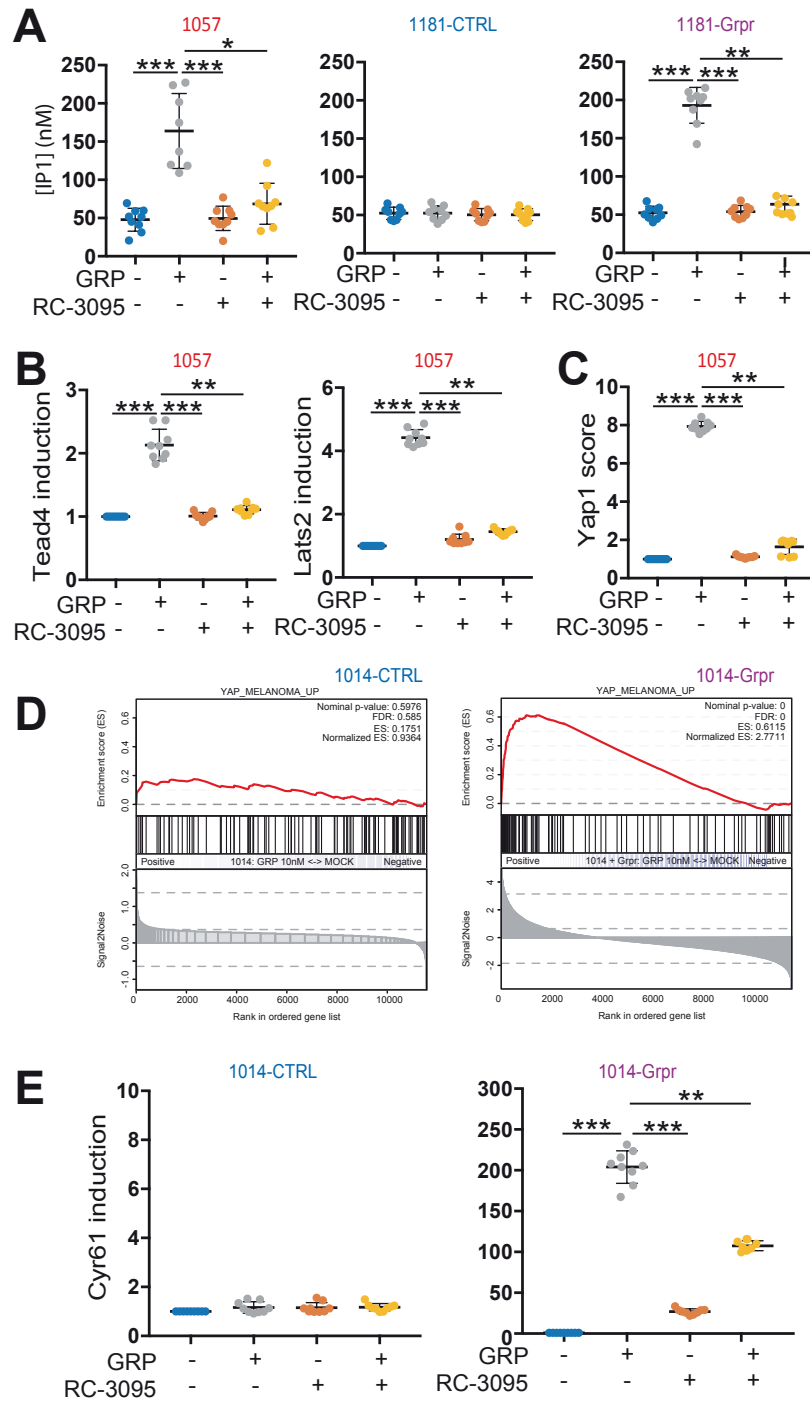


Figure 4S: GRPR activation by GRP promotes YAP1 transcriptional program.

IP1 concentration (A) of 1057 (left), 1181-Ctrl (middle) and 1181-Grpr (right) with 10nM GRP (lane 1), 1 μ M RC-3095 (lane 2) or both (lane3). Data represented as mean \pm SD. Induction of Yap1 targets (B) Tead4 (left), Lats2 (middle) in the 1057 GRPRpos melanoma cell line after stimulation with 10 nM GRP (lane 1), 1 μ M RC-3095 (lane 2) or both (lane3). Quantification of Yap1 score (C) in 1057 GRPRpos melanoma cell line after stimulation with 10 nM GRP (lane 1), 1 μ M RC-3095 (lane 2) or both (lane3). Enrichment by GSEA of the YAP1 signature (D) after GRP stimulation of 1014-Ctrl (left) and 1014-Grpr (right) murine melanoma cell lines. Induction of the Yap1 target Cyr61 (E) in the 1014-Ctrl (left) and 1014-Grpr (right) murine melanoma cell lines. Data are represented as mean \pm SD.

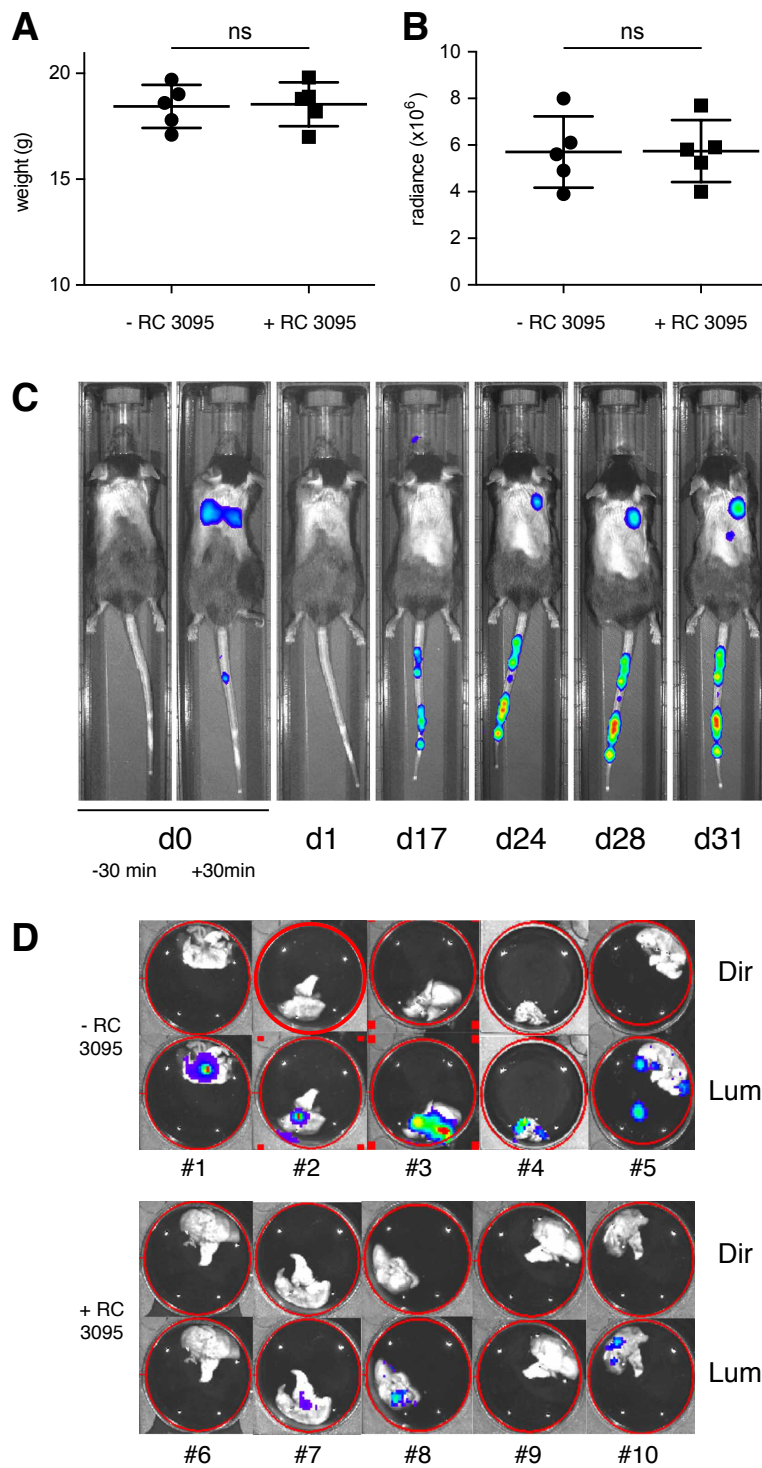


Figure 6S: RC antagonist inhibits the growth and number of lung GRPR positive melanoma metastasis.

Randomization in 2 groups according to the weight (A) and to the radiance (B) Representative images of C57BL/6 mice injected intravenously with 1057Luc melanoma cells analyzed with the IVIS Spectrum Imaging System at different time points (C). d means day. Note that at day 31, signal was detected. After dissection, metastasis can occur in the liver and in the kidney (see signal appearing at day 31 out of the lung. Detection of luminescence of the lungs after sacrifice and dissection of RC treated (n#6 to #10) or not (n#1 to #5) mice. Lum means luminescence, Dir means direct.

Supplementary Tables

Table S1: Description of the cell lines

Cell line	Sex	Genotype	Grpr expression (TPM)	Cdh1 expression (TPM)
1057	Female	Tyr::NRAS ^{Q61K} ; Cdkn2a ^{+/-} ; TyrCreA ^o ; Cdh1 ^{F/F}	327	0
1064	Female	Tyr::NRAS ^{Q61K} ; Cdkn2a ^{+/-} ; TyrCreA ^o ; Cdh1 ^{F/F}	1190	0
1181	male	Tyr::NRAS ^{Q61K} ; Cdkn2a ^{+/-} ; ρ^o ; Cdh1 ^{F/F}	0	17
1181-CTRL	male	Tyr::NRAS ^{Q61K} ; Cdkn2a ^{+/-} ; TyrCreA ^o ; Cdh1 ^{F/F} ; CMV::tGFP	0	16
1181-Grpr	male	Tyr::NRAS ^{Q61K} ; Cdkn2a ^{+/-} ; TyrCreA ^o ; Cdh1 ^{F/F} ; CMV::Grpr/tGFP	18	14
1014	Female	Tyr::NRAS ^{Q61K}	0	6
1014-CTRL	Female	Tyr::NRAS ^{Q61K} ; CMV::tGFP	0	7
1014-Grpr	Female	Tyr::NRAS ^{Q61K} ; CMV::Grpr/tGFP	880	5
MDA-MB-435S	Female	BRAFV600E; CDKN2A ^{-/-} ; TP53G266E	3	0
501-mel	Female	BRAFV600E; CDKN2A ^{-/-} ; PTEN ^{-/-}	0	3
501-Mel-CTRL	Female	BRAFV600E; CDKN2A ^{-/-} ; PTEN ^{-/-} ; CMV::eGFP; PGK::HygroR	0	3
501-mel-GRPR	Female	BRAFV600E; CDKN2A ^{-/-} ; PTEN ^{-/-} ; CMV::GRPR/eGFP; PGK::HygroR	380	3.5

Table S2: Primer used for the PCR & RT-qPCR

RT-qPCR quantification		Primer forward		Primer reverse		Product size	Concentration	PCR conditions
Gene	Name	Sequence	nName	Sequence				
Grpr	LL2955	AGTGGGGGTGTCTTCACACT	LL2956	TCAGGGCATGGGATGCCTGGAT	95bp	150nM	Standard RT-qPCR	
Cdh1	LL1267	AGCCATTGCCAAGTACATCC	LL1268	GCAACGAATCCCTCAAAGAC	147bp	300nM	Standard RT-qPCR	
Cyr61	LL2914	TTCTTTTCAACCCTCTGCAC	LL2915	GACTGGTCTGGGGATTCT	239bp	600nM	Standard RT-qPCR	
Tead4	LL3241	TGATGCAGAGGGTGTATGGA	LL3242	TTCCCTGTCTGAGCTTGAT	533bp	900nM	Standard RT-qPCR	
Lats2	LL3245	GAGTATCGAAGCTGCCTGG	LL3246	TGGTAGGATGGGAGTGTTC	98bp	600nM	Standard RT-qPCR	
Gapdh	LL1615	CAAGCTTCTGGTGAAGGA	LL1616	TGCCTCATCTTAGGCTTTGTA	188bp	300nM	Standard RT-qPCR	
GRPR	LL3234	CTGATCCAGAGTCTTACAA	LL3235	CGGTACAGTAGATGACATGA	152bp	600nM	Standard RT-qPCR	
TBP	LL521	CACGAACACGGCAGTACTGATT	LL522	TTTTCTTCTGCGAGTCTGGAC	89bp	300nM	Standard RT-qPCR	

Table S3: PCR & qPCR conditions

Classic 58		
Temperature	time	number of cycle
94°C	05:00	1X
94°C	01:00	3X
58°C	01:00	
72°C	01:00	30X
94°C	00:45	
58°C	00:30	
72°C	00:30	1X
72°C	10:00	
Classic 56		
Temperature	time	number of cycle
94°C	05:00	1X
94°C	01:00	3X
56°C	01:00	
72°C	01:00	30X
94°C	00:45	
56°C	00:30	
72°C	00:30	1X
72°C	10:00	
Standard RT-qPCR		
Temperature	time	number of cycle
50°C	02:00	1X
95°C	10:00	40X
95°C	00:15	
60°C	01:00	
95°C	00:15	
60°C	01:00	
95°C	00:15	1X

Table S4 : Genesets used for the GSEA analysis

YAP_melanoma_UP		Pigmentation	NCS like	Invasion	MSC
From Zhang et al. Oncogene 2020		From Rambow et al.Cell, 2018	From Rambow et al.Cell, 2018	From Rambow et al.Cell, 2018	From Rambow et al.Cell, 2018
GJA5	TUFT1	SNAI2	SEMA3B	VCAN	SLC7A8
AL844908.5	GADD45B	RAB27A	IGF1	TNC	DLX5
CCN1	SYT1	TYR	ATP1A2	BCAT1	TRIM67
ITGB2	NTNG1	GPR143	VCAN	FOSL2	ARMC7
RP11-799021.1	NTNG2	TYRP1	NGFR	UNC5B	CD36
SH3RF2	SLFN12	MLPH	ITGA6	CCL2	PAX3
S1PR1	LYPD6	MLANA	SLC22A17	COL1A1	RNF121
VGLL3	DNAJC6	APOE	PDGFB	SH2B3	SLC25A48
RP11-68819.1	HSD17B7	TRPM1	PLAT	MGP	IP6K3
RP11-16M8.2	HSD17B7P2	EDNRB	TMEM176B	VEGFA	UBXN10
RP11-463H12.2	CAVIN1	KIT	COL1A1	LOX	MYORG
NGF	SH2D5	SLC45A2	CNN3	FGF1	LSMEM1
THBS1	DSE	FABP7	ADGB	PDGFRB	FRAT2
KRTAP2-3	PRKCA	PMEL	ATP1B2	IGFBP5	ATP6AP1L
RP11-320G24.1	CLCF1	SLC24A5	MATN2	ERRF1	
GREM1	STAMBPL1		SYT11	PRDX1	
ZNF804A	RRAS2		ANXA1	TGFB1	
AJUBA	TSC2D2		LAMC1	IL13RA2	
NRG1	HMG2		GFRA3	SOX4	
SLC6A11	FSTL3		RSPO3	NES	
ZNF542P	CTC-529P8.1		GFRA1	LOXL2	
TGFB2	RP11-274J7.2		ADAMTS4	SPRY2	
WTIP	HMG2-AS1		MPZ	CDH13	
BCAS1	AC063955.1		GFRA2	LMO4	
IL6	B3GALT2		PRIMA1	RG55	
CCN2	F2R		A2M	RG516	
FGF1	SNAPC1		NRXN1	DLX1	
AC079145.4	SMURF2		CADM1	SLIT2	
TTC9	AC017002.1		SLITRK6	GPC3	
BDNF	ARHGAP23		THBS2	ADM	
RP11-224O19.2	SMAD3		COL4A1	EDNRA	
ADRB2	LIMA1		IL1RAP	CYSLTR2	
FST	STC2		S100A4	DDAH1	
WWC1	PM20D2		NLGN3	PLXDC1	
RP11-131L23.1	FOSL1		L1CAM	VSNL1	
ZNF404	PAWR		ITGA1	COL1A2	
PLEKHA7	CTNNA1		AQP1	DLC1	
ADM	PALLD			AXL	
CDC42EP2	DUSP14			ANGPTL4	
HBEGF	WWC2			IGFBP6	
AC009237.1	FAM53A			COL3A1	
RP3-399L15.3	NUDCD1			FABP4	
AOX1	UAP1			CDH2	
5_8S_rRNA.3	COL12A1			PTGER4	
CNN2	CCL2			NDNF	
ANKRD30B	FLRT2			NR2F1	
DDAH1	PLOD2			BGN	
ATP6V0A4	TES			TGM2	
FJX1	PLAUR			TMSB4X	
DLC1	BICC1				
DLEC1	MAFF				
DYNLL1	ADAMTS1				
PDCD1LG2	RP11-79I23.2				
SLC8A1	ABL2				
IL11	CDR2				
AC006213.1	CYTH3				
ZNF714	FMN2				
CRIM1	PDLIM1				
IL7R	BCL9L				
GPR176	SYDE1				
AMOTL2	PNPLA3				
PLSCR4	DRAM1				
NAV3	METRNL				
BEX1	TGM2				
FAT4	RFTN1				
DKK1	RP11-21M7.1				
CCL20	TIGD2				
ANKRD1	FSTL1				
RND3	EVA1C				
SERPINB2	ELL2				
NUAK1	RBMS2				
LATS2	ARID5B				
TPM1	NEDD4L				
EPHA2	RAI14				
SYNPO	CHML				
SYDE2	RBMS3				
IRS1	MARCHF3				
ZNF620	POLR1G				
AC069292.6	LIMCH1				
RP5-862P8.2	MYO1B				
JDP2	CYTOR				
MYBL1	CNN3				
HHEX	SRGAP1				
CXCL8	CCDC80				
LINC01505	EFNA5				
TEAD4	SERTAD4-AS1				
GADD45A	AC068491.4				
LOXL2	RAB30				
ZNF45	RDH10				

Discussion

A. Importance de la E-cadhérine dans le mélanome

E-cadhérine avait été décrite dans de nombreux cancers comme le cancer du sein ou le cancer gastrique comme étant un gène suppresseur de métastases (Corso et al., 2013, 2018). Dans le mélanome, seules des corrélations cliniques avaient été établies (Danen et al., 1996; Pećina-Slaus et al., 2007; Tucci et al., 2007; Venza et al., 2016). Le modèle murin de mélanome développé dans cette thèse est le premier modèle adressant le rôle de *Cdh1* dans toutes les étapes de la formation du mélanome. Ce modèle montre que la perte d'E-cad induit un risque accru de produire des métastases d'environ 3 fois sans correction par le sexe. La production de ces métastases est également largement favorisée par la perte d'E-cad avec presque 7 fois plus de métastases produites par poumon envahi. Nos résultats sont confortés par les résultats de Shields et coll. qui ont montré que l'induction de l'expression de CDH1 dans les cellules B16 induisait une diminution de la formation de métastases pulmonaires (Shields et al., 2019).

Quel que soit le contexte génétique (notre cohorte de métastases pulmonaires de mélanome ou la cohorte du TCGA), une anti-corrélation d'expression CDH1/GRPR est présente. Par contre, nous avons noté un dimorphisme sexuel dans le modèle de mélanome quant à la formation de métastases. En effet, la perte d'E-cad augmente le risque de formation de métastases pulmonaires de presque 4 lorsque les souris sont femelles, mais seulement de 1,6 lorsque les souris sont mâles. Le sexe impacte aussi le nombre des foyers métastatiques augmentant à la fois la formation des micro- et des macro-métastases. Ces considérations inédites ne sont pas observées dans la base de données du TCGA, mais le faible nombre de cas de tumeurs primaires ne permet pas de réaliser des statistiques sur la survie et la rechute des patientes atteintes de mélanome ayant perdu l'expression d'E-cadhérine. Cette information est d'autant plus compliquée à obtenir étant donné que l'expression d'E-cadhérine est très forte dans les kératinocytes de l'épiderme et les prélèvements sont souvent contaminés par des résidus épidermiques. Les données du TCGA, issues de bases de données obtenues par méthode de RNAseq « bulk », sont donc contaminées par des cellules qui vont perturber l'établissement de seuil d'expression pour définir les statuts E-cad haut et E-cad bas. La généralisation de l'étude menée sur notre petite cohorte de patients atteints de mélanome pourrait aider à valider l'importance de l'analyse des données en fonction du genre comme recommandé par le NIH pour

éviter le biais dans l'interprétation des données. Ces dimorphismes n'ont pas été identifiés dans la littérature, car bien au contraire les femmes semblent avoir des mélanomes moins agressifs (Bellenghi et al., 2020; Mervic et al., 2011; Nosrati and Wei, 2014; Schwartz et al., 2019). Les raisons avancées sont doubles : (i) les hommes cumulent généralement les facteurs de risque ce qui participent à la dégradation de leur qualité de vie, leur capacité à résister au mélanome et au développement tumoral (ii) une action du microenvironnement, particulièrement des hormones où notamment les estrogènes réguleraient négativement la croissance tumorale et favoriserait l'immunité sur site tandis que les androgènes favoriseraient la formation de métastases (Chen et al., 2018; McQuade and Davies, 2018; Wang et al., 2017; Zhao et al., 2018). Nos résultats semblent donc aller à l'encontre de ces données. Ceci peut être dû au fait que nos modèles sont épurés de nombreux facteurs de risques externes (UVs, tabagisme, alcoolisme, exposition à des xénobiotiques, ...). Il est à souligner que le pronostic de survie, en fonction de l'expression de GRPR est nettement défavorable chez les femmes et pas chez les hommes.

L'effet de l'expression de la E-cadhérine sur la sensibilité à l'anoïkis est en faveur de l'effet de sa perte sur la progression tumorale. La présence de nombreuses métastases montre que les cellules sont capables de ne pas entrer en apoptose. Cette résistance à l'anoïkis est probablement due à l'expression de GRPR.

Enfin, la capacité des cellules à pousser à faible densité est historiquement liée à l'expression d'E-cad (Li et al., 2010a; Padmanaban et al., 2019). Nos résultats *in vitro* suggèrent totalement l'inverse avec une absence quasi-totale de la capacité de cloner de nos lignées de mélanome murin exprimant E-cad. A l'inverse, les lignées de mélanome Δ E-cad ont, elles, une capacité clonogénique avec une pénétrance de 100%.

Le modèle développé est assez rigide dans le sens où il ne permet pas de moduler l'expression d'E-cad comme elle pourrait l'être normalement lorsqu'elle est régulée par la méthylation. Les conséquences d'une réactivation d'E-cad dans les métastases pulmonaires seraient intéressantes à observer, mais difficile à mettre en place techniquement. Ce modèle ne serait pertinent qu'à une condition, que la réexpression d'E-cad *in vitro* n'impacte pas l'expression de GRPR.

B. Rôle de GRPR dans la progression du mélanome

Notre étude a montré que l'expression de GRPR est capable par elle-même d'induire les métastases de mélanome. Nous avons identifié également l'action de GRPR sur différents processus cellulaires importants de la progression tumorale comme la croissance cellulaire, la résistance à l'anoïkis, la clonogénicité, l'invasion cellulaire. Nos résultats montrent également que l'expression de GRPR est exclusive chez les souris femelles ΔE -cad. Cette expression de GRPR chez les femelles est notre explication principale au dimorphisme sexuel quant à la formation des métastases pulmonaires de mélanome. L'importance de ce dimorphisme est vérifiée dans les données de l'étude TCGA où les patientes qui portent des mélanomes exprimant fortement GRPR ont tendance à décéder plus rapidement et surtout avec une progression est plus rapide. Ces données viennent de patients non-traités (ou traités avec des molécules inefficaces comme la dacarbazine) donc ici le terme de progression ne se fait pas par référence à la rechute d'un patient sous thérapie, mais à la réapparition de nouvelles métastases après la chirurgie et/ou l'enrôlement du patient dans l'essai clinique. Cela indique que l'expression de GRPR favorise la formation des métastases de mélanome chez la femme en cohérence avec nos données. L'effet chez les hommes est diamétralement opposé, semblant diminuer la progression tumorale. Cet effet n'est pas vu dans nos modèles murins, car les cellules Ecad dans les cellules GRPRneg 1181 sont mâles et produisent quand même des métastases après l'expression ectopique de GRPR. Il faut également adresser un point à propos de la base de données du TCGA, en particulier dans le cas du mélanome. Celle-ci a été réalisée avant l'arrivée des nouvelles thérapies au tournant des années 2010 et donc les patients inclus ne représentent pas du tout l'état de la clinique actuel du mélanome. De plus, sa composition est biaisée vers les métastases ganglionnaires et loco-régionales cutanées qui sont loin d'être les plus délétères pour la survie du patient. La base de données est donc peu informative sur la biologie des métastases à distance. La réalisation d'un TCGA « bis », composé de patients traités et de métastases des organes profonds pourrait être particulièrement intéressante pour améliorer les connaissances sur le mélanome. L'absence de cette base de données contenant un grand nombre de métastases pulmonaires ou dans d'autres organes ne nous permet pas de conclure *in silico* sur la prévalence de l'expression de GRPR dans les métastases non pulmonaires.

Pour vérifier si GRPR est le seul déterminant dans la capacité acquise des cellules à former des métastases, le croisement des lignées utilisées avec des lignées de souris invalidées pour Grpr

(Hampton et al., 1998) ou Grp (Barry et al., 2020) nous permettrait de statuer clairement sur le rôle de GRPR dans la mélanomagenèse. On s'attend à voir une nette diminution de la formation de métastases dans les souris femelles.

GRPR induit la croissance cellulaire, comme dans de nombreux autres cancers (Elshafae et al., 2016; Li et al., 2010b; Moody et al., 2003; Yano et al., 1992) (Elshafae et al., 2016; Li et al., 2010b; Moody et al., 2003; Yano et al., 1992). L'effet de cette croissance est, il est vrai modéré, 20-25% de cellules en plus après 2 jours de stimulation en culture. Il serait intéressant de connaître les déterminants de cette croissance et différencier un effet pro-prolifératif d'effets anti-apoptotique. Nos résultats préliminaires semblent aller majoritairement vers une résistance à l'apoptose plutôt qu'une action en faveur de la prolifération. Cet effet sur la survie est également à mettre en parallèle de l'effet sur la capacité à cloner des cellules. L'induction de l'expression de GRPR est suffisante pour permettre aux cellules GRPRneg 1181 qui n'avaient cette capacité clonogénique de l'acquérir. Dans des modèles déjà capables de cloner (501-Mel, 1014), l'induction de GRPR augmente significativement cette capacité clonogénique. L'impact de ces deux processus cellulaires sur la formation du mélanome expliquerait notamment le nombre très important de micro-métastases. Ces cellules auraient leur survie augmentée et seraient capables de s'implanter très efficacement dans les poumons.

GRPR induit l'invasion cellulaire dans le mélanome comme cela avait été montré précédemment dans d'autres cancers ou modèles cellulaires (Clarimundo et al., 2017; Elshafae et al., 2016). Cette invasion peut expliquer l'invasion de la tumeur primaire vers l'environnement, mais également l'invasion des organes cibles. Cependant, concernant la sortie des cellules de la peau, il faut noter deux éléments qui peuvent contrecarrer cette hypothèse : (i) la peau n'exprime pas de GRP et donc pas de ligand à même d'activer GRPR et donc d'attirer les cellules de mélanome exprimant GRPR (Fagerberg et al., 2014; The Cancer Genome Atlas Network, 2015). (ii) les concentrations sanguines de GRP sont bien en deçà de l'EC50 du récepteur. En effet GRPR a une EC50 autour de 0,5 nM alors que les concentrations sanguines sont plus de l'ordre de 0.05nM maximum (Grimsholm et al., 2005; Jönsson et al., 2006). Cette différence d'un log10 est probablement trop faible pour induire l'activation du récepteur. Ainsi le rôle de GRPR est principalement dans la croissance des cellules de mélanome GRPRpos dans les poumons.

GRPR favorise la résistance à l'anoïkis. Ces résultats sont encore préliminaires et n'ont pas encore été répliqués 3 fois, mais le fait que les cellules humaines et murines montrent les mêmes effets nous encourage à croire en ses résultats. Dans le processus métastatique du mélanome, cet effet de résistance à l'anoïkis se situe probablement lors de la circulation des cellules dans les vaisseaux et l'arrivée des cellules dans le poumon.

GRPR active la signalisation YAP1. Cette signalisation a été associée dans le mélanome avec l'invasion, l'anoïkis et la formation de métastases (Ma et al., 2021; Nallet-Staub et al., 2014; Zhang et al., 2020c; Zhao et al., 2021). Les effets sur la croissance sont encore discutés, mais ils semblent qu'ils soient réservés aux mélanomes uvéaux uniquement (Ma et al., 2021; Zhang et al., 2020c). Ces processus cellulaires régulés par YAP1 sont en parfaite adéquation avec les observations faites sur l'activation de GRPR ce qui suggère que l'activité oncogénique de GRPR passe principalement par YAP1. Cette hypothèse mérite néanmoins d'être testée en utilisant l'inhibiteur de YAP1, la vertéporfine ou l'inhibition génétique de l'expression de YAP1 sur les processus cellulaires décrits plus haut après activation de GRPR par la GRP. Des tests inverses dans le but de vérifier que YAP1 régule tous ces processus dans notre modèle de mélanome pourront également être entrepris à l'aide de l'expression du quintuple mutant YAP^{5A} insensible à la dégradation induite par la phosphorylation par la voie Hippo.

Notre modèle de mélanome est l'un des premiers à proposer un mécanisme d'activation de YAP1 dans le mélanome cutané et le premier à proposer un mécanisme en dehors de l'apparition de mutation dans cette même pathologie. L'autre mécanisme est l'apparition de mutations somatiques ciblant les sérines cibles des kinases LAST1/2, derniers effecteurs de la voie Hippo. Ces sérines sont mutées en alanine (mutations S61A, S127A, S164A et S397A) (Zhang et al., 2019). Ce mécanisme en dehors de l'apparition de mutations permet une meilleure plasticité cellulaire et donc une plus grande adaptation de la cellule cancéreuse à son environnement et aux traitements même si l'effet observé sera moins intense comparé aux mutations.

D'autres signalisations sont mises en jeu. Des résultats préliminaires ont montré une légère suractivation de la voie MAPK en réponse à la GRP dans nos lignées murines. Nous avons également pu écarter l'activation d'AKT par GRP. Des tests kinases réalisés à l'aide de la technologie de PamChip® sont en cours de réalisation pour définir quelles sont les kinases activées. Ces tests seront mis en relation avec les signatures transcriptomiques obtenues dans

nos lignées pour identifier les voies de signalisations cellulaires induites par l'activation de GRPR. Ces voies pourront identifier de nouvelles protéines clefs de la progression tumorale du mélanome. Les voies activées pourront également être ciblées en complément ou en remplacement de l'inhibition de GRPR pour le traitement du mélanome.

Notre modèle est également le deuxième modèle de mélanome cutané à proposer un ciblage de la localisation des métastases par des ligands endogènes. Ce mécanisme avec déjà été suggéré avec un autre RCPGs dans le mélanome cutané. En effet CCR4 est capable de diriger le mélanome vers des métastases cérébrales (Klein et al., 2017). Il serait intéressant de vérifier l'action de GRPR sur la formation de métastases dans d'autres organes et plus particulièrement ceux exprimant la GRP comme le cerveau que nos cellules GRPR pos sont capables de coloniser à faible fréquence après injection des cellules dans la veine de la queue des souris (<10%). L'utilisation d'injection stéréotaxiques directement dans le cerveau, permettrait de vérifier si l'on retrouve les mêmes mécanismes, nos modèles cellulaires étant trop agressifs pour des injections autres ou pour étudier la formation de métastases spontanées, ce qui ne laisse pas le temps à d'éventuelles métastases cérébrales de s'établir. Il faut néanmoins savoir que la GRP dans le tissu nerveux est un neurotransmetteur (Barry et al., 2020) dont l'expression est certainement limitée aux synapses et n'est pas libre en dehors de la survenue de potentiel d'action (et encore cette libération reste limitée à l'espace inter-synaptique). Il n'est donc pas certain que la GRP du cerveau soit disponible pour attirer ou favoriser la survie des cellules de mélanomes.

C. Importance de l'inhibition de GRPR dans la progression du mélanome

Notre étude a mis en lumière l'effet de l'inhibition de GRPR sur la formation des métastases, le traitement par le RC-3095 diminuant dramatiquement le nombre de foyers métastatiques. Ces résultats poussent en faveur de l'utilisation d'antagoniste de GRPR dans le traitement du mélanome, mais ont aussi permis de valider le rôle de l'activation GRPR par la GRP dans la formation des métastases pulmonaires. Il faut néanmoins discuter de l'efficacité de ces molécules dans la prise en charge du mélanome. Pour l'instant nous avons seulement mis en évidence l'impact sur la formation des métastases avec une prise en charge précoce. Il faudrait tester l'effet d'antagoniste de GRPR sur des métastases déjà bien établies. Néanmoins, si le profil toxicologique et pharmacocinétique des inhibiteurs est correct, les inhibiteurs pourraient être utilisés comme adjuvant en plus de la résection tumorale afin de protéger les poumons de

colonisation métastatique ou de la réduire, les poumons étant particulièrement impactés par la formation des métastases de mélanome (Barth et al., 1995; Zekri et al., 2017).

Il y a cependant un écueil important à l'utilisation des antagonistes de GRPR en cliniques : actuellement aucune des molécules disponibles n'est réellement adaptée. Le RC-3095 est rapidement dégradé *in vivo*, ce qui oblige à multiplier les injections pour avoir un profil pharmacologique intéressant (González et al., 2009; Szepeshazi et al., 1997). De plus, du fait de son activité en tant qu'agoniste partiel, le RC-3095 a montré une grande toxicité dans un essai clinique de phase I (Schwartzmann et al., 2006).

Un autre antagoniste de GRPR a été utilisé, le PD-176252, mais il est inutilisable en clinique, car trop lipophile, impossible d'être absorbé, y compris après injection intra-parentérale. Cette donnée remet en question une partie de la littérature qui lui trouve notamment un effet anti-tumoral *in vivo* même si l'on peut toujours imaginer qu'il est en fait une pro-drogue métabolisée par les bactéries digestives. Il faudrait donc générer de nouvelles molécules. Deux techniques complémentaires s'offrent à nous : (i) un criblage pour permettre de trouver des « Hits » qui serviront de base structurale pour des pharmacomodulations ultérieures. (ii) la cristallographie du récepteur pour comprendre les déterminants à l'échelle de la molécule définissant l'état activé ou inactivé de GRPR et d'identifier les acides aminés interagissant avec les ligands. Cette cristallisation sera également d'une grande aide pour la pharmacomodulation des « hits » afin de l'orienter. Ces « hits » pharmacomodulés deviendront des « leads » qui pourront être testés sur les modèles *in vitro* et *in vivo* que nous avons générés. Ces molécules au-delà de leur aspect anti-tumoral, pourraient avoir une action anti-prurit et être utilisées dans de nombreuses pathologies courantes de la peau comme le psoriasis ou l'eczéma.

Au-delà de l'utilisation d'antagonistes de GRPR pour leur action directe anti-tumorale, celle-ci peut être couplée avec d'autres molécules, voir un radio-ligand pour augmenter l'effet anti-tumoral ou avoir une approche diagnostique. Cette approche a été beaucoup développée pour GRPR en le couplant avec des radionucléides. Le couplage avec des radionucléides comme le ^{68}Ga permet de détecter les cellules par PET/CT dans l'organisme ou avec le ^{177}Lu entraînant une action anti-tumorale par irradiation. Cette approche a déjà été réalisée chez des patientes atteintes de cancers du sein ou de la prostate avec de bons résultats (Advanced Accelerator Applications, 2021; Zang et al., 2018, 2020; Zhang et al., 2018). Le couplage peut également être fait avec des molécules qui vont exercer une action thérapeutique, on peut notamment citer l'AN-215 combinant un antagoniste de GRPR et une anthracycline (Engel et al., 2005). Pour finir,

l'utilisation d'agoniste de GRPR peut permettre de cibler les cellules cancéreuses et induire l'internaliser de vésicules contenant des molécules thérapeutiques (Akbar et al., 2019).

La signalisation de l'endothéline a été associée avec la résistance aux inhibiteurs de MAPK dans le mélanome (Asundi et al., 2014; Schäfer et al., 2021; Smith et al., 2017b). GRPR partage la même signalisation $G\alpha_q$ en aval que le récepteur à l'endothéline. Il est donc possible de GRPR possède également ce même effet en faveur de la résistance au traitement par inhibiteurs de la voie MAPK. De premiers résultats obtenus au laboratoire vont dans ce sens. La stimulation par la GRP augmentant d'un facteur environ 4 l'IC50 de la binimétinib mesurée en test de viabilité MTT (Figure 37).

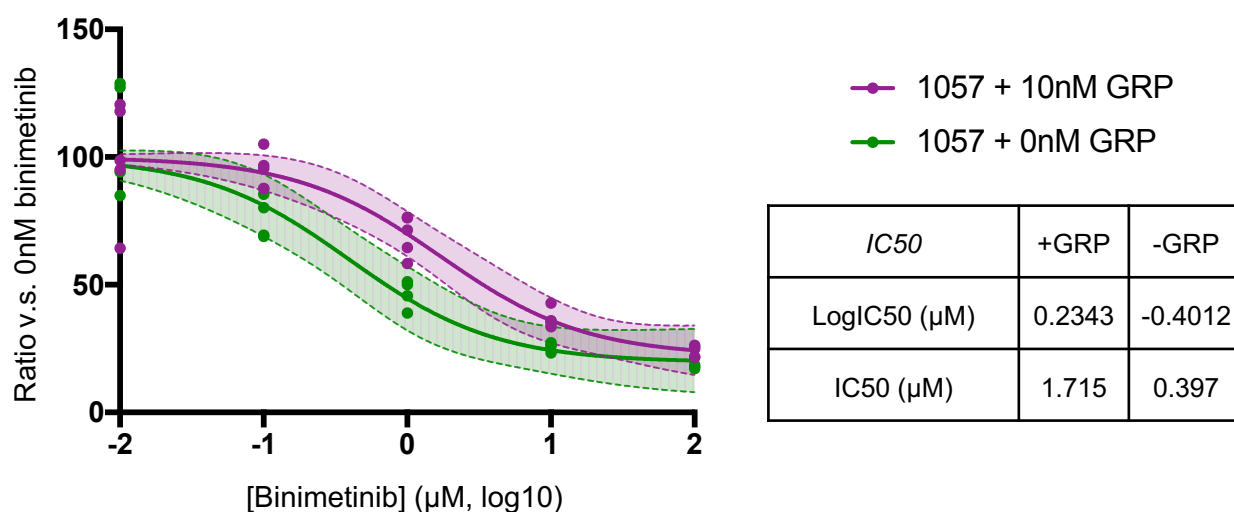


Figure 37: Croissance des cellules de mélanome GRPR pos 1057 stimulées par la GRP et traitées par la binimétinib

La binimétinib est un inhibiteur de MEK1/2. Les IC50 ont été calculées par l'application d'un modèle de régression logistique à 4 paramètres. N=2

D. Mécanismes moléculaires conduisant à l'expression de GRPR

Les mécanismes qui conduisent à l'expression de GRPR après la perte d'expression de E-cad ne sont pas encore connus. Les études transcriptomiques des tumeurs et des cellules murines ont pu identifier des corrélations avec l'expression de Notch3 et du récepteur aux estrogènes Esr1. Pour ce dernier nous avons pu identifier qu'il existe deux populations : (i) une population E-cad neg / Grpr pos / Esr1 pos et (ii) une population E-cad pos / Grpr neg / Esr1 neg (Figure 38). Son profil d'expression permettrait d'expliquer l'expression de GRPR uniquement dans les mélanomes Δ E-cad chez la femme et donc le dimorphisme observé quant à la formation des métastases et l'expression de GRPR.

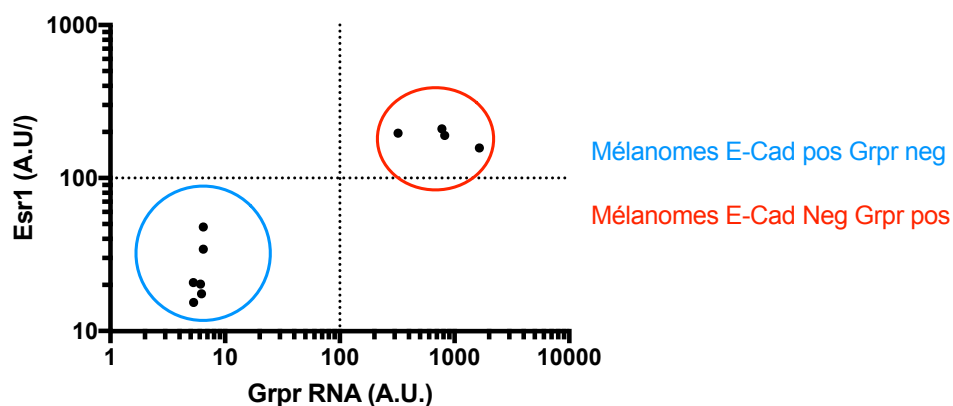


Figure 38: Expression de Grpr et d'Esr1 dans les lignées cellulaires de mélanomes murins établies au laboratoire.

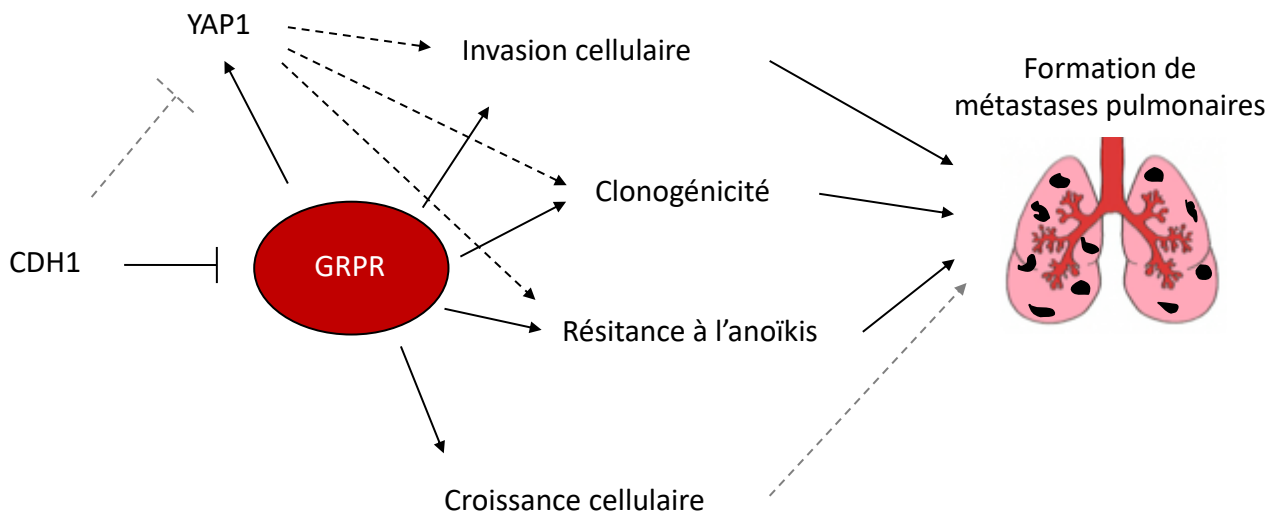
On distingue 2 populations (i) une population E-cad neg / Grpr pos / Esr1 pos cerclée de rouge et (ii) une population E-cad pos / Grpr neg / Esr1 neg cerclée de bleu.

Cette expression de Esr1 est très intéressante lorsque mis en parallèle avec les récents travaux menés dans des neurones dans le cadre de la démangeaison. Takanami et ses collègues ont montré que le récepteur aux estrogènes alpha, codé par *Esr1* se fixe au promoteur de GRPR (Takanami et al., 2021). Cette fixation entraîne l'augmentation de l'expression de GRPR. Il est également intéressant de noter par ailleurs que les estrogènes augmentent également l'expression de la GRP dans leurs modèles, mais de manière probablement indirecte. Selon ces résultats, la perte d'E-cadhérine dans le mélanome en présence d'ESR1 chez les femmes activerait l'expression de GRPR. Dans cette idée, il serait intéressant de comparer les niveaux d'expression de Grp dans les poumons des souris mâles et femelles. On peut imaginer que l'expression de Grp dans les poumons de souris femelles soit plus élevée et donc favorise, du côté du ligand également, cette interaction GRP-GRPR pro-métastatique.

D'autres facteurs de transcription ont été corrélés avec l'expression de GRPR comme RUNX2 ou BACH1, mais à ce jour aucune corrélation exacte n'a été faite. Il est intéressant de noter que la liaison de ces facteurs de transcription sur les régions régulatrices d'ESR1 et de GRPR a été montrée par expérience de CHIP-seq en dehors du contexte du mélanome (Lachmann et al., 2010). La régulation de GRPR pourrait donc être due à l'action conjuguée de ces facteurs.

Les seuls éléments que l'on peut dès à présent écarter sont des mutations de gènes ou des différences de méthylations du promoteur de GRPR. La régulation de l'expression de GRPR par β -caténine, qui aurait pu être envisagée dans le cadre de la perte d'E-cad, semble exclue, car il n'a pas été retrouvé de signature β -caténine associée à GRPR aussi bien dans les mélanomes murins que dans les mélanomes humains.

Conclusion



La perte d'E-Cadhérine conduit à la formation des métastases de mélanome via l'expression de GRPR. L'activation de GRPR va conduire à l'activation de processus cellulaires très importants dans la progression tumorale qui vont engendrer la formation des métastases de mélanome dans les poumons. Ce récepteur couplé aux protéines-G peut être ciblé et son inhibition provoque une diminution drastique de la formation des métastases pulmonaires de mélanomes. Ces résultats montrent que GRPR pourrait être une cible intéressante dans le traitement du mélanome malin.

Bibliographie

- Aban, C.E., Lombardi, A., Neiman, G., Biani, M.C., La Greca, A., Waisman, A., Moro, L.N., Sevlever, G., Miriuka, S., and Luzzani, C. (2021). Downregulation of E-cadherin in pluripotent stem cells triggers partial EMT. *Sci Rep* *11*, 2048.
- Abreu, N., Acosta-Ruiz, A., Xiang, G., and Levitz, J. (2021). Mechanisms of differential desensitization of metabotropic glutamate receptors. *Cell Reports* *35*, 109050.
- Abrisqueta, M., Herraiz, C., Pérez Oliva, A.B., Sanchez-Laorden, B.L., Olivares, C., Jiménez-Cervantes, C., and García-Borrón, J.C. (2013). Differential and competitive regulation of human melanocortin 1 receptor signaling by β -arrestin isoforms. *J Cell Sci* *126*, 3724–3737.
- Advanced Accelerator Applications (2021). A Phase I/IIa Open-label, Multi-center Study to Evaluate the Safety, Tolerability, Whole-body Distribution, Radiation Dosimetry and Anti-tumor Activity of [¹⁷⁷Lu]-NeoB Administered in Patients With Advanced Solid Tumors Known to Overexpress Gastrin-releasing Peptide Receptor (GRPR) (clinicaltrials.gov).
- Aiba, Y., Oh-hora, M., Kiyonaka, S., Kimura, Y., Hijikata, A., Mori, Y., and Kurosaki, T. (2004). Activation of RasGRP3 by phosphorylation of Thr-133 is required for B cell receptor-mediated Ras activation. *Proc Natl Acad Sci U S A* *101*, 16612–16617.
- Akbar, M.J., Lukasewicz Ferreira, P.C., Giorgetti, M., Stokes, L., and Morris, C.J. (2019). Bombesin receptor-targeted liposomes for enhanced delivery to lung cancer cells. *Beilstein J Nanotechnol* *10*, 2553–2562.
- Akeson, M., Sainz, E., Mantey, S.A., Jensen, R.T., and Battey, J.F. (1997). Identification of four amino acids in the gastrin-releasing peptide receptor that are required for high affinity agonist binding. *J Biol Chem* *272*, 17405–17409.
- Aktary, Z., McMahon, M., and Larue, L. (2017). Animal Models of Melanoma. In *Melanoma*, D.E. Fisher, and B.C. Bastian, eds. (New York, NY: Springer), pp. 1–31.
- Alewijnse, A.E., Timmerman, H., Jacobs, E.H., Smit, M.J., Roovers, E., Cotecchia, S., and Leurs, R. (2000). The effect of mutations in the DRY motif on the constitutive activity and structural instability of the histamine H₂ receptor. *Mol Pharmacol* *57*, 890–898.
- Alexander, S.P., Christopoulos, A., Davenport, A.P., Kelly, E., Mathie, A., Peters, J.A., Veale, E.L., Armstrong, J.F., Faccenda, E., Harding, S.D., et al. (2019). THE CONCISE GUIDE TO PHARMACOLOGY 2019/20: G protein-coupled receptors. *Br J Pharmacol* *176*, S21–S141.
- Algazi, A.P., Esteve-Puig, R., Nosrati, A., Hinds, B., Hobbs-Muthukumar, A., Nandoskar, P., Ortiz-Urda, S., Chapman, P.B., and Daud, A. (2018). Dual MEK/AKT inhibition with trametinib and GSK2141795 does not yield clinical benefit in metastatic NRAS-mutant and wild-type melanoma. *Pigment Cell Melanoma Res* *31*, 110–114.
- Allen, C.E., Merad, M., and McClain, K.L. (2018). Langerhans-Cell Histiocytosis. *N Engl J Med* *379*, 856–868.
- Ambrosini, G., Pratilas, C.A., Qin, L.-X., Tadi, M., Surriga, O., Carvajal, R.D., and Schwartz, G.K. (2012). Identification of unique MEK-dependent genes in GNAQ mutant uveal melanoma involved in cell growth, tumor cell invasion and MEK-resistance. *Clin Cancer Res* *18*, 3552–3561.
- Annala, S., Feng, X., Shridhar, N., Eryilmaz, F., Patt, J., Yang, J., Pfeil, E.M., Cervantes-Villagrana, R.D., Inoue, A., Häberlein, F., et al. (2019). Direct targeting of G α q and G α 11 oncoproteins in cancer cells. *Sci Signal* *12*, eaau5948.

Aoude, L.G., Wadt, K.A.W., Pritchard, A.L., and Hayward, N.K. (2015). Genetics of familial melanoma: 20 years after CDKN2A. *Pigment Cell Melanoma Res* 28, 148–160.

Aprikian, A.G., Tremblay, L., Han, K., and Chevalier, S. (1997). Bombesin stimulates the motility of human prostate-carcinoma cells through tyrosine phosphorylation of focal adhesion kinase and of integrin-associated proteins. *International Journal of Cancer* 72, 498–504.

Arang, N., and Gutkind, J.S. (2020). G Protein-Coupled receptors and heterotrimeric G proteins as cancer drivers. *FEBS Letters* 594, 4201–4232.

Arita, Y., O'Driscoll, K.R., and Weinstein, I.B. (1992). Growth of Human Melanocyte Cultures Supported by 12-O-Tetradecanoylphorbol-13-acetate Is Mediated through Protein Kinase C Activation. *Cancer Res* 52, 4514–4521.

Artinger, K.B., and Monsoro-Burq, A.H. (2021). Neural crest multipotency and specification: power and limits of single cell transcriptomic approaches. *Fac Rev* 10, 38.

Arulanandam, R., Vultur, A., Cao, J., Carefoot, E., Elliott, B.E., Truesdell, P.F., Larue, L., Feracci, H., and Raptis, L. (2009). Cadherin-cadherin engagement promotes cell survival via Rac1/Cdc42 and signal transducer and activator of transcription-3. *Mol Cancer Res* 7, 1310–1327.

Ascierto, P.A., Dréno, B., Larkin, J., Ribas, A., Liskay, G., Maio, M., Mandalà, M., Demidov, L., Stroyakovskiy, D., Thomas, L., et al. (2021). 5-Year Outcomes with Cobimetinib plus Vemurafenib in BRAF V600 Mutation-Positive Advanced Melanoma: Extended Follow-up of the coBRIM Study. *Clin Cancer Res*.

Asundi, J., Lacap, J.A., Clark, S., Nannini, M., Roth, L., and Polakis, P. (2014). MAPK Pathway Inhibition Enhances the Efficacy of an Anti-Endothelin B Receptor Drug Conjugate by Inducing Target Expression in Melanoma. *Mol Cancer Ther* 13, 1599–1610.

Atkins, M.B., Kunkel, L., Sznol, M., and Rosenberg, S.A. (2000). High-dose recombinant interleukin-2 therapy in patients with metastatic melanoma: long-term survival update. *Cancer J Sci Am* 6 Suppl 1, S11-14.

Attwood, T.K., and Findlay, J.B. (1994). Fingerprinting G-protein-coupled receptors. *Protein Eng* 7, 195–203.

Avizienyte, E., Wyke, A.W., Jones, R.J., McLean, G.W., Westhoff, M.A., Brunton, V.G., and Frame, M.C. (2002). Src-induced de-regulation of E-cadherin in colon cancer cells requires integrin signalling. *Nat Cell Biol* 4, 632–638.

Azam, S., Haque, Md.E., Jakaria, Md., Jo, S.-H., Kim, I.-S., and Choi, D.-K. (2020). G-Protein-Coupled Receptors in CNS: A Potential Therapeutic Target for Intervention in Neurodegenerative Disorders and Associated Cognitive Deficits. *Cells* 9, 506.

Bagnato, A., and Natali, P.G. (2004). Endothelin receptors as novel targets in tumor therapy. *J Transl Med* 2, 16.

Balaji Rangunathrao, V.A., Vellingiri, V., Anwar, M., Akhter, M.Z., and Mehta, D. (2020). S1PR1 and VEGFR2 - a synergy that promotes tumor angiogenesis? *Mol Cell Oncol* 7, 1746131.

Baljinnyam, E., Umemura, M., De Lorenzo, M.S., Xie, L.-H., Nowycky, M., Iwatsubo, M., Chen, S., Goydos, J.S., and Iwatsubo, K. (2011). G $\beta\gamma$ subunits inhibit Epac-induced melanoma cell migration. *BMC Cancer* 11, 256.

Bang, J., and Zippin, J.H. (2021). Cyclic adenosine monophosphate (cAMP) signaling in melanocyte pigmentation and melanomagenesis. *Pigment Cell Melanoma Res* 34, 28–43.

- Bardoni, R., Shen, K.-F., Li, H., Jeffry, J., Barry, D.M., Comitato, A., Li, Y.-Q., and Chen, Z.-F. (2019). Pain Inhibits GRPR Neurons via GABAergic Signaling in the Spinal Cord. *Sci Rep* 9, 15804.
- Barry, D.M., Liu, X.-T., Liu, B., Liu, X.-Y., Gao, F., Zeng, X., Liu, J., Yang, Q., Wilhelm, S., Yin, J., et al. (2020). Exploration of sensory and spinal neurons expressing gastrin-releasing peptide in itch and pain related behaviors. *Nat Commun* 11, 1397.
- Barth, A., Wanek, L.A., and Morton, D.L. (1995). Prognostic factors in 1,521 melanoma patients with distant metastases. *J. Am. Coll. Surg.* 181, 193–201.
- Basith, S., Cui, M., Macalino, S.J.Y., Park, J., Clavio, N.A.B., Kang, S., and Choi, S. (2018). Exploring G Protein-Coupled Receptors (GPCRs) Ligand Space via Cheminformatics Approaches: Impact on Rational Drug Design. *Frontiers in Pharmacology* 9, 128.
- Bautista, R.-M.F., Carter, K.M., Jarrett, S.G., Napier, D., Wakamatsu, K., Ito, S., and D’Orazio, J.A. (2020). Cutaneous pharmacologic cAMP induction induces melanization of the skin and improves recovery from ultraviolet injury in melanocortin 1 receptor-intact or heterozygous skin. *Pigment Cell Melanoma Res* 33, 30–40.
- Baxter, L.L., Watkins-Chow, D.E., Pavan, W.J., and Loftus, S.K. (2019). A curated gene list for expanding the horizons of pigmentation biology. *Pigment Cell Melanoma Res* 32, 348–358.
- Baynash, A.G., Hosoda, K., Giaid, A., Richardson, J.A., Emoto, N., Hammer, R.E., and Yanagisawa, M. (1994). Interaction of endothelin-3 with endothelin-B receptor is essential for development of epidermal melanocytes and enteric neurons. *Cell* 79, 1277–1285.
- Beaulieu, J.-M., Sotnikova, T.D., Marion, S., Lefkowitz, R.J., Gainetdinov, R.R., and Caron, M.G. (2005). An Akt/beta-arrestin 2/PP2A signaling complex mediates dopaminergic neurotransmission and behavior. *Cell* 122, 261–273.
- Beebe, S.J., Salomonsky, P., Holroyd, C., and Becker, D. (1993). Differential expression of cyclic AMP-dependent protein kinase isozymes in normal human melanocytes and malignant melanomas. *Cell Growth & Differentiation* 4, 1005.
- Bellenghi, M., Puglisi, R., Pontecorvi, G., De Feo, A., Carè, A., and Mattia, G. (2020). Sex and Gender Disparities in Melanoma. *Cancers (Basel)* 12, 1819.
- Benham-Pyle, B.W., Pruitt, B.L., and Nelson, W.J. (2015). Mechanical strain induces E-cadherin-dependent Yap1 and β -catenin activation to drive cell cycle entry. *Science* 348, 1024–1027.
- Bertolotto, C., Abbe, P., Hemesath, T.J., Bille, K., Fisher, D.E., Ortonne, J.P., and Ballotti, R. (1998). Microphthalmia gene product as a signal transducer in cAMP-induced differentiation of melanocytes. *J Cell Biol* 142, 827–835.
- Block, E. (2018). Molecular Basis of Mammalian Odor Discrimination: A Status Report. *J Agric Food Chem* 66, 13346–13366.
- Bonacci, T.M., Ghosh, M., Malik, S., and Smrcka, A.V. (2005). Regulatory interactions between the amino terminus of G-protein betagamma subunits and the catalytic domain of phospholipase Cbeta2. *J Biol Chem* 280, 10174–10181.
- Bonaventure, J., Domingues, M.J., and Larue, L. (2013). Cellular and molecular mechanisms controlling the migration of melanocytes and melanoma cells. *Pigment Cell Melanoma Res* 26, 316–325.
- Bonet, C., Luciani, F., Ottavi, J.-F., Leclerc, J., Jouenne, F.-M., Boncompagni, M., Bille, K., Hofman, V., Bossis, G., Marco de Donatis, G., et al. (2017). Deciphering the Role of Oncogenic MITFE318K in Senescence Delay and Melanoma Progression. *J Natl Cancer Inst* 109.

- Boniface, K., Seneschal, J., Picardo, M., and Taïeb, A. (2018). Vitiligo: Focus on Clinical Aspects, Immunopathogenesis, and Therapy. *Clinic Rev Allerg Immunol* 54, 52–67.
- Borsotti, P., Ghilardi, C., Ostano, P., Silini, A., Dossi, R., Pinessi, D., Foglieni, C., Scatolini, M., Lacial, P.M., Ferrari, R., et al. (2015). Thrombospondin-1 is part of a Slug-independent motility and metastatic program in cutaneous melanoma, in association with VEGFR-1 and FGF-2. *Pigment Cell & Melanoma Research* 28, 73–81.
- Bosenberg, M., Muthusamy, V., Curley, D.P., Wang, Z., Hobbs, C., Nelson, B., Nogueira, C., Horner II, J.W., DePinho, R., and Chin, L. (2006). Characterization of melanocyte-specific inducible Cre recombinase transgenic mice. *Genesis* 44, 262–267.
- Bouillaud, F., Hammad, N., and Schwartz, L. (2021). Warburg Effect, Glutamine, Succinate, Alanine, When Oxygen Matters. *Biology* 10, 1000.
- Boukhedouni, N., Martins, C., Darrigade, A.-S., Drullion, C., Rambert, J., Barrault, C., Garnier, J., Jacquemin, C., Thiolat, D., Lucchese, F., et al. Type-1 cytokines regulate MMP-9 production and E-cadherin disruption to promote melanocyte loss in vitiligo. *JCI Insight* 5, e133772.
- Bourgognon, J.-M., Schiavon, E., Salah-Uddin, H., Skrzypiec, A.E., Attwood, B.K., Shah, R.S., Patel, S.G., Mucha, M., Challiss, R.A.J., Forsythe, I.D., et al. (2013). Regulation of Neuronal Plasticity and Fear by a Dynamic Change in PAR1 – G Protein Coupling in the Amygdala. *Mol Psychiatry* 18, 1136–1145.
- Bourillon, A., Hu, H.-H., Hetet, G., Lacapere, J.-J., André, J., Descamps, V., Basset-Seguin, N., Ogbah, Z., Puig, S., Saiag, P., et al. (2013). Genetic variation at KIT locus may predispose to melanoma. *Pigment Cell Melanoma Res* 26, 88–96.
- Boussadia, O., Kutsch, S., Hierholzer, A., Delmas, V., and Kemler, R. (2002). E-cadherin is a survival factor for the lactating mouse mammary gland. *Mech Dev* 115, 53–62.
- Braeuer, R.R., Zigler, M., Villares, G.J., Dobroff, A.S., and Bar-Eli, M. (2011). Transcriptional control of melanoma metastasis: The importance of the tumor microenvironment. *Seminars in Cancer Biology* 21, 83–88.
- Brault, C., Zerbib, Y., Delette, C., Marc, J., Gruson, B., Marolleau, J.P., and Maizel, J. (2018). The Warburg Effect as a Type B Lactic Acidosis in a Patient With Acute Myeloid Leukemia: A Diagnostic Challenge for Clinicians. *Front Oncol* 8, 232.
- Brown, J.R., and DuBois, R.N. (2005). COX-2: a molecular target for colorectal cancer prevention. *J Clin Oncol* 23, 2840–2855.
- Bunney, T.D., and Katan, M. (2006). Phospholipase C epsilon: linking second messengers and small GTPases. *Trends Cell Biol* 16, 640–648.
- Burger, J.A., and Kipps, T.J. (2006). CXCR4: a key receptor in the crosstalk between tumor cells and their microenvironment. *Blood* 107, 1761–1767.
- Buscà, R., and Ballotti, R. (2000). Cyclic AMP a Key Messenger in the Regulation of Skin Pigmentation. *Pigment Cell Research* 13, 60–69.
- Cai, D., Chen, S.-C., Prasad, M., He, L., Wang, X., Choesmel-Cadamuro, V., Sawyer, J.K., Danuser, G., and Montell, D.J. (2014). Mechanical Feedback through E-Cadherin Promotes Direction Sensing during Collective Cell Migration. *Cell* 157, 1146–1159.
- Capra, J., and Eskelinen, S. (2017). Correlation between E-cadherin interactions, survivin expression, and apoptosis in MDCK and ts-Src MDCK cell culture models. *Lab Invest* 97, 1453–1470.

Cargnello, M., and Roux, P.P. (2011). Activation and Function of the MAPKs and Their Substrates, the MAPK-Activated Protein Kinases. *Microbiol Mol Biol Rev* 75, 50–83.

Carlino, M.S., Fung, C., Shahheydari, H., Todd, J.R., Boyd, S.C., Irvine, M., Nagrial, A.M., Scolyer, R.A., Kefford, R.F., Long, G.V., et al. (2015). Preexisting MEK1P124 mutations diminish response to BRAF inhibitors in metastatic melanoma patients. *Clin Cancer Res* 21, 98–105.

Carlino, M.S., Menzies, A.M., Atkinson, V., Cebon, J.S., Jameson, M.B., Fitzharris, B.M., McNeil, C.M., Hill, A.G., Ribas, A., Atkins, M.B., et al. (2020). Long-term Follow-up of Standard-Dose Pembrolizumab Plus Reduced-Dose Ipilimumab in Patients with Advanced Melanoma: KEYNOTE-029 Part 1B. *Clin Cancer Res* 26, 5086–5091.

Carroll, R.E., Ostrovskiy, D., Lee, S., Danilkovich, A., and Benya, R.V. (2000). Characterization of gastrin-releasing peptide and its receptor aberrantly expressed by human colon cancer cell lines. *Mol Pharmacol* 58, 601–607.

Catalanotti, F., Cheng, D.T., Shoushtari, A.N., Johnson, D.B., Panageas, K.S., Momtaz, P., Higham, C., Won, H.H., Harding, J.J., Merghoub, T., et al. (2017). PTEN Loss-of-Function Alterations Are Associated With Intrinsic Resistance to BRAF Inhibitors in Metastatic Melanoma. *JCO Precision Oncology* 1–15.

Ceraudo, E., Horioka, M., Mattheisen, J.M., Hitchman, T.D., Moore, A.R., Kazmi, M.A., Chi, P., Chen, Y., Sakmar, T.P., and Huber, T. (2021). Direct evidence that the GPCR CysLTR2 mutant causative of uveal melanoma is constitutively active with highly biased signaling. *J Biol Chem* 296, 100163.

Chan, A.S.L., and Wong, Y.H. (2005). Gq-mediated activation of c-Jun N-terminal kinase by the gastrin-releasing peptide-preferring bombesin receptor is inhibited upon costimulation of the Gs-coupled dopamine D1 receptor in COS-7 cells. *Mol Pharmacol* 68, 1354–1364.

Chang, C.-H., Tsai, R.-K., Tsai, M.-H., Lin, Y.-H., and Hirobe, T. (2014). The roles of Frizzled-3 and Wnt3a on melanocyte development: In vitro studies on neural crest cells and melanocyte precursor cell lines. *Journal of Dermatological Science* 75, 100–108.

Chang, S.-H., Ai, Y., Breyer, R.M., Lane, T.F., and Hla, T. (2005). The prostaglandin E2 receptor EP2 is required for cyclooxygenase 2-mediated mammary hyperplasia. *Cancer Res* 65, 4496–4499.

Chanson, L., Brownfield, D., Garbe, J.C., Kuhn, I., Stampfer, M.R., Bissell, M.J., and LaBarge, M.A. (2011). Self-organization is a dynamic and lineage-intrinsic property of mammary epithelial cells. *Proc Natl Acad Sci U S A* 108, 3264–3269.

Chao, C., Ives, K., Hellmich, H.L., Townsend, C.M., and Hellmich, M.R. (2009). Gastrin-releasing peptide receptor in breast cancer mediates cellular migration and interleukin-8 expression. *J Surg Res* 156, 26–31.

Chapman, P.B., Robert, C., Larkin, J., Haanen, J.B., Ribas, A., Hogg, D., Hamid, O., Ascierto, P.A., Testori, A., Lorigan, P.C., et al. (2017). Vemurafenib in patients with BRAFV600 mutation-positive metastatic melanoma: final overall survival results of the randomized BRIM-3 study. *Ann Oncol* 28, 2581–2587.

Chatzinasiou, F., Lill, C.M., Kypreou, K., Stefanaki, I., Nicolaou, V., Spyrou, G., Evangelou, E., Roehr, J.T., Kodela, E., Katsambas, A., et al. (2011). Comprehensive field synopsis and systematic meta-analyses of genetic association studies in cutaneous melanoma. *J Natl Cancer Inst* 103, 1227–1235.

Chen, P.-W., and Kroog, G.S. (2004). Alterations in receptor expression or agonist concentration change the pathways gastrin-releasing peptide receptor uses to regulate extracellular signal-regulated kinase. *Mol Pharmacol* 66, 1625–1634.

- Chen, C.P., Posy, S., Ben-Shaul, A., Shapiro, L., and Honig, B.H. (2005a). Specificity of cell-cell adhesion by classical cadherins: Critical role for low-affinity dimerization through beta-strand swapping. *Proc Natl Acad Sci U S A* *102*, 8531–8536.
- Chen, J., Wu, F., Shi, Y., Yang, D., Xu, M., Lai, Y., and Liu, Y. (2019). Identification of key candidate genes involved in melanoma metastasis. *Mol Med Rep* *20*, 903–914.
- Chen, J., Zhou, X., Yang, J., Sun, Q., Liu, Y., Li, N., Zhang, Z., and Xu, H. (2020). Circ-GLI1 promotes metastasis in melanoma through interacting with p70S6K2 to activate Hedgehog/GLI1 and Wnt/ β -catenin pathways and upregulate Cyr61. *Cell Death Dis* *11*, 1–16.
- Chen, P., Sheikh, S., Ahmad, A., Ali, S.M., Ahmad, M.U., and Ahmad, I. (2018). Orally administered endoxifen inhibits tumor growth in melanoma-bearing mice. *Cell Mol Biol Lett* *23*, 3.
- Chen, S., Zhu, H., Wetzell, W.J., and Philbert, M.A. (1996). Spontaneous melanocytosis in transgenic mice. *J Invest Dermatol* *106*, 1145–1151.
- Chen, X., Wu, Q., Depeille, P., Chen, P., Thornton, S., Kalirai, H., Coupland, S.E., Roose, J.P., and Bastian, B.C. (2017). RasGRP3 Mediates MAPK Pathway Activation in GNAQ Mutant Uveal Melanoma. *Cancer Cell* *31*, 685–696.e6.
- Chen, Z., Singer, W.D., Sternweis, P.C., and Sprang, S.R. (2005b). Structure of the p115RhoGEF rgRGS domain-Galpha13/i1 chimera complex suggests convergent evolution of a GTPase activator. *Nat Struct Mol Biol* *12*, 191–197.
- Choi, K.Y., Chang, K., Pickel, J.M., Badger, J.D., and Roche, K.W. (2011). Expression of the metabotropic glutamate receptor 5 (mGluR5) induces melanoma in transgenic mice. *Proc Natl Acad Sci U S A* *108*, 15219–15224.
- Chua, V., Lapadula, D., Randolph, C., Benovic, J.L., Wedegaertner, P.B., and Aplin, A.E. (2017). Dysregulated GPCR Signaling and Therapeutic Options in Uveal Melanoma. *Mol Cancer Res* *15*, 501–506.
- Clarimundo, V.S., Farinon, M., Pedó, R.T., Teixeira, V.O.N., Nör, C., Gulko, P.S., Xavier, R.M., and de Oliveira, P.G. (2017). Gastrin-releasing peptide and its receptor increase arthritis fibroblast-like synoviocytes invasiveness through activating the PI3K/AKT pathway. *Peptides* *95*, 57–61.
- Cohen, J.N., Yeh, I., Mully, T.W., LeBoit, P.E., and McCalmont, T.H. (2020). Genomic and Clinicopathologic Characteristics of PRKAR1A-inactivated Melanomas: Toward Genetic Distinctions of Animal-type Melanoma/Pigment Synthesizing Melanoma. *Am J Surg Pathol* *44*, 805–816.
- Coma, E., Guiriguet, C., Mora, N., Marzo-Castillejo, M., Benítez, M., Méndez-Boo, L., Fina, F., Fàbregas, M., Mercadé, A., and Medina, M. (2021). Impact of the COVID-19 pandemic and related control measures on cancer diagnosis in Catalonia: a time-series analysis of primary care electronic health records covering about five million people. *BMJ Open* *11*, e047567.
- Cooper, D.M.F. (2003). Regulation and organization of adenylyl cyclases and cAMP. *Biochem J* *375*, 517–529.
- Cornelio, D.B., Roesler, R., and Schwartzmann, G. (2007). Gastrin-releasing peptide receptor as a molecular target in experimental anticancer therapy. *Ann Oncol* *18*, 1457–1466.
- Corso, G., Carvalho, J., Marrelli, D., Vindigni, C., Carvalho, B., Seruca, R., Roviello, F., and Oliveira, C. (2013). Somatic mutations and deletions of the E-cadherin gene predict poor survival of patients with gastric cancer. *J Clin Oncol* *31*, 868–875.
- Corso, G., Figueiredo, J., La Vecchia, C., Veronesi, P., Pravettoni, G., Macis, D., Karam, R., Lo Gullo,

- R., Provenzano, E., Toesca, A., et al. (2018). Hereditary lobular breast cancer with an emphasis on E-cadherin genetic defect. *J Med Genet* 55, 431–441.
- Coulombe, P., and Meloche, S. (2007). Atypical mitogen-activated protein kinases: Structure, regulation and functions. *Biochimica et Biophysica Acta (BBA) - Molecular Cell Research* 1773, 1376–1387.
- Cousin, H. (2017). Cadherins function during the collective cell migration of *Xenopus* Cranial Neural Crest cells: revisiting the role of E-cadherin. *Mechanisms of Development* 148, 79–88.
- Cox, J.L., Lancaster, T., and Carlson, C.G. (2002). Changes in the motility of B16F10 melanoma cells induced by alterations in resting calcium influx. *Melanoma Research* 12, 211–219.
- Cozzi, S.-J., Parsons, P.G., Ogbourne, S.M., Pedley, J., and Boyle, G.M. (2006). Induction of senescence in diterpene ester-treated melanoma cells via protein kinase C-dependent hyperactivation of the mitogen-activated protein kinase pathway. *Cancer Res* 66, 10083–10091.
- Czepielewski, R.S., Porto, B.N., Rizzo, L.B., Roesler, R., Abujamra, A.L., Pinto, L.G., Schwartzmann, G., Cunha, F. de Q., and Bonorino, C. (2012). Gastrin-releasing peptide receptor (GRPR) mediates chemotaxis in neutrophils. *Proc Natl Acad Sci U S A* 109, 547–552.
- Dal Lago, L., D’Hondt, V., and Awada, A. (2008). Selected combination therapy with sorafenib: a review of clinical data and perspectives in advanced solid tumors. *Oncologist* 13, 845–858.
- Damsky, W., and Bosenberg, M. (2017). Melanocytic nevi and melanoma: unraveling a complex relationship. *Oncogene* 36, 5771–5792.
- Damsky, W.E., Curley, D.P., Santhanakrishnan, M., Rosenbaum, L.E., Platt, J.T., Gould Rothberg, B.E., Taketo, M.M., Dankort, D., Rimm, D.L., McMahon, M., et al. (2011). β -catenin signaling controls metastasis in Braf-activated Pten-deficient melanomas. *Cancer Cell* 20, 741–754.
- Danen, E.H., de Vries, T.J., Morandini, R., Ghanem, G.G., Ruitter, D.J., and van Muijen, G.N. (1996). E-cadherin expression in human melanoma. *Melanoma Res* 6, 127–131.
- Daniel, C.W., Strickland, P., and Friedmann, Y. (1995). Expression and functional role of E- and P-cadherins in mouse mammary ductal morphogenesis and growth. *Dev Biol* 169, 511–519.
- Danson, C.M., Pocha, S.M., Bloomberg, G.B., and Cory, G.O. (2007). Phosphorylation of WAVE2 by MAP kinases regulates persistent cell migration and polarity. *J Cell Sci* 120, 4144–4154.
- Davies, M.A. (2012). The Role of the PI3K-AKT Pathway in Melanoma. *The Cancer Journal* 18, 142.
- De la Fuente, M., Del Rio, M., and Hernanz, A. (1993). Stimulation of natural killer and antibody-dependent cellular cytotoxicity activities in mouse leukocytes by bombesin, gastrin-releasing peptide and neuromedin C: involvement of cyclic AMP, inositol 1,4,5-trisphosphate and protein kinase C. *J Neuroimmunol* 48, 143–150.
- De Santis, G., Miotti, S., Mazzi, M., Canevari, S., and Tomassetti, A. (2009). E-cadherin directly contributes to PI3K/AKT activation by engaging the PI3K-p85 regulatory subunit to adherens junctions of ovarian carcinoma cells. *Oncogene* 28, 1206–1217.
- Del Rio, M., and De la Fuente, M. (1994). Chemoattractant capacity of bombesin, gastrin-releasing peptide and neuromedin C is mediated through PKC activation in murine peritoneal leukocytes. *Regul Pept* 49, 185–193.
- Del Rio, M., Hernanz, A., and de la Fuente, M. (1994). Bombesin, gastrin-releasing peptide, and neuromedin C modulate murine lymphocyte proliferation through adherent accessory cells and

activate protein kinase C. *Peptides* 15, 15–22.

Delmas, V., Pla, P., Feracci, H., Thiery, J.P., Kemler, R., and Larue, L. (1999). Expression of the cytoplasmic domain of E-cadherin induces precocious mammary epithelial alveolar formation and affects cell polarity and cell-matrix integrity. *Dev Biol* 216, 491–506.

Delmas, V., Martinuzzi, S., Bourgeois, Y., Holzenberger, M., and Larue, L. (2003). Cre-mediated recombination in the skin melanocyte lineage. *Genesis* 36, 73–80.

Delyon, J., Servy, A., Laugier, F., André, J., Ortonne, N., Battistella, M., Mourah, S., Bensussan, A., Lebbé, C., and Dumaz, N. (2017). PDE4D promotes FAK-mediated cell invasion in BRAF-mutated melanoma. *Oncogene* 36, 3252–3262.

Demunter, A., De Wolf-Peeters, C., Degreef, H., Stas, M., and van den Oord, J.J. (2001). Expression of the endothelin-B receptor in pigment cell lesions of the skin. Evidence for its role as tumor progression marker in malignant melanoma. *Virchows Arch* 438, 485–491.

Deng, W., Balazs, L., Wang, D.-A., Van Middlesworth, L., Tigyi, G., and Johnson, L.R. (2002). Lysophosphatidic acid protects and rescues intestinal epithelial cells from radiation- and chemotherapy-induced apoptosis. *Gastroenterology* 123, 206–216.

Deng, W., Shuyu, E., Tsukahara, R., Valentine, W.J., Durgam, G., Gududuru, V., Balazs, L., Manickam, V., Arsura, M., VanMiddlesworth, L., et al. (2007). The lysophosphatidic acid type 2 receptor is required for protection against radiation-induced intestinal injury. *Gastroenterology* 132, 1834–1851.

Denning, M.F. (2012). Specifying protein kinase C functions in melanoma. *Pigment Cell & Melanoma Research* 25, 466–476.

Deraredj Nadim, W., Hassanaly, S., Bénédicti, H., Kieda, C., Grillon, C., and Morisset-Lopez, S. (2021). The GTPase-activating protein-related domain of neurofibromin interacts with MC1R and regulates pigmentation-mediated signaling in human melanocytes. *Biochemical and Biophysical Research Communications* 534, 758–764.

Derksen, P.W.B., Liu, X., Saridin, F., van der Gulden, H., Zevenhoven, J., Evers, B., van Beijnum, J.R., Griffioen, A.W., Vink, J., Krimpenfort, P., et al. (2006). Somatic inactivation of E-cadherin and p53 in mice leads to metastatic lobular mammary carcinoma through induction of anoikis resistance and angiogenesis. *Cancer Cell* 10, 437–449.

Dessauer, C.W., Scully, T.T., and Gilman, A.G. (1997). Interactions of Forskolin and ATP with the Cytosolic Domains of Mammalian Adenylyl Cyclase *. *Journal of Biological Chemistry* 272, 22272–22277.

Deutsch, G.B., Flaherty, D.C., Kirchoff, D.D., Bailey, M., Vitug, S., Foshag, L.J., Faries, M.B., and Bilchik, A.J. (2017). Association of Surgical Treatment, Systemic Therapy, and Survival in Patients With Abdominal Visceral Melanoma Metastases, 1965-2014: Relevance of Surgical Cure in the Era of Modern Systemic Therapy. *JAMA Surgery* 152, 672–678.

Dillenburg-Pilla, P., Patel, V., Mikelis, C.M., Zárate-Bladés, C.R., Doçi, C.L., Amornphimoltham, P., Wang, Z., Martin, D., Leelahavanichkul, K., Dorsam, R.T., et al. (2015). SDF-1/CXCL12 induces directional cell migration and spontaneous metastasis via a CXCR4/Gαi/mTORC1 axis. *FASEB J* 29, 1056–1068.

Dissanayake, S.K., Wade, M., Johnson, C.E., O'Connell, M.P., Leotlela, P.D., French, A.D., Shah, K.V., Hewitt, K.J., Rosenthal, D.T., Indig, F.E., et al. (2007). The Wnt5A/Protein Kinase C Pathway Mediates Motility in Melanoma Cells via the Inhibition of Metastasis Suppressors and Initiation of an Epithelial to Mesenchymal Transition *. *Journal of Biological Chemistry* 282, 17259–17271.

Dobroff, A.S., Wang, H., Melnikova, V.O., Villares, G.J., Zigler, M., Huang, L., and Bar-Eli, M. (2009). Silencing cAMP-response Element-binding Protein (CREB) Identifies CYR61 as a Tumor Suppressor Gene in Melanoma. *Journal of Biological Chemistry* 284, 26194–26206.

Donohue, P.J., Sainz, E., Akesson, M., Kroog, G.S., Mantey, S.A., Battey, J.F., Jensen, R.T., and Northup, J.K. (1999). An aspartate residue at the extracellular boundary of TMII and an arginine residue in TMVII of the gastrin-releasing peptide receptor interact to facilitate heterotrimeric G protein coupling. *Biochemistry* 38, 9366–9372.

D’Orazio, J.A., Nobuhisa, T., Cui, R., Arya, M., Spry, M., Wakamatsu, K., Igras, V., Kunisada, T., Granter, S.R., Nishimura, E.K., et al. (2006). Topical drug rescue strategy and skin protection based on the role of Mc1r in UV-induced tanning. *Nature* 443, 340–344.

Dorsky, R.I., Moon, R.T., and Raible, D.W. (1998). Control of neural crest cell fate by the Wnt signalling pathway. *Nature* 396, 370–373.

Dorsky, R.I., Raible, D.W., and Moon, R.T. (2000). Direct regulation of nacre, a zebrafish MITF homolog required for pigment cell formation, by the Wnt pathway. *Genes Dev.* 14, 158–162.

Drury, L.J., Ziarek, J.J., Gravel, S., Veldkamp, C.T., Takekoshi, T., Hwang, S.T., Heveker, N., Volkman, B.F., and Dwinell, M.B. (2011). Monomeric and dimeric CXCL12 inhibit metastasis through distinct CXCR4 interactions and signaling pathways. *Proc Natl Acad Sci U S A* 108, 17655–17660.

Du, L., Anderson, A., Nguyen, K., Ojeda, S.S., Ortiz-Rivera, I., Nguyen, T.N., Zhang, T., Kaoud, T.S., Gray, N.S., Dalby, K.N., et al. (2019). JNK2 Is Required for the Tumorigenic Properties of Melanoma Cells. *ACS Chem Biol* 14, 1426–1435.

Dubuc, C., Savard, M., Bovenzi, V., Lessard, A., Fortier, A., Côté, J., Neugebauer, W., Rizzolio, F., Geha, S., Giordano, A., et al. (2018). Targeting intracellular B2 receptors using novel cell-penetrating antagonists to arrest growth and induce apoptosis in human triple-negative breast cancer. *Oncotarget* 9, 9885–9906.

Dumaz, N., Hayward, R., Martin, J., Ogilvie, L., Hedley, D., Curtin, J.A., Bastian, B.C., Springer, C., and Marais, R. (2006). In Melanoma, RAS Mutations Are Accompanied by Switching Signaling from BRAF to CRAF and Disrupted Cyclic AMP Signaling. *Cancer Res* 66, 9483–9491.

Dumaz, N., Bagot, M., and Bensussan, A. (2011). [When CRAF takes over BRAF in melanoma]. *Med Sci (Paris)* 27, 817–819.

Dummer, R., Schadendorf, D., Ascierto, P.A., Arance, A., Dutriaux, C., Giacomo, A.M.D., Rutkowski, P., Vecchio, M.D., Gutzmer, R., Mandala, M., et al. (2017). Binimetinib versus dacarbazine in patients with advanced NRAS-mutant melanoma (NEMO): a multicentre, open-label, randomised, phase 3 trial. *The Lancet Oncology* 18, 435–445.

Dummer, R., Flaherty, K., Robert, C., Arance, A.M., de Groot, J.W., Garbe, C., Gogas, H., Gutzmer, R., Krajsová, I., Liskay, G., et al. (2021). Five-year overall survival (OS) in COLUMBUS: A randomized phase 3 trial of encorafenib plus binimetinib versus vemurafenib or encorafenib in patients (pts) with BRAF V600-mutant melanoma. *JCO* 39, 9507–9507.

Dunn, K.J., Williams, B.O., Li, Y., and Pavan, W.J. (2000). Neural crest-directed gene transfer demonstrates Wnt1 role in melanocyte expansion and differentiation during mouse development. *Proc Natl Acad Sci U S A* 97, 10050–10055.

Eddy, K., and Chen, S. (2021). Glutamatergic Signaling a Therapeutic Vulnerability in Melanoma. *Cancers (Basel)* 13, 3874.

Elshafae, S.M., Hassan, B.B., Supsavhad, W., Dirksen, W.P., Camiener, R.Y., Ding, H., Tweedle, M.F.,

- and Rosol, T.J. (2016). Gastrin-releasing peptide receptor (GRPr) promotes EMT, growth, and invasion in canine prostate cancer. *Prostate* 76, 796–809.
- Elste, A.P., and Petersen, I. (2010). Expression of proteinase-activated receptor 1-4 (PAR 1-4) in human cancer. *J Mol Histol* 41, 89–99.
- Emanuel, R.L., Torday, J.S., Mu, Q., Asokanathan, N., Sikorski, K.A., and Sunday, M.E. (1999). Bombesin-like peptides and receptors in normal fetal baboon lung: roles in lung growth and maturation. *American Journal of Physiology-Lung Cellular and Molecular Physiology* 277, L1003–L1017.
- Engel, J.B., Schally, A.V., Halmos, G., Baker, B., Nagy, A., and Keller, G. (2005). Targeted cytotoxic bombesin analog AN-215 effectively inhibits experimental human breast cancers with a low induction of multi-drug resistance proteins. *Endocr Relat Cancer* 12, 999–1009.
- Erdmann, F., Wellbrock, M., Trübenbach, C., Spix, C., Schrappe, M., Schüz, J., Grabow, D., and Eichinger, M. (2021). Impact of the COVID-19 pandemic on incidence, time of diagnosis and delivery of healthcare among paediatric oncology patients in Germany in 2020: Evidence from the German Childhood Cancer Registry and a qualitative survey. *The Lancet Regional Health – Europe* 9.
- Erspamer, V., Erpamer, G.F., and Inselvini, M. (1970). Some pharmacological actions of alytesin and bombesin. *J Pharm Pharmacol* 22, 875–876.
- Estrada, Y., Dong, J., and Ossowski, L. (2009). Positive crosstalk between ERK and p38 in melanoma stimulates migration and in vivo proliferation. *Pigment Cell Melanoma Res* 22, 66–76.
- Fagerberg, L., Hallström, B.M., Oksvold, P., Kampf, C., Djureinovic, D., Odeberg, J., Habuka, M., Tahmasebpoor, S., Danielsson, A., Edlund, K., et al. (2014). Analysis of the Human Tissue-specific Expression by Genome-wide Integration of Transcriptomics and Antibody-based Proteomics *. *Molecular & Cellular Proteomics* 13, 397–406.
- Fajardo, A.M., Piazza, G.A., and Tinsley, H.N. (2014). The Role of Cyclic Nucleotide Signaling Pathways in Cancer: Targets for Prevention and Treatment. *Cancers (Basel)* 6, 436–458.
- Fang, J., Lu, Y., Ouyang, K., Wu, G., Zhang, H., Liu, Y., Chen, Y., Lin, M., Wang, H., Jin, L., et al. (2009). Specific Antibodies Elicited by a Novel DNA Vaccine Targeting Gastrin-Releasing Peptide Inhibit Murine Melanoma Growth In Vivo. *Clinical and Vaccine Immunology* 16, 1033–1039.
- Farshad, A., Burg, G., Panizzon, R., and Dummer, R. (2002). A retrospective study of 150 patients with lentigo maligna and lentigo maligna melanoma and the efficacy of radiotherapy using Grenz or soft X-rays. *Br J Dermatol* 146, 1042–1046.
- Feng, X., Degese, M.S., Iglesias-Bartolome, R., Vaque, J.P., Molinolo, A.A., Rodrigues, M., Zaidi, M.R., Ksander, B.R., Merlino, G., Sodhi, A., et al. (2014). Hippo-Independent Activation of YAP by the GNAQ Uveal Melanoma Oncogene through a Trio-Regulated Rho GTPase Signaling Circuitry. *Cancer Cell* 25, 831–845.
- Ferber, E.C., Kajita, M., Wadlow, A., Tobiansky, L., Niessen, C., Ariga, H., Daniel, J., and Fujita, Y. (2008). A role for the cleaved cytoplasmic domain of E-cadherin in the nucleus. *J Biol Chem* 283, 12691–12700.
- Flem-Karlsen, K., McFadden, E., Omar, N., Haugen, M.H., Øy, G.F., Ryder, T., Gullestad, H.P., Hermann, R., Mælandsmo, G.M., and Flørenes, V.A. (2020). Targeting AXL and the DNA Damage Response Pathway as a Novel Therapeutic Strategy in Melanoma. *Mol Cancer Ther* 19, 895–905.
- Foskett, J.K., White, C., Cheung, K.-H., and Mak, D.-O.D. (2007). Inositol trisphosphate receptor

Ca²⁺ release channels. *Physiol Rev* 87, 593–658.

Freitas, J.T., Lopez, J., Llorian, C., Boroni, M., and Kos, L. (2021). The immunosuppressive role of Edn3 overexpression in the melanoma microenvironment. *Pigment Cell Melanoma Res*.

Frey, U., Fritz, A., Rotterdam, S., Schmid, K., Potthoff, A., Altmeyer, P., Siffert, W., and Brockmeyer, N. (2010). GNAS1 T393C polymorphism and disease progression in patients with malignant melanoma. *Eur J Med Res* 15, 422–427.

Frey, U.H., Alakus, H., Wohlschlaeger, J., Schmitz, K.J., Winde, G., van Calcker, H.G., Jöckel, K.-H., Siffert, W., and Schmid, K.W. (2005a). GNAS1 T393C polymorphism and survival in patients with sporadic colorectal cancer. *Clin Cancer Res* 11, 5071–5077.

Frey, U.H., Eisenhardt, A., Lümmer, G., Rübber, H., Jöckel, K.-H., Schmid, K.W., and Siffert, W. (2005b). The T393C polymorphism of the G alpha s gene (GNAS1) is a novel prognostic marker in bladder cancer. *Cancer Epidemiol Biomarkers Prev* 14, 871–877.

Frixen, U.H., Behrens, J., Sachs, M., Eberle, G., Voss, B., Warda, A., Löchner, D., and Birchmeier, W. (1991). E-cadherin-mediated cell-cell adhesion prevents invasiveness of human carcinoma cells. *J Cell Biol* 113, 173–185.

Fu, Y., Rathod, D., and Patel, K. (2020). Protein kinase C inhibitor anchored BRD4 PROTAC PEGylated nanoliposomes for the treatment of vemurafenib-resistant melanoma. *Experimental Cell Research* 396, 112275.

Fukuhara, S., Murga, C., Zohar, M., Igishi, T., and Gutkind, J.S. (1999). A novel PDZ domain containing guanine nucleotide exchange factor links heterotrimeric G proteins to Rho. *J Biol Chem* 274, 5868–5879.

Gallagher, S.J., Rambow, F., Kumasaka, M., Champeval, D., Bellacosa, A., Delmas, V., and Larue, L. (2013). Beta-catenin inhibits melanocyte migration but induces melanoma metastasis. *Oncogene* 32, 2230–2238.

Gandhi, S., and Bronner, M.E. (2021). Seq Your Destiny: Neural Crest Fate Determination in the Genomic Era. *Annu Rev Genet*.

Garbe, C., Amaral, T., Peris, K., Hauschild, A., Arenberger, P., Bastholt, L., Bataille, V., Del Marmol, V., Dréno, B., Fargnoli, M.C., et al. (2020). European consensus-based interdisciplinary guideline for melanoma. Part 1: Diagnostics - Update 2019. *Eur J Cancer* 126, 141–158.

Garcia, R.J., Ittah, A., Mirabal, S., Figueroa, J., Lopez, L., Glick, A.B., and Kos, L. (2008). Endothelin 3 induces skin pigmentation in a keratin-driven inducible mouse model. *J Invest Dermatol* 128, 131–142.

García-Borrón, J.C., Abdel-Malek, Z., and Jiménez-Cervantes, C. (2014). MC1R, the cAMP pathway and the response to solar UV: Extending the horizon beyond pigmentation. *Pigment Cell Melanoma Res* 27, 699–720.

Goding, C.R., and Arnheiter, H. (2019). MITF—the first 25 years. *Genes Dev* 33, 983–1007.

González, N., Mantey, S.A., Pradhan, T.K., Sancho, V., Moody, T.W., Coy, D.H., and Jensen, R.T. (2009). Characterization of putative GRP- and NMB-receptor antagonist's interaction with human receptors. *Peptides* 30, 1473–1486.

Gorbulev, V., Akhundova, A., Büchner, H., and Fahrenholz, F. (1992). Molecular cloning of a new bombesin receptor subtype expressed in uterus during pregnancy. *Eur J Biochem* 208, 405–410.

Grill, C., Benzekri, L., Rubod, A., Aktary, Z., Ezzedine, K., Taïeb, A., Gauthier, Y., Larue, L., and

- Delmas, V. (2018). Epidermal melanocytes in segmental vitiligo show altered expression of E-cadherin, but not P-cadherin. *Br J Dermatol* 178, 1204–1206.
- Grimaldi, A.M., Simeone, E., Giannarelli, D., Muto, P., Falivene, S., Borzillo, V., Giugliano, F.M., Sandomenico, F., Petrillo, A., Curvietto, M., et al. (2014). Abscopal effects of radiotherapy on advanced melanoma patients who progressed after ipilimumab immunotherapy. *Oncoimmunology* 3, e28780.
- Grimaldi, C., Schumacher, I., Boquet-Pujadas, A., Tarbashevich, K., Vos, B.E., Bandemer, J., Schick, J., Aalto, A., Olivo-Marin, J.-C., Betz, T., et al. (2020). E-cadherin focuses protrusion formation at the front of migrating cells by impeding actin flow. *Nat Commun* 11, 5397.
- Grimsholm, O., Rantapää-Dahlqvist, S., and Forsgren, S. (2005). Levels of gastrin-releasing peptide and substance P in synovial fluid and serum correlate with levels of cytokines in rheumatoid arthritis. *Arthritis Research & Therapy* 7, R416.
- Guida, S., Guida, G., and Goding, C.R. (2021). MC1R Functions, Expression, and Implications for Targeted Therapy. *Journal of Investigative Dermatology*.
- Guilloteau, P., Meuth-Metzinger, V.L., Morisset, J., and Zabielski, R. (2006). Gastrin, cholecystokinin and gastrointestinal tract functions in mammals. *Nutrition Research Reviews* 19, 254–283.
- Guo, L., Wu, X., Zhang, Y., Wang, F., Li, J., and Zhu, J. (2019). Protective effects of gastrin-releasing peptide receptor antagonist RC-3095 in an animal model of hepatic ischemia/reperfusion injury. *Hepatology Research* 49, 247–255.
- Gupta, S., and Yap, A.S. (2021). How adherens junctions move cells during collective migration. *Fac Rev* 10, 56.
- Gurevich, V.V., and Gurevich, E.V. (2015). Arrestins: Critical Players in Trafficking of Many GPCRs. *Prog Mol Biol Transl Sci* 132, 1–14.
- Gutkind, J.S., Novotny, E.A., Brann, M.R., and Robbins, K.C. (1991). Muscarinic acetylcholine receptor subtypes as agonist-dependent oncogenes. *Proc Natl Acad Sci U S A* 88, 4703–4707.
- Halata, Z., Baumann, K.I., and Grim, M. (2008). 6.02 - Merkel Cells. In *The Senses: A Comprehensive Reference*, R.H. Masland, T.D. Albright, T.D. Albright, R.H. Masland, P. Dallos, D. Oertel, S. Firestein, G.K. Beauchamp, M. Catherine Bushnell, A.I. Basbaum, et al., eds. (New York: Academic Press), pp. 33–38.
- Hamm, H.E. (1998). The Many Faces of G Protein Signaling *. *Journal of Biological Chemistry* 273, 669–672.
- Hampton, L.L., Ladenheim, E.E., Akesson, M., Way, J.M., Weber, H.C., Sutliff, V.E., Jensen, R.T., Wine, L.J., Arnheiter, H., and Battey, J.F. (1998). Loss of bombesin-induced feeding suppression in gastrin-releasing peptide receptor-deficient mice. *Proc Natl Acad Sci U S A* 95, 3188–3192.
- Hanahan, D., and Weinberg, R.A. (2000). The hallmarks of cancer. *Cell* 100, 57–70.
- Hanahan, D., and Weinberg, R.A. (2011). Hallmarks of Cancer: The Next Generation. *Cell* 144, 646–674.
- Hanoune, J., and Defer, N. (2001). Regulation and role of adenylyl cyclase isoforms. *Annu Rev Pharmacol Toxicol* 41, 145–174.
- Haraguchi, M., Fukushige, T., Kanekura, T., and Ozawa, M. (2019). E-cadherin loss in RMG-1 cells inhibits cell migration and its regulation by Rho GTPases. *Biochem Biophys Rep* 18, 100650.

Harding, R.M., Healy, E., Ray, A.J., Ellis, N.S., Flanagan, N., Todd, C., Dixon, C., Sajantila, A., Jackson, I.J., Birch-Machin, M.A., et al. (2000). Evidence for variable selective pressures at MC1R. *Am J Hum Genet* 66, 1351–1361.

Hari, L., Brault, V., Kléber, M., Lee, H.-Y., Ille, F., Leimeroth, R., Paratore, C., Suter, U., Kemler, R., and Sommer, L. (2002). Lineage-specific requirements of β -catenin in neural crest development. *J Cell Biol* 159, 867–880.

Hari, L., Miescher, I., Shakhova, O., Suter, U., Chin, L., Taketo, M., Richardson, W.D., Kassaris, N., and Sommer, L. (2012). Temporal control of neural crest lineage generation by Wnt/ β -catenin signaling. *Development* 139, 2107–2117.

Hart, M.J., Jiang, X., Kozasa, T., Roscoe, W., Singer, W.D., Gilman, A.G., Sternweis, P.C., and Bollag, G. (1998). Direct stimulation of the guanine nucleotide exchange activity of p115 RhoGEF by Galph13. *Science* 280, 2112–2114.

Hasegawa, M., Hosaka, T., Kojima, K., Nishimura, Y., Nakajima, Y., Kimura-Someya, T., Shirouzu, M., Sudo, Y., and Yoshizawa, S. (2020). A unique clade of light-driven proton-pumping rhodopsins evolved in the cyanobacterial lineage. *Sci Rep* 10, 16752.

Hauschild, A., Grob, J.-J., Demidov, L.V., Jouary, T., Gutzmer, R., Millward, M., Rutkowski, P., Blank, C.U., Miller, W.H., Kaempgen, E., et al. (2012). Dabrafenib in BRAF-mutated metastatic melanoma: a multicentre, open-label, phase 3 randomised controlled trial. *Lancet* 380, 358–365.

He, M., Bakken, T., Kassimova, A., Boshoff, C., Philpott, N., and Cannon, M.L. (2012). Focal adhesion kinase is required for KSHV vGPCR signaling. *Mol Carcinog* 51, 339–351.

Hernández-Martínez, R., Ramkumar, N., and Anderson, K.V. (2019). p120-catenin regulates WNT signaling and EMT in the mouse embryo. *PNAS* 116, 16872–16881.

Heuberger, J., and Birchmeier, W. (2010). Interplay of Cadherin-Mediated Cell Adhesion and Canonical Wnt Signaling. *Cold Spring Harb Perspect Biol* 2, a002915.

Hildebrand, P., Lehmann, F.S., Ketterer, S., Christ, A.D., Stingelin, T., Beltinger, J., Gibbons, A.H., Coy, D.H., Calam, J., Larsen, F., et al. (2001). Regulation of gastric function by endogenous gastrin releasing peptide in humans: studies with a specific gastrin releasing peptide receptor antagonist. *Gut* 49, 23–28.

Hiramoto, K., Murata, T., Shimizu, K., Morita, H., Inui, M., Manganiello, V.C., Tagawa, T., and Arai, N. (2014). Role of phosphodiesterase 2 in growth and invasion of human malignant melanoma cells. *Cell Signal* 26, 1807–1817.

Hitchman, T.D., Bayshtok, G., Ceraudo, E., Moore, A.R., Lee, C., Jia, R., Wang, N., Pachai, M.R., Shoushtari, A.N., Francis, J.H., et al. (2021). Combined Inhibition of G α q and MEK Enhances Therapeutic Efficacy in Uveal Melanoma. *Clin Cancer Res* 27, 1476–1490.

Hodis, E., Watson, I.R., Kryukov, G.V., Arold, S.T., Imielinski, M., Theurillat, J.-P., Nickerson, E., Auclair, D., Li, L., Place, C., et al. (2012). A landscape of driver mutations in melanoma. *Cell* 150, 251–263.

Horn, S., Figl, A., Rachakonda, P.S., Fischer, C., Sucker, A., Gast, A., Kadel, S., Moll, I., Nagore, E., Hemminki, K., et al. (2013). TERT promoter mutations in familial and sporadic melanoma. *Science* 339, 959–961.

Hoshi, N., Langeberg, L.K., Gould, C.M., Newton, A.C., and Scott, J.D. (2010). Interaction with AKAP79 modifies the cellular pharmacology of PKC. *Mol Cell* 37, 541–550.

Hosoda, K., Hammer, R.E., Richardson, J.A., Baynash, A.G., Cheung, J.C., Giaid, A., and Yanagisawa,

M. (1994). Targeted and natural (piebald-lethal) mutations of endothelin-B receptor gene produce megacolon associated with spotted coat color in mice. *Cell* 79, 1267–1276.

Hsu, M.-Y., Meier, F.E., Nesbit, M., Hsu, J.-Y., Van Belle, P., Elder, D.E., and Herlyn, M. (2000). E-Cadherin Expression in Melanoma Cells Restores Keratinocyte-Mediated Growth Control and Down-Regulates Expression of Invasion-Related Adhesion Receptors. *The American Journal of Pathology* 156, 1515–1525.

Hu, W., Jin, L., Jiang, C.C., Long, G.V., Scolyer, R.A., Wu, Q., Zhang, X.D., Mei, Y., and Wu, M. (2013). AEBP1 upregulation confers acquired resistance to BRAF (V600E) inhibition in melanoma. *Cell Death Dis* 4, e914–e914.

Huang, J.L.-Y., Urtatiz, O., and Van Raamsdonk, C.D. (2015). Oncogenic G Protein GNAQ Induces Uveal Melanoma and Intravasation in Mice. *Cancer Res* 75, 3384–3397.

Huang, R.Y.-J., Wong, M.K., Tan, T.Z., Kuay, K.T., Ng, A.H.C., Chung, V.Y., Chu, Y.-S., Matsumura, N., Lai, H.-C., Lee, Y.F., et al. (2013). An EMT spectrum defines an anoikis-resistant and spheroidogenic intermediate mesenchymal state that is sensitive to e-cadherin restoration by a src-kinase inhibitor, saracatinib (AZD0530). *Cell Death Dis* 4, e915–e915.

Huang, W.-L., Li, Z., Lin, T.-Y., Wang, S.-W., Wu, F.-J., and Luo, C.-W. (2016). Thyrostimulin-TSHR signaling promotes the proliferation of NIH:OVCAR-3 ovarian cancer cells via trans-regulation of the EGFR pathway. *Sci Rep* 6, 27471.

Hunger-Glaser, I., Salazar, E.P., Sinnott-Smith, J., and Rozengurt, E. (2003). Bombesin, lysophosphatidic acid, and epidermal growth factor rapidly stimulate focal adhesion kinase phosphorylation at Ser-910: requirement for ERK activation. *J Biol Chem* 278, 22631–22643.

Hunt, N.C., Douglas-Jones, A.G., Jasani, B., Morgan, J.M., and Pignatelli, M. (1997). Loss of E-cadherin expression associated with lymph node metastases in small breast carcinomas. *Virchows Arch* 430, 285–289.

Hussussian, C.J., Struewing, J.P., Goldstein, A.M., Higgins, P.A., Ally, D.S., Sheahan, M.D., Clark, W.H., Tucker, M.A., and Dracopoli, N.C. (1994). Germline p16 mutations in familial melanoma. *Nat Genet* 8, 15–21.

Hwang, S., Zimmerman, N.P., Agle, K.A., Turner, J.R., Kumar, S.N., and Dwinell, M.B. (2012). E-cadherin Is Critical for Collective Sheet Migration and Is Regulated by the Chemokine CXCL12 Protein During Restitution *. *Journal of Biological Chemistry* 287, 22227–22240.

IARC (2006). Exposure to artificial uv radiation and skin cancer (Lyon: International Agency For Research On Cancer).

Ieranò, C., D’Alterio, C., Giarra, S., Napolitano, M., Rea, G., Portella, L., Santagata, A., Trotta, A.M., Barbieri, A., Campani, V., et al. (2019). CXCL12 loaded-dermal filler captures CXCR4 expressing melanoma circulating tumor cells. *Cell Death Dis* 10, 562.

Ikeya, M., Lee, S.M.K., Johnson, J.E., McMahon, A.P., and Takada, S. (1997). Wnt signalling required for expansion of neural crest and CNS progenitors. *Nature* 389, 966–970.

Inoue, A., Raimondi, F., Kadji, F.M.N., Singh, G., Kishi, T., Uwamizu, A., Ono, Y., Shinjo, Y., Ishida, S., Arang, N., et al. (2019). Illuminating G-Protein-Coupling Selectivity of GPCRs. *Cell* 177, 1933-1947.e25.

Iwasaki, T., Yamauchi, M., Liang, Z., Itai, A., Sakaguchi, M., Nagano, T., Kamada, S., and Oka, M. (2017). TPA inhibits melanoma growth through inactivation of STAT3 through protein tyrosine phosphatases. *Journal of Dermatological Science* 86, e94.

- Jacquelot, N., Duong, C.P.M., Belz, G.T., and Zitvogel, L. (2018). Targeting Chemokines and Chemokine Receptors in Melanoma and Other Cancers. *Front Immunol* 9, 2480.
- Jaeger, N., Czepielewski, R.S., Bagatini, M., Porto, B.N., and Bonorino, C. (2017). Neuropeptide gastrin-releasing peptide induces PI3K/reactive oxygen species-dependent migration in lung adenocarcinoma cells. *Tumour Biol* 39, 1010428317694321.
- Janiszewska, M., Primi, M.C., and Izard, T. (2020). Cell adhesion in cancer: Beyond the migration of single cells. *J Biol Chem* 295, 2495–2505.
- Jayachandran, A., Anaka, M., Prithviraj, P., Hudson, C., McKeown, S.J., Lo, P.-H., Vella, L.J., Goding, C.R., Cebon, J., and Behren, A. (2014). Thrombospondin 1 promotes an aggressive phenotype through epithelial-to-mesenchymal transition in human melanoma. *Oncotarget* 5, 5782–5797.
- Jensen, R.T., and Gardner, J.D. (1981). Identification and characterization of receptors for secretagogues on pancreatic acinar cells. *Fed Proc* 40, 2486–2496.
- Jensen, R.T., Moody, T., Pert, C., Rivier, J.E., and Gardner, J.D. (1978). Interaction of bombesin and litorin with specific membrane receptors on pancreatic acinar cells. *Proc Natl Acad Sci U S A* 75, 6139–6143.
- Jensen, R.T., Battey, J.F., Spindel, E.R., and Benya, R.V. (2008). International Union of Pharmacology. LXVIII. Mammalian Bombesin Receptors: Nomenclature, Distribution, Pharmacology, Signaling, and Functions in Normal and Disease States. *Pharmacol Rev* 60, 1–42.
- Johannessen, C.M., Boehm, J.S., Kim, S.Y., Thomas, S.R., Wardwell, L., Johnson, L.A., Emery, C.M., Stransky, N., Cogdill, A.P., Barretina, J., et al. (2010). COT drives resistance to RAF inhibition through MAP kinase pathway reactivation. *Nature* 468, 968–972.
- Johannessen, C.M., Johnson, L.A., Piccioni, F., Townes, A., Frederick, D.T., Donahue, M.K., Narayan, R., Flaherty, K.T., Wargo, J.A., Root, D.E., et al. (2013). A melanocyte lineage program confers resistance to MAP kinase pathway inhibition. *Nature* 504, 138–142.
- Johansson, P., Aoude, L.G., Wadt, K., Glasson, W.J., Warriar, S.K., Hewitt, A.W., Kiilgaard, J.F., Heegaard, S., Isaacs, T., Franchina, M., et al. (2016). Deep sequencing of uveal melanoma identifies a recurrent mutation in PLCB4. *Oncotarget* 7, 4624–4631.
- Johnson, J.E., Goulding, R.E., Ding, Z., Partovi, A., Anthony, K.V., Beaulieu, N., Tazmini, G., Cornell, R.B., and Kay, R.J. (2007). Differential membrane binding and diacylglycerol recognition by C1 domains of RasGRPs. *Biochem J* 406, 223–236.
- Jönsson, E., Forsman, A., Einarsdottir, I.E., Egnér, B., Ruohonen, K., and Björnsson, B.T. (2006). Circulating levels of cholecystokinin and gastrin-releasing peptide in rainbow trout fed different diets. *Gen Comp Endocrinol* 148, 187–194.
- Jørgensen, K., Skrede, M., Cruciani, V., Mikalsen, S.-O., Slipicevic, A., and Flørenes, V.A. (2005). Phorbol ester phorbol-12-myristate-13-acetate promotes anchorage-independent growth and survival of melanomas through MEK-independent activation of ERK1/2. *Biochem Biophys Res Commun* 329, 266–274.
- Kamb, A., Gruis, N.A., Weaver-Feldhaus, J., Liu, Q., Harshman, K., Tavtigian, S.V., Stockert, E., Day, R.S., Johnson, B.E., and Skolnick, M.H. (1994). A cell cycle regulator potentially involved in genesis of many tumor types. *Science* 264, 436–440.
- Kashatus, D.F. (2013). Ral GTPases in tumorigenesis: emerging from the shadows. *Exp Cell Res* 319, 2337–2342.
- Kawakami, A., and Fisher, D.E. (2017). The master role of microphthalmia-associated

transcription factor in melanocyte and melanoma biology. *Lab Invest* 97, 649–656.

Kefford, R., Beith, J.M., Van Hazel, G.A., Millward, M., Trotter, J.M., Wyld, D.K., Kusic, R., Shreeniwas, R., Morganti, A., Ballmer, A., et al. (2007). A Phase II study of bosentan, a dual endothelin receptor antagonist, as monotherapy in patients with stage IV metastatic melanoma. *Invest New Drugs* 25, 247–252.

Kefford, R.F., Clingan, P.R., Brady, B., Ballmer, A., Morganti, A., and Hersey, P. (2010). A randomized, double-blind, placebo-controlled study of high-dose bosentan in patients with stage IV metastatic melanoma receiving first-line dacarbazine chemotherapy. *Molecular Cancer* 9, 69.

Kelley, M.J., Linnoila, R.I., Avis, I.L., Georgiadis, M.S., Cuttitta, F., Mulshine, J.L., and Johnson, B.E. (1997). Antitumor activity of a monoclonal antibody directed against gastrin-releasing peptide in patients with small cell lung cancer. *Chest* 112, 256–261.

Kelly, P., Stemmler, L.N., Madden, J.F., Fields, T.A., Daaka, Y., and Casey, P.J. (2006a). A role for the G12 family of heterotrimeric G proteins in prostate cancer invasion. *J Biol Chem* 281, 26483–26490.

Kelly, P., Moeller, B.J., Juneja, J., Booden, M.A., Der, C.J., Daaka, Y., Dewhirst, M.W., Fields, T.A., and Casey, P.J. (2006b). The G12 family of heterotrimeric G proteins promotes breast cancer invasion and metastasis. *Proc Natl Acad Sci U S A* 103, 8173–8178.

Kemler, R. (1992). Classical cadherins. *Semin Cell Biol* 3, 149–155.

Khaled, M., Levy, C., and Fisher, D.E. (2010). Control of melanocyte differentiation by a MITF–PDE4D3 homeostatic circuit. *Genes Dev* 24, 2276–2281.

Kim, A., and Cohen, M.S. (2016). The discovery of vemurafenib for the treatment of BRAF-mutated metastatic melanoma. *Expert Opin Drug Discov* 11, 907–916.

Kim, N.-G., Koh, E., Chen, X., and Gumbiner, B.M. (2011). E-cadherin mediates contact inhibition of proliferation through Hippo signaling-pathway components. *Proc Natl Acad Sci U S A* 108, 11930–11935.

Kirkwood, J.M., Ibrahim, J.G., Sosman, J.A., Sondak, V.K., Agarwala, S.S., Ernstoff, M.S., and Rao, U. (2001). High-dose interferon alfa-2b significantly prolongs relapse-free and overall survival compared with the GM2-KLH/QS-21 vaccine in patients with resected stage IIB-III melanoma: results of intergroup trial E1694/S9512/C509801. *J Clin Oncol* 19, 2370–2380.

Kirova, Y.M., Chen, J., Rabarijaona, L.I., Piedbois, Y., and Le Bourgeois, J.P. (1999). Radiotherapy as palliative treatment for metastatic melanoma. *Melanoma Res* 9, 611–613.

Kirschner, L.S., Carney, J.A., Pack, S.D., Taymans, S.E., Giatzakis, C., Cho, Y.S., Cho-Chung, Y.S., and Stratakis, C.A. (2000). Mutations of the gene encoding the protein kinase A type I-alpha regulatory subunit in patients with the Carney complex. *Nat Genet* 26, 89–92.

Klein, A., Sagi-Assif, O., Meshel, T., Telerman, A., Izraely, S., Ben-Menachem, S., Bayry, J., Marzese, D.M., Ohe, S., Hoon, D.S.B., et al. (2017). CCR4 is a determinant of melanoma brain metastasis. *Oncotarget* 8, 31079–31091.

Kleinau, G., Neumann, S., Grüters, A., Krude, H., and Biebermann, H. (2013). Novel insights on thyroid-stimulating hormone receptor signal transduction. *Endocr Rev* 34, 691–724.

Kleinboelting, S., Diaz, A., Moniot, S., van den Heuvel, J., Weyand, M., Levin, L.R., Buck, J., and Steegborn, C. (2014). Crystal structures of human soluble adenylyl cyclase reveal mechanisms of catalysis and of its activation through bicarbonate. *Proc Natl Acad Sci U S A* 111, 3727–3732.

Koboldt, D.C., Fulton, R.S., McLellan, M.D., Schmidt, H., Kalicki-Veizer, J., McMichael, J.F., Fulton, L.L., Dooling, D.J., Ding, L., Mardis, E.R., et al. (2012). Comprehensive molecular portraits of human breast tumours. *Nature* *490*, 61–70.

Koikov, L., Starner, R.J., Swope, V.B., Upadhyay, P., Hashimoto, Y., Freeman, K.T., Knittel, J.J., Haskell-Luevano, C., and Abdel-Malek, Z.A. (2021). Development of hMC1R Selective Small Agonists for Sunless Tanning and Prevention of Genotoxicity of UV in Melanocytes. *J Invest Dermatol* *141*, 1819–1829.

Körner, M., Waser, B., Rehmann, R., and Reubi, J.C. (2014). Early over-expression of GRP receptors in prostatic carcinogenesis. *Prostate* *74*, 217–224.

von Koschembahr, A.M., Swope, V.B., Starner, R.J., and Abdel-Malek, Z.A. (2015). Endothelin-1 protects human melanocytes from UV-induced DNA damage by activating JNK and p38 signalling pathways. *Exp Dermatol* *24*, 269–274.

Kostenis, E., Pfeil, E.M., and Annala, S. (2020). Heterotrimeric Gq proteins as therapeutic targets? *Journal of Biological Chemistry* *295*, 5206–5215.

Kourtidis, A., Ngok, S.P., and Anastasiadis, P.Z. (2013). p120 catenin: an essential regulator of cadherin stability, adhesion-induced signaling, and cancer progression. *Prog Mol Biol Transl Sci* *116*, 409–432.

Krauthammer, M., Kong, Y., Ha, B.H., Evans, P., Bacchiocchi, A., McCusker, J.P., Cheng, E., Davis, M.J., Goh, G., Choi, M., et al. (2012). Exome sequencing identifies recurrent somatic RAC1 mutations in melanoma. *Nat Genet* *44*, 1006–1014.

Kreiseder, B., Orel, L., Bujnow, C., Buschek, S., Pflueger, M., Schuett, W., Hundsberger, H., de Martin, R., and Wiesner, C. (2013). α -Catulin downregulates E-cadherin and promotes melanoma progression and invasion. *International Journal of Cancer* *132*, 521–530.

Krupnick, J.G., Goodman, O.B., Keen, J.H., and Benovic, J.L. (1997). Arrestin/clathrin interaction. Localization of the clathrin binding domain of nonvisual arrestins to the carboxy terminus. *J Biol Chem* *272*, 15011–15016.

Kumar, U., and Singh, S. (2020). Role of Somatostatin in the Regulation of Central and Peripheral Factors of Satiety and Obesity. *Int J Mol Sci* *21*, 2568.

Kumar, S., Park, S.H., Cieply, B., Schupp, J., Killiam, E., Zhang, F., Rimm, D.L., and Frisch, S.M. (2011). A Pathway for the Control of Anoikis Sensitivity by E-Cadherin and Epithelial-to-Mesenchymal Transition ∇ . *Mol Cell Biol* *31*, 4036–4051.

Kumasaka, M.Y., Yajima, I., Hossain, K., Iida, M., Tsuzuki, T., Ohno, T., Takahashi, M., Yanagisawa, M., and Kato, M. (2010). A Novel Mouse Model for De novo Melanoma. *Cancer Res* *70*, 24–29.

Kunz, M., Moeller, S., Koczan, D., Lorenz, P., Wenger, R.H., Glocker, M.O., Thiesen, H.-J., Gross, G., and Ibrahim, S.M. (2003). Mechanisms of Hypoxic Gene Regulation of Angiogenesis Factor Cyr61 in Melanoma Cells *. *Journal of Biological Chemistry* *278*, 45651–45660.

Kuphal, S., Poser, I., Jobin, C., Hellerbrand, C., and Bosserhoff, A.K. (2004). Loss of E-cadherin leads to upregulation of NF κ B activity in malignant melanoma. *Oncogene* *23*, 8509–8519.

Kwon, H., Kim, J., and Jho, E.-H. (2021). Role of the Hippo pathway and mechanisms for controlling cellular localization of YAP/TAZ. *FEBS J*.

Kwong, J., Kulbe, H., Wong, D., Chakravarty, P., and Balkwill, F. (2009). An antagonist of the chemokine receptor CXCR4 induces mitotic catastrophe in ovarian cancer cells. *Mol Cancer Ther* *8*, 1893–1905.

- La Porta, C.A., Porro, D., and Comolli, R. (1998). Opposite effects of TPA on G1/S transition and on cell size in the low metastatic B16F1 with respect to high metastatic BL6 murine melanoma cells. *Cancer Lett* 132, 159–164.
- Lachmann, A., Xu, H., Krishnan, J., Berger, S.I., Mazloom, A.R., and Ma'ayan, A. (2010). ChEA: transcription factor regulation inferred from integrating genome-wide ChIP-X experiments. *Bioinformatics* 26, 2438–2444.
- Ladenheim, E.E., Taylor, J.E., Coy, D.H., Moore, K.A., and Moran, T.H. (1996). Hindbrain GRP receptor blockade antagonizes feeding suppression by peripherally administered GRP. *American Journal of Physiology-Regulatory, Integrative and Comparative Physiology* 271, R180–R184.
- Ladenheim, E.E., Hampton, L.L., Whitney, A.C., White, W.O., Battey, J.F., and Moran, T.H. (2002). Disruptions in feeding and body weight control in gastrin-releasing peptide receptor deficient mice. *J Endocrinol* 174, 273–281.
- Lahav, R., Heffner, G., and Patterson, P.H. (1999). An endothelin receptor B antagonist inhibits growth and induces cell death in human melanoma cells in vitro and in vivo. *Proc Natl Acad Sci U S A* 96, 11496–11500.
- Lahav, R., Suvà, M.-L., Rimoldi, D., Patterson, P.H., and Stamenkovic, I. (2004). Endothelin receptor B inhibition triggers apoptosis and enhances angiogenesis in melanomas. *Cancer Res* 64, 8945–8953.
- Lämmermann, T., and Kastenmüller, W. (2019). Concepts of GPCR-controlled navigation in the immune system. *Immunological Reviews* 289, 205–231.
- Larkin, J., Chiarion-Sileni, V., Gonzalez, R., Grob, J.-J., Rutkowski, P., Lao, C.D., Cowey, C.L., Schadendorf, D., Wagstaff, J., Dummer, R., et al. (2019). Five-Year Survival with Combined Nivolumab and Ipilimumab in Advanced Melanoma. *New England Journal of Medicine* 381, 1535–1546.
- Larue, L., and Bellacosa, A. (2005). Epithelial-mesenchymal transition in development and cancer: role of phosphatidylinositol 3' kinase/AKT pathways. *Oncogene* 24, 7443–7454.
- Larue, L., and Delmas, V. (2006). The WNT/Beta-catenin pathway in melanoma. *Front Biosci* 11, 733–742.
- Larue, L., Ohsugi, M., Hirchenhain, J., and Kemler, R. (1994). E-cadherin null mutant embryos fail to form a trophectoderm epithelium. *PNAS* 91, 8263–8267.
- Larue, L., Antos, C., Butz, S., Huber, O., Delmas, V., Dominis, M., and Kemler, R. (1996). A role for cadherins in tissue formation. *Development* 122, 3185–3194.
- Larue, L., de Vuyst, F., and Delmas, V. (2013). Modeling melanoblast development. *Cell. Mol. Life Sci.* 70, 1067–1079.
- Laurette, P., Strub, T., Koludrovic, D., Keime, C., Le Gras, S., Seberg, H., Van Otterloo, E., Imrichova, H., Siddaway, R., Aerts, S., et al. (2015). Transcription factor MITF and remodeler BRG1 define chromatin organisation at regulatory elements in melanoma cells. *ELife* 4, e06857.
- Lee, E., Salic, A., Krüger, R., Heinrich, R., and Kirschner, M.W. (2003). The Roles of APC and Axin Derived from Experimental and Theoretical Analysis of the Wnt Pathway. *PLOS Biology* 1, e10.
- Lee, H.-Y., Kléber, M., Hari, L., Brault, V., Suter, U., Taketo, M.M., Kemler, R., and Sommer, L. (2004). Instructive Role of Wnt/ β -Catenin in Sensory Fate Specification in Neural Crest Stem Cells. *Science* 303, 1020–1023.

- Lehrer, E.J., Peterson, J., Brown, P.D., Sheehan, J.P., Quiñones-Hinojosa, A., Zaorsky, N.G., and Trifiletti, D.M. (2019). Treatment of brain metastases with stereotactic radiosurgery and immune checkpoint inhibitors: An international meta-analysis of individual patient data. *Radiother Oncol* 130, 104–112.
- Leiter, U., Stadler, R., Mauch, C., Hohenberger, W., Brockmeyer, N.H., Berking, C., Sunderkötter, C., Kaatz, M., Schatton, K., Lehmann, P., et al. (2019). Final Analysis of DeCOG-SLT Trial: No Survival Benefit for Complete Lymph Node Dissection in Patients With Melanoma With Positive Sentinel Node. *J Clin Oncol* 37, 3000–3008.
- Leopoldt, D., Hanck, T., Exner, T., Maier, U., Wetzker, R., and Nürnberg, B. (1998). Gβγ Stimulates Phosphoinositide 3-Kinase-γ by Direct Interaction with Two Domains of the Catalytic p110 Subunit *. *Journal of Biological Chemistry* 273, 7024–7029.
- Levine, L., Lucci, J.A., Pazdrak, B., Cheng, J.-Z., Guo, Y.-S., Townsend, C.M., and Hellmich, M.R. (2003). Bombesin stimulates nuclear factor kappa B activation and expression of proangiogenic factors in prostate cancer cells. *Cancer Res* 63, 3495–3502.
- Li, J., Zhao, X., Wang, D., He, W., Zhang, S., Cao, W., Huang, Y., Wang, L., Zhou, S., and Luo, K. (2016a). Up-regulated expression of phospholipase C, β1 is associated with tumor cell proliferation and poor prognosis in hepatocellular carcinoma. *Onco Targets Ther* 9, 1697–1706.
- Li, L., Wang, B.H., Wang, S., Moalim-Nour, L., Mohib, K., Lohnes, D., and Wang, L. (2010a). Individual Cell Movement, Asymmetric Colony Expansion, Rho-Associated Kinase, and E-Cadherin Impact the Clonogenicity of Human Embryonic Stem Cells. *Biophysical Journal* 98, 2442–2451.
- Li, P., Sun, T., Yuan, Q., Pan, G., Zhang, J., and Sun, D. (2016b). The expressions of NEDD9 and E-cadherin correlate with metastasis and poor prognosis in triple-negative breast cancer patients. *Onco Targets Ther* 9, 5751–5759.
- Li, X., Lv, Y., Yuan, A., Yi, S., Ma, Y., and Li, Z. (2010b). Gastrin-releasing peptide promotes the growth of HepG2 cells via EGFR-independent ERK1/2 activation. *Oncol Rep* 24, 441–448.
- Lin, D.-C., Xu, L., Ding, L.-W., Sharma, A., Liu, L.-Z., Yang, H., Tan, P., Vadgama, J., Karlan, B.Y., Lester, J., et al. (2013). Genomic and functional characterizations of phosphodiesterase subtype 4D in human cancers. *Proc Natl Acad Sci U S A* 110, 6109–6114.
- Lin, Y., Jian, X., Lin, Z., Kroog, G.S., Mantey, S., Jensen, R.T., Battey, J., and Northup, J. (2000). Two amino acids in the sixth transmembrane segment of the mouse gastrin-releasing peptide receptor are important for receptor activation. *J Pharmacol Exp Ther* 294, 1053–1062.
- Liu, F., Visser, M., Duffy, D.L., Hysi, P.G., Jacobs, L.C., Lao, O., Zhong, K., Walsh, S., Chaitanya, L., Wollstein, A., et al. (2015). Genetics of skin color variation in Europeans: genome-wide association studies with functional follow-up. *Hum Genet* 134, 823–835.
- Liu, Q., Tong, D., Liu, G., Yi, Y., Zhang, D., Zhang, J., Zhang, Y., Huang, Z., Li, Y., Chen, R., et al. (2017). Carney complex with PRKAR1A gene mutation. *Medicine (Baltimore)* 96, e8999.
- Liu, W.F., Nelson, C.M., Pirone, D.M., and Chen, C.S. (2006). E-cadherin engagement stimulates proliferation via Rac1. *J Cell Biol* 173, 431–441.
- Liu, X., Carlisle, D.L., Swick, M.C., Gaither-Davis, A., Grandis, J.R., and Siegfried, J.M. (2007). Gastrin-releasing peptide activates Akt through the epidermal growth factor receptor pathway and abrogates the effect of gefitinib. *Exp Cell Res* 313, 1361–1372.
- Loh, C.-Y., Chai, J.Y., Tang, T.F., Wong, W.F., Sethi, G., Shanmugam, M.K., Chong, P.P., and Looi, C.Y.

- (2019). The E-Cadherin and N-Cadherin Switch in Epithelial-to-Mesenchymal Transition: Signaling, Therapeutic Implications, and Challenges. *Cells* 8, 1118.
- Long, G.V., Fung, C., Menzies, A.M., Pupo, G.M., Carlino, M.S., Hyman, J., Shahheydari, H., Tembe, V., Thompson, J.F., Saw, R.P., et al. (2014). Increased MAPK reactivation in early resistance to dabrafenib/trametinib combination therapy of BRAF-mutant metastatic melanoma. *Nat Commun* 5, 5694.
- Long, G.V., Flaherty, K.T., Stroyakovskiy, D., Gogas, H., Levchenko, E., Braud, F. de, Larkin, J., Garbe, C., Jouary, T., Hauschild, A., et al. (2017). Dabrafenib plus trametinib versus dabrafenib monotherapy in patients with metastatic BRAF V600E/K-mutant melanoma: long-term survival and safety analysis of a phase 3 study. *Annals of Oncology* 28, 1631–1639.
- Lou, H., Lu, J., Choi, E.B., Oh, M.H., Jeong, M., Barmettler, S., Zhu, Z., and Zheng, T. (2017). Expression of IL-22 in the Skin Causes Th2-Biased Immunity, Epidermal Barrier Dysfunction, and Pruritus via Stimulating Epithelial Th2 Cytokines and the GRP Pathway. *The Journal of Immunology* 198, 2543–2555.
- Luciani, F., Champeval, D., Herbette, A., Denat, L., Aylaj, B., Martinozzi, S., Ballotti, R., Kemler, R., Goding, C.R., De Vuyst, F., et al. (2011). Biological and mathematical modeling of melanocyte development. *Development* 138, 3943–3954.
- Lui, J.W., Moore, S.P.G., Huang, L., Ogomori, K., Li, Y., and Lang, D. (2021). YAP facilitates melanoma migration through regulation of actin-related protein 2/3 complex subunit 5 (ARPC5). *Pigment Cell Melanoma Res.*
- Luke, J.J., Flaherty, K.T., Ribas, A., and Long, G.V. (2017). Targeted agents and immunotherapies: optimizing outcomes in melanoma. *Nature Reviews Clinical Oncology* 14, 463–482.
- Luttrell, L.M., Ferguson, S.S., Daaka, Y., Miller, W.E., Maudsley, S., Della Rocca, G.J., Lin, F., Kawakatsu, H., Owada, K., Luttrell, D.K., et al. (1999). Beta-arrestin-dependent formation of beta2 adrenergic receptor-Src protein kinase complexes. *Science* 283, 655–661.
- Luttrell, L.M., Roudabush, F.L., Choy, E.W., Miller, W.E., Field, M.E., Pierce, K.L., and Lefkowitz, R.J. (2001). Activation and targeting of extracellular signal-regulated kinases by β -arrestin scaffolds. *PNAS* 98, 2449–2454.
- Lyon, A.M., and Tesmer, J.J.G. (2013). Structural Insights into Phospholipase C- β Function. *Mol Pharmacol* 84, 488–500.
- Lyons, J., Bastian, B.C., and McCormick, F. (2013). MC1R and cAMP signaling inhibit cdc25B activity and delay cell cycle progression in melanoma cells. *Proc Natl Acad Sci U S A* 110, 13845–13850.
- Ma, M., Dai, J., Tang, H., Xu, T., Yu, S., Si, L., Cui, C., Sheng, X., Chi, Z., Mao, L., et al. (2019). MicroRNA-23a-3p Inhibits Mucosal Melanoma Growth and Progression through Targeting Adenylate Cyclase 1 and Attenuating cAMP and MAPK Pathways. *Theranostics* 9, 945–960.
- Ma, Y., Wang, L., He, F., Yang, J., Ding, Y., Ge, S., Fan, X., Zhou, Y., Xu, X., and Jia, R. (2021). LACTB suppresses melanoma progression by attenuating PP1A and YAP interaction. *Cancer Lett* 506, 67–82.
- Magro, C.M., Neil Crowson, A., Desman, G., and Zippin, J.H. (2012). Soluble Adenylyl Cyclase Antibody Profile as a Diagnostic Adjunct in the Assessment of Pigmented Lesions. *Arch Dermatol* 148, 335–344.
- Mahajan, A., Ahmed, S., McAleer, M.F., Weinberg, J.S., Li, J., Brown, P., Settle, S., Prabhu, S.S., Lang,

- F.F., Levine, N., et al. (2017). Post-operative stereotactic radiosurgery versus observation for completely resected brain metastases: a single-centre, randomised, controlled, phase 3 trial. *Lancet Oncol* 18, 1040–1048.
- Marambaud, P., Shioi, J., Serban, G., Georgakopoulos, A., Sarnier, S., Nagy, V., Baki, L., Wen, P., Efthimiopoulos, S., Shao, Z., et al. (2002). A presenilin-1/ γ -secretase cleavage releases the E-cadherin intracellular domain and regulates disassembly of adherens junctions. *EMBO J* 21, 1948–1956.
- Marasigan, V., Güvenç, C., van den Oord, J.J., Stas, M., Boecxstaens, V., Bechter, O., Wolter, P., Lambrechts, D., and Garmyn, M. (2019). Melanoma susceptibility variant rs869330 in the MTAP gene is associated with melanoma outcome. *Melanoma Res* 29, 590–595.
- Marín, Y.E., Namkoong, J., Cohen-Solal, K., Shin, S.-S., Martino, J.J., Oka, M., and Chen, S. (2006). Stimulation of oncogenic metabotropic glutamate receptor 1 in melanoma cells activates ERK1/2 via PKCepsilon. *Cell Signal* 18, 1279–1286.
- Marquette, A., André, J., Bagot, M., Bensussan, A., and Dumaz, N. (2011). ERK and PDE4 cooperate to induce RAF isoform switching in melanoma. *Nat Struct Mol Biol* 18, 584–591.
- Marrone, B.F., Meurer, L., Moretto, A., Kleina, W., and Schwartzmann, G. (2013). Expression of gastrin-releasing peptide receptor in patients with cutaneous malignant melanoma. *Clin Exp Dermatol* 38, 707–712.
- Martin, E.L., Rens-Domiano, S., Schatz, P.J., and Hamm, H.E. (1996). Potent peptide analogues of a G protein receptor-binding region obtained with a combinatorial library. *J Biol Chem* 271, 361–366.
- Martínez-Vicente, I., Abrisqueta, M., Herraiz, C., Jiménez-Cervantes, C., García-Borrón, J.C., and Olivares, C. (2020). Functional characterization of a C-terminal splice variant of the human melanocortin 1 receptor. *Exp Dermatol* 29, 610–615.
- Matsuoka, H., Tsubaki, M., Yamazoe, Y., Ogaki, M., Satou, T., Itoh, T., Kusunoki, T., and Nishida, S. (2009). Tamoxifen inhibits tumor cell invasion and metastasis in mouse melanoma through suppression of PKC/MEK/ERK and PKC/PI3K/Akt pathways. *Experimental Cell Research* 315, 2022–2032.
- Mattei, J., Achcar, R.D., Cano, C.H., Macedo, B.R., Meurer, L., Batlle, B.S., Groshong, S.D., Kulczynski, J.M., Roesler, R., Dal Lago, L., et al. (2014). Gastrin-releasing peptide receptor expression in lung cancer. *Arch Pathol Lab Med* 138, 98–104.
- Mayumi, N., Watanabe, E., Norose, Y., Watari, E., Kawana, S., Geijtenbeek, T.B.H., and Takahashi, H. (2013). E-cadherin interactions are required for Langerhans cell differentiation. *Eur J Immunol* 43, 270–280.
- Maziarz, M., Leyme, A., Marivin, A., Luebbers, A., Patel, P.P., Chen, Z., Sprang, S.R., and Garcia-Marcos, M. (2018). Atypical activation of the G protein G α q by the oncogenic mutation Q209P. *J Biol Chem* 293, 19586–19599.
- McDermott, D., Lebbé, C., Hodi, F.S., Maio, M., Weber, J.S., Wolchok, J.D., Thompson, J.A., and Balch, C.M. (2014). Durable benefit and the potential for long-term survival with immunotherapy in advanced melanoma. *Cancer Treatment Reviews* 40, 1056–1064.
- McDonald, P.H., Chow, C.-W., Miller, W.E., Laporte, S.A., Field, M.E., Lin, F.-T., Davis, R.J., and Lefkowitz, R.J. (2000). β -Arrestin 2: A Receptor-Regulated MAPK Scaffold for the Activation of JNK3. *Science* 290, 1574–1577.

- McDonald, T.J., Jörnvall, H., Nilsson, G., Vagne, M., Ghatei, M., Bloom, S.R., and Mutt, V. (1979). Characterization of a gastrin releasing peptide from porcine non-antral gastric tissue. *Biochem Biophys Res Commun* *90*, 227–233.
- McQuade, J.L., and Davies, M.A. (2018). Estrogen returns to the stage in melanoma. *Pigment Cell & Melanoma Research* *31*, 554–555.
- Meloche, S., and Pouysségur, J. (2007). The ERK1/2 mitogen-activated protein kinase pathway as a master regulator of the G1- to S-phase transition. *Oncogene* *26*, 3227–3239.
- Mendoza, M.C., Er, E.E., Zhang, W., Ballif, B.A., Elliott, H.L., Danuser, G., and Blenis, J. (2011). ERK-MAPK drives lamellipodia protrusion by activating the WAVE2 regulatory complex. *Mol Cell* *41*, 661–671.
- Mervic, L., Leiter, U., Meier, F., Eigentler, T., Forschner, A., Metzler, G., Bartenjev, I., Büttner, P., and Garbe, C. (2011). Sex differences in survival of cutaneous melanoma are age dependent: an analysis of 7338 patients. *Melanoma Research* *21*, 244–252.
- Mesri, E.A., Cesarman, E., and Boshoff, C. (2010). Kaposi's sarcoma herpesvirus/ Human herpesvirus-8 (KSHV/HHV8), and the oncogenesis of Kaposi's sarcoma. *Nat Rev Cancer* *10*, 707–719.
- Mikesh, L.M., Kumar, M., Erdag, G., Hogan, K.T., Molhoek, K.R., Mayo, M.W., and Slingluff, C.L. (2010). Evaluation of Molecular Markers of Mesenchymal Phenotype in Melanoma. *Melanoma Res* *20*, 485–495.
- Miller, W.E., Maudsley, S., Ahn, S., Khan, K.D., Luttrell, L.M., and Lefkowitz, R.J. (2000). beta-arrestin1 interacts with the catalytic domain of the tyrosine kinase c-SRC. Role of beta-arrestin1-dependent targeting of c-SRC in receptor endocytosis. *J Biol Chem* *275*, 11312–11319.
- Minami, K., Ueda, N., Ishimoto, K., and Tsujiuchi, T. (2020). Lysophosphatidic acid receptor-2 (LPA2)-mediated signaling enhances chemoresistance in melanoma cells treated with anticancer drugs. *Mol Cell Biochem* *469*, 89–95.
- Minamino, N., Kangawa, K., and Matsuo, H. (1983). Neuromedin B: a novel bombesin-like peptide identified in porcine spinal cord. *Biochem Biophys Res Commun* *114*, 541–548.
- Minamino, N., Kangawa, K., and Matsuo, H. (1984). Neuromedin C: a bombesin-like peptide identified in porcine spinal cord. *Biochem Biophys Res Commun* *119*, 14–20.
- Mitra, D., Luo, X., Morgan, A., Wang, J., Hoang, M.P., Lo, J., Guerrero, C.R., Lennerz, J.K., Mihm, M.C., Wargo, J.A., et al. (2012). An ultraviolet-radiation-independent pathway to melanoma carcinogenesis in the red hair/fair skin background. *Nature* *491*, 449–453.
- Mo, J.-S., Yu, F.-X., Gong, R., Brown, J.H., and Guan, K.-L. (2012). Regulation of the Hippo-YAP pathway by protease-activated receptors (PARs). *Genes Dev.* *26*, 2138–2143.
- Mobley, A.K., Braeuer, R.R., Kamiya, T., Shoshan, E., and Bar-Eli, M. (2012). Driving transcriptional regulators in melanoma metastasis. *Cancer Metastasis Rev* *31*, 621–632.
- Modlin, I.M., Lamers, C.B., and Walsh, J.H. (1981). Stimulation of canine pancreatic polypeptide, gastrin, and gastric acid secretion by ranatensin, litorin, bombesin nonapeptide and substance P. *Regul Pept* *1*, 279–288.
- Molina-Ortiz, I., Bartolomé, R.A., Hernández-Varas, P., Colo, G.P., and Teixidó, J. (2009). Overexpression of E-cadherin on Melanoma Cells Inhibits Chemokine-promoted Invasion Involving p190RhoGAP/p120ctn-dependent Inactivation of RhoA *. *Journal of Biological Chemistry* *284*, 15147–15157.

- Möller, I., Murali, R., Müller, H., Wiesner, T., Jakkett, L.A., Scholz, S.L., Cosgarea, I., van de Nes, J.A., Sucker, A., Hillen, U., et al. (2017). Activating cysteinyl leukotriene receptor 2 (CYSLTR2) mutations in blue nevi. *Mod Pathol* *30*, 350–356.
- Molven, A., Grimstvedt, M.B., Steine, S.J., Harland, M., Avril, M.-F., Hayward, N.K., and Akslen, L.A. (2005). A large Norwegian family with inherited malignant melanoma, multiple atypical nevi, and CDK4 mutation. *Genes, Chromosomes and Cancer* *44*, 10–18.
- Montaner, S., Kufareva, I., Abagyan, R., and Gutkind, J.S. (2013). Molecular mechanisms deployed by virally encoded G protein-coupled receptors in human diseases. *Annu Rev Pharmacol Toxicol* *53*, 331–354.
- Moody, T.W., Staley, J., Zia, F., Coy, D.H., and Jensen, R.T. (1992). Neuromedin B binds with high affinity, elevates cytosolic calcium and stimulates the growth of small-cell lung cancer cell lines. *J Pharmacol Exp Ther* *263*, 311–317.
- Moody, T.W., Leyton, J., Garcia-Marin, L., and Jensen, R.T. (2003). Nonpeptide gastrin releasing peptide receptor antagonists inhibit the proliferation of lung cancer cells. *Eur J Pharmacol* *474*, 21–29.
- Moody, T.W., Ramos-Alvarez, I., Moreno, P., Mantey, S.A., Ridnour, L., Wink, D., and Jensen, R.T. (2017). Endothelin causes transactivation of the EGFR and HER2 in non-small cell lung cancer cells. *Peptides* *90*, 90–99.
- Moore, A.R., Ran, L., Guan, Y., Sher, J.J., Hitchman, T.D., Zhang, J.Q., Hwang, C., Walzak, E.G., Shoushtari, A.N., Monette, S., et al. (2018). GNA11 Q209L Mouse Model Reveals RasGRP3 as an Essential Signaling Node in Uveal Melanoma. *Cell Rep* *22*, 2455–2468.
- Morgat, C., MacGrogan, G., Brouste, V., Vélasco, V., Sévenet, N., Bonnefoi, H., Fernandez, P., Debled, M., and Hindié, E. (2017). Expression of Gastrin-Releasing Peptide Receptor in Breast Cancer and Its Association with Pathologic, Biologic, and Clinical Parameters: A Study of 1,432 Primary Tumors. *J Nucl Med* *58*, 1401–1407.
- Morin, P.J., Sparks, A.B., Korinek, V., Barker, N., Clevers, H., Vogelstein, B., and Kinzler, K.W. (1997). Activation of beta-catenin-Tcf signaling in colon cancer by mutations in beta-catenin or APC. *Science* *275*, 1787–1790.
- Müller, J., Krijgsman, O., Tsoi, J., Robert, L., Hugo, W., Song, C., Kong, X., Possik, P.A., Cornelissen-Steijger, P.D.M., Geukes Foppen, M.H., et al. (2014). Low MITF/AXL ratio predicts early resistance to multiple targeted drugs in melanoma. *Nat Commun* *5*, 5712.
- Nagalla, S.R., Barry, B.J., Creswick, K.C., Eden, P., Taylor, J.T., and Spindel, E.R. (1995). Cloning of a receptor for amphibian [Phe¹³]bombesin distinct from the receptor for gastrin-releasing peptide: identification of a fourth bombesin receptor subtype (BB4). *Proc Natl Acad Sci U S A* *92*, 6205–6209.
- Nagarsheth, N., Wicha, M.S., and Zou, W. (2017). Chemokines in the cancer microenvironment and their relevance in cancer immunotherapy. *Nat Rev Immunol* *17*, 559–572.
- Nakagawa, T., Hocart, S.J., Schumann, M., Tapia, J.A., Mantey, S.A., Coy, D.H., Tokita, K., Katsuno, T., and Jensen, R.T. (2005). Identification of key amino acids in the gastrin-releasing peptide receptor (GRPR) responsible for high affinity binding of gastrin-releasing peptide (GRP). *Biochem Pharmacol* *69*, 579–593.
- Nallet-Staub, F., Marsaud, V., Li, L., Gilbert, C., Dodier, S., Bataille, V., Sudol, M., Herlyn, M., and Mauviel, A. (2014). Pro-invasive activity of the Hippo pathway effectors YAP and TAZ in cutaneous melanoma. *J Invest Dermatol* *134*, 123–132.

Nam, J.-S., Ino, Y., Sakamoto, M., and Hirohashi, S. (2002). Src family kinase inhibitor PP2 restores the E-cadherin/catenin cell adhesion system in human cancer cells and reduces cancer metastasis. *Clin Cancer Res* 8, 2430–2436.

Narayan, S., Draviam, E., Rajaraman, S., and Singh, P. (1991). High-affinity binding sites for bombesin on mouse colonic mucosal membranes. *Mol Cell Biochem* 106, 31–39.

Narita, M., Murata, T., Shimizu, K., Nakagawa, T., Sugiyama, T., Inui, M., Hiramoto, K., and Tagawa, T. (2007). A role for cyclic nucleotide phosphodiesterase 4 in regulation of the growth of human malignant melanoma cells. *Oncology Reports* 17, 1133–1139.

Nathanson, K.L., Martin, A.-M., Wubbenhorst, B., Greshock, J., Letrero, R., D’Andrea, K., O’Day, S., Infante, J.R., Falchook, G.S., Arkenau, H.-T., et al. (2013). Tumor genetic analyses of patients with metastatic melanoma treated with the BRAF inhibitor dabrafenib (GSK2118436). *Clin Cancer Res* 19, 4868–4878.

Nell, R.J., Menger, N.V., Versluis, M., Luyten, G.P.M., Verdijk, R.M., Madigan, M.C., Jager, M.J., and van der Velden, P.A. (2021). Involvement of mutant and wild-type CYSLTR2 in the development and progression of uveal nevi and melanoma. *BMC Cancer* 21, 164.

Nemlich, Y., Baruch, E.N., Besser, M.J., Shoshan, E., Bar-Eli, M., Anafi, L., Barshack, I., Schachter, J., Ortenberg, R., and Markel, G. (2018). ADAR1-mediated regulation of melanoma invasion. *Nat Commun* 9, 2154.

Neto, A., and Ceol, C.J. (2018). Melanoma-associated GRM3 variants dysregulate melanosome trafficking and cAMP signaling. *Pigment Cell & Melanoma Research* 31, 115–119.

Nie, X., Liu, H., Liu, L., Wang, Y.-D., and Chen, W.-D. (2020). Emerging Roles of Wnt Ligands in Human Colorectal Cancer. *Frontiers in Oncology* 10, 1341.

Niebergall-Roth, E., and Singer, M.V. (2001). Central and peripheral neural control of pancreatic exocrine secretion. *J Physiol Pharmacol* 52, 523–538.

Niessen, C.M. (2007). Tight junctions/adherens junctions: basic structure and function. *J Invest Dermatol* 127, 2525–2532.

Niessen, C.M., Leckband, D., and Yap, A.S. (2011). Tissue Organization by Cadherin Adhesion Molecules: Dynamic Molecular and Cellular Mechanisms of Morphogenetic Regulation. *Physiological Reviews* 91, 691–731.

Nishina, H., Nimota, K., Kukimoto, I., Maehama, T., Takahashi, K., Hoshino, S., Kanaho, Y., and Katada, T. (1995). Significance of Thr182 in the nucleotide-exchange and GTP-hydrolysis reactions of the alpha subunit of GTP-binding protein Gi2. *J Biochem* 118, 1083–1089.

Nosrati, A., and Wei, M.L. (2014). Sex disparities in melanoma outcomes: The role of biology. *Archives of Biochemistry and Biophysics* 563, 42–50.

Nsengimana, J., Laye, J., Fila, A., O’Shea, S., Muralidhar, S., Poźniak, J., Droop, A., Chan, M., Walker, C., Parkinson, L., et al. (2018). β -Catenin-mediated immune evasion pathway frequently operates in primary cutaneous melanomas. *J Clin Invest* 128, 2048–2063.

Oakley, R.H., Laporte, S.A., Holt, J.A., Caron, M.G., and Barak, L.S. (2000). Differential Affinities of Visual Arrestin, β Arrestin1, and β Arrestin2 for G Protein-coupled Receptors Delineate Two Major Classes of Receptors*. *Journal of Biological Chemistry* 275, 17201–17210.

Oas, R.G., Nanes, B.A., Esimai, C.C., Vincent, P.A., García, A.J., and Kowalczyk, A.P. (2013). p120-catenin and β -catenin differentially regulate cadherin adhesive function. *Mol Biol Cell* 24, 704–714.

- O'Hayre, M., Vázquez-Prado, J., Kufareva, I., Stawiski, E.W., Handel, T.M., Seshagiri, S., and Gutkind, J.S. (2013). The Emerging Mutational Landscape of G-proteins and G-protein Coupled Receptors in Cancer. *Nat Rev Cancer* 13, 412–424.
- Ohtani, Y., Harada, T., Funasaka, Y., Nakao, K., Takahara, C., Abdel-Daim, M., Sakai, N., Saito, N., Nishigori, C., and Aiba, A. (2008). Metabotropic glutamate receptor subtype-1 is essential for in vivo growth of melanoma. *Oncogene* 27, 7162–7170.
- Oka, M., Kikkawa, U., and Nishigori, C. (2008). Protein kinase C-betaII represses hepatocyte growth factor-induced invasion by preventing the association of adapter protein Gab1 and phosphatidylinositol 3-kinase in melanoma cells. *J Invest Dermatol* 128, 188–195.
- Okereke, I. (2015). Surgical management of malignant melanoma of the lung. *Melanoma Manag* 2, 301–303.
- Oliveira, P.G., Grespan, R., Pinto, L.G., Meurer, L., Brenol, J.C.T., Roesler, R., Schwartzmann, G., Cunha, F.Q., and Xavier, R.M. (2011). Protective effect of RC-3095, an antagonist of the gastrin-releasing peptide receptor, in experimental arthritis. *Arthritis Rheum* 63, 2956–2965.
- Omori, K., and Kotera, J. (2007). Overview of PDEs and Their Regulation. *Circulation Research*.
- Onder, T.T., Gupta, P.B., Mani, S.A., Yang, J., Lander, E.S., and Weinberg, R.A. (2008). Loss of E-cadherin promotes metastasis via multiple downstream transcriptional pathways. *Cancer Res* 68, 3645–3654.
- Ostojić, J., Yoon, Y.-S., Sonntag, T., Nguyen, B., Vaughan, J.M., Shokhirev, M., and Montminy, M. (2021). Transcriptional co-activator regulates melanocyte differentiation and oncogenesis by integrating cAMP and MAPK/ERK pathways. *Cell Reports* 35, 109136.
- Pace, A.M., Wong, Y.H., and Bourne, H.R. (1991). A mutant alpha subunit of Gi2 induces neoplastic transformation of Rat-1 cells. *Proc Natl Acad Sci U S A* 88, 7031–7035.
- Padmanaban, V., Krol, I., Suhail, Y., Szczerba, B.M., Aceto, N., Bader, J.S., and Ewald, A.J. (2019). E-cadherin is required for metastasis in multiple models of breast cancer. *Nature* 573, 439–444.
- Paradis, J.S., Acosta, M., Saddawi-Konefka, R., Kishore, A., Lubrano, S., Gomes, F., Arang, N., Tiago, M., Coma, S., Wu, X., et al. (2021). Synthetic Lethal Screens Reveal Cotargeting FAK and MEK as a Multimodal Precision Therapy for GNAQ-Driven Uveal Melanoma. *Clin Cancer Res* 27, 3190–3200.
- Paraiso, K.H.T., Xiang, Y., Rebecca, V.W., Abel, E.V., Chen, Y.A., Munko, A.C., Wood, E., Fedorenko, I.V., Sondak, V.K., Anderson, A.R.A., et al. (2011). PTEN loss confers BRAF inhibitor resistance to melanoma cells through the suppression of BIM expression. *Cancer Res* 71, 2750–2760.
- Parisiadou, L., Fassa, A., Fotinopoulou, A., Bethani, I., and Efthimiopoulos, S. (2004). Presenilin 1 and cadherins: stabilization of cell-cell adhesion and proteolysis-dependent regulation of transcription. *Neurodegener Dis* 1, 184–191.
- Park, H.Y., Russakovsky, V., Ohno, S., and Gilchrist, B.A. (1993). The beta isoform of protein kinase C stimulates human melanogenesis by activating tyrosinase in pigment cells. *J Biol Chem* 268, 11742–11749.
- Park, H.-Y., Wu, H., Killoran, C.E., and Gilchrist, B.A. (2004). The receptor for activated C-kinase-I (RACK-I) anchors activated PKC-beta on melanosomes. *J Cell Sci* 117, 3659–3668.
- Pascale, R.M., Calvisi, D.F., Simile, M.M., Feo, C.F., and Feo, F. (2020). The Warburg Effect 97 Years after Its Discovery. *Cancers* 12, 2819.

- Patel, M., Kawano, T., Suzuki, N., Hamakubo, T., Karginov, A.V., and Kozasa, T. (2014). $G\alpha_{13}$ /PDZ-RhoGEF/RhoA Signaling Is Essential for Gastrin-Releasing Peptide Receptor-Mediated Colon Cancer Cell Migration. *Mol Pharmacol* *86*, 252–262.
- Patel, O., Dumesny, C., Shulkes, A., and Baldwin, G.S. (2007). C-Terminal Fragments of the Gastrin-Releasing Peptide Precursor Stimulate Cell Proliferation via a Novel Receptor. *Endocrinology* *148*, 1330–1339.
- Pathria, G., Garg, B., Garg, K., Wagner, C., and Wagner, S.N. (2016). Dual c-Jun N-terminal kinase-cyclin D1 and extracellular signal-related kinase-c-Jun disjunction in human melanoma. *Br J Dermatol* *175*, 1221–1231.
- Patton, E.E., Widlund, H.R., Kutok, J.L., Kopani, K.R., Amatruda, J.F., Murphey, R.D., Berghmans, S., Mayhall, E.A., Traver, D., Fletcher, C.D.M., et al. (2005). BRAF mutations are sufficient to promote nevi formation and cooperate with p53 in the genesis of melanoma. *Curr Biol* *15*, 249–254.
- Pećina-Slaus, N., Zigmund, M., Kusec, V., Martić, T.N., Cacić, M., and Slaus, M. (2007). E-cadherin and beta-catenin expression patterns in malignant melanoma assessed by image analysis. *J. Cutan. Pathol.* *34*, 239–246.
- Pereira, P.J.S., Machado, G.D.B., Danesi, G.M., Canevese, F.F., Reddy, V.B., Pereira, T.C.B., Bogo, M.R., Cheng, Y.-C., Laedermann, C., Talbot, S., et al. (2015). GRPR/PI3Ky: Partners in Central Transmission of Itch. *J. Neurosci.* *35*, 16272–16281.
- Peres, J., Damerell, V., Chauhan, J., Popovic, A., Desprez, P.-Y., Galibert, M.-D., Goding, C.R., and Prince, S. (2021). TBX3 Promotes Melanoma Migration by Transcriptional Activation of ID1, which Prevents Activation of E-Cadherin by MITF. *J Invest Dermatol* *141*, 2250-2260.e2.
- Perrot, C.Y., Gilbert, C., Marsaud, V., Postigo, A., Javelaud, D., and Mauviel, A. (2013). GLI2 cooperates with ZEB1 for transcriptional repression of CDH1 expression in human melanoma cells. *Pigment Cell Melanoma Res* *26*, 861–873.
- Perry, S.J., Baillie, G.S., Kohout, T.A., McPhee, I., Magiera, M.M., Ang, K.L., Miller, W.E., McLean, A.J., Conti, M., Houslay, M.D., et al. (2002). Targeting of Cyclic AMP Degradation to β 2-Adrenergic Receptors by β -Arrestins. *Science* *298*, 834–836.
- Persson, K., Pacini, G., Sundler, F., and Ahrén, B. (2002). Islet function phenotype in gastrin-releasing peptide receptor gene-deficient mice. *Endocrinology* *143*, 3717–3726.
- Petit, V., and Larue, L. (2016). Any route for melanoblasts to colonize the skin! *Experimental Dermatology* *25*, 669–673.
- Petit, V., Raymond, J., Alberti, C., Pouteaux, M., Gallagher, S.J., Nguyen, M.Q., Aplin, A.E., Delmas, V., and Larue, L. (2019). C57BL/6 congenic mouse NRASQ61K melanoma cell lines are highly sensitive to the combination of Mek and Akt inhibitors in vitro and in vivo. *Pigment Cell & Melanoma Research* *32*, 829–841.
- Pettersson, M., and Ahrén, B. (1987). Gastrin releasing peptide (GRP): effects on basal and stimulated insulin and glucagon secretion in the mouse. *Peptides* *8*, 55–60.
- Pfeil, E.M., Brands, J., Merten, N., Vögtle, T., Vescovo, M., Rick, U., Albrecht, I.-M., Heycke, N., Kawakami, K., Ono, Y., et al. (2020). Heterotrimeric G Protein Subunit $G\alpha_q$ Is a Master Switch for $G\beta\gamma$ -Mediated Calcium Mobilization by Gi-Coupled GPCRs. *Mol Cell* *80*, 940-954.e6.
- Pinski, J., Schally, A.V., Halmos, G., and Szepeshazi, K. (1993). Effect of somatostatin analog RC-160 and bombesin/gastrin releasing peptide antagonist RC-3095 on growth of PC-3 human prostate-cancer xenografts in nude mice. *Int J Cancer* *55*, 963–967.

- Pla, P., and Monsoro-Burq, A.H. (2018). The neural border: Induction, specification and maturation of the territory that generates neural crest cells. *Dev Biol* 444 Suppl 1, S36–S46.
- Plagge, A., Kelsey, G., and Germain-Lee, E.L. (2008). Physiological functions of the imprinted *Gnas* locus and its protein variants *Gas* and *XLas* in human and mouse. *Journal of Endocrinology* 196, 193–214.
- Pollock, P.M., Cohen-Solal, K., Sood, R., Namkoong, J., Martino, J.J., Koganti, A., Zhu, H., Robbins, C., Makalowska, I., Shin, S.-S., et al. (2003). Melanoma mouse model implicates metabotropic glutamate signaling in melanocytic neoplasia. *Nat Genet* 34, 108–112.
- Poser, I., Domínguez, D., Herreros, A.G. de, Varnai, A., Buettner, R., and Bosserhoff, A.K. (2001). Loss of E-cadherin Expression in Melanoma Cells Involves Up-regulation of the Transcriptional Repressor Snail *. *Journal of Biological Chemistry* 276, 24661–24666.
- Poulikakos, P.I., Persaud, Y., Janakiraman, M., Kong, X., Ng, C., Moriceau, G., Shi, H., Atefi, M., Titz, B., Gabay, M.T., et al. (2011). RAF inhibitor resistance is mediated by dimerization of aberrantly spliced BRAF(V600E). *Nature* 480, 387–390.
- Prasad, M.S., Charney, R.M., and García-Castro, M.I. (2019). Specification and formation of the neural crest: Perspectives on lineage segregation. *Genesis* 57, e23276.
- Prickett, T.D., Wei, X., Cardenas-Navia, I., Teer, J.K., Lin, J.C., Walia, V., Gartner, J., Jiang, J., Cherukuri, P.F., Molinolo, A., et al. (2011). Exon capture analysis of G protein-coupled receptors identifies activating mutations in *GRM3* in melanoma. *Nat Genet* 43, 1119–1126.
- Ragnarsson, L., Andersson, Å., Thomas, W.G., and Lewis, R.J. (2019). Mutations in the NPxxY motif stabilize pharmacologically distinct conformational states of the α 1B- and β 2-adrenoceptors. *Sci Signal* 12, eaas9485.
- Ramahi, E., Choi, J., Fuller, C.D., and Eng, T.Y. (2013). Merkel Cell Carcinoma. *Am J Clin Oncol* 36, 299–309.
- Rashid, S., and Tsao, H. (2021). Effect of the COVID-19 Pandemic on Delayed Skin Cancer Services. *Dermatol Clin* 39, 627–637.
- Rate, W.R., Solin, L.J., and Turrisi, A.T. (1988). Palliative radiotherapy for metastatic malignant melanoma: brain metastases, bone metastases, and spinal cord compression. *Int J Radiat Oncol Biol Phys* 15, 859–864.
- Rizeq, B., and Malki, M.I. (2020). The Role of CCL21/CCR7 Chemokine Axis in Breast Cancer Progression. *Cancers (Basel)* 12, 1036.
- Robert, C., Ribas, A., Schachter, J., Arance, A., Grob, J.-J., Mortier, L., Daud, A., Carlino, M.S., McNeil, C.M., Lotem, M., et al. (2019a). Pembrolizumab versus ipilimumab in advanced melanoma (KEYNOTE-006): post-hoc 5-year results from an open-label, multicentre, randomised, controlled, phase 3 study. *The Lancet Oncology* 20, 1239–1251.
- Robert, C., Grob, J.J., Stroyakovskiy, D., Karaszewska, B., Hauschild, A., Levchenko, E., Chiarion Sileni, V., Schachter, J., Garbe, C., Bondarenko, I., et al. (2019b). Five-Year Outcomes with Dabrafenib plus Trametinib in Metastatic Melanoma. *New England Journal of Medicine* 381, 626–636.
- Robertson, A.G., Shih, J., Yau, C., Gibb, E.A., Oba, J., Mungall, K.L., Hess, J.M., Uzunangelov, V., Walter, V., Danilova, L., et al. (2017). Integrative Analysis Identifies Four Molecular and Clinical Subsets in Uveal Melanoma. *Cancer Cell* 32, 204–220.e15.
- Robles-Espinoza, C.D., Harland, M., Ramsay, A.J., Aoude, L.G., Quesada, V., Ding, Z., Pooley, K.A.,

- Pritchard, A.L., Tiffen, J.C., Petljak, M., et al. (2014). POT1 loss-of-function variants predispose to familial melanoma. *Nat Genet* *46*, 478–481.
- Rodien, P., Ho, S.-C., Vlaeminck, V., Vassart, G., and Costagliola, S. (2003). Activating mutations of TSH receptor. *Ann Endocrinol (Paris)* *64*, 12–16.
- Rodríguez, C.I., and Setaluri, V. (2018). EPAC mediates the dual role of cAMP signaling in melanoma. *Oncoscience* *6*, 283–284.
- Rodríguez, C.I., Castro-Pérez, E., Prabhakar, K., Block, L., Longley, B.J., Wisinski, J.A., Kimple, M.E., and Setaluri, V. (2017). EPAC–RAP1 Axis-Mediated Switch in the Response of Primary and Metastatic Melanoma to Cyclic AMP. *Mol Cancer Res* *15*, 1792–1802.
- Rodríguez, C.I., Castro-Pérez, E., Longley, B.J., and Setaluri, V. (2018). Elevated cyclic AMP levels promote BRAFCA/Pten-/- mouse melanoma growth but pCREB is negatively correlated with human melanoma progression. *Cancer Lett* *414*, 268–277.
- Roh, M.R., Eliades, P., Gupta, S., and Tsao, H. (2015). Genetics of melanocytic nevi. *Pigment Cell & Melanoma Research* *28*, 661–672.
- Rovati, G.E., Capra, V., and Neubig, R.R. (2007). The Highly Conserved DRY Motif of Class A G Protein-Coupled Receptors: Beyond the Ground State. *Mol Pharmacol* *71*, 959–964.
- van Roy, F., and Berx, G. (2008). The cell-cell adhesion molecule E-cadherin. *Cell Mol Life Sci* *65*, 3756–3788.
- Rozenberg, A., Inoue, K., Kandori, H., and Bédj, O. (2021). Microbial Rhodopsins: The Last Two Decades. *Annu Rev Microbiol* *75*, 427–447.
- Rozengurt, E. (1998). Signal transduction pathways in the mitogenic response to G protein-coupled neuropeptide receptor agonists. *J Cell Physiol* *177*, 507–517.
- Ruff, M., Schiffmann, E., Terranova, V., and Pert, C.B. (1985). Neuropeptides are chemoattractants for human tumor cells and monocytes: a possible mechanism for metastasis. *Clin Immunol Immunopathol* *37*, 387–396.
- Saito, H., Yasumoto, K.-I., Takeda, K., Takahashi, K., Fukuzaki, A., Orikasa, S., and Shibahara, S. (2002). Melanocyte-specific microphthalmia-associated transcription factor isoform activates its own gene promoter through physical interaction with lymphoid-enhancing factor 1. *J Biol Chem* *277*, 28787–28794.
- Sakamoto, H., Matsuda, K.-I., Zuloaga, D.G., Hongu, H., Wada, E., Wada, K., Jordan, C.L., Breedlove, S.M., and Kawata, M. (2008). Sexually dimorphic gastrin releasing peptide system in the spinal cord controls male reproductive functions. *Nat Neurosci* *11*, 634–636.
- Sakamoto, H., Takanami, K., Zuloaga, D.G., Matsuda, K., Jordan, C.L., Breedlove, S.M., and Kawata, M. (2009a). Androgen Regulates the Sexually Dimorphic Gastrin-Releasing Peptide System in the Lumbar Spinal Cord that Mediates Male Sexual Function. *Endocrinology* *150*, 3672–3679.
- Sakamoto, H., Matsuda, K.-I., Zuloaga, D.G., Nishiura, N., Takanami, K., Jordan, C.L., Breedlove, S.M., and Kawata, M. (2009b). Stress Affects a Gastrin-Releasing Peptide System in the Spinal Cord That Mediates Sexual Function: Implications for Psychogenic Erectile Dysfunction. *PLOS ONE* *4*, e4276.
- Salic, A., Lee, E., Mayer, L., and Kirschner, M.W. (2000). Control of beta-catenin stability: reconstitution of the cytoplasmic steps of the wnt pathway in *Xenopus* egg extracts. *Mol Cell* *5*, 523–532.

- Samson, K. (2015). Melanoma: Immunotherapy-Induced Vitiligo Documented as Linked to Better Outcomes. *Oncology Times* 37, 64–65.
- Sánchez-Más, J., Guillo, L.A., Zanna, P., Jiménez-Cervantes, C., and García-Borrón, J.C. (2005). Role of G protein-coupled receptor kinases in the homologous desensitization of the human and mouse melanocortin 1 receptors. *Mol Endocrinol* 19, 1035–1048.
- Sandhu, S., McNeil, C.M., LoRusso, P., Patel, M.R., Kabbarah, O., Li, C., Sanabria, S., Flanagan, W.M., Yeh, R.-F., Brunstein, F., et al. (2020). Phase I study of the anti-endothelin B receptor antibody-drug conjugate DEDN6526A in patients with metastatic or unresectable cutaneous, mucosal, or uveal melanoma. *Invest New Drugs* 38, 844–854.
- Sassone-Corsi, P. (2012). The Cyclic AMP Pathway. *Cold Spring Harb Perspect Biol* 4, a011148.
- Schäfer, A., Haenig, B., Erupathil, J., Strickner, P., Sabato, D., Welford, R.W.D., Klaeyle, L., Simon, E., Krepler, C., Brafford, P., et al. (2021). Inhibition of endothelin-B receptor signaling synergizes with MAPK pathway inhibitors in BRAF mutated melanoma. *Oncogene* 40, 1659–1673.
- Schechtman, D., and Mochly-Rosen, D. (2001). Adaptor proteins in protein kinase C-mediated signal transduction. *Oncogene* 20, 6339–6347.
- Schepsky, A., Bruser, K., Gunnarsson, G.J., Goodall, J., Hallsson, J.H., Goding, C.R., Steingrimsdottir, E., and Hecht, A. (2006). The microphthalmia-associated transcription factor Mitf interacts with beta-catenin to determine target gene expression. *Mol. Cell. Biol.* 26, 8914–8927.
- Schiffner, S., Chen, S., Becker, J.C., and Bosserhoff, A.-K. (2012). Highly pigmented Tg(Grm1) mouse melanoma develops non-pigmented melanoma cells in distant metastases. *Exp Dermatol* 21, 786–788.
- Schönwasser, D.C., Marais, R.M., Marshall, C.J., and Parker, P.J. (1998). Activation of the mitogen-activated protein kinase/extracellular signal-regulated kinase pathway by conventional, novel, and atypical protein kinase C isoforms. *Mol Cell Biol* 18, 790–798.
- Schubert, M.L., Hightower, J., Coy, D.H., and Makhlof, G.M. (1991). Regulation of acid secretion by bombesin/GRP neurons of the gastric fundus. *Am J Physiol* 260, G156-160.
- Schwartzmann, G., DiLeone, L.P., Horowitz, M., Schunemann, D., Cancelli, A., Pereira, A.S., Richter, M., Souza, F., da Rocha, A.B., Souza, F.H., et al. (2006). A phase I trial of the bombesin/gastrin-releasing peptide (BN/GRP) antagonist RC3095 in patients with advanced solid malignancies. *Invest New Drugs* 24, 403–412.
- Schwartz, M.R., Luo, L., and Berwick, M. (2019). Sex Differences in Melanoma. *Curr Epidemiol Rep* 6, 112–118.
- Scott, M.C., Wakamatsu, K., Ito, S., Kadekaro, A.L., Kobayashi, N., Groden, J., Kavanagh, R., Takakuwa, T., Virador, V., Hearing, V.J., et al. (2002). Human melanocortin 1 receptor variants, receptor function and melanocyte response to UV radiation. *J Cell Sci* 115, 2349–2355.
- Sellers, L.A., Alderton, F., Carruthers, A.M., Schindler, M., and Humphrey, P.P. (2000). Receptor isoforms mediate opposing proliferative effects through gbetagamma-activated p38 or Akt pathways. *Mol Cell Biol* 20, 5974–5985.
- Seneschal, J., Boniface, K., D’Arino, A., and Picardo, M. (2021). An update on Vitiligo pathogenesis. *Pigment Cell & Melanoma Research* 34, 236–243.
- Senese, N.B., Rasenick, M.M., and Traynor, J.R. (2018). The Role of G-proteins and G-protein Regulating Proteins in Depressive Disorders. *Front Pharmacol* 9, 1289.

- Sengelaub, C.A., Navrazhina, K., Ross, J.B., Halberg, N., and Tavazoie, S.F. (2016). PTPRN2 and PLC β 1 promote metastatic breast cancer cell migration through PI(4,5)P $_2$ -dependent actin remodeling. *EMBO J* 35, 62–76.
- Shaffer, S.M., Dunagin, M.C., Torborg, S.R., Torre, E.A., Emert, B., Krepler, C., Beqiri, M., Sproesser, K., Brafford, P.A., Xiao, M., et al. (2017). Rare cell variability and drug-induced reprogramming as a mode of cancer drug resistance. *Nature* 546, 431–435.
- Shah, K.V., Chien, A.J., Yee, C., and Moon, R.T. (2008). CTLA-4 Is a Direct Target of Wnt/ β -Catenin Signaling and Is Expressed in Human Melanoma Tumors. *Journal of Investigative Dermatology* 128, 2870–2879.
- Shalaeva, D.N., Galperin, M.Y., and Mulkidjanian, A.Y. (2015). Eukaryotic G protein-coupled receptors as descendants of prokaryotic sodium-translocating rhodopsins. *Biol Direct* 10, 63.
- Shan, L., Emanuel, R.L., Dewald, D., Torday, J.S., Asokanathan, N., Wada, K., Wada, E., and Sunday, M.E. (2004). Bombesin-like peptide receptor gene expression, regulation, and function in fetal murine lung. *American Journal of Physiology-Lung Cellular and Molecular Physiology* 286, L165–L173.
- Shapiro, L., and Weis, W.I. (2009). Structure and Biochemistry of Cadherins and Catenins. *Cold Spring Harb Perspect Biol* 1, a003053.
- Sharma, A., Trivedi, N.R., Zimmerman, M.A., Tuveson, D.A., Smith, C.D., and Robertson, G.P. (2005). Mutant V599E-Raf Regulates Growth and Vascular Development of Malignant Melanoma Tumors. *Cancer Res* 65, 2412–2421.
- Shaulian, E., and Karin, M. (2001). AP-1 in cell proliferation and survival. *Oncogene* 20, 2390–2400.
- Shenoy, S.K., and Lefkowitz, R.J. (2003). Multifaceted roles of beta-arrestins in the regulation of seven-membrane-spanning receptor trafficking and signalling. *Biochem J* 375, 503–515.
- Shi, H., Hugo, W., Kong, X., Hong, A., Koya, R.C., Moriceau, G., Chodon, T., Guo, R., Johnson, D.B., Dahlman, K.B., et al. (2014). Acquired Resistance and Clonal Evolution in Melanoma during BRAF Inhibitor Therapy. *Cancer Discov* 4, 80–93.
- Shields, B.D., Koss, B., Taylor, E.M., Storey, A.J., West, K.L., Byrum, S.D., Mackintosh, S.G., Edmondson, R., Mahmoud, F., Shalin, S.C., et al. (2019). Loss of E-Cadherin Inhibits CD103 Antitumor Activity and Reduces Checkpoint Blockade Responsiveness in Melanoma. *Cancer Res* 79, 1113–1123.
- Shriver, S.P., Bourdeau, H.A., Gubish, C.T., Tirpak, D.L., Davis, A.L.G., Luketich, J.D., and Siegfried, J.M. (2000). Sex-Specific Expression of Gastrin-Releasing Peptide Receptor: Relationship to Smoking History and Risk of Lung Cancer. *JNCI: Journal of the National Cancer Institute* 92, 24–33.
- Skalhegg, B.S., and Tasken, K. (2000). Specificity in the cAMP/PKA signaling pathway. Differential expression, regulation, and subcellular localization of subunits of PKA. *Front Biosci* 5, D678–693.
- Smith, M.P., Rowling, E.J., Miskolczi, Z., Ferguson, J., Spoerri, L., Haass, N.K., Sloss, O., McEntegart, S., Arozarena, I., von Kriegsheim, A., et al. (2017a). Targeting endothelin receptor signalling overcomes heterogeneity driven therapy failure. *EMBO Mol Med* 9, 1011–1029.
- Smith, M.P., Rowling, E.J., Miskolczi, Z., Ferguson, J., Spoerri, L., Haass, N.K., Sloss, O., McEntegart, S., Arozarena, I., von Kriegsheim, A., et al. (2017b). Targeting endothelin receptor signalling overcomes heterogeneity driven therapy failure. *EMBO Mol Med* 9, 1011–1029.

Smith, R., Healy, E., Siddiqui, S., Flanagan, N., Steijlen, P.M., Rosdahl, I., Jacques, J.P., Rogers, S., Turner, R., Jackson, I.J., et al. (1998). Melanocortin 1 receptor variants in an Irish population. *J Invest Dermatol* *111*, 119–122.

Smrcka, A.V., Hepler, J.R., Brown, K.O., and Sternweis, P.C. (1991). Regulation of polyphosphoinositide-specific phospholipase C activity by purified Gq. *Science* *251*, 804–807.

Snyder, A., Makarov, V., Merghoub, T., Yuan, J., Zaretsky, J.M., Desrichard, A., Walsh, L.A., Postow, M.A., Wong, P., Ho, T.S., et al. (2014). Genetic Basis for Clinical Response to CTLA-4 Blockade in Melanoma. *New England Journal of Medicine* *371*, 2189–2199.

Spangler, B., Vardimon, L., Bosserhoff, A.K., and Kuphal, S. (2011). Post-transcriptional regulation controlled by E-cadherin is important for c-Jun activity in melanoma. *Pigment Cell Melanoma Res* *24*, 148–164.

Sparks, A.B., Morin, P.J., Vogelstein, B., and Kinzler, K.W. (1998). Mutational analysis of the APC/beta-catenin/Tcf pathway in colorectal cancer. *Cancer Res* *58*, 1130–1134.

Spindel, E.R., Giladi, E., Brehm, P., Goodman, R.H., and Segerson, T.P. (1990). Cloning and functional characterization of a complementary DNA encoding the murine fibroblast bombesin/gastrin-releasing peptide receptor. *Mol Endocrinol* *4*, 1956–1963.

Spranger, S., Bao, R., and Gajewski, T.F. (2015). Melanoma-intrinsic β -catenin signalling prevents anti-tumour immunity. *Nature* *523*, 231–235.

Squires, P.E., Meloche, R.M., and Buchan, A.M. (1999). Bombesin-evoked gastrin release and calcium signaling in human antral G cells in culture. *Am J Physiol* *276*, G227–237.

Sun, J., Lu, F., He, H., Shen, J., Messina, J., Mathew, R., Wang, D., Sarnaik, A.A., Chang, W.-C., Kim, M., et al. (2014). STIM1- and Orai1-mediated Ca^{2+} oscillation orchestrates invadopodium formation and melanoma invasion. *J Cell Biol* *207*, 535–548.

Sun, T., Jiao, L., Wang, Y., Yu, Y., and Ming, L. (2018). SIRT1 induces epithelial-mesenchymal transition by promoting autophagic degradation of E-cadherin in melanoma cells. *Cell Death Dis* *9*, 1–10.

Sun, Y.-G., Zhao, Z.-Q., Meng, X.-L., Yin, J., Liu, X.-Y., and Chen, Z.-F. (2009). Cellular basis of itch sensation. *Science* *325*, 1531–1534.

Sung, H., Ferlay, J., Siegel, R.L., Laversanne, M., Soerjomataram, I., Jemal, A., and Bray, F. (2021). Global Cancer Statistics 2020: GLOBOCAN Estimates of Incidence and Mortality Worldwide for 36 Cancers in 185 Countries. *CA: A Cancer Journal for Clinicians* *71*, 209–249.

Suomivuori, C.-M., Latorraca, N.R., Wingler, L.M., Eismann, S., King, M.C., Kleinhenz, A.L.W., Skiba, M.A., Staus, D.P., Kruse, A.C., Lefkowitz, R.J., et al. (2020). Molecular mechanism of biased signaling in a prototypical G protein-coupled receptor. *Science* *367*, 881–887.

Sutherland, E.W., and Rall, T.W. (1958). Fractionation and characterization of a cyclic adenine ribonucleotide formed by tissue particles. *J Biol Chem* *232*, 1077–1091.

Suzuki, I., Cone, R.D., Im, S., Nordlund, J., and Abdel-Malek, Z.A. (1996). Binding of melanotropic hormones to the melanocortin receptor MC1R on human melanocytes stimulates proliferation and melanogenesis. *Endocrinology* *137*, 1627–1633.

Suzuki, N., Nakamura, S., Mano, H., and Kozasa, T. (2003). G α 12 activates Rho GTPase through tyrosine-phosphorylated leukemia-associated RhoGEF. *Proc Natl Acad Sci U S A* *100*, 733–738.

- Swope, V.B., and Abdel-Malek, Z.A. (2016). Significance of the Melanocortin 1 and Endothelin B Receptors in Melanocyte Homeostasis and Prevention of Sun-Induced Genotoxicity. *Front Genet* 7, 146.
- Swope, V.B., Starner, R.J., Rauck, C., and Abdel-Malek, Z.A. (2020). Endothelin-1 and α -melanocortin have redundant effects on global genome repair in UV-irradiated human melanocytes despite distinct signaling pathways. *Pigment Cell & Melanoma Research* 33, 293–304.
- Szepeshazi, K., Schally, A.V., Halmos, G., Lamharzi, N., Groot, K., and Horvath, J.E. (1997). A single in vivo administration of bombesin antagonist RC-3095 reduces the levels and mRNA expression of epidermal growth factor receptors in MXT mouse mammary cancers. *PNAS* 94, 10913–10918.
- Taché, Y., Marki, W., Rivier, J., Vale, W., and Brown, M. (1981). Central Nervous System Inhibition of Gastric Secretion in the Rat by Gastrin-Releasing Peptide, a Mammalian Bombesin. *Gastroenterology* 81, 298–302.
- Tagliabue, E., Gandini, S., Bellocco, R., Maisonneuve, P., Newton-Bishop, J., Polsky, D., Lazovich, D., Kanetsky, P.A., Ghiorzo, P., Gruis, N.A., et al. (2018). MC1R variants as melanoma risk factors independent of at-risk phenotypic characteristics: a pooled analysis from the M-SKIP project. *Cancer Manag Res* 10, 1143–1154.
- Takada, R., Satomi, Y., Kurata, T., Ueno, N., Norioka, S., Kondoh, H., Takao, T., and Takada, S. (2006). Monounsaturated Fatty Acid Modification of Wnt Protein: Its Role in Wnt Secretion. *Developmental Cell* 11, 791–801.
- Takahashi, M., Li, Y., Dillon, T.J., and Stork, P.J.S. (2017). Phosphorylation of Rap1 by cAMP-dependent Protein Kinase (PKA) Creates a Binding Site for KSR to Sustain ERK Activation by cAMP. *Journal of Biological Chemistry* 292, 1449–1461.
- Takanami, K., Uta, D., Matsuda, K.I., Kawata, M., Carstens, E., Sakamoto, T., and Sakamoto, H. (2021). Estrogens influence female itch sensitivity via the spinal gastrin-releasing peptide receptor neurons. *Proc Natl Acad Sci U S A* 118, e2103536118.
- Tamate, H.B., and Takeuchi, T. (1984). Action of the e Locus of Mice in the Response of Pheomelanin Hair Follicles to α -Melanocyte-Stimulating Hormone in Vitro. *Science* 224, 1241–1242.
- Tamura, A., Halaban, R., Moellmann, G., Cowan, J.M., Lerner, M.R., and Lerner, A.B. (1987). Normal murine melanocytes in culture. *In Vitro Cell Dev Biol* 23, 519–522.
- Tan, S., Zhao, Z., Qiao, Y., Zhang, B., Zhang, T., Zhang, M., Qi, J., Wang, X., Meng, M., and Zhou, Q. (2021). Activation of the tumor suppressive Hippo pathway by triptonide as a new strategy to potently inhibit aggressive melanoma cell metastasis. *Biochemical Pharmacology* 185, 114423.
- Tanaka, Y., Sano, T., Qian, Z.R., and Hirokawa, M. (2004). Expression of adhesion molecules and cytokeratin 20 in merkel cell carcinomas. *Endocr Pathol* 15, 117–129.
- Tang, A., Amagai, M., Granger, L.G., Stanley, J.R., and Uddy, M.C. (1993). Adhesion of epidermal Langerhans cells to keratinocytes mediated by E-cadherin. *Nature* 361, 82–85.
- Tanimura, S., and Takeda, K. (2017). ERK signalling as a regulator of cell motility. *The Journal of Biochemistry* 162, 145–154.
- Tarlé, R.G., Silva de Castro, C.C., do Nascimento, L.M., and Mira, M.T. (2015). Polymorphism of the E-cadherin gene CDH1 is associated with susceptibility to vitiligo. *Exp Dermatol* 24, 300–302.
- Tas, F. (2012). Metastatic Behavior in Melanoma: Timing, Pattern, Survival, and Influencing

Factors.

Taskén, K., Skålhegg, B.S., Taskén, K.A., Solberg, R., Knutsen, H.K., Levy, F.O., Sandberg, M., Orstavik, S., Larsen, T., Johansen, A.K., et al. (1997). Structure, function, and regulation of human cAMP-dependent protein kinases. *Adv Second Messenger Phosphoprotein Res* 31, 191–204.

Taylor, S.J., Chae, H.Z., Rhee, S.G., and Exton, J.H. (1991). Activation of the beta 1 isozyme of phospholipase C by alpha subunits of the Gq class of G proteins. *Nature* 350, 516–518.

Teixeira, C., Stang, S.L., Zheng, Y., Beswick, N.S., and Stone, J.C. (2003). Integration of DAG signaling systems mediated by PKC-dependent phosphorylation of RasGRP3. *Blood* 102, 1414–1420.

The Cancer Genome Atlas Network (2015). Genomic Classification of Cutaneous Melanoma. *Cell* 161, 1681–1696.

Thomas, S.M., Grandis, J.R., Wentzel, A.L., Gooding, W.E., Lui, V.W.Y., and Siegfried, J.M. (2005). Gastrin-Releasing Peptide Receptor Mediates Activation of the Epidermal Growth Factor Receptor in Lung Cancer Cells. *Neoplasia* 7, 426–431.

Thul, P.J., Åkesson, L., Wiking, M., Mahdessian, D., Geladaki, A., Ait Blal, H., Alm, T., Asplund, A., Björk, L., Breckels, L.M., et al. (2017). A subcellular map of the human proteome. *Science* 356, eaal3321.

Tian, X., Liu, Z., Niu, B., Zhang, J., Tan, T.K., Lee, S.R., Zhao, Y., Harris, D.C.H., and Zheng, G. (2011). E-Cadherin/ β -Catenin Complex and the Epithelial Barrier. *J Biomed Biotechnol* 2011, 567305.

Tizpa, E., Young, H.J., Bonjoc, K.-J.C., Chang, C.-W., Liu, Y., Foulks, J.M., and Chaudhry, A. (2020). Role of AXL in metastatic melanoma and impact of TP-0903 as a novel therapeutic option for melanoma brain metastasis. *JCO* 38, e22021–e22021.

Tod, B.M., Schneider, J.W., Bowcock, A.M., Visser, W.I., and Kotze, M.J. (2020). The tumor genetics of acral melanoma: What should a dermatologist know? *JAAD International* 1, 135–147.

Tong, G.-X., Mody, K., Wang, Z., Hamele-Bena, D., Nikiforova, M.N., and Nikiforov, Y.E. (2015). Mutations of TSHR and TP53 Genes in an Aggressive Clear Cell Follicular Carcinoma of the Thyroid. *Endocr Pathol* 26, 315–319.

Tsopanoglou, N.E., and Maragoudakis, M.E. (2004). Role of thrombin in angiogenesis and tumor progression. *Semin Thromb Hemost* 30, 63–69.

Tsubaki, M., Matsuoka, H., Yamamoto, C., Kato, C., Ogaki, M., Satou, T., Itoh, T., Kusunoki, T., Tanimori, Y., and Nishida, S. (2007). The protein kinase C inhibitor, H7, inhibits tumor cell invasion and metastasis in mouse melanoma via suppression of ERK1/2. *Clin Exp Metastasis* 24, 431–438.

Tucci, M. g., Lucarini, G., Brancorsini, D., Zizzi, A., Pugnali, A., Giacchetti, A., Ricotti, G., and Biagini, G. (2007). Involvement of E-cadherin, β -catenin, Cdc42 and CXCR4 in the progression and prognosis of cutaneous melanoma. *British Journal of Dermatology* 157, 1212–1216.

Tunggal, J.A., Helfrich, I., Schmitz, A., Schwarz, H., Günzel, D., Fromm, M., Kemler, R., Krieg, T., and Niessen, C.M. (2005). E-cadherin is essential for in vivo epidermal barrier function by regulating tight junctions. *EMBO J* 24, 1146–1156.

Udey, M.C. (1997). Cadherins and Langerhans cell immunobiology. *Clin Exp Immunol* 107 Suppl 1, 6–8.

Uhlen, M., Zhang, C., Lee, S., Sjöstedt, E., Fagerberg, L., Bidkhori, G., Benfeitas, R., Arif, M., Liu, Z.,

Edfors, F., et al. (2017). A pathology atlas of the human cancer transcriptome. *Science* 357, ean2507.

Umemura, M., Baljinnyam, E., Feske, S., De Lorenzo, M.S., Xie, L.-H., Feng, X., Oda, K., Makino, A., Fujita, T., Yokoyama, U., et al. (2014). Store-operated Ca²⁺ entry (SOCE) regulates melanoma proliferation and cell migration. *PLoS One* 9, e89292.

Urtatiz, O., Cook, C., Huang, J.L.-Y., Yeh, I., and Van Raamsdonk, C.D. (2020). GNAQQ209L expression initiated in multipotent neural crest cells drives aggressive melanoma of the central nervous system. *Pigment Cell & Melanoma Research* 33, 96–111.

Vallorosi, C.J., Day, K.C., Zhao, X., Rashid, M.G., Rubin, M.A., Johnson, K.R., Wheelock, M.J., and Day, M.L. (2000). Truncation of the β -Catenin Binding Domain of E-cadherin Precedes Epithelial Apoptosis during Prostate and Mammary Involution *. *Journal of Biological Chemistry* 275, 3328–3334.

Van Allen, E.M., Wagle, N., Sucker, A., Treacy, D.J., Johannessen, C.M., Goetz, E.M., Place, C.S., Taylor-Weiner, A., Whittaker, S., Kryukov, G.V., et al. (2014). The genetic landscape of clinical resistance to RAF inhibition in metastatic melanoma. *Cancer Discov* 4, 94–109.

Van Allen, E.M., Miao, D., Schilling, B., Shukla, S.A., Blank, C., Zimmer, L., Sucker, A., Hillen, U., Foppen, M.H.G., Goldinger, S.M., et al. (2015). Genomic correlates of response to CTLA-4 blockade in metastatic melanoma. *Science* 350, 207–211.

Van Raamsdonk, C.D., Bezrookove, V., Green, G., Bauer, J., Gaugler, L., O'Brien, J.M., Simpson, E.M., Barsh, G.S., and Bastian, B.C. (2009). Frequent somatic mutations of GNAQ in uveal melanoma and blue naevi. *Nature* 457, 599–602.

Van Raamsdonk, C.D., Griewank, K.G., Crosby, M.B., Garrido, M.C., Vemula, S., Wiesner, T., Obenaus, A.C., Wackernagel, W., Green, G., Bouvier, N., et al. (2010). Mutations in GNA11 in uveal melanoma. *N Engl J Med* 363, 2191–2199.

Vaqu e, J.P., Dorsam, R.T., Feng, X., Iglesias-Bartolome, R., Forsthoefel, D.J., Chen, Q., Debant, A., Seeger, M.A., Ksander, B.R., Teramoto, H., et al. (2013). A genome-wide RNAi screen reveals a Trio-regulated Rho GTPase circuitry transducing mitogenic signals initiated by G protein-coupled receptors. *Mol Cell* 49, 94–108.

Veloso, E.S., Gonalves, I.N.N., Silveira, T.L., Espirito Santo, J.T., Figueiredo, L.V., Varaschin, M.S., Cassali, G.D., Del Puerto, H.L., and Ferreira, E. (2020). ZEB and Snail expression indicates epithelial-mesenchymal transition in canine melanoma. *Res Vet Sci* 131, 7–14.

Venza, M., Visalli, M., Catalano, T., Biondo, C., Beninati, C., Teti, D., and Venza, I. (2016). DNA methylation-induced E-cadherin silencing is correlated with the clinicopathological features of melanoma. *Oncology Reports* 35, 2451–2460.

Verfaillie, A., Imrichova, H., Atak, Z.K., Dewaele, M., Rambow, F., Hulselmans, G., Christiaens, V., Svetlichnyy, D., Luciani, F., Van den Mooter, L., et al. (2015). Decoding the regulatory landscape of melanoma reveals TEADS as regulators of the invasive cell state. *Nat Commun* 6, 6683.

Verrier, F., An, S., Ferrie, A.M., Sun, H., Kyoung, M., Deng, H., Fang, Y., and Benkovic, S.J. (2011). GPCRs regulate the assembly of a multienzyme complex for purine biosynthesis. *Nat Chem Biol* 7, 909–915.

Viegas, C.S.B., Costa, R.M., Santos, L., Videira, P.A., Silva, Z., Ara ujo, N., Macedo, A.L., Matos, A.P., Vermeer, C., and Simes, D.C. (2017). Gla-rich protein function as an anti-inflammatory agent in monocytes/macrophages: Implications for calcification-related chronic inflammatory diseases. *PLoS One* 12, e0177829.

- Villares, G.J., Zigler, M., Wang, H., Melnikova, V.O., Wu, H., Friedman, R., Leslie, M.C., Vivas-Mejia, P.E., Lopez-Berestein, G., Sood, A.K., et al. (2008). Targeting melanoma growth and metastasis with systemic delivery of liposome-incorporated protease-activated receptor-1 small interfering RNA. *Cancer Res* 68, 9078–9086.
- Vleminckx, K., Vakaet, L., Mareel, M., Fiers, W., and van Roy, F. (1991). Genetic manipulation of E-cadherin expression by epithelial tumor cells reveals an invasion suppressor role. *Cell* 66, 107–119.
- Vogt, S., Grosse, R., Schultz, G., and Offermanns, S. (2003). Receptor-dependent RhoA activation in G12/G13-deficient cells: genetic evidence for an involvement of Gq/G11. *J Biol Chem* 278, 28743–28749.
- Voris, J.P., Sitailo, L.A., Rahn, H.R., Defnet, A., Gerds, A.T., Sprague, R., Yadav, V., Caroline Le Poole, I., and Denning, M.F. (2010). Functional alterations in protein kinase C beta II expression in melanoma. *Pigment Cell Melanoma Res* 23, 216–224.
- Wada, E., Way, J., Shapira, H., Kusano, K., Lebacqz-Verheyden, A.M., Coy, D., Jensen, R., and Battery, J. (1991). cDNA cloning, characterization, and brain region-specific expression of a neuromedin-B-preferring bombesin receptor. *Neuron* 6, 421–430.
- Wadt, K.A.W., Aoude, L.G., Krogh, L., Sunde, L., Bojesen, A., Grønskov, K., Wartacz, N., Ek, J., Tolstrup-Andersen, M., Klarskov-Andersen, M., et al. (2015). Molecular Characterization of Melanoma Cases in Denmark Suspected of Genetic Predisposition. *PLOS ONE* 10, e0122662.
- Wagenaar, R.A., Crawford, H.C., and Matrisian, L.M. (2001). Stabilized β -Catenin Immortalizes Colonic Epithelial Cells. *Cancer Res* 61, 2097–2104.
- Wagner, R.Y., Luciani, F., Cario-André, M., Rubod, A., Petit, V., Benzekri, L., Ezzedine, K., Lepreux, S., Steingrimsson, E., Taieb, A., et al. (2015). Altered E-Cadherin Levels and Distribution in Melanocytes Precede Clinical Manifestations of Vitiligo. *Journal of Investigative Dermatology* 135, 1810–1819.
- Wagner, W., Kania, K.D., Blauz, A., and Ciszewski, W.M. (2017). The lactate receptor (HCAR1/GPR81) contributes to doxorubicin chemoresistance via ABCB1 transporter up-regulation in human cervical cancer HeLa cells. *J Physiol Pharmacol* 68, 555–564.
- Waldo, G.L., Boyer, J.L., Morris, A.J., and Harden, T.K. (1991). Purification of an ALF4- and G-protein beta gamma-subunit-regulated phospholipase C-activating protein. *J Biol Chem* 266, 14217–14225.
- Walsh, D.A., Perkins, J.P., and Krebs, E.G. (1968). An Adenosine 3',5'-Monophosphate-dependant Protein Kinase from Rabbit Skeletal Muscle. *Journal of Biological Chemistry* 243, 3763–3765.
- Wang, H., Liu, W., Black, S., Turner, O., Daniel, J.M., Dean-Colomb, W., He, Q.P., Davis, M., and Yates, C. (2016). Kaiso, a transcriptional repressor, promotes cell migration and invasion of prostate cancer cells through regulation of miR-31 expression. *Oncotarget* 7, 5677–5689.
- Wang, Y., Ou, Z., Sun, Y., Yeh, S., Wang, X., Long, J., and Chang, C. (2017). Androgen receptor promotes melanoma metastasis via altering the miRNA-539-3p/USP13/MITF/AXL signals. *Oncogene* 36, 1644–1654.
- Watson, I.R., Li, L., Cabeceiras, P.K., Mahdavi, M., Gutschner, T., Genovese, G., Wang, G., Fang, Z., Tepper, J.M., Stemke-Hale, K., et al. (2014). The RAC1 P29S hotspot mutation in melanoma confers resistance to pharmacological inhibition of RAF. *Cancer Res* 74, 4845–4852.
- Waugh, D.J.J., and Wilson, C. (2008). The interleukin-8 pathway in cancer. *Clin Cancer Res* 14,

6735–6741.

Weis, W.I., and Kobilka, B.K. (2018). The Molecular Basis of G Protein–Coupled Receptor Activation. *Annu Rev Biochem* 87, 897–919.

Wells, C.D., Liu, M.-Y., Jackson, M., Gutowski, S., Sternweis, P.M., Rothstein, J.D., Kozasa, T., and Sternweis, P.C. (2002). Mechanisms for reversible regulation between G13 and Rho exchange factors. *J Biol Chem* 277, 1174–1181.

Wettschureck, N., and Offermanns, S. (2005). Mammalian G proteins and their cell type specific functions. *Physiol Rev* 85, 1159–1204.

White, J.R., Thompson, D.T., Koch, K.E., Kiriazov, B.S., Beck, A.C., van der Heide, D.M., Grimm, B.G., Kulak, M.V., and Weigel, R.J. (2021). AP-2 α -Mediated Activation of E2F and EZH2 Drives Melanoma Metastasis. *Cancer Res* 81, 4455–4470.

Wiesner, T., Obenauf, A.C., Murali, R., Fried, I., Griewank, K.G., Ulz, P., Windpassinger, C., Wackernagel, W., Loy, S., Wolf, I., et al. (2011). Germline mutations in BAP1 predispose to melanocytic tumors. *Nat Genet* 43, 1018–1021.

Willert, K., Brown, J.D., Danenberg, E., Duncan, A.W., Weissman, I.L., Reya, T., Yates, J.R., and Nusse, R. (2003). Wnt proteins are lipid-modified and can act as stem cell growth factors. *Nature* 423, 448–452.

Wingler, L.M., and Lefkowitz, R.J. (2020). Conformational Basis of G Protein-Coupled Receptor Signaling Versatility. *Trends in Cell Biology* 30, 736–747.

Wu, Y., Lin, Y., Liu, H., and Li, J. (2008). Inhibition of invasion and up-regulation of E-cadherin expression in human malignant melanoma cell line A375 by (-)-epigallocatechin-3-gallate. *J. Huazhong Univ. Sci. Technol. [Med. Sci.]* 28, 356.

Xu, C., Zhao, H., Chen, H., and Yao, Q. (2015). CXCR4 in breast cancer: oncogenic role and therapeutic targeting. *Drug Des Devel Ther* 9, 4953–4964.

Yajima, I., Belloir, E., Bourgeois, Y., Kumasaka, M., Delmas, V., and Larue, L. (2006). Spatiotemporal gene control by the Cre-ERT2 system in melanocytes. *Genesis* 44, 34–43.

Yamashita, N., Tokunaga, E., Iimori, M., Inoue, Y., Tanaka, K., Kitao, H., Saeki, H., Oki, E., and Maehara, Y. (2018). Epithelial Paradox: Clinical Significance of Coexpression of E-cadherin and Vimentin With Regard to Invasion and Metastasis of Breast Cancer. *Clinical Breast Cancer* 18, e1003–e1009.

Yano, T., Pinski, J., Groot, K., and Schally, A.V. (1992). Stimulation by Bombesin and Inhibition by Bombesin/Gastrin-releasing Peptide Antagonist RC-3095 of Growth of Human Breast Cancer Cell Lines. *Cancer Res* 52, 4545–4547.

Yano, T., Pinski, J., Szepeshazi, K., Halmos, G., Radulovic, S., Groot, K., and Schally, A.V. (1994). Inhibitory effect of bombesin/gastrin-releasing peptide antagonist RC-3095 and luteinizing hormone-releasing hormone antagonist SB-75 on the growth of MCF-7 MIII human breast cancer xenografts in athymic nude mice. *Cancer* 73, 1229–1238.

York, J.R., and McCauley, D.W. (2020). The origin and evolution of vertebrate neural crest cells. *Open Biology* 10, 190285.

Young, D., Waitches, G., Birchmeier, C., Fasano, O., and Wigler, M. (1986). Isolation and characterization of a new cellular oncogene encoding a protein with multiple potential transmembrane domains. *Cell* 45, 711–719.

- Yu, F.-X., Zhao, B., Panupinthu, N., Jewell, J.L., Lian, I., Wang, L.H., Zhao, J., Yuan, H., Tumaneng, K., Li, H., et al. (2012a). Regulation of the Hippo-YAP pathway by G-protein-coupled receptor signaling. *Cell* 150, 780–791.
- Yu, F.-X., Zhao, B., Panupinthu, N., Jewell, J.L., Lian, I., Wang, L.H., Zhao, J., Yuan, H., Tumaneng, K., Li, H., et al. (2012b). Regulation of the Hippo-YAP pathway by G-protein coupled receptor signaling. *Cell* 150, 780–791.
- Yu, F.-X., Luo, J., Mo, J.-S., Liu, G., Kim, Y.C., Meng, Z., Zhao, L., Peyman, G., Ouyang, H., Jiang, W., et al. (2014). Mutant Gq/11 promote uveal melanoma tumorigenesis by activating YAP. *Cancer Cell* 25, 822–830.
- Zabelskii, D., Dmitrieva, N., Volkov, O., Shevchenko, V., Kovalev, K., Balandin, T., Soloviov, D., Astashkin, R., Zinovev, E., Alekseev, A., et al. (2021). Structure-based insights into evolution of rhodopsins. *Commun Biol* 4, 1–12.
- Zaccolo, M., Zerio, A., and Lobo, M.J. (2021). Subcellular Organization of the cAMP Signaling Pathway. *Pharmacol Rev* 73, 278–309.
- Zang, J., Mao, F., Wang, H., Zhang, J., Liu, Q., Peng, L., Li, F., Lang, L., Chen, X., and Zhu, Z. (2018). ⁶⁸Ga-NOTA-RM26 PET/CT in the Evaluation of Breast Cancer: A Pilot Prospective Study. *Clin Nucl Med* 43, 663–669.
- Zang, J., Liu, Q., Sui, H., Guo, H., Peng, L., Li, F., Lang, L., Jacobson, O., Zhu, Z., Mao, F., et al. (2020). Combined ⁶⁸Ga-NOTA-Evans Blue Lymphoscintigraphy and ⁶⁸Ga-NOTA-RM26 PET/CT Evaluation of Sentinel Lymph Node Metastasis in Breast Cancer Patients. *Bioconjug Chem* 31, 396–403.
- Zehir, A., Benayed, R., Shah, R.H., Syed, A., Middha, S., Kim, H.R., Srinivasan, P., Gao, J., Chakravarty, D., Devlin, S.M., et al. (2017). Mutational Landscape of Metastatic Cancer Revealed from Prospective Clinical Sequencing of 10,000 Patients. *Nat Med* 23, 703–713.
- Zekri, J., Marples, M., Taylor, D., Kandukurti, K., McParland, L., and Brown, J.E. (2017). Complications of bone metastases from malignant melanoma. *J Bone Oncol* 8, 13–17.
- Zhai, P., Yamamoto, M., Galeotti, J., Liu, J., Masurekar, M., Thaisz, J., Irie, K., Holle, E., Yu, X., Kupersmidt, S., et al. (2005). Cardiac-specific overexpression of AT1 receptor mutant lacking G α _q/G β _i causes hypertrophy and bradycardia in transgenic mice. *The Journal of Clinical Investigation* 115, 3045–3056.
- Zhan, T., Rindtorff, N., and Boutros, M. (2017). Wnt signaling in cancer. *Oncogene* 36, 1461–1473.
- Zhang, H., Kong, Q., Wang, J., Jiang, Y., and Hua, H. (2020a). Complex roles of cAMP–PKA–CREB signaling in cancer. *Experimental Hematology & Oncology* 9, 32.
- Zhang, H., Luginina, A., Mishin, A., Baidya, M., Shukla, A.K., and Cherezov, V. (2021). Structural insights into ligand recognition and activation of angiotensin receptors. *Trends Pharmacol Sci* 42, 577–587.
- Zhang, J., Mao, F., Niu, G., Peng, L., Lang, L., Li, F., Ying, H., Wu, H., Pan, B., Zhu, Z., et al. (2018). ⁶⁸Ga-BBN-RGD PET/CT for GRPR and Integrin $\alpha\beta$ ₃ Imaging in Patients with Breast Cancer. *Theranostics* 8, 1121–1130.
- Zhang, J., Zhang, Q., Yang, Y., and Wang, Q. (2020b). Association Between Succinate Receptor SUCNR1 Expression and Immune Infiltrates in Ovarian Cancer. *Front Mol Biosci* 7, 150.
- Zhang, X., Tang, J.Z., Vergara, I.A., Zhang, Y., Szeto, P., Yang, L., Mintoff, C., Colebatch, A., McIntosh, L., Mitchell, K.A., et al. (2019). Somatic Hypermutation of the YAP Oncogene in a Human

Cutaneous Melanoma. *Mol Cancer Res* 17, 1435–1449.

Zhang, X., Yang, L., Szeto, P., Abali, G.K., Zhang, Y., Kulkarni, A., Amarasinghe, K., Li, J., Vergara, I.A., Molania, R., et al. (2020c). The Hippo pathway oncoprotein YAP promotes melanoma cell invasion and spontaneous metastasis. *Oncogene* 39, 5267–5281.

Zhao, B., Xie, J., Zhou, X., Zhang, L., Cheng, X., and Liang, C. (2021). YAP activation in melanoma contributes to anoikis resistance and metastasis. *Exp Biol Med (Maywood)* 246, 888–896.

Zhao, L., Huang, S., Mei, S., Yang, Z., Xu, L., Zhou, N., Yang, Q., Shen, Q., Wang, W., Le, X., et al. (2018). Pharmacological activation of estrogen receptor beta augments innate immunity to suppress cancer metastasis. *Proc Natl Acad Sci U S A* 115, E3673–E3681.

Zhao, X., Geltinger, C., Kishikawa, S., Ohshima, K., Murata, T., Nomura, N., Nakahara, T., and Yokoyama, K.K. (2000). Treatment of mouse melanoma cells with phorbol 12-myristate 13-acetate counteracts mannosylerythritol lipid-induced growth arrest and apoptosis. *Cytotechnology* 33, 123–130.

Zhou, J., Chen, J., Zhong, R., Mokotoff, M., Shultz, L.D., and Ball, E.D. (2006). Targeting gastrin-releasing peptide receptors on small cell lung cancer cells with a bispecific molecule that activates polyclonal T lymphocytes. *Clin Cancer Res* 12, 2224–2231.

Zhou, Q., Yang, D., Wu, M., Guo, Y., Guo, W., Zhong, L., Cai, X., Dai, A., Jang, W., Shakhnovich, E.I., et al. (2019). Common activation mechanism of class A GPCRs. *ELife* 8, e50279.

Zhu, D., Hunter, S.B., Vertino, P.M., and Van Meir, E.G. (2011). Overexpression of MBD2 in glioblastoma maintains epigenetic silencing and inhibits the antiangiogenic function of the tumor suppressor gene BAI1. *Cancer Res* 71, 5859–5870.

Zhu, D., Osuka, S., Zhang, Z., Reichert, Z.R., Yang, L., Kanemura, Y., Jiang, Y., You, S., Zhang, H., Devi, N.S., et al. (2018a). BAI1 Suppresses Medulloblastoma Formation by Protecting p53 from Mdm2-Mediated Degradation. *Cancer Cell* 33, 1004-1016.e5.

Zhu, G.-J., Song, P.-P., Zhou, H., Shen, X.-H., Wang, J.-G., Ma, X.-F., Gu, Y.-J., Liu, D.-D., Feng, A.-N., Qian, X.-Y., et al. (2018b). Role of epithelial-mesenchymal transition markers E-cadherin, N-cadherin, β -catenin and ZEB2 in laryngeal squamous cell carcinoma. *Oncology Letters* 15, 3472–3481.

Zigler, M., Kamiya, T., Brantley, E.C., Villares, G.J., and Bar-Eli, M. (2011). PAR-1 and Thrombin: The Ties that Bind the Microenvironment to Melanoma Metastasis. *Cancer Res* 71, 6561–6566.

Zlotnik, A., Burkhardt, A.M., and Homey, B. (2011). Homeostatic chemokine receptors and organ-specific metastasis. *Nat Rev Immunol* 11, 597–606.

Zouboulis, C.C. (2000). Human skin: an independent peripheral endocrine organ. *Horm Res* 54, 230–242.

Annexes

A. Participation à d'autres projets

I. C57BL/6 congenic mouse NRAS Q61K melanoma cell lines are highly sensitive to the combination of Mek and Akt inhibitors *in vitro* and *in vivo*

Article publié en novembre 2019

Résumé :

Les mutations NRAS sont fréquentes dans le mélanome, mais difficiles à traiter. Les patients porteurs de mélanomes mutés NRAS n'ont pas de thérapies spécifiques à leur disposition. Nous avons établi des cellules de mélanome et de mélanocyte de souris à partir d'un modèle murin C57BL/6 NRASQ61K. Ces lignées cellulaires peuvent être utilisées ensuite pour des études pré-cliniques et fondamentales de mélanome porteur de mutation NRAS. Le fait que ces lignées soient syngéniques C57BL/6 permet de travailler dans un environnement immunocompétent plus proche de la réalité immunologique du patient. Pour faire la preuve de concept de l'intérêt de nos cellules, nous avons analysé le protéome et identifier une activation des voies AKT et MAPK. Nous avons montré ensuite que la co-inhibition de ces deux voies a un effet additif sur la croissance cellulaire *in vitro* et *in vivo*.

Ma participation à ce projet a été dans la réalisation d'analyse bio-informatique d'une part en analysant le transcriptome des lignées établies pour observer les différences entre mélanocytes et mélanomes et pour caractériser les cellules, mais aussi en analysant le RPPA en identifiant des déficits de phosphorylation d'AKT et de ERK lors de l'inhibition génétique de NRAS dans ces lignées. J'ai également pris une part active dans les expériences *in vivo* en assurant une partie des traitements et des analyses des souris et du suivi des tumeurs.

ORIGINAL ARTICLE

C57BL/6 congenic mouse NRAS^{Q61K} melanoma cell lines are highly sensitive to the combination of Mek and Akt inhibitors in vitro and in vivo

Valérie Petit^{1,2,3} | Jeremy Raymond^{1,2,3} | Christophe Alberti^{1,2,3} | Marie Pouteaux^{1,2,3} | Stuart J. Gallagher^{1,2,3} | Mai Q. Nguyen⁴ | Andrew E. Aplin^{4,5}  | Véronique Delmas^{1,2,3} | Lionel Larue^{1,2,3} 

¹INSERM U1021, Normal and Pathological Development of Melanocytes, Institut Curie, PSL Research University, Orsay, France

²CNRS UMR 3347, Univ Paris-Sud, Univ Paris-Saclay, Orsay, France

³Equipe Labellisée Ligue Contre le Cancer, Orsay, France

⁴Department of Cancer Biology, Thomas Jefferson University, Philadelphia, PA, USA

⁵Sidney Kimmel Cancer Center, Philadelphia, PA, USA

Correspondence

Lionel Larue
Email: lionel.larue@curie.fr

Funding information

Ligue Contre le Cancer; Fondation ARC; Institut Carnot; INCa; ITMO Cancer; ANR Labex CelTisPhyBio, Grant/Award Number: ANR-11-LABX-0038 and ANR-10-IDEX-0001-02; MENRT; Department of Defense, Grant/Award Number: W81XWH-18-1-0224; Sheldon G. Adelson Medical Research Foundation; NCI Cancer Center, Grant/Award Number: CA16672

Abstract

RAS is frequently mutated in various tumors and known to be difficult to target. NRAS^{Q61K/R} are the second most frequent mutations found in human skin melanoma after BRAF^{V600E}. Aside from surgery, various approaches, including targeted therapies, immunotherapies, and combination therapies, are used to treat patients carrying NRAS mutations, but they are inefficient. Here, we established mouse NRAS^{Q61K} melanoma cell lines and genetically derived isografts (GDIs) from Tyr::NRAS^{Q61K} mouse melanoma that can be used in vitro and in vivo in an immune-competent environment (C57BL/6) to test and discover novel therapies. We characterized these cell lines at the cellular, molecular, and oncogenic levels and show that NRAS^{Q61K} melanoma is highly sensitive to the combination of Mek and Akt inhibitors. This pre-clinical model shows much potential for the screening of novel therapeutic strategies for patients harboring NRAS mutations that have limited therapeutic options and resulted in poor prognoses.

KEYWORDS

binimetinib, MK-2206 2HCl, mouse model, PD-0325901, S6

1 | INTRODUCTION

Skin melanoma is a malignant tumor that develops from melanocytes, the cells that produce melanin, which are responsible for skin pigmentation. Skin melanoma is a multifactorial disease; risk factors are related to the environment, lifestyle and conditions (chronic or intermittent sun exposure), and individual risk factors (ethnicity, genetic factors, skin pigmentation, abundant nevi). Cutaneous melanoma ranks 9th among all cancers of men and women combined, accounting for 15,404 and 287,723 new cases in France in 2017 (68 million

inhabitants) and worldwide in 2018, respectively (Bray et al., 2018; Jéhannin-Ligier et al., 2017). Its incidence has been steadily increasing in most Caucasian populations over the last 50 years. Various classifications of melanoma have been implemented based on clinical, anatomical, histopathological, and, more recently, molecular genetic criteria. Cutaneous melanoma is currently molecularly classified into four major classes: (a) "BRAF mutated" (50% of patients), (b) "NRAS mutated" (25% of patients), (c) "NF1 mutated" (10% of patients), and (d) "others" for approximately 15% (Cancer Genome Atlas Network, 2015).

Surgery is still the primary treatment for most skin cancers but is ineffective in advanced melanoma cases, in which tumors have spread beyond the skin to the lymphatic system, blood circulation, or other parts of the body. Chemotherapy and radiation have been routinely used without objective responses.

In recent years, two parallel approaches have been successful. The first is immunotherapy with ipilimumab or nivolumab/pembrolizumab (monoclonal antibodies directed against CTLA4 or PD1 proteins, respectively) or the two in combination. This approach can be very effective, but a maximum of 60% of patients respond to this type of treatment for reasons that are unknown. The second approach consists of targeted therapy for molecular abnormalities involved in cancer initiation/progression. This therapeutic approach emerged directly from major advances in our understanding of the biology of melanoma, knowledge of signaling pathways, and dissection of the molecular genetics of the disease. In particular, mutated BRAF inhibitors, such as Vemurafenib®, have demonstrated their ability to inhibit the very high activity of the BRAF^{V600X} form. These inhibitors are effective in patients whose melanoma is mutated for this kinase, but not when the melanoma is mutated for NRAS or NF1.

Melanomas carrying mutations for NRAS are aggressive tumors, with thick lesions, a high mitotic index, and a high rate of metastases in lymph nodes. To date, there is no targeted therapy for NRAS, mainly due to the nature of this protein. Here, we established and characterized mouse NRAS^{Q61K} melanoma cell lines and genetically derived isografts (GDIs) from Tyr::NRAS^{Q61K} mouse melanoma. We then evaluated their sensitivity to a combination of Mek and Akt inhibitors.

2 | MATERIALS AND METHODS

2.1 | Establishment of cell lines

RAS90 [McNRAS1] and RAS91A [McNRAS2] melanocyte cell lines were obtained from Tyr::NRAS^{Q61K} transgenic mice that were backcrossed to C57BL/6 and established as previously described (Ackermann et al., 2005; Delmas et al., 2007; Longvert et al., 2011). The Melan-a, 9v [McWT1], and 14d [McWT2] C57BL/6 melanocyte cell lines have been previously described (Bennett, Cooper, & Hart, 1987; Delmas et al., 2007). The 1007 [MaNRAS1] and 1014 [MaNRAS2] melanoma cell lines were established from melanoma arising from a male and female Tyr::NRAS^{Q61K} transgenic mouse, respectively. Small pieces ($\approx 10 \text{ mm}^3$) of Tyr::NRAS^{Q61K} primary tumors were cleaned, washed in PBS, and subcutaneously implanted into the neck pad of C57BL/6 mice. Once the implanted tumor reached a volume of $\approx 1 \text{ cm}^3$, it was removed from the mouse, tumors were dissociated as single cells prior to establishing them in culture as previously described (Gallagher et al., 2011).

2.2 | Cell culture

Melanoma cell lines were maintained at 37°C in complete medium, consisting of Ham's F12 medium supplemented with 10% fetal calf

Significance

The establishment of novel congenic mouse melanoma cell lines and GDIs mutated for NRAS is a key step toward evaluating various therapies, as RAS tumors are still difficult to target. Proper use of these models will limit the number of therapies that enter clinical phase 1 trials to increase the success rate and thereby reduce the astronomical financial costs of phase 3.

serum, 5 mM L-glutamine, and antibiotics (100 U/ml penicillin and 100 µg/ml streptomycin), in a humidified atmosphere containing 5% CO₂. Melanocyte cell lines were maintained under the same conditions in the presence of 200 nM TPA (tetradecanoyl phorbol acetate, Sigma). The Melan-a and Melan-c mouse melanocyte and melanoma cell lines were kindly provided by Dr. D. Bennett (Bennett et al., 1989, 1987).

2.3 | DNA genotyping

Genomic DNA was extracted from melanocyte and melanoma cell lines and column-purified with the QIAamp Kit (Qiagen). The presence of the Tyr::NRAS^{Q61K} transgene was determined after amplifying and genotyping the appropriate DNA. Fragments containing the NRAS Q61K human sequence were amplified by PCR with primers LL1086 (5'-GAT CCC ACC ATA GAG GAT / T3') and LL1087 (5'-CTG GCG TAT TTC TCT TAC C-3'). This PCR consisted of 35 cycles at 94°C for 45 s, 56°C for 30 s, and 72°C for 30 s, and generated a product of 399 bp. The gender of the cells (XX or XY) was determined using a combined Smcy and Smcx PCR with primers: LL362 (5'-TGA AGC TTT TGG CTT TGA G-3') and LL363 (5'-CCG CTG CCA AAT TCT TTG G-3'). This PCR consisted of 35 cycles at 94°C for 1 min, 55°C for 30 s, and 72°C for 30 s, and generated products of 280 and 310 bp for males (XY) but only 310 bp for females (XX) (Pla et al., 2004).

2.4 | Growth curves and clonogenic assays

Growth curves were established by seeding six-well tissue culture plates with 10⁵ cells in complete medium with or without 200 nM TPA. Three images were taken per well at 24, 48, and 72 hr after seeding. Images were also taken just after cell attachment to determine the exact number of seeded cells per well. Cells were manually counted from images (cell counter plugin—*ImageJ*). For the growth curves established in the presence of the inhibitors, binimetinib, PD-0325901, or MK-2206 2HCl, the inhibitors were added 24 hr after seeding. The doubling time (Dt) was determined using the formula $Dt = (t_2 - t_1) \times (\log(2)/\log(q_2/q_1))$, with q_1 = to the quantity of cells at time t_1 and q_2 = to the quantity of cells at time t_2 .

For clonogenic assays, six-well tissue culture plates were seeded with 500 cells in complete medium. The medium was changed 24 hr

after cell seeding and replaced with complete medium containing the indicated concentrations of binimetinib, PD-0325901, or MK-2206 2HCl. This medium was left on the cells for either 1 hr and replaced with new complete medium or left unchanged. After 15 days of incubation, colonies were fixed with 4% PFA (paraformaldehyde), stained with crystal violet in 10% ethanol, and counted on images. Experiments were performed in triplicate.

2.5 | Melanin determination

To determine the amount of melanin per cell line, cells were counted, pelleted, and solubilized by incubation in 1 ml 1 M NaOH for 2 hr at 80°C. Samples were then centrifuged at 15,300 g for 10 min at room temperature and the absorbance of the supernatants measured at 470 nm. Melanin content was determined by comparison with a standard curve generated for synthetic melanin (Sigma).

2.6 | Western blot analysis

Whole-cell lysates were prepared from melanocytes and melanoma cell lines in ice-cold RIPA buffer supplemented with complete protease inhibitor cocktail and PhosStop phosphatase inhibitor cocktail (Roche). For Western blotting, 20 µg total protein was separated on a 15% denaturing acrylamide SDS-PAGE gel and the proteins transferred to a nitrocellulose membrane. Membranes were blocked in 5% non-fat milk in Tris-buffered saline supplemented with 0.01% Tween-20 (TBST) and probed with primary antibodies overnight. The signal was detected using peroxidase-conjugated anti-mouse or anti-rabbit secondary antibodies and enhanced chemiluminescence (ECL; Thermo Fisher). The primary antibodies used were against Erk (Cell Signaling, 9102), p-Erk (Thr202/Thr204, Cell Signaling, 9106), Akt (Cell Signaling, 2938), p-Akt (Ser473, Cell Signaling 3787), S6 (Cell Signaling, 2317), pS6 (Ser235/236, Cell Signaling, 4857), and β-actin (Sigma, A5441). All antibodies were used at a dilution of 1/1,000, except β-actin (1/10,000). For NRAS siRNA knockdown experiments, proteins were extracted with Laemmli sample buffer, resolved by SDS-PAGE, and transferred to PVDF membranes. Immunoreactivity was detected using HRP-conjugated secondary antibodies (Calbiotech) and chemiluminescence HRP-recognizing substrates (Thermo Scientific) on a VersaDoc Multi-Imager. The primary antibodies used were against NRAS (Santa Cruz, sc-519, dilution 1/1,000) and actin (Sigma-Aldrich, A2066, dilution 1/5,000).

2.7 | Mice and iso-/xenografts

C57BL/6 and Swiss nude mice were purchased from Charles River Laboratories (France). All animals were housed under specific pathogen-free conditions in the animal facility. Animal care, use, and experimental procedures were conducted in accordance with recommendations of the European Community (86/609/EEC) and Union (2010/63/UE) and the French National Committee (87/848). The ethics committee of the Curie Institute in compliance with the

institutional guidelines approved animal care and use. Xenograft experiments were performed as previously described (Grille et al., 2003). The 1014 melanoma cells were injected subcutaneously either in the flank of female Swiss nude mice, at a concentration of 8×10^5 cells per flank, or in the flank of female C57BL/6 mice at a concentration of 10^5 cells per flank. The 1007 melanoma cells were injected subcutaneously in the flank of male C57BL/6 mice at a concentration of 10^5 cells per flank. Tumor size was measured by caliper every 2–3 days and the volume (v) estimated as $(\text{length} \times \text{width} \times \text{height})/2$.

2.8 | Gene expression RT-PCR

RNA was extracted from mouse melanocyte (9v, 14d, R90, and R91a) and mouse melanoma (1007 and 1014) cell lines using the miRNeasy Kit (Qiagen, #217004). M-MLV reverse transcriptase (Invitrogen) was used according to the manufacturer's protocol to synthesize cDNA from 1 µg total RNA in combination with random hexamers. The cDNA was used as template for PCR with the NRAS primers LL1086 (5'-GAT CCC ACC ATA GAG GAT / T3') and LL1087 (5'-CTG GCG TAT TTC TCT TAC C-3'), amplified, and revealed with ethidium bromide.

2.9 | Transcriptomic analysis

RNA was extracted from mouse melanocyte (9v, 14d, R90, and R91a) and mouse melanoma (1007 and 1014) cell lines using the miRNeasy kit (Qiagen, #217004). RNA integrity (RIN) was measured using an Agilent Bioanalyser 2100 (Agilent Technologies). The minimum threshold for RNA integrity was fixed at $RIN \geq 9$. RNA concentration was measured using a NanoDrop (ND-2000, Thermo Fischer). Complementary RNA (cRNA) was synthesized using the GeneChip 3'IVT Plus Reagent Kit (Thermo Fisher, #902415), according to the manufacturer's protocol. In brief, total RNA was first reverse-transcribed using a T7-Oligo(dT) promoter primer for first-strand cDNA synthesis. After RNaseH treatment and second-strand cDNA synthesis, the double-stranded cDNA was purified and served as template for subsequent in vitro transcription (IVT). The IVT reaction was carried out in the presence of T7 RNA polymerase and a biotinylated nucleotide analog/ribonucleotide mix for cRNA amplification and biotin labeling. The biotinylated cRNA targets were then cleaned up, fragmented, and 11 µg cRNA hybridized to a single GeneChip® Mouse Genome 430 2.0 Array (Affymetrix, #900495). After washing and staining, using the Affymetrix Fluidics Station 450 (Affymetrix, # 00-0079), the probe arrays were scanned using an Affymetrix GeneChip Scanner 3000 (Affymetrix, # 00-0210). Microarray analysis was conducted using R and package available on Bioconductor (<http://www.bioconductor.org>). Data were normalized using the robust multichip average algorithm (RMA) from package OLIGO (Carvalho & Irizarry, 2010) and annotated using A4PREPROC (Talloen & Verbeke, 2018) and MOUSE4302.DB. The principal component analysis was performed using the

packages FACTOMINER (Le, Josse, & Husson, 2008) and FACTOEXTRA (Kassambara & Mundt, 2017). The differential analysis (D.A.) to compare NRAS melanocytes and NRAS melanomas was performed using the LIMMA package (Ritchie et al., 2015). A heatmap to display the results of the D.A. was generated using the PHEATMAP (Kolde, 2018) and GPLOTS packages. Genes with an adjusted p -value under .01 and absolute log₂ fold change over 3 were chosen for drawing the heatmap. The volcano plot depicting the D.A. results was generated using the GGPLOT2 (Wickham, 2016) and GGPEL packages. Gene ontology and enriched pathway analysis were performed using the CLUSTERPROFILER package (Yu, Wang, Han, & He, 2012).

2.10 | Reverse-phase protein array (RPPA) analysis

Cell lysates were prepared and analyzed by RPPA, as previously described (Tibes et al., 2006), with 304 antibodies. Triplicate normalized RPPA data were transformed for use with Gene Set Enrichment Analysis (GSEA) software using gene ontology gene sets available from MSigDB (Cambridge, MA), as previously described. A storey value <0.05 and log₂ fold change >0.32193 were used as cutoffs for determining significance. Unsupervised and supervised hierarchical

clustering heatmaps were produced using log₂-transformed sample expression data for antibody lists constructed from either significance cutoffs or a priori pathway information. Calculations were performed using MATLAB® (v2017b).

2.11 | RNA interference

Cells (200,000) were plated in six-well plates and transfected for 4 hr with chemically synthesized siRNA at a final concentration of 25 nmol/L using Lipofectamine™ RNAiMax (Invitrogen). The medium was then replaced with TPA-free medium and replenished at day 3 if the experiments lasted for more than 3 days. Cell growth was monitored using the Incucyte® system for an additional 5 days post-transfection. NRAS siRNA #1 (5'-CAC CAU AGA GGA UUC UUA CUU-3') and NRAS siRNA #2 (5'-GCA AGU GUG AUU UGC CAA CA-3') were purchased from Dharmacon Inc.

2.12 | Inhibitor treatment in vitro and in vivo

PD-0325901, binimetinib, and MK-2206 2HCl were purchased from Selleckchem. For the in vitro studies, the drugs were dissolved in

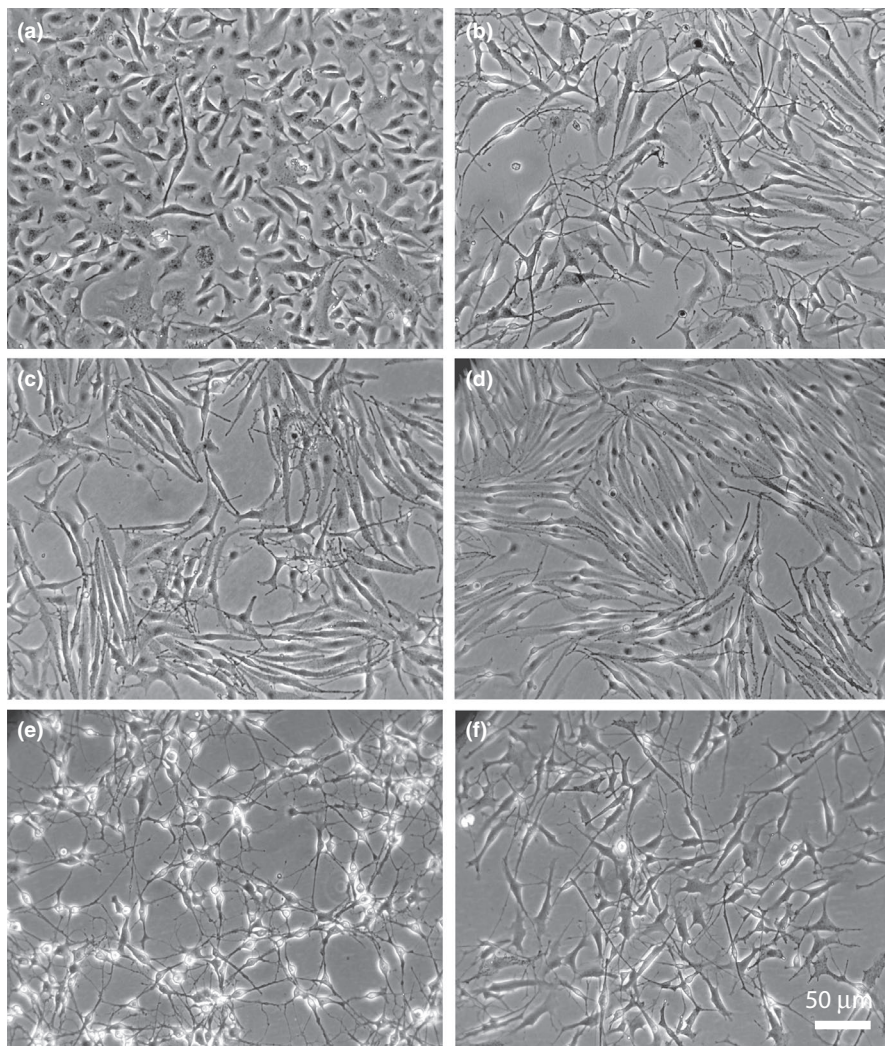


FIGURE 1 General morphology of the melanocyte and melanoma cell lines. Phase contrast images of melanocyte and melanoma cell lines. (a) Melan-a cells, (b) 9v cells, (c) R90 cells, (d) R91a cells, (e) 1007 melanoma cells, and (f) 1014 melanoma cells. Scale bar = 50 μ m

TABLE 1 Characteristics of C57BL/6 cell lines of the melanocyte lineage

Name of the cell line	Abbreviation	Genotype	Gender	Reference
McWT1 [9v]	9v	WT	Male	Delmas et al. (2007)
McWT2 [14d]	14d	WT	Female	Delmas et al. (2007)
McNRAS1 [90]	R90	Tyr::NRAS ^{Q61K} /o	Male	This article
McNRAS2 [91A]	R91a	Tyr::NRAS ^{Q61K} /o	Male	This article
MaNRAS1 [1007]	1007	Tyr::NRAS ^{Q61K} /o	Male	This article
MaNRAS2 [1014]	1014	Tyr::NRAS ^{Q61K} /o	Female	This article
Melan-a	Melan-a	WT	Female	Bennett et al. (1987)

Note: The official names of the established cell lines are given with their genotypes and genders.

DMSO as 10 mM stock solutions, stored at -20°C , and adjusted to the final concentration with culture medium. DMSO was used as the vehicle control for the in vitro studies. For the in vivo studies, the drugs were resuspended in 1% CMC (carboxymethyl cellulose) plus 0.5% Tween-80 and administered by oral gavage. Binimetinib was used at a dose of 10 mg/kg per day and MK-2206 2HCl at a dose of 15 mg/kg per day. The resuspension solution (1% CMC plus 0.5% Tween-80) was used as the vehicle control (mock). Injected mice were treated daily from day 21 post-injection for 21 consecutive days. Mice were sacrificed when the tumor volume reached more than 2 cm^3 .

3 | RESULTS

We established melanocyte cell lines in culture from one-day-old C57BL/6 wild-type and Tyr::NRAS^{Q61K} pups. Tyr::NRAS^{Q61K} transgenic mice express the human NRAS protein mutated on amino acid 61, driven by the mouse tyrosinase promoter (Ackermann et al., 2005). The rate of success in establishing these cell lines was similar (approximately 30%), indicating that the presence of the NRAS mutation does not influence immortalization of these cells in culture. The morphology of the two novel NRAS^{Q61K} melanocyte cell lines McNRAS1 [90] (or R90) and McNRAS2 [91a] (or R91a) is similar to that of wild-type Melan-a, McWT1 [9v] (or 9v), and McWT2 [14d] (or 14d) melanocyte cell lines, dendritic and pigmented (Figure 1a-d; Figure S1a; Table 1). These results suggest that these cells retained their principal melanocytic characteristics. The R90 and R91a melanocyte cell lines contain and express the human NRAS^{Q61K} oncogene (Figure S1b,c). Tumors arising from 1-year-old Tyr::NRAS^{Q61K} mice were engrafted into 2-month-old C57BL/6 mice and collected after growth. They were divided into 10-mm^3 cubes prior to either freezing in liquid nitrogen in the presence of FCS/DMSO to generate GDIs or establishing them in culture in the presence of medium containing TPA. The morphology of the melanoma cell lines (MaNRAS1 [1007] (or 1007) and

MaNRAS2 [1014] (or 1014) is similar to melanocyte cell lines, and they are pigmented (Figure 1e,f; Figure S1a). The 1007 and 1014 melanoma cell lines contain and express the human NRAS^{Q61K} oncogene (Figure S1b,c). The 9v, R90, R91a, and 1007 melanocyte/melanoma cell lines were established from male mice and the 14d and 1014 melanocyte/melanoma cell lines from female mice; the sex of these cell lines was confirmed by PCR (Table 1).

It is well established that the growth of mouse melanocytes requires mitogenic factors in addition to the standard medium conditions (Bennett et al., 1987; Larue & Mintz, 1990). TPA, a phorbol ester that activates PKC signaling, is used to promote melanocyte growth in vitro. As PKC activates Mapk signaling, we evaluated the requirement of TPA for the growth of 9v wild-type melanocytes, R90 and R91a NRAS^{Q61K} melanocytes, and 1007 and 1014 NRAS^{Q61K} melanoma cells (Figure 2). As expected, wild-type 9v melanocytes did not grow without TPA and their doubling time in the presence of TPA was approximately 40 hr. The R90 and R91a NRAS^{Q61K} melanocytes were unable to grow without TPA, suggesting that NRAS^{Q61K} did not sufficiently activate the MAP kinase pathway to promote cell growth. The doubling times of R90 and R91a NRAS^{Q61K} melanocytes were similar to that of wild-type 9v melanocytes, both in the presence or absence of TPA. Based on this criterion, R90 and R91a melanocytes are not transformed. The 1007 and 1014 melanoma cell lines were able to grow both in the presence and absence of TPA. However, the doubling time of 1007 cells appeared to be higher in the absence of TPA (40 hr vs. 50 hr), which was not true of 1014 cells.

We injected 1014 melanoma cells into female C57BL/6 and nude mice to evaluate their potential to grow in vivo. The injection of 10^5 1014 cells in 2-month-old female C57BL/6 mice was sufficient to reproducibly generate melanomas (Figure 3a). However, injection of the same number of 1014 cells (10^5) into nude mice resulted in very few mice presenting tumors. The optimal number of cells to obtain reproducible growth in nude mice was 8×10^5 (Figure 3b). We did not evaluate the cause of this difference between C57BL/6 and nude mice, but it may be due to the action of NK cells, as they are

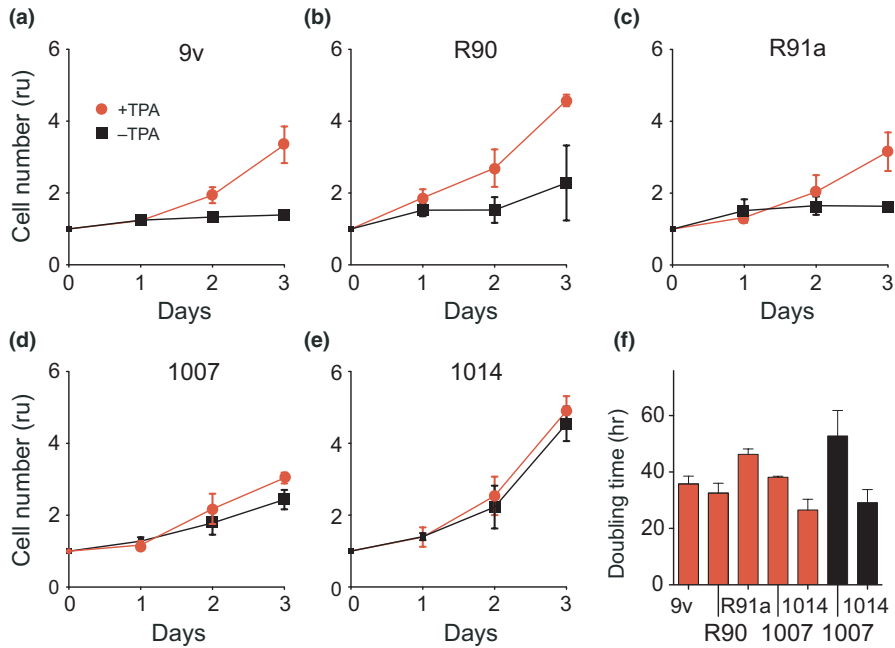


FIGURE 2 Growth dependence of the melanocyte and melanoma cell lines on TPA in vitro. (a-e) In vitro growth curves of the various cell lines over 3 days in the presence (red) or absence (black) of 200 nM TPA. a, 9v cells; b, R90 cells; c, R91a cells; d, 1007 cells; and e, 1014 cells. Results are expressed as the ratio of cells at each timepoint over the number of cells plated at the beginning of the experiment (time 0) and represent the average \pm SD of three to five independent experiments. (f) Doubling time (in hours) of each cell population during exponential growth in the presence (red) or absence (black) of 200 nM TPA. Each bar represents the mean \pm SD of at least three independent measurements

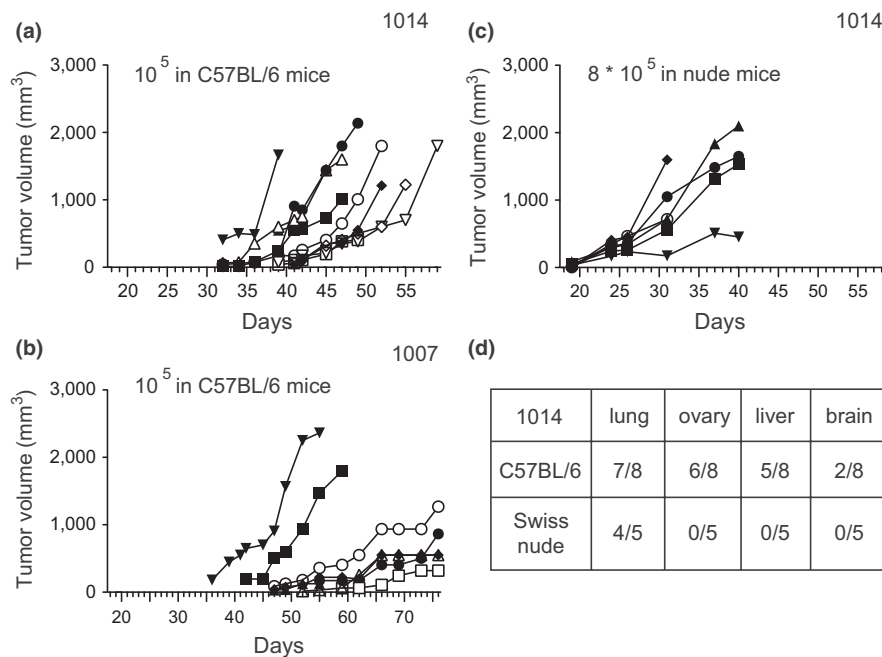
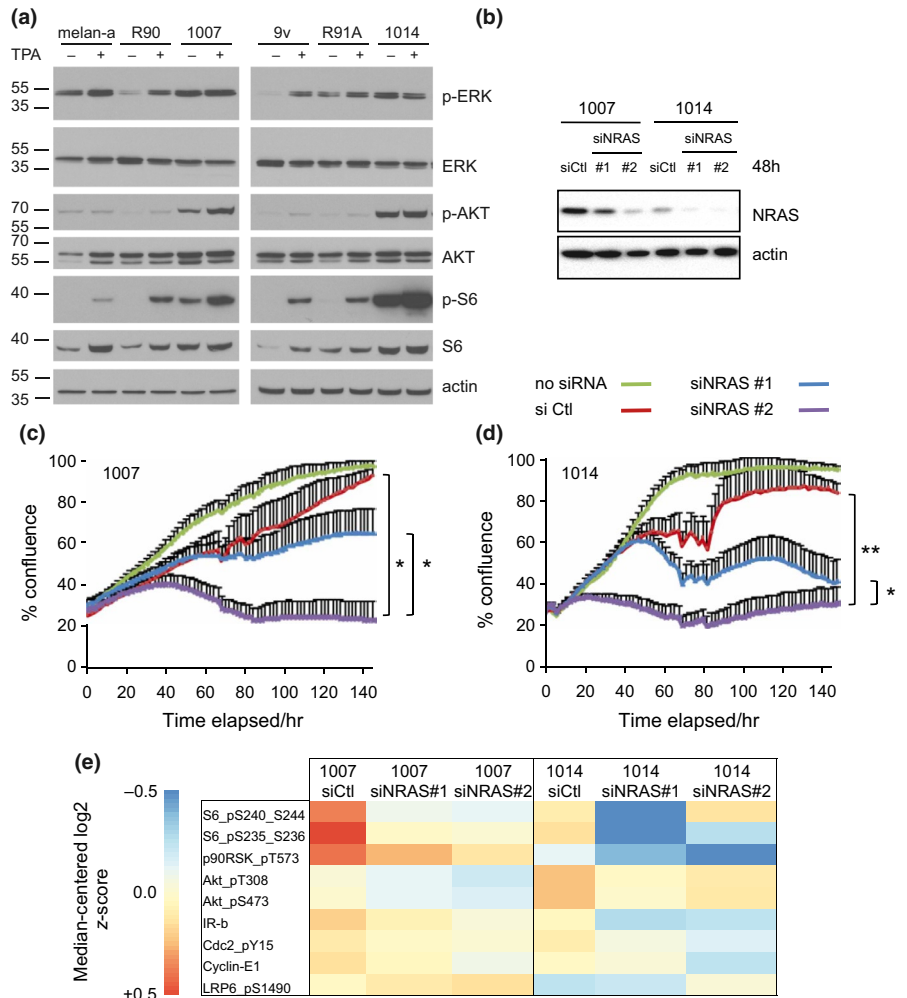


FIGURE 3 Growth of the 1007 and 1014 melanoma cell lines in vivo. Established 1014 (a) and 1007 (b) melanoma cells were injected subcutaneously in the flanks of female and male C57BL/6 mice (10^5 cells per side) and allowed to form tumors. Tumor size was measured by caliper and calculated as $(\text{length} \times \text{width} \times \text{height})/2$. Each curve represents the growth of a tumor in a specific mouse. (c) Established 1014 melanoma cells were injected subcutaneously in the flanks of Swiss nude female mice (8×10^5 cells per side) and allowed to form tumors. Tumor size was measured by caliper and calculated as $(\text{length} \times \text{width} \times \text{height})/2$. Each curve represents the growth of a tumor in a specific mouse. (d) Established 1014 melanoma cells were injected in the tail vein of female C57BL/6 or Swiss nude mice (5×10^5 cells per mouse) and allowed to form metastases. Results represent the number of mice bearing lung, ovary, liver, and/or brain metastases per mouse injected

more robust and potent in nude mice than C57BL/6 mice. We performed similar experiments with 1007 melanoma cells. They were able to grow in C57BL/6 mice, but took longer to appear, ≈ 45 days for 1007 versus ≈ 30 days for 1014 (Figure 3c). Finally, 1014 melanoma cells could form lung, ovary, liver, and brain metastases

when 5×10^5 cells were injected in the tail veins of C57BL/6 mice (Figure 3d). 1007 melanoma cells were unable to colonize the lungs when injected in the tail vein of nude mice (5-month follow-up). Four million R90 or R91a cells were injected into six C57BL/6 mice; none presented tumors after 5 months.

FIGURE 4 Analysis of signaling pathways by Western blotting. (a) Cells were grown in the presence or absence of 200 nM TPA and lysed 48 hr after seeding. Total cell extracts were subjected to Western blot analysis using the mentioned antibodies. Actin was used as a loading control. (b) 1007 and 1014 cells (200,000) were transfected with non-targeting or NRAS-targeting siRNAs and grown in TPA-free media for 48 hr. Lysates were collected and analyzed by western blotting. 1007 (c) and 1014 (d) cells (200,000) were transfected with non-targeting (siCtl) or NRAS-targeting siRNAs and grown in TPA-free media for 144 hr. A non-transfected control was also included. Growth was monitored using the IncuCyte® system ($n = 4$; error bars indicate the standard error; * $p < .05$, ** $p < .01$; p -values were determined by comparing the area under the curve). (e) Reverse-phase protein array (RPPA) analysis of the indicated cell lines transfected with non-targeting or NRAS-targeting siRNAs and grown in TPA-free media for 48 hr. Expression levels are presented as the NormLog2 median-centered z-score



Overall, these results show that the NRAS melanocyte cell lines (R90 and R91a) are not transformed, which is not true of the two NRAS melanoma cell lines (1007 and 1014). However, 1007 melanoma cells appear to be less aggressive than 1014 melanoma cells, based on these criteria (dependence on TPA, growth, and metastasis formation in mice).

We next performed transcriptomic analysis of the wild-type (9v and 14d) and NRAS (R90 and R91a) melanocyte cell lines and NRAS melanoma (1007 and 1014) cell lines (Table S1). We first evaluated the levels of the seven key transcription factors for human melanocyte/melanoma (Rambow et al., 2015). The levels of the common melanocytic mRNAs (Mitf, Pax3, Sox10, and Tfap2a) were similar in these cell lines and validated the melanocytic origin of all the cell lines, whereas the levels of Lef1 and Dlx2 were barely detectable. However, the level of Gas7 was significantly higher (adjusted p -value = 4.75×10^{-3} with a log2 fold change of 3.00) in the melanoma than melanocyte cell lines (Figure S2a-g). We validated the induction of Gas7 mRNA synthesis in the melanoma cell lines relative to that in melanocyte cell lines by RT-qPCR (Figure S2h). PCA analysis showed the melanocyte cell lines (9v, 14d, R90, and R91a) to cluster together, distant from the 1007 and 1014 melanoma cell lines (Figure S3a). The most differentially expressed genes (log2 fold change >3), with

an adjusted p -value < .01 between melanocytes and melanoma, are given as a heatmap (Figure S3b). As expected, Gas7, Chd4, Fscn1, Tubb5, Igfbp4, and Pik3cd emerged were induced and Mecom, Atrx, Nrcam, and Nfix repressed in the melanoma cells. We generated a volcano plot after comparing the NRAS melanocyte (R90 and R91a) and melanoma (1007 and 1014) cell lines (Figure S3b). GO, KEGG, and MSigDB analysis was performed on 889 differentially expressed genes defined from the differences between NRAS^{Q61K} melanocyte and NRAS^{Q61K} melanoma cell lines (FC > 1 and adjusted p -value < .05). These analyses revealed the main differences between the NRAS^{Q61K} melanocyte and NRAS^{Q61K} melanoma cell lines to be associated with chromatin organization, the mRNA machinery, and cytoskeleton modifications (Figure S4).

The second dimension of the PCA showed the 1007 and 1014 melanoma cells to be different (Table S2). These results were not surprising, as Tyr::NRAS^{Q61K} melanoma could be divided into two classes by transcriptomic analysis (data not shown). GO analysis showed that the 1007 melanoma cells express higher levels of genes associated with sugar metabolism, including that of glucose, carbohydrates, hexose, and monosaccharide, than 1014 melanoma cells.

NRAS controls the Mapk and PI3K signaling pathways. We thus evaluated the level of proteins of these two pathways (Erk, p-Erk,

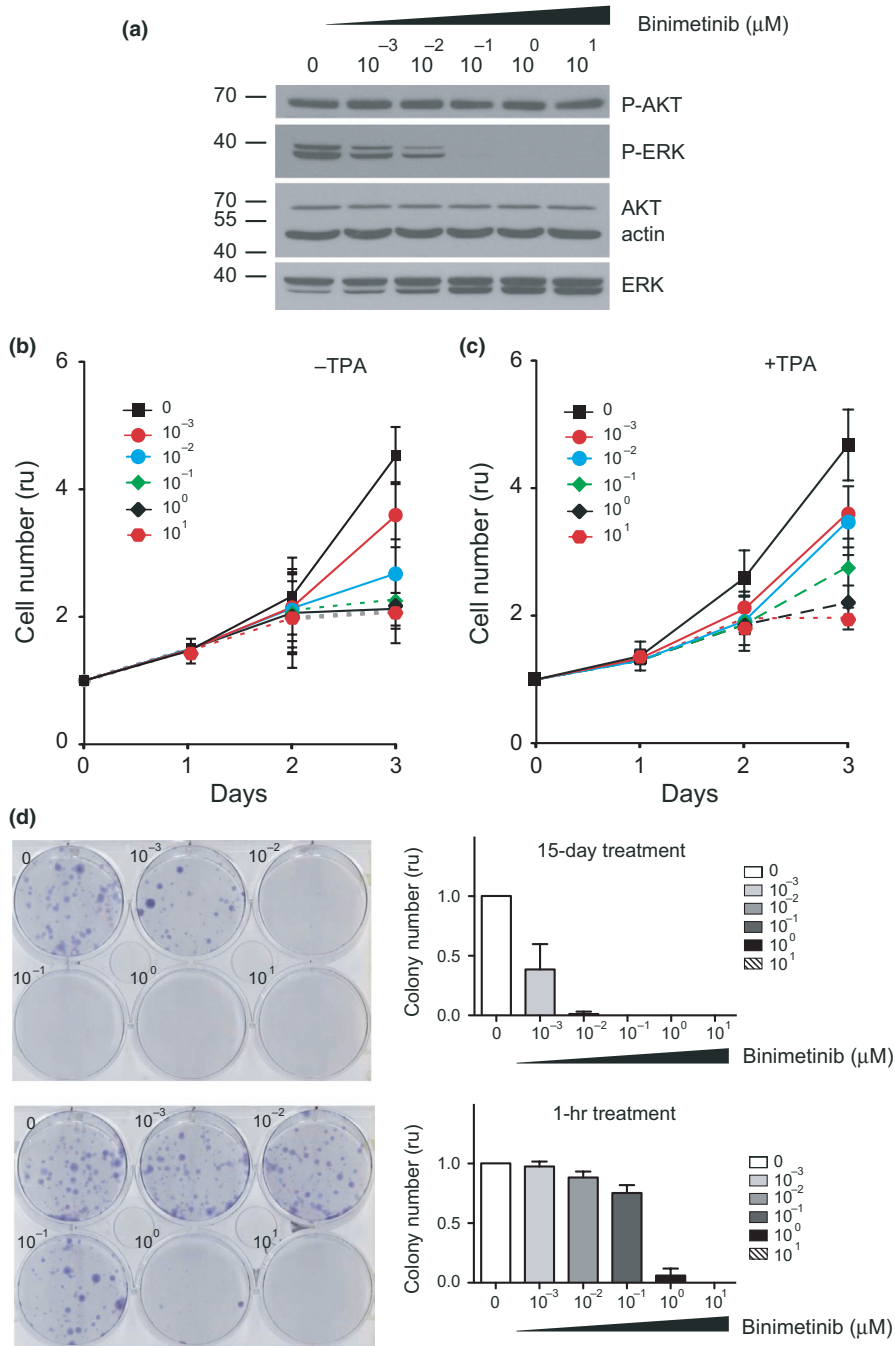
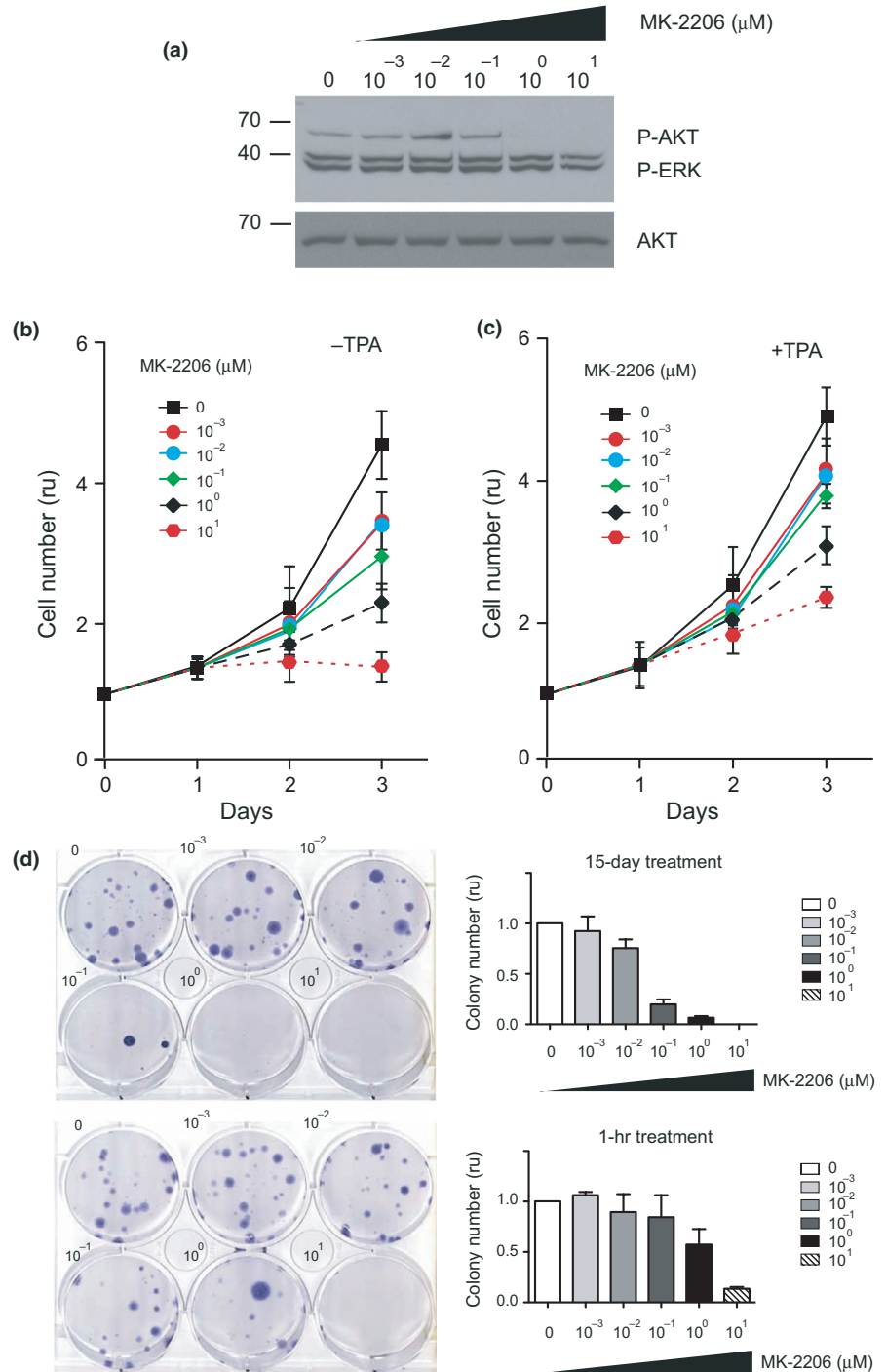


FIGURE 5 The Mek inhibitor binimetinib inhibits the growth of the 1014 melanoma cell line in vitro. (a) Western blot analysis of 1014 cells exposed to binimetinib at the indicated concentrations for 1 hr before lysis, using the antibodies mentioned at the right of the panel. (b, c) Growth curves of 1014 melanoma cells cultivated in the absence (b) or presence (c) of 200 nM TPA, with or without the Mek inhibitor binimetinib at the indicated concentrations. The inhibitor was added 24 hr after plating. Results are expressed as the ratio of the number of cells for each timepoint over the number of cells plated at the beginning of the experiment (time 0). (d) Clonogenic growth of 1014 cells in the presence or absence of the Mek inhibitor binimetinib. Cells were seeded at cloning density (500 cells per six-well dish) at day 0. Binimetinib was added 24 hr after plating, at the indicated concentrations, in complete medium and the medium left either for 14 days or 1 hr and then replaced by complete medium. Crystal violet-stained colonies were counted on images. Representative images of the colonies of three experiments are shown. Results are expressed as the relative amount compared with the vehicle control-treated samples and represent the average \pm SD of three independent experiments

Akt, p-Akt, S6, and p-S6) in the melanocyte and melanoma cell lines in the presence or absence of TPA (Figure 4a). The levels of Erk and Akt were similar in the cell lines in the presence or absence of TPA. An increase in the levels of p-Akt and p-Erk was not induced by TPA treatment of the melanoma cells. However, the level of S6 was higher in the melanocyte cell lines in the presence of TPA, but this induction was modest or not observed in the melanoma cell lines. The mechanism by which the level of S6 protein in melanocytes is induced in the presence of TPA is still unknown. The level of p-S6 was higher in the presence of TPA in all cell lines as expected (Trevillyan, Kulkarni, & Byus, 1984). p-S6 and p-Akt were barely detectable in the 9v, R90, and R91a melanocyte cell lines in the absence of TPA.

Next, we evaluated the requirement for NRAS on cell growth in the NRAS melanoma cell lines. We knocked down NRAS in both the 1007 and 1014 cells at 48 hr using two independent siRNAs (Figure 4b). Knockdown was associated with a reduction in cell confluency relative to control knockdowns (Figure 4c,d). siRNA #2 led to a larger reduction in cell growth than siRNA #1. We then used RPPA to examine the signaling changes with >300 phospho- and total protein antibodies. The levels of nine epitopes were affected after reducing the level of NRAS in both the 1007 and 1014 melanoma cells (Figure 4e; Figure S5). Upon knockdown of NRAS, there was a significant reduction in the NRAS effectors p-S6 (S235-236), p-p90 RSK (T573), and insulin receptor in both cell lines. The reduction in NRAS

FIGURE 6 The Akt inhibitor MK-2206 2HCl inhibits the growth of the 1014 melanoma cell line in vitro. (a) Western blot analysis of 1014 cells exposed to MK-2206 2HCl at the indicated concentrations for 1 hr before lysis, using the antibodies mentioned at the right of the panel. (b, c) Growth curves of 1014 melanoma cells cultivated in the absence (b) or presence (c) of 200 nM TPA, with or without the Akt inhibitor MK-2206 2HCl at the indicated concentrations. The inhibitor was added 24 hr after plating. Results are expressed as the ratio of the number of cells at each timepoint over the number of cells plated at the beginning of the experiment (time 0). (d) Clonogenic growth of 1014 cells in the presence or absence of the Akt inhibitor MK-2206 2HCl. Cells were seeded at cloning density (500 cells per six-well dish) at day 0. MK-2206 2HCl was added 24 hr after plating, at the indicated concentrations in complete medium, and the medium left either for 14 days or 1 hr and replaced by complete medium. Crystal violet-stained colonies were counted on images. Representative images of the colonies of three experiments are shown. Results are expressed as the relative amount compared with the vehicle control-treated samples and represent the average \pm SD of three independent experiments



levels can also induce a reduction in the level of phosphorylation of Akt (T308 and S473), CDC2-pY15, CYCLIN E1, and S6-pS240/S244 and an increase in the level of LRP6-pS1490. Thus, the Mapk and Akt signaling pathways are dependent on the presence of the activated form of human NRAS^{Q61K} in these melanoma cell lines.

We evaluated the action of binimetinib (a Mek inhibitor) and MK-2206 2HCl (an Akt inhibitor) on 1014 melanoma cells in vitro and in vivo. As expected, binimetinib had a dose-dependent effect on the phosphorylation of Erk and no effect on the phosphorylation of Akt (Figure 5a). We evaluated the growth of 1014 melanoma cells in the presence or absence of TPA and in the presence

of various doses of binimetinib (Figure 5b,c). A minimum of 10⁻³ μM binimetinib was required to affect the growth of 1014 melanoma cells in the presence or absence of TPA. We evaluated the cytotoxicity of binimetinib against 1014 melanoma cells using a colony-forming assay. Binimetinib was added to the cells 1 hr before allowing them to form colonies for 15 days (Figure 5d). Under these conditions, 1 μM binimetinib was sufficient to reduce the number of colonies by approximately 90%. Moreover, 0.01 μM binimetinib had a similar effect when the drug was present for the entire period of growth. We obtained similar results with another Mek inhibitor, PD-0325901 (Figure S6). Similarly, MK-2206 2HCl

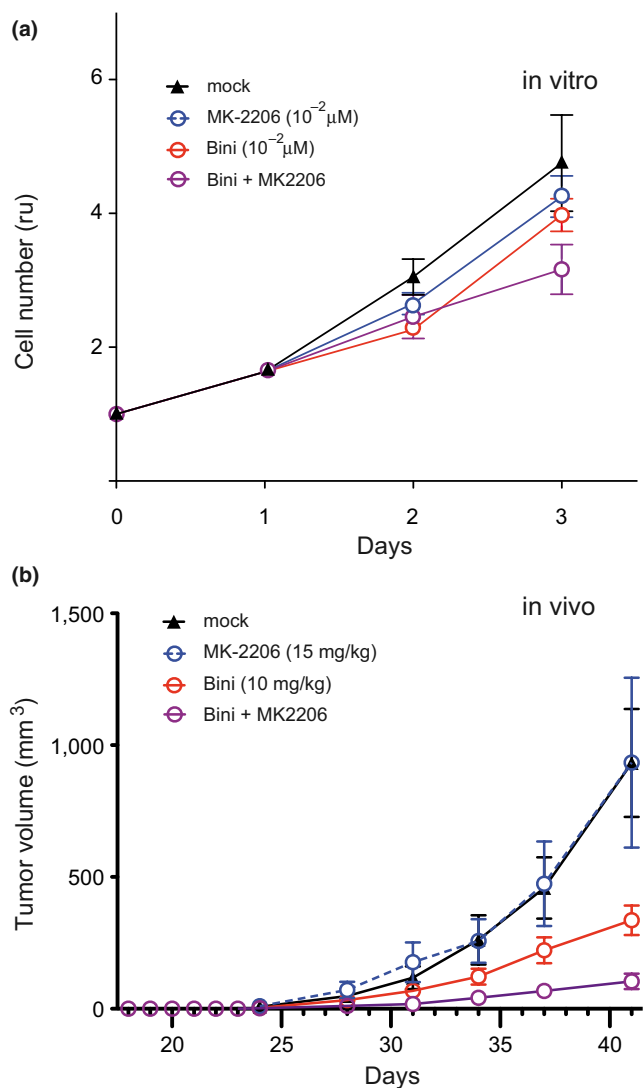


FIGURE 7 In vivo tumor growth in the presence of Mek and/or Akt inhibitors. (a) Growth curves of 1014 melanoma cells cultivated with the Akt inhibitor MK-2206 2HCl, Mek inhibitor binimetinib, or both at the indicated concentrations or no inhibitor. Inhibitors were added 24 hr after plating. Results are expressed as the ratio of the number of cells at each timepoint over the number of cells plated at the beginning of the experiment (time 0). These experiments were performed in the absence of TPA. (b) Established 1014 melanoma cells were injected subcutaneously in the flanks of female C57BL/6 mice (10^5 cells per side). At day 21, the mice were assigned to four treatment groups (12 mice per group): vehicle only (mock), binimetinib only, MK-2206 2HCl only, and binimetinib and MK-2206 2HCl. Mice were treated by oral gavage for 21 consecutive days with binimetinib at 10 mg/kg per day and/or MK-2206 2HCl at 15 mg/kg per day. Tumor size was measured by caliper every 2–3 days and calculated as (length \times width \times height)/2. Arrows indicate the beginning and end of treatment. Results are expressed as mean tumor volumes \pm SEM for each treatment group. Growth curves for each individual tumor are shown in Figure S6

had a dose-dependent effect on the phosphorylation of Akt and no effect on the phosphorylation of Erk (Figure 6a). We evaluated the growth of 1014 melanoma cells in the presence or absence of TPA and in the presence of various doses of MK-2206 (Figure 6b,c).

In the absence of TPA, the action of MK-2206 on the growth of the cells was observable at a very low dose (10^{-3} nM). However, 10 nM MK-2206 was required to block the growth of these cells. In the presence of TPA, the effect of MK-2206 on 1014 melanoma cells was slightly less than in its absence. We evaluated the cytotoxicity of MK-2206 against 1014 melanoma cells using a colony-forming assay. MK-2206 was added to the cells for 1 hr before allowing them to form colonies for 15 days (Figure 6d). Under these conditions, 10 nM MK-2206 was sufficient to reduce the number of colonies by approximately 90%.

We then evaluated the action of MK-2206 and binimetinib on the growth of 1014 melanoma cells in vitro and in vivo in C57BL/6 mice (Figure 7; Figure S7). In vitro, the action of the two compounds on 1014 cell growth after 3 days of treatment was additive (Figure 7a). In vivo, MK-2206 did not affect the growth of melanoma cells at a dose of 15 mg/kg, whereas binimetinib efficiently inhibited tumor growth at a dose of 10 mg/kg. Importantly, the combination of MK-2206 and binimetinib was remarkably efficient in stopping the growth of NRAS melanoma in vivo (Figure 7b).

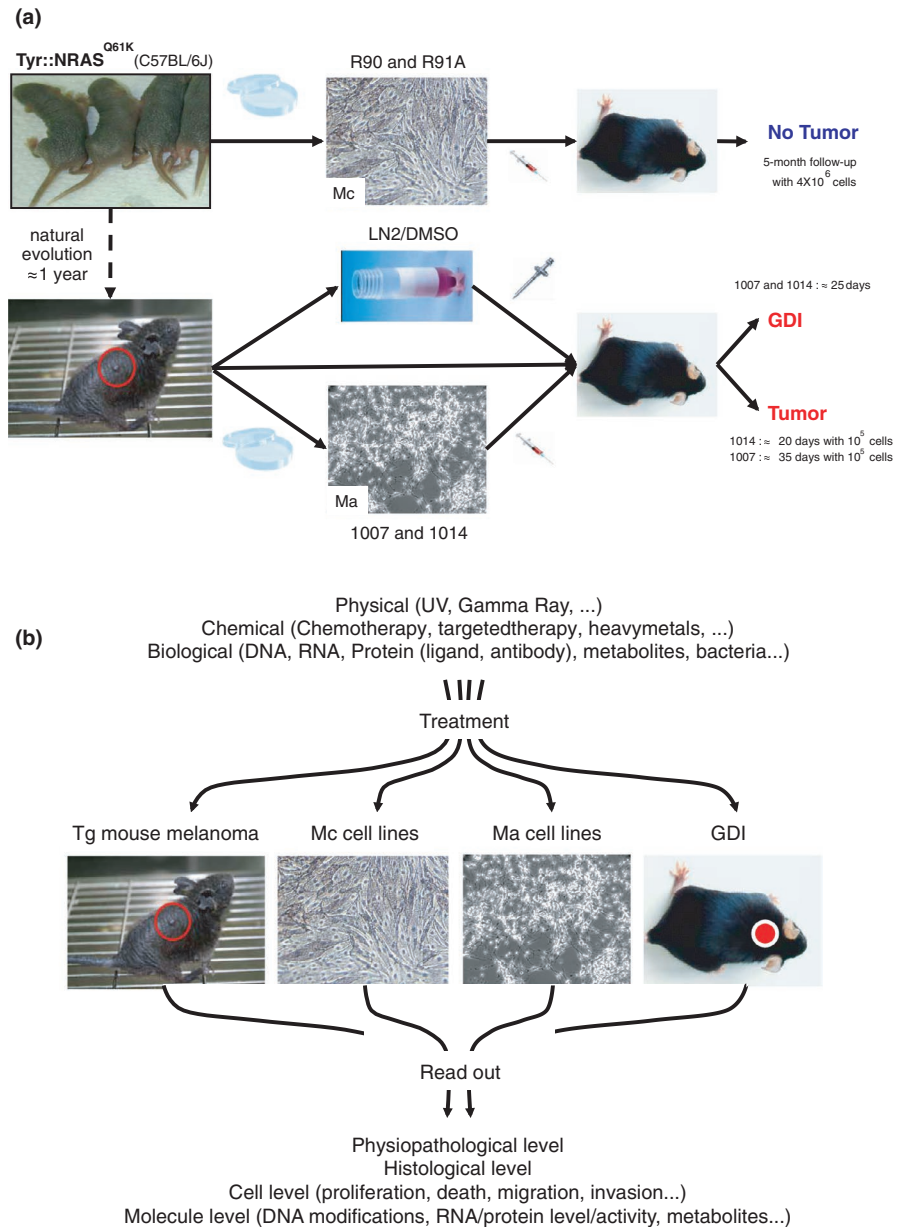
4 | DISCUSSION

The establishment of genetically coherent mouse, tumor, and cell line (transformed and non-transformed) models is of great importance for better understanding the physiology, pathophysiology, and cell and molecular biology associated with genetic and/or micro-environmental and/or environmental modifications in an immune-competent environment. Moreover, such coherent models are of importance for the testing of novel therapies (Figure 8).

In the case of melanoma, various mouse cell lines have been established for years, including Cloudman S-91 and B16 cells (Cloudman, 1941; Harding & Passey, 1930). Today, B16 is still the most popular mouse melanoma cell line and is used throughout the world. Indeed, B16 melanoma cells have been cited approximately 7,000 times, according to the Web of Science (January 2019), and in 2018, B16 melanoma cells appeared in at least 320 publications. Several B16 melanoma subclones have been derived from the original one, including B16.F1, B16.F10, and B16.C3. B16 melanoma cell lines have the advantage of being syngeneic to C57BL/6, growing subcutaneously in C57BL/6 or nude mice, forming metastasis in the lung, being amenable to genetic manipulation, and remaining pigmented. However, this model was generated after multiple aggressive treatments (B. Mintz, personal communication). Thus, the B16 melanoma cell model is not relevant to human skin melanoma, as the mutations do not reflect the human mutations and the key signaling pathways involved in melanomagenesis are profoundly different between this cell line and human melanoma. However, despite its shortcomings, it should not be forgotten that the B16 melanoma cell line has allowed researchers to shed light on numerous crucial processes.

The generation of transgenic mice has allowed the establishment of mouse melanoma models (for review see (Aktary,

FIGURE 8 Establishment of the mouse NRAS melanoma model and functional tests. (a) Mouse melanocyte (Mc) and melanoma (Ma) cell lines were established in culture from P1 newborn transgenic (tg) pups and primary melanomas, respectively. Mouse melanocyte and melanoma cell lines were subcutaneously injected into C57BL/6 mice to evaluate their ability to grow in vivo. Melanoma tumors were frozen in liquid nitrogen (LN2) in the presence of fetal calf serum/DMSO (90/10, v/v) prior to thawing, washing, and implantation in C57BL/6 mice to generate genetically derived isografts (GDIs). One hundred thousand established 1007 and 1014 melanoma cells were injected subcutaneously in the flanks of C57BL/6 mice to generate tumors in approximately 1 month. (b) Tg animals, Mc, Ma, and GDIs can be subjected to physical, chemical, and biological treatment. Various readouts can be performed



Mcmahon, & Larue, 2018; Larue & Beermann, 2007)). Melanoma cell lines have already been established from some of them. For example, the groups of Constance Brinckerhoff and Marcus Bosenberg established a series of Braf^{V600E} melanoma cell lines, known as D4M and YUMM (Jenkins et al., 2014; Meeth, Wang, Micevic, Damsky, & Bosenberg, 2016), and that of Thomas Tüting established melanoma cell lines expressing the oncogenic form of CDK4^{R24C} (Bald et al., 2014).

We decided to focus on the NRAS mutation, as this mutation is frequently found in human melanoma and involved in melanoma initiation. Furthermore, no targeted therapy for NRAS mutations is yet available nor C57BL/6 congenic mouse NRAS melanoma cells. Recently, it was shown that the compound ZT-12-037-01 can inhibit the serine–threonine kinase STK19, which phosphorylates NRAS on serine S89, leading to its activation (Yin et al., 2019). This new target and compound are promising and may constitute a way to inhibit

NRAS activation in melanoma. The Tyr::NRAS^{Q61K} mouse melanoma line was previously generated by the group of Friedrich Beermann (Ackermann et al., 2005). We backcrossed the initial Tyr::NRAS^{Q61K} mice to male and female C57BL/6J mice more than 12 times to achieve a minimum of 99.95% C57BL/6J, allowing the establishment of a C57BL/6J congenic Tyr::NRAS^{Q61K} mouse line (Longvert et al., 2011). Here, we established and characterized a coherent C57BL/6 mouse NRAS melanoma model, including melanocyte cell lines, melanoma cell lines, GDIs, and the transgenic mouse melanoma model that was already available. We characterized this model at the cellular, molecular, and oncogenic levels.

In vitro, we evaluated the action of Mek and Akt inhibitors in the presence and absence of TPA, as this phorbol ester is known to modify various cellular activities, including proliferation, differentiation, migration, and invasion (Denning, 2012). At the molecular level, TPA activates diacylglycerol (DAG), which in turn activates

multiple PKC isoforms, triggering Mapk/Mek/Erk signaling, as well as GSK3-beta and IKK-beta signaling. Aside from the activation of proliferation, PKC enzymes profoundly influence actin cytoskeleton organization and several PKC isoforms have been shown to colocalize with various specific components of the actin, vimentin, and/or tubulin cytoskeleton (Szalay et al., 2001). The activation of these PKC isoforms and subsequent cytoskeletal reorganization may strongly influence the efficacy/availability of Mek inhibitors. However, our results did not show the mixture of TPA and Mek/Akt inhibitors to have much of an effect on the growth of these cells.

The action of the combination of Mek and Akt inhibitors on this mouse NRAS melanoma model was very efficient. Nonetheless, it is highly probable that the combination of Mek and Akt inhibitors on NRAS melanoma patients is not sufficient. Indeed, trametinib and GSK2141795 were used in combination on NRAS and "WT" human melanoma patients to inhibit Mek and Akt, respectively (Algazi et al., 2018). However, no clinical benefit in NRAS-metastatic patient was observed. These results may reveal different issues: (a) These drugs were not sufficiently specific, (b) the protocol of administration was suboptimal, and/or (c) the strategy was not ideal. Indeed, human melanoma is highly genetically and epigenetically unstable (Goodall et al., 2008; Hoek & Goding, 2010; Lawrence et al., 2013). Targeting these two signaling pathways may not be sufficient in this context, as these tumors may carry other abnormalities (genetic or not) that induce natural neo-resistance to these inhibitors. Complementary (combinatory) therapies, including immune therapy, NRAS targeted therapy, or even radiotherapy, could be beneficial for patients. Better molecular knowledge of the patients and their tumors would also be beneficial to optimally adapt treatment (Najem et al., 2017). For example, the immune checkpoint inhibitors, anti CTLA-4 and anti-PD1/PDL1, can be used in combination with Mek inhibitors with a certain level of success on NRAS-mutated melanoma in vivo. Moreover, the combination of Mek inhibitor, trametinib, and radiotherapy on NRAS-mutated melanoma prolonged G1 arrest and premature senescence in vitro, is well-tolerated, and reduces tumor growth in vivo. Furthermore, the combination of a Mek inhibitor and the reactivation of p53 NRAS-mutated melanoma cells show a strong synergistic effect. Overall, we provide the proof of concept that this NRAS melanoma model can be used to test novel therapies.

In conclusion, we have no doubt that the proper use of the mouse NRAS^{Q61K} melanoma mouse model (cell lines and GDI) will allow the scientific community to better evaluate melanoma progression and efficiently test novel therapies.

ACKNOWLEDGMENTS

This work was supported by the Ligue Contre le Cancer, Fondation ARC, Institut Carnot, INCa, and ITMO Cancer and is under the program "Investissements d'Avenir" launched by the French Government and implemented by ANR Labex CeTisPhyBio (ANR-11-LABX-0038 and ANR-10-IDEX-0001-02

PSL). JR is supported by a fellowship from MENRT. Work in the Aplin Lab was supported by grants from Department of Defense (W81XWH-18-1-0224) and the Dr. Miriam and Sheldon G. Adelson Medical Research Foundation. The RPPA studies were performed at the Functional Proteomics Core Facility at The University of Texas MD Anderson Cancer Center, which is supported by a NCI Cancer Center Support Grant (CA16672). We thank the members of the laboratory "Normal and Pathological Development of Melanocytes." We also thank the staff in charge of the animal facilities of the Institut Curie, especially Pauline Dubreuil. A.E. Aplin reports receiving a commercial research grant from Pfizer Inc. (2013-2017) and has ownership interest in patent number 9880150.

CONFLICT OF INTEREST

The authors declare that they have no conflict of interest.

ORCID

Andrew E. Aplin  <https://orcid.org/0000-0001-5967-0939>

Lionel Larue  <https://orcid.org/0000-0002-2010-6107>

REFERENCES

- Ackermann, J., Fruttschi, M., Kaloulis, K., Mckee, T., Trumpp, A., & Beermann, F. (2005). Metastasizing melanoma formation caused by expression of activated N-RasQ61K on an INK4a-deficient background. *Cancer Research*, *65*, 4005–4011.
- Aktary, Z., McMahon, M., & Larue, L. (2018). Animal models of melanoma. In D. Fisher, & B. Bastian (Eds.), *Melanoma*. New York, NY:Springer.
- Algazi, A. P., Esteve-Puig, R., Nosrati, A., Hinds, B., Hobbs-Muthukumar, A., Nandoskar, P., ... Daud, A. (2018). Dual MEK/AKT inhibition with trametinib and GSK2141795 does not yield clinical benefit in metastatic NRAS-mutant and wild-type melanoma. *Pigment Cell and Melanoma Research*, *31*, 110–114. <https://doi.org/10.1111/pcmr.12644>
- Bald, T., Quast, T., Landsberg, J., Rogava, M., Glodde, N., Lopez-Ramos, D., ... Tüting, T. (2014). Ultraviolet-radiation-induced inflammation promotes angiogenesis and metastasis in melanoma. *Nature*, *507*, 109–113. <https://doi.org/10.1038/nature13111>
- Bennett, D. C., Cooper, P. J., Dexter, T. J., Devlin, L. M., Heasman, J., & Nester, B. (1989). Cloned mouse melanocyte lines carrying the germline mutations albino and brown: Complementation in culture. *Development*, *105*, 379–385.
- Bennett, D. C., Cooper, P. J., & Hart, I. R. (1987). A line of non-tumorigenic mouse melanocytes, syngeneic with the B16 melanoma and requiring a tumour promoter for growth. *International Journal of Cancer*, *39*, 414–418. <https://doi.org/10.1002/ijc.2910390324>
- Bray, F., Ferlay, J., Soerjomataram, I., Siegel, R. L., Torre, L. A., & Jemal, A. (2018). Global cancer statistics 2018: GLOBOCAN estimates of incidence and mortality worldwide for 36 cancers in 185 countries. *CA: A Cancer Journal for Clinicians*, *68*, 394–424. <https://doi.org/10.3322/caac.21492>
- Cancer Genome Atlas Network (2015). Genomic classification of cutaneous melanoma. *Cell*, *161*, 1681–1696.
- Carvalho, B. S., & Irizarry, R. A. (2010). A framework for oligonucleotide microarray preprocessing. *Bioinformatics*, *26*, 2363–2367. <https://doi.org/10.1093/bioinformatics/btq431>

- Cloudman, A. M. (1941). The effect of an extra-chromosomal influence upon transplanted spontaneous tumors in mice. *Science*, *93*, 380–381. <https://doi.org/10.1126/science.93.2416.380>
- Delmas, V., Beermann, F., Martinuzzi, S., Carreira, S., Ackermann, J., Kumasaka, M., ... Larue, L. (2007). Beta-catenin induces immortalization of melanocytes by suppressing p16INK4a expression and cooperates with N-Ras in melanoma development. *Genes and Development*, *21*, 2923–2935. <https://doi.org/10.1101/gad.450107>
- Denning, M. F. (2012). Specifying protein kinase C functions in melanoma. *Pigment Cell and Melanoma Research*, *25*, 466–476. <https://doi.org/10.1111/j.1755-148X.2012.01015.x>
- Gallagher, S. J., Luciani, F., Berlin, I., Rambow, F., Gros, G., Champeval, D., ... Larue, L. (2011). General strategy to analyse melanoma in mice. *Pigment Cell and Melanoma Research*, *24*, 987–988. <https://doi.org/10.1111/j.1755-148X.2011.00907.x>
- Goodall, J., Carreira, S., Denat, L., Kobi, D., Davidson, I., Nuciforo, P., ... Goding, C. R. (2008). Brn-2 represses microphthalmia-associated transcription factor expression and marks a distinct subpopulation of microphthalmia-associated transcription factor-negative melanoma cells. *Cancer Research*, *68*, 7788–7794. <https://doi.org/10.1158/0008-5472.CAN-08-1053>
- Grille, S. J., Bellacosa, A., Upson, J., Klein-Szanto, A. J., Van Roy, F., Lee-Kwon, W., ... Larue, L. (2003). The protein kinase Akt induces epithelial mesenchymal transition and promotes enhanced motility and invasiveness of squamous cell carcinoma lines. *Cancer Research*, *63*, 2172–2178.
- Harding, H. E., & Passey, R. D. (1930). A transplantable melanoma of the mouse. *The Journal of Pathology and Bacteriology*, *33*, 417–427. <https://doi.org/10.1002/path.1700330219>
- Hoek, K. S., & Goding, C. R. (2010). Cancer stem cells versus phenotype-switching in melanoma. *Pigment Cell and Melanoma Research*, *23*, 746–759. <https://doi.org/10.1111/j.1755-148X.2010.00757.x>
- Jéhannin-Ligier, K., Dantony, E., Bossard, N., Molinié, F., Defossez, G., Daubisse-Marliac, L., ... Uhry, Z. (2017). *Projection de l'incidence et de la mortalité par cancer en France métropolitaine en 2017*. Rapport technique. Saint-Maurice: Santé publique France. 80p.
- Jenkins, M. H., Steinberg, S. M., Alexander, M. P., Fisher, J. L., Ernstoff, M. S., Turk, M. J., ... Brinckerhoff, C. E. (2014). Multiple murine BRAF(V600E) melanoma cell lines with sensitivity to PLX4032. *Pigment Cell and Melanoma Research*, *27*, 495–501.
- Kassambara, A., & Mundt, F. (2017). *factoextra: Extract and visualize the results of multivariate data analyses*. R package version 1.0.5.
- Kolde, R. (2018). *heatmap: Pretty heatmaps*. R package version 1.0.12.
- Larue, L., & Beermann, F. (2007). Cutaneous melanoma in genetically modified animals. *Pigment Cell Research*, *20*, 485–497. <https://doi.org/10.1111/j.1600-0749.2007.00411.x>
- Larue, L., & Mintz, B. (1990). Pigmented cell lines of mouse albino melanocytes containing a tyrosinase cDNA with an inducible promoter. *Somatic Cell and Molecular Genetics*, *16*, 361–368. <https://doi.org/10.1007/BF01232464>
- Lawrence, M. S., Stojanov, P., Polak, P., Kryukov, G. V., Cibulskis, K., Sivachenko, A., ... Getz, G. (2013). Mutational heterogeneity in cancer and the search for new cancer-associated genes. *Nature*, *499*, 214–218. <https://doi.org/10.1038/nature12213>
- Le, S., Josse, J., & Husson, F. (2008). FactoMineR: An R package for multivariate analysis. *Journal of Statistical Software*, *25*, 1–18.
- Longvert, C., Gros, G., Beermann, F., Marais, R., Delmas, V., & Larue, L. (2011). Murine cutaneous melanoma models. Importance of the genetic background. *Annales de Pathologie*, *31*, S70–S73.
- Meeth, K., Wang, J. X., Micevic, G., Damsky, W., & Bosenberg, M. W. (2016). The YUMM lines: A series of congenic mouse melanoma cell lines with defined genetic alterations. *Pigment Cell and Melanoma Research*, *29*, 590–597. <https://doi.org/10.1111/pcmr.12498>
- Najem, A., Krayem, M., Perdrix, A., Kerger, J., Awada, A., Journe, F., & Ghanem, G. (2017). New drug combination strategies in melanoma: Current status and future directions. *Anticancer Research*, *37*, 5941–5953.
- Pla, P., Solov'eva, O., Moore, R., Alberti, C., Kunisada, T., & Larue, L. (2004). Dct:lacZ ES cells: A novel cellular model to study melanocyte determination and differentiation. *Pigment Cell Research*, *17*, 142–149. <https://doi.org/10.1046/j.1600-0749.2003.00121.x>
- Rambow, F., Job, B., Petit, V., Gesbert, F., Delmas, V., Seberg, H., ... Larue, L. (2015). New functional signatures for understanding melanoma biology from tumor cell lineage-specific analysis. *Cell Reports*, *13*, 840–853. <https://doi.org/10.1016/j.celrep.2015.09.037>
- Ritchie, M. E., Phipson, B., Wu, D., Hu, Y., Law, C. W., Shi, W., & Smyth, G. K. (2015). limma powers differential expression analyses for RNA-seq and microarray studies. *Nucleic Acids Research*, *43*, e47. <https://doi.org/10.1093/nar/gkv007>
- Szalay, J., Bruno, P., Bhati, R., Adjodha, J., Schueler, D., Summerville, V., & Vazeos, R. (2001). Associations of PKC isoforms with the cytoskeleton of B16F10 melanoma cells. *Journal of Histochemistry and Cytochemistry*, *49*, 49–66. <https://doi.org/10.1177/002215540104900106>
- Talloe, W., & Verbeke, T. (2018). *a4Preproc: Automated affymetrix array analysis preprocessing package*. R package version 1.30.0.
- Tibes, R., Qiu, Y., Lu, Y., Hennessy, B., Andreeff, M., Mills, G. B., & Kornblau, S. M. (2006). Reverse phase protein array: Validation of a novel proteomic technology and utility for analysis of primary leukemia specimens and hematopoietic stem cells. *Molecular Cancer Therapeutics*, *5*, 2512–2521. <https://doi.org/10.1158/1535-7163.MCT-06-0334>
- Trevillyan, J. M., Kulkarni, R. K., & Byus, C. V. (1984). Tumor-promoting phorbol esters stimulate the phosphorylation of ribosomal protein S6 in quiescent Reuber H35 hepatoma cells. *Journal of Biological Chemistry*, *259*, 897–902.
- Wickham, H. (2016). *ggplot2: Elegant graphics for data analysis*. New York, NY: Springer-Verlag.
- Yin, C., Zhu, B. O., Zhang, T., Liu, T., Chen, S., Liu, Y. U., ... Cui, R. (2019). Pharmacological targeting of STK19 inhibits oncogenic NRAS-driven melanomagenesis. *Cell*, *176*(1113–1127), e16. <https://doi.org/10.1016/j.cell.2019.01.002>
- Yu, G., Wang, L. G., Han, Y., & He, Q. Y. (2012). clusterProfiler: An R package for comparing biological themes among gene clusters. *OMICS: A Journal of Integrative Biology*, *16*, 284–287. <https://doi.org/10.1089/omi.2011.0118>

SUPPORTING INFORMATION

Additional supporting information may be found online in the Supporting Information section at the end of the article.

How to cite this article: Petit V, Raymond J, Alberti C, et al. C57BL/6 congenic mouse NRAS^{Q61K} melanoma cell lines are highly sensitive to the combination of MEK and AKT inhibitors in vitro and in vivo. *Pigment Cell Melanoma Res*. 2019;00:1–13. <https://doi.org/10.1111/pcmr.12807>

II. BRN2 is a non-canonical melanoma tumor-suppressor








Article publié en juin 2021

Résumé :

Le facteur de transcription BRN2 est associé à la progression dans la mélanomagenèse, mais son rôle dans l'initiation est peu connu. Nous avons généré, au laboratoire, modèle murin de mélanome haplo-insuffisant pour BRN2 dans un contexte BrafV600E PtenF/+. Nous avons montré que l'haplo-insuffisance de BRN2 favorise l'initiation et la progression du mélanome. Nous avons montré à l'échelle moléculaire que BRN2 induit directement l'expression de PTEN et réprime en conséquence la signalisation PI3K. Nous avons également montré un rôle dans l'invasion cellulaire de l'haplo-insuffisance de BRN2.

Ma participation à cette étude a concerné toutes les analyses transcriptomiques réalisées aussi bien sur les tumeurs que sur les cellules. J'ai pu mettre en évidence que l'haplo-insuffisance de BRN2 induit l'expression de signature d'invasion, validée ensuite *in vitro*. Cet effet pro-invasif explique la formation de métastases ganglionnaires observée *in vivo*. Cet effet pro-invasif peut être dû à l'expression d'*Axl*, car ce gène est surexprimé dans les mélanomes et les cellules établies en culture haplo-insuffisantes pour Brn2.

BRN2 is a non-canonical melanoma tumor-suppressor

Michael Hamm^{1,2,3,13}, Pierre Sohier ^{1,2,3,13}, Valérie Petit^{1,2,3,13}, Jérémy H. Raymond^{1,2,3},
Véronique Delmas ^{1,2,3}, Madeleine Le Coz^{1,2,3}, Franck Gesbert^{1,2,3}, Colin Kenny⁴, Zackie Aktary^{1,2,3},
Marie Pouteaux^{1,2,3}, Florian Rambow^{1,2,3}, Alain Sarasin⁵, Nisamanee Charoenchon^{1,2,3,6}, Alfonso Bellacosa⁷,
Luis Sanchez-del-Campo ⁸, Laura Mosteo⁸, Martin Lauss⁹, Dies Meijer ¹⁰, Eirikur Steingrimsón¹¹,
Göran B. Jönsson⁹, Robert A. Cornell⁴, Irwin Davidson ^{4,12}, Colin R. Goding ⁸✉ & Lionel Larue ^{1,2,3}✉

While the major drivers of melanoma initiation, including activation of NRAS/BRAF and loss of *PTEN* or *CDKN2A*, have been identified, the role of key transcription factors that impose altered transcriptional states in response to deregulated signaling is not well understood. The POU domain transcription factor BRN2 is a key regulator of melanoma invasion, yet its role in melanoma initiation remains unknown. Here, in a *Braf*^{V600E} *Pten*^{F/+} context, we show that *BRN2* haplo-insufficiency promotes melanoma initiation and metastasis. However, metastatic colonization is less efficient in the absence of Brn2. Mechanistically, BRN2 directly induces *PTEN* expression and in consequence represses PI3K signaling. Moreover, MITF, a BRN2 target, represses *PTEN* transcription. Collectively, our results suggest that on a *PTEN* heterozygous background somatic deletion of one *BRN2* allele and temporal regulation of the other allele elicits melanoma initiation and progression.

¹Institut Curie, Université PSL, CNRS UMR3347, Inserm U1021, Normal and Pathological Development of Melanocytes, Orsay, France. ²Université Paris-Saclay, CNRS UMR3347, Inserm U1021, Signalisation radiobiologie et cancer, Orsay, France. ³Équipes Labellisées Ligue Contre le Cancer, Paris, France. ⁴Department of Anatomy and Cell biology, Carver College of Medicine, University of Iowa, Iowa City, IA, USA. ⁵Laboratory of Genetic Instability and Oncogenesis, UMR8200 CNRS, Gustave Roussy, Université Paris-Sud, Villejuif, France. ⁶Department of Pathobiology, Faculty of Science, Mahidol University, Bangkok, Thailand. ⁷Cancer Epigenetics Program, Fox Chase Cancer Center, Philadelphia, PA, USA. ⁸Ludwig Institute for Cancer Research, Nuffield Department of Clinical Medicine, University of Oxford, Headington, Oxford, UK. ⁹Department of Oncology, Clinical Sciences Lund, Lund University and Skåne University Hospital, Lund, Sweden. ¹⁰Centre of Neuroregeneration, University of Edinburgh, Edinburgh, UK. ¹¹Department of Biochemistry and Molecular Biology, and Department of Anatomy, BioMedical Center, Faculty of Medicine, University of Iceland, Reykjavik, Iceland. ¹²Department of Functional Genomics and Cancer, Institut de Génétique et de Biologie Moléculaire et Cellulaire, CNRS/INSERM/UNISTRA, 1 Rue Laurent Fries, 67404 Illkirch, Cedex, France. ¹³These authors contributed equally: M Hamm, P Sohier, V Petit. ✉email: colin.goding@ludwig.ox.ac.uk; lionel.larue@curie.fr

Cancer initiation is triggered by the activation of oncogenic signaling combined with senescence bypass. Yet while many typical oncogenes and tumor suppressors that affect cancer initiation have been identified, cancer initiation is likely to be modulated by additional genetic events. Understanding how non-classical driver mutations may impact cancer initiation is a key issue that has been relatively underexplored. Melanoma, a highly aggressive skin cancer, arises through the acquisition of well-defined genetic and epigenetic modifications in oncogenes and tumor suppressors and represents an excellent model system to address this key question.

As a highly genetically unstable cancer type, the initiation of melanoma requires the induction of melanocyte proliferation, which is mediated by several major founder mutations, the most common of which are *BRAF*^{V600E} and *NRAS*^{Q61K/R1.2}. However, activation of *BRAF* or *NRAS* is insufficient to promote melanoma initiation without senescence bypass mediated by additional founder mutations or expression changes of several genes including *p16*^{INK4A}, *CTNBN1*, *PTEN*, or *MDM4*^{3–7}.

The transcription factor *BRN2*, also known as *POU3F2* and *N-OCT3*, plays a critical role in neurogenesis and drives proliferation in a range of cancer types with neural or neuroendocrine origins, including glioblastoma, neuroblastoma, small cell lung cancer, and neuroendocrine prostate cancer^{8–10}. In the melanocyte lineage, *BRN2* is not detected in melanoblasts *in vivo* but is heterogeneously expressed in naevi and melanoma^{11–14}. *In vitro* studies have shown that *BRN2* expression is induced by a range of melanoma-associated signaling pathways including activation of the mitogen-activated protein kinase (MAPK) pathway downstream from *BRAF*, the PI3K pathway, the LEF- β -catenin axis, as well as FGF, TNF- α , EDN3, and SCF signaling^{14–17}. Consistent with *BRN2* being expressed in a predominantly mutually exclusive pattern with the Microphthalmia-associated transcription factor (MITF)¹³ that plays a crucial role in melanoma proliferation¹⁸, *BRN2* is repressed by MITF via miR-211¹⁹. However, the relationship between MITF and *BRN2* is complex. For example, *BRN2* was recently found to be regulated by E2F1, a cell cycle-regulated transcription factor that is also a target for MITF, and both *BRN2* and MITF are regulated by PAX3 and WNT/ β -catenin^{15,16,20–24}. Indeed, both *BRN2* and MITF can regulate expression of *AXL*^{21,25}, with *BRN2* repressing *AXL* expression, thus enabling some cells in human melanoma to adopt an *AXL*^{High}, *MITF*^{Low} and *BRN2*^{Low} state²⁵. The activation of *BRN2* expression in a specific subset of melanoma cells in response to all three major signaling pathways (MAPK, PI3K/*PTEN*, and β -catenin) linked to melanoma initiation (early proliferation and bypass/escape senescence) and progression (including late proliferation and metastatic dissemination) suggests that *BRN2* is likely to have a critical role in disease progression²⁶. Most notably, *BRN2* has been associated with *MITF*^{Low} senescent or slow-cycling cells¹¹, and identified as a key regulator of melanoma invasion and anoikis *in vitro*^{13,27,28} and in *in vivo* xenograft experiments^{20,29,30}. Mechanistically, the ability of *BRN2* to promote invasion has been linked to its ability to control expression of PDE5A-mediated cell contractility, phosphorylation of myosin light chain 2, repression of MITF and PAX3, and cooperation with bi-allelic loss of *CDKN2A*^{13,20,27,30}. However, despite abundant information linking *BRN2* to melanoma proliferation and invasiveness *in vitro* and in xenograft experiments, the impact of *BRN2* on melanoma initiation and progression *in vivo* has never been assessed.

In this work, we show that *BRN2* acts as a tumor suppressor during melanoma initiation and progression in a *BRAF-PTEN* context since *BRN2* and MITF regulate positively and negatively the transcription of *PTEN*, respectively.

Results

BRN2 loss or low expression correlates with reduced survival and worse prognosis. Although *BRN2* has been implicated in melanoma invasiveness, and its expression is highly regulated, whether and how it may contribute to melanoma initiation or incidence is not understood. To evaluate the prevalence of *BRN2* loss in human skin cutaneous melanoma (SKCM), we retrieved copy-number alteration (CNA) data for *BRN2* in SKCM metastases (stage IV) from the Cancer Genome Atlas (TCGA, <https://cancergenome.nih.gov/>). The *BRN2* locus showed mono-allelic loss in 53% and bi-allelic loss in 2.7% of all patient samples ($n = 367$, Fig. 1A). Only a minority ($n = 29$ of 367, corresponding to 7.9%) of SKCM samples showed a copy-number gain ($n = 27$)/amplification ($n = 2$) for *BRN2*. We did not further analyze these samples since the expression of *BRN2* was slightly increased but not statistically different ($p = 0.26$, test of Kruskal-Wallis with a Dunn correction) between tumors that gained and/or amplified this locus compared to the normal situation. We screened a panel of human melanoma cell lines available in our laboratory ($n = 23$) for deletions that affect the *BRN2* locus by comparative genomic hybridization. The *BRN2* locus showed mono-allelic loss in 48% (11 out of 23) of the human melanoma cell lines and no bi-allelic loss, comparable to the TCGA-data (Supplementary Fig. 1A, Supplementary Data 1). Notably, *BRN2* mRNA levels were significantly lower in SKCM metastases with bi-allelic *BRN2* loss (Supplementary Fig. 1B). The mono- and bi-allelic loss of *BRN2* was frequently associated with a large segmental deletion of the long arm of chromosome 6 (Chr.6q) in SKCM metastases and in our cell line panel (Fig. 1B, Supplementary Fig. 1C, Supplementary Data 2). From the TCGA, patients carrying the monoallelic loss of *BRN2* in metastases displayed a trend to have a shorter overall survival than those with diploid status (Fig. 1C). These results were validated using an independent cohort of 108 regional metastases previously described³¹ (Fig. 1D). Moreover, we evaluated the number of *BRN2* alleles in nevi and melanoma that arose from these nevi using publically available data³². It appears that 28% (5 out of 18) or 22% (4 out of 18) of melanomas presented either a mono-allelic loss or a gain of *BRN2* respectively compared to nevi (Supplementary Fig. 1D). The situation is clearly complex, but we may conclude that *BRN2* mono-allelic loss can occur during the early steps of melanomagenesis.

We next assessed the correlation between *BRN2* mRNA levels and overall patient survival to evaluate the effect of *BRN2* mono-allelic loss on melanoma progression. We established “*BRN2*-high” and “*BRN2*-low” patient groups based on RNA-seq data available from the TCGA (*BRN2* subgroups defined as *BRN2*-low (≤ 1 transcript per million reads [TPM]) and *BRN2* expressed/high (> 1 TPM)). Patients in the “*BRN2*-low” group displayed significantly shorter overall survival than those of the “*BRN2*-high” group (Fig. 1E). Overall, the *BRN2* locus, frequently associated with a large segmental deletion, is lost (mono- and bi-allelic) in $\approx 60\%$ of human SKCM metastases and correlates with significantly reduced overall survival. Since *CCNC*, *ROS1* and *ARID1B* loci are distal to *BRN2* on chromosome 6, and are known to be involved in melanomagenesis, we evaluated the overall survival of these patients according to the presence and the level of mRNA expression of the corresponding genes. We observed no significant difference between the presence or absence of these three genes or their expression (Supplementary Fig. 1E–L). Finally, we compared the loss of 6q with the mono-allelic loss (MAL) of *BRN2* (Supplementary Fig. 1M) and found that 6q loss is associated with a worse prognostic than *BRN2* mono-allelic loss. This result indicates, as suspected, that other gene(s) located on 6q are of importance in melanomagenesis. Taken together, these data indicate that in human melanoma

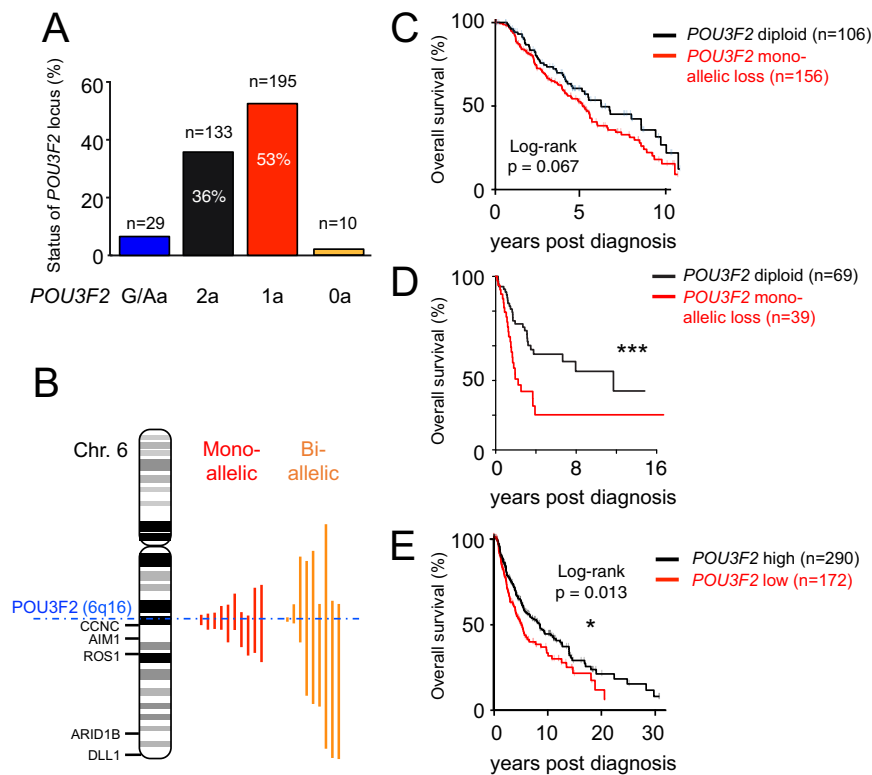


Fig. 1 One *BRN2* allele is frequently lost in human melanoma and reduced *BRN2* mRNA level correlates with reduced overall survival. **A** Bar graph showing the status of the *BRN2* locus in human skin cutaneous melanoma (SKCM) metastases (stage IV). Copy-number alterations (CNAs) were estimated using the GISTIC algorithm. Two alleles (2a in black), one allele (1a in red), no allele (0a in orange), and gain and/or amplification (G/Aa in blue) of the *BRN2* locus are given. **B** Pictogram showing the extent of segmental deletions (red or orange vertical lines) that affect the *BRN2* locus on Chr.6q16 (dashed blue horizontal line) in SKCM metastases. **C** Kaplan-Meier curves comparing 10-year overall survival of SKCM patients diploid for *BRN2* (black line, $n = 106$) or those with mono-allelic (red $n = 156$). The TCGA CNA-data set was analyzed ($n = 309$). Diploid vs. Mono-allelic loss: log-rank (Mantel-cox) test ($p = 0.067$). Data were retrieved from TCGA on August 8, 2019. **D** Kaplan-Meier curves comparing melanoma patients with diploid status or mono-allelic loss of *BRN2* in 108 regional metastatic melanoma patients ($p = 0.001$, log-rank test)³¹ and unpublished data. **E** Kaplan-Meier curves comparing 30-year overall survival of SKCM patients to *BRN2* mRNA levels. Log-rank (Mantel-Cox) test ($p = 0.03$). Data were retrieved from TCGA on August 8, 2019. Significance was defined as * ($p < 0.05$) and *** ($p \leq 0.001$).

BRN2 loss/low expression is associated with an adverse outcome for the patient.

Co-occurrence of *BRN2* loss with mono-allelic loss of *PTEN*.

We next determined whether *BRN2* loss co-occurs with melanoma driver mutations by examining the TCGA CNA-data set and human melanoma cell-line panel. There was no significant correlation between *BRAF* or *NRAS* mutation and *BRN2* loss (mono- or bi-allelic), neither in human melanoma samples nor the human cell-line panel (Supplementary Fig. 2A,B). We then searched for co-occurring CNAs of other known melanoma-associated genes and found that mono-allelic loss of *BRN2* co-occurred with mono-allelic loss of *PTEN* in approximately 40% of the human melanoma samples in TCGA and in the human cell-line panel (Supplementary Fig. 2C,D). We next evaluated the concomitant *BRN2* locus alterations, *BRAF/NRAS* mutations, and *CDKN2A/PTEN* alterations and found the most frequent genetic constellation that co-occurs with *BRN2* loss in melanoma to be *BRAF*^{V600X} mutation together with mono-allelic *PTEN* loss (Supplementary Fig. 2E). Finally, we compared the overall survival of human patients with a loss of one allele of *PTEN* who also had a loss of *BRN2* (monoallelic loss = MAL) with a loss of one allele of *PTEN* and no loss of *BRN2* (*BRN2*-normal). In this context, patients with loss of *BRN2* showed significantly lower overall survival than *BRN2*-normal patients (Supplementary Fig. 1N).

In conclusion, in human melanoma, the loss of *BRN2* is preferentially associated with *BRAF* mutation together with *PTEN* loss.

Loss of *BRN2* drives melanomagenesis in vivo. These data suggesting that the loss of *BRN2* might be of importance in melanoma prompted us to evaluate the potential causal role of *BRN2* in melanomagenesis in vivo by examining whether heterozygous (het) or homozygous (hom) loss of *Brn2* affects melanoma initiation and/or progression in a mouse model. Note however, that while genetic loss of *BRN2* might be important, the complex regulation of *BRN2* expression driven by melanoma-associated signaling pathways might also play a major role, especially given that melanoma cells within a single tumor can exhibit both high and very low *BRN2* expression^{13,20}. We therefore developed an inducible genetically engineered mouse model system for generating *Brn2*-deficient melanoma driven by the most common alterations in human SKCM (*Braf*^{V600E} and *Pten* loss). Specifically, we used *Tyr::Cre*^{Ert2^{fl}/Lar}; *Braf*^{V600E/+} (called *Braf* from hereon) and *Tyr::Cre*^{Ert2^{fl}/Lar}; *Braf*^{V600E/+}; *Pten*^{F/+} (called *Braf-Pten* from hereon) mice carrying a tamoxifen-inducible Cre-recombinase under the control of the tyrosinase promoter^{33–35}. This model system allows melanocyte lineage-specific induction of a *BRAF*^{V600E} mutation and mono-allelic deletion of *Pten* for *Braf-Pten* mice. Cre-mediated defloxxing leads to activation of the *Braf*^{V600E} oncogene, inducing nevus

and spontaneous melanoma formation in *Braf* mice, reproducing many of the cardinal histological and molecular features of human melanoma³⁶. Bi-allelic and mono-allelic loss of *PTEN* reduces tumor latency in *Braf*^{V600E}- and *NRAS*^{Q61K}-driven mouse melanoma models^{3,37}.

Using these models, we studied the effect of *Brn2* insufficiency (het and hom) on in vivo melanomagenesis by introducing the floxed *Brn2* locus into the genome by appropriate crossings (Supplementary Fig. 3A)³⁸. Specifically, we generated the mouse lines *Tyr::Cre*^{ERT2^o}; *Braf*^{V600E/+}; *Brn2*^{+/+} (*Braf*-*Brn2*-WT), *Tyr::Cre*^{ERT2^o}; *Braf*^{V600E/+}; *Brn2*^{F/+} (*Braf*-*Brn2*-het), *Tyr::Cre*^{ERT2^o}; *Braf*^{V600E/+}; *Brn2*^{F/F} (*Braf*-*Brn2*-hom), *Tyr::Cre*^{ERT2^o}; *Braf*^{V600E/+}; *Pten*^{F/+}; *Brn2*^{+/+} (*Braf*-*Pten*-*Brn2*-WT), *Tyr::Cre*^{ERT2^o}; *Braf*^{V600E/+}; *Pten*^{F/+}; *Brn2*^{F/+} (*Braf*-*Pten*-*Brn2*-het) and *Tyr::Cre*^{ERT2^o}; *Braf*^{V600E/+}; *Pten*^{F/+}; *Brn2*^{F/F} (*Braf*-*Pten*-*Brn2*-hom). Cre-mediated defloxing of *Braf*, *Pten*, and *Brn2* loci was induced by topical application of tamoxifen during the first 3 days after birth (Supplementary Fig. 3B). All mice were monitored for the appearance and growth rate of the first tumor, as well as for the number of tumors/mouse. Note that the ability to generate either homo- or heterozygous *Brn2* KOs will mimic not only mono or biallelic loss in humans, but also reflect the variable levels of BRN2 observed within human tumors^{13,20}. In the absence of *PTEN* (*Pten*^{F/F}) on a *Braf*^{V600E} background, the appearance of the tumors was too rapid to observe any difference between *Brn2* +/+, *Brn2* F/+ or *Brn2* F/F mice.

Braf-*Brn2*-WT/het/hom mice showed no differences in the appearance of the first tumor, number of tumors/mouse or the tumor growth rate from those of *Braf*-WT mice (Fig. 2, Supplementary Fig. 3C). However, compared to *Braf*-*Pten*-*Brn2*-WT, *Braf*-*Pten*-*Brn2*-het/hom mice significantly increased the number of tumors/mouse and the tumor growth rate, but not the timing of the appearance of the first tumor (Fig. 2, Supplementary Fig. 3D). We verified that *Brn2*, *Braf*, and *Pten* were correctly defloxed in the resulting melanomas (Supplementary Fig. 3E,F). In summary, our data show that *Brn2* acts as a tumor suppressor in vivo. As it has been shown in humans and mice, induction of early proliferation induced by the presence of the *BRAF*^{V600E} mutation leads to senescence, but it can be bypassed when the level of *Pten* is reduced^{3,37,39,40}. It is important to note that in the absence of *Pten* in the physiological context, proliferation of melanoblasts and melanocytes is not induced as the reduction/lack of *Pten* promotes proliferation once the cells are transformed^{3,41}. On a *Braf*-*Pten* context the loss/reduction of *Brn2* appears to induce melanoma initiation after promoting proliferation and bypass/escape of senescence, and then allows the tumor growth as was previously showed in vivo^{3,37}.

Reduction of BRN2 levels increases proliferation in vivo and in vitro. The effect of *Brn2* loss on tumor growth prompted us to investigate whether *Brn2* loss increases intra-tumor proliferation. Staining sections for Ki-67, a marker of cycling cells, revealed that melanomas from *Braf*-*Pten*-*Brn2*-het/hom mice displayed a significantly higher number of Ki-67⁺ cells than *Braf*-*Pten*-*Brn2*-WT melanomas (Fig. 3A,B). To confirm this result, we injected *Braf*-*Pten*-*Brn2* mice with bromodeoxyuridine (BrdU) two hours prior to euthanization, to determine whether melanoma cells were slow or fast-dividing. *Braf*-*Pten*-*Brn2* melanomas had a significantly higher number of BrdU⁺ cells when *Brn2* was heterozygous or homozygous (Fig. 3C,D). These results indicated that heterozygous loss of *Pten* combined with heterozygous/homozygous loss of *Brn2* promotes melanoma proliferation in vivo.

We next assessed whether *Brn2* knockdown favors proliferation in vitro and whether this mechanism is conserved (i) between human and mouse and (ii) between transformed and

non-transformed cells using Dauv-1 human melanoma cell line, and the Melan-a mouse melanocyte cell line. These cell lines express both *Pten* and *Brn2* mRNA and protein (Supplementary Table 1). Dauv-1 cells carry a *BRAF*^{V600E/+} mutation identical to that used in the mouse melanoma model system, and Melan-a cells are WT for *Braf*. siRNA-mediated knockdown of *Brn2* significantly increased cell number 72 h after transfection of both cell lines (Fig. 3E–G). *Brn2* knockdown, assessed by western blot, led to an increase in cyclin D1 protein levels in both cell lines, but did not alter cyclin D1 mRNA levels, suggesting a regulation of cyclin D1 at the protein level (Fig. 3F–H). Overall, the reduction of the *Brn2* protein induces cell proliferation of the melanocytic lineage in vivo and in vitro.

Colony formation assays in vitro are classically used to show the importance of a gene in tumorigenesis, and indicate that a single cell may survive in vitro and proliferate to form a colony. Previous work has demonstrated that a reduction in *Brn2* levels in melanoma cells has no effect on colony formation^{42,43}. However, to test this in our model, mouse melanoma cell lines were established and characterized from the different independent *Braf*-*Pten*-*Brn2* C57BL/6J mouse melanoma; the m50 and m6 cell lines were *Brn2*-WT, m59, and m36 were *Brn2*-het, and m82 and m8 were *Brn2*-hom (Supplementary Fig. 4A–F). The presence or absence of *Brn2* did not decrease the ability of these melanoma cell lines to grow in syngeneic mice (Supplementary Table 2). In other words, it appears that the absence of *Brn2* in these melanoma cells does not affect the implantation of the cells on the body wall, the proliferation after their transformation or the induction of angiogenesis in an immunocompetent environment. We evaluated the capacity of the m50 (*Brn2* WT), m59 (het), and m82 (hom) cells to generate colonies and observed, in agreement with previous observations obtained using BRN2 depletion, that the three cell lines have similar abilities to form colonies (Supplementary Fig. 4G). Moreover, re-expression of *Brn2* using lentivirus infection in two independent m8 and m82 *Braf*-*Pten*-*Brn2*-hom mouse melanoma cell lines, also indicated that BRN2 does not affect their capacity to form colonies under these conditions (Supplementary Fig. 4H, I). In conclusion, as shown in human cell lines, the number of colony forming units is independent of the presence or absence of *Brn2* and consequently this assay is uninformative regarding the role of *Brn2* in melanomagenesis.

We also evaluated the activity of *BRAF*^{V600} (PLX4720), MEK (Binimetinib), and PI3K (LY294002) inhibitors on the capacities of m50, m59 and m82 mouse melanoma cell lines to form CFU and determined the IC50 of these drugs (Supplementary Fig. 4J–O). Consistent with observations suggesting that BRN2 may suppress cell death⁴³, *Brn2*-het/hom cells are more sensitive than WT cells to these three drugs. We also evaluated the cooperativity of PLX4720 and LY294002 using various concentrations of each drug, but we did not observe any cooperation/synergy of these two drugs.

Mono-allelic loss of *Brn2* induces melanoma metastasis. We next evaluated the effects of *Brn2* on metastasis formation in vivo. Since human SKCM is known to spread to proximal lymph nodes (LNs), we assessed the presence of pigmented cells in the inguinal LNs of tumor-bearing *Braf*-*Pten*-*Brn2* mice. Specifically, we estimated the volume of the various metastases present in LNs and the number of pigmented areas after haematoxylin & eosin (HE) staining of LN sections (Fig. 4A–C). All *Braf*-*Pten*-*Brn2* mice, irrespective of BRN2 status, showed the presence of pigmented cells in both inguinal LNs. However, the LN volume of *Braf*-*Pten*-*Brn2*-het mice was significantly higher than that of *Braf*-*Pten*-*Brn2*-WT and *Braf*-*Pten*-*Brn2*-hom (Fig. 4A, B). Similarly, *Braf*-

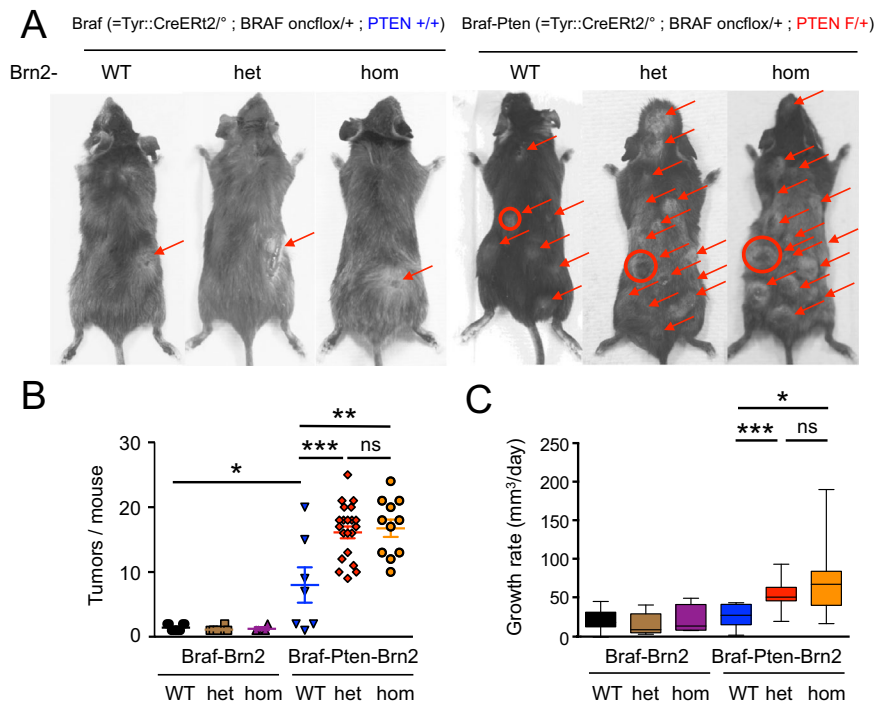


Fig. 2 Brn2 loss potentiates melanomagenesis in Braf-Pten mice. **A** Macroscopic pictures of the dorsal view of mice with cutaneous melanomas carrying mutations in the melanocyte lineage for Braf, Pten, and Brn2 after tamoxifen induction at birth (p1, p2, and p3 – see Supplementary Fig. 3). *Tyr::CreERT2^{fl}*; *Braf^{V600E/+}*; *Pten^{+/+}* (= Braf), *Pten^{F/+}* (= Pten), *Brn2^{+/+}* (=Brn2-WT), *Brn2^{F/+}* (= Brn2-het), and *Brn2^{F/F}* (= Brn2-hom). Tumors are highlighted with arrows and the sizes of the first growing tumors to appear are proportional to the diameters of the circles. F means floxed allele. **B** All Braf ($n = 9$), Braf-Brn2-het ($n = 8$), and Braf-Brn2-hom ($n = 4$) mice produced cutaneous melanomas and their number was similar (1 to 2 tumors/mouse). All Braf-Pten-Brn2-WT ($n = 7$), Braf-Pten-Brn2-het ($n = 21$), and Braf-Pten-Brn2-hom ($n = 11$) mice produced cutaneous melanomas. Note that in the absence of Pten (*Pten^{F/F}*), the appearance of the melanoma was too rapid to observe any difference between Brn2-WT, Brn2-het, and Brn2-hom mice. Each dot corresponds to an individual mouse. As control, mice of different genetic backgrounds were produced and not induced with tamoxifen Braf [$n = 12$], Braf-Brn2-het [$n = 25$], Braf-Brn2-hom [$n = 11$], Braf-Pten [$n = 7$], Braf-Pten-Brn2-het [$n = 13$], and Braf-Pten-Brn2-hom [$n = 6$]; none of them developed melanoma after 18 months, except one Braf-Pten-Brn2-het mouse that developed one melanoma after 12 months. None of the mice that were wild-type for *Braf* displayed any obvious phenotype, irrespective of the status of *Pten* or *Brn2*, including melanomagenesis and hyperpigmentation. **C** Growth rates of the first tumor appearing in each mouse for Braf-Brn2-WT, Braf-Brn2-het, Braf-Brn2-hom, Braf-Pten-Brn2-WT, Braf-Pten-Brn2-het, and Braf-Pten-Brn2-hom mice. The number of tumors is determined all along the life of the mouse by checking the mice a minimum of twice a week. Statistical analysis was performed using the two-tailed unpaired *t* test. ns = non-significant, * $p < 0.05$, ** $p < 0.01$, and *** $p < 0.001$. Data are presented as mean values \pm SEM. Braf-Pten-Brn2-het mice were euthanized in average 1.3 weeks after appearance of the first tumors with an average of 16 tumors/mouse. Similar results were obtained with Braf-Pten-Brn2-hom mice. Braf-Pten-Brn2-WT mice were euthanized at 4 weeks with an average of 8 tumors even though they did not reach a total volume of 2 cm³ except for one mouse that was euthanized earlier (3 weeks).

Pten-Brn2-het LNs showed a higher number of pigmented areas per mm² than Braf-Pten-Brn2-WT/hom mice (Fig. 4C).

To verify that the pigmented cells in the lymph nodes did not arise from cells in which the Cre recombinase had not worked efficiently, we tested whether these pigmented cells were properly defloxed for Brn2. The targeted Brn2-flox allele, used in our mouse model, has an eGFP-cassette inserted downstream of the floxed *Brn2* locus (Fig. 4D). Thus the production of eGFP occurs once the upstream *Brn2* gene is defloxed. Consistent with correct defloxing of *Brn2*, pigmented areas of LNs expressed GFP in Braf-Pten-Brn2-het/hom mice, but not Braf-Pten-Brn2-WT mice (Fig. 4E). The pigmented cells present in Braf-Pten-Brn2-WT and Braf-Pten-Brn2-het LNs also expressed Sox10, a melanocytic marker (Fig. 4E), that co-localized with eGFP-expression in Braf-Pten-Brn2-het mice confirming the melanocytic origin of the pigmented cells observed.

To get a better understanding of melanomagenesis in the various Brn2-WT/het/hom situations, we performed a transcriptomic analysis of the various Brn2 tumors and cell lines (Supplementary Data 3 and 4). The ontology enrichment analysis indicated that the Braf-Pten-Brn2-het tumors were more inflamed than the Braf-Pten-Brn2-WT tumors with increased neutrophil-

associated gene expression (Supplementary Fig. 5A). It also suggests that the extracellular-matrix was actively remodeled and that these Braf-Pten-Brn2-het tumors were more subject to angiogenesis (Supplementary Fig. 5A). Pathway enrichment analysis supported these results as inflammatory gene expression signatures are enriched from both the WikiPathways and KEGG databases (Supplementary Fig. 5B,C). Significantly, the PI3K/AKT pathway was enriched in the Braf-Pten-Brn2-het tumors compared to the Braf-Pten-Brn2-WT in both WikiPathways and KEGG databases (Supplementary Fig. 5B,C), suggesting that AKT could be more phosphorylated in the Braf-Pten-Brn2-het tumors. This assumption was verified by Western-blot analysis where phosphorylation of AKT on S473, a surrogate of the AKT activity, and the phosphorylation of S6 on S235/236 were significantly increased in Braf-Pten-Brn2-het/hom tumors compared to Braf-Pten-Brn2-WT tumors (Supplementary Fig. 5D).

Gene Set Enrichment Analysis (GSEA) using the melanoma invasive signature from Verfaillie⁴⁴ indicated that Braf-Pten-Brn2-het tumors and cell lines were more invasive than Braf-Pten-Brn2-hom tumors and cell lines (Fig. 4F). Moreover, from the GO, WikiPathways and KEGG 2019 analyses of the mouse melanoma tumors, the immune system (cytokine, neutrophil,

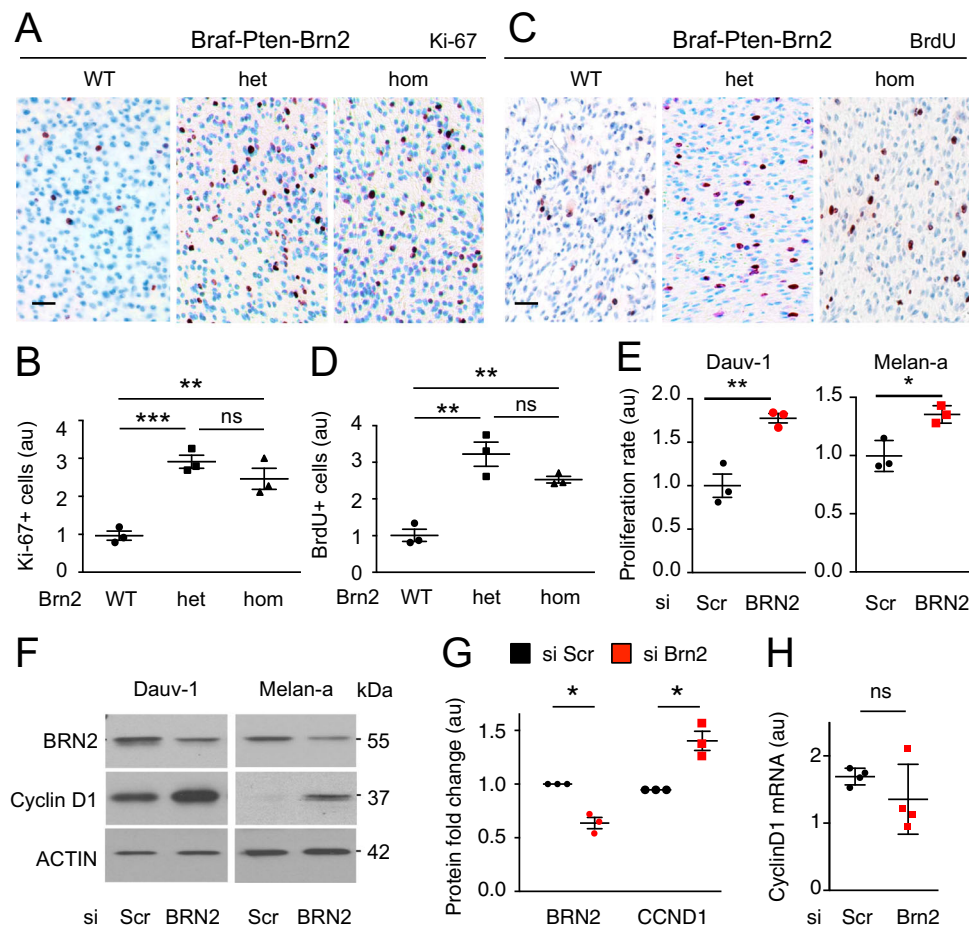


Fig. 3 BRN2-het/hom induces proliferation in vitro and in vivo. **A–D** Representative photomicrographs of Ki-67 (**a**) and BrdU (**c**) stainings of BraF-Pten-Brn2-WT/het/hom tumors. Ki-67⁺ cells are stained in red. Nuclei are stained in blue. Scale bar = 40 μ m. Quantification of ($n = 3$) Ki-67+ (**B**) and BrdU (**D**) stainings of (**A**) and (**C**), respectively. Scale bar = 40 μ m. Each dot represents the result for one tumor. (**e**) Growth rate is induced in Dauv-1 and Melan-a cell lines after reduction of Brn2 using siBRN2 and siScr as control (Scr = scramble). Three independent biological and technical experiments were performed for each cell line and for each condition. **F–H** Brn2 knock down induces Cyclin D1 protein but not its mRNA in melanocytes. **F** Western blot analysis for Brn2, Cyclin D1, and actin after reduction of Brn2 in Dauv-1 and Melan-a cells. Experiments were performed independently three times. One representative western blot is shown (raw data are presented in Supplementary Fig. 8). Quantification of protein (**G**) and mRNA (**H**) levels for Dauv-1 cells after siRNA-mediated knockdown ($n = 3$, independent experiments). For the proteins, all values were normalized against the background and corresponding actin loading control for each sample. Quantification was performed using *Image-J* software. For mRNA, all values were normalized against those of TBP. au = arbitrary units. Statistical analysis was performed using the two-tailed unpaired (**B**, **D**, **E**, **H**) and paired (**G**) *t* tests. ns = non-significant, * $p < 0.05$, ** $p < 0.01$, and *** $p < 0.001$. Data are presented as mean values \pm SEM.

macrophage) and angiogenesis are induced in BraF-Pten-Brn2-het tumors compared to BraF-Pten-Brn2-WT tumors (Supplementary Fig. 5A–C). This information suggests that BraF-Pten-Brn2-het cells have more potential to metastasize than BraF-Pten-Brn2-WT and BraF-Pten-Brn2-hom cells. In this respect, we tested the capacity of BraF-Pten-Brn2-hom (m82) mouse melanoma cell lines re-expressing or not Brn2 (m82 and m82 + Brn2) to invade matrigel in 3D. In the presence of ectopic Brn2, the m82 Brn2 KO melanoma cell lines have more ability to invade (Fig. 4G and Supplementary Fig. 4I). Since AXL, a receptor tyrosine kinase (RTK), is associated with melanoma metastasis⁴⁵, we also evaluated the level of Axl in mouse melanoma tumors and cells. BraF-Pten-Brn2-het cells produce slightly more Axl mRNA than Brn2-WT/hom (Fig. 4H). This upregulation does not affect genes that are in *Cis* of Axl suggesting a specific regulation of Axl in a BraF-Pten-Brn2-het context (Supplementary Fig. 5E–G). Moreover, when the levels of both BRN2 and MITF are reduced in human melanoma cell lines, the level of AXL mRNA is induced (Supplementary Fig. 6D,H,L,P,T). More precisely the level of AXL is slightly, but significantly, higher in Gerlach and DAUV-1 cell

lines in which the level of AXL is already very high, and is higher in SK28 and 501Mel cell lines in which the level of AXL is much lower than in Gerlach and DAUV-1 cell lines.

In conclusion, compared with BraF-Pten-Brn2-WT mice, melanoma initiation is promoted in both BraF-Pten-Brn2-het/hom mice, but metastasis is promoted only in BraF-Pten-Brn2-het mice. These observations are consistent with the fact that on a Brn2-het/hom background melanoma initiation (proliferation and bypass/escape of senescence) is induced and melanoma invasion and/or survival is inhibited on a Brn2-hom background.

BRN2 binds to the PTEN promoter and BRN2 loss leads to the reduction of PTEN transcription. The PI3K-AKT pathway is induced in melanoma and its induction abrogates BRAF^{V600E}-induced senescence^{46,47}. The loss of *Pten*, a suppressor of the PI3K pathway, induces melanoma initiation and proliferation in vivo^{3,37}. Since our BraF-Pten mouse melanoma model retained one functional allele of *Pten*, we hypothesized that *Brn2* loss would induce less expression from the WT *Pten* allele, leading to

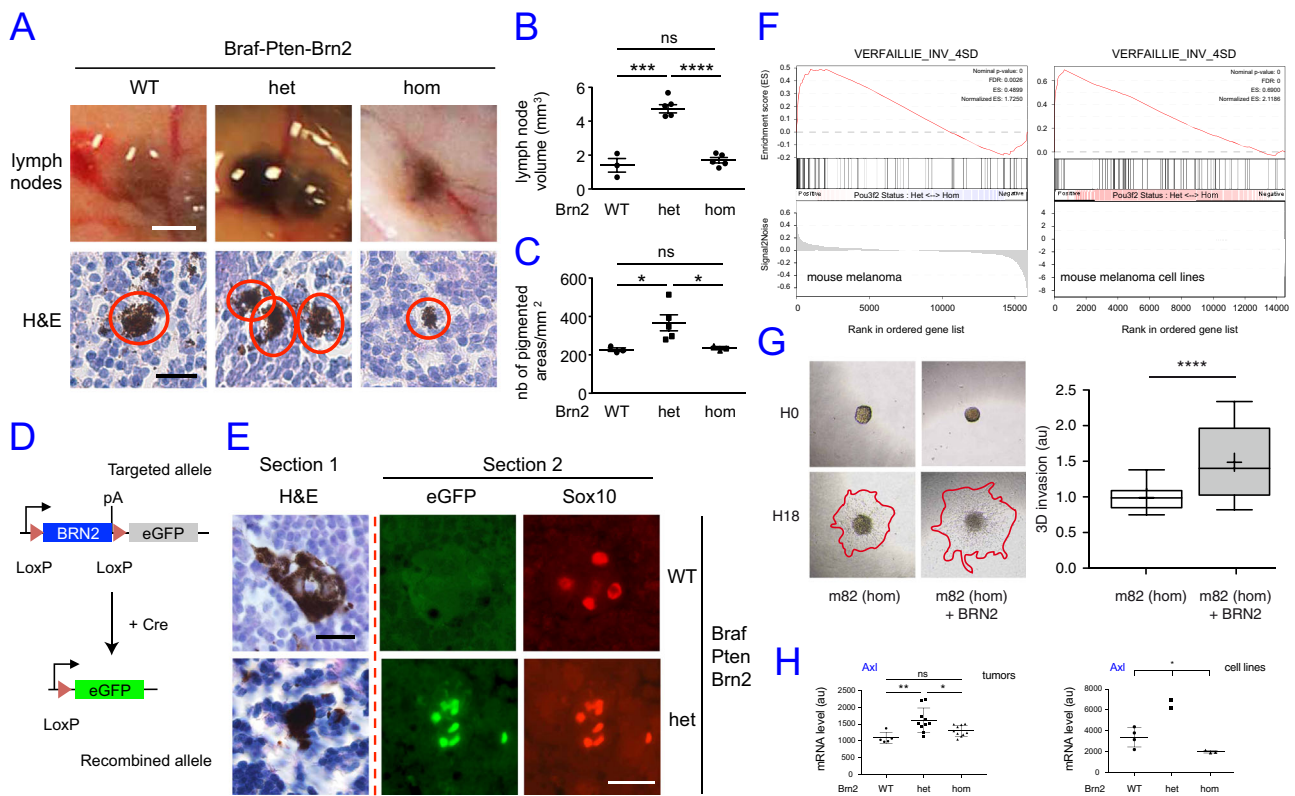


Fig. 4 Mono-allelic loss of *Brn2* induces melanoma metastasis. **A** Upper panel: Representative photomicrographs of in situ inguinal lymph nodes (LN) of *Braf-Pten-Brn2*-WT/het/hom mice. Scale bar = 1 mm. The pigmented volume (mm^3) was estimated for each LN. Lower panel: Representative photomicrographs of haematoxylin & eosin (H&E) staining of LNs containing pigmented cells. Scale bar = 20 μm . **B** Quantification of the pigmented volume of inguinal LNs in the upper panel of Figure (A). $n = 3, 5, 5$ and 5 for WT, het, and hom. **(c)** Quantification of the pigmented areas per mm^2 of inguinal LNs in the lower panel of Figure (A). Pigmented areas > 50 μm^2 were considered. $n = 3, 5,$ and 3 for WT, het, and hom. **D** Scheme showing the defloxing strategy of *Brn2* in melanocytes of the primary tumor that releases eGFP expression upon the defloxing of *Brn2*. **E** Representative photomicrographs of serial LN sections of *Braf-Pten-Brn2*-WT and *Braf-Pten-Brn2*-het mice stained with H&E and the melanocyte marker Sox10. H&E staining was evaluated for one section and GFP (green channel) and Sox10 staining (red channel) evaluated for an adjacent section. Scale bar = 20 μm . **F** A melanoma invasive signature was significantly enriched in the *Braf-Pten-Brn2*-het tumors (left) and in the *Braf-Pten-Brn2*-het melanoma cell lines (right) compared to their *Braf-Pten-Brn2*-hom counterparts. **G** Left: photomicrographs of m82 and m82-BRN2 mouse melanoma cells embedded as spheroids in 600 $\mu\text{g}/\text{mL}$ matrigel at t0 (H0) and 18 hrs after (H18). Right: Boxes and plots represent the area of invasion (red lines on photomicrographs) quantified with *ImageJ* ($n = 54$ for m82 cells and $n = 56$ for m82-BRN2 cells). P value < 0.0001. au = arbitrary unit. **H** *Axl* mRNA is significantly overexpressed in *Braf-Pten-Brn2*-het melanoma and melanoma cell lines ($n = 10$ and 2, respectively) compared to the *Braf-Pten-Brn2*-WT ($n = 5$ and 4, respectively) and *Braf-Pten-Brn2*-hom ($n = 10$ and 3, respectively) tumors. Statistical analysis was performed using the two-tailed unpaired *t* test for (B), (C), (G), and (H) (tumors) and an Anova test for H (cell lines). Data are presented as mean values \pm SEM for (B) and (C), sd for (H), and Box and whiskers (median, min to max) for (G). ns = non-significant, * $p < 0.05$, *** $p < 0.001$, **** $p < 0.0001$.

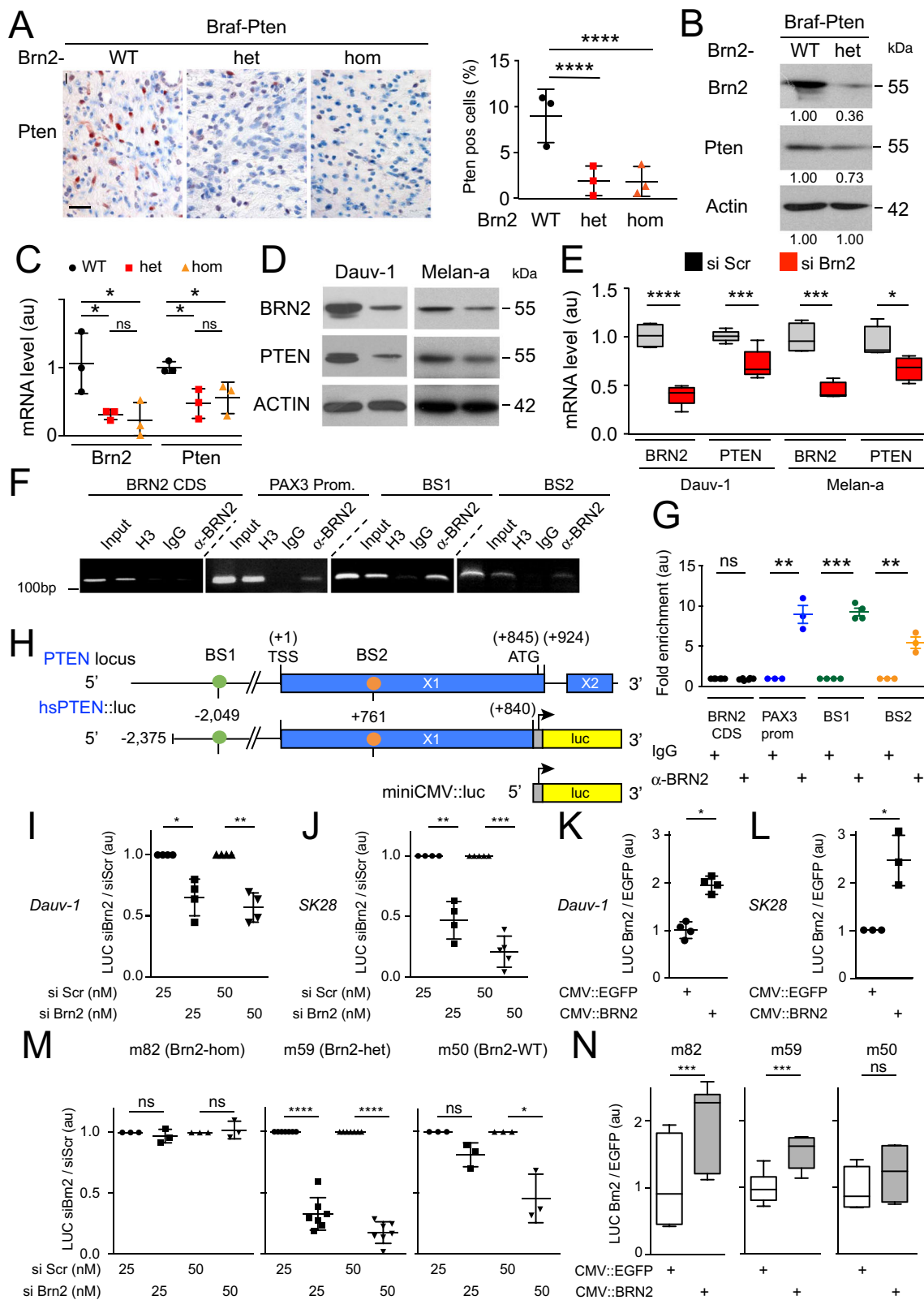
the increased PI3K-AKT signaling observed (Supplementary Fig. 5D) and consequent melanoma initiation and proliferation. We therefore evaluated the number of Pten positive cells in the various *Braf-Pten* tumors by immunohistochemistry and found that *Braf-Pten-Brn2*-het/hom tumors showed fewer Pten-pos cells than *Braf-Pten-Brn2*-WT tumors (Fig. 5A). This result was verified by western blotting of *Braf-Pten* tumor samples. The reduction of *Brn2* correlates with the reduction of *Pten* in *Braf-Pten-Brn2*-het tumors compared to the *Braf-Pten-Brn2*-WT tumors (Fig. 5B). In accordance with the reduced protein levels, the mRNA levels of *Brn2* and *Pten* were significantly lower in *Braf-Pten-Brn2*-het/hom tumors than in *Braf-Pten-Brn2*-WT tumors, suggesting regulation of *Pten* at the transcriptional level (Fig. 5C).

Next, we evaluated the mechanism of *Pten* repression mediated by reduced levels of *Brn2* in the human Dauv-1, Gerlach, SK28, and 501Mel melanoma cell lines and in the non-transformed mouse Melan-a cell line. siRNA-mediated *BRN2* knockdown led to significantly reduced *PTEN* protein and mRNA levels in cell

lines having high *BRN2* expression (Fig. 5D, E and Supplementary Fig. 6). In cells with lower level of *BRN2* (501Mel), the reduction of *PTEN* was not observed.

We examined the *PTEN* promoter for *BRN2* binding sites conserved between humans and mice to determine whether *BRN2* acts directly on *PTEN* and detected two potential *Brn2* binding sites (BS1 and BS2) at the positions—2049 and +761 (numbering relative to TSS). Chromatin-immunoprecipitation (ChIP) for *BRN2*, performed on Dauv-1 melanoma cell extracts, followed by qPCR, revealed quantitative *BRN2* binding to both binding sites, comparable to *BRN2* binding on the *PAX3* promoter (Fig. 5F–H). IgG was used as a negative control.

To evaluate *Pten* promoter activity in response to *BRN2*, we cloned a 3.2-kb-human *Pten* promoter fragment containing the two *BRN2* binding sites upstream the luciferase gene to generate the *hsPten::Luciferase* reporter construct (Fig. 5H). The analysis of human *PTEN* promoter activity showed an intrinsic activity of *hsPten::Luciferase* in human melanoma cells (Supplementary Fig. 7A, B). A consistent repression of *PTEN* transcription was



observed when a smart-pool of siBRN2 was added. In contrast, PTEN transcription was activated following co-transfection of a BRN2 expression vector compared to empty vector in Dauv-1 and SK28 cell lines in luciferase assay (Fig. 5I–L). We performed similar experiments with the mouse PTEN promoter, which was cloned upstream of the luciferase construct (Supplementary Fig. 7C–F); Brn2 activated Pten transcription in three mouse melanoma cell

lines (m82, m59, and m50) (Fig. 5M, N). In conclusion, BRN2 directly induces PTEN transcription.

MITF binds the PTEN locus and represses PTEN transcription. The MITF gene encodes a key transcription factor that plays a major role in melanocyte and melanoma biology¹⁸. Several

Fig. 5 Brn2 binds to the Pten promoter and Brn2 loss leads to Pten transcription reduction. **A** Representative photomicrographs of immunohistochemistry staining of Pten (red) in Braf-Pten-Brn2-WT and Braf-Pten-Brn2 mouse melanomas are shown. Scale bar = 40 μ m. Three independent tumors for each genotype were used for these experiments and three independent sections were used for each tumor. A 2-way ANOVA with Dunnett's multiple comparisons tests were performed. The percentage of Pten⁺ cells in WT and mutant tumors is shown. **B** Western blot analysis of Brn2, Pten and actin for Braf-Pten-WT and Braf-Pten-Brn2 from at least three tumors of each genotype. One representative example is presented, raw data are presented in Supplementary Fig. 8. The relative intensities of the band were estimated with ImageJ. **C** RT-qPCR of Brn2 and Pten from Braf-Pten-WT and Braf-Pten-Brn2 melanomas. Three independent mouse melanomas per genotype were analyzed. Data were normalized against the values of Gapdh. au = arbitrary unit. **D** Western blot analysis of BRN2, PTEN and ACTIN from Dauv-1 human melanoma cells and Melan-a mouse melanocytes after siRNA mediated knockdown. A representative western blot is shown, raw data are presented in Supplementary Fig. 8. Scr = Scramble. **E** RT-qPCR of BRN2 and PTEN from human melanoma cells (Dauv-1) and mouse melanocytes (Melan-a) after siRNA-mediated knockdown. Specific primers were used for human and mouse samples. Dauv-1 ($n = 6$), Melan-a ($n = 4$), independent experiments. Data were normalized against the values for TBP (Dauv-1) or Gapdh (Melan-a). **F** ChIP assays of BRN2 binding to the PTEN promoter in Dauv-1 melanoma cells. All data shown are representative of at least three independent assays. **G** Quantification of the ChIP-qPCR, plotted and normalized against IgG as the reference. au = arbitrary unit. $n = 6, 3, 4,$ and 3 for BRN2 CDS, PAX3 prom, BS1 and BS2, respectively. **H** Scheme of the human PTEN promoter containing two BRN2 binding sites (BS) represented as colored circles. Note that BS are conserved between humans and mice. TSS = transcription start site. Exons (X) 1 and 2 are shown as horizontal rectangles. The translation start site (ATG) and the end of exon 1 are indicated. All numbering is relative to the TSS (+1). Representation of the reporter luciferase (luc) construct with or without PTEN promoter. **I-N** Human and mouse PTEN promoter activities were evaluated in human Dauv-1 (**I, K**), SK28 (**J, L**), and in mouse m82 [Brn2-hom], m59 [Brn2-het], and m50 [Brn2-WT] (**M, N**) melanoma cell lines either in the presence of siScr (scramble) or siBrn2 (smart-pool) (**I, J, M**) or in the presence of expression vector of BRN2 (CMV::BRN2) (**L, N**). The experiments were independently performed four (**I, J, K**) and three (**L**) times. They were performed three independent times for m82 and m50, seven for m59 (**M**), and seven times for m82, six for m59 and four for m50 (**N**). Statistical analysis was performed using the two-tailed unpaired t test for (**C**), (**E**), (**G**) and paired t test for (**I-N**). Data are presented as mean values \pm SEM for (**C**), (**E**), (**G**), **I-M** Box and whiskers (median, min to max) for N . ns = non-significant, $*p < 0.05$, $***p < 0.001$, and $****p < 0.0001$.

studies have reported that *MITF* transcription is directly repressed by BRN2 whereas a reduction in BRN2 levels leads to increased MITF levels^{13,27,48}, while another study showed that BRN2 induces MITF⁴⁹. Likely both results are correct due to the versatile role of BRN2 as a transcription regulator whose activity may be dependent on context including genetic status and/or the environment^{21,26,27}.

Knowing the importance of MITF in the melanocyte lineage, we analyzed the consequences of modulation of MITF expression on PTEN. Using siRNA-mediated *MITF* knockdown in three human melanoma cell lines expressing high levels of MITF (501mel, SK28, HBL) led to a significant increase of PTEN protein and mRNA levels (Fig. 6A, B). In cells expressing lower levels of MITF, such as Gerlach and Dauv-1, we did not observe an increase of PTEN (Supplementary Fig. 6C, G). Next, to determine if MITF directly regulates PTEN expression through proximal enhancers we performed Cleavage Under Targets and Release Using Nuclease (CUT&RUN) with antibodies to MITF, as previously described,⁵⁰ and to H3K27Ac, revealing active chromatin, and against H3K4me3, revealing active and poised promoters, in SK28 cell lines that were wild type for *MITF* (*MITF*-WT) or had loss of function mutations in all alleles of it (Δ MITF) (Fig. 6C)⁵⁰. An MITF peak is present within the gene body of *PTEN* (intron 4), and a second one is 114 kb downstream of the *PTEN* transcriptional start site (TSS) (i.e., +114 kb). Both MITF peaks were centered on an M-box motif (5'-TCATGTG-3'). At both intron-4 and +114 kb MITF peaks, the H3K27Ac signal was unchanged in Δ MITF mutant cell lines. However, six distal enhancers (painted light blue) exhibited a twofold greater H3K27ac signal in MITF mutant cell lines compared to wild-type cell lines (+140 kb, +210 kb, +230 kb, +253 kb, +301 kb and +317 kb), suggesting increased transcription of *PTEN* in the former. We confirmed the +140 kb MITF peak after performing a quantitative ChIP experiments on 501Mel cells expressing MITF-HA (Fig. 6D, E), using Tyrosinase (TYR) and PRM1 as positive and negative controls respectively. Overall, reduction of MITF results in an increase in PTEN mRNA expression. As such, it is plausible that Brn2 induces *Pten* transcription through two different, but concurrent mechanisms: (i) directly through BRN2 binding to the *PTEN* promoter to induce its transcription and (ii) indirectly via BRN2 modulating (repressing/inducing depending

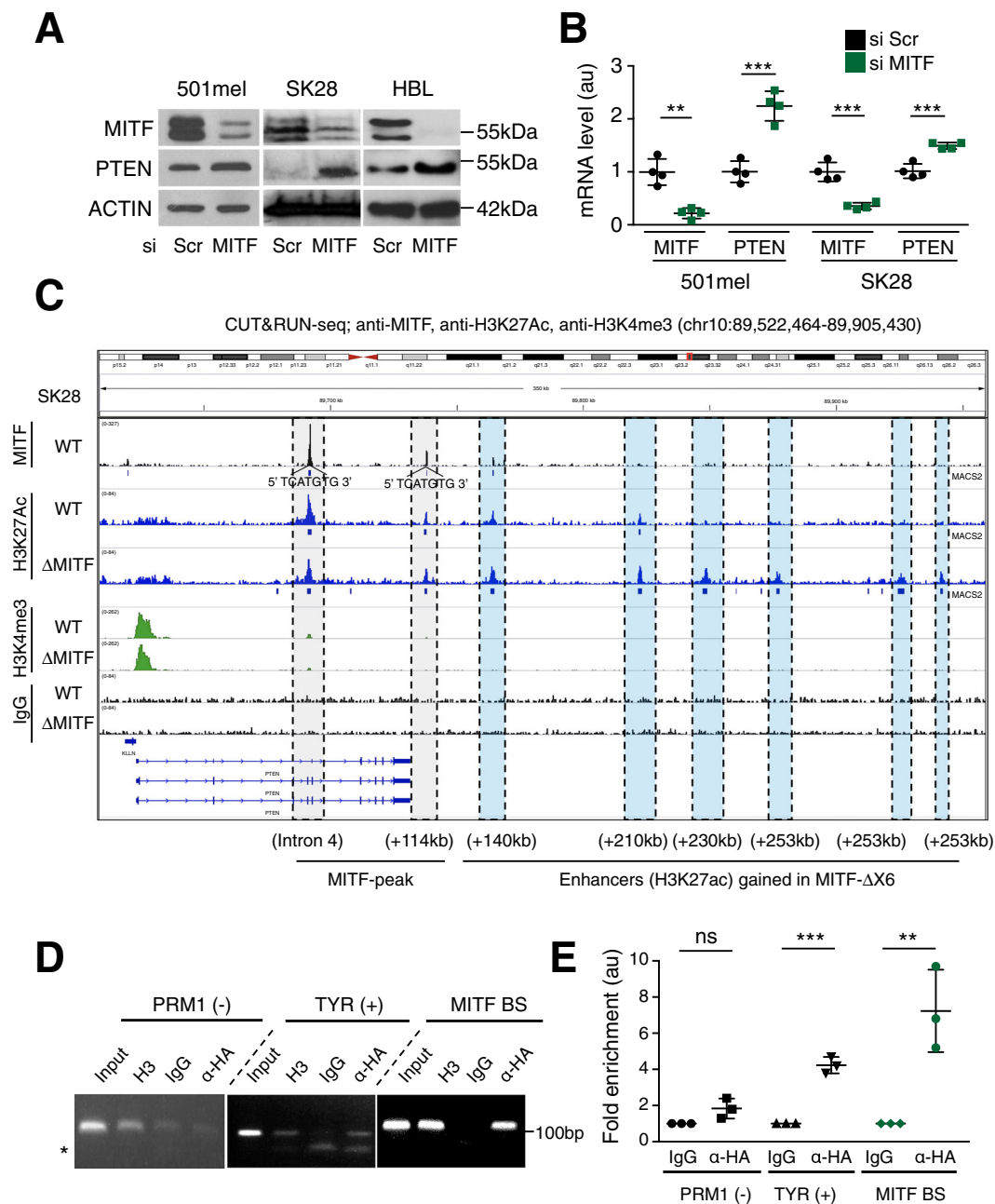
of the situation) MITF expression, with MITF binding to the 3' end of *PTEN* to inhibit its transcription. In the absence of BRN2, these mechanisms are disrupted and *PTEN* transcription is downregulated in our conditions. In conclusion, MITF represses directly *PTEN* transcription.

Overall, our results are consistent with a model in which reduction of BRN2 reduces PTEN transcription in vitro and in vivo, thus ramping up PI3K signaling and inducing both the initiation of melanoma and the formation of metastases.

Discussion

A well-established principle of cancer biology is that tumors are initiated by a combination of oncogene activation together with loss of tumor suppressor expression or activity. In melanoma, key oncogenic drivers, such as BRAF and NRAS, have been well defined. Loss of P16 or PTEN tumor suppressor activity is required to bypass oncogene-induced senescence and permit melanoma initiation. However, while inactivation of tumor suppressors by mutation has been extensively studied, it is less well understood how their activity may be modulated by changes in their mRNA expression mediated by key melanoma-associated transcription factors. At this point, it is important to note that factors involved in melanoma initiation will not automatically reflect/translate into overall survival. Here, we identify BRN2, a key transcription factor lying downstream of three melanoma-associated signaling pathways (WNT/ β -catenin, MAPK, and PI3K), as a tumor suppressor that functions to regulate PTEN expression. Thus, monoallelic loss of *Brn2* promotes melanoma initiation in a *Braf*^{V600E}/*Pten*^{F/+} background where mono-allelic loss of *Pten* sensitizes cells to loss of *Brn2*.

Previous work has primarily linked BRN2 to melanoma migration and invasion in vitro and in xenograft experiments^{13,20,42,51}, but its role during melanoma initiation and proliferation in vivo and in normal melanocytes had not been determined. We report that, consistent with BRN2 playing a key role as a tumor suppressor in melanomagenesis, its locus is frequently lost in human skin cutaneous melanoma (SKCM) metastases, independently of their NRAS or BRAF status, and that BRN2 status contributes to overall patient survival. Significantly, the overall survival of patients with a mono-allelic loss of PTEN is higher when the BRN2 locus is intact.



Although these observations are consistent with *BRN2* affecting human melanoma initiation and progression, loss of the *BRN2* locus is frequently associated with large segmental deletions that affect the long arm of chromosome 6 (6q) as it was observed in 14 out of 53, and 9 out of 32 out of primary melanoma and in 17 out of 21 melanoma cell lines^{52–54}, and confirmed in this study on a total of 205 out of 338 melanomas, and 11 out of 25 melanoma cell lines. It has already been shown that the loss of 6q was associated with a worse prognosis⁵². According to our observations, the loss of 6q is more detrimental for the overall survival than the focal loss of the *BRN2* locus (Fig. 1 and Supplementary Fig. 1). Moreover, in vitro studies have shown that several genes are linked to melanomagenesis in the co-deleted region, including *ARID1B*, *CCNC*, and *ROS1*, although none have yet been shown to be functionally important in melanoma in vivo^{48,55–61}. Similarly, we analysed the SKCM TCGA study to evaluate the overall survival comparing the mono allelic loss and the diploid state for *CCNC*, *ROS1* and *ARID1B* (Fig. S1).

There is no statistical significance for *CCNC* ($p = 0.086$), *ROS1* ($p = 0.27$), or *ARID1B* ($p = 0.66$).

Thus, it might be argued that any of the genes located in this frequently deleted region may be acting to modulate melanoma initiation or progression. However, our functional mouse molecular genetics models show conclusively that the heterozygous or homozygous loss of *Brn2* promotes melanoma initiation and initial growth. Similarly, our transcriptomic analysis showed that the mRNA levels of the seven genes in the region co-deleted in humans (*Arid1b*, *Mchr2*, *Ccnc*, *Cdk19*, *Dll1*, *Ros1*, and *Crybg1/Aim1*) were not affected in the mouse tumors (Braf-Pten-Brn2-WT, Braf-Pten-Brn2-het and Braf-Pten-Brn2-hom). Collectively, these results strongly suggest that the reduction/loss of *Brn2* levels is a critical event that cooperates with heterozygous *Pten* to promote the initiation and growth of melanoma, independently of the co-deleted genes in melanoma. Finally, independent initiation events are promoted when the level of *Brn2* is lower than normal -heterozygous or homozygous- since the number of

Fig. 6 MITF binds downstream of *PTEN* gene, MITF loss induces its transcription, and enhancers flanking *PTEN* are activated in MITF-depleted cells. A

Western blot analysis of MITF and PTEN from human melanoma cells (501mel, SK28, and HBL) after siRNA-mediated knockdown. Actin was used as a loading control. A representative western blot is shown, raw data are presented in Supplementary Fig. 8. The molecular weight is indicated in kDa. Scr = Scrambled. **B** RT-qPCR of MITF and PTEN from human melanoma cells (501mel and SK28) after siRNA-MITF and Scr knockdown. All values were normalized against TBP. The analysis was performed on three independent experiments with technical triplicates, au = arbitrary unit. **C** Screenshot of IGV genome browser (GRCH37/hg19) visualization of MITF, H3K27Ac and H3K4me3 binding to the *PTEN* locus in SkMel28 cell lines that are MITF-WT or mutant (i.e., MITF- $\Delta X6 = \Delta MITF$). Blue boxes below MITF and H3K27Ac tracks: signal above IgG background (i.e., peaks) called by MACS2. PTEN and downstream regions are shown, blue arrows indicate strand orientation and horizontal rectangles the exons. Y-axes are scaled per antibody sample. Anti-MITF CUT&RUN peaks present in WT cells that harbor an M-Box binding motif are painted gray. Six distal enhancers (painted light blue) exhibited a twofold greater H3K27ac signal in MITF mutant cell lines compared to wild-type cell lines. At least two CUT&RUN biological replicates were performed for MITF, H3K27ac, and H3K4me3. **D** ChIP assays of MITF binding downstream of *PTEN* in 501mel human melanoma cells stably expressing HA-Tagged MITF (location +140 kb). ChIP assays are performed using an antibody against HA and analyzed after a 30-cycle PCR (exponential phase). The tyrosinase promoter (*TYR*) and *PRM1* were used as positive and negative controls, respectively. Input represents approximately 3% of the input used for the ChIP assay. H3 (histone H3) and IgG (Immunoglobulin G) were used as positive and negative technical controls for each region of interest, respectively. The oligonucleotides, their positions on the genome, and sizes of the amplified fragments are shown in Supplementary Tables 3 and 4. All data shown are representative of three independent assays. * corresponds to the remaining oligonucleotides. **E** Quantification of the ChIP-qPCR presented in (**D**) is plotted and normalized against IgG as a reference. au = arbitrary unit. PRM1 (-): PRM1 (negative control), TYR (+): tyrosinase promoter (positive control). Statistical analysis was performed using the two-tailed unpaired *t* test. Data are presented as mean values \pm SD. ns = non-significant, **p* < 0.05, ***p* < 0.01, and ****p* < 0.001.

independent melanoma is higher in *Braf*-*Pten*-*Brn2*-het/hom mice than in *Braf*-*Pten*-*Brn2*-WT mice (Fig. 2B). Our observations are therefore consistent with BRN2 acting as a tumor suppressor in melanoma, and are in full agreement with the predominantly mutually exclusive pattern of BRN2 and Ki-67 in situ staining of invasive melanoma²⁰.

The presence of *Braf*^{V600E} promotes proliferation prior to inducing senescence and the loss of *Pten* results in senescence bypass^{3,34,37}. As such, we believe that the increased proliferation and tumor-initiation frequency observed in our *Braf*^{V600E}/*Pten*^{F/+} model arising as a consequence of the reduction of *Brn2*, is likely to occur as a consequence of the ability of *Brn2* to activate *Pten* expression and suppress PI3K signaling either directly or potentially indirectly via *Mitf* repression during early melanomagenesis. In other words, inactivation of *Brn2* or a reduction in its expression would lead to low expression of the remaining *Pten* allele and as a consequence increase the probability of senescence bypass. This explanation fits with the fact that in the absence of *Pten* on a *Braf*^{V600E} background, the appearance of the tumors is too rapid to observe any difference between *Brn2* +/+, *Brn2* F/+ or *Brn2* F/F. According to our model the transcription regulation by *Brn2* and *Mitf* would not affect the level of *Pten* since it is already lost. Moreover, in a context in which *Pten* is diploid (WT) and *Brn2* is reduced (het or hom), the downregulation of *Pten* would be limited and not sufficient to act efficiently as a tumor-suppressor.

Although it might be argued that the increase in visible tumor number in a *Braf*-*Pten*-*Brn2*-het and -hom might be a consequence of the increased proliferation caused by reduction/loss of *Brn2*, as evidenced by the increased proportion of Ki-67 positive cells within tumors, we feel this is unlikely. For welfare reasons the *Braf*-*Pten*-*Brn2*-WT mice were euthanized with tumors (total volume 2 cm³) after 4 weeks with about 8 tumors per mouse; by contrast the *Braf*-*Pten*-*Brn2*-het/hom mice were euthanized after 1.3 weeks with about 17 tumors per mouse of a similar size to the WT. Since tumor size is similar in the WT and *Brn2* mutants, this indicates that the total number of cells in the WT and mutant tumors is similar and have undergone a similar number of cell divisions (though this occurred in a shorter time in the mutant). Since the WT and mutants have undergone a similar number of cell divisions, if proliferation were responsible for any increase in number of visible tumors then at 4 weeks the numbers of tumors in the WT should be the same as in the mutant at 1.3 weeks, whereas in fact, the tumor numbers in the WT were

around 50% of those in the *Brn2* mutants. Although we do not want to rule out a contribution of proliferation, the more likely explanation is that the reduction of BRN2 promotes the bypass of senescence (by reducing the level of *Pten*) or/and promotes survival of proliferating melanoma cells at the early stages of initiation.

Our in vivo data therefore reveal that melanocyte-specific *Brn2* reduction in *Braf*-*Pten* mice promotes the initiation and progression of melanoma. Melanoma initiation is promoted after proliferation is induced through various proteins including *Mitf* and senescence bypassed in this case through reduction of the level of *Pten*. Melanoma progression is induced by promoting invasion when the level of *Brn2* is intermediate after inducing *Axl* and modulating the immune system. In the future, we will have to evaluate the kinase activity of *Axl* in this context, and the consequences of its inhibition *in cellulo* and *in vivo* to understand the *Mitf*/*Brn2*/*Axl ménage à trois*. Altogether, we establish *Brn2* as a central tumor suppressor, acting at different steps of melanomagenesis, and complement numerous other studies showing the effect of *Brn2* on invasion^{13–15,20,29,51}.

Brn2 heterozygous mice were more prone to form LN metastases efficiently than mice that were *Brn2* WT when *Pten* was already heterozygous. The efficiency of the metastasis process depends on the status of *Brn2* as the number and size of each micro-metastasis was greater in *Brn2* heterozygous than *Brn2* wild-type melanoma. This is important as mono-allelic loss of *BRN2* in human, corresponding to *BRN2* heterozygous melanoma, occurs in 53% of human melanoma. In *Brn2* wild-type melanoma, the change of the level/activity of *Brn2* is possible but the amount of protein found in *Brn2* wild-type melanoma absorbs better transient *Brn2* depletion than in *Brn2* heterozygous melanoma.

Some residual *Brn2* activity might be required for efficient melanoma progression. On one hand, *Braf*-*Pten*-*Brn2*-het and *Braf*-*Pten*-*Brn2*-hom melanomas proliferate faster, and on the other hand, according to our results (Fig. 4F,G) *Braf*-*Pten*-*Brn2*-hom melanomas have a reduced ability to invade compared to *Braf*-*Pten*-*Brn2*-het melanomas. Moreover, the lack of *BRN2* reduces migration and increases the rate of apoptosis and/or anoikis^{20,28,43}. In a more speculative way, one may think that optimal melanoma progression may be associated with a series of proliferative and invasive phases. In the absence of *BRN2*, cells are “fixed” in one stage and cannot switch from “proliferative” to “invasive” states. These cells are mainly proliferative and poorly

invasive as we observed in *Braf*-*Pten*-*Brn2*-hom situation. In the presence of *Brn2* as WT [two alleles] or heterozygous [one allele], the corresponding mRNA and protein concentrations can be positively and negatively modulated by external/internal factors. The modulation of the level of *Brn2* is more sensitive on a heterozygous background than on a WT background.

Altogether, one may understand that melanoma grows faster and forms melanoma when *Brn2* expression is not too high (proliferation handicap) but at the same time not too low (migration/invasion/survival handicap). Indeed, on the one hand, *Brn2*-het and *Brn2*-hom melanomas proliferate faster, and on the other hand, *Brn2*-hom melanomas are handicapped to invade (Fig. 4F,G), to migrate²⁰ and to die by anoikis²⁸.

The formation of metastases is a multistep process in which cells proliferating in the primary tumor, and surviving the metastatic process, must undergo a switch to an invasive phenotype prior to a switch to a proliferative phenotype on site. Since the switch from proliferation to invasion, and back, has been associated with the activity of *MITF*, it is possible that for efficient metastatic colonization cells must be able to modulate *MITF* expression via *BRN2*. In this respect, it is especially important to note that *BRN2* has been identified as a key regulator of *MITF*^{13,49}. Consistent with the observation that *MITF* and *BRN2* are frequently observed in mutually exclusive populations in melanoma, and that *BRN2* may act in vivo as an *MITF* repressor¹³, we have observed that in a non-tumoral context, the specific knock-out of *Brn2* in vivo in melanocytes increases the level of *Mitf* (publication in preparation). Importantly, during progression of mouse *Braf*-*Pten* melanoma *Mitf* levels are modulated. During the initial phase of growth, melanoma cells are pigmented, indicative of *Mitf* activity, but later in situ they lose pigmentation and ability to produce *Mitf*⁶². Although the reduction of *Brn2* in *Braf*-*Pten*-*Brn2* primary melanoma is not sufficient to re-induce *Mitf* mRNA and pigmentation in all cells of these primary melanomas, the *Braf*-*Pten* melanoma cells that formed LN metastases were pigmented and re-expressed *Sox10*, a key transcription activator of *Mitf*. Thus, during progression of *Braf*-*Pten* melanomas *Mitf* is produced during initial growth and subsequently repressed during the second phase, before being re-expressed in LN metastases. It seems therefore likely that one role of the residual *BRN2* in the heterozygotes may be to facilitate the modulation of *MITF* expression during metastatic spread.

It has been shown that *BRAF* and *PI3K* induce *BRN2*^{15,16}. In consequence, it was expected that the level of *BRN2* would decrease in the presence of such inhibitors. In addition, in the presence or absence of *BRN2*, melanoma cells are either more resistant or more sensitive to *BRAF* inhibitors, respectively^{28,43}. This sensitivity would be associated with the function of *BRN2* in DNA repair⁴³.

Although here we have focused on the role of *BRN2* in melanoma, *BRN2* is also expressed in a number of other cancer types including small cell lung cancer, neuroblastoma, glioblastoma and neuroendocrine prostate cancer^{8–10}. While *BRN2*-mediated regulation of *MITF* is not likely to be important for non-melanoma cancers that do not express *MITF*, the ability of *BRN2* to modulate *PTEN* expression uncovered here may play an equally important role in promoting the initiation and progression of these cancer types. In this respect the inducible knockout mice described here may represent an important tool to examine the role of *BRN2* in non-melanoma cancers.

In conclusion, our results identify *Brn2* as a key tumor suppressor through its ability to modulate *Pten* expression that, given the high prevalence of monoallelic mutations, is likely to play a key role in initiation of human melanoma and likely other *BRN2*-expressing cancer types. Since *BRN2* expression is activated by *PI3K* signaling via *PAX3*¹⁶, its ability to suppress *PI3K* signaling

by increasing *PTEN* expression may also provide cells with a negative feedback loop to control the *PI3K* pathway. Moreover activation of *BRN2* by *MAPK* signaling downstream *BRAF*¹⁵ as well as *WNT*/ β -catenin signaling¹⁴, may also permit coordination between these pathways and the *PTEN*/*PI3K* axis. Finally, given the importance of *BRN2* in melanomagenesis identified here as well as its frequent heterozygosity, it may be important to further explore whether tumors with low *BRN2* expression may be more susceptible to *PI3K* pathway inhibition, as it was shown for *MAPK* inhibitors. In this respect, this mouse model of *BRN2*-deficient melanoma could be useful for the pre-clinical testing of inhibitors for clinical development especially since it has been shown that *BRN2* is involved in DNA repair⁴³.

Methods

TCGA data mining. All TCGA data sets for somatic mutations, copy number alterations (CNAs), RNA levels, and clinical data for skin cutaneous melanoma and other cancers were retrieved from <http://www.cbioportal.org> on August, 2019. CNAs were calculated using the GISTIC algorithm. Samples with GISTIC copy-number values of “-1” were considered to have mono-allelic loss and those with GISTIC copy number values of “-2” to have bi-allelic loss. GISTIC copy number values > “+1” were considered as amplification. The TCGA datasets used were the: CNA-data set ($n = 367$), Seq-Data set ($n = 473$), Clark level data set ($n = 461$), and Breslow index data set ($n = 316$). mRNA levels were calculated from RNA sequencing read counts using RNA-Seq V2 RSEM and normalized to transcripts per million reads (TPM).

Copy number analysis. Copy number data for the regional metastatic cohort used in Fig. 1D was obtained from a previous study⁶³. Briefly, DNA sequencing data of 1,500 cancer genes were used to generate copy number data. Copy number log ratios of sequenced exons were generated from bam files of tumor-normal pairs using CONTRA 2.03⁶⁴, with default parameters. Exons with insufficient coverage in the normal sample were removed. Copy number data were segmented using GLAD⁶⁵. We used cut-off of -0.3 to determine mono-allelic loss of *BRN2*.

Copy number data with matched nevus-melanoma pairs used in Supplementary Fig. 1D was obtained from a previous study³². Log2 copy ratio values were processed using the PureCN R package⁶⁶ to estimate tumor purity and copy number.

Level of expression of *BRN2* mRNA in melanoma patients. *BRN2* mRNA levels were obtained from RNA sequencing data analyzed using the RNA Seq V2 RSEM pipeline as transcripts per million reads (TPM).

Mouse models. Mice were bred and maintained in the specific pathogen-free mouse colony of the Institut Curie, in accordance with the institute's regulations and French and European Union laws. Mice were bred and maintained in the specific pathogen-free mouse colony of the Institut Curie, in accordance with the institute's regulations and French and European Union laws. The transgenic *Tyr::Cre^{ERT2}* (031281—B6N.Cg-Tg(Tyr-cre/ERT2)1Lru/J), *Braf^{V600E/+}*, *Pten* (006440 - B6.129S4-Ptentm1Hwu/J) and *Brn2* mice have been described and characterized elsewhere^{33–35,38,67}. All mouse lines were backcrossed onto a C57BL/6 background for more than ten generations. All desired combinations of genotypes were obtained through crosses. Mice were born with the expected ratio of Mendelian inheritance and no changes in gender ratios were observed. Experimental mice were of both genders and no apparent phenotypic differences between genders were observed. No statistical methods were used to predetermine sample size. The sample size was sufficient to measure the effect size for all experiments presented in this study. The experiments were not randomized, and the investigators were not blinded to allocation during the experiments and outcome assessment. Mice were housed in a certified animal facility with a 12-hour light/dark cycle in a temperature-controlled room (22 ± 1 °C) with free access to water and food.

Growth of the mouse melanoma cell lines in syngeneic mice. C57BL/6 mice were purchased from Charles River Laboratories. Twenty-four C57BL/6 mice were injected with *Brn2* +/+ [m6 and m50], *Brn2* F/+ [m36 and m59], and *Brn2* F/F [m8 and m82] mouse melanoma cell lines. The cells were resuspended in PBS and 10⁵ cells (100 μ L) subcutaneously implanted into the flanks of seven-week-old C57BL/6 mice using a 27-gauge needle. Presence of tumors was detected from day 15 to 50, it was independent of the genotypes.

Ethical rules. Animal care, use, and experimental procedures were conducted in accordance with recommendations of the European Community (86/609/EEC) and Union (2010/63/UE) and the French National Committee (87/848). Animal care and use were approved by the ethics committee of the Curie Institute in compliance with the institutional guidelines. Experimental procedures were specifically

approved by the ethics committee of the Institut Curie CEEA-IC #118 (CEEA-IC 2016-001) in compliance with the international guidelines.

Mouse genotyping. Mouse biopsies were digested overnight at 55°C using 200 ng proteinase K (Roche, #11 243 233 001) in 500 µL lysis buffer containing 16 mM [NH₄]₂ SO₄, 67 mM Tris-HCl [pH 8.8 at 25 °C], 0.01% [v/v] Tween-20, in deionized H₂O. Proteinase K was inactivated for 20 min at 95 °C. Primers and PCR conditions are described (Supplementary Tables 3 and 4). PCR products were separated by agarose (Invitrogen, #15510027) gel electrophoresis. Genotyping were performed accordingly (Supplementary Tables 3 and 4).

In vivo gene activation/deletion and melanoma monitoring. Newborn mice were treated dorsally with 20 µL/day/mouse tamoxifen (Sigma, T5648, working concentration 20 µg/mL in DMSO) for the first three consecutive days after birth. Non-tamoxifen-induced mice of the same genotype were used as controls. After the application of tamoxifen, the mice were evaluated for the appearance of tumors and their progression once per week or more frequently if required. Developing skin excrescences > 3 mm diameter were considered to be melanomas, and validated after growth. Mice were euthanized and autopsied four weeks after tumor appearance or once the tumors reached 2 cm³. Melanoma-specific survival curves were estimated from the day of euthanasia. Mouse melanomas were excised, rinsed in cold phosphate-buffered saline (PBS, Euromedex, ET330-A) and divided into four parts, two snap-frozen in liquid nitrogen for subsequent transcriptomic and western blot analysis and two fixed in 4% paraformaldehyde (PFA, Euromedex, 15714-S) and embedded in paraffin or OCT (VWR, #00411243) for histological analysis and immunostaining. Inguinal lymph nodes were fixed in 4% PFA and embedded in paraffin or OCT for histological analysis and immunostaining.

Detection of defloxing from mouse melanoma tissue. DNA extraction from paraffin-embedded melanoma sections (10 µm) was performed using the QIAamp DNA FFPE Tissue Kit (Qiagen, #56404), according to the manufacturer's instructions. A PCR using DNA extracted from each tumor was performed to verify the mouse genotype and proper defloxing of the modified genes (see Key Resource Table and Supplementary Tables 3 and 4 for PCR conditions and primers sequences).

Immunohistochemistry of mouse melanoma and inguinal lymph nodes.

Paraffin-embedded mouse melanomas were sectioned into 7-µm-thick transverse sections and stained with hematoxylin/eosin (H&E), as previously described⁶⁸. For immunostaining, sections were deparaffinized, rinsed in Tris-buffered saline (TBS; 20 mM Tris (Sigma: T-1503) pH7.6), 150 mM NaCl (OSI, A4321152), containing 0.1% [v/v] Tween-20 (VWR 8221840500) (TBST), depigmented with H₂O₂ (Sigma, H1009) for 15 min, boiled for 20 min in 10 mM sodium citrate (VWR, 1120051000), and blocked with TBST containing 3% bovine serum albumin (BSA, Sigma A9418). Sections were incubated overnight at 4 °C in TBST containing 3% BSA with antibodies against Ki-67 (Nova-Costra, NCL-Ki67p), BrdU (BD Biosciences, #555627), or PTEN (Cell signaling, #9559). The sections were then incubated in secondary biotinylated anti-rabbit or anti-mouse antibodies for 2 h at room temperature (RT). AEC (Sigma-Aldrich, A6926) was used to reveal bound antibody according to the manufacturer's instructions. All sections were counterstained with hematoxylin. Images were captured using a ZEISS Axio Imager 2 with Axiocam 506 color cameras. Image analysis was performed using ZEISS ZEN, Adobe Photoshop, and ImageJ software. Quantifications of Ki-67 and BrdU stainings were determined as a percentage. The percentage of Ki-67⁺ and BrdU⁺ cells from three fields (1000–2000 cells/field) from three independent tumors per genotype was determined and normalized.

Immunofluorescence of mouse inguinal lymph nodes. OCT-embedded lymph nodes were sectioned into 7-µm-thick transverse sections and rinsed in TBST, depigmented with H₂O₂ (Sigma, H1009) for 15 min, boiled for 20 min in 10 mM sodium citrate (VWR, 1120051000) and blocked with TBST containing 3% BSA (Sigma A9418). Sections were incubated overnight at 4 °C in TBST containing 3% BSA with antibodies against SOX10 (Abcam, ab155279). Sections were then incubated in secondary donkey anti-mouse 647 (Abcam, ab150107) and goat anti-rabbit IgG (H&L)-Affinity Pure, DyLight® 650 Conjugate (GtxRb-003-E650NHSX) antibodies for 2 h at RT. All sections were counterstained with DAPI (0.5 µg/mL in ethanol, Sigma, D9542). Images were captured using a ZEISS Axio Imager 2 with Axiocam 506 color cameras. Image analysis was performed using ZEISS ZEN, Adobe Photoshop, and ImageJ software.

Protein extraction from tumors. All steps were performed at 4 °C. Tissues were transferred to a tube containing 2.8-mm stainless steel beads and 1 mL RIPA buffer supplemented with sodium orthovanadate (Sigma, S6508). Complete protease inhibitor (Roche, #11873580001) and Phostop (Roche, #04906837001) were added. Tissues were homogenized three times for 3 min using the BeadBug™ homogenizer at 4 °C, followed by a brief centrifugation at 17,949 g for 1 min at 4 °C. Supernatants were transferred and centrifuged for 20 min at 15,294 × g. Supernatants

were collected and incubated with 200 µL previously PBS-washed G-Sepharose beads (GE Healthcare, #17-0618-01) for 2 h. Samples were centrifuged at 15,294 × g for 5 min and quantified using the Bradford assay.

Microarray analysis. Only one tumor per mouse was considered and corresponding to the biggest one. Tumors had the same size since we harvested tumors for transcriptomic analyses when they reached a size of 1 cm³. RNA from mouse melanomas (5 Braf-Pten-Brn2-WT, 10 Braf-Pten-Brn2-het, and 10 Braf-Pten-Brn2-hom) and mouse melanoma cell lines (4 Braf-Pten-Brn2-WT, 2 Braf-Pten-Brn2-het, and 3 Braf-Pten-Brn2-hom) established from the mouse melanoma tumors was extracted using the miRNeasy Kit (Qiagen, #217004). RNA Integrity was assessed using an Agilent BioAnalyzer 2100 (Agilent Technologies), only RNA with a RIN > 7 were kept for the analysis. RNA concentrations were measured using a NanoDrop (NanoDrop Technologies). Complementary RNA (cRNA) was synthesized using the GeneChip 3'UT Plus reagent Kit (ThermoFisher, #902415), according to the manufacturer's protocol. In brief, total RNA was first reverse transcribed using a T7-Oligo(dT) promoter primer for first-strand cDNA synthesis. After RNase H treatment and second-strand cDNA synthesis, the double-stranded cDNA was purified and served as template for subsequent in vitro transcription (IVT). The IVT reaction was carried out in the presence of T7 RNA polymerase and a biotinylated nucleotide analog/ribonucleotide mix for cRNA amplification and biotin labeling. The biotinylated cRNA targets were then cleaned up, fragmented, and 11 µg cRNA hybridized to mouse MOE430 gene expression Affymetrix microarrays (Affymetrix, #900443). After washing and staining, using the Affymetrix fluidics station 450 (Affymetrix, # 00-0079), the probe arrays were scanned using an Affymetrix GeneChip Scanner 3000 (Affymetrix, # 00-0210).

The microarray data were normalized using the RMA (Robust Multichip Average) function of the edgeR package⁶⁹. For genes targeted by multiple probesets, only the most variant probeset was kept. Differentially expressed gene analysis was performed with R, for the cell lines and the tumors using the limma package⁷⁰ available from Bioconductor (<http://www.bioconductor.org>). An enriched gene-ontology (Gene-Ontology Biological-Process, 2018) and pathway (WikiPathways human, 2019 & KEGG human, 2019) analysis was performed on the 296 genes found overexpressed in the Braf-Pten-Brn2-het compared to the Braf-Pten-Brn2-WT using Enrichr⁷¹. Gene-set enrichment analysis (GSEA) was performed using the "Verfaillie" signature⁴⁴. These signatures originally containing too much genes (>1,000) were reduced to fit to the GSEA algorithm by selecting the most differentially expressed genes based on their fold change, a threshold of 4 standard deviation was selected. For the tumors analysis the GSEA was run with one thousand permutations gene set based. For the analysis of the cell lines, the run pre-ranked function of the GSEA software was used using one thousand permutations gene set based. The genes were ranked according to their statistic t coming from the differential analysis results. The enrichment score (ES) reflects the degree to which a given gene set is represented in a ranked list of genes. Calculation of the ES is based on walking down a ranked list of genes and adjusting a running-sum statistic based on the presence of absence of a gene in the gene set. The magnitude of the increment represents the correlation of the gene with the phenotype. P values were estimated by gene-based permutation. GSEA normalizes the enrichment score for each gene set to account for the variation in set sizes, yielding a normalized enrichment score (NES). Only gene set with a NES absolute > 1.7 and a FDR < 0.01 were considered.

Cell lines. Melan-a and C57BL/6 9 v cells were grown in Ham's F12 media (GIBCO 11765054) supplemented with 10% fetal calf serum (FCS, GIBCO, 10270106), 1% Penicillin-Streptomycin (GIBCO, 15140), and 200 nM TPA (Sigma, P 8139)⁴. 501mel, 501mel-MITF-HA, HBL, SK-Mel-28, SK-Mel-28 Δex6, and Dauv-1 cells were grown in RPMI 1640 media (GIBCO, 11875101) supplemented with 10% FCS (GIBCO, 10270106) and 1% Penicillin-Streptomycin (GIBCO, 15140)^{50,72–74}. SK28Δex6 melanoma cells lacking Mitf was previously produced⁵⁰. Cells are routinely tested for the absence of mycoplasmas using MycoAlert (Lonza). Mouse melanoma cell lines were established as previously described⁷⁵. The genetic status and the level of expression of key genes of these cell lines is given in Supplementary Table 1.

Genomic DNA extraction from cell culture. Genomic DNA was extracted from melanoma cell lines using the AllPrep DNAMini Kit (Qiagen, #80204) or QIAamp Kit (QIAGEN) according to manufacturer's instructions. The DNA region for BRAF and NRAS was amplified by PCR and submitted for sequencing (see for primers and conditions in the Key Resource Table and Supplementary Tables 3 and 4).

siRNA-mediated knock-down. siRNA targeting human BRN2 and MITF was purchased from Dharmacon as a SMART-pool mix of four sequences. siRNA targeting PTEN was purchased from Santa Cruz Biotech. Si Scramble (siSCR), with no known human or mouse targets, was purchased from Eurofins Genomics (Supplementary Table 5). All sequences and product references are listed in Supplementary Table 6. Briefly, cells were transfected with Lipofectamin2000 with 200 pmol siRNA or siSCR and assayed for mRNA expression or protein content 48 or 72 h post-transfection.

Cell counting. Phase-contrast pictures of cells were taken using a Zeiss Axiovert 135 microscope with an AxioCam MRC camera. Cells were counted using a LUNA automated cell counter (L10001) and cell-counting slides (L12001).

Clonogenic assays. For clonogenic assays, six-well tissue culture plates were seeded with 500 cells in complete medium. The medium was changed 24 h after cell seeding and replaced with complete medium containing the indicated concentrations of Binimetinib (Selleck), MK-2206 2HCl (Selleck), LY294002 (Calbiochem) or PLX4720 (Axon Medchem). After 9 days of incubation, colonies were fixed with 4% PFA (paraformaldehyde), stained with Crystal violet in 10% ethanol, and counted on images. IC50 were determined for each pharmacological agent and for each cell line using the number of colonies in mock treated condition as the top response. Cell lines have been treated with Binimetinib from 10^{-3} to 100 μM , with PLX4720 from 10^{-3} to 100 μM , with LY294002 from 5.10^{-3} to 50 μM and with MK-2206 from 10^{-3} to 10 μM . We used the resulted sigmoidal curves to calculate the IC50 with Graphpad Prism. Experiments were performed at least in triplicate.

Western blotting and detection. Whole-cell lysate was prepared from human melanoma cell lines using RIPA buffer supplemented with sodium orthovanadate (Sigma S 6508), complete inhibitor (Roche, #11873580001), and Phostop (Roche, #04906837001). SDS-PAGE was carried out on homemade 10% polyacrylamide protein gels. Following the transfer of the proteins, the nitrocellulose membranes were blocked in TBST with 5% non-fat dry milk for 1.5 h at RT and then probed with antibodies against BRN2 (Cell signaling, #12137), MITF (Abcam, ab12039), β -actin (Sigma, A5441), cyclin D1 (Cell signaling, #2926), PTEN (Cell signaling, #9559), phospho-S6 (Cell signaling, #4857), S6 (Cell signaling, #2317), phospho-AKT (Cell signaling, #3787), AKT (Cell signaling, #4685), or vinculin (Sigma, V9131). Primary antibodies were applied in TBST/5% non-fat dry milk overnight at 4 °C and visualized using secondary antibodies (HRP-conjugated goat anti-rabbit IgG, Jackson, 111-035-003 and HRP-conjugated goat anti-mouse IgG, Jackson, 115-035-003) in TBST/5% non-fat dry milk for 1 h at RT. Blots were incubated in ECL (Pierce, #34075) and revealed in the dark using ECL hyperfilm (GE Healthcare, RPN3103K). All primary antibodies were used at a dilution of 1/1,000, except β -actin and vinculin (1/5,000). All secondary antibodies were used at a dilution of 1/20,000. PAGERuler (ThermoFisher, #26616) was used as the molecular marker. Quantification of the western blots was performed using *ImageJ* software. Quantification of the western blots was performed using *ImageJ* software. See Supplementary table 7.

Chromatin immunoprecipitation. ChIP experiments were performed as previously described⁴, and see Supplementary Table 6. ChIP assays of BRN2 binding to the *PTEN* promoter. ChIP assays were performed using an antibody against BRN2 and analyzed after 30-cycle PCR in exponentially growing phase of Dauv-1 melanoma cells. *PAX3* promoter (prom.) and *Brn2* coding sequences (CDS) were used as positive and negative controls, respectively. Input represents approximately 0.4% of the input used for the ChIP assay. H3 (histone H3) and IgG (Immunoglobulin G) were used as positive and negative controls for each region of interest, respectively. The oligonucleotides, their position on the genome, and the sizes of the amplified fragments are given in Supplementary Tables 3 and 4.

RNA extraction and (ChIP) RT-qPCR. Tissues were crushed with a mortar and pestle, and stainless steel beads. Qiazol was used to homogenize the samples prior extracting RNA using the miRNeasy Kit. Purified RNA was reversed transcribed using M-MLV Reverse Transcriptase. Real-time quantitative PCR (qPCR) was performed using iTaq™ Universal SYBR Green Supermix. Each sample was run in technical triplicates and the quantified RNA normalized against TBP (human) or Gapdh (mouse) as housekeeping transcripts (Supplementary Tables 3 and 4).

CUT&RUN. Anti-MITF, anti-H3K27Ac and anti-H3K4Me3 Cleavage Under Targets and Release Using Nuclease (CUT&RUN) sequencing was performed in SK28 melanoma cell lines that are MITF-WT or null (Δ MITF) as described⁷⁶, with minor modifications. Cells (~75–80% confluent) were harvested by cell scraping (Corning), centrifuged at 600 × g (Eppendorf, centrifuge 5424) and washed in calcium-free wash-buffer (20 mM HEPES, pH7.5, 150 mM NaCl, 0.5 mM spermidine and protease inhibitor cocktail, cComplete Mini, EDTA-free Roche). Pre-activated Concanavalin A-coated magnetic beads (Bangs Laboratories Inc) were added to 100 μL cell suspensions (2×10^5 cells) and incubated at 4 °C for 15 min. Antibody dilution buffer (wash-buffer with 2 mM EDTA and 0.03% digitonin) containing anti-MITF (Sigma, HPA003259, 1:100), anti-H3K27Ac (Millipore, 07-360, 1:100), anti-H3K4Me3 (Millipore, 05-745 R, 1:100) and Rabbit IgG (Millipore, 12-370, 1:100) was added and cells were incubated at 4 °C overnight. The next day, cells were placed on a magnetic rack and washed twice in dig-wash buffer (wash buffer containing 0.025% digitonin). pAG-MNase at a concentration of 500 $\mu\text{g}/\text{mL}$ was added and cells were incubated at 4 °C for 30 mins (pAG-MNase was purified in Dr. Robert Cornell's research group at the University of Iowa). The pAG-MNase reactions were quenched with 2X Stop buffer (340 mM NaCl, 867 mM EDTA, 4 mM EGTA, 0.05% Digitonin, 100 $\mu\text{g}/\text{mL}$ RNase A and 50 $\mu\text{g}/\text{mL}$ Glycogen). Released DNA fragments were Phosphatase K (1 $\mu\text{L}/\text{mL}$, Thermo Fisher Scientific)

treated at 50 °C for 1 hr and purified by phenol/chloroform-extracted and ethanol-precipitated. Fragment sizes were analyzed using a 2100 Bioanalyzer (Agilent). All CUT&RUN experiments were performed in duplicate.

Library preparation and data analysis. CUT&RUN-seq libraries were prepared using the KAPA Hyper Prep Kit (Roche). Quality control post-library amplification was conducted using the 2100 Bioanalyzer (Agilent). Fragment analysis and fragments sizes were compared pre- and post-library amplification to insure correct size selection. Libraries were pooled to equimolar concentrations and sequenced with paired-end 100 bp reads on an Illumina HiSeq X platform. Paired-end FastQ files were processed through FastQC (Babraham Bioinformatics) for quality control. Reads were trimmed using Trim Galore Version 0.6.3 (Developed by Felix Krueger at the Babraham Institute), Bowtie2 version 2.1.0⁷⁷ was used to map the reads against the hg19 genome assembly and MACS2 Version 2.1.1.20160309.6 was used to call peaks. The mapping parameters and peak calling analysis was performed as previously described^{76,78} using IgG samples as background control. The DeepTools function “BAMcoverage”⁷⁹ was used to generate normalized (–RPKM) BigWigs files for visualization on Integrative Genomics Viewer (IGV)⁸⁰.

Luciferase assays. Human (–2,375 to +840) and murine (–2136 to +936) Pten-promoter fragments were cloned upstream 56 bp of CMV promoter conferring a very weak basal activity upstream luciferase (miniCMV::Luc, VectorBuilder) to generate hsPTEN::Luc (#1282) and mmPTEN::Luc (#1283) reporter vectors. Cells at 70% confluence were transiently transfected in twelve-well plates, using 2 μL of Lipofectamin2000 (Invitrogen), 500 ng of total plasmid DNA 200 ng Pten::Luc reporter plasmids (#1282 or #1283) or miniCMV::Luc reporter (#1281), 200 ng of the expression vectors CMV::EGFP-Brn2 (#896) or CMV::EGFP (#1042) (equimolar) as a control²⁷; 100 ng of the HSV-TK:renilla luciferase construct (#894) in Opti-MEM medium (Gibco). Luciferase activity and renilla luciferase activity were determined 48 h after transfection. Luciferase activity was normalized against renilla luciferase activity.

Software. GraphPad PRISM, R version 3.6.3 (R Foundation for Statistical Computing, Vienna, Austria), Adobe Illustrator, Adobe Photoshop, and Microsoft Power Point software were used to analyze data and generate all graphs and figures.

Quantification and statistical analysis. Cell culture-based experiments were performed in at least biological triplicate and validated three times as technical triplicates. *P* values for the comparison of two groups were calculated using the unpaired Student t-test or Mann-Whitney test. *P* values for the comparison of multiple groups were calculated using the analysis of variance (ANOVA) and Fisher's least significant difference tests. *P*-values for categorical data were calculated using the Chi-square test. *P*-values for the comparison of Kaplan–Meier curves were calculated using the log-rank (Mantel–Cox) or Gehan–Breslow–Wilcoxon test giving weight to the early events. *P* values were reported as computed by Prism 6.

Reporting summary. Further information on research design is available in the Nature Research Reporting Summary linked to this article.

Data availability

Microarray gene expression data that support the findings of this study have been deposited in Gene Expression Omnibus (GEO) with the accession codes [GSE126524](https://www.ncbi.nlm.nih.gov/geo/query/acc.cgi?acc=GSE126524) and [GSE163085](https://www.ncbi.nlm.nih.gov/geo/query/acc.cgi?acc=GSE163085). The TCGA Skin Cutaneous Melanoma data referenced during the study are available in a public repository from the National Cancer Institute (NCI) Genomic Data Commons (GDC) website (<https://portal.gdc.cancer.gov>). Cut&Run assay data that support the findings of this study have been deposited in Gene Expression Omnibus (GEO) with the accession codes [GSE153020](https://www.ncbi.nlm.nih.gov/geo/query/acc.cgi?acc=GSE153020). The accession number for the sequencing data reported in this paper is dbGaP: phs001550.v1.p1. All the other data supporting the findings of this study are available within the article and its supplementary information/data files and from the corresponding author upon reasonable request. A reporting summary for this article is available as a Supplementary Information file. The data that support the findings of this study are available from the corresponding author upon reasonable request. All details concerning antibodies, chemicals, critical commercial assays, cell lines, model organisms, oligonucleotides, and software and algorithms can be found in Supplementary Table 7a–g. Source data are provided with this paper.

Received: 24 April 2019; Accepted: 27 May 2021;

Published online: 17 June 2021

References

1. Davies, H. et al. Mutations of the BRAF gene in human cancer. *Nature* **417**, 949–954 (2002).

2. Eskandarpour, M. et al. Frequency of UV-inducible NRAS mutations in melanomas of patients with germline CDKN2A mutations. *J. Natl. Cancer Inst.* **95**, 790–798 (2003).
3. Conde-Perez, A. et al. A caveolin-dependent and PI3K/AKT-independent role of PTEN in beta-catenin transcriptional activity. *Nat. Commun.* **6**, 8093 (2015).
4. Delmas, V. et al. Beta-catenin induces immortalization of melanocytes by suppressing p16INK4a expression and cooperates with N-Ras in melanoma development. *Genes Dev.* **21**, 2923–2935 (2007).
5. Bennett, D. C. Genetics of melanoma progression: the rise and fall of cell senescence. *Pigment Cell Melanoma Res.* **29**, 122–140 (2016).
6. Gray-Schopfer, V. C. et al. Cellular senescence in naevi and immortalisation in melanoma: a role for p16? *Br. J. Cancer* **95**, 496–505 (2006).
7. Gembarska, A. et al. MDM4 is a key therapeutic target in cutaneous melanoma. *Nat. Med.* **18**, 1239–1247 (2012).
8. Schreiber, E. et al. Astrocytes and glioblastoma cells express novel octamer-DNA binding proteins distinct from the ubiquitous Oct-1 and B cell type Oct-2 proteins. *Nucleic Acids Res.* **18**, 5495–5503 (1990).
9. Bishop, J. L. et al. The master neural transcription factor BRN2 is an androgen receptor-suppressed driver of neuroendocrine differentiation in prostate cancer. *Cancer Disco.* **7**, 54–71 (2017).
10. Ishii, J. et al. POU domain transcription factor BRN2 is crucial for expression of ASCL1, ND1 and neuroendocrine marker molecules and cell growth in small cell lung cancer. *Pathol. Int.* **63**, 158–168 (2013).
11. Chitsazan, A. et al. Unexpected high levels of BRN2/POU3F2 expression in human dermal melanocytic nevi. *J. Invest. Dermatol.* **140**, 1299–1302 e4 (2020).
12. Colombo, S., Champeval, D., Rambow, F. & Larue, L. Transcriptomic analysis of mouse embryonic skin cells reveals previously unreported genes expressed in melanoblasts. *J. Invest. Dermatol.* **132**, 170–178 (2012).
13. Goodall, J. et al. Brn-2 represses microphthalmia-associated transcription factor expression and marks a distinct subpopulation of microphthalmia-associated transcription factor-negative melanoma cells. *Cancer Res.* **68**, 7788–7794 (2008).
14. Goodall, J. et al. Brn-2 expression controls melanoma proliferation and is directly regulated by beta-catenin. *Mol. Cell Biol.* **24**, 2915–2922 (2004).
15. Goodall, J. et al. The Brn-2 transcription factor links activated BRAF to melanoma proliferation. *Mol. Cell Biol.* **24**, 2923–2931 (2004).
16. Bonvin, E., Falletta, P., Shaw, H., Delmas, V. & Goding, C. R. A phosphatidylinositol 3-kinase-Pax3 axis regulates Brn-2 expression in melanoma. *Mol. Cell Biol.* **32**, 4674–4683 (2012).
17. Cook, A. L., Smith, A. G., Smit, D. J., Leonard, J. H. & Sturm, R. A. Co-expression of SOX9 and SOX10 during melanocytic differentiation in vitro. *Exp. Cell Res.* **308**, 222–235 (2005).
18. Goding, C. R. & Arnheiter, H. MITF—the first 25 years. *Genes Dev.* **33**, 983–1007 (2019).
19. Boyle, G. M. et al. Melanoma cell invasiveness is regulated by miR-211 suppression of the BRN2 transcription factor. *Pigment Cell Melanoma Res.* **24**, 525–537 (2011).
20. Zeng, H. et al. Bi-allelic Loss of CDKN2A initiates melanoma invasion via BRN2 activation. *Cancer Cell* **34**, 56–68 e9 (2018).
21. Smith, M. P. et al. A PAX3/BRN2 rheostat controls the dynamics of BRAF mediated MITF regulation in MITF(high)/AXL(low) melanoma. *Pigment Cell Melanoma Res.* **32**, 280–291 (2019).
22. Potterf, S. B., Furumura, M., Dunn, K. J., Arnheiter, H. & Pavan, W. J. Transcription factor hierarchy in Waardenburg syndrome: regulation of MITF expression by SOX10 and PAX3. *Hum. Genet.* **107**, 1–6 (2000).
23. Bondurand, N. et al. Interaction among SOX10, PAX3 and MITF, three genes altered in Waardenburg syndrome. *Hum. Mol. Genet.* **9**, 1907–1917 (2000).
24. Vivas-Garcia, Y. et al. Lineage-restricted regulation of SCD and fatty acid saturation by MITF controls melanoma phenotypic plasticity. *Mol. Cell* **77**, 120–139 (2020).
25. Simmons, J. L., Neuendorf, H. M. & Boyle, G. M. BRN2 and MITF together impact AXL expression in melanoma. *Exp. Dermatol.* <https://doi.org/10.1111/exd.14225> (2020).
26. Fane, M. E., Chhabra, Y., Smith, A. G. & Sturm, R. A. BRN2, a POUerful driver of melanoma phenotype switching and metastasis. *Pigment Cell Melanoma Res.* **32**, 9–24 (2019).
27. Berlin, I. et al. Phosphorylation of BRN2 modulates its interaction with the Pax3 promoter to control melanocyte migration and proliferation. *Mol. Cell Biol.* **32**, 1237–1247 (2012).
28. Pierce, C. J. et al. BRN2 expression increases anoikis resistance in melanoma. *Oncogenesis* **9**, 64 (2020).
29. Pinner, S. et al. Intravital imaging reveals transient changes in pigment production and Brn2 expression during metastatic melanoma dissemination. *Cancer Res.* **69**, 7969–7977 (2009).
30. Arozarena, I. et al. In melanoma, beta-catenin is a suppressor of invasion. *Oncogene* **30**, 4531–4543 (2011).
31. Cirenajwis, H. et al. NF1-mutated melanoma tumors harbor distinct clinical and biological characteristics. *Mol. Oncol.* **11**, 438–451 (2017).
32. Shain, A. H. et al. Genomic and transcriptomic analysis reveals incremental disruption of key signaling pathways during melanoma evolution. *Cancer Cell* **34**, 45–55 (2018).
33. Yajima, I. et al. Spatiotemporal gene control by the Cre-ERT2 system in melanocytes. *Genesis* **44**, 34–43 (2006).
34. Dhomen, N. et al. Oncogenic Braf induces melanocyte senescence and melanoma in mice. *Cancer Cell* **15**, 294–303 (2009).
35. Lesche, R. et al. Cre/loxP-mediated inactivation of the murine Pten tumor suppressor gene. *Genesis* **32**, 148–149 (2002).
36. Dhomen, N. et al. Inducible expression of (V600E) Braf using tyrosinase-driven Cre recombinase results in embryonic lethality. *Pigment Cell Melanoma Res.* **23**, 112–120 (2010).
37. Dankort, D. et al. Braf(V600E) cooperates with Pten loss to induce metastatic melanoma. *Nat. Genet.* **41**, 544–552 (2009).
38. Jaegle, M. et al. The POU proteins Brn-2 and Oct-6 share important functions in Schwann cell development. *Genes Dev.* **17**, 1380–1391 (2003).
39. Bennett, D. C. Human melanocyte senescence and melanoma susceptibility genes. *Oncogene* **22**, 3063–3069 (2003).
40. Michaloglou, C. et al. BRAFE600-associated senescence-like cell cycle arrest of human naevi. *Nature* **436**, 720–724 (2005).
41. Puig, I. et al. Deletion of Pten in the mouse enteric nervous system induces ganglioneuromatosis and mimics intestinal pseudoobstruction. *J. Clin. Invest.* **119**, 3586–3596 (2009).
42. Simmons, J. L., Pierce, C. J., Al-Ejeh, F. & Boyle, G. M. MITF and BRN2 contribute to metastatic growth after dissemination of melanoma. *Sci. Rep.* **7**, 10909 (2017).
43. Herbert, K. et al. BRN2 suppresses apoptosis, reprograms DNA damage repair, and is associated with a high somatic mutation burden in melanoma. *Genes Dev.* **33**, 310–332 (2019).
44. Verfaillie, A. et al. Decoding the regulatory landscape of melanoma reveals TEADS as regulators of the invasive cell state. *Nat. Commun.* **6**, 6683 (2015).
45. Muller, J. et al. Low MITF/AXL ratio predicts early resistance to multiple targeted drugs in melanoma. *Nat. Commun.* **5**, 5712 (2014).
46. Davies, M. A. et al. Integrated molecular and clinical analysis of AKT activation in metastatic melanoma. *Clin. Cancer Res.* **15**, 7538–7546 (2009).
47. Vredeveld, L. C. et al. Abrogation of BRAFV600E-induced senescence by PI3K pathway activation contributes to melanomagenesis. *Genes Dev.* **26**, 1055–1069 (2012).
48. Thurber, A. E. et al. Inverse expression states of the BRN2 and MITF transcription factors in melanoma spheres and tumour xenografts regulate the NOTCH pathway. *Oncogene* **30**, 3036–3048 (2011).
49. Wellbrock, C. et al. Oncogenic BRAF regulates melanoma proliferation through the lineage specific factor MITF. *PLoS ONE* **3**, e2734 (2008).
50. Dilshat, R. et al. MITF reprograms the extracellular matrix and focal adhesion in melanoma. *Elife* **10**, e63093 (2021).
51. Thomson, J. A. et al. The Brn-2 gene regulates the melanocytic phenotype and tumorigenic potential of human melanoma cells. *Oncogene* **11**, 691–700 (1995).
52. Healy, E. et al. Prognostic significance of allelic losses in primary melanoma. *Oncogene* **16**, 2213–2218 (1998).
53. Bastian, B. C., LeBoit, P. E., Hamm, H., Brocker, E. B. & Pinkel, D. Chromosomal gains and losses in primary cutaneous melanomas detected by comparative genomic hybridization. *Cancer Res.* **58**, 2170–2175 (1998).
54. Guan, X. Y. et al. Detection of chromosome 6 abnormalities in melanoma cell lines by chromosome arm painting probes. *Cancer Genet. Cytogenet.* **107**, 89–92 (1998).
55. Lee, J. J. et al. Targeted next-generation sequencing reveals high frequency of mutations in epigenetic regulators across treatment-naive patient melanomas. *Clin. Epigenetics* **7**, 59 (2015).
56. Shain, A. H. et al. Exome sequencing of desmoplastic melanoma identifies recurrent NFKBIE promoter mutations and diverse activating mutations in the MAPK pathway. *Nat. Genet.* **47**, 1194–1199 (2015).
57. Saito, Y. et al. Endogenous melanin-concentrating hormone receptor SLC-1 in human melanoma SK-MEL-37 cells. *Biochem. Biophys. Res. Commun.* **289**, 44–50 (2001).
58. Cifola, I. et al. Comprehensive genomic characterization of cutaneous malignant melanoma cell lines derived from metastatic lesions by whole-exome sequencing and SNP array profiling. *PLoS One* **8**, e63597 (2013).
59. Zhang, J. P. et al. Notch ligand Delta-like 1 promotes the metastasis of melanoma by enhancing tumor adhesion. *Braz. J. Med Biol. Res.* **47**, 299–306 (2014).
60. Wiesner, T. et al. Kinase fusions are frequent in Spitz tumours and spitzoid melanomas. *Nat. Commun.* **5**, 3116 (2014).
61. Ray, M. E., Su, Y. A., Meltzer, P. S. & Trent, J. M. Isolation and characterization of genes associated with chromosome-6 mediated tumor suppression in human malignant melanoma. *Oncogene* **12**, 2527–2533 (1996).

62. Laurette, P. et al. Transcription factor MITF and remodeler BRG1 define chromatin organisation at regulatory elements in melanoma cells. *Elife* **4** (2015).
63. Cirenajwis, H. et al. Molecular stratification of metastatic melanoma using gene expression profiling: Prediction of survival outcome and benefit from molecular targeted therapy. *Oncotarget* **6**, 12297–12309 (2015).
64. Li, J. et al. CONTRA: copy number analysis for targeted resequencing. *Bioinformatics* **28**, 1307–1313 (2012).
65. Hupe, P., Stransky, N., Thiery, J. P., Radvanyi, F. & Barillot, E. Analysis of array CGH data: from signal ratio to gain and loss of DNA regions. *Bioinformatics* **20**, 3413–3422 (2004).
66. Riester, M. et al. PureCN: copy number calling and SNV classification using targeted short readsequencing. *Source Code Biol. Med.* **11**, 13 (2016).
67. Aktary, Z., Corvelo, A., Estrin, C. & Larue, L. Sequencing two Tyr::CreER(T2) transgenic mouse lines. *Pigment Cell Melanoma Res.* **33**, 426–434 (2020).
68. Gallagher, S. J. et al. General strategy to analyse melanoma in mice. *Pigment Cell Melanoma Res.* **24**, 987–988 (2011).
69. Robinson, M. D., McCarthy, D. J. & Smyth, G. K. edgeR: a bioconductor package for differential expression analysis of digital gene expression data. *Bioinformatics* **26**, 139–140 (2010).
70. Ritchie, M. E. et al. Limma powers differential expression analyses for RNA-seq and microarray studies. *Nucleic Acids Res.* **43**, e47 (2015).
71. Chen, E. Y. et al. Enrichr: interactive and collaborative HTML5 gene list enrichment analysis tool. *BMC Bioinforma.* **14**, 128 (2013).
72. Strub, T. et al. Essential role of microphthalmia transcription factor for DNA replication, mitosis and genomic stability in melanoma. *Oncogene* **30**, 2319–2332 (2011).
73. Ghanem, G. E., Comunale, G., Libert, A., Vercammen-Grandjean, A. & Lejeune, F. J. Evidence for alpha-melanocyte-stimulating hormone (alpha-MSH) receptors on human malignant melanoma cells. *Int. J. Cancer* **41**, 248–255 (1988).
74. Rambow, F. et al. New functional signatures for understanding melanoma biology from tumor cell lineage-specific analysis. *Cell Rep.* **13**, 840–853 (2015).
75. Petit, V. et al. C57BL/6 congenic mouse NRAS(Q61K) melanoma cell lines are highly sensitive to the combination of Mek and Akt inhibitors in vitro and in vivo. *Pigment Cell Melanoma Res.* **32**, 829–841 (2019).
76. Skene, P. J. & Henikoff, S. An efficient targeted nuclease strategy for high-resolution mapping of DNA binding sites. *Elife* **6**, e21856 (2017).
77. Langmead, B. & Salzberg, S. L. Fast gapped-read alignment with Bowtie 2. *Nat. Methods* **9**, 357–359 (2012).
78. Meers, M. P., Tenenbaum, D. & Henikoff, S. Peak calling by sparse enrichment analysis for CUT&RUN chromatin profiling. *Epigenetics Chromatin* **12**, 42 (2019).
79. Ramírez, F. et al. deepTools2: a next generation web server for deep-sequencing data analysis. *Nucleic Acids Res.* **44**, W160–W165 (2016).
80. Robinson, J. T. et al. Integrative genomics viewer. *Nat. Biotechnol.* **29**, 24–26 (2011).

Acknowledgements

We are grateful to Dorothy C Bennett, Ghanem Ghanem, Florence Faure, and Meenhard Herlyn for providing cell lines. Hong Wu for providing Pten flox mice. We thank the Institut Curie staff responsible for the animal colony (especially P. Dubreuil), and the histology (S. Leboucher), FACS (C. Lasgi), and PICT-IBiSA imaging (C. Lovo) facilities.

This work was supported by the Ligue nationale contre le cancer, INCa, ITMO Cancer, Fondation ARC (PGA), and is under the program «Investissements d’Avenir» launched by the French Government and implemented by ANR Labex CellTisPhyBio (ANR-11-LBX-0038 and ANR-10-IDEX-0001-02 PSL). M.H. had a fellowship from PSL and FRM, P.S. had a fellowship from INSERM, and M.L.C. had a fellowship from FRM. C.R.G. was supported by the Ludwig Institute for Cancer Research. RC was supported in part by a grant from the National Institutes of Health (AR062547, RAC) and a postdoctoral fellowship from the American Association for Anatomy (CK). E.S. was supported from the Research Fund of Iceland (184861-053). L.L. and E.S. are supported by a Jules Verne grant.

Author contributions

M.H., P.S., V.P., J.R., V.D., M.L.C., C.K., M.P., F.R., N.C., A.S., L.S.C., L.M., M.L., and G.B.J. conducted the experiments M.H., P.S., R.A.C., C.R.G. and L.L. designed the experiments M.H., P.S., V.P., F.G., V.D., Z.A., A.S., A.B., I.D., C.R.G., and L.L. wrote and reviewed the manuscript C.R.G., and L.L. secured the funding D.M. and E.S. provided reagents I.D., A.S., C.R.G. provided expertise and feedback

Competing interests

The authors declare no competing interests.

Additional information

Supplementary information The online version contains supplementary material available at <https://doi.org/10.1038/s41467-021-23973-5>.

Correspondence and requests for materials should be addressed to C.R.G. or L.L.

Peer review information *Nature Communications* thanks Rugang Zhang and the other, anonymous, reviewer(s) for their contribution to the peer review of this work. Peer reviewer reports are available.

Reprints and permission information is available at <http://www.nature.com/reprints>

Publisher’s note Springer Nature remains neutral with regard to jurisdictional claims in published maps and institutional affiliations.



Open Access This article is licensed under a Creative Commons Attribution 4.0 International License, which permits use, sharing, adaptation, distribution and reproduction in any medium or format, as long as you give appropriate credit to the original author(s) and the source, provide a link to the Creative Commons license, and indicate if changes were made. The images or other third party material in this article are included in the article’s Creative Commons license, unless indicated otherwise in a credit line to the material. If material is not included in the article’s Creative Commons license and your intended use is not permitted by statutory regulation or exceeds the permitted use, you will need to obtain permission directly from the copyright holder. To view a copy of this license, visit <http://creativecommons.org/licenses/by/4.0/>.

© The Author(s) 2021

III. Efficacy of Targeted Radionuclide Therapy Using [131 I]ICF01012 in 3D Pigmented BRAF- and NRAS-Mutant Melanoma Models and *In Vivo* NRAS-Mutant Melanoma

Article publié en mars 2021

Résumé :

L'équipe de F. Degoul, à Clermont a mis au point un radiotracer ciblant la mélanine, [131I]ICF01012, qu'il développe dans un but de thérapie par radionucléides ciblés. Ils ont pu montrer que ce radiotracer coopérait *in vitro* pour inhiber la croissance des cellules de mélanome. Ils ont également montré que le radiotracer était capable de réduire la croissance de lignées de mélanome murine *in vivo*. Des hypothèses ont été émises pour expliquer l'effet anti-tumoral observé comme l'activation de p53, l'augmentation de l'oxydation et de l'inflammation.

Dans ce projet, j'ai été en charge des analyses des tumeurs avec les études transcriptomiques qui ont abouti aux différentes hypothèses pouvant expliquer l'effet anti-tumoral.

Article

Efficacy of Targeted Radionuclide Therapy Using [¹³¹I]ICF01012 in 3D Pigmented BRAF- and NRAS-Mutant Melanoma Models and In Vivo NRAS-Mutant Melanoma

Hussein Akil ^{1,2}, Mercedes Quintana ^{1,†}, Jérémy H. Raymond ^{3,4,5,†}, Tommy Billoux ⁶,
Valentin Benboubker ¹, Sophie Besse ¹, Philippe Auzeloux ¹, Véronique Delmas ^{3,4,5}, Valérie Petit ^{3,4,5},
Lionel Larue ^{3,4,5}, Michel D'Incan ^{1,7}, Françoise Degoul ^{1,8,‡} and Jacques Rouanet ^{1,7,*,‡}

¹ INSERM U1240, University of Clermont Auvergne, 58 rue Montalembert, 63000 Clermont-Ferrand, France; hussein.akil@unilim.fr (H.A.); mercedes.quintana@inserm.fr (M.Q.); vbenboubker@chu-clermontferrand.fr (V.B.); sophie.besse@inserm.fr (S.B.); philippe.auzeloux@inserm.fr (P.A.); mdincan@chu-clermontferrand.fr (M.D.); francoise.degoul@inserm.fr (F.D.)

² CNRS 7276, INSERM U1262, 2 rue du Pr Descottes, 87025 Limoges, France

³ INSERM U1021, Normal and Pathological Development of Melanocytes, Institut Curie, PSL Research University, Campus Universitaire, 91898 Orsay, France; jeremy.raymond@curie.fr (J.H.R.); veronique.delmas@curie.fr (V.D.); valerie.petit@curie.fr (V.P.); lionel.larue@curie.fr (L.L.)

⁴ Campus Universitaire, University Paris-Sud, University Paris-Saclay, CNRS UMR3347, 91898 Orsay, France

⁵ Equipes Labellisées-Ligue Contre le Cancer, Campus Universitaire, 91898 Orsay, France

⁶ Cirmen, Centre Jean Perrin, 58 rue Montalembert, 63000 Clermont-Ferrand, France; Tommy.BILLOUX@clermont.unicancer.fr

⁷ Department of Dermatology and Oncodermatology, CHU Estaing, 1 Place Aubrac, 63000 Clermont-Ferrand, France

⁸ CNRS 6293 INSERM U1103, University of Clermont Auvergne, 28, Place Henri Dunant, 63000 Clermont-Ferrand, France

* Correspondence: jrouanet@chu-clermontferrand.fr

† These authors contributed equally to this work.

‡ These authors contributed equally to this work.



Citation: Akil, H.; Quintana, M.; Raymond, J.H.; Billoux, T.; Benboubker, V.; Besse, S.; Auzeloux, P.; Delmas, V.; Petit, V.; Larue, L.; et al. Efficacy of Targeted Radionuclide Therapy Using [¹³¹I]ICF01012 in 3D Pigmented BRAF- and NRAS-Mutant Melanoma Models and In Vivo NRAS-Mutant Melanoma. *Cancers* **2021**, *13*, 1421. <https://doi.org/10.3390/cancers13061421>

Academic Editors: Tadashi Watabe, Frederik Lars Giesel and Elif Hindić

Received: 24 December 2020

Accepted: 16 March 2021

Published: 20 March 2021

Publisher's Note: MDPI stays neutral with regard to jurisdictional claims in published maps and institutional affiliations.



Copyright: © 2021 by the authors. Licensee MDPI, Basel, Switzerland. This article is an open access article distributed under the terms and conditions of the Creative Commons Attribution (CC BY) license (<https://creativecommons.org/licenses/by/4.0/>).

Simple Summary: Targeted radionuclide therapy (TRT) aims to selectively deliver radioactive molecules to tumor cells. For this purpose, we deliver iodine-131 ([¹³¹I]) to melanoma cells by using our laboratory-developed melanin specific radiotracer, the ICF01012. Approximately 50% and 20%–30% of human melanomas have activating mutation in BRAF or NRAS genes, respectively. These mutations lead to a constitutive activation of the MAPK/ERK pathway, which is known to be involved in tumor cells' radioresistance. In this work, we showed using 3D in vitro tumor models, an additive efficiency of combining [¹³¹I]ICF01012-TRT and MAPK/ERK inhibitors in BRAF- and NRAS-mutant melanoma cells. In mice bearing NRAS^{Q61K}-mutated melanoma, TRT induced an impressive decrease in tumor growth, as well as a highly extended survival. Additionally, we showed that TRT reduces the metastatic capacity of melanoma, especially through lymph-node dissemination. These results are therefore of great interest, especially for patients with NRAS-mutant metastatic melanoma who currently lack specific efficient therapies.

Abstract: Purpose: To assess the efficiency of targeted radionuclide therapy (TRT), alone or in combination with MEK inhibitors (MEKi), in melanomas harboring constitutive MAPK/ERK activation responsible for tumor radioresistance. Methods: For TRT, we used a melanin radiotracer ([¹³¹I]ICF01012) currently in phase 1 clinical trial (NCT03784625). TRT alone or combined with MEKi was evaluated in three-dimensional melanoma spheroid models of human BRAF^{V600E} SK-MEL-3, murine NRAS^{Q61K} 1007, and WT B16F10 melanomas. TRT in vivo biodistribution, dosimetry, efficiency, and molecular mechanisms were studied using the C57BL/6J-NRAS^{Q61K} 1007 syngeneic model. Results: TRT cooperated with MEKi to increase apoptosis in both BRAF- and NRAS-mutant spheroids. NRAS^{Q61K} spheroids were highly radiosensitive towards [¹³¹I]ICF01012-TRT. In mice bearing NRAS^{Q61K} 1007 melanoma, [¹³¹I]ICF01012 induced a significant extended survival (92 vs. 44 days, $p < 0.0001$), associated with a 93-Gy tumor deposit, and reduced lymph-node

metastases. Comparative transcriptomic analyses confirmed a decrease in mitosis, proliferation, and metastasis signatures in TRT-treated vs. control tumors and suggest that TRT acts through an increase in oxidation and inflammation and P53 activation. Conclusion: Our data suggest that [¹³¹I]ICF01012-TRT and MEKi combination could be of benefit for advanced pigmented BRAF-mutant melanoma care and that [¹³¹I]ICF01012 alone could constitute a new potential NRAS-mutant melanoma treatment.

Keywords: targeted radionuclide therapy; MEK inhibitors; BRAF mutation; NRAS mutation; melanoma spheroid model

1. Introduction

Cutaneous malignant melanoma is one of the most lethal forms of skin cancer. It develops from epidermal melanocytes responsible for melanin synthesis [1]. These pigments protect melanocytes and neighboring keratinocytes from deoxyribonucleic acid (DNA) double-strand breaks by forming a shield that absorbs reactive oxygen species (ROS) induced by ultraviolet (UV) radiation. The main signaling pathway involved in melanoma-genes is that of mitogen-activated protein kinases (MAPK), along with the associated *Rat sarcoma* GTPase (RAS)/*rapidly accelerated fibrosarcoma* protein(RAF)/mitogen-activated extracellular signal-regulated kinase kinase (MEK)/*extracellular signal-related kinase* (ERK proteins) [1,2]. Somatic mutations in genes encoding protein actors of this phosphorylation cascade constitutively activate the MAPK pathway: mutations in *BRAF*, neurofibromin 1 (*NF1*), *NRAS*, and *c-KIT* are the most frequent, representing 50, 20, 20, and 2% of melanomas, respectively [3]. Most (70 to 90%) mutations in *BRAF* lead to the substitution of valine by glutamic acid at position 600 in *BRAF* (V600E). Mutations in *NRAS* gene occur in 20–30% of melanomas, at codon 61 for ≈90% of the cases, resulting in a change in amino acid Q61K (45%) and Q61R (35%) while Q61L and Q61H modifications were lower (20%). Other genetic alterations in *NRAS* gene G12R/D/A/V occurred at a low rate (≈10%) [3,4].

Based on these molecular characteristics of the melanoma, specific *BRAF* (V600E) ATP-competitive inhibitors, such as vemurafenib [5] or dabrafenib [6] have been developed and have shown remarkable clinical efficacy in *BRAF*(V600E) melanoma tumors. Despite the initial positive effects on melanoma progression, these selective inhibitors often lead to the development of rapid neo/acquired resistance, resulting in either reactivation of the MAPK signaling pathway or activation of PI3K signaling pathway [2,7,8], usually within 6 to 8 months of treatment [9]. Several mechanisms involved in resistance to *BRAF* inhibitors have been identified and a number of strategies combining them with MEK inhibitors have been tested in multiple phase 3 trials. For example, the COMBI-d and COMBI-v trials studied the efficiency of combining dabrafenib with a MEK inhibitor, trametinib, compared to dabrafenib or vemurafenib alone [9]. Five-year pooled analyses [10] showed that this combination leads to a progression free survival (PFS) rate of 19%, with a median PFS of 11.1 months, and an overall survival (OS) rate of 34%, with median OS of 25.9 months. For patients receiving only dabrafenib or vemurafenib, the 5-year PFS rate was 13% and 9%, respectively; the 5-year OS rate was 27% and 23%, respectively, confirming the long-term interest of combining *BRAF* and MEK inhibitors. The phase 3 coBRIM [11] trial compared vemurafenib and cobimetinib vs. placebo and vemurafenib and obtained a median PFS of 12.6 months for the combination vs. 7.2 months for vemurafenib alone. The overall response rate (ORR) was 70% vs. 50% and median OS was 22.5 vs. 17.4 months. The most recent trial [12,13] (COLUMBUS) assessed the combination of binimetinib (MEK inhibitor) with encorafenib (*BRAF* inhibitor). This study showed the best efficiency for a *BRAF*/MEK combination versus vemurafenib alone and a very low number of adverse events, such as photosensitivity or fever. The combination showed an ORR of 64% and median PFS of 14.9 vs. 7.3 and 9.6 months for vemurafenib and encorafenib, respectively [13]. OS was 33.6 months for the combination vs. 16.9 months

for vemurafenib ($p \leq 0.0001$) [13]. Moreover, the number of secondary cutaneous cancers was lower with combination therapy in both trials. These significant clinical benefits have made combined BRAF and MEK inhibitors the new standard for advanced and metastatic V600E BRAF-mutated melanoma treatment. There are no clinically approved inhibitors for NRAS mutant melanomas. Initial clinical trials have tested farnesyl transferase inhibitors (FTIs), which block the lipid post-translational modification of RAS required for its activity. One such FTI (tipifarnib) was clinically tested but showed no significant clinical benefit [14]. The NRAS inhibitor salirasib, which modifies RAS-GTP binding to cell membranes by competition, has not been assessed in a clinical trial for melanoma [15]. MEK inhibitors have been tested in preclinical and clinical studies with promising results. However, the phase 3 NEMO trial, which compared binimetinib to dacarbazine, failed to show a benefit on OS (11 vs. 10 months, hazard ratio (HR) 1.00 (95% CI (0.75–1.33)); one-sided $p = 0.50$) although there was an extension of PFS (2.8 vs. 1.5 months, HR 0.62 (95% CI [0.47–0.80]); one-sided $p < 0.001$) [16]. Recruiting has been halted due to poor results. Thus, immune checkpoint inhibitors [9] are currently the sole treatment available for patients with NRAS melanoma.

Targeted radionuclide therapy (TRT) consists in delivering radiopharmaceuticals to tumor cells by targeting specific characteristics [17]. [^{131}I]ICF01012 is a melanin-targeting compound that has already shown its efficiency by reducing tumor growth and enhancing survival in various syngeneic and xenograft pigmented melanoma models with wild-type or mutant BRAF [18–21], whereas injection of [^{131}I] alone or of non-labeled ICF01012 in mice bearing B16 melanomas did not modify mice survival and tumor growth [21]. In addition, biodistribution studies and secondary ion mass spectrometry (SIMS) technique have confirmed a specific accumulation of [^{131}I]ICF01012 in pigmented tissues/cells and in acidic organelles [18–23]. [^{131}I]ICF01012 can also reduce melanoma metastases, mainly by modifying pseudo-epithelial-mesenchymal transition mechanisms, in vitro and in vivo, in murine and human melanoma cell lines [24]. We have also shown that TRT using [^{131}I]ICF01012 induces first a decrease and then an insignificant increase in ERK phosphorylation [18], suggesting a mechanism of radioresistance through activation of the MAPK pathway.

The association of targeted therapies and radiation has already shown positive results in preclinical [25,26] and clinical studies [27]. Indeed, BRAF and MEK inhibitors have been shown to increase melanoma-cell radiosensitivity [25]. Hecht et al. have confirmed that combined radiotherapy and administration of BRAF inhibitors is tolerable, with an acceptable increase in toxicity [27]. We developed a three-dimensional (3D) melanoma spheroid approach for in vitro studies of TRT to mimic tumor architecture and better model the consequences of irradiation [24]. Here, we investigated the effect of combining MEK inhibitors with [^{131}I]ICF01012-TRT in an in vitro 3D spheroid model. We further studied the efficiency of [^{131}I]ICF01012-TRT in vivo using the syngenic NRAS^{Q61K} 1007-mutant melanoma allograft model corresponding to the human NRAS^{Q61K} mutation [28].

2. Materials and Methods

2.1. Cell Lines, Culture Conditions and Spheroid Collection

Human SK-MEL-3 and murine B16F10 melanoma cell lines were purchased from the American Type Culture Collection (ATCC). SK-MEL-3 cells were maintained as monolayer using culture medium consisting of McCoy's 5A medium (Invitrogen, Cergy Pontoise, France) supplemented with 15% fetal calf serum (FCS) (Eurobio, Les Ulis, France), and $4 \mu\text{g } \mu\text{L}^{-1}$ gentamycin (Invitrogen) at 37°C in a humidified incubator containing 5% CO_2 . B16F10 cells were maintained as monolayer using culture medium consisting of DMEM-Glutamax medium (Invitrogen) supplemented with 10% FCS (Eurobio), and $4 \mu\text{g } \mu\text{L}^{-1}$ gentamycin (Invitrogen) at 37°C in a humidified incubator containing 5% CO_2 . The NRAS^{Q61K} 1007 (also named NRAS 1007) murine cell line was cultured as previously described [28]. Melanoma spheroids were generated as previously described [24].

Spheroids were harvested between 1 and 72 h post- ^{131}I ICF01012 removal, frozen in N_2 , and stored at -80°C during the radioactive decay (80 days; 10 times the half-life of the iodine-131 isotope) for Western blot analysis or fixed in 70% ethanol for cell-cycle studies.

2.2. ^{131}I ICF01012 TRT and MEK Inhibitor Treatment of Spheroids

^{131}I iodine was purchased from Perkin Elmer (Waltham, MA, USA) or Izotop (Budapest, Hungary). Radiolabeling of ICF01012 was performed as previously described [23]. For the ^{131}I ICF01012 alone experiments, each spheroid was irradiated at day 6 of culture with 37 kBq of ^{131}I ICF01012/100 μL of cell culture medium (without FCS). The addition of medium alone was used as a control. After 1 h of incubation, the irradiation medium was removed and replaced by complete medium supplemented with 0.5% methylcellulose. For the ^{131}I ICF01012 and MEK inhibitors (MEKi) combinations, each spheroid was pre-treated for 2 h with cobimetinib (GDC-0973) (Selleckchem (Houston, TX, USA), 100 nM, SK-MEL-3 spheroids), GDC-0623 (Selleckchem, 50 nM, B16F10, and NRAS 1007 spheroids), or dimethyl sulfoxide (DMSO) (control and ^{131}I ICF01012 alone groups) on day 6 of culture. Then, each spheroid was irradiated according to the above-mentioned protocol with cell culture medium containing the corresponding MEKi (MEKi alone or TRT + MEKi groups) or DMSO (control DMSO or TRT alone groups). Spheroids were then incubated from 1 to 72 h.

2.3. Colony Formation Assay

Twenty-four hours after irradiation in combination with MEKi (as described above for the combination ^{131}I ICF01012 and MEKi), 60 spheroids/condition were collected and centrifuged (50 g, 5 min). Supernatants were removed and spheroids were dissociated with 500 μL collagenase IV (0.2%; Sigma Aldrich, Saint-Quentin Fallavier, France) during 30 min at 37°C . Cells were re-suspended, counted, and seeded in 6 well plates with a 2 mL final volume of complete culture medium containing the corresponding MEKi (TRT + MEKi and MEKi groups) or DMSO (TRT and control groups). SK-MEL3 cells were seeded at 7200 cells/well, NRAS 1007 at 5000 cells/well, and B16F10 at 400 cells/well. After 3 days of incubation, culture medium was removed and replaced by complete culture medium without DMSO or MEKi. After 18 days of incubation for SK-MEL3, 15 days for NRAS 1007, and 8 days for B16F10 cells, medium was removed and colonies were rinsed once with PBS. Colonies were then fixed by methanol absolute during 3 min then revealed with 0.5% crystal violet aqueous solution. The counting of colonies was realized using the ImageJ software. Plating efficiency (PE) and survival fraction (SF) were determined as described [29].

2.4. Apoptosis Assay

Apoptosis was measured by the detection of cytoplasmic soluble nucleosomes using a colorimetric assay, Cell Death Detection ELISAPLUS (Sigma Aldrich) according to the manufacturer's instructions. Absorbance was measured at 405–490 nm dual wavelengths.

2.5. Cell Cycle Analysis

Spheroids were dissociated with collagenase IV (0.2%; Sigma Aldrich) during 30 min at 37°C . Cells were then fixed in 70% ethanol and stored at -20°C . After complete radioactive decay, cells were washed twice with PBS then 50 μL of Ribonuclease A (100 $\mu\text{g mL}^{-1}$; Sigma-Aldrich) and 450 μL of propidium iodide (50 $\mu\text{g mL}^{-1}$; Sigma-Aldrich) were added. After 15 min of incubation in the dark at room temperature, cell cycle was analyzed using a flow cytometer (BD Accuri C6 Plus, BD Biosciences, Le Pont de Claix, France).

2.6. Western Blotting

Western blot analysis was carried out as previously described [30]. The following primary antibodies (Abs) were used: anti-phospho-H2A.X (S139) (1/2000), anti-H2A.X (1/1000), anti-phospho-ERK1/2 (Thr202/Tyr204) (1/2000), anti-ERK1/2 (1/2000), anti-

phospho-MEK1/2 (Ser217/221) (1/2000), and anti-MEK1/2 (1/2000) from Cell Signaling Technology (Danvers, MA, USA), and anti-PARP-1 (1/200; Santa Cruz Biotechnology, (Dallas, TX, USA)) and anti-Actin (1/10,000; Sigma-Aldrich). The following secondary Abs were used: anti-rabbit-HRP (1/5000) and anti-mouse-HRP (1/5000 and 1/10,000 for actin) from SouthernBiotech (Nanterre, France). The Western blots were scanned using ChemiDoc imaging system (Bio-Rad, Marnes-la-Coquette, France). The densitometric analyses were performed using an *ImageJ* software (National Institutes of Health, Bethesda, MD, USA) (accessed on 11 November 2020).

2.7. Murine Models

This investigation conformed to the Guide for the Care and Use of Laboratory Animals published by the US National Institutes of Health (8th edition, 2011). All experiments were conducted in accordance with the relevant guidelines and regulations and approved by both the local ethics committee of Clermont-Ferrand (C2E2A n°002) and the French Ministry of Education and Research (approval n°12211-2017111613576925). NRAS 1007 melanoma cells (1×10^5) in 100 μ L of saline solution were injected subcutaneously in the right flank of five-week-old C57BL/6J male mice purchased from Charles River Laboratories (Ecully, France). Three different in vivo experiment using [131 I]ICF01012 were realized: a biodistribution and dosimetry study using 3 animals per time (n = 15), a survival study (n = 28), and a mechanistic study (n = 15) including single-photon emission computed tomography (SPECT-CT) imaging, melanin quantification, lymph nodes, and transcriptomic analyses.

2.8. Biodistribution Study

Thirty-six days following tumor implantation, 15 mice received an intra-venous (i.v.) injection of 0.37 MBq [131 I]ICF01012. Three mice were sacrificed per timepoint (1, 3, 6, 24, and 72 h) prior to removing and weighing the organs and tumors. Their radioactivity was analyzed using a γ -counter (Wizard 1480, Perkin Elmer) and the gamma counting data were corrected for physical decay and background. The percentage of injected activity in tumors was determined by the ratio of counted activity per organ divided by the organ weight (% IA/g).

2.9. Dosimetry

The dose was assessed from organ activity measured at each timepoint (1, 3, 6, 24, and 72 h, n = 3 per timepoint).

The percentage of injected activity curves $\%IA(t) = \frac{Activity(t)}{weight \cdot Activity_{injected}}$ were calculated for each organ. Curves were adjusted using MatLab software (TheMathWorks, Natick, MA, USA): tumor: $y = a(1 - \exp^{-bt})\exp^{-ct}$; eyes: $y = a(1 - \exp^{-bt})\exp^{-\lambda_{physique}t}$ with $\lambda_{physique} = \frac{\ln 2}{T_{physique}(h)}$; other organs (bi-exponential): $y = a.\exp^{-bt} + c.\exp^{-dt}$.

The MatLab adjustment parameters were: Method: NonlinearLeastSquare; Robust: Bisquare; Algorithm: Trust-Region. Cumulative activity confidence intervals were assessed by bootstrapping (adjustment with a 153-fit simulation and the leave-one-and-two-out method) and 95% CI, with the 2.5 and 97.5 percentiles. Mouse and human doses were calculated with MIRD21 formalism, using S factors from Perrot et al. [31] for mice and Olinda factors and organ weights for humans [32].

2.10. [131 I]ICF01012 Treatment

C57BL/6J mice were injected intravenously with either 18.5 MBq/100 μ L of [131 I]ICF01012 (TRT groups) or 100 μ L saline (control groups) 36 days after tumor implantation. Mice were sacrificed before the tumor volume reached 1500 mm³ for survival study or 10 days after TRT injection for mechanistic analyses (including SPECT-CT imaging, melanin quantification, lymph nodes and transcriptomic analyses). Mice were homogeneously randomized between control and treated groups according to mice weight and tumor size, seven days

after cells injection (survival study: TRT: n = 14, control: n = 14; mechanistic study: TRT: n = 8, control: n = 10).

Body weight and tumor volume were measured three times a week until tumor volume reached 1000 mm³ and then, daily (For mice weight and tumor volume at start of experiment and endpoint for survival and mechanical studies, see Supplementary Table S1). Potential toxicities were evaluated daily with a scoring grid, exploring general condition, behavior changes, and skin toxicities. Mice were sacrificed when tumor volume reached approximately 1500 mm³ or at experiment time.

Tumor volume was calculated from the measurement of two perpendicular diameters using a caliper according to the formula $L \times S^2/2$, where L and S are the largest and smallest diameters, respectively, expressed in millimeters.

The doubling time was calculated individually for each animal. Tumor growth has an exponential function ($N = N_0 \cdot e^{at}$), the doubling time (DT) is calculated using the formula $DT = \ln 2/a$, where “N” represents the volume of the tumor, “N₀” represents the volume of the tumor at time 0, “a” represents the slope of the exponential phase, and “t” the time (in days).

2.11. SPECT-CT Imaging

Multimodal SPECT-CT imaging was performed using a NanoScan SPECT/CT camera (Mediso Ltd., Budapest, Hungary) equipped with four detectors and multi pinhole collimation (APT62). Mice were placed in a Multicell Mouse L bed (Mediso Ltd.) with temperature control (37 °C). SPECT-CT imaging was performed on representative mice (n = 2 at 1 h and 6 h and n = 5 at 24 h, 72 h, and 168 h) of each group at different time points (i.e., 1 h, 6 h, 24 h, 72 h and 168 h) after the injections of [¹³¹I]ICF01012. Nucline software (Mediso Ltd.) was used for image acquisitions and reconstructions (Nucline 3.00.018). CT parameters were as follows: helical scan with 480 projections (300 ms per projection), 50 kV, 590 uA, pitch 1.0, binning 1:4, and field of view: max. SPECT images were acquired within the CT scan range, with a standard resolution. The time per projection was determined in accordance to the detected radioactivity (most frequently used: 30 s). SPECT image reconstruction was conducted using TeraTomo3D (Nucline v3.00.018) with high dynamic range. Regularization filters, reconstruction resolution and iterations were set to “medium”. Additional corrections were performed during reconstruction: Monte Carlo correction quality was set to “high”; attenuation: based on CT attenuation map and scatter corrections; activity decay correction: during acquisition time lapse.

2.12. Melanin Determination

For melanin assays, tumors were excised 10 days after [¹³¹I]ICF01012 irradiation, frozen in N₂, and stored at −80 °C for radioactive decay (80 days; 10 times the half-life of the iodine-131 isotope). Eumelanin and pheomelanin analyses were performed as previously described [33].

2.13. RT-qPCR Analyses

Inguinal and axillar lymph nodes (LNs) were collected 10 days after [¹³¹I]ICF01012 irradiation, frozen in N₂, and stored at −80 °C. After complete radioactive decay, ribonucleic acid (RNA) was extracted (RNA Extraction Kit, Macherey Nagel) and the amounts measured by spectrophotometry (MultiskanGo, ThermoFisher, FisherScientific, Illkirch, France). Complementary DNA (cDNA) was synthesized from 250 ng RNA using the ThermoScript kit (ThermoFisher). Quantitative PCR (qPCR) reactions were performed in triplicate with Master Mix SybrGreen using an Applied BioSystems StepOne Plus device. Primers and annealing conditions are described in Supplementary Table S2. Results are expressed according to the $\Delta\Delta CT$ method after normalization against the glyceraldehyde 3-phosphate dehydrogenase (GAPDH) housekeeping gene.

2.14. Transcriptomic Analysis

According to Petit et al. [28], RNA from mouse melanomas (Control: $n = 6$, TRT: $n = 6$) was extracted using the miRNeasy Kit (Qiagen, Courtaboeuf, France, #217004). RNA integrity was assessed using an Agilent BioAnalyser 2100 (Agilent Technologies, Les Ulis, France), only RNA with a RNA integrity number (RIN) > 7 were kept for the analysis. This threshold led to the sequencing of 6 controls and 3 treated tumors. RNA concentrations were measured using a NanoDrop (NanoDrop Technologies, Wilmington, DA, USA). RNA sequencing libraries were prepared from 1 μg of total RNA using the Illumina TruSeq Stranded mRNA Library preparation kit that allows to perform a strand specific sequencing. A first step of polyA selection using magnetic beads is done to focus sequencing on polyadenylated transcripts. After fragmentation, cDNA synthesis was performed and resulting fragments were used for dA-tailing followed by ligation of TruSeq indexed adapters. PCR amplification was finally achieved to generate the final barecoded cDNA libraries (12 amplification cycles). The 9 libraries were equimolarly pooled and subjected to qPCR quantification using the KAPA library quantification kit (Roche). Sequencing was carried out on the NovaSeq 6000 instrument from Illumina based on a 2×100 cycles mode (paired-end reads, 100 bases) using an S1 flow cell in order to obtain around 35 million clusters (70 million raw paired-end reads) per sample. Reads were mapped to the mouse reference genome (gencode m13 version-GRCm38.p5) using STAR [34]. STAR was also used to determine the expression matrix. Expression matrix was first filtered by expression level to keep only sufficiently expressed genes using the edgeR package [35]. Principal component analysis (PCA) was performed using FactomineR [36]. 3D PCA animated gif was made with the help of the pca3d package (<https://cran.r-project.org/web/packages/pca3d/index.html>) (accessed on June 2020). The significance of the clustering was evaluated using PERMANNOVA. The deconvolution was conducted using the R-package mcp-counter [37]. To the gene set distributed with the package have been added two gene sets containing genes respectively specific of melanocytes (*Mitf*, *Pax3*, *Mc1r*, *Rxrg*, and *Tspan10*) and of keratinocytes (*Flg*, *Krt1*, *Dsc1*, *Sprr1b*, and *Krt14*) in the skin. Differential gene expression was performed with R following the limma-voom pipeline using the limma package [38]. edgeR and limma packages are both available from Bioconductor (<http://www.bioconductor.org>) (accessed on June 2020). The threshold for significantly differentially expressed genes was set as an absolute fold-change $>$ two times the standard deviation of the fold-change and an adjusted p -value < 0.05 . The volcano plot depicting the results was generated using the R package ggplot2 [39]. The interactive volcano plot was made with the plotly R package [40]. Gene-ontology and enriched pathway analysis were performed using Enrichr [41] on genes found overexpressed by the differential analysis either in the TRT-treated tumors or in the control tumors (also designed as CTRL-treated tumors). Gene-set enrichment analysis (GSEA) was performed using three collections from the Molecular Signatures Database (MSigDB v7.2): H (Hallmark), C2 (curated gene sets), and C5 (ontology gene sets), and a gene set describing the different sub-population in melanoma [42]. One thousand permutations gene set-based were made per analysis. The enrichment score (ES) reflects the degree to which a given gene set is represented in a ranked list of genes. Calculation of the ES is based on walking down a ranked list of genes and adjusting a running-sum statistic based on the presence of absence of a gene in the gene set. The magnitude of the increment represents the correlation of the gene with the phenotype. p -values were estimated by gene-based permutation. GSEA normalizes the enrichment score for each gene set to account for the variation in set sizes, yielding a normalized enrichment score (NES). Only gene sets with an NES > 2 and an FDR < 0.01 were considered.

2.15. Statistical Analyses

Statistical analyses were performed with GraphPad (Addinsoft, New York, NY, USA) and StatView (Abacus concepts, Southfield, MI, USA) software using Log-rank for survival analyses, Student's t tests for animal experiments, and two-way analysis of variance

(ANOVA) associated with post-hoc Tukey's multiple comparison test for in vitro experiments. A p -value < 0.05 was considered to represent statistically significant differences.

3. Results

3.1. MEKi Radio-Sensitizes BRAF- and NRAS-Mutant Melanoma Spheroids for [¹³¹I]ICF01012 by Increasing Apoptosis

We first defined a 100-nM dose of cobimetinib to treat human melanoma SK-MEL-3 spheroids and a 50-nM dose of GDC-0623 for both the NRAS 1007 and B16F10 murine melanoma spheroids (Supplementary Figure S1). We further assessed the efficiency of combining TRT with MEKi using apoptosis assay. We showed that combining TRT with MEKi increased the apoptotic ratio of SK-MEL-3 spheroids by nearly 2-fold at 4 hours (h) post-irradiation and 22-fold at 24 h relative to either treatment alone: DMSO ($p = 10^{-4}$), MEKi ($p = 5 \times 10^{-4}$), or TRT ($p = 5 \times 10^{-4}$) (Figure 1A). These results also showed a supra-additive mechanism. This effect was confirmed by Western blot analysis of cleaved poly (ADP-ribose) polymerase 1 (PARP-1) protein expression (Figure 1B). At 24 h post-irradiation, apoptotic ratio of NRAS 1007 spheroids (Figure 1A) treated with TRT + MEKi was nearly 15-fold higher than those treated with DMSO ($p < 0.0001$), MEKi alone ($p < 10^{-4}$), or TRT alone ($p < 10^{-4}$). Cleaved PARP-1 analysis also showed such radiosensitization, with increased levels of cleaved PARP-1 protein expression at 4 and 24 h post-irradiation (Figure 1B). These results highlight the high radiosensitivity of NRAS 1007 spheroids to TRT, which can be enhanced using MEKi. Consistent with our previous findings [18], a small percentage of B16F10 cells entered into apoptosis following TRT. As expected, MEKi did not induce significant apoptosis in these wild-type BRAF/NRAS spheroids (Figure 1A). These results were also confirmed by Western blot analysis, showing the absence of PARP-1 cleavage induction (Figure 1B).

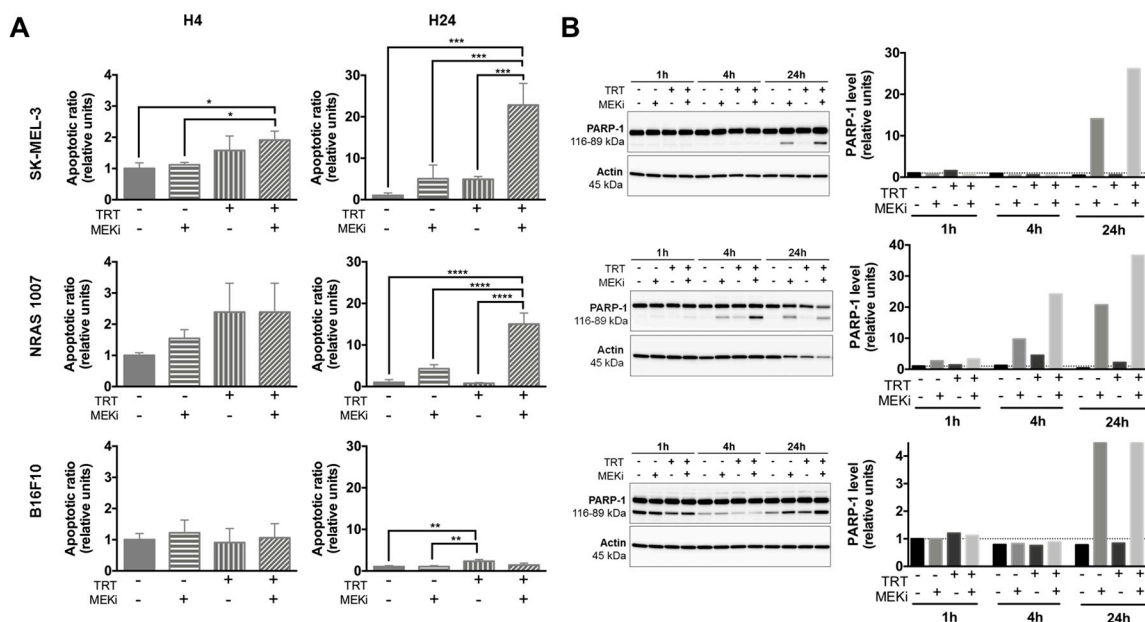


Figure 1. Apoptosis assays ($n = 3$) on melanoma spheroids after treatment with [¹³¹I]ICF01012-targeted radionuclide therapy (TRT), MEK inhibitors (MEKi), or both. Results are presented as mean \pm SD (A). (A) Apoptosis was assessed by quantification of soluble nucleosomes in cells using an ELISA cell death for SK-MEL-3, NRAS 1007, and B16F10. (B) Western blot analysis of cleaved PARP-1 in SK-MEL-3, NRAS 1007, and B16F10 spheroids treated with TRT, MEKi, or both. Actin was used as a protein-loading control. For Western blot, spheroids from 3 different experiments were pooled. For Western blot graphs, y-scales are not identical between cell lines. (* $p < 0.05$, ** $p < 0.01$, *** $p < 0.001$, **** $p < 0.0001$).

These data suggest that, except for B16F10 spheroids, MEKi and TRT can cooperate to increase apoptosis in melanoma cells with a constitutively activated MAPK pathway (SK-

MEL-3 and NRAS 1007). Nonetheless, we were not able to confirm this radiosensitization effect with clonogenic assays (Supplementary Figure S2). This could be explained by the selection of MEKi-resistant cells and/or the loss of apoptotic cells initiated after spheroid dissociation prior to cell seeding. However, it should be noted that NRAS 1007 spheroids demonstrated very high radiosensitivity to [¹³¹I]ICF01012, with the complete extinction of clonogenic survival for spheroids treated with TRT (compared to control: $p < 0.0001$, Supplementary Figure S2). The low apoptotic ratios with TRT are probably linked to the fact that TRT efficiency relies on mitotic catastrophe [18], characterized by a phase G2/M cell-cycle arrest. Cell-cycle arrest was indeed observed for SK-MEL-3 cells treated by TRT (Supplementary Figure S3), whereas a decrease in the S-phase was observed with MEKi treatment. The association of MEKi and TRT decreased the G2/M arrest due to fewer proliferating cells in S phase.

3.2. MEKi Inhibits [¹³¹I]ICF01012-Induced ERK1/2 Phosphorylation in BRAF- and NRAS-Mutant Melanoma Spheroid Models

We assessed the levels of constitutive and [¹³¹I]ICF01012-induced phosphorylated ERK1/2 (p-ERK) by Western blot analysis. All spheroids displayed high basal levels of p-ERK. For SK-MEL-3 and 1007 spheroids, such high basal p-ERK levels are likely due to BRAF and NRAS mutations. B16F10 spheroids are wild-type for BRAF and NRAS. Thus, the high basal level of p-ERK is most likely due to the 3D spheroid cell-culture model. Indeed, it has been described that cell-cell contacts and interactions between cells are enhanced by the 3D spatial organization of the cells, which influences the signal transduction pathways and biological functions [43]. This hypothesis was confirmed by comparing the basal p-ERK expression in B16F10 spheroids to that of cells grown in 2D monolayer culture system (Supplementary Figure S4). In addition, it has been shown that increased cell-cell contact or hypoxia could activate the MAPK pathway [44]. TRT treatment of SK-MEL-3 spheroids slightly increased the level of p-ERK protein at 4 h and then at 72 h post-irradiation (Figure 2A). However, treatment with MEKi resulted in complete and maintained inhibition of constitutive and TRT-induced p-ERK. Treatment of NRAS 1007 spheroids with TRT increased p-ERK expression at 24 h post-irradiation, whereas MEKi alone or combined with [¹³¹I]ICF01012 completely inhibited constitutive and TRT-induced p-ERK expression (Figure 2A). This increase of p-ERK at 24 h post-irradiation could be explained by the high radiosensitivity of NRAS 1007 cells growing in spheroids, which could lead to cell death and selection of resistant cells. TRT did not increase p-ERK levels in B16F10 spheroids, except for a slight increase at 24 h post-irradiation (Figure 2A).

3.3. MEKi Enhances the Radiosensitivity of BRAF- and NRAS-Mutant Melanoma Spheroids, Leading to Increased DNA Double-Strand Breaks

We investigated whether the radio-sensitizing effect of MEKi was also due to DNA damage by performing Western blot analysis of the phosphorylated form of H2A histone family member X (γ H2A.X) protein levels. The irradiation of SK-MEL-3 spheroids by [¹³¹I]ICF01012 induced an increase in the level of γ H2A.X Serine 139 (Ser139) protein, indicating an increase in DNA double-strand breaks from 1 to 48 h post-irradiation (Figure 2B). Combining MEKi with TRT induced an increase in the level of γ H2A.X(Ser139) after 24 (1.1-fold increase) and 48 h (1.1-fold increase) of irradiation relative to that with TRT alone. Treatment of SK-MEL-3 spheroids with MEKi alone also increased the level of γ H2A.X at 24 and 48 h post-treatment. This can be explained by the induction of apoptosis in these spheroids and confirms the results obtained with the apoptosis assay and Western blot analysis of the cleaved PARP-1 protein (Figure 1A,B). Combining MEKi and TRT enhanced the level of γ H2A.X(Ser139) in NRAS 1007 spheroids after 1 h of irradiation (0.8-fold increase) relative to TRT treatment alone and they remained higher up to 48 h post-irradiation (3.4-fold increase) (Figure 2C). In accordance with our previous data [24], [¹³¹I]ICF01012-TRT alone induced increased levels of γ H2A.X in B16F10 spheroids. However, combining MEKi with TRT failed to radio-sensitize BRAF and NRAS wild-type B16F10 spheroids (Figure 2B).

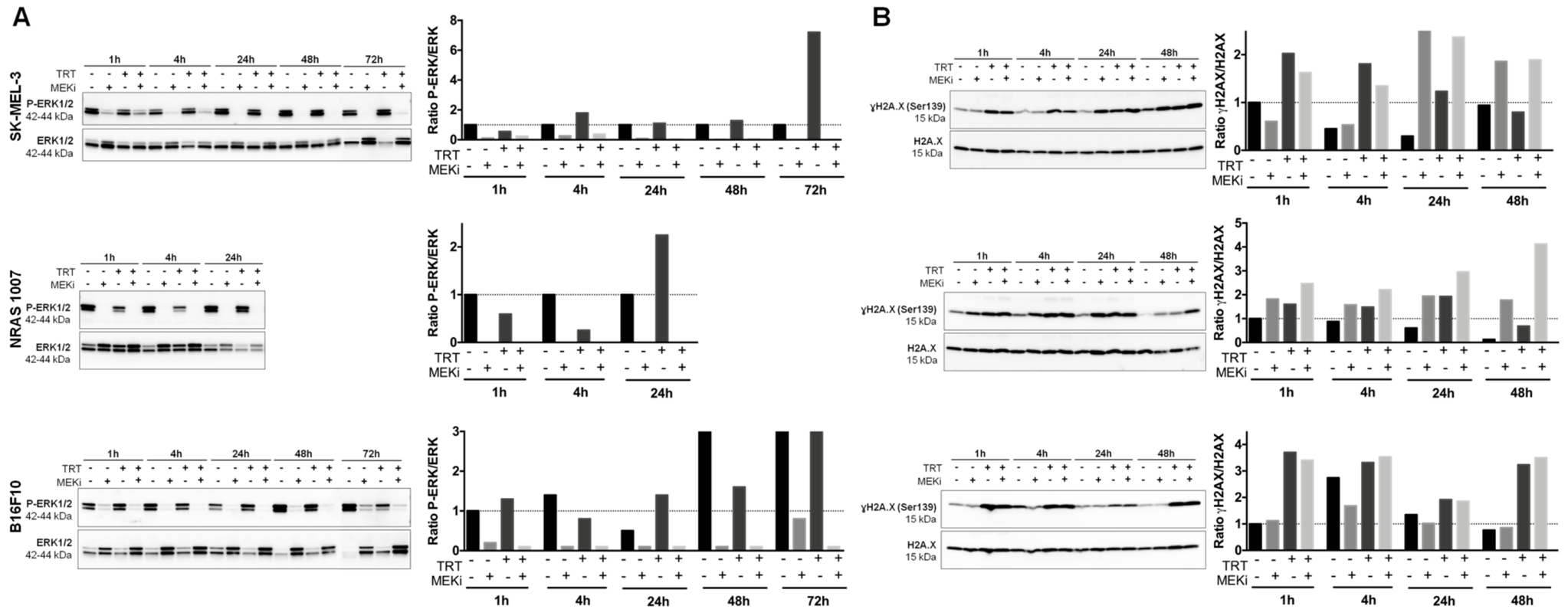


Figure 2. Quantification of p-ERK expression and analysis of DNA damage in melanoma spheroids following treatment with [¹³¹I]ICF01012-TRT, MEKi, or both. (A) Western blot analysis of P-ERK1/2 and ERK1/2 of total cellular protein extracted from SK-MEL-3, NRAS 1007, and B16F10 spheroids treated or not with TRT, MEKi, or both for the indicated times. The density of each P-ERK1/2 band was corrected using the density of the corresponding total ERK1/2 band. All values were normalized to the control (1 h). (B) The expression of phospho-H2A.X (γ H2A.X) and total H2A.X were analyzed by Western blotting for SK-MEL-3, NRAS 1007, and B16F10 spheroids treated or not with TRT, MEKi, or both for the indicated times. The density of each γ H2A.X band was corrected using the density of the corresponding total H2A.X band. For Western blot, spheroids from 3 different experiments were pooled. In graphs, y-scales are not identical between cell lines.

3.4. [¹³¹I]ICF01012 Accumulates in NRAS 1007 Tumors, with a Favorable Dosimetry for TRT

SPECT-CT imaging (Figure 3A) showed rapid and persistent accumulation of [¹³¹I]ICF01012 in tumors, which was maximal at 6 h post-injection. As expected, non-saturated thyroid showed intense fixation from 6 to 72 h post-injection. Specific [¹³¹I]ICF01012 fixation was observed in the eyes, which contain both types of melanin. One hour after injection, [¹³¹I]ICF01012 accumulated in the bladder and was completely eliminated after 24 h. The biodistribution in the tumor showed rapid and persistent accumulation of [¹³¹I]ICF01012 over 72 h (16.1% IA/g) (Figure 3B), which was maximal at 6 h post-injection (28.5% IA/g).

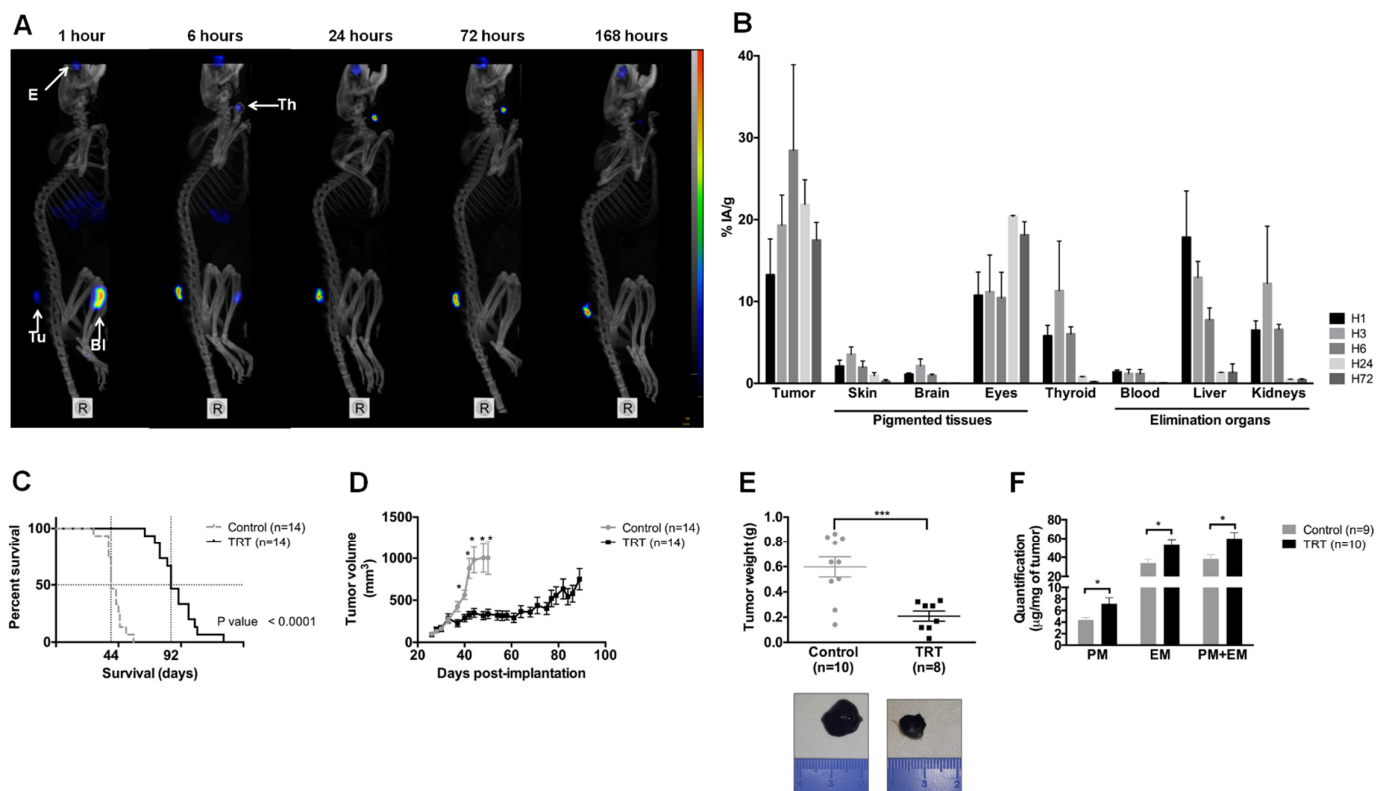


Figure 3. [¹³¹I]ICF01012 biodistribution and efficiency in an NRAS-mutant murine model. Results are presented as mean \pm SD (D,F) and as median, 1st quartile, and 3rd quartile (E). (A) Maximum intensity projection from SPECT-CT imaging of the same mouse from 1 h post-injection to 168 h shows tumor (Tu), eyes (E), thyroid (Th), and bladder (Bl) fixation of [¹³¹I]ICF01012. (B) Biodistribution of [¹³¹I]ICF01012, expressed as the percentage of injected activity/gram, was determined for each timepoint and each non-target organ by activity count ($n = 3$ mice per timepoint). (C,D) Survival curve (C) and tumor growth (D) were determined using 14 animals for each group. (E) Tumor weight for 10 control mice and eight TRT-treated mice, sacrificed 10 days after treatment, illustrated by 2 tumors representative of observed differences between control and TRT tumors. (F) Pheomelanin (PM) and eumelanin (EM) were quantified for nine control tumors and 10 TRT tumors. (* $p < 0.05$, *** $p < 0.001$).

We determined the absorbed dose for NRAS 1007 tumors and non-targeted organs from biodistribution studies (Figure 3B and Supplementary Table S3) after i.v. injection of 0.37 MBq [¹³¹I]ICF01012 and calculated the dosimetry for certain organs using S -values (Supplementary Table S4). The dose used for the therapeutic injection (18.5 Gy) showed high delivery of [¹³¹I]ICF01012 to the tumor (93.2 Gy) relative to the other organs. A low absorbed dose was deposited in excretion organs, such as the kidneys and liver (1.8 Gy and 4.3 Gy, respectively). The absorbed dose for the thyroid was very high (228.1 Gy), as potassium iodide was not used to block iodine absorption by the thyroid. As we used C57BL/6 mice, the dose delivered to the pigmented eyes was also very high (137.5 Gy), as expected.

An injected activity of 3.7 GBq is classically considered as a standard therapeutic dose in human iodine-TRT protocols. Based on this activity, [¹³¹I]ICF01012 dosimetry for humans extrapolated using Olinda S-values (Table 1) did not show toxic levels for the studied organs. Total body irradiation was evaluated to be 0.021 Gy.

Table 1. Extrapolated [¹³¹I]ICF01012 dosimetry for humans: absorbed dose (Gy/MBq) and dose (Gy) for 3.7 GBq extrapolated using Olinda S-values.

Organ/Tissue	Absorbed Dose (Gy·GBq ⁻¹)	Dose for 3.7 GBq (Gy)
Adrenals	0.006	0.023
Brain	0.007	0.025
Gall bladder	0.010	0.037
Lower large intestine	0.021	0.079
Small Intestine	0.048	0.176
Stomach	0.043	0.159
Upper large intestine	0.021	0.078
Heart	0.012	0.044
Kidneys	0.055	0.203
Liver	0.064	0.238
Lungs	0.028	0.105
Muscle	0.003	0.009
Ovaries	0.007	0.026
Pancreas	0.008	0.028
Red Marrow	0.003	0.010
Skin	0.001	0.004
Spleen	0.062	0.229
Testes	0.012	0.044
Thymus	0.002	0.007
Thyroid	0.044	0.163
Urinary Bladder	0.184	0.682
Total body	0.006	0.021

3.5. [¹³¹I]ICF01012 Induces Significant Tumor Regression and Extended Survival for Mice Bearing NRAS 1007 Tumors

[¹³¹I]ICF01012 significantly prolonged the survival of mice bearing NRAS mutant tumors relative to the control group (Figure 3C, median survival: 92 vs. 44 days, $p < 10^{-4}$). This was associated with slowed tumor growth from day 5 post-[¹³¹I]ICF01012 injection (Figure 3D). The doubling time of treated tumors was five-times longer than that of the control group (DT = 26.23 vs. 5.177 days⁻¹, $p < 10^{-4}$). Ten days post-[¹³¹I]ICF01012 treatment, the tumor weight was significantly lower in the treated group (Figure 3E, 0.208 vs. 0.598 g, $p = 7 \times 10^{-4}$). Consistent with our previous finding using SK-MEL-3 tumors [24], [¹³¹I]ICF01012-TRT induced a significant 1.5-fold increase of both pheomelanin (control: 4.39 vs. TRT: 7.19 µg/mg) and eumelanin (33.97 vs. 53.05 µg/mg) levels (Figure 3F). However, the proportion of pheomelanin (11.71% vs. 12.52%) and eumelanin (88.29% vs. 87.48%) positive tumors was similar for control and TRT-treated animals, respectively. Interestingly, we did not evidence significant loss of weight, alterations of general condition, vitiligo, or changes in behavior that could suggest any ocular toxicity.

3.6. [¹³¹I]ICF01012 Reduces Lymph-Node Metastases in the NRAS 1007 Model

We observed macroscopic melanin-pigmented LN metastases. [¹³¹I]ICF01012 treatment decreased the number of macroscopically invaded LNs in mice (Figure 4A,B: 0.875 vs. 1.70, $p = 0.0310$). Indeed, all mice presented at least one metastatic LN in the control group, whereas 37.5% of the mice in the TRT-treated group did not (Figure 4C). The proportion of mice with two invaded LNs was also higher in the control group (Figure 4C, 70% vs. 25%). Concerning the topography, 62% of inguinal and 25% of axillary right LNs were metastatic in the treated mice versus 90% and 80% in the control group, respec-

tively (Figure 4D, $p = 0.0306$). Assessment of the biodistribution and SPECT-CT imaging (Figure 4E,F) confirmed that [^{131}I]ICF01012 was present in the LNs. [^{131}I]ICF01012 uptake was significantly higher in metastatic LNs, which was maximal at 6 h post-[^{131}I]ICF01012 injection, corresponding to the highest uptake of the tumor and confirming the presence of melanin in the metastatic LNs. We assessed specific molecular melanoma markers by RT-qPCR analysis to assess the presence of melanoma cells in the LNs [45]. The expression of melanin biosynthesis-related genes, such as premelanosome gene (*pMel*), dopachrome tautomerase (*Trp2* (*Dct*)), and *tyrosinase* (*Tyr*) was significantly higher in metastatic LNs (Figure 4G) ($p = 0.0062$, $p = 0.0428$, $p = 0.0115$, respectively). The levels of mRNA corresponding to these genes in the metastatic LNs were similar between the TRT-treated and control groups. These results provide evidence for [^{131}I]ICF01012 uptake by metastatic LNs and its efficiency to reduce the spread of melanoma throughout the lymphatic system.

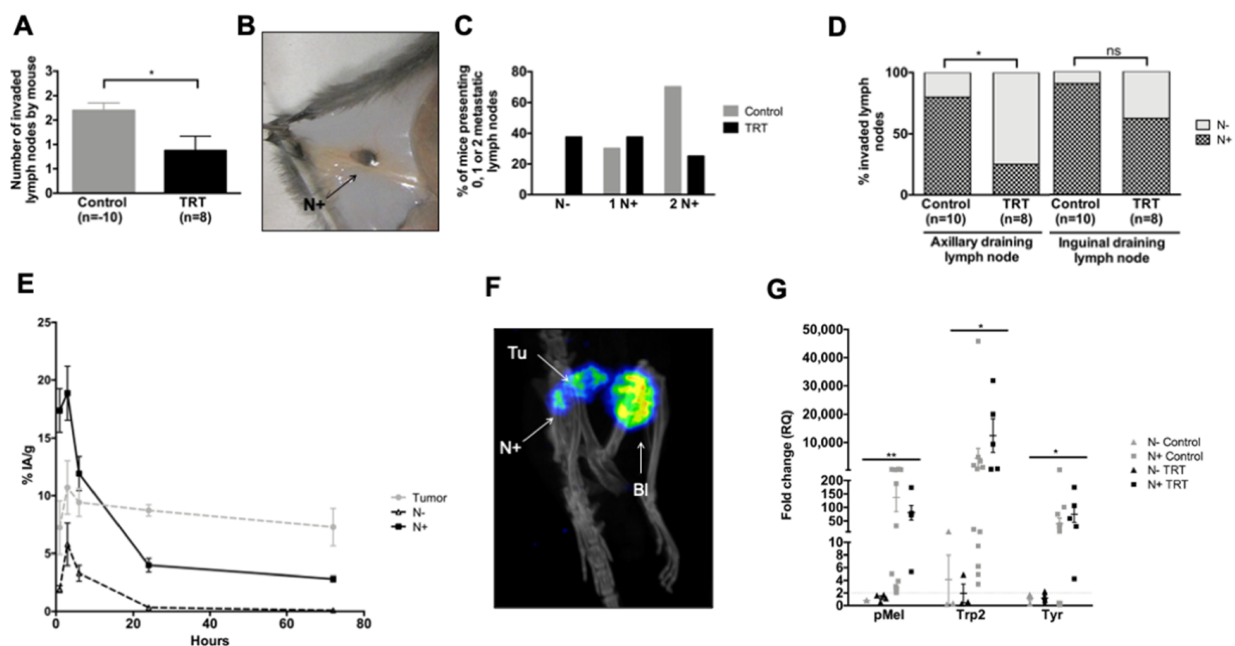


Figure 4. [^{131}I]ICF01012 decreases lymph-node dissemination. Results are presented as mean \pm SD (A,E) and as median, 1st quartile, and 3rd quartile (G). (A–E) The numbering and topographic location of metastatic LNs (N+) were determined for each mouse 10 days after treatment (10 control, 8 TRT): number of N+ per mouse (A), typical N+ (B), proportion of mice presenting 0 (N–), 1, or 2 N+ (C), repartition of invaded LNs (D). The radioactivity present in (T) tumors and (N+) (E) was determined during biodistribution studies on three mice per timepoint (1, 3, 6, 24, and 72 hours after injection): 24 LNs were macroscopically metastatic (N+) and 32 were non-metastatic (N–). (F) Visualization of an N+ by SPECT-CT imaging (T: tumor, N: lymph node, Bl: bladder). (G). *Trp2*, *pMel*, and *Tyr* gene expression in axillary and inguinal draining LNs was measured by RT-qPCR in 18 N+ (control group: $n = 13$ and TRT group: $n = 5$) and 7 N– (control group: $n = 3$ and TRT group: $n = 4$). LNs were considered to be metastatic when they showed a ≥ 2 -fold change for at least two genes. (* $p < 0.05$, ** $p < 0.01$).

3.7. [^{131}I]ICF01012 Modifies Oxidative Stress, Inflammatory, and P53 Signatures

We next performed transcriptomic analysis of TRT-treated and control tumors. First, deconvolution analyses showed the TRT-treated tumors to contain fewer melanocytes (Figure 5A) and more keratinocytes (Figure 5B) than control tumors, demonstrating the antitumoral activity of [^{131}I]ICF01012. Intriguingly, we observed a significant enrichment of dendritic cell-related genes in TRT-treated tumors relative to the control group (Figure 5C). These modifications were not present for other cell types, such as, for example, neutrophils, (Figure 5D and Supplementary Figure S5). Principal component analysis (PCA) showed that TRT-treated tumors form a significant cluster ($p = 0.014$) separate from the controls (Figure 5E) as PCA plots (Supplementary Video S1). We performed differential analysis to compare TRT-treated and control tumors. In total, 316 genes were upregulated and

331 downregulated in TRT-treated vs. control tumors with a fold-change > 2SD and an adjusted *p*-value < 0.05 (Figure 5F).

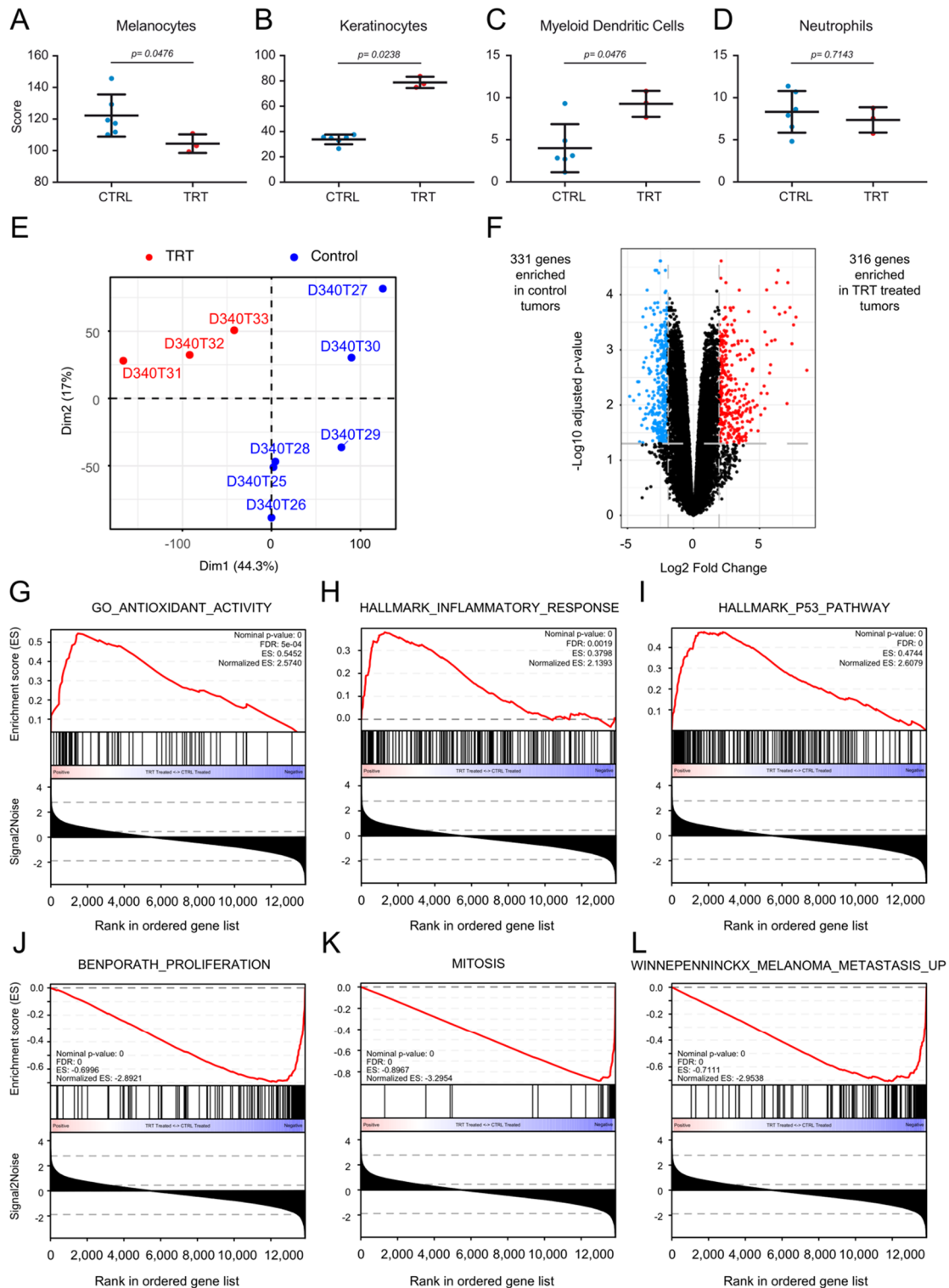


Figure 5. Bioinformatics analysis of treated and non-treated tumors. (A–D) Deconvolution results comparing the enrichment of various cell populations between six control-treated tumors and three TRT-treated tumors. Results for the three significantly enriched cell populations: melanocytes (A), keratinocytes (B), and myeloid dendritic cells (C) and one of the non-modified populations, (neutrophils) (D), are depicted. (E) Principal component analysis (PCA) showing a clear demarcation between TRT-treated tumors and mock-treated tumors. (F) Volcano-plot depicting the differential analysis results between TRT-treated tumors and control tumors. Differentially expressed genes were defined as genes with an adjusted

p -value < 0.05 and a fold-change > 2 SD of the fold change (<https://www.ncbi.nlm.nih.gov/geo/query/acc.cgi?acc=GSE162536>) (accessed on June 2020). In total, 316 genes were enriched in TRT-treated tumors vs. 331 in mock-treated tumors. An interactive volcano plot is presented in Supplementary Figure S6. (G–L) Gene-set enrichment results from gene-set enrichment analysis (GSEA). The gene sets enriched in TRT-treated tumors were related to antioxidant activity (G), an inflammatory response (H), and activation of the P53 pathway (I). The gene sets enriched in control tumors were related to proliferation (J), mitosis (K), and melanoma metastasis (L).

An interactive volcano plot is presented in Supplementary Figure S6. The differentially expressed genes are also listed in Supplementary Table S5. Pathway and ontology enrichment analysis by over-representation were conducted on the BioPlanet (BioPlanet 2019) and Gene Ontology (GO-Biological Pathways 2018) databases, respectively, using the 316 and 331 differentially expressed genes. The 331 genes enriched in the control tumors mapped to pathways and ontologies involved in the cell cycle, cell proliferation, and cell replication (Supplementary Figure S7A,B). Interestingly, the 316 genes significantly overexpressed in TRT-treated tumors mapped to pathways related to lipid and folate metabolism (Supplementary Figure S7C). The ontologies enriched in TRT-treated tumors were related to lipid metabolism and the presence of more keratinocytes in the samples (Supplementary Figure S7D). Gene-set enrichment analysis (GSEA) was conducted to document the mechanism of action of [131 I]ICF01012. The results suggest the involvement of oxidative stress pathways (Figure 5G) and inflammation (Figure 5H) and activation of the p53 signaling pathway (Figure 5I). The gene sets enriched in the control tumors reflected the effect observed during the follow-up of tumor growth in mice, with an enrichment of proliferation (Figure 5J) and mitosis (Figure 5K) signatures. A signature of metastatic melanoma was also significantly enriched in control tumors relative to TRT tumors (Figure 5L). These bioinformatics data indeed correlate perfectly with our *in vivo* observations.

4. Discussion

MAPK pathway activation has been shown to play a role in external beam radiation therapy (EBRT) radioresistance [46] but is still poorly documented in TRT. We have previously shown that [131 I]ICF01012 induces an initial decrease in p-ERK levels and then a non-significant increase in a B16BL6 model, suggesting potential radioresistance mechanisms [18]. Here, we evaluated the potential of combining TRT with an MEK inhibitor to overcome MAPK-mediated radioresistance in a panel of melanoma 3D spheroid models that mimic tumor architecture. We used the SK-MEL-3 (BRAF^{V600E}) and NRAS 1007 (NRAS^{Q61K}) cell lines, which exhibit a constitutively activated MAPK pathway, and the B16F10 cell line (wild-type BRAF/NRAS).

Here, we show that combining TRT with MEKi can overcome such activation by reducing ERK phosphorylation in BRAF- and NRAS-mutant melanoma. In addition, the inhibition of ERK phosphorylation significantly enhanced apoptosis in BRAF- and NRAS-mutant melanoma spheroids, but not the wild-type BRAF/NRAS spheroid model. However, combining MEKi with TRT did not modify the clonogenic capacity and subsequently the survival fraction of BRAF mutant spheroids. Such a residual survival fraction may indicate that the process selected a number of MEKi- and/or TRT-resistant cells. However, colony forming assay showed that [131 I]ICF01012-TRT alone was able to induce complete inhibition of the clonogenic survival capacity of NRAS 1007 cells, highlighting their high radiosensitivity. Furthermore, aside from the total melanin content being similar (Supplementary Figure S8B), [131 I]ICF01012 uptake by NRAS 1007 spheroids was significantly lower than that of B16F10 spheroids (Supplementary Figure S8A), reinforcing the hypothesis of the intrinsic radiosensitivity of these cells. Complementary studies on other NRAS mutant melanoma cell lines are required to show that such high TRT radiosensitivity is related to NRAS mutation, although previous EBRT studies have reported increased radiosensitivity *in vitro* [47] and *in vivo* [48] when NRAS is mutated. As expected, com-

binning MEKi with TRT had no effect on the clonogenic capacity or apoptosis of BRAF and NRAS wild-type B16F10 spheroids.

It has been shown that MEKi (trametinib)-induced EBRT radiosensitization is related to the acquisition of senescence and perturbation of the cell cycle, with a decrease in the proportion of cells in S phase and a blockade in the G1 phase [25]. However, no effect on apoptosis, delayed DNA damage repair, or mitotic catastrophe has been described. Our results demonstrate that combining MEKi with TRT induces a similar decrease in the proportion of cells in S phase in BRAF spheroids and an increase in DNA double-strand breaks in NRAS spheroids. However, we showed that combining MEKi with TRT induces a marked increase in apoptosis of BRAF- and NRAS-mutant melanoma cells, which could be specific to TRT irradiation or related to the spheroid 3D architecture. These results suggest that the addition of MEKi to TRT radio-sensitizes melanoma cells in our spheroid model by increasing DNA damage and apoptosis in BRAF- and NRAS-mutant cells. Although the spheroids mimic 3D tumor architecture, this model does not fully reflect the complexity of the tumor with neoangiogenesis and the active microenvironment (including cancer-associated fibroblast and the immune infiltrate), components that may impact the MAPK signaling pathway. The observed radio-sensitization in BRAF- and NRAS-mutant melanoma cells lines treated with TRT and MEKi combination will need, in the future, to be assessed by *in vivo* studies using human BRAF- and NRAS-mutant melanoma xenografts. The use of MAPK inhibitors to radio-sensitize tumors to TRT appears to be a promising strategy in BRAF- and NRAS-mutant melanoma, although the lack of an *in vivo* study to confirm the results is the main limitation of this work.

We used the syngeneic NRAS^{Q61K} 1007 model [28], which mimics the human NRAS-mutant model [49], to address the efficiency of [¹³¹I]ICF01012-TRT in this pigmented melanoma. NRAS^{Q61K} 1007 tumors clearly accumulate a sufficient amount of [¹³¹I]ICF01012 to improve the efficiency of TRT, with an absorbed dose in the supra-therapeutic range (94 Gy), as the curative dose for EBRT is 50 to 60 Gy. The extrapolated dosimetry to humans does not suggest major toxicity, as the absorbed doses of non-target organs remained within the recommended limits, as previously reported for extrapolated doses from a rabbit bio-distribution study [50]. The main concern with TRT using [¹³¹I]ICF01012 is potential ocular toxicity due to a high absorbed dose related to [¹³¹I]ICF01012 fixation on the melanin present in the choroid and retinal pigment epithelium. However, [¹³¹I]ICF01012 rabbit dosimetry extrapolated to humans has shown that the absorbed dose in the eyes remains acceptable [50]. Furthermore, the first clinical trial using a similar radiolabeled melanin-binding molecule showed clear clinical improvement for 2 of 5 patients with metastatic melanoma and did not report any ocular toxicity [51]. In the present NRAS-mutant melanoma model, [¹³¹I]ICF01012-TRT dramatically increased mouse survival and reduced tumor growth. These observations clearly have to be confirmed using other NRAS-mutant tumors. There are several possible explanations for such high radiosensitivity compared to our previous results on B16 tumors [18,20,21]. One is that the proportion of pheomelanin in NRAS mutant tumors (11.67% in the control tumors) is clearly higher than that in the B16BL6 tumor (1.61%) [33], which could considerably increase TRT-induced oxidative stress [52]. Previously, TLDA-analysis in B16BL6 tumors showed a significant increase in antioxidant enzyme expression (GPx1, heme oxygenase, SOD3) in treated tumors three days post-TRT [18]. This is fully supported by the present transcriptomic analysis, which emphasizes the increase in antioxidant gene expression in treated vs. control tumors. It could also be related to the enhancement of immunogenicity by radiation, as we already demonstrated for the B16F10 melanoma model [53], also consistent with the increased expression of inflammatory genes shown by transcriptomics. Additional studies need to be conducted to confirm that these pathways are involved in the NRAS^{Q61K} 1007 response to [¹³¹I]ICF01012-TRT, as modified lipid metabolism has already been reported to alter the efficiency of radioimmunotherapy [54]. In previous studies, we showed that TRT reduces hematogenous dissemination, especially lung invasion [21], by modifying pseudoepithelial-mesenchymal transition pEMT-mechanisms [24]. Here, we demonstrate, for the

first time, that [¹³¹I]ICF01012 penetrates the lymphatic system and limits LN metastases. Transcriptomic analyses also support the reduction of the metastatic capacity of melanoma by [¹³¹I]ICF01012-TRT.

5. Conclusions

In conclusion, this study reinforces the potential of [¹³¹I]ICF01012-TRT in the management of pigmented metastatic melanoma, especially its capacity to reduce metastatic dissemination. Future experiments that aim to clarify the mechanisms underpinning such high radiosensitivity to [¹³¹I]ICF01012-TRT will likely lead to a specific clinical trial including patients harboring NRAS metastatic melanoma, following the ongoing dose-escalation phase 1 study MELRIV1 (NCT03784625).

Supplementary Materials: The following are available online at <https://www.mdpi.com/2072-6694/13/6/1421/s1>, Figure S1: Determination of the optimal dose of MEKi (Cobimetinib and GDC-0623) for the treatment of ^{V600E}BRAF SK-MEL-3, ^{Q61K}NRAS 1007, and ^{WT}BRAF/NRAS B16F10 melanoma spheroids. Figure S2: Colony formation (n = 3) on melanoma spheroids after treatment with [¹³¹I]ICF01012-TRT, MEKi, or both. Figure S3: Cell-cycle analysis of SK-MEL-3 spheroids treated with TRT alone or in combination with MEKi. Figure S4: Western blot analysis of P-ERK1/2 and ERK1/2 of total cellular protein extracted from B16F10 cells that have been cultured in a 2D monolayer culture system. Figure S5: Deconvolution analyses of major immune cells subset. Figure S6: Interactive volcano plot depicting the differential analysis results between TRT treated tumors and Control tumors (see HTML file). Figure S7: Pathways and gene ontology analyses. Figure S8: [¹³¹I]ICF01012 uptake by spheroids and melanin content in spheroids. Table S1: Mice weight and tumor volume at start of experiment and endpoint for survival and mechanistical studies. Table S2: Primer sequences. Table S3: [¹³¹I]ICF01012 biodistribution in non-target organs in mice. Table S4: [¹³¹I]ICF01012 dosimetry in mice. Table S5: Differential mRNA expression analysis of treated vs. non-treated tumors. Video S1: Principal component analysis (PCA) of the three first dimensions of treated and non-treated tumors (see mp4 file).

Author Contributions: Conceptualization, H.A., F.D., and J.R.; data curation, H.A., F.D., and J.R.; formal analysis, H.A., M.Q., J.H.R., T.B., L.L., F.D., and J.R.; funding acquisition, H.A., L.L., F.D., and J.R.; investigation, H.A., M.Q., J.H.R., T.B., V.B., S.B., P.A., V.D., V.P., L.L., M.D., F.D., and J.R.; methodology, H.A., M.Q., J.H.R., and J.R.; project administration, H.A., F.D., and J.R.; resources, T.B., P.A., V.D., and V.P.; software, J.H.R.; supervision, H.A., F.D., and J.R.; validation, H.A., L.L., F.D., and J.R.; visualization, H.A., J.H.R., F.D., and J.R.; writing—original draft, H.A., F.D., and J.R.; writing—review and editing, H.A., L.L., M.D., F.D., and J.R. All authors have read and agreed to the published version of the manuscript.

Funding: This work was supported by recurrent INSERM and UCA funding and the Ligue Régionale Contre le Cancer (2015 and 2016). H. AKIL was supported by a fellowship from the Auvergne Regional council and the European Community. J. ROUANET was supported by a doctoral fellowship granted by the SFD (French Society for Dermatology). The work of L.L.'s group was supported by the Ligue Contre le Cancer, Fondation ARC, Institut Carnot, INCa, ITMO Cancer, CNRS, INSERM, the French National Research Agency through the "Investments for the Future" program (France-BioImaging, ANR-10-INSB-04), and the program "Investissements d'Avenir" launched by the French Government and implemented by the ANR Labex CelTisPhyBio (ANR-11-LABX-0038 and ANR-10-IDEX-0001-02 PSL).

Institutional Review Board Statement: This investigation was conducted according to the Guide for the Care and Use of Laboratory Animals published by the US National Institutes of Health (8th edition, 2011). All experiments were conducted in accordance with the relevant guidelines and regulations and approved by both the local ethics committee of Clermont-Ferrand (C2E2A n°002) and the French Ministry of Education and Research (approval n°12211-2017111613576925).

Informed Consent Statement: Not applicable.

Data Availability Statement: The data generated by the transcriptomic study (Table S3) have been deposited in the Gene Expression Omnibus of the NCBI and are accessible through GEO Series accession number GSE162536 (<https://www.ncbi.nlm.nih.gov/geo/query/acc.cgi?acc=GSE162536>). This series contains the raw reads (fastq) and aligned-reads (BAM) of nine tumors (3 treated and

6 non-treated), as well as the gene expression read counts and TPM values. The other data presented in this study are available on request from the corresponding author.

Acknowledgments: We thank A Briat from the Ivia Platform for help with the SPECT-CT imaging. We are grateful to A Cayre and M Roche from the anatomopathological department of the Jean Perrin Center and C Vacchias from the confocal imaging facilities (CLIC platform). High-throughput sequencing was performed by the ICGex NGS platform of the Institut Curie, supported by the grants ANR-10-EQPX-03 (Equipex) and ANR-10-INBS-09-08 (France Génomique Consortium) from the Agence Nationale de la Recherche (“Investissements d’Avenir” program), the Canceropole Ile-de-France, and the SiRIC-Curie program-SiRIC Grant INCa-DGOS-4654.

Conflicts of Interest: The authors declare no conflict of interest.

References

1. Paluncic, J.; Kovacevic, Z.; Jansson, P.J.; Kalinowski, D.; Merlot, A.M.; Huang, M.L.; Lok, H.C.; Sahni, S.; Lane, D.J.; Richardson, D.R. Roads to melanoma: Key pathways and emerging players in melanoma progression and oncogenic signaling. *Biochim. Biophys. Acta* **2016**, *1863*, 770–784. [[CrossRef](#)] [[PubMed](#)]
2. Savoia, P.; Fava, P.; Casoni, F.; Cremona, O. Targeting the ERK signaling pathway in melanoma. *Int. J. Mol. Sci.* **2019**, *20*, 1483. [[CrossRef](#)]
3. Reddy, B.Y.; Miller, D.M.; Tsao, H. Somatic driver mutations in melanoma. *Cancer* **2017**, *123*, 2104–2117. [[CrossRef](#)] [[PubMed](#)]
4. Gesbert, F.; Larue, L. Cutaneous melanoma: From rationalized models to patients care. *Med. Sci.* **2018**, *34*, 407–416. [[CrossRef](#)]
5. McArthur, G.A.; Chapman, P.B.; Robert, C.; Larkin, J.; Haanen, J.B.; Dummer, R.; Ribas, A.; Hogg, D.; Hamid, O.; Ascierto, P.A.; et al. Safety and efficacy of vemurafenib in BRAF(V600E) and BRAF(V600K) mutation-positive melanoma (BRIM-3): Extended follow-up of a phase 3, randomised, open-label study. *Lancet Oncol.* **2014**, *15*, 323–332. [[CrossRef](#)]
6. Hauschild, A.; Grob, J.J.; Demidov, L.V.; Jouary, T.; Gutzmer, R.; Millward, M.; Rutkowski, P.; Blank, C.U.; Miller, W.H., Jr.; Kaempgen, E.; et al. Dabrafenib in BRAF-mutated metastatic melanoma: A multicentre, open-label, phase 3 randomised controlled trial. *Lancet* **2012**, *380*, 358–365. [[CrossRef](#)]
7. Prasad, C.P.; Mohapatra, P.; Andersson, T. Therapy for BRAFi-Resistant Melanomas: Is WNT5A the Answer? *Cancers* **2015**, *7*, 1900–1924. [[CrossRef](#)] [[PubMed](#)]
8. Kunz, M.; Holzner, M. The impact of melanoma genetics on treatment response and resistance in clinical and experimental studies. *Cancer Metastasis Rev.* **2017**, *36*, 53–75. [[CrossRef](#)]
9. Mason, R.; Au, L.; Ingles Garcés, A.; Larkin, J. Current and emerging systemic therapies for cutaneous metastatic melanoma. *Expert Opin. Pharm.* **2019**, *20*, 1135–1152. [[CrossRef](#)]
10. Robert, C.; Grob, J.J.; Stroyakovskiy, D.; Karaszewska, B.; Hauschild, A.; Levchenko, E.; Chiarion Sileni, V.; Schachter, J.; Garbe, C.; Bondarenko, I.; et al. Five-year outcomes with dabrafenib plus trametinib in Metastatic Melanoma. *N. Engl. J. Med.* **2019**. [[CrossRef](#)]
11. Ascierto, P.A.; McArthur, G.A.; Dreno, B.; Atkinson, V.; Liskay, G.; Di Giacomo, A.M.; Mandala, M.; Demidov, L.; Stroyakovskiy, D.; Thomas, L.; et al. Cobimetinib combined with vemurafenib in advanced BRAF(V600)-mutant melanoma (coBRIM): Updated efficacy results from a randomised, double-blind, phase 3 trial. *Lancet Oncol.* **2016**, *17*, 1248–1260. [[CrossRef](#)]
12. Dummer, R.; Ascierto, P.A.; Gogas, H.J.; Arance, A.; Mandala, M.; Liskay, G.; Garbe, C.; Schadendorf, D.; Krajsova, I.; Gutzmer, R.; et al. Overall survival in patients with BRAF-mutant melanoma receiving encorafenib plus binimetinib versus vemurafenib or encorafenib (COLUMBUS): A multicentre, open-label, randomised, phase 3 trial. *Lancet Oncol.* **2018**, *19*, 1315–1327. [[CrossRef](#)]
13. Dummer, R.; Ascierto, P.A.; Gogas, H.J.; Arance, A.; Mandala, M.; Liskay, G.; Garbe, C.; Schadendorf, D.; Krajsova, I.; Gutzmer, R.; et al. Encorafenib plus binimetinib versus vemurafenib or encorafenib in patients with BRAF-mutant melanoma (COLUMBUS): A multicentre, open-label, randomised phase 3 trial. *Lancet Oncol.* **2018**, *19*, 603–615. [[CrossRef](#)]
14. Gajewski, T.F.; Salama, A.K.; Niedzwiecki, D.; Johnson, J.; Linette, G.; Bucher, C.; Blaskovich, M.A.; Sebt, S.M.; Haluska, F. Phase II study of the farnesyltransferase inhibitor R115777 in advanced melanoma (CALGB 500104). *J. Transl. Med.* **2012**, *10*, 246. [[CrossRef](#)]
15. Smalley, K.S.; Eisen, T.G. Farnesyl transferase inhibitor SCH66336 is cytostatic, pro-apoptotic and enhances chemosensitivity to cisplatin in melanoma cells. *Int. J. Cancer* **2003**, *105*, 165–175. [[CrossRef](#)]
16. Dummer, R.; Schadendorf, D.; Ascierto, P.A.; Arance, A.; Dutriaux, C.; Di Giacomo, A.M.; Rutkowski, P.; Del Vecchio, M.; Gutzmer, R.; Mandala, M.; et al. Binimetinib versus dacarbazine in patients with advanced NRAS-mutant melanoma (NEMO): A multicentre, open-label, randomised, phase 3 trial. *Lancet Oncol.* **2017**, *18*, 435–445. [[CrossRef](#)]
17. Norain, A.; Dadachova, E. Targeted radionuclide therapy of melanoma. *Semin. Nucl. Med.* **2016**, *46*, 250–259. [[CrossRef](#)]
18. Degoul, F.; Borel, M.; Jacquemot, N.; Besse, S.; Communal, Y.; Mishellany, F.; Papon, J.; Penault-Llorca, F.; Donnarieix, D.; Doly, M.; et al. In vivo efficacy of melanoma internal radionuclide therapy with a ¹³¹I-labelled melanin-targeting heteroarylcarboxamide molecule. *Int. J. Cancer* **2013**, *133*, 1042–1053. [[CrossRef](#)]
19. Viillard, C.; Perrot, Y.; Boudhraa, Z.; Jouberton, E.; Miot-Noirault, E.; Bonnet, M.; Besse, S.; Mishellany, F.; Cayre, A.; Maigne, L.; et al. [¹²³I]ICF01012 melanoma imaging and [¹³¹I]ICF01012 dosimetry allow adapted internal targeted radiotherapy in preclinical melanoma models. *Eur. J. Dermatol.* **2015**, *25*, 29–35. [[CrossRef](#)]

20. Bonnet, M.; Mishellany, F.; Papon, J.; Cayre, A.; Penault-Llorca, F.; Madelmont, J.C.; Miot-Noirault, E.; Chezal, J.M.; Moins, N. Anti-melanoma efficacy of internal radionuclide therapy in relation to melanin target distribution. *Pigment Cell Melanoma Res.* **2010**, *23*, e1–e11. [[CrossRef](#)]
21. Bonnet-Duquennoy, M.; Papon, J.; Mishellany, F.; Labarre, P.; Guerquin-Kern, J.L.; Wu, T.D.; Gardette, M.; Maublant, J.; Penault-Llorca, F.; Miot-Noirault, E.; et al. Targeted radionuclide therapy of melanoma: Anti-tumoural efficacy studies of a new ¹³¹I labelled potential agent. *Int. J. Cancer* **2009**, *125*, 708–716. [[CrossRef](#)]
22. Viillard, C.; Chezal, J.M.; Mishellany, F.; Ranchon-Cole, I.; Pereira, B.; Herbette, A.; Besse, S.; Boudhraa, Z.; Jacquemot, N.; Cayre, A.; et al. Targeting DNA repair by coDbait enhances melanoma targeted radionuclide therapy. *Oncotarget* **2016**, *7*, 12927–12936. [[CrossRef](#)] [[PubMed](#)]
23. Chezal, J.M.; Papon, J.; Labarre, P.; Lartigue, C.; Galmier, M.J.; Decombat, C.; Chavignon, O.; Maublant, J.; Teulade, J.C.; Madelmont, J.C.; et al. Evaluation of radiolabeled (hetero)aromatic analogues of N-(2-diethylaminoethyl)-4-iodobenzamide for imaging and targeted radionuclide therapy of melanoma. *J. Med. Chem.* **2008**, *51*, 3133–3144. [[CrossRef](#)] [[PubMed](#)]
24. Akil, H.; Rouanet, J.; Viillard, C.; Besse, S.; Auzeloux, P.; Chezal, J.M.; Miot-Noirault, E.; Quintana, M.; Degoul, F. Targeted radionuclide therapy decreases melanoma lung invasion by modifying epithelial-mesenchymal transition-like mechanisms. *Transl. Oncol.* **2019**, *12*, 1442–1452. [[CrossRef](#)] [[PubMed](#)]
25. Schick, U.; Kyula, J.; Barker, H.; Patel, R.; Zaidi, S.; Gregory, C.; Hafsi, H.; Roulstone, V.; Deutsch, E.; McLaughlin, M.; et al. Trametinib radiosensitises RAS- and BRAF-mutated melanoma by perturbing cell cycle and inducing senescence. *Radiother. Oncol.* **2015**, *117*, 364–375. [[CrossRef](#)]
26. Marampon, F.; Ciccarelli, C.; Zani, B.M. Biological Rationale for Targeting MEK/ERK Pathways in anti-cancer therapy and to potentiate tumour responses to radiation. *Int. J. Mol. Sci.* **2019**, *20*, 2530. [[CrossRef](#)] [[PubMed](#)]
27. Hecht, M.; Zimmer, L.; Loquai, C.; Weishaupt, C.; Gutzmer, R.; Schuster, B.; Gleisner, S.; Schulze, B.; Goldinger, S.M.; Berking, C.; et al. Radiosensitization by BRAF inhibitor therapy-mechanism and frequency of toxicity in melanoma patients. *Ann. Oncol.* **2015**, *26*, 1238–1244. [[CrossRef](#)]
28. Petit, V.; Raymond, J.; Alberti, C.; Pouteaux, M.; Gallagher, S.J.; Nguyen, M.Q.; Aplin, A.E.; Delmas, V.; Larue, L. C57BL/6 congenic mouse NRAS(Q61K) melanoma cell lines are highly sensitive to the combination of Mek and Akt inhibitors in vitro and in vivo. *Pigment Cell Melanoma Res.* **2019**. [[CrossRef](#)]
29. Buch, K.; Peters, T.; Nawroth, T.; Sanger, M.; Schmidberger, H.; Langguth, P. Determination of cell survival after irradiation via clonogenic assay versus multiple MTT Assay—a comparative study. *Radiat. Oncol.* **2012**, *7*, 1. [[CrossRef](#)]
30. Akil, H.; Abbaci, A.; Lalloue, F.; Bessette, B.; Costes, L.M.; Domballe, L.; Charreau, S.; Guilloteau, K.; Karayan-Tapon, L.; Bernard, F.X.; et al. IL22/IL-22R pathway induces cell survival in human glioblastoma cells. *PLoS ONE* **2015**, *10*, e0119872. [[CrossRef](#)]
31. Perrot, Y.; Degoul, F.; Auzeloux, P.; Bonnet, M.; Cachin, F.; Chezal, J.M.; Donnarieix, D.; Labarre, P.; Moins, N.; Papon, J.; et al. Internal dosimetry through GATE simulations of preclinical radiotherapy using a melanin-targeting ligand. *Phys. Med. Biol.* **2014**, *59*, 2183–2198. [[CrossRef](#)]
32. Stabin, M.G. Developments in the internal dosimetry of radiopharmaceuticals. *Radiat. Prot. Dosim.* **2003**, *105*, 575–580. [[CrossRef](#)]
33. Rioux, B.; Rouanet, J.; Akil, H.; Besse, S.; Debiton, E.; Bouchon, B.; Degoul, F.; Quintana, M. Determination of eumelanin and pheomelanin in melanomas using solid-phase extraction and high performance liquid chromatography-diode array detection (HPLC-DAD) analysis. *J. Chromatogr. B Analyt. Technol. Biomed. Life Sci.* **2019**, *1113*, 60–68. [[CrossRef](#)]
34. Dobin, A.; Davis, C.A.; Schlesinger, F.; Drenkow, J.; Zaleski, C.; Jha, S.; Batut, P.; Chaisson, M.; Gingeras, T.R. STAR: Ultrafast universal RNA-seq aligner. *Bioinformatics* **2012**, *29*, 15–21. [[CrossRef](#)]
35. Robinson, M.D.; McCarthy, D.J.; Smyth, G.K. edgeR: A Bioconductor package for differential expression analysis of digital gene expression data. *Bioinformatics* **2010**, *26*, 139–140. [[CrossRef](#)]
36. Lê, S.; Josse, J.; Husson, F. FactoMineR: An R Package for Multivariate Analysis. *J. Stat. Softw.* **2008**, *25*, 1–18. [[CrossRef](#)]
37. Becht, E.; Giraldo, N.A.; Lacroix, L.; Buttard, B.; Elarouci, N.; Petitprez, F.; Selves, J.; Laurent-Puig, P.; Sautès-Fridman, C.; Fridman, W.H.; et al. Estimating the population abundance of tissue-infiltrating immune and stromal cell populations using gene expression. *Genome Biol.* **2016**, *17*, 218. [[CrossRef](#)] [[PubMed](#)]
38. Ritchie, M.E.; Phipson, B.; Wu, D.; Hu, Y.; Law, C.W.; Shi, W.; Smyth, G.K. Limma powers differential expression analyses for RNA-sequencing and microarray studies. *Nucleic Acids Res.* **2015**, *43*, e47. [[CrossRef](#)] [[PubMed](#)]
39. Wickham, H. *Ggplot2: Elegant Graphics for Data Analysis*; Springer: New York, NY, USA, 2009.
40. Sievert, C. *Interactive Web-based Data Visualization with R, Plotly, and Shiny*; CRC Press, Taylor and Francis Group: Boca Raton, FL, USA, 2020.
41. Chen, E.Y.; Tan, C.M.; Kou, Y.; Duan, Q.; Wang, Z.; Meirelles, G.V.; Clark, N.R.; Ma’ayan, A. Enrichr: Interactive and collaborative HTML5 gene list enrichment analysis tool. *BMC Bioinform.* **2013**, *14*, 128. [[CrossRef](#)] [[PubMed](#)]
42. Rambow, F.; Rogiers, A.; Marin-Bejar, O.; Aibar, S.; Femel, J.; Dewaele, M.; Karras, P.; Brown, D.; Chang, Y.H.; Debiec-Rychter, M.; et al. Toward minimal residual disease-directed therapy in melanoma. *Cell* **2018**, *174*, 843–855.e819. [[CrossRef](#)] [[PubMed](#)]
43. Edmondson, R.; Broglie, J.J.; Adcock, A.F.; Yang, L. Three-dimensional cell culture systems and their applications in drug discovery and cell-based biosensors. *Assay Drug Dev. Technol.* **2014**, *12*, 207–218. [[CrossRef](#)]
44. Kumar, S.M.; Zhang, G.; Bastian, B.C.; Arcasoy, M.O.; Karande, P.; Pushparajan, A.; Acs, G.; Xu, X. Erythropoietin receptor contributes to melanoma cell survival in vivo. *Oncogene* **2012**, *31*, 1649–1660. [[CrossRef](#)] [[PubMed](#)]

45. Sorensen, M.R.; Pedersen, S.R.; Lindkvist, A.; Christensen, J.P.; Thomsen, A.R. Quantification of B16 melanoma cells in lungs using triplex Q-PCR—a new approach to evaluate melanoma cell metastasis and tumor control. *PLoS ONE* **2014**, *9*, e87831. [[CrossRef](#)]
46. Munshi, A.; Ramesh, R. Mitogen-activated protein kinases and their role in radiation response. *Genes Cancer* **2013**, *4*, 401–408. [[CrossRef](#)] [[PubMed](#)]
47. Pomp, J.; Ouwerkerk, I.J.; Hermans, J.; Wondergem, J.; Cornelisse, C.J.; Leer, J.W.; Schrier, P.I. The influence of the oncogenes NRAS and MYC on the radiation sensitivity of cells of a human melanoma cell line. *Radiat Res.* **1996**, *146*, 374–381. [[CrossRef](#)] [[PubMed](#)]
48. Rutter, C.E.; Johung, K.L.; Yao, X.; Lu, A.Y.; Jilaveanu, L.B.; Yu, J.B.; Contessa, J.N.; Kluger, H.M.; Chiang, V.L.S.; Bindra, R.S. Demonstration of differential radiosensitivity based upon mutation profile in metastatic melanoma treated with stereotactic radiosurgery. *J. Radiosurg. SBRT* **2016**, *4*, 97–106. [[PubMed](#)]
49. Conde-Perez, A.; Larue, L. Human relevance of NRAS/BRAF mouse melanoma models. *Eur. J. Cell Biol.* **2014**, *93*, 82–86. [[CrossRef](#)] [[PubMed](#)]
50. Jouberton, E.; Perrot, Y.; Dirat, B.; Billoux, T.; Auzeloux, P.; Cachin, F.; Chezal, J.M.; Filaire, M.; Labarre, P.; Miot-Noirault, E.; et al. Radiation dosimetry of [¹³¹I]ICF01012 in rabbits: Application to targeted radionuclide therapy for human melanoma treatment. *Med. Phys.* **2018**, *45*, 5251–5262. [[CrossRef](#)]
51. Mier, W.; Kratochwil, C.; Hassel, J.C.; Giesel, F.L.; Beijer, B.; Babich, J.W.; Friebe, M.; Eisenhut, M.; Enk, A.; Haberkorn, U. Radiopharmaceutical therapy of patients with metastasized melanoma with the melanin-binding benzamide 131I-BA52. *J. Nucl. Med.* **2014**, *55*, 9–14. [[CrossRef](#)]
52. Napolitano, A.; Panzella, L.; Monfrecola, G.; d’Ischia, M. Pheomelanin-induced oxidative stress: Bright and dark chemistry bridging red hair phenotype and melanoma. *Pigment. Cell Melanoma Res.* **2014**, *27*, 721–733. [[CrossRef](#)] [[PubMed](#)]
53. Rouanet, J.; Benboubker, V.; Akil, H.; Hennino, A.; Auzeloux, P.; Besse, S.; Pereira, B.; Delorme, S.; Mansard, S.; D’Incan, M.; et al. Immune checkpoint inhibitors reverse tolerogenic mechanisms induced by melanoma targeted radionuclide therapy. *Cancer Immunol. Immunother.* **2020**, *69*, 2075–2088. [[CrossRef](#)] [[PubMed](#)]
54. Ladjohounlou, R.; Lozza, C.; Pichard, A.; Constanzo, J.; Karam, J.; Le Fur, P.; Deshayes, E.; Boudousq, V.; Paillas, S.; Busson, M.; et al. Drugs that modify cholesterol metabolism alter the p38/JNK-mediated targeted and nontargeted response to alpha and auger radioimmunotherapy. *Clin. Cancer Res.* **2019**, *25*, 4775–4790. [[CrossRef](#)] [[PubMed](#)]

IV. CLEC12B Decreases Melanoma Proliferation by Repressing Signal Transducer and Activator of Transcription 3

Article publié en juillet 2021

Résumé :

Nos collaborateurs de Nice de l'équipe de Thierry Passeron ont identifié un gène dont le niveau d'expression diminuait au cours de la formation du mélanome primaire, CLEC12B, en étant significativement réduit dans les métastases de mélanomes. Ce profil d'expression suggère un effet suppresseur de tumeur. En collaboration avec notre laboratoire, ils ont pu montrer que l'expression de CLEC12B diminue la croissance des cellules de mélanome *in vivo* alors que sa perte d'expression favorise la croissance cellulaire *in vivo*. Il a été montré que l'action de CLEC12B passe par l'inhibition de STAT1/3/5 et l'activation des facteurs impliqués dans la régulation négative du cycle cellulaire P53/p21/p27.

J'ai pris part à ce projet en analysant des bases de données publiques et en conseillant sur leur utilisation.

CLEC12B Decreases Melanoma Proliferation by Repressing Signal Transducer and Activator of Transcription 3

Henri Montaudie^{1,2}, Laura Sormani¹, Bérengère Dadone-Montaudie^{3,4}, Marjorie Heim¹, Nathalie Cardot-Leccia³, Meri K. Tulic¹, Guillaume Beranger¹, Anne-Sophie Gay⁵, Delphine Debayle⁵, Yann Cheli⁶, Jérémy H. Raymond^{7,8,9}, Pierre Sohier^{7,8,9}, Valérie Petit^{7,8,9}, Stéphane Rocchi¹, Franck Gesbert^{7,8,9}, Lionel Larue^{7,8,9,10} and Thierry Passeron^{1,2,10}

The potential role of *CLEC12B*, a gene predominantly expressed by skin melanocytes discovered through transcriptomic analysis, in melanoma is unknown. In this study, we show that *CLEC12B* expression is lower in melanoma and melanoma metastases than in melanocytes and benign melanocytic lesions and that its decrease correlates with poor prognosis. We further show that *CLEC12B* recruits SHP2 phosphatase through its immunoreceptor tyrosine-based inhibition motif domain, inactivates signal transducer and activator of transcription 1/3/5, increases p53/p21/p27 expression/activity, and modulates melanoma cell proliferation. The growth of human melanoma cells overexpressing *CLEC12B* in nude mice after subcutaneous injection is significantly decreased compared with that in the vehicle control group and is associated with decreased signal transducer and activator of transcription 3 phosphorylation and increased p53 levels in the tumors. Reducing the level of *CLEC12B* had the opposite effect. We show that *CLEC12B* represses the activation of the signal transducer and activator of transcription pathway and negatively regulates the cell cycle, providing a proliferative asset to melanoma cells.

Journal of Investigative Dermatology (2021) ■, ■-■; doi:10.1016/j.jid.2021.05.035

INTRODUCTION

Targeted therapy and immune checkpoint inhibitors have dramatically changed the landscape of melanoma treatment. Nevertheless, despite such progress, melanoma still ranks

among the most aggressive and deadly human cancers. Many patients still fail to respond to these drugs, and only a subset of them (~50% depending on regimen) truly benefit from these new therapies (Michielin et al., 2019). These limitations highlight the need for a better understanding of the pathogenesis of melanoma to provide new therapeutic targets and strategies.

We performed a transcriptional analysis of vitiligo skin to further characterize the pathophysiological mechanisms involved in this disease (Regazzetti et al., 2015). By comparing biopsies taken from lesional skin (characterized by the total absence of melanocytes), nonlesional skin, and skin from healthy subjects, we highlighted a strong decrease in the expression of key enzymes involved in melanogenesis. We found that *CLEC12B*, a type II transmembrane protein (4933425B16Rik or UNQ5782), is differentially expressed lesional skin compared with the expression in the nonlesional skin of these patients and that of healthy volunteers, with a magnitude comparable with that of the major melanocytic genes, including dopachrome tautomerase gene *DCT*, *TYRP1*, and *TYR*. *CLEC12B* encodes a C lectin receptor containing an intracellular immunoreceptor tyrosine-based inhibitory motif (ITIM) domain reported to be expressed by myeloid cells (Hoffmann et al., 2007). Our laboratory recently showed that *CLEC12B* in the skin is selectively and strongly expressed by melanocytes in the epidermis and negatively regulates melanogenesis (Sormani et al., unpublished data).

In this study, we show lower expression of *CLEC12B* in melanoma cell lines and in melanoma metastases than in normal human melanocytes or benign melanocytic lesions

¹Team 12, Study of the melanocytic differentiation applied to vitiligo and melanoma: from the patient to the molecular mechanisms, Centre Méditerranéen de Médecine Moléculaire (C3M), Institut national de la santé et de la recherche médicale (INSERM) U1065, Université Nice Côte d'Azur, Nice, France; ²Department of Dermatology, Centre hospitalier universitaire (CHU) de Nice, Université Nice Côte d'Azur, Nice, France; ³Department of Pathology, Université Nice Côte d'Azur, Nice, France; ⁴Laboratory of Solid Tumors Genetics, Institute for Research on Cancer and Aging of Nice, CNRS UMR 7284/ Institut national de la santé et de la recherche médicale (INSERM) U1081, CHU Nice, Université Nice Côte d'Azur, Nice, France; ⁵IPMC, CNRS, Université Côte d'Azur, Sophia Antipolis, France; ⁶Team 1, Biology and pathologies of melanocytes, Centre Méditerranéen de Médecine Moléculaire (C3M), Institut national de la santé et de la recherche médicale (INSERM) U1065, Université Nice Côte d'Azur, Nice, France; ⁷Normal and Pathological Development of Melanocytes, Institut Curie, Institut national de la santé et de la recherche médicale (INSERM) U1021, PSL Research University, Paris, France; ⁸UMR 3347, CNRS, Université Paris-Saclay, Paris, France; and ⁹Equipe Labellisée Ligue Contre le Cancer, Paris, France

¹⁰These authors contributed equally to this work.

Correspondence: Thierry Passeron, Department of Dermatology and Centre Méditerranéen de Médecine Moléculaire (C3M), Institut national de la santé et de la recherche médicale (INSERM) U1065, Université Nice Côte d'Azur, 151 route Saint-Antoine de Ginestière, 06200 Nice, France. E-mail: passeron@unice.fr

Abbreviations: ITIM, immunoreceptor tyrosine-based inhibition motif; Ov, overexpressing vector; Sh, silencing vector; STAT, signal transducer and activator of transcription; WT, wild-type

Received 2 April 2020; revised 18 May 2021; accepted 24 May 2021; accepted manuscript published online XXX; corrected proof published online XXX

(nevi), and this expression correlates with significantly lower overall survival of patients. We further show that CLEC12B, through recruitment of SHP2 through its ITIM domain, strongly inhibits melanoma proliferation in vitro and in a nude-mouse xenograft model by inhibiting the phosphorylation of signal transducer and activator of transcription (STAT) 1, 3, and 5. Overall, these data show that the decreased expression of CLEC12B in melanoma cells increases STATs activation and confers to those cells a proliferative asset.

RESULTS

We investigated the clinical significance of *CLEC12B* in melanoma by first comparing *CLEC12B* mRNA levels in five human melanoma cell lines (A375, MeWo, Mel501, Skmel28, and WM9), tumor cells were established in short-term culture from three patient metastases (1, 2 and 3) and normal human melanocytes. The genetic background of the cells is presented (Supplementary Table S1). Although variable in their expression, all the eight melanoma cell cultures showed significantly lower expression of *CLEC12B* than normal human melanocytes (Figure 1a). We further compared the expression of *CLEC12B* in tissue samples. First, a comparison of the differential mRNA expression of *CLEC12B* in melanoma samples with that of normal skin using the Gene Expression Profiling Interactive Analysis database revealed a significantly decreased expression of *CLEC12B* in melanoma tissues ($P < 0.0001$) (Supplementary Figure S1a); the same observation was made in another RNA-sequencing dataset (Supplementary Figure S1b). We also evaluated the expression of *CLEC12B* in another public database (Kunz et al., 2018), which confirms the decrease of *CLEC12B* expression in melanoma compared with that in nevi; interestingly, a variable expression of *CLEC12B* during the different stages of melanomagenesis is observed (Supplementary Figure S1c). We further assessed the protein expression using benign and malignant melanocytic tumors from patients ($n = 44$). Immunohistochemical analysis of CLEC12B revealed strong, diffuse cytoplasmic expression in melanocytes of the normal skin and benign melanocytic lesions (junctional and dermal nevi) (Figure 1b) and moderate to high expression in thin melanomas (Figure 1b). Conversely, expression was weak or undetectable in thick melanomas (Figure 1b) and in various metastases (Figure 1b). The immunohistochemical data are summarized in Supplementary Table S2. We used the human melanoma dataset generated by The Cancer Genome Atlas to analyze whether overall survival was associated with *CLEC12B* mRNA levels. The Kaplan–Meier survival analysis for patients in this dataset showed that those with high *CLEC12B* expression (red curve) had significantly higher median survival than those with low expression (blue curve, Log-rank test, $P = 0.006$) (Figure 1c). Overall, these correlative data suggest that *CLEC12B* may play a role in melanoma progression.

We evaluated the biological function of *CLEC12B* in melanoma by examining the effect of its modulation on melanoma cell proliferation and colony formation. We established stable melanoma cell lines with overexpressing vector (Ov)-*CLEC12B* by lentiviral transduction or with silencing vector

(Sh) *CLEC12B* (Supplementary Figure S2a). After Ov *CLEC12B*, we detected a specific 43-kDa band by western blot analysis (Supplementary Figure S2b). This was surprising because the theoretical molecular weight of *CLEC12B* is approximately 32 kDa. We thus performed proteomic analysis, which confirmed that the upper 43-kDa band corresponded to the CLEC12B protein (Supplementary Figure S2c). Treatment of the Ov-*CLEC12B* A375 melanoma cell line with tunicamycin, an inhibitor of N-glycosylation, showed a shift from 43 to 32 kDa. These results suggest that the observed 43-kDa band corresponds to an N-glycosylated form of *CLEC12B* (Supplementary Figure S2d). Because it was difficult to assess the expression of *CLEC12B* in melanoma cells by western blot analysis because the basal level of *CLEC12B* in the A375 and MeWo melanoma cell lines was too low, Sh*CLEC12B* was confirmed by RT-qPCR analysis for all experiments. Ov *CLEC12B* by lentiviral transduction inhibited cell proliferation by ~60%, and conversely, Sh*CLEC12B* promoted the proliferation of the A375 and MeWo human melanoma cell lines by 100% and ~60%, respectively (Figure 1d, upper panel). In accordance with these results, we analyzed the doubling time in A375 and MeWo melanoma cells after overexpressing or reducing CLEC12B. The doubling time of A375 was 22 hours in empty vector controls, 33 hours when Ov *CLEC12B*, and 16.5 hours when repressing it. Similarly, doubling time of MeWo cells was 31 hours in controls, 99 hours when Ov *CLEC12B*, and 21 hours when repressing it. We also assessed the impact of the modulation of *CLEC12B* levels on the ability of melanoma cells to form colonies. We observed ~45% fewer colonies in Ov-*CLEC12B* A375 and MeWo melanoma cells than in those carrying the control vector (Figure 1d, lower panel) and the opposite effect after Sh*CLEC12B*, showing ~100% more colony-forming units for A375 and ~60% for MeWo cells than those with control vector (Figure 1d, lower panel). Interestingly, despite low basal levels of *CLEC12B* in melanoma cells, a further decrease of its expression using short hairpin RNA still increased the proliferation and the colony formation. Overall, these results show that *CLEC12B* inhibits proliferation and colony formation in melanoma cell lines.

Hoffmann et al. (2007) showed that the inhibitory function of *CLEC12B* is mediated by recruitment of the Y phosphatases SHP1/2 to its ITIM domain on receptor phosphorylation in human epithelial embryonic kidney 293T cells. Because SHP2 has been shown to play a role in cancer, particularly in melanoma (Cai et al., 2015; Hill et al., 2019; Zhang et al., 2015), unlike SHP1 that is implicated in inflammatory diseases (Chong and Maiese, 2007), we thus focused on SHP2. In addition, SHP2 induces its own rapid dephosphorylation, and after activation, SHP2 becomes dephosphorylated (Stein-Gerlach et al., 1995). Ov-*CLEC12B* induced the dephosphorylation of SHP2 (Y542) in both A375 and MeWo cells (Figure 2a, upper panel), and phosphorylated SHPY542 levels were significantly higher in Sh*CLEC12B* cells (Figure 2a, lower panel). We further generated a point mutant of *CLEC12B* by exchanging the ITIM Y with phenylalanine (Ov-mutant). Coimmunoprecipitation assays showed an interaction between *CLEC12B* and SHP2 in melanoma cells. Moreover, the recruitment of SHP2 by *CLEC12B* dramatically decreased when using the Ov-mutant (Figure 2b). As

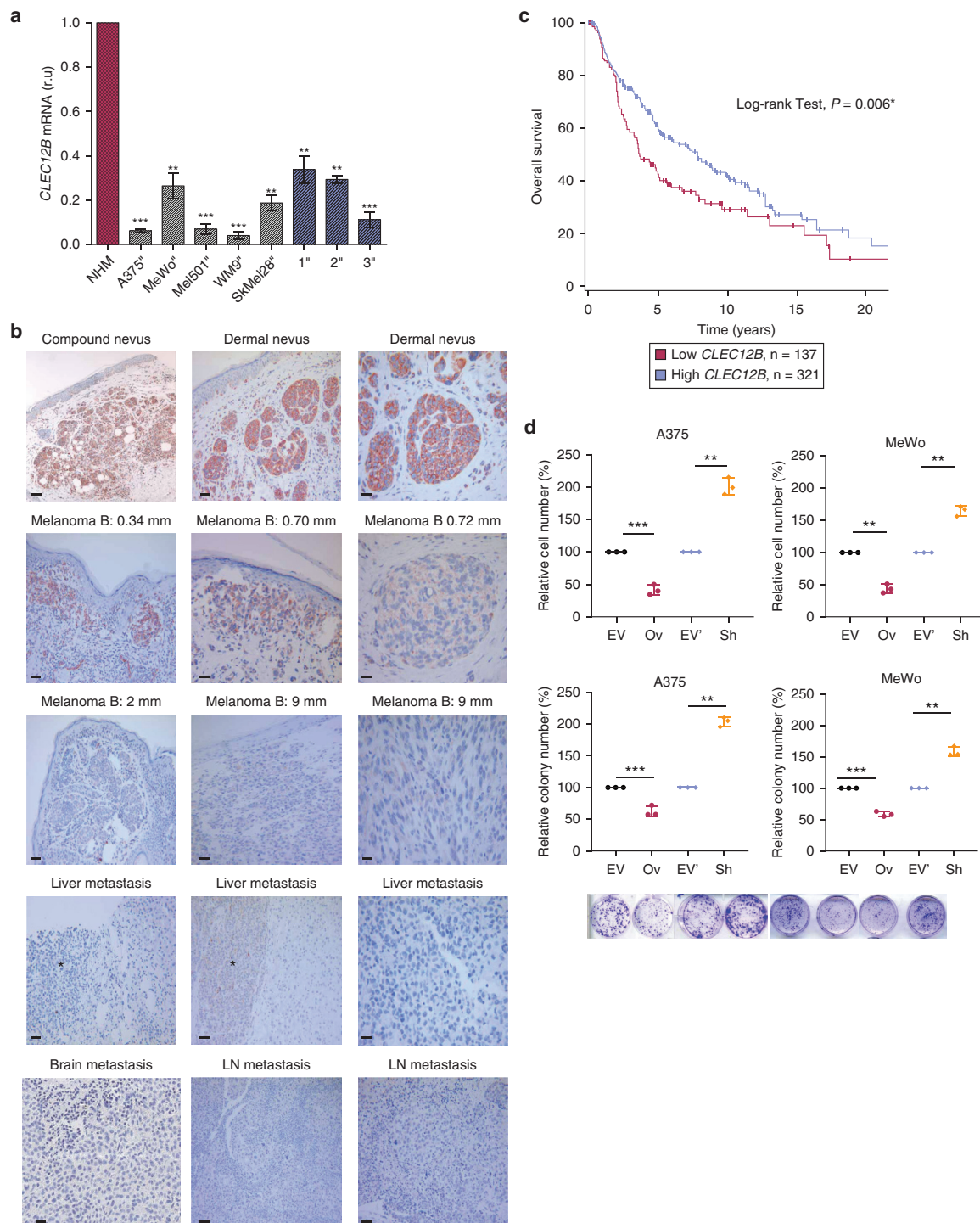


Figure 1. CLEC12B modulation shows clinical significance in melanoma, and its overexpression inhibits the proliferation and colony formation of melanoma cell lines. (a) The relative levels of *CLEC12B* mRNA were examined in human melanoma samples (A375, MeWo, Mel501, WM9, and Skmel28) cells extracted from three patients with metastases (1, 2, 3) and in NHMs by qPCR. The qPCR results were normalized to those of the house-keeping gene *SB34* and expressed as the fold change in mRNA level relative to that of NHM. (b) Immunohistochemical analysis of *CLEC12B* was performed on nevi samples ($n = 12$, B1–B3), primitive thin melanomas ($n = 11$, B4–B6), primitive thick melanomas ($n = 9$, B7–B9), and melanoma metastases ($n = 12$, B10–B15). Asterisk (*) indicates the tumor cells. Bar = 200 μm . (c) Kaplan–Meier survival curves for *CLEC12B* high tumors ($n = 321$, red curve) versus *CLEC12B* low tumors ($n = 137$, blue curve). Data were extracted from the Tumor Cancer Genome Atlas database ($n = 458$ samples from primary and metastatic melanoma). High-level expression of *CLEC12B* was defined as ≥ 1 TPM, and low-level expression was defined as < 1 TPM. The human melanoma cell lines A375 and MeWo were transfected with a puromycin-resistance vector and either a lentivirus Ov-*CLEC12B* or its control EV or a lentivirus Sh*CLEC12B* or its control EV'. (d) Effect of *CLEC12B* Ov or Sh on the proliferation of A375 and MeWo melanoma cells (upper panel). (d) Effect of *CLEC12B* Ov or Sh on colony formation of A375 and MeWo melanoma cells (lower panel). For each experiment, the number of cells and the number of colonies are expressed as the percentage of those transduced with the vector alone (100%). Data are shown as the mean \pm SD of three biological replicates. Differences between groups were tested using the nonparametric Mann–Whitney test and considered significant when $P < 0.05$. * $P < 0.05$, ** $P < 0.001$, *** $P < 0.0001$. B, Breslow thickness; EV, empty vector; LN, lymph node; NHM, normal human melanocyte; Ov, overexpressing; ru, relative unit; Sh, silencing vector; TPM, transcripts per million kilobases.

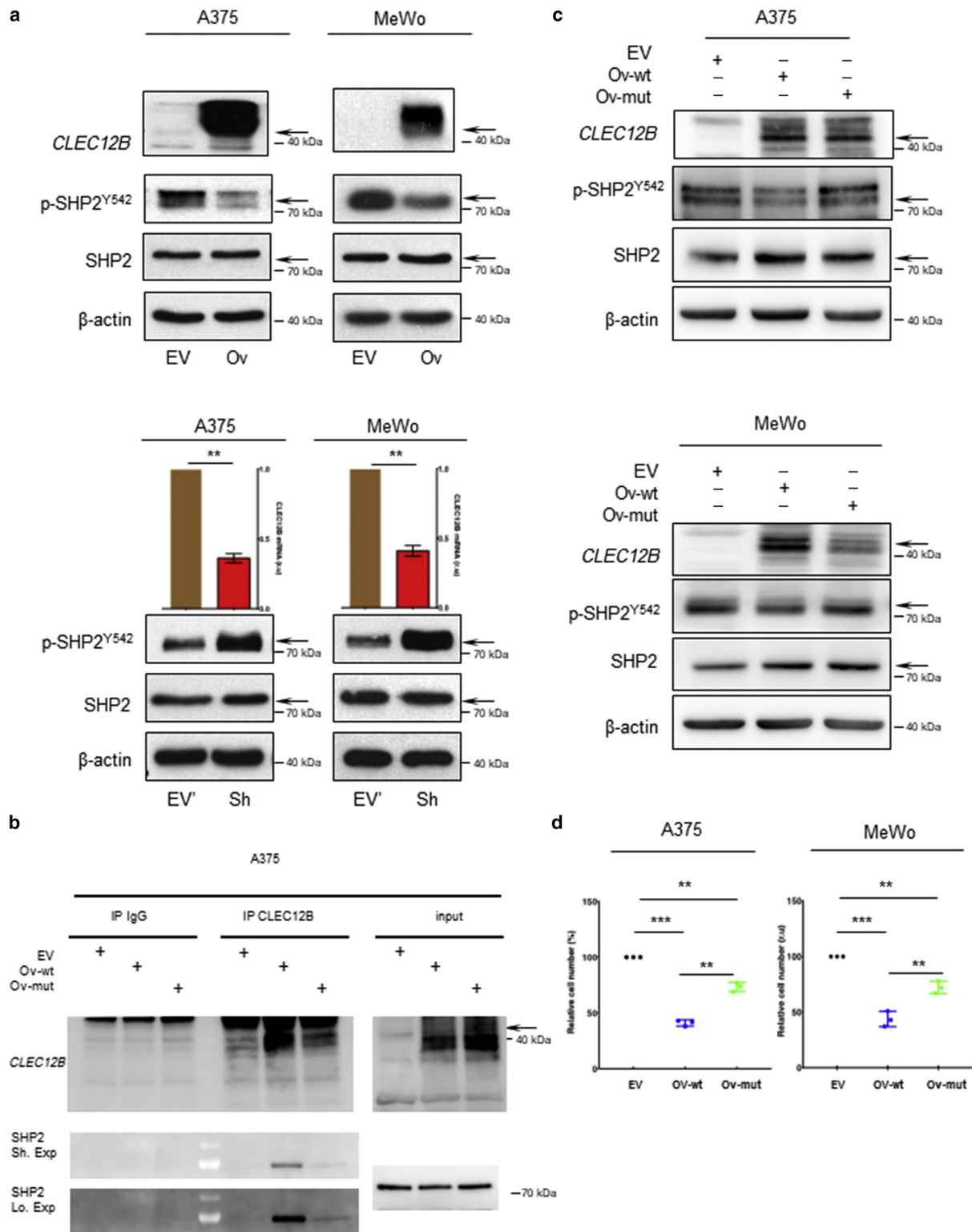


Figure 2. CLEC12B recruits and activates phosphatase SHP2 in melanoma cells through its ITIM domain. (a) The effects of *CLEC12B* modulation (upper panel: Ov, lower panel: Sh) on the phosphorylation status of SHP2 (Y542) were analyzed in A375 and MeWo melanoma cells. β -Actin was used as the loading control. Sh*CLEC12B* was confirmed by quantitative real-time reverse transcriptase–PCR, as shown in the histograms. (b) Lentiviral infection was used to Ov wt *CLEC12B* or an ITIM Ov-mut of *CLEC12B* in A375 cells. Lysates were immunoprecipitated using control IgG or anti-*CLEC12B* antibodies, and the samples were analyzed by western blotting for coimmunoprecipitated SHP-2 and total immunoprecipitated *CLEC12B*. (c) The effects of Ov-mut transduced A375 (upper panel) and MeWo (lower panel) cells on the phosphorylation status of SHP2 (Y542) were analyzed by western blotting. β -Actin was used as a loading control. (d) Effect of Ov-mut on the proliferation of A375 (left panel) and MeWo (right panel) melanoma cells lines. For each experiment, the number of cells and the number of colonies are expressed as the percentage of those transduced with the vector alone (100%). Data are shown as the mean \pm SD of three biological replicates. Differences between groups were tested using the nonparametric Mann–Whitney test and considered significant when $P < 0.05$. * $P < 0.05$, ** $P < 0.001$, *** $P < 0.0001$. EV, empty vector; ITIM, immunoreceptor tyrosine-based inhibition motif; Ov, overexpressing vector; mut, mutant; Sh, silencing vector; wt, wild-type.

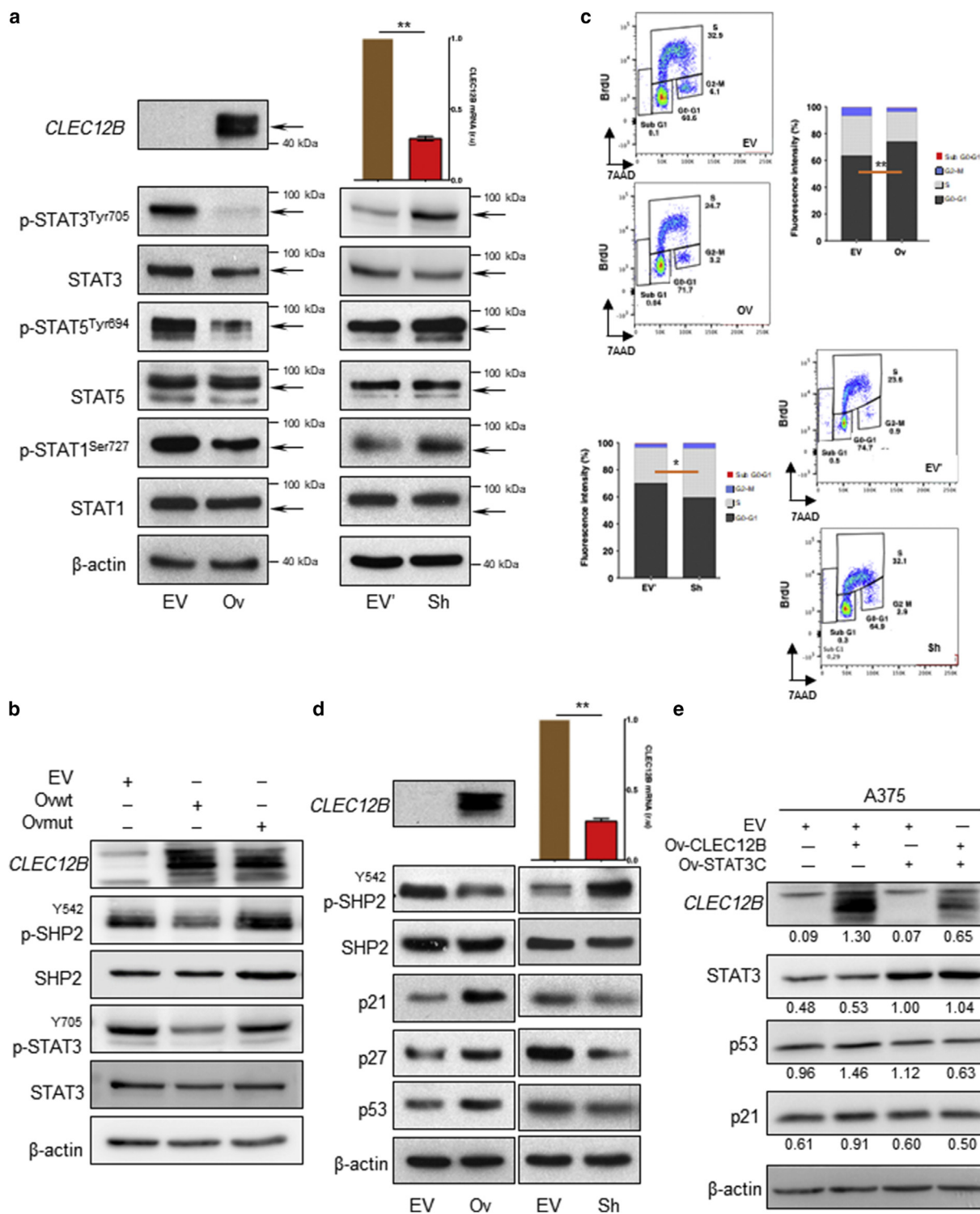


Figure 3. *CLEC12B* inhibits the activation of STAT1, STAT3, and STAT5 and increases the expression of p21/p53 and p27. (a) The effects of *CLEC12B* modulation (left panel: Ov, right panel: Sh) on the phosphorylation status of STAT1, STAT3, and STAT5 in A375 cells were analyzed by western blotting. β -Actin was used as the loading control. Sh*CLEC12B* was confirmed by QRT-PCR as shown in the histograms. (b) The effect of Ov-mut transduced A375 on the phosphorylation status of STAT3 was analyzed by western blotting. β -Actin was used as a loading control. (c) Flow cytometry analysis of Ov-*CLEC12B* (upper panel, histograms on the right correspond to the mean of three independent experiments) or Sh (lower panel, histograms on the left correspond to the mean of three independent experiments) A375 cells with BrdU incorporation after cell cycle synchronization. (d) The effects of *CLEC12B* modulation (left panel: Ov, right panel: Sh) on p53, p21, and p27 levels in A375 cells were analyzed by western blotting. β -Actin was used as the loading control. Sh*CLEC12B* was confirmed by QRT-PCR, as shown by the histograms. (e) The effects of Ov-*CLEC12B* on p53 and p21 after expressing STAT3 phosphorylated tyrosine (Y705E) mimic on p53 and p21 in A375 cells were analyzed by western blotting. β -Actin was used as the loading control. Differences between groups were tested using the nonparametric Mann-Whitney test and considered significant when $P < 0.05$. * $P < 0.05$, ** $P < 0.001$, *** $P < 0.0001$. EV, empty vector; mut, mutant; Ov, overexpressing vector; QRT-PCR, quantitative real-time reverse transcriptase-PCR; Sh, silencing vector; STAT, signal transducer and activator of transcription; wt, wild-type.

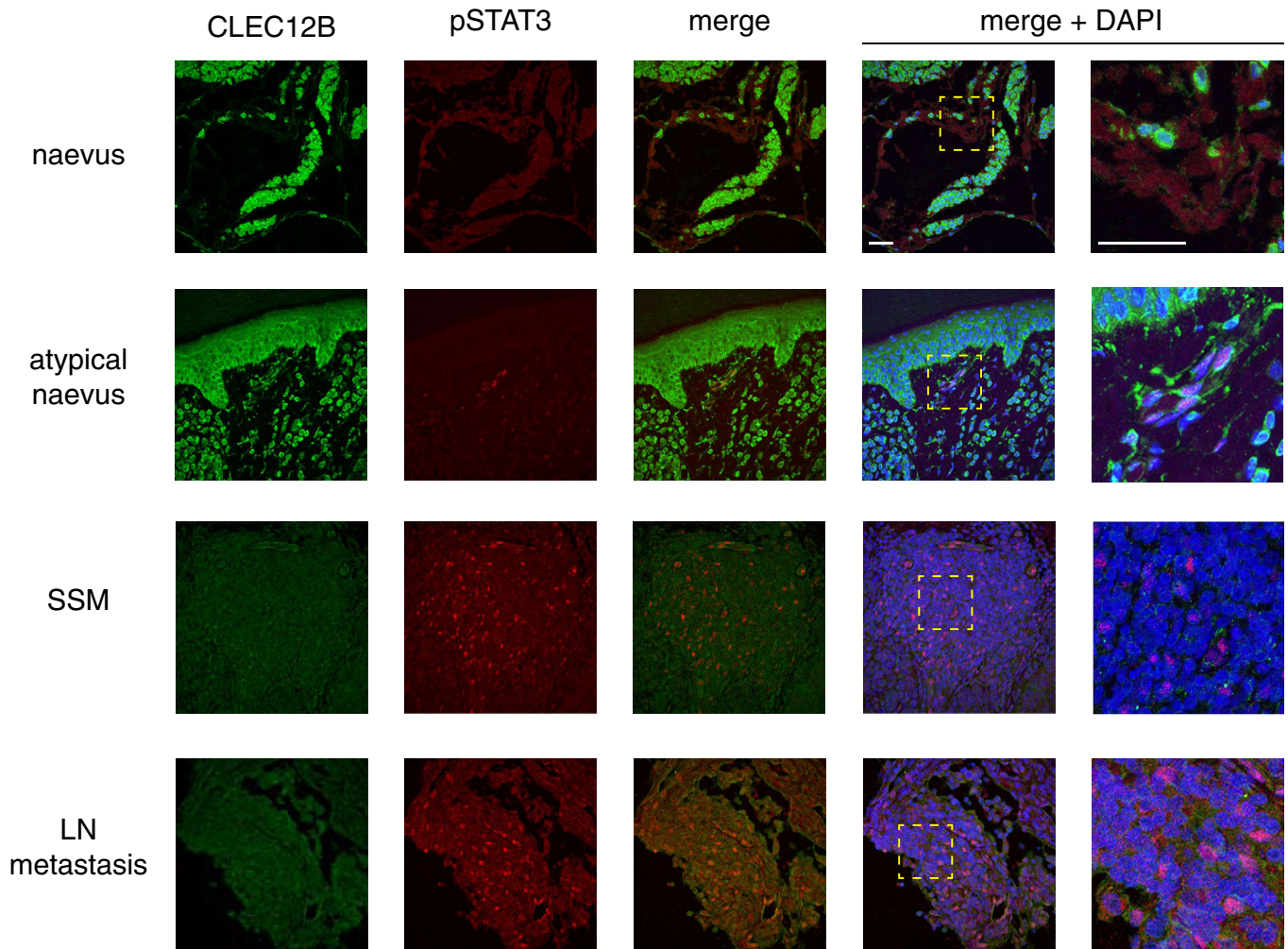


Figure 4. STAT3 phosphorylated tyrosine Y705 has an inverse expression with CLEC12B in human tumor samples. Immunofluorescence analyses of tumor samples, showing that dermal nevus and atypical nevus with high levels of CLEC12B (green staining) are negative for pSTAT3 (red staining), whereas primary melanoma (SSM; with Breslow thickness = 2 mm) and LN metastasis negative for CLEC12B express pSTAT3 (red staining). Bar = 40 μ m. LN, lymph node; pSTAT, phosphorylated signal transducer and activator of transcription; SSM, superficial spreading melanoma

expected, the effect on phosphorylated SHP2Y542 observed after Ov-CLEC12B no longer occurred with the Ov-mutant, either in A375 or MeWo cells (Figure 2c, upper and lower panels, respectively). Ov-CLEC12B with an altered ITIM domain had a significantly lower antiproliferative effect than overexpression of the wild-type (WT) form (Figure 2d), both in A375 and in MeWo melanoma cell lines. Overall, these data show that CLEC12B directly recruits and activates SHP2 through its ITIM domain in melanoma cells.

SHP2 plays a dual role in cancer because it stimulates the MAPK pathway but inhibits the STATs (Li et al., 2012). The Jak/STAT signaling pathway plays a crucial role in melanoma, and in general, it is constitutively activated during melanoma progression (Thomas et al., 2015). SHP2 appears to play a critical role in regulating the Jak/STAT pathway in cancer, particularly in melanoma (Cai et al., 2015; Frankson et al., 2017; Kim et al., 2018). We thus assessed whether modulating CLEC12B levels can affect the Jak/STAT pathway. STAT1, STAT3, and STAT5 phosphorylation were significantly lower in Ov-CLEC12B A375 cells than in those carrying the control vector (Figure 3a, left panel). In contrast, Sh-mediated

CLEC12B downmodulation promoted the phosphorylation of STAT1, STAT3, and STAT5 (Figure 3a, right panel). We observed the same effects on the activation of STATs in MeWo cells (Supplementary Figure S3). SHP2 also appears to regulate the MAPK pathway (Grossmann et al., 2010; Li et al., 2012), especially in melanoma cells not harboring mutations in BRAF or NRAS. However, we did not observe any modification of extracellular signal-regulated kinase or phosphorylated extracellular signal-regulated kinase when we modulated CLEC12B expression in A375 (BRAF^{V600E}, NRAS-WT) or MeWo (BRAF-WT, NRAS-WT) cells (Supplementary Figure S4). We further aimed to assess whether the inhibition of the STATs was due to the recruitment of SHP2 by CLEC12B. Use of the altered ITIM mutant of CLEC12B showed that the decrease of phosphorylated SHP2 observed after Ov-CLEC12B was accompanied by lower phosphorylation of STAT3 (Figure 3b) and that these effects were lost when the Ov-mutant was expressed. Overall, our results show that the recruitment of SHP2 by CLEC12B may activate SHP2, which in turn leads to the dephosphorylation of STATs and lower proliferative capacity of the cells. STAT3 has a

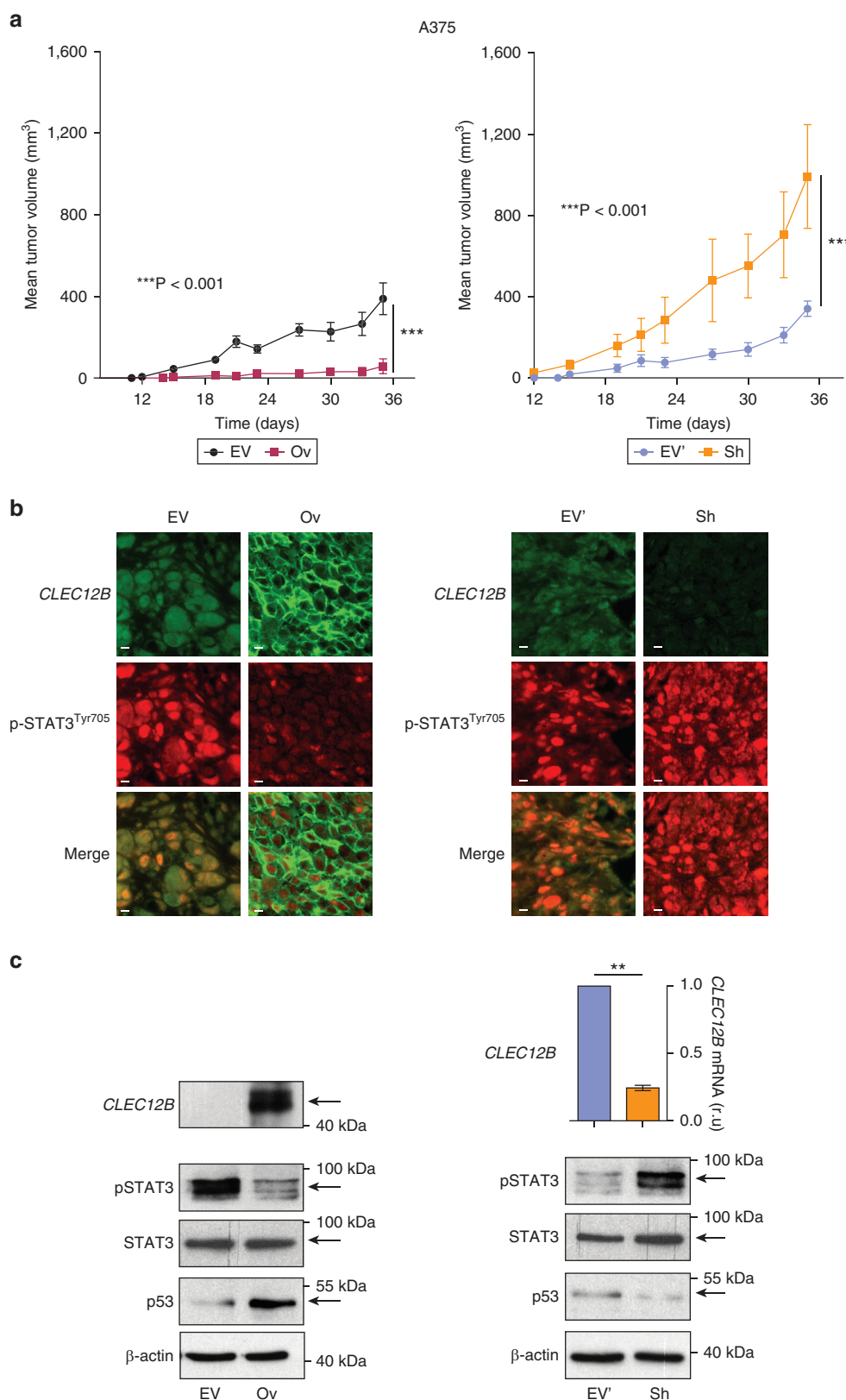


Figure 5. *CLEC12B* inhibits A375 melanoma cell xenograft tumor growth in vivo and decreases the level of pSTAT3. A total of 4×10^6 cells ($100 \mu\text{l}$) were subcutaneously engrafted into the flank of Swiss nude mice, and tumor growth was measured at various time points. (a) The tumor volume of Ov-*CLEC12B* compared with that of EV (left panel) and Sh*CLEC12B* compared with that of EV' (right panel) were measured three times per week until day 36, when the mice were killed. Differences between groups were tested using the nonparametric Mann-Whitney test and considered significant when $P < 0.05$. * $P < 0.05$, ** $P < 0.001$, *** $P < 0.0001$. (b) Immunofluorescence analyses of pSTAT3 of tumor samples in Ov-*CLEC12B* injected mice compared with that of those injected with cells containing the EV (left panel) and in Sh*CLEC12B* injected mice compared with that of those injected with cells containing the EV' (right panel). Bar = $200 \mu\text{m}$. (c) Western blot analyses of STAT3 and p53 were performed with protein extracted from A375 tumor samples. β -Actin was used as the loading control. Sh*CLEC12B* was confirmed by quantitative real-time reverse transcriptase-PCR, as shown in the histograms. * $P < 0.05$, ** $P < 0.001$, *** $P < 0.0001$. EV, empty vector; Ov, overexpressing vector; pSTAT, phosphorylated signal transducer and activator of transcription; r.u., relative unit; Sh, silencing vector; STAT, signal transducer and activator of transcription.

demonstrated role in the regulation of p53/p21/p27. We further studied the role of *CLEC12B* in the cell cycle to better understand the mechanisms involved in its regulation of melanoma cell proliferation. The percentage of cells in the

G0–G1 phase of the cell cycle increased significantly in Ov-*CLEC12B* A375 cells (Figure 3c, upper panel). In contrast, the percentage of cells in the S phase decreased significantly in Sh*CLEC12B* cells (Figure 3c, lower panel). In accordance

with these results, western blot analysis showed elevated levels of p21, p27, and p53 in Ov-*CLEC12B* A375 cells (Figure 3d, left panel). Conversely, the level of these proteins was reduced when *CLEC12B* was silenced (Figure 3d, right panel). We also explored the effect of *CLEC12B* modulation in skMEL28 and M229 melanoma cell lines, which are inactivated for p53 and have shown similar effects on proliferation to those of p53 WT cells (data not shown). Furthermore, we have shown that p21 is increased independently of p53 and, importantly, that in cell lines mutated or not for p53, the inhibition of phosphorylated STAT3 mediates the effects of *CLEC12B* (Supplementary Figure S5). These results are in accordance with data from literature reporting that STAT3 acts on p53 but also directly on p21 (Humbert et al., 2015). Furthermore, using a lentivirus expressing a constitutively active form of STAT3, we were able to rescue the effects of Ov-*CLEC12B* on the levels of p53 and p21, allowing us to conclude that the effects of *CLEC12B* modulation observed are directly related to STAT3 (Figure 3e). Moreover, immunofluorescence staining of tissues, including nevi, primary melanoma, and lymph node metastases, revealed that the phosphorylated Y Y705 levels of STAT3 were inversely correlated with the level of *CLEC12B* (Figure 4). These data strongly support that the STAT3 is the major effector of *CLEC12B* regulation of proliferation.

Finally, we analyzed the tumorigenic properties of *CLEC12B* in Swiss nude mice. Tumor size was monitored for 36 days after inoculation of A375 cell lines transduced with an empty vector, an Ov-*CLEC12B*, or an Sh. In accordance with the in vitro results, tumor growth and volume in the Ov group were significantly lower than in the vehicle control group empty vector and the opposite was true for Sh compared with the corresponding empty vector (Figure 5a, left and right panels, respectively). Immunofluorescence analyses of the tumor samples showed that *CLEC12B* lowered the level of phosphorylated STAT3 in vivo (Figure 5b, left panel, and Supplementary Figure S6). Western blot analysis of the protein extracted from the tumors confirmed that Ov-*CLEC12B* decreased the phosphorylated STAT3 and increased p53 levels (Figure 5c, left panel), whereas the opposite was true after Sh*CLEC12B* (Figure 5b and c, right panels).

DISCUSSION

CLEC12B, a C-type lectin receptor, mainly known for its role in myeloid cells (Hoffmann et al., 2007), remains poorly studied and characterized. *CLEC12B* is also a gene predominantly expressed by melanocytes in the skin that has profound effects on melanogenesis (Sormani et al., unpublished data). In this study, we also show that *CLEC12B* plays an important role in human melanoma. *CLEC12B* has a marked effect on melanoma proliferation by activating SHP2 and downstream STAT3 signaling. In accordance with these antiproliferative effects, we observed a significant decrease in *CLEC12B* expression in melanoma in multiple public databases and confirmed this in tissues from patients with melanoma. The decreased *CLEC12B* expression is mostly observed in the late stages of the disease and in metastases, whereas most cells of thin melanoma still expressed *CLEC12B*. This suggests that the decrease of *CLEC12B* is not involved in the transformation of melanocytic cells but

confers proliferative assets in later stages when cells are getting more dedifferentiated.

STATs mediate essential signaling pathways and are involved in many cancers (Groner and von Manstein, 2017; Heppler and Frank, 2017). Among the STATs, STAT3 appears to be of critical importance in several solid cancers, including melanoma (Liu et al., 2018; Xie et al., 2006). SHP2 is the main inhibitor of STAT3 by inducing its dephosphorylation (Bard-Chapeau et al., 2011; Kim et al., 2018). *CLEC12B* appears to be of great interest in counteracting melanoma by recruiting SHP2 and acting downstream of STATs, notably phosphorylated STAT3. Although data on the oncogenic role of STAT3 are unambiguous, the role of SHP2 in cancer remains uncertain, showing both oncogenic and tumor-suppressive properties (Frankson et al., 2017; Kim et al., 2018; Zhang et al., 2015). Most of the beneficial effects of SHP2 are associated with its regulation of STATs. *PTPN11*, which encodes SHP2, acts as an oncogene through its activation of the MAPK pathway in *BRAF* WT melanomas (Hill et al., 2019). Furthermore, SHP2 inhibitors have been reported to reduce tumor growth in a xenografted mouse model of melanoma by preventing MAPK activation (Zhang et al., 2016). However, *PTPN11* shows either tumor-promoting or -suppressing roles, depending on the context (Li et al., 2012). Thus, in hepatocarcinoma, SHP2 acts as a tumor suppressor gene by inhibiting the activation of STAT3 (Bard-Chapeau et al., 2011). We observed no modification of extracellular signal-regulated kinase or phosphorylated extracellular signal-regulated kinase levels when *CLEC12B* was overexpressed or downregulated in melanoma cells (WT or *BRAF* mutated). Importantly, *CLEC12B* induced transient activation of SHP2, which rapidly dephosphorylated itself, as previously reported (Stein-Gerlach et al., 1995). Most *PTPN11* mutations in melanoma are missense mutations clustered in the interacting portions of the amino N-SH2 and phosphorylated Y phosphatase domains, leading to a constitutively active conformation (Tartaglia et al., 2001). It is possible that in melanoma, in which the MAPK pathway is highly modulated by many proteins, transient activation of SHP2 by *CLEC12B* may not affect the activation of the MAPK pathway. On the other hand, phosphatases, particularly SHP2, are the main endogenous regulators of STAT3 activation. Altogether, our data show that *CLEC12B* regulates melanoma growth by recruiting SHP2 that further inactivates STAT3 and downstream induces a p53-independent increase of p21. This is in accordance with our in vitro but also in vivo results that show a profound reduction of tumor growth associated with inhibition of phosphorylated STAT3 expression in Ov-*CLEC12B* tumor cells. These marked antiproliferative in vivo effects suggest that *CLEC12B* may have additional roles in melanoma cells and in melanocytes in general, fostering new fields of research.

Overall, we show that the recruitment of SHP2 by *CLEC12B* through its ITIM domain strongly decreases STAT activation in vitro and in vivo, thus leading to a marked decrease in tumor growth. Thus, *CLEC12B* provides a

potential marker for melanoma progression and prognosis and appears as a potential new therapeutic target.

MATERIALS AND METHODS

A comprehensive and detailed description of all methods used in this study is also provided in the [Supplementary Materials and Methods](#).

Cell lines

The human melanoma cell lines A375 (CRL-1619), MeWo (≠HTB-65), and SKMEL28 (HTB-72) were purchased from the ATCC (Molsheim, France). M229 was a kind gift from S. Tartare-Deckert (Université Nice Côte d'Azur, INSERM, U1065, Centre Méditerranéen de Médecine Moléculaire, Nice, France) (Gembarska et al., 2012).

Normal human melanocytes were obtained from the foreskin of young children undergoing circumcision. Patient melanoma cells were extracted from tissues obtained from surgical waste from patients diagnosed with metastatic melanoma ([Supplementary Table S1](#)).

Human materials

For all patient samples, written informed consent was obtained from each patient, and the study was approved by the hospital ethics committee (Nice Hospital Center and University of Nice, Sophia Antipolis, France, number 210-2998).

Lentivirus production and transduction

For the overexpression of *CLEC12B*, we used *CLEC12B* Lentiviral Vector pLenti-GIII-CMV-GFP-2A-Puro (catalog number LV796325, Applied Biological Materials, Richmond, Canada) custom (CDS of *CLEC12B* accession number NM_001129998 - transcript variant 1) and the control plasmid pLenti-CMV-GFP-2A-Puro-Blank Vector (Applied Biological Materials) (LV590). For the Sh*CLEC12B*, we used MISSION shRNA plasmid DNA (Sigma-Aldrich, St. Louis, MO). For the overexpression of STAT3, we used the Lentiviral construct EF.STAT3C.Ubc.GFP (gift from Linzhao Cheng, Addgene plasmid # 24983).

Site-directed mutagenesis of CLEC12B

The CLEC12B Y→F mutation was generated by site-directed mutagenesis (QuikChange II XL Site-Directed Mutagenesis; Stratagene, Agilent Technologies, Les Ulis, France), according to the kit manufacturer's instructions. The following primers were used (the substituted nucleotides are shown in bold and underlined): CLEC12B Y→F-forward: 5'-GTCTGAAGAAGTGACCTTCGCGA-CACTCACATTTTC-3' and CLEC12B Y→F-reverse: 5'-GAAATGTGAGTGTCGCGAAGGTCACCTTCTTCAGAC-3'. Mutations were verified by DNA sequencing (MWG-Eurofins; Eurofins Genomics Germany GmbH, Ebersberg, Germany).

In vivo experiments

Animal care and use for this study were performed in accordance with the recommendations of the European Community (2010/63/UE) for the care and use of laboratory animals. Experimental procedures were specifically approved by the ethics committee of the Institut Curie CEEA-IC #118 (CEEA-IC 2016-001) in compliance with the international guidelines.

Statistical analyses

Statistical analyses were performed using GraphPad Prism 6 software (GraphPad Software, San Diego, CA). Mann-Whitney nonparametric analysis was used to test unpaired differences between two groups.

Statistical significance is represented in the figures as * $P < 0.05$, ** $P < 0.001$, or *** $P < 0.0001$.

Data availability statement

Datasets related to this article are public (GSE112509, GSE4587); they were not generated from our laboratories and are cited appropriately.

ORCIDiS

Henri Montaudié: <https://orcid.org/0000-0002-0528-4829>
 Laura Sormani: <http://orcid.org/0000-0002-0838-2088>
 Bérengère Dadone-Montaudié: <http://orcid.org/0000-0002-0339-4602>
 Marjorie Heim: <http://orcid.org/0000-0002-7858-4822>
 Nathalie Cardot-Leccia: <http://orcid.org/0000-0001-8192-8545>
 Meri K. Tulic: <http://orcid.org/0000-0002-2661-2369>
 Guillaume Beranger: <http://orcid.org/0000-0001-8770-864X>
 Anne-Sophie Gay: <http://orcid.org/0000-0002-2229-5271>
 Delphine Debayle: <http://orcid.org/0000-0003-2807-9198>
 Yann Cheli: <http://orcid.org/0000-0001-9839-4332>
 Jérémy H. Raymond: <http://orcid.org/0000-0002-8712-895X>
 Pierre Sohier: <http://orcid.org/0000-0002-2341-6848>
 Valérie Petit: <http://orcid.org/0000-0003-1645-9396>
 Stéphane Rocchi: <http://orcid.org/0000-0002-0943-1304>
 Franck Gesbert: <http://orcid.org/0000-0002-5800-8385>
 Lionel Larue: <http://orcid.org/0000-0002-2010-6107>
 Thierry Passeron: <http://orcid.org/0000-0002-0797-6570>

CONFLICT OF INTEREST

The authors state no conflict of interest.

ACKNOWLEDGMENTS

We sincerely thank Sophie Leboucher (Institut Curie, Centre de Recherche, Plateforme d'Histologie, Paris, France) for her help with the immunofluorescence staining, Charlène Lasli (Institut Curie, Plateforme Cytométrie, Paris, France) for her help with the cytometry analysis, and Sandrine Destree and Arnaud Borderie for their help with the immunohistochemical analysis. This work was supported by the Institut national de la santé et de la recherche médicale and grants from the French Society of Dermatology, Collège des Enseignants en Dermatologie de France, Ligue Contre le Cancer, INCa, ITMO Cancer, and Fondation ARC and is under the program Investissements d'Avenir launched by the French Government and implemented by the ANR Labex CelTisPhyBio (ANR-11-LABX-0038 and ANR-10-IDEX-0001-02 PSL).

AUTHOR CONTRIBUTIONS

Conceptualization: LL, TP; Formal Analysis: PS, JHR; Funding Acquisition: LL, TP; Investigation: HM, MH, BDM, NCL, GB, ASG, DD, YC, VP, FG, LS; Supervision: LL, TP; Validation: HM, LL, TP; Visualization: HM, LL, TP; Writing - Original Draft Preparation: HM, LL, TP; Writing - Review and Editing: FG, MKT, BDM, PS, JHR, SR

SUPPLEMENTARY MATERIAL

Supplementary material is linked to the online version of the paper at www.jidonline.org, and at <https://doi.org/10.1016/j.jid.2021.05.035>.

REFERENCES

- Bard-Chapeau EA, Li S, Ding J, Zhang SS, Zhu HH, Princen F, et al. Ptpn11/Shp2 acts as a tumor suppressor in hepatocellular carcinogenesis. *Cancer Cell* 2011;19:629–39.
- Cai T, Kuang Y, Zhang C, Zhang Z, Chen L, Li B, et al. Glucose-6-phosphate dehydrogenase and NADPH oxidase 4 control STAT3 activity in melanoma cells through a pathway involving reactive oxygen species, c-SRC and SHP2. *Am J Cancer Res* 2015;5:1610–20.
- Chong ZZ, Maiese K. The Src homology 2 domain tyrosine phosphatases SHP-1 and SHP-2: diversified control of cell growth, inflammation, and injury. *Histol Histopathol* 2007;22:1251–67.
- Frankson R, Yu ZH, Bai Y, Li Q, Zhang RY, Zhang ZY. Therapeutic targeting of oncogenic tyrosine phosphatases. *Cancer Res* 2017;77:5701–5.
- Gembarska A, Luciani F, Fedele C, Russell EA, Dewaele M, Villar S, et al. MDM4 is a key therapeutic target in cutaneous melanoma. *Nat Med* 2012;18:1239–47.
- Groner B, von Manstein V. Jak Stat signaling and cancer: opportunities, benefits and side effects of targeted inhibition. *Mol Cell Endocrinol* 2017;451:1–14.

- Grossmann KS, Rosário M, Birchmeier C, Birchmeier W. The tyrosine phosphatase Shp2 in development and cancer. *Adv Cancer Res* 2010;106:53–89.
- Heppler LN, Frank DA. Targeting oncogenic transcription factors: therapeutic implications of endogenous STAT inhibitors. *Trends Cancer* 2017;3:816–27.
- Hill KS, Roberts ER, Wang X, Marin E, Park TD, Son S, et al. *PTPN11* plays oncogenic roles and is a therapeutic target for *BRAF* wild-type melanomas. *Mol Cancer Res* 2019;17:583–93.
- Hoffmann SC, Schellack C, Textor S, Konold S, Schmitz D, Cerwenka A, et al. Identification of CLEC12B, an inhibitory receptor on myeloid cells. *J Biol Chem* 2007;282:22370–5.
- Humbert L, Ghozlan M, Canaff L, Tian J, Lebrun JJ. The leukemia inhibitory factor (LIF) and p21 mediate the TGF β tumor suppressive effects in human cutaneous melanoma. *BMC Cancer* 2015;15:200.
- Kim M, Morales LD, Jang IS, Cho YY, Kim DJ. Protein tyrosine phosphatases as potential regulators of STAT3 signaling. *Int J Mol Sci* 2018;19:2708.
- Kunz M, Löffler-Wirth H, Dannemann M, Willscher E, Doose G, Kelso J, et al. RNA-seq analysis identifies different transcriptomic types and developmental trajectories of primary melanomas. *Oncogene* 2018;37:6136–51.
- Li S, Hsu DD, Wang H, Feng GS. Dual faces of SH2-containing protein-tyrosine phosphatase Shp2/PTPN11 in tumorigenesis. *Front Med* 2012;6:275–9.
- Liu J, Qu X, Shao L, Hu Y, Yu X, Lan P, et al. Pim-3 enhances melanoma cell migration and invasion by promoting STAT3 phosphorylation. *Cancer Biol Ther* 2018;19:160–8.
- Michielin O, van Akkooi ACJ, Ascierto PA, Dummer R, Keilholz U, ESMO Guidelines Committee. Cutaneous melanoma: ESMO Clinical Practice Guidelines for diagnosis, treatment and follow-up[†]. *Ann Oncol* 2019;30:1884–901.
- Regazzetti C, Joly F, Marty C, Rivier M, Mehl B, Reiniche P, et al. Transcriptional analysis of vitiligo skin reveals the alteration of WNT pathway: a promising target for repigmenting vitiligo patients. *J Invest Dermatol* 2015;135:3105–14.
- Stein-Gerlach M, Kharitonov A, Vogel W, Ali S, Ullrich A. Protein-tyrosine phosphatase 1D modulates its own state of tyrosine phosphorylation. *J Biol Chem* 1995;270:24635–7.
- Tartaglia M, Mehler EL, Goldberg R, Zampino G, Brunner HG, Kremer H, et al. Mutations in *PTPN11*, encoding the protein tyrosine phosphatase SHP-2, cause Noonan syndrome [published correction appears in *Nat Genet* 2001;29:491 and *Nat Genet* 2002;30:123]. *Nat Genet* 2001;29:465–8.
- Thomas SJ, Snowden JA, Zeidler MP, Danson SJ. The role of JAK/STAT signalling in the pathogenesis, prognosis and treatment of solid tumours. *Br J Cancer* 2015;113:365–71.
- Xie TX, Huang FJ, Aldape KD, Kang SH, Liu M, Gershenwald JE, et al. Activation of stat3 in human melanoma promotes brain metastasis. *Cancer Res* 2006;66:3188–96.
- Zhang J, Zhang F, Niu R. Functions of Shp2 in cancer. *J Cell Mol Med* 2015;19:2075–83.
- Zhang RY, Yu ZH, Zeng L, Zhang S, Bai Y, Miao J, et al. SHP2 phosphatase as a novel therapeutic target for melanoma treatment. *Oncotarget* 2016;7:73817–29.

B. Revue : Targeting GPCRs & their signaling as a therapeutic option in melanoma

Targeting GPCRs & their signaling as a therapeutic option in melanoma

J.H.Raymond, V. Delmas, L.Larue^{1,2,3}

(1) Institut Curie, PSL Research University, INSERM U1021, Normal and Pathological Development of Melanocytes, Orsay, France, (2) Univ Paris-Saclay, CNRS UMR 3347, Orsay, France, (3) Equipe Labellisée Ligue Contre le Cancer

Abstract

G protein-coupled receptors (GPCRs) serve prominent roles in melanocyte lineage physiology, with an impact at all stages of development, as well as on mature melanocyte functions. GPCR ligands are present in the skin and regulate melanocyte homeostasis, including pigmentation. The role of GPCRs in the regulation of pigmentation and, consequently, protection against external aggression, such as ultraviolet radiation, has long been established. However, evidence of new functions of GPCRs directly in melanomagenesis has been highlighted in recent years. GPCRs are coupled, through their intracellular domains, to heterotrimeric G proteins, which induce cellular signaling through various pathways. Such signaling modulates essential cellular processes of melanomagenesis, such as proliferation and migration. GPCR-associated signaling in melanoma can be activated by the binding of paracrine factors to their receptors or directly by activating mutations. In this review, we present melanoma-associated alterations of GPCRs and their downstream signaling and discuss the various preclinical models used to evaluate new therapeutic approaches against GPCR activity in melanoma. Recent striking advances in our understanding of the structure, function, and regulation of GPCRs will undoubtedly broaden treatment options in melanoma in the future.

Introduction

G protein-coupled receptors (GPCRs) participate in intercellular communication by receiving extracellular stimuli from the microenvironment. They then amplify and transduce the signal, passing it on to the nucleus, where it triggers an appropriate cellular response. GPCRs can bind to a wide variety of ligands (hormones, proteins, peptides, amino acids, lipids, nucleotides, xenobiotics, etc.) and regulate numerous essential physiological processes during development and in adult life. GPCRs are the largest receptor family in the mammalian genome, with over 800 members (Hu et al., 2017). The GPCR family is composed of receptors that share a common structure consisting of seven transmembrane helices and are associated with a heterotrimeric G protein. These receptors are known to regulate many essential physiological processes and their aberrant expression or activity can contribute to human disease, including cancer. GPCRs are among the most common drug targets because they can be activated or blocked by low molecular weight molecules that have a very strong interaction with their receptors. Their importance in drug discovery is demonstrated by the fact that nearly 60% of drugs in the developmental stage and 36% of currently marketed drugs target human GPCRs, representing ~700 molecules (Hauser et al., 2017). However, only 10 molecules are used in cancer therapy and none have yet been approved for melanoma (Usman et al., 2020).

Melanoma is a skin cancer that arises from melanocytes, the cells responsible for pigmentation. It affects more than 320,000 people worldwide each year, resulting in the death of nearly 60,000 patients (Sung et al., 2021). According to the International Agency for Research on Cancer of the WHO, the incidence is expected to continue to rise in the coming years, reaching half a million patients by 2040. Mortality estimates are also on the rise, with 97,000 deaths estimated for 2040, despite the appearance of new therapies in the second half of the 2010s (Sung et al., 2021). These treatments are based on two approaches: 1) inhibition of the MAPK/ERK pathway in melanoma using a combination of BRAF and MEK activation inhibitors – targeted therapy (TT) - and 2) inhibition of immune cell exhaustion using the checkpoint inhibitors iCTL4 and iPD1 – immunotherapy (IT) - (Luke et al., 2017). Although these treatments have significantly increased patient survival, they do not prevent half of patients from relapsing (Carlino et al., 2021). Furthermore, despite significant recent progress in both targeted therapies and immunotherapies for treating advanced-stage disease, the long-term prognosis for patients with cutaneous melanoma is still poor. An effective,

reliable cure of melanoma undoubtedly requires further therapeutic innovation. Moreover, 40-60% patients are not responsive to current treatments.

GPCRs play crucial roles in various physiological processes, including neurotransmission, cardiac and sensory function, immune responses, and regulation of the pigmentary system. Aside from its cosmetic role, pigmentation is a natural sunscreen that potently absorbs ultraviolet radiation (UVR) and is among the most important factors that determine UV sensitivity and melanoma risk. The melanin pigments responsible for the color of the skin and hair are synthesized within the melanosomes of melanocytes. In the epidermis, melanosomes synthesized by melanocytes are transferred to keratinocytes to allow homogenous pigmentation and protection of the entire skin against UVR. Melanocytes, keratinocytes, and dermal fibroblasts communicate with each other via secreted factors and cell-to-cell contact. The crosstalk of the various signaling pathways between these cells constitutes a complex network that controls pigmentation and melanocyte homeostasis. Genetics and *in vitro* studies have identified loci that regulate pigmentation, among them, certain key regulators belonging to the GPCR family. For example, the identification of the mouse extension locus (extension, recessive yellow, or *Mc1r*) associated with cloning of the melanocortin 1 receptor (*MC1R*) gene in human melanocytes identified this GPCR as the primary regulator of pigment synthesis. Apart from its effects on melanin production and, consequently, UVR protection, the *MC1R* has functions extending beyond pigmentation that explain how *MC1R* activity is directly involved in multiple aspects of melanomagenesis.

In contrast to epidermal melanocytes, which have a long life span and low proliferative capacity during adult life, the precursor cells of melanocytes, called melanoblasts, proliferate and actively migrate during embryonic development to colonize the entire skin. Many signaling molecules/ligands are required during all stages of melanocyte development. These ligands educate neural crest cells (NCCs) to specify the melanocytic fate and instruct melanoblasts to proliferate, migrate, survive, and home (final destination) prior to terminal differentiation into pigmented melanocytes. Approximately 100 genes have been shown to be specifically involved in melanocyte development, among them, two GPCRs that play a key role, the ET3/EDNRB (endothelin 3 ligand and its receptor, endothelin receptor type B) and WNT/FZL/ β -catenin (Wnt1/3A and frizzled receptors, with one of its mediators, β -catenin). Of note, the molecular and cellular mechanisms involved in the proliferation

and migration of melanoblasts during development and those of melanoma cells during tumor progression are often closely related. Therefore, it is not surprising to find that key regulators of melanocyte development are also important players of melanomagenesis. The objective of this review is to provide an update on the GPCRs that have an important, well-identified role in melanomagenesis and to discuss the therapeutic strategies that have been used.

1. Impact of GPCRs on melanoma initiation and progression

1.a. Melanomagenesis

During a multi-step process, known as melanomagenesis, skin melanocytes are transformed into melanoma. Briefly, the first steps consist of the benign proliferation of melanocytes to form a nevus, in which the melanocytes are grouped together and lose their characteristic contacts with keratinocytes. The melanocytes in the nevus eventually stop proliferating and become senescent. As melanomagenesis continues, nevus melanocytes are able to bypass senescence and enter the radial growth phase (RGP), where they typically superficially proliferate toward the basement membrane of the epidermis. These primary steps can be defined as "melanoma initiation". Then, during the vertical growth phase (VGP), melanoma cells continue to actively proliferate and acquire migratory and invasive properties, allowing them to cross the basement membrane and invade the dermis. The cells eventually acquire metastatic characteristics as they enter the bloodstream and/or lymphatic vessels and eventually colonize various tissues and organs. These latter stages can be considered as the "progression" of the disease. Melanomagenesis is associated with changes in many cellular processes, such as proliferation, immortalization, pseudo-epithelial-mesenchymal transition, migration, and invasion. Cutaneous melanomas are molecularly classified into four groups based on their mutations: BRAF, RAS, NF1, and the "triple wildtype". All four genomic subtypes of cutaneous melanoma are associated with aberrant activation of the MAPK and/or PI3K/AKT pathway that supports tumor cell growth, proliferation, survival, and anti-apoptotic signals.

The only effective way to demonstrate the causal role of a gene in tumor initiation is to use animal models. Their use allows a better understanding of tumor progression in a physiological context. Indeed, it is very difficult, if not impossible, to reproduce the cell-cell organization and microenvironment *in vitro*. However, simple or

complex *in vitro* models are very useful for deciphering the involvement of key genetic elements in various cellular processes but cannot be used to determine the causal role of a gene in tumorigenesis because (i) established melanoma cell lines are often derived from metastases in which the cells have already undergone a complete transformation process, (ii) the cells are grown on plastic, without their microenvironment, and (iii) colonization of distant organs is very difficult or impossible to assess. Various animal models allow evaluation of the proliferation and bypass of senescence (initiation) and invasion and metastasis (progression). Several animal models have been used to better understand melanomagenesis, including mouse, dog, pig, horse, chicken, and zebrafish. In this review, we focus on the currently best studied mouse models for melanomagenesis.

1.b. GPCRs in melanoma

GPCRs regulate many key biological functions, such as cell differentiation, proliferation, migration, and metabolic activity. Thus, it is not surprising that they play a role in tumorigenesis, including melanomagenesis (Lee and Chen, 2008). There are four main mechanisms by which GPCRs can drive tumorigenesis: (i) excess ligand availability, (ii) excess GPCR expression, (iii) activating mutations in GPCRs, and (iv) activating mutations in G α proteins.

The role of certain GPCRs during melanomagenesis has been studied using natural (or chemically induced) mouse mutants of genes of interest or novel engineered gain- and loss-of-function mutants. A list of mouse mutants with pigmentation phenotypes is available and regularly updated (<http://www.ifpcs.org/colorgenes/>) (Baxter et al. 2019). In the case of genetically modified mutants, targeting of the melanocytic lineage is performed using tyrosinase (Tyr), tyrosinase related protein 1 (Typr1), dopachrome tautomerase (Dct), or microphthalmia-associated transcription factor (Mitf) promoters/enhancers in the transgenic constructs (Aktary et al., 2018). Cre recombinase is used to generate conditional mutants, which are required when genes are essential in other lineages and/or during development: Tyr::Cre, Tyr::CreER^{T2-Lar}, and Tyr::CreER^{T2-Bos} (Delmas et al, 2003; Yajima et al., 2006; Bosenberg et al., 2006).

The known GPCRs involved in melanomagenesis are presented in the following section. The role of certain GPCRs in melanocyte transformation is predictable, given their key function in melanocyte development and homeostasis (ET/EDNRB,

MSH/MC1R, WNT/FZD), whereas the involvement of others in melanomagenesis was less expected (GLU).

1.b.1. Endothelin receptor type B

The endothelin (ET) system consists of two class A G-protein-coupled receptors, endothelin receptors type A and B (EDNRA and EDNRB, respectively) and their three similar peptide ligands, endothelin-1, -2, and -3 (ET1, 2,3). The EDNRB is the predominant receptor expressed by melanocytes/melanomas and binds all ETs with the same affinity. *Edn3* and *EdnrB* were first found to play a major role during the development of melanocytes from NCCs using genetic knockout mouse models and then, by analogy, of the classic mouse mutants, piebald and lethal spotting (Baynash et al., 1994; Hosoda et al., 1994). Indeed, *EdnrB* and *Edn3* genetically engineered mice (GEM) are both allelic to the spontaneous mouse mutations that occur at the piebald and lethal spotting loci. Recessive mutants at either of these loci give rise to similar phenotypes consisting of differing degrees of hypopigmentation and aganglionic megacolon due to the absence of enteric ganglia, which have the same neural crest embryonic origin as melanocytes. Reciprocally, increased expression of *Edn3* in the epidermis leads to increased numbers of melanocytes and hyperpigmentation (Garcia et al.; 2008). Germline *EdnrB* deletion does not lead to tumorigenesis but to the absence of melanocytes, mainly in the dermis. The role of *EdnrB* in melanomagenesis has been evaluated in the context of oncogenic *GNAQ*^{Q209L} signaling (see next paragraph). The expression of *GNAQ*^{Q209L} (encoding for Gq) is not sufficient to replace *EdnrB* signaling during embryonic development, suggesting that Gq may not be the only G protein activated downstream of *EdnrB* (or other signaling pathways). Using a conditional knockout approach, *GNAQ*^{Q209L}-induced melanomagenesis is inhibited in the absence of *EdnrB*, including lung metastases (*Mitf-cre/+*; *Rosa-fs-GNAQ*^{Q209L/+}; *EdnrB*^{F/F} background). Intriguingly, germline haploinsufficiency for *EdnrB* has the opposite effect in the RET mouse melanoma model (*Metallothionein-1/RFP-RET*; *EdnrB* (+/-) mice), in which it accelerates tumorigenesis, with an increase in lung metastases (Kumasaka et al., 2010). These two mouse models are of interest and clearly show that *EdnrB* expression affects melanomagenesis but have the disadvantage of representing an uncommon oncogenic situation in cutaneous melanoma, consisting of haploinsufficiency or the lack of *EdnrB* combined with a *GNAQ*^{Q209L} driver mutation or with increased RET signaling, which is not observed in

human melanoma, reducing the clinical relevance of this model.

Interest in *Ednrb* in melanoma stems primarily from early observations in humans showing that EDNBR expression was positively associated with cutaneous melanoma progression; EDNBR mRNA and protein levels were found to increase from common nevi to dysplastic nevi and from primary to metastatic melanoma (Demunter, 2001). Consistent with this observation, *in vitro* experiments showed that ET promoted melanoma cell proliferation, migration, and invasion and that EDNBR inhibitors reduced melanoma cell growth and survival in culture and xenografts (Asundi 2011; Lahav 1999, 2004). However, overexpression of *Ednrb* alone or combined with driver mutations was not performed in mice to genetically address its role in tumorigenesis.

Another aspect of ET signaling in melanoma is its activity in DNA repair, which has a role in reducing the genotoxic effect of UVR (Swope et al., 2019). Indeed, ET signaling increases intracellular Ca^{2+} mobilization, and downstream activation of the stress-induced MAP kinases JNK and p38, which enhances the repair of cyclobutane pyrimidines (CPDs), the major form of DNA photoproducts, in UV-irradiated human melanocytes (von Koschembahr et al., 2015). Finally, a recent study has suggested that ET signaling has a multifunctional role in melanoma, acting on both tumorigenic and stromal cells, where it mediates immunosuppression (Freitas et al., 2021). Thus, although the role of EDNBR signaling is relatively well understood during melanocyte development, its role in malignant transformation is much less clear, as it acts in multiple signaling pathways and is context dependent. Thus, it is not surprising that therapies that target EDNBR have thus far not been very successful. Small-molecule inhibitors of EDNBR, A-192621 and BQ788, were shown to inhibit the growth and survival of melanoma cells in culture and in xenografts (Bagnato et al., 2004; Lahav et al., 1999; 2004). However, the dual EDNRA/EDNBR antagonist, Bosentan, was tested in phase II clinical trials and failed to produce a robust response in cutaneous melanoma patients in the clinic, either alone or in combination with dacarbazine (Kefford et al., 2007, 2010). Similarly, A-192621 treatment of mice expressing *Ednrb* in the context of oncogenic GNAQ^{Q209L} showed no effect on tumorigenesis, whereas haploinsufficiency for *Ednrb* reduced it. Targeting EDNBR with an antibody-drug conjugate (DEDN6526A) is currently being tested in phase I (Sandhu S, 2020). It would be of great interest to generate a mouse model that reflects the human *EdnRB* situation in cutaneous melanoma: overexpression of *EdnRB* (human and mouse) in

melanocytes/melanoma combined with oncogenic BRAF^{V600E} or NRAS^{Q61K/R}, the major driver mutations in human cutaneous melanoma. Such models would allow a better understanding of the effect of Ednrb overexpression on melanomagenesis, the study of its downstream signaling, and the testing inhibitors in a human relevant preclinical mouse model before clinical trials.

1.b.2. The melanocortin receptor

Melanocytes exhibit a receptor (MC1R) that controls melanogenesis. The MC1R belongs to a small subfamily of GPCRs, classified into five subtypes (MCR1-5) that contribute to important physiological processes. MC1R is the only melanocortin receptor expressed in melanocytes. MC1R is a class A receptor and coupled to G_s protein. MC1R binds to the pro-opiomelanocortin-derived peptide α -melanocyte-stimulating hormone (α -MSH), resulting in the activation of downstream signaling cascades in a cAMP-PKA-dependent manner (Garcia-Borrón 2014). Upon UV exposure, α -MSH is released by keratinocytes, leading to stimulation of the MC1R at the melanocyte membrane, the activation of protein kinase A (PKA), and ultimately, to increased cAMP levels. An important target of cAMP is the transcription factor CREB (cAMP-responsive element-binding protein), which becomes phosphorylated and then activates the promoter of the *MITF*, which in turn up-regulates the transcription of the melanogenesis enzyme genes *Tyr*, *Tyrp1*, and *Dct*, as well as those regulating other cellular processes, including proliferation, invasion and metabolism (Bertolotto et al., 1998, Goding and Arnheiter 2019). MC1R is the product of the gene located at the *extension* locus and stimulates the synthesis of the pigment, eumelanin (black, brown). The loss-of-function mutation in this locus, *recessive yellow* (*e/e*), results in the production of pheomelanin (yellow, red) instead of eumelanin (Tamate and Takeuchi, 1984). An MC1R antagonist is the agouti signaling protein (ASP). Mutations in the mouse *Agouti* gene that cause increased and ectopic expression of ASIP (*viable yellow*, *A^{VY}*) result in yellow coat color, similar to the phenotype of *e/e* mice, as well as obesity due to ASIP binding to the MC4R. In humans, more than 200 MC1R variants have been identified and high numbers of natural MC1R variants are strongly associated with pigmentary phenotypes, providing evidence that the MC1R is the main determinant of human pigmentation and central to eu- and pheo-melanin regulation (Garcia-Borrón 2014). Similarly to mice, MC1R variants in humans can result in the

reduction of receptor activity and a shift in melanin synthesis from eumelanin to pheomelanin. MC1R is inactivated in people with red hair, due to mutation(s) that make(s) them more susceptible to melanoma than dark-skinned individuals. For example, variants of the gene encoding *MC1R*, mainly R151C, R160W, and D294H, have been shown to be associated with light and poorly pigmented skin (Smith et al., 1998), whereas the WT form is associated with dark, highly pigmented skin (Harding et al., 2000; Scott et al., 2002). These variants decrease the sensitivity of the receptor and binding of the hormone α -MSH, produced by keratinocytes in response to UVR. Epidemiology studies have strongly established that the *MC1R* functions as a melanoma predisposition gene. However, it is still not clear whether this is due to the lack of eumelanin, with photoprotective and antioxidant activities, or the expression of pheomelanin, which is known to amplify UVA-induced reactive oxygen species (ROS), or other functions not related to pigmentation. Indeed, pheomelanin was shown to promote melanomagenesis via the induction of oxidative DNA damage, without exposure to any carcinogens, such as UVR, in mice harboring the activating *Braf*^{V600E} mutation combined with *MC1R*^{e/e} (Mitra et al., 2012). Thus, loss of function of *MC1R* promotes initiation in UV-independent manner, demonstrating its tumor suppressor activity and a key role in the initiation of melanoma. Apart from its central role in pigment switching, it is now recognized that *MC1R* has non-pigmentary roles in antioxidant defenses and DNA-repair mechanisms (Swope and Abdel-Malek 2016). The cAMP pathway enhances melanocyte nucleotide excision repair (NER) activity, which operates by a « cut and patch » mechanism, to remove UV lesions. Activation of the *MC1R* by α -MSH binding results in phosphorylation of the DNA damage sensors ataxia telangiectasia mutated (ATM) and Rad3 related (ATR), as well as recruitment of the xeroderma pigmentosum complementing proteins XPC (Group C) and XPA (Group A) (Swope et al. 2020). Consistent with *MC1R* promoting DNA damage repair, impairment of the NER pathway in subjects carrying a *MC1R* loss-of function mutation has been observed. Additional non-pigmentation-related effects of *MC1R* can be attributed to the activation of MITF expression, which controls genes involved in DNA damage repair, chromosome stability, and centromere integrity (Guida and Goding, 2021).

Therapies involving defective *MC1R* signaling aim to restore its activities. Mouse mutants of *MC1R* have been characterized for years and can be used to

evaluate therapies for better protection against UVR. Topical application of the cAMP permeable-inducer forskolin onto mice harboring loss-of-function mutations or haploinsufficiency of $Mc1r^{e/e}$ stimulated eumelanogenesis and induced UV-resistance (D’Orazio et al., 2006, Bautista et al., 2020). These studies confirmed epidemiological studies suggesting that MC1R haploinsufficiency increases mutagenic susceptibility to UVR and melanoma risk. Another therapeutic approach is to use MC1R agonists to increase pigmentation, antioxidant defense, and DNA repair. The best-known analogue is NDP-MSH, which is 100 times more potent than α -MSH and is currently used to treat photosensitivity diseases, such as erythropoietic protoporphyria (EPP). A very promising analog is the tripeptide (LK-514), which is $> 10^5$ times more selective for MC1R than other melanocortin receptors (Koikov 2021). The challenge of MC1R-based therapies is to use an analog that is highly specific to MC1R to prevent toxic effects due to the activation of other receptors and to avoid targeting expression of MC1R in non-melanocytes.

1.b.3. Glutamate receptors

Glutamate is the most abundant excitatory neurotransmitter in the human central nervous system, where it plays a critical role in intercellular communication. Glutamate receptors are also expressed in tissues outside of the nervous system and are involved in the modulation of various normal and pathological processes. The glutamate receptor family is divided into two major groups: ionotropic glutamate receptors (iGluRs) and metabotropic glutamate receptors (mGluRs). The mGluRs belong to the class C family of GPCRs, characterized by a large, globular, extracellular ligand-binding domain. The mGluR family consists of eight members (mGluR1-8), which are organized by sequence homology, signaling effectors, and general localization. Group I mGluRs, consisting of mGluR1 and mGluR5, are multi-coupling receptors that can signal through both the $G\alpha_q$ and $G\alpha_{i/o}$ pathways. Group II mGluRs consist of mGluR2 and mGluR3 and couple to the $G\alpha_{i/o}$ pathway. Group III mGluRs consist of mGluR4, mGluR6, mGluR7, and mGluR8 and couple to $G\alpha_{i/o}$ signaling pathways. Three members of the metabotropic glutamate receptors (mGluR1, mGluR5, mGluR3) have been clearly identified as regulators of melanomagenesis (see for review Eddy and Chen 2021).

The involvement of metabotropic glutamate receptors in melanomagenesis was initially revealed by chance in a complex study using insertional mutagenesis, leading

to aberrant expression of **mGluR1**. Surprisingly, the mouse developed metastatic melanoma, whereas mGluR1 is not detected in normal melanocytes in mice (Chen 1996). Confirming this initial observation, transgenic mice containing mGluR1 under the control of the Dct promoter (Dct::Grm1) developed melanoma with 100% penetrance (Pollock et al., 2003). Initially, no distant organ metastases were observed but disseminated cells were later detected in distant organs, such as the lung and liver (Schiffner et al. 2012). A conditional transgenic model using the tetracycline-regulated system to express mGluR1 in adulthood demonstrated that mGluR1 expression is required not only for the initiation of melanoma initiation but also for its progression *in vivo* (Ohtani Y et al., 2008). The gene encoding the human receptor (*GRM1*) is altered in melanoma by point mutations, amplification, and/or deletions. In humans, GRM1 expression is not detected in normal melanocytes but it is expressed in 80% of metastatic melanoma or cell lines. Chen et al. showed that mGluR1 and GRM1 expression results from activation of the MAPK and PI3K/AKT pathways, the main pathways activated in melanoma (Eddy and Chen 2021). Melanomas expressing mGluR1 show elevated levels of glutamate in the tumor microenvironment, contributing to hyperactivation of the receptor and its downstream effectors. The identification of this autocrine loop between mGluR1 expression and the secretion of glutamate led to clinical trials to test riluzole, known to reduce glutamate release and thus reduce activation of the receptor. No objective responses were observed. However, riluzole monotherapy showed more immune cell infiltrates in stable disease patients than those with progressive disease, suggesting that combining riluzole with immune checkpoint blockade therapy could enhance the efficacy of either agent alone. However, this has not yet been tested.

In contrast to mGluR1, **mGluR5** is normally expressed in both normal melanocytes and melanoma tumors. Transgenic mice overexpressing mGluR5 (Tyrop1-Grm5) present with multiple melanoma located on the tail, with 100% penetrance and metastases, demonstrating that mGluR5 drives melanoma initiation and progression (Choi et al., 2012). Of note, mice with mGluR1 or mGluR5 melanoma both exhibit tumor formation on the hairless skin, including the pinnae and tails, rather than on trunk areas, as observed for BRAF^{V600E} and NRAS^{Q61K} induced melanoma, suggesting that the origin of the transformed cell may not be identical (epidermal vs. hair follicle). No information concerning GRM5 in humans is available.

Exon capture sequencing of 734 GPCRs in malignant melanoma showed that

a third glutamate receptor, *GRM3* (encoding for **mGluR3**), is frequently mutated in human melanoma. The identification of the same mutation as G18E/R or M518I in multiple individuals suggests that these mutations may be “drivers” of the oncogenic process. Mutant GRM3 selectively regulates the phosphorylation of MEK, leading to increased anchorage-independent growth and migration (Prickett et al., 2011). Mutated GRM3 cells are more sensitive to MEK inhibitors. To date, no transgenic models with GRM3 mutants to study its effect on cellular transformation and sensitivity to MEK inhibitors have been developed. GRM3 mutants may contribute to melanomagenesis through cross talk between the cAMP and MAPK signaling pathways (Neto and Ceol 2018). The misexpression of two other glutamate receptors, **mGluR4** and **mGluR8**, has been detected in melanoma but their precise role has not yet been clearly demonstrated (Eddy and Chen, 2021). Over 60% of human melanomas express mGluRs, indicating the importance of glutamatergic signals in this type of tumor. It appears that glutamate receptors are not only involved in neuronal signaling and neuronal disorders but also in the transformation of the originating neural crest-derived cells, melanocytes, into melanoma.

1.b.4. The Wnt/Frizzled receptor

The Wnt (fusion of the words wingless and integrated) pathway is one of the most important signaling pathways during embryonic development and adult homeostasis and its deregulation has often been linked to cancer. Wnt proteins activate at least three different intracellular signaling pathways: the Wnt/ β -catenin (or canonical), Wnt/ Ca^{2+} , and Wnt/planar polarity pathways. The type of Wnt protein secreted determines which of these three signaling cascades is activated. The Wnt family contains at least 19 secreted cysteine-rich glycoproteins in humans. Wnt proteins bind to target cells via two families of receptors: the seven transmembrane receptors Frizzled (Fzd) and LDL-receptor-related proteins. The Frizzled (FZDs) receptors are comprised of ten members (FZD1–FZD10), most of which are coupled to the **β -catenin** (bcat) canonical signaling pathway. FZD receptors are frequently overexpressed in tumor tissues relative to normal tissues and are potentially associated with a poor prognosis. No FZD overexpression has been directly linked to melanoma, but its associated signaling with β -catenin clearly plays a central role in melanomagenesis. The Wnt pathway has been widely studied and reviewed. Here we provide the current

knowledge of Wnt/FZD signaling in melanoma, especially through the activity of bcat, which is encoded by *Ctnnb1* (Zhan et al., 2017 ; Larue and Delmas, 2006).

The Wnt/bcat pathway is essential for melanocyte development from NCCs (Dorsky et al., 1998). No natural mutants involving members of the WNT/bcat pathway have been found. Thus, evidence of the involvement of this pathway in melanocyte development comes from studies using newly engineered mice. WNT1 and WNT3a are expressed in the dorsal portion of the neural tube and bcat in melanoblasts at all stages of development. In particular, the ligands Wnt1 and Wnt3a are required for the specification, expansion, and differentiation of melanoblasts from NCCs (Ikeya et al., 1997; Dunn et al., 2000). bcat itself has been directly implicated in melanoblast determination in several models, with varying effects depending on the temporality of its activation (Dorsky et al., 2000; Hari et al., 2002). In mice, loss of bcat from pre-migratory NCCs (*Wnt1::Cre; Ctnnb1^{ex2-6^{F/F}}*) or melanoblasts (*Tyr::Cre; Ctnnb1^{ex2-6^{F/F}}*) induces the disappearance of melanoblasts (Hari et al., 2002; Luciani et al., 2011). Early activation of bcat signaling in pre-migratory NCCs via the use of a bcat-stabilizing template (*Wnt1::Cre; Ctnnb1 Δ ex3*) favors the sensory neuronal lineage at the expense of the melanocytic lineage (Hari et al., 2002; Lee et al., 2004b). On the contrary, activation in migratory NCCs (*Sox10::Cre; Ctnnb1^{ex3^{F/+}}*) promotes the melanocytic lineage, with the appearance of ectopic melanocytes in target organs of other lineages (Hari et al., 2012). The expression of a stabilized form of bcat (*Tyr::bcataut-mut-nls-egfp*) leads to mice with a ventral white coat area associated with a defect in melanoblast migration (Gallagher et al., 2013). Various bcat targets have been shown to be involved in cell proliferation and include the ubiquitous genes *Myc* and *CyclinD1* and the melanocyte-specific gene *Mitf-M*. The CMYC and cyclin D1 proteins induce cell proliferation. MITF-M is a regulator of cell-cycle genes, with opposing functions: it can exert either an antiproliferative or a proliferative effect, depending on the cellular context. In bcat-sta melanoblasts, stabilised bcat increases MITF-M levels, which may interfere with bcat transactivation, inhibiting the activation of CMYC and CyclinD1 and therefore reducing proliferation. bcat and MITF-M levels are likely maintained within a very narrow range during melanoblast development, with any reduction or increase, such as those observed in the bcat mutants, altering melanoblast proliferation. The multiplicity of roles for bcat raises questions about the nature of the mechanisms that allow a single signaling pathway to control so many different processes during development and tissue homeostasis. β -catenin has the ability to regulate the

transcription of numerous genes to exert its diverse roles. However, transcriptional responses to Wnt/bcat signaling are often highly specific to a given developmental stage, tissue, or cell lineage.

Melanoma was one of the first cancers in which *CTNNB1* mutations were identified. In mouse models, the activation of WNT/bcat signaling participates in the initiation of melanomagenesis but is not, alone, sufficient for initiation. Expression of a stabilized mutated bcat in melanocytes associated with a mutated human NRAS oncogene, constitutively activating the MAPK pathway, in a mouse model (Tyr::NRAS^{Q61K/°}; Tyr::bcat-mut/[°]) led to accelerated onset and increased the number of melanomas (Delmas et al., 2007). This property has been linked to the increased immortalization of melanocytes *in vitro* by the repression of p16 expression. In a *Braf*^{V600E}; *Pten*^{-/-}; *bcat*-KO (Tyr::CreER^{T2-Bos}; *Braf*^{CA}; *Pten*^{F/F}; *Ctnnb1ex2-6*^{F/F}) mouse model, in which β-catenin is inactivated, the occurrence of melanoma is strongly delayed relative to that in a *Braf*^{V600E}; *Pten*^{-/-} model (Damsky et al., 2011). In a *Braf*^{V600E}; *Pten*^{-/-}; *bcat*-STA (Tyr::CreER^{T2-Bos}; *Braf*^{CA}; *Pten*^{F/F}; *Ctnnb1ex3*^{F/F}) mouse model, in which bcat is activated, the occurrence of melanoma is accelerated (Damsky et al., 2011). In mouse models of *Braf*^{V600E}, *Pten*^{-/-}, and NRAS^{Q61R} melanoma, bcat activation increases the number of lung metastases, whereas bcat inactivation decreases the number of lymph-node and lung metastases (Damsky et al., 2011; Gallagher et al., 2013). In conclusion, the activation of bcat increases both the initiation and progression of melanoma in mouse models. Of note, in humans, several studies have linked the Wnt/bcat pathway to the antitumor immune response in melanoma (Shah et al., 2008; Spranger et al., 2015; Nsengimara et al., 2018).

1.b.5. Other GPCRs

Other GPCRs have been implicated in melanomagenesis, but their role in melanomagenesis has not been extensively evaluated, particularly *in vivo* using genetically modified mouse models.

* The protease-activated receptors (PARs) are a family of GPCRs comprised of four members (PAR1–4) involved in the regulation of various cellular processes, including inflammation and coagulation. Cleavage of **PAR1** (also known as the thrombin receptor) by thrombin activates the receptor and downstream signaling through multiple heterotrimeric G proteins such as Gq, Gi/o, and G12/13. In turn, MAPK, the phosphatidylinositol 3-kinase (PI3-K) signaling pathway, and

phospholipase C- β (PLC- β) are activated. Elevated PAR-1 expression during melanoma progression has been suggested to promote key processes that contribute to melanoma metastasis. Targeting PAR-1 reduced tumor growth and the metastases of melanoma cells in xenograft experiments (Villares et al., 2008). Overexpression of PAR-1, as well as the continuous activation of thrombin, promotes the upregulation of genes involved in adhesion, invasion, angiogenesis, and metastasis (Zigler et al., 2011). As PAR-1 signaling affects both melanoma cells and their microenvironment, it was considered to be an attractive therapeutic target for the treatment of melanoma patients. However therapeutic trials were not continue in melanoma due to the activity of PAR1 in coagulation.

* Chemokine receptors belong to the GPCR family and are classified into four groups, CXCR, CCR, XCR, and CX3CR. Each receptor can bind to several chemokines. A variety of chemokine receptors are expressed on the surface of both immune and tumor cells. Expression of **CXCR4**, **CCR7**, and **CCR10** on the surface of melanoma cells is associated with a poor prognosis (Jacquelot et al., 2018). Aside from their critical role in the immune response, chemokines and their receptors have been studied for their capacity to guide cancer cells to specific organs. Chemokines have chemotactic properties and can attract melanoma cells expressing their corresponding receptors. High concentrations of CXCL12, the ligand of CXCR4, are produced in the lungs and injected CXCR4-expressing B16 melanoma cells are able to efficiently colonize the lung. Such colonization is reduced in the presence of T22, a specific inhibitor of CXCR4 (Drury et al., 2011). In addition, a commercially available dermal filler, hyaluronic acid (HA)-based gel, loaded with CXCL12 was able to recruit and trap CXCR4-expressing B16 melanoma cells injected into mice, consequently leading to a reduction in lung metastases (Ierano et al., 2019). One hundred and thirty-eight (138) clinical trials with CXCR4 inhibitors are being/have been performed, none of which include(d) melanoma. In mice, the overexpression of CCR7 or CCR10 in B16 melanoma cells was shown to increase metastasis to the lymph nodes, which was blocked by neutralizing its ligand, CCL21, using a specific antibody (Jacquelot et al., 2018). However, most of these experiments used mouse B16 melanoma cells, which are not necessarily the best representative of human melanoma. The effect of the various chemokines on the immune response is not discussed here.

2. GPCR associated signaling in melanoma

The activation of GPCRs leads to modulation of the activity of cellular signaling pathways, marked by the production of second messengers. The first element of such signaling is the heterotrimeric G proteins to which these receptors are coupled through their intracellular domain. These G proteins consist of three subunits, $G\alpha$, $G\beta$, and $G\gamma$ (Hamm, 1998). The C-terminal subunit of the GPCR is responsible for the selectivity of receptor/G protein binding (Hamm, 1998; Martin et al., 1996). The G subunit is also responsible for the selectivity of downstream signaling pathways (Wettschureck and Offermanns, 2005). There is a total of 21 G subunits grouped into four subfamilies: $G\alpha_s$, $G\alpha_{i/o}$, $G\alpha_{q/11}$, and $G\alpha_{12/13}$.

GPCRs generally couple to a specific G protein but may interact with several different G proteins (Harding et al., 2000; Inoue et al., 2019). Coupling appears to be cell-dependent. Thus, a careful analysis of the downstream signaling is required for each cell type. Binding of a ligand to its GPCR causes a conformational change in the GPCR that is transmitted to the $G\alpha$ subunit, which exchanges the GDP to a GTP molecule. The binding of GTP induces the dissociation of $G\alpha$ from the $G\beta$ - $G\gamma$ subunits of the receptor. This dimer then modulates the activity of other intracellular proteins (Hamm, 1998). The $G\alpha$ GTP and $G\beta$ / $G\gamma$ complexes then generate different intracellular signals that included cAMP, inositol tri-phosphate, diacyl-glycerol, and Rho proteins. The different signaling pathways activated by GPCRs are detailed in Figure 1.

2.a. Signaling via cAMP

cAMP was the first second messenger to be discovered and regulates many downstream cellular processes (Sutherland and Rall, 1958, Sassone-Corsi 2012). Two classes of G subunit modulate intracellular cAMP levels, $G\alpha_s$ and $G\alpha_{i/o}$, with diametrically opposed effects (Wettschureck and Offermanns, 2005; Zaccolo et al., 2021). The enzyme responsible for cAMP production, adenylyl cyclase (ADCY), is a membrane-associated enzyme that converts ATP to cAMP (Hanoune and Defer, 2001; Zaccolo et al., 2021). The difference between $G\alpha_s$ and $G\alpha_{i/o}$ is due to the difference in the binding domain on the adenylyl cyclase: members of the $G\alpha_s$ family bind to the C2 intracellular domain of the adenylyl cyclase, which then activate its enzymatic activity, ultimately leading to an increase in intracellular cAMP levels (Dessauer et al., 1997). Conversely, members of the $G\alpha_{i/o}$ family bind to the C1 intracellular domain of the adenylyl cyclase, thereby inhibiting its activity.

The heterotrimeric G protein subfamily $G\alpha_s$ is composed of three members: $G\alpha_s$ and $G\alpha_{sxl}$, two splice variants of the *GNAS* gene, and $G\alpha_{olf}$, encoded by the *GNAL* gene (Wettschureck and Offermanns, 2005). Only $G\alpha_s$ is expressed in melanocytes and melanoma (Plagge et al., 2008) and is activated by an associated receptor, such as the MC1R (Sánchez-Más et al., 2005). Gain-of-function mutations of *GNAS* are clustered at amino-acids R201 and Q227, located in the pocket where GTPase activity is located, and induce the loss of intrinsic GTPase activity and maintain the $G\alpha_s$ protein in an activated state. Mutations of *GNAS* are frequently found in various tumors of the pancreas, kidney, and stomach but are more anecdotal in melanoma, affecting less than 1% of cases (Innamorati et al. 2018, The Cancer Genome Atlas Network, 2015). More strikingly, the *GNAS* T393C SNP polymorphism is associated with tumor progression in metastatic melanoma (Frey et al., 2010), as well as in other cancers, such as colorectal cancer or bladder cancer (Frey et al., 2005a, 2005b). The effect of this polymorphism on the activity of $G\alpha_s$ has not been evaluated nor on the oncogenic process. However, this observation suggests that $G\alpha_s$ inactivation favors melanoma progression.

The $G\alpha_{i/0}$ heterotrimeric G protein subfamily is composed of eight members: $G\alpha_{i1}$, $G\alpha_{i2}$, $G\alpha_{i3}$, $G\alpha_0$, $G\alpha_z$, $G\alpha_{t-r}$, $G\alpha_{t-c}$, and $G\alpha_{gust}$. However, only $G\alpha_{i1}$, $G\alpha_{i2}$, and $G\alpha_{i3}$ are expressed in melanocytes and melanoma, and encoded respectively by *GNAI1-3* (The Cancer Genome Atlas Network, 2015; Thul et al., 2017; Uhlen et al., 2017; Wettschureck and Offermanns, 2005). Gain-of-function mutations of *GNAI2* are clustered at amino-acids R179 and T182 and lead to constitutive activation of the $G\alpha_{i2}$ subunit by increasing the GTP binding capacity (Nishina et al., 1995; Pace et al., 1991). *GNAI2* is mostly involved in cell injury and inflammatory responses but these activating mutations can lead to tumors, depending on the cellular context, due to increased MAPK activity. $G\alpha_{i2}$ R179 and T182 mutations are found in 1.4% of melanoma patients (The Cancer Genome Atlas Network, 2015) but their impact has not yet been evaluated.

$G\alpha_s$ and $G\alpha_{i/0}$ directly regulate adenylyl cyclase. There are ten (10) enzymes encoded by ten (10) different *ADCY1-10* genes (Cooper, 2003 2017). All are membrane bound via their two series of six transmembrane helices (TM1 and TM2), followed by a cytoplasmic domain (C1 and C2, respectively). Only *ADCY10*, which is soluble, differs from the others, as its activation is GPCR independent, being activated

by bicarbonate and calcium (Kleinboelting et al., 2014). Most adenylate cyclases are expressed in melanoma, with the exception of ADCY5 and ADCY8 (The Cancer Genome Atlas Network, 2015; Uhlen et al., 2017). The expression of ADCY10 is unclear because, although teams have found the protein by IHC, databases suggest that the mRNA is absent (Magro et al., 2012; The Cancer Genome Atlas Network, 2015). It has been shown that metastatic melanomas express more ADCY1 mRNA than primary melanomas and that a high level of ADCY1 expression correlates with a poorer prognosis (Chen et al., 2019). Consistent with this observation, the silencing of ADCY1 *in vitro* in mucosal melanoma cell lines decreases the ability of cells to form clones in a colony-formation assay, as well as their migratory and invasive capacity (Ma et al., 2019). In xenograft experiments, decreased ADCY1 expression decreased subcutaneous cell growth, as well as colonization of the lung after the injection of melanoma cells into the tail vein of NOD/SCID mice (Ma et al., 2019). More generally, stimulation of adenylate cyclase activity by forskolin promotes tumor growth in the *Braf^{CA}/Pten^{-/-}* melanoma mouse model, whereas its pharmacological inhibition by SQ22536 leads to a decrease in tumor growth in a MAPK pathway-independent manner (Rodríguez et al., 2017, 2018). However, treatment of human primary and metastatic melanoma cell lines with SQ22536, even at high concentrations, does not alter cell survival. This implies that the targeting of transmembrane adenylate cyclase is not a feasible therapeutic strategy on its own. Adenylate cyclase activity is also involved in resistance to MAPK inhibitors. Indeed, treating BRAF^{V600E} melanoma cells with forskolin increases ADCY9 expression and cAMP synthesis, leading to greater resistance to MAPK inhibition (Johannessen et al., 2013).

The intracellular concentration of cAMP is negatively regulated by phosphodiesterases (PDEs), which hydrolyze cAMP to AMP, thus controlling the amplitude and duration of the signal. There are 11 families of PDEs (PDE1-11) encoded by a total of 21 different genes (Omori and Kotera, 2007). Specific PDE isoforms are located in different subcellular compartments, where they regulate cAMP levels. Indeed, cAMP does not freely diffuse across the cell but is rather produced in subcellular compartments. This feature has important consequences, allowing only appropriate targets to be activated in microdomains (Bang and Zippin, 2021).

In melanocytes, phosphodiesterase 4 (PD4E), more specifically its variant PD4ED3, is a direct target of MC1R-cAMP signaling, constituting a negative feedback mechanism (Khaled et al. 2010). Blocking PDE4D3 activity in conjunction with forskolin

treatment can efficiently restore cAMP levels and pigmentation in MC1R^{e/e} mice. In melanoma, the expression of numerous PDEs has been reported and their effect was initially shown on cell proliferation (Dumaz et al., 2011; Lin et al., 2013). Their specific functions in BRAF or NRAS-mutated melanoma highlight the connection between the cAMP and MAPK pathways (see below). The overexpression of PDE4 and, therefore, the inhibition of cAMP signaling is critical for MAPK activation by oncogenic RAS in melanoma (Dumaz et al., 2006; Marquette et al., 2011). In BRAF-mutated melanoma, the inhibition of PDE4 activity by pharmacological inhibitors or RNA interference decreases melanoma cell invasion by interacting with the focal adhesion kinase FAK (Delyon et al., 2017). Overall, 3.5% of solid tumors (including melanoma) have homozygous microdeletions of PDE4D associated with increased expression and a tumor-promoting effect (Lin et al., 2013). PDE4D expression is elevated in advanced melanoma and negatively associated with survival. More generally, inhibiting cAMP signaling through the expression of phosphodiesterases (PDE1, PDE2, PDE4, and PDE8) is associated with oncogenic progression in melanoma (Bang and Zippln, 2021). Whether phosphodiesterase inhibitors can prevent proliferation, invasion, or migration in melanoma needs to be evaluated in the future.

The main target of cAMP is protein kinase A (PKA) (Walsh et al., 1968; Wettschureck and Offermanns, 2005). PKA is a serine/threonine kinase composed of four subunits: two regulatory and two catalytic. There are four isoforms for both the regulatory (**RI α** , **RI β** , **RII α** , and **RII β**) and catalytic subunits (**C α** , **C β** , **C γ** , and **PRKX**), each isoform showing individual localization and specificity. All are expressed in melanocytes and melanomas (Skalhegg and Tasken, 2000). Binding of cAMP to the regulatory subunits induces their dissociation from the catalytic units, which become active and phosphorylate downstream targets (Taskén et al., 1997). More than 70% of patients with familial Carney complex carry three mutations associated with pathogenic features (82c->t, 491_492 deltg, c.709-2_709-7 delattttt) in the *PRKAR1A* gene, which encodes the RI α subunit (Liu et al., 2017). This mutation induces a dominant-negative action of the the regulatory subunit and in consequence a constitutive activation of the catalytic subunit of PKA. This autosomal dominant multiple neoplastic syndrome is marked by mottled pigmentation of the skin (Kirschner et al., 2000). Inactivating mutations of *PRKAR1A* lead to constitutive activation of the cAMP-PKA pathway through the loss of regulation of the catalytic subunits of PKA. In melanoma, mutations are found in 1.4% of cases, as well as loss of heterozygosity in 11.8% of patients (The

Cancer Genome Atlas Network, 2015). Furthermore, loss of function of *PRKAR1A* is found in epithelioid pigmented melanocytomas, a rare intermediate/borderline form of melanoma (Cohen et al., 2020). By comparing PKA activity in primary and metastatic melanoma cells, Beebe and colleagues suggested that PKA activity is higher in melanoma metastases (Beebe et al., 1993). The pharmacological inhibition of PKA induces the growth and invasion of melanoma cells (Hiramoto et al., 2014).

A large number of cytosolic and nuclear proteins have been identified as substrates for PKA (Sassone-Corsi, 2012). Importantly, PKA is located at the crossroads between cAMP and MAPK/ERK. Constitutive activation of cAMP leads to the phosphorylation and inactivation of CRAF by PKA in melanoma (Marquette et al., 2011). CRAF is important in maintaining activation of the MAPK pathway in RAS-mutated cancers because ERK1/2 has a negative feedback action through the phosphorylation of BRAF, which causes its inhibition (Dumaz et al., 2006; Lyons et al., 2013; Marquette et al., 2011). As a consequence, activation of MAPK pathways through CRAF requires that the cAMP pathway in melanoma cells be inactivated to release cAMP-mediated inhibition of CRAF. PKA can also directly phosphorylate BRAF on serine 365, dislocating the RAS/BRAF/KSR complex and thus activating BRAF (Takahashi et al., 2017). The catalytic α subunit renders BRAF^{V600E} melanoma cells resistant to MAPK inhibitors (Johannessen et al., 2013). The CRT3 protein, a co-activator of CREB that is phosphorylated and activated by PKA and ERK (Ostojic et al., 2021), lies at the interface between signaling through the cAMP and MAPK pathways. A knock-out mouse model for *Crc3* showed graying of the coat due to defects in melanocyte maturation (Ostojic et al., 2021). Mutations in *CRCT3* have been identified in 23% of human melanomas, most leading to an increase in its expression and activity and reduced patient survival (Ostojic et al., 2021). Thus, CRT3 inhibition could be beneficial for such patients.

The regulation of transcription by PKA is mainly achieved by the phosphorylation of CREB. CREB phosphorylation leads to dimerization of this transcription factor and its subsequent binding to cAMP response elements (CRE) in target genes and its interaction with transcription co-activators, such as CREB-binding protein (CBP) and p300. CRE binding sites are located in the promoter regions of many genes, including the master melanocyte regulator MITF (Bertolotto et al., 1998; Buscà and Ballotti, 2000). MITF regulates numerous major cellular processes, including pigmentation, growth, survival, migration, and invasion essential for melanogenesis

and melanomagenesis (Goding and Arnheiter, 2019). In melanoma, CREB overexpression is associated with transition from the radial to vertical growth phase (Mobley et al., 2012).

The inhibition of CREB in melanoma cell lines was shown to decrease metastasis formation after injection into the tail veins of mice (Xie et al., 1997; Dobroff et al., 2009). This loss of metastatic potential can be explained, in particular, by the loss of expression of the metalloproteinase MMP2 and the adhesion molecule MCAM/MUC18. Surprisingly, CREB, which generally acts as a transactivator, negatively regulates the transcription factor AP2 α and the gene encoding cysteine-rich protein 61 (CCN1/CYR61). In early publications, these two genes were considered to be tumor suppressor genes in melanoma but more recent studies have proposed that AP2 α and CYR61 facilitate melanoma progression (Braeuer et al., 2011; Chen et al., 2020; White et al., 2021). The RNA-editing enzyme adenosine deaminase acting on RNA1 (ADAR1) has been recently identified as a new target of CREB. Silencing ADAR1 enhances the invasiveness of melanoma cells (Nemlich et al., 2018). CREB has been associated with resistance to MAPK inhibitors. Phospho-CREB is restored in relapsing melanomas previously treated by MAPK inhibitors, possibly by the up-regulation of adipocyte enhancer-binding protein 1, AEBP1 (Johannessen et al., 2013). (Hu et al., 2013).

cAMP also targets the cAMP-activated exchange protein (**EPAC**) (Zhang et al., 2020a). EPAC is a guanine nucleotide exchange factor (GEF) for small GTPases, e.g. RAP1 (Ras-related protein 1). Activation of RAP1 occurs through the exchange of GDP for GTP (Sassone-Corsi, 2012; Zhang et al., 2020a). The consequences of EPAC activation on the growth of melanoma are still unclear and reports are conflicting. Indeed, pharmacological activation of EPAC using an EPAC-specific cAMP analog increases the growth of HMG cells (Narita et al., 2007) but has no effect on PMP melanoma (Hiramoto et al., 2014). The use of shRNA targeting Rap1 increases the growth and survival of cells derived from primary but not metastatic melanomas (Rodríguez et al., 2017). The current hypothesis is that the EPAC-Rap1 pathway is anti-proliferative in metastatic melanoma and pro-proliferative in primary melanoma (Rodríguez and Setaluri, 2018).

The last major effectors of cAMP are the cAMP-dependent ion channels: the cyclic nucleotide-gated ion channel (CNG) and the hyperpolarization-activated cyclic nucleotide-gated channel (HCN) (Fajardo et al., 2014; Zhang et al., 2020a). These

channels are relatively nonselective cation channels and have not yet been studied in melanoma.

2.b. Signaling via inositol tri-phosphate and diacyl-glycerol

Cellular levels of inositol tri-phosphate (IP3) and diacyl-glycerol are highly regulated by the stimulation of GPCRs of the $G\alpha_{q/11}$ class. This class contains four members: $G\alpha_q$, $G\alpha_{11}$, $G\alpha_{14}$, and $G\alpha_{16}$ (Wettschureck and Offermanns, 2005). All can be expressed in melanocytes and melanoma but only $G\alpha_q$ and $G\alpha_{11}$ are highly expressed in these cells (The Cancer Genome Atlas Network, 2015; Uhlen et al., 2017). Activation of the receptor induces the exchange of GDP bound to the alpha subunit for GTP, resulting in activation of this subunit. Mutations affecting G proteins of the $G\alpha_{q/11}$ class are almost systematically found in uveal melanoma, of which approximately 90% of metastatic uveal melanomas are mutated for $G\alpha_q$ or $G\alpha_{11}$ affecting mainly glutamine 209 in both proteins, but also, to a lesser extent, arginine 183 (Robertson et al., 2017; Van Raamsdonk et al., 2010). **GNAQ**, which is encoding $G\alpha_q$, is mutated in 50 to 85% of non-epithelial melanocytic lesions, including blue nevi and leptomeningeal melanocytic neoplasms, and **GNA11**, which is encoding $G\alpha_{11}$, mutations are more frequent in uveal melanomas. (Urtatiz and Van Raamsdonk 2016). These mutations are found at lower frequencies (~1-6%) In other types of cutaneous melanoma (O'Hayre et al., 2013; The Cancer Genome Atlas Network, 2015). Q209L/P and R183C/Q mutations in GNAQ or GNA11 affect the GTPase domain (Maziarz et al., 2018) but only Q209L/P mutations have actually been characterized. These mutations reduce the GTPase activity of the $G\alpha_q$ subunit and cause hyperactive signaling (Maziarz et al., 2018). Regardless of the tumor context, the mutations are mutually exclusive (Robertson et al., 2017) and are also mutually exclusive with BRAF and NRAS mutations. Of note, in uveal melanoma, mutations of CYSLTR2 (L129G), encoding a $G\alpha_{q/11}$ -coupled GPCR, are found in a mutually exclusive manner with $G\alpha_q$ and $G\alpha_{11}$ mutations in approximately 3% of patients. This mutation is also present in blue nevi (Möller et al., 2017; Robertson et al., 2017). This CYSLTR2^{L129G} mutation constitutively activates the receptor and thus downstream signaling. Depending on the murine models used and the cells targeted (neural crest cells or melanoblasts), embryonic $G\alpha_q^{\text{Q209L}}$ expression is able to induce a range of lesions from dermal hyperpigmentation to leptomeningeal melanocytoma, nevi, and dermal melanoma to

malignant uveal melanomas with lung invasion (Huang et al., 2015; Urtatiz et al., 2020). Similarly, postnatal expression of $G\alpha_{11}^{Q209L}$ in melanocytes induces hyperpigmented melanocytic lesions in the uveal tract, skin, and leptomeninges that progress to melanoma with lung invasion (Moore et al., 2018). Mice transplanted under the skin with $G\alpha_q$ mutated melanoma cells show inhibition of MAPK signaling and tumor growth following treatment with FR900359 (Annala et al., 2019). To date, the inhibition of uveal melanoma with FR900359 appears to be more potent than inhibition with YM254890 (Kostenis et al., 2020). The activation of $G\alpha_{q/11}$ is a mechanism of resistance to MAPK pathway inhibition through the overexpression of c-Jun (Ambrosini et al., 2012). These data are consistent with the gain in resistance to MAPK inhibitors shown by activation of EDNRB (Asundi et al., 2014). Conversely, inhibition of G_q by YM-254890 resulted in inhibition of MAPK signaling, with evidence of a rebound after 24 hours in xenograft experiments of uveal melanoma. Combined treatment with YM-254890 and a MEK inhibitor led to sustained MAPK inhibition and tumor shrinkage (Hitchman et al., 2021). A combination of PKC and MEK1 inhibitors is currently under clinical evaluation for solid tumors harboring GNAQ/11 mutations or PRKS fusions. (Phase I/II trials: NCT03947385).

The primary target of $G\alpha_{q/11}$ subunits is phospholipase C beta ($PLC\beta$) (Smrcka et al., 1991; Taylor et al., 1991; Waldo et al., 1991). This subfamily is encoded by four genes (*PLCB1-4*) encoding seven proteins, all of which have two isoforms, except $PLC\beta_3$ (Lyon and Tesmer, 2013). All $PLC\beta$ s are likely expressed in cutaneous melanoma (The Cancer Genome Atlas Network, 2015), whereas, only the *PLCB2-4* genes are expressed in uveal melanoma (Robertson et al., 2017). $PLC\beta$ s function by hydrolyzing membrane phosphatidylinositol-4,5-bisphosphates (PIP2) into inositol-1,4,5 trisphosphate (IP3) and diacyl glycerol (DAG) (Chua et al., 2017). $PLCB4$ mutations occur in approximately 5% of uveal melanoma and are mutually exclusive with *GNAQ*, *GNA11*, and *CYSLTR2* mutations (Johansson et al., 2016). $PLC\beta_4^{D630Y}$ mutations affect the Y domain of the catalytic core of $PLC4$ (Johansson et al., 2016). Their effect has not been precisely studied, but their exclusivity with the *GNAQ*, *GNA11*, and *CYSLTR2* mutations and its being downstream of these proteins suggest that $PLC\beta_4$ mutations have a similar effect on the oncogenicity of uveal melanomas (Johansson et al., 2016). Outside of the context of melanoma, the other PLC s have often been

shown to be associated with tumor progression en activation la migration ou en modulant l'immunité (Li et al., 2016; Sengelaub et al., 2016).

One of the two secondary messengers produced by PLCs is DAG, which remains anchored in the membrane. Phorbol esters, such as 12-O-tetradecanoyl phorbol-13-acetate (TPA) and phorbol 12-myristate 13-acetate (PMA), are synthetic analogues of DAG. TPA is essential for melanocyte growth *in vitro* (Arita et al., 1992; Petit et al., 2019; Tamura et al., 1987). Interestingly, the effect of TPA on the proliferation of melanoma cell lines appears to be cell dependent (Cooper, 2003; Iwasaki et al., 2017; Jørgensen et al., 2005; La Porta et al., 1998; Petit et al., 2019). PMA increases cell survival and invasion and resistance to anoikis (Dissanayake et al., 2007; Jørgensen et al., 2005; Zhao et al., 2000). TPA and PMA activate the PKC and MAPK pathways (Jørgensen et al., 2005). The other secondary messenger produced by PLCs is IP3. The binding of IP3 to the IP3 receptor (IP3R) increases intracellular Ca²⁺ levels (Foskett et al., 2007). Calcium release induced by IP3 supports melanoma cell migration and invasion (Cox et al., 2002; Sun et al., 2014; Umemura et al., 2014).

DAG and calcium activate protein kinase C by binding to the C1 and C2 domains of PKC, respectively (Denning, 2012). There are nine genes that encode PKC: PKC α , PKC β , PKC γ , PKC δ , PKC θ , PKC ϵ , PKC η , PKC ι , and PKC ζ (Denning, 2012). They are divided into three classes according to their activation mechanism. The classical PKCs (cPKCs) consist of PKC α , PKC β , and PKC γ and are activated by calcium and DAGs. The novel PKCs (nPKCs) (PKC δ , PKC θ , PKC ϵ , PKC η) are activated by DAGs alone. Atypical PKCs (aPKCs) (PKC ι and PKC ζ) are not activated by calcium or DAGs (Denning, 2012). At least one PKC from each class is expressed in melanoma cells, except PKC γ (Denning, 2012; The Cancer Genome Atlas Network, 2015). PKC activity is regulated by the presence of their substrates and cofactors and their recruitment by scaffolding proteins, such as receptor for activated kinases C (RACK) or protein kinase A scaffolding protein 5 (AKAP5) (Hoshi et al., 2010; Park et al., 2004; Schechtman and Mochly-Rosen, 2001; Voris et al., 2010). PKC regulates invasion of melanoma cells but the various members have different effects: PKC α and PKC δ induce melanoma migration, invasion, and lung colonization (Matsuoka et al., 2009). Conversely, PKC β decreases invasion and promotes cell differentiation and pigmentation (Oka et al., 2008; Park et al., 1993). There are frequent mutations in *PRKCB* and loss of expression in melanoma but their impact on PKC β activity has not been evaluated

(Voris et al., 2010; The Cancer Genome Atlas Network, 2015). Similarly, the effect of PKC on cell growth is dependent of the isotype (Lau et al., 2012; Chen et al., 2017; Mhaidat et al., 2017).

Among the targets of PKC is Ras guanine-releasing protein 3 (RASGRP3), a guanine nucleotide exchange factor for RAS family proteins (Chen et al., 2017; Moore et al., 2018). PKC phosphorylates RASGRP3 on Thr 133, which contributes to its activation in conjunction with DAG binding (Aiba et al., 2004; Johnson et al., 2007; Teixeira et al., 2003). The inhibition of RASGRP3 induces the loss of GTP binding to RAS and thus its activity (Chen et al., 2017; Moore et al., 2018). This decrease in activity is accompanied by a decrease in MAPK pathway activity associated with a decrease in cell proliferation (Moore et al., 2018). This molecular mechanism may explain the activation of the MAPK pathway seen after PKC activation (Cozzi et al., 2006; Marín et al., 2006; Schönwasser et al., 1998; Tsubaki et al., 2007). PKC ϵ and PKC η are able to shunt the pharmacological inhibition of BRAF^{V600E}, rendering melanoma cells resistant to these drugs (Johannessen et al., 2010). Consistent with this finding, the use of PKC inhibitors inhibits the survival and migration of melanoma cells resistant to vemurafenib (Fu et al., 2020).

The activity of Yes-associated protein 1 (YAP1) is positively regulated by many GPCRs but negatively regulated by the Hippo pathway (Kwon et al., 2021; Yu et al., 2012a). In uveal melanoma, YAP1 is activated by Gq, inducing cell growth and survival (Huang et al., 2015; Yu et al., 2014; Feng et al., 2014). Inhibition of YAP activity by verteporfin reduces tumor growth (Feng et al., 2014; Yu et al., 2014). Gq activates the guanine nucleotide exchange factor TRIO, which in turn activates the small GTPases RhoA and Rac1 (Feng et al., 2014; Vaqué et al., 2013). This likely has a dual action: (i) the activation of FAK, which in turn inhibits the LATS1/2 kinase of the Hippo pathway, inactivating the action of YAP1, and (ii) the direct activation of YAP1 by releasing this angiomin transcription factor (AMOT) (Feng et al., 2014; Paradis et al., 2021). In uveal melanoma, the activation of Rho and Rac is linked to the activation of the MAP kinases JNK & p38 (Vaqué et al., 2013). JNK and p38 phosphorylate c-Jun and induce the expression of AP-1 targets (Shaulian and Karin, 2001). Phosphorylation of c-Jun induces cell proliferation via AP1 targets that regulate the cell cycle, such as cyclin D1, p53, p21cip1/Waf1, p19ARF, and p16 (Du et al., 2019; Estrada et al., 2009; Pathria et al., 2016; Shaulian and Karin, 2001). Activation of p38 and JNK are likely to be involved in mechanisms of resistance to MAPK inhibitors (Du et al., 2019; Estrada

et al., 2009). In cutaneous melanoma, the activation of YAP1 is required for cell invasion (Ma et al., 2021; Nallet-Staub et al., 2014; Zhang et al., 2020b; Zhao et al., 2021), as well as viability and resistance to anoikis (Ma et al., 2021; Nallet-Staub et al., 2014; Zhao et al., 2021). Although the effect of YAP1 on invasion is clearly documented, its effect on melanoma growth is still debated (Ma et al., 2021; Zhang et al., 2020c). YAP1 activity has also been shown to be associated with cell migration via regulation of the arp2/3 complex 3 (Lui et al., 2021; Ma et al., 2021). The invasive phenotype of melanoma cells has been correlated with the activation signature of YAP (Zhang et al., 2020b). *In vivo*, YAP1 activation induces the formation of very large numbers of metastases in the lungs after the injection of cells carrying the activating mutation of YAP1-5SA under the skin of mice (Zhang et al., 2020b). Lung colonization after the injection of cells into the tails of mice also decreases when YAP1 levels are genetically decreased (Nallet-Staub et al., 2014; Zhao et al., 2021). Most interestingly, inhibition of the Hippo pathway replicates this effect, favoring lung colonization (Tan et al., 2021). The pro-invasive action of YAP1 is mediated through the transcription of a number of its targets, such as CCN1, AXL, and THBS1 (Zhang et al., 2020b). These targets are well known in melanoma. AXL expression is associated with tumor growth and cell invasion and migration and has also been shown to be associated with resistance to MAPK inhibitors (Flem-Karlsen et al., 2020; Müller et al., 2014; Tizpa et al., 2020). CCN1 has been shown to be associated with increased metastatic potential and angiogenesis (Chen et al., 2020; Kunz et al., 2003). Genetic inhibition of THBS1 is associated with decreased cell invasion (Jayachandran et al., 2014; Borsotti et al., 2015). YAP1 requires the transcriptional cofactors TEAD1-4 to bind to its targets. Genetic inhibition of TEAD1-4 recapitulates the *in vitro* effects of YAP1 on invasion, with a clear decrease in the invasive capacity of melanoma cells (Verfaillie et al., 2015). TEAD1-4 are also involved in resistance to MAPK inhibitors and inhibition of all four TEADs sensitizes cells to these inhibitors (Verfaillie et al., 2015).

2.c. Signaling via $G\alpha_{12/13}$

The third major pathway of GPCR signaling involved in melanoma is the pathway involving $G\alpha_{12/13}$ (Wettschureck and Offermanns, 2005). This class of G subunits has two members, $G\alpha_{12}$ and $G\alpha_{13}$, encoded by the **GNA12** and **GNA13** genes, respectively. The expression of these genes is ubiquitous (The Cancer Genome Atlas

Network, 2015; Uhlen et al., 2017; Wettschureck and Offermanns, 2005). Activation of these subunits activates Rho-GEFs, such as leukemia-associated Rho-GEF (LARG) or p115 Rho-GEF (Hart et al., 1998; Suzuki et al., 2003). Activation is achieved by the attachment of the G12/13 subunit to the RH domain of Rho-GEFs (Chen et al., 2005). Once activated, Rho-GEFs induce RhoA activation (Suzuki et al., 1996; Fukuhara et al., 1999; Wells et al., 2002; Vogt et al., 2003). Rho is a converging point for $G\alpha_{12/13}$ and $G\alpha_{q/11}$ signaling (Vogt et al., 2003). Signaling induced downstream occurs through the activation of YAP1, as described above (Yu et al., 2012b). $G\alpha_{12/13}$ signaling has been poorly analyzed in the context of melanoma. PAR1 and 2 receptors, coupled to $G\alpha_{12/13}$ proteins, are expressed in melanoma (Elste and Petersen, 2010). Activation of PAR1 receptors by its ligand TRAP6 induces the activation of YAP1 in a HEK293A cell model (Mo et al., 2012). YAP1 activation subsequently leads to activation of RhoA and inhibition of LATS1 (Mo et al., 2012). Similar to $G\alpha_{q/11}$ signaling, $G\alpha_{12/13}$ signaling appears to increase invasion and migration while not altering cell growth (Kelly et al., 2006a, 2006b). However, these results were obtained in breast and prostate cancer and need to be confirmed in melanoma. Of note, activation of LPA receptors (LPA1-LPA6), coupled to $G_{12/13}$ receptors, is still poorly documented in melanoma, although it has been reported to enhance chemoresistance to drugs and increase the survival of melanoma cells in vitro (Minami et al., 2020).

2.d. Signaling via WNT/ β -catenin

The canonical WNT pathway is activated only in response to the formation of a complex containing WNT, FZD, and LRP. WNT proteins are difficult to purify in an active form and only a few antibodies are available for their detection. The WNT proteins most studied in the context of β -catenin activation in melanocyte/melanoma are WNT1 and WNT3a. WNT5a has different roles and acts as an antagonist or agonist of the canonical WNT/ β -catenin pathway, depending on the cellular context. WNT proteins are subject to post-translational modifications, including glycosylation and lipid modifications. Acylation on conserved serine and cysteine residues is required for WNT secretion and efficient binding to the Frizzled receptor (Willert et al., 2003; Takada et al., 2006). In the basal state, axin protein interacts through distinct domains with GSK-3, CK1 α , APC, and β -catenin. Axin is considered to be the limiting component of the β -catenin destruction complex (Salic et al., 2000; Lee et al., 2003).

Modulation of its levels would therefore be an effective way to regulate β -catenin destruction. APC is a large protein that interacts with both β -catenin and axin. It contains three axin-binding domains, interposed between armadillo repeat domains (ARMs), which bind to β -catenin. β -catenin is sequentially phosphorylated by CK1 α and GSK-3 on serines (S) and threonines (T) (S45, T41, S37, and S33) in the N-terminal region of the protein. β -catenin binds to and is ubiquitinated by β -TRCP1 before being degraded by the proteasome.

Binding of the WNT ligand leads to the dimerization of Frizzled with the coreceptor LRP5/6. This dimerization results in a conformational change of the receptors, leading to relocalization of the degradation complex to the cell membrane under the double interaction of axin with DVL (itself associated with Frizzled) and with the cytoplasmic end of LRP. Such membrane relocalization decreases the activity of the degradation complex, such that the amount of unphosphorylated cytoplasmic β -catenin rapidly increases. The stabilization of cytoplasmic β -catenin results in an increase in nuclear β -catenin. The balance between the amount of cytoplasmic and nuclear β -catenin is dynamic, resulting from multiple mechanisms of transport and retention between the two compartments. In the nucleus, β -catenin binds to the T-cell factor (TCF)/lymphoid enhancer-binding factor (LEF) family of transcription factors, which themselves are already associated with DNA. In the absence of β -catenin, TCF factors interact with transcriptional co-repressors of the Groucho/transducin-like enhancer of split (TLE) family and repress the expression of their target genes. Nuclear accumulation of β -catenin leads to the association of TCF with β -catenin, resulting in dissociation from Groucho/TLE1 and allowing the recruitment of other coactivators for transcriptional activation through its C-terminal transcriptional activation domain. Many transcription factors outside the TCF/LEF family of transcription factors have been reported to be capable of associating with β -catenin to activate or repress transcription. In melanocytes/melanoma, MITF interacts with β -catenin and redirects β -catenin-mediated transcriptional activity from canonical Wnt/ β -target genes to specific MITF target genes to activate their transcription. Other levels of cross-signaling between the WNT/ β -catenin pathway and MITF have been described. For example, it has been shown that β -catenin/TCF transcriptionally upregulates MITF expression (Dorsky et al., 2000). It has also been shown that MITF-M binds to and upregulates its own promoter through a direct interaction with LEF1 (Saito et al., 2002). Therefore, it would appear to be difficult to target β -catenin in melanoma without affecting MITF expression

and/or activity. MITF could potentially be an attractive target for melanoma therapy but the drug-targeting of MITF is highly challenging. As mentioned already, MITF is considered to be the "master gene" of melanocyte differentiation and has an essential role in the proliferation, survival, senescence, migration, invasion, DNA repair, and metabolism of melanoma cells (Kawakami and Fisher, 2017; Goding and Arnheiter, 2019). *Mitf* expression is regulated by multiple signaling pathways outside of the canonical Wnt/ β -catenin pathway, such as the cAMP/CREB, YAP1/PAX3, TGF β /GLI2, TNF/NF κ B pathways, and transcription factors, such as SOX10 and BRN2, themselves regulated by multiple pathways in melanoma. The basic concept in melanoma is that the proliferative and invasive states are defined, in part, by the high level/activity of MITF and low level/activity MITF, respectively. High and low MITF level/activity co-exist in melanoma tumors and the switch in MITF expression (high and low) is reversible and responsible for melanoma heterogeneity and plasticity. MITF is also involved in the resistance to BRAF inhibitors. One current view for the therapeutic strategy is to increase MITF levels and therefore those of melanoma antigens, such as MART-1 and GP-100, to increase the recognition of melanoma cells by T cells and improve the immune response (Ballotti et al., 2020). In any case, therapeutic strategies have to address the versatility and heterogeneity of melanoma cells.

2.e. Signaling via G β /G γ subunits

The activation of GPCRs mainly induces the activation of G α subunits, but also that of the G β /G γ complex. There are five G β subunits (G β ₁₋₅) in humans encoded by the *GNB1-5* genes. All except *GNB5* are expressed in melanoma (Wettschureck and Offermanns, 2005). There are 16 G γ subunits encoded by the *GNG1-16* genes, of which only G γ ₂, G γ ₄, G γ ₅, G γ ₆, G γ ₇, G γ ₁₀, G γ ₁₁, and G γ ₁₂ are expressed in melanoma (The Cancer Genome Atlas Network, 2015; Uhlen et al., 2017; Wettschureck and Offermanns, 2005). The significance of G β /G γ signaling in melanoma has not yet been fully assessed. There are two major molecular mechanisms induced by G β /G γ subunits: the modulation of cytosolic calcium concentrations and phosphoinositide 3-kinase (PI3K) signaling (Baljinnyam et al., 2011; Pfeil et al., 2020; New et al., 2007; Sellers et al., 2000). Calcium increase is due to PLC β activation (Bonacci et al., 2005). G β /G γ subunits bind to p110, the catalytic subunit of PI3K, and induce its activation (Leopoldt et al., 1998). PI3K activation induces AKT activation and increases cell

survival (Sellers et al., 2000). Given the known importance of the PI3K/AKT pathways in melanoma, its regulation by G β /G γ subunits needs to be further analyzed.

2.f. Biased signaling

At the end of the 1990s, it was observed that Src family tyrosine kinases are recruited by β -arrestins (encoded by *ARRB1-2* genes) to the adrenergic receptor 2a member of the GPCR family (Luttrell et al., 1999). Surprisingly, the binding of protein kinases induced activation of the MAPK/ERK pathway only if the receptor was internalized (Luttrell et al., 1999; Miller et al., 2000). Other observations in the mid-2000s showed that such signaling was non-canonical and independent of G proteins. Indeed, the activation of GPCRs activates three types of proteins: G proteins, GPCR protein kinases (GRKs), and arrestins. GRKs and arrestins are the most important elements involved in the termination of GPCR activation. GRKs phosphorylate the receptor on its C-terminal residues, which prevents the activation of G proteins (Krupnick et al., 1997). Such phosphorylation recruits the non-visual arrestins, β -arrestin 1 & 2, which in turn recruit clathrin, resulting in receptor internalization by clathrin coated-pits (Gurevich and Gurevich, 2015; Krupnick et al., 1997; Shenoy and Lefkowitz, 2003). Depending on the affinity of the GPCR/ β -arrestin complex, receptors can be recycled or degraded in the proteasome (Oakley et al., 2000). In early endosomes, the GPCR/ β -arrestin complex is able to form a signalosome by recruiting signaling proteins, such as members of the MAPK pathway (Miller and Lefkowitz, 2001; Shenoy and Lefkowitz, 2003, 2005). Several pathways can be activated, such as the MAPK/ERK and Src pathways (Luttrell et al., 1999; Zhai et al., 2005), AKT (Beaulieu et al., 2005), MAPK/JNK (McDonald et al., 2000), MAPK/p38 (Luttrell et al., 2001), or PDEs (Perry et al., 2002).

GRK-arrestin signaling has been poorly studied in melanoma. β -arrestin2 is able to bias MC1R signaling by promoting activation of the MAPK pathway towards that of cAMP-dependent signaling (Abrisqueta et al., 2013). A transcript of the MC1R (MC1R-203) naturally promotes such biased signaling toward the MAPK pathway (Martínez-Vicente et al., 2020). Mutants of metabolic glutamate receptors (mGluR3^{G848E}) can promote such biased signaling, characterized by prolonged internalization of the receptor (Abreu et al., 2021). This mutation is found in rare cases of cutaneous melanoma (< 1%) (The Cancer Genome Atlas Network, 2015). Conversely, in uveal

melanoma, the *CYSLTR2*^{L129Q} mutation forces signaling via $G\alpha_{q/11}$ and disfavors β -arrestin-biased signaling (Ceraudo et al., 2021). GPCR signaling is certainly much more complex than that presented here. Their interactions with GRKs and arrestins and the dynamics of their desensitization add another level of complexity that needs to be investigated in the future.

3. Perspectives of targeting GPCRs in melanoma

The molecular and cellular consequences of the activation of GPCRs in melanoma clearly indicate that they could be interesting targets for therapy. Targeting GPCRs has the advantage of seeking readily available membrane molecules instead of signaling proteins with molecules that need to cross the plasma membrane without deteriorating the intracellular environment and/or endocytotic vesicles and lysosomes (Bhullar et al., 2018; Menichetti et al., 2019; Sharma et al., 2018).

3.a. Limitation of available tools

Large-scale sequencing conducted by the cancer genome atlas consortium (TCGA) has shown that approximately 92% of the melanoma patients tested had at least one nonsense or missense mutation of at least one non-olfactory GPCR (Liu et al., 2019; The Cancer Genome Atlas Network, 2015). Each melanoma patient has an average of 10 mutated GPCRs (Liu et al., 2019; The Cancer Genome Atlas Network, 2015). The receptor function of the vast majority of these mutations is uncharacterized. A number of genes encoding GPCRs appear to be frequently mutated, such as *ADGRV1*, which is mutated in approximately 30% of patients but for which only a few recurrent mutations are found. None of these mutations are present at a high frequency in cutaneous melanoma - none exceeding 1%, with the most frequent being the uncharacterized *GPR139*^{R217C} mutation (Liu et al., 2019; The Cancer Genome Atlas Network, 2015). These data suggests that if we cannot offer patients a personalized and targeted therapy (one patient = one mutation = one drug), patients could be grouped by activated signaling for therapy that is still targeted but less personalized. This less direct choice of therapy would consider the positioning of the GPCR within the signaling pathways and targeting of the downstream node(s) (Campbell and Smrcka, 2018). Such a therapeutic option would also be attractive in the setting of patients who do not have mutated GPCRs but rather mutations in downstream signaling elements.

Receptor activation may result by a mechanism independent of the presence of a mutation in the gene. This could be related to overexpression or de novo expression of a receptor, which would induce a higher basal level of receptor activity, or activation of the receptor by the production of its ligand in the environment (Chidiac et al., 1994; de Ligt et al., 2000; Pozvek et al., 1997). Binding of the ligand to the receptor may occur in the primary melanoma in an autocrine/paracrine mode, with ligand production by the melanoma cell or by cells in the microenvironment (Wu et al., 2019). For example, activation of EDNRB by ET-1 secreted by surrounding melanoma cells induces reactivation of the MAPK pathway after BRAFi treatment (Smith et al., 2017). In this model, ET is secreted by melanoma cells and activates EDNRB in an autocrine and/or paracrine manner (Smith et al., 2017). Alternatively, ligand production may only occur at the metastatic site and thus only affect metastasis formation and not melanoma initiation (Ben-Baruch, 2009; Chen et al., 2018). Ligand production may attract tumor cells into the target tissue by chemoattraction, promote cell survival and/or proliferation, or induce resistance to drugs. In this perspective, ET-1 is highly expressed in the lungs and can promote the colonization of melanoma cells that express EDNRB in this organ. The reactivation of MAPK pathways by expression of EDNRB may occur at primary sites, as well as in distant organs. Ligand-dependent tissue expression can be observed, in particular, in the lungs, where only 50 highly expressed ligands are found (Fagerberg et al., 2014; Forrest et al., 2014; Melé et al., 2015; Pierson et al., 2015; Thul et al., 2017). An important limitation is our lack of knowledge about the level of gene expression in melanoma cells that colonize distant organs. Transcriptomic analyses would be extremely useful in determining which GPCRs are expressed in melanoma in distant metastases. The correlation of GPCR expression data in melanoma at sites of metastasis with expression in the target tissue of ligands for these GPCRs would allow the selection of potential receptors of interest.

An alternative to transcriptional analysis is likely to be the identification of GPCRs at metastatic sites on the basis of protein expression. However, the identification of GPCRs by immunolabeling is difficult, due to the small exposed area of extracellular epitopes and very high conformational variability, or by conventional mass spectrometry, as receptors are not readily isolatable from membranes (Jo and Jung, 2016; Latorraca et al., 2017; Pauwels et al., 2021).

The improvement of antibody-isolation technologies associated with our knowledge of GPCRs will lead to the generation of new, more selective antibodies.

The development of nanobodies appears to be promising for the detection and targeting of GPCRs (Alhosaini et al., 2021). The major limitation in the high-throughput identification of GPCRs via mass spectrometry is the depletion of GPCRs from mass spectrometry samples. This bias can be avoided by performing surfaceomes, which will significantly enrich samples for membrane glycoproteins and thus potentially reveal the expression of GPCRs (Kuhlmann et al., 2018; Pauwels et al., 2021; Sun et al., 2021). Finally, GPCRs can also be indirectly identified by analyzing cell-binding ligands rather than the receptors directly (Qin et al., 2018).

Data mining of the literature generates databases, such as TCGA. To date, current databases have been extremely useful for the identification of driver mutations in melanoma and prognostic biomarkers. However they are composed of 80% primary tumors or skin or lymphatic metastases (Liu et al., 2019; The Cancer Genome Atlas Network, 2015) and visceral, bone, and nervous system melanoma metastases are poorly represented. The presence of characteristic and highly aggressive mutations in distant metastasis may be hidden by the small sample size. Furthermore, current databases were generated before the generalization of current treatments and the samples constituting the large databases came from patients who were naive to any treatment with MAPK or checkpoint inhibitors. The changes in genetic/epigenetic expression due to such treatments could involve the activation of GPCR expression or the selection of subclones in which GPCR signaling is activated. The generation of databases enriched with samples from distant metastases and patients treated with MAPK and immune checkpoint, inhibitors would be of great interest to the scientific community.

Large-scale high-throughput screening using RNA interference or CRISPR-Cas9 could be performed to identify the dependence of melanoma cells on GPCRs for growth or invasion. Such screens can also be performed *in vivo*. To evaluate the role of specific GPCR, transplantation of genetically modified cells into animals would reveal the role of this GPCR in internal organs colonization and its role in melanoma progression (Crotty and Pipkin, 2015). Such screening could also be performed by generating transgenic animal models, but the experiments would become extremely complex, time consuming and expensive. Zebrafish may be a suitable model for these types of studies. Indeed, it is relatively easy to generate and maintain large groups of transgenic animals (Driever et al., 1996; Haffter et al., 1996; Keatinge et al., 2021; Trubiroha et al., 2018). Furthermore zebrafish express many of the GPCRs expressed

in humans, as well as their signaling machinery (Howe et al., 2013; Langenhan et al., 2015). In addition, there are already many melanoma models that could be used to test genetic modifications in melanoma-producing animals, for example, to assess the pro-metastatic effect (Frantz and Ceol, 2020; Patton et al., 2005, 2021).

3.b. Novel Structures and drug design approaches

To target efficiently GPCR, two parallel and complementary approaches are used: binding on GPCR of compounds that includes small molecules, antibodies and radiotherapies, and structure determination of the proteins. The structure of GPCR can be elucidated using X-ray crystallography, Cryo-EM, NMR and artificial intelligence.

A better knowledge of GPCR structure and molecular ligand-receptor interactions is critical for structure-based molecule design and the design of new receptor-activating agonist or antagonist molecules (Lee et al., 2018). Such structural knowledge needs to be as accurate as possible and is currently acquired by two main experimental methods and one predictive method (García-Nafría and Tate, 2020; Lee et al., 2018).

The first three-dimensional structure of a GPCR, rhodopsin, was solved by X-ray crystallization in 2000 (Okada et al., 2000). This method requires obtaining stable crystals of the receptor extracted from its membrane in solution, which has been a major obstacle to structure determination (Tate and Schertler, 2009). This problem has been solved by modifying GPCRs to make them more stable while retaining their activity (Lebon et al., 2011; Rosenbaum et al., 2007; Tate, 2010; Tate and Schertler, 2009). This can be achieved, for example, by fusing the T4 lysozyme protein as a replacement for intracellular loop 3 (Rosenbaum et al., 2007) or by mutating the receptor to thermostabilize it (Lebon et al., 2011). A new technique for crystal structure resolution has recently been developed, X-ray-free electron laser (XFEL) crystallography. The use of lasers reduces the size of the crystals required and, therefore, increases their stability (Ishchenko et al., 2019; Liu and Lee, 2019).

Crystallization has been completed by cryo-electromicroscopy (Cryo-EM). Significant improvements in detectors and structure determination algorithms have enabled the resolution of structures at the particle scale (McMullan et al., 2016; Vinothkumar and Henderson, 2016; Zivanov et al., 2018). Cryo-EM does not require the formation of crystals, as the receptors are directly vitrified after purification, but requires more computational time to solve the structure, resulting in lower resolution

(Congreve et al., 2020; Danev et al., 2021; García-Nafría and Tate, 2020; Zhang et al., 2021). These various constraints and the relative novelty of these techniques mean that, currently, the structure of only 20% of non-olfactory GPCRs has been solved (Congreve et al., 2020). Nuclear magnetic resonance (NMR) allows the acquisition of dynamic data and thus complements the data from the fixed structures of crystallography and Cryo-EM (Shimada et al., 2019).

More recently, advances in artificial intelligence have made it possible to approach structures using machine learning. Protein structure prediction was revolutionized in 2021 by the publication of the algorithms, not specific to GPCRs, *AlphaFold2* and *RoseTTA*, which generated highly accurate three-dimensional structures of proteins (Baek et al., 2021; Jumper et al., 2021; Tunyasuvunakool et al., 2021). These algorithms are completed by GPCR-specific algorithms, such as the already developed arsenal, which is specific to the GPCR field (Bender et al., 2020; Esguerra et al., 2016; Worth et al., 2017; Zhang et al., 2015). Nonetheless, although these algorithms all regularly perform well, they can still be improved. GPCRs differ, particularly in their loops, which results in a deficit for machine-learning algorithms and thus low confidence in the models and often false predictions (Bender et al., 2020; Mullard, 2021). Generating and publishing more receptor structures will increase both direct knowledge about receptors and knowledge about other receptors via increased substrates for algorithms and in-silico prediction. Predictions of molecular anchors in receptors can also be made by site-directed mutagenesis (SDM) studies to find amino acids that interact with known ligands of the receptor (Potterton et al., 2018; Zhou et al., 2019). Crystallization and SDM techniques can be used synergistically to better understand the binding of the molecule to the receptor and produce much more refined and/or efficient molecules (Di Roberto et al., 2017; Potterton et al., 2018; Zhou et al., 2019).

For the development of an effective therapy, stable, receptor-specific agonists or antagonists must be found. The screening of drug libraries is performed to find molecular scaffolds capable of binding to receptors and modulating their activity (Hughes et al., 2011). Screening can be performed using affinity assays by assessing the ability of molecules to bind to the target as purified proteins, on whole cells expressing the target, or on isolated membranes (von Ahsen and Bömer, 2005; Jones et al., 2020; Kitaeva et al., 2020). Purified proteins are free of binding to secondary targets, but the ability of the molecules to cross a membrane is not analyzed. Moreover,

the presence of the membrane is often necessary for receptor stability (Jones et al., 2020).

Affinity tests are based on the ability of molecules to displace - and replace on the receptor - a reference ligand known to bind the receptor. Detection is either by radio-labeling of the reference ligand, regularly labeled with iodine-125 or tritium (González et al., 2009; Uehara et al., 2011; Zhang and Xie, 2012) or by fluorescence resonance energy transfer (FRET), in which both the reference ligand and the receptor are bound to a fluorophore that allows resonance from one molecule to the other (Maurel et al., 2008; Valencia et al., 2017). Such screening is only able to identify ligands that bind to the same site as the competitor. To overcome this bias, the analysis of the activity of various elements of GPCR signaling, such as IP1 concentration for the $G\alpha_q$ pathway or cAMP for the $G\alpha_s$ pathway, can be jointly performed on a large scale (Titus et al., 2008; Trinquet et al., 2011). The activity of molecules on downstream G-protein signaling pathways can also be assessed using kinase assays from protein extracts or purified protein or by FRET (Katsuya et al., 2018; Lotta et al., 2019; Zindel et al., 2019). These screens can be virtually performed with high efficiency if the receptor structure is known (Liu and Jockers, 2020; Shoichet and Kobilka, 2012; Stein et al., 2020). The hits that are found are generally of low affinity for their targets and require optimization to be usable (Hughes et al., 2011). They will then need to undergo pharmaco-modulation that will be directed through structural data and docking algorithms to result in lead generation (Ebalunode et al., 2011; Green et al., 2021; Neves et al., 2018). These leads will have to be tested *in vivo* to verify their pharmacokinetic parameters (absorption, distribution, metabolism, elimination) at the risk of obtaining only molecules incapable of producing an effect *in vivo* and condemned to be used only as an *in vitro* tool (Chung et al., 2004; Guan et al., 2018). Molecules identified as leads can be used to verify the efficacy of these molecules on the cellular and molecular processes of melanoma progression, as well as on the formation of metastasis and resistance to treatment.

In addition to small chemical molecules, GPCRs can be targeted by monoclonal antibodies. Several have been generated and approved as therapeutic targets, such as mogamulizumab, a humanized antibody against chemokine receptor type 4. The advantage of using monoclonal antibodies in treating diseases is notable because they have a long half-life.

Finally, targeted radiotherapy is currently being developed and constitutes a promising strategy to target GPCRs in cancer. The radioactivity is delivered to a specific tumor by means of a systemic injection. For melanoma treatment, targeted treatment can be achieved by labeling small molecules, such as melanin ligands, peptides that recognize a specific receptor (MC1R), or antibodies (anti-melanin, anti-GD3)(Akil et al., 2021). The efficacy of targeted radiotherapy depends on the dose delivered, which in turn depends on the radionuclide used and the time that the labeled compound remains associated with the target. Targeted radiotherapy is highly relevant for the treatment of disseminated lesions and overcoming tumor heterogeneity through cross-fire irradiation with α -radionuclides characterized by a decay spectrum of between a few nanometers and 2mm. The reception of adequate doses of radiation from neighboring receptor-expressing cells can kill tumor cells lacking the targeted receptor in the tumor. This property is particularly important for melanoma, in which gene expression is often heterogeneous. Targeted radiotherapy of the somatostatin receptor is used for the clinical treatment of neuroendocrine tumors. The same strategy could be adapted for targeting GPCRs in melanoma.

References

- Abreu, N., Acosta-Ruiz, A., Xiang, G., and Levitz, J. (2021). Mechanisms of differential desensitization of metabotropic glutamate receptors. *Cell Reports* 35, 109050.
- Abrisqueta, M., Herraiz, C., Pérez Oliva, A.B., Sanchez-Laorden, B.L., Olivares, C., Jiménez-Cervantes, C., and García-Borrón, J.C. (2013). Differential and competitive regulation of human melanocortin 1 receptor signaling by β -arrestin isoforms. *J Cell Sci* 126, 3724–3737.
- von Ahsen, O., and Bömer, U. (2005). High-Throughput Screening for Kinase Inhibitors. *ChemBioChem* 6, 481–490.
- Aiba, Y., Oh-hora, M., Kiyonaka, S., Kimura, Y., Hijikata, A., Mori, Y., and Kurosaki, T. (2004). Activation of RasGRP3 by phosphorylation of Thr-133 is required for B cell receptor-mediated Ras activation. *Proc Natl Acad Sci U S A* 101, 16612–16617.
- Ambrosini, G., Pratilas, C.A., Qin, L.-X., Tadi, M., Surriga, O., Carvajal, R.D., and Schwartz, G.K. (2012). Identification of unique MEK-dependent genes in GNAQ mutant uveal melanoma involved in cell growth, tumor cell invasion and MEK-resistance. *Clin Cancer Res* 18, 3552–3561.
- Annala, S., Feng, X., Shridhar, N., Eryilmaz, F., Patt, J., Yang, J., Pfeil, E.M., Cervantes-Villagrana, R.D., Inoue, A., Häberlein, F., et al. (2019). Direct targeting of G α q and G α 11 oncoproteins in cancer cells. *Sci Signal* 12, eaau5948.

- Arita, Y., O'Driscoll, K.R., and Weinstein, I.B. (1992). Growth of Human Melanocyte Cultures Supported by 12-O-Tetradecanoylphorbol-13-acetate Is Mediated through Protein Kinase C Activation. *Cancer Res* 52, 4514–4521.
- Asundi, J., Lacap, J.A., Clark, S., Nannini, M., Roth, L., and Polakis, P. (2014). MAPK Pathway Inhibition Enhances the Efficacy of an Anti-Endothelin B Receptor Drug Conjugate by Inducing Target Expression in Melanoma. *Mol Cancer Ther* 13, 1599–1610.
- Baek, M., DiMaio, F., Anishchenko, I., Dauparas, J., Ovchinnikov, S., Lee, G.R., Wang, J., Cong, Q., Kinch, L.N., Schaeffer, R.D., et al. (2021). Accurate prediction of protein structures and interactions using a three-track neural network. *Science* 373, 871–876.
- Baljinnyam, E., Umemura, M., De Lorenzo, M.S., Xie, L.-H., Nowycky, M., Iwatsubo, M., Chen, S., Goydos, J.S., and Iwatsubo, K. (2011). Gβγ subunits inhibit Epac-induced melanoma cell migration. *BMC Cancer* 11, 256.
- Beaulieu, J.-M., Sotnikova, T.D., Marion, S., Lefkowitz, R.J., Gainetdinov, R.R., and Caron, M.G. (2005). An Akt/beta-arrestin 2/PP2A signaling complex mediates dopaminergic neurotransmission and behavior. *Cell* 122, 261–273.
- Beebe, S.J., Salomonsky, P., Holroyd, C., and Becker, D. (1993). Differential expression of cyclic AMP-dependent protein kinase isozymes in normal human melanocytes and malignant melanomas. *Cell Growth & Differentiation* 4, 1005.
- Ben-Baruch, A. (2009). Site-specific metastasis formation. *Cell Adh Migr* 3, 328–333.
- Bender, B.J., Marlow, B., and Meiler, J. (2020). Improving homology modeling from low-sequence identity templates in Rosetta: A case study in GPCRs. *PLoS Comput Biol* 16, e1007597.
- Bonacci, T.M., Ghosh, M., Malik, S., and Smrcka, A.V. (2005). Regulatory interactions between the amino terminus of G-protein betagamma subunits and the catalytic domain of phospholipase Cbeta2. *J Biol Chem* 280, 10174–10181.
- Borsotti, P., Ghilardi, C., Ostano, P., Silini, A., Dossi, R., Pinessi, D., Foglieni, C., Scatolini, M., Lacal, P.M., Ferrari, R., et al. (2015). Thrombospondin-1 is part of a Slug-independent motility and metastatic program in cutaneous melanoma, in association with VEGFR-1 and FGF-2. *Pigment Cell & Melanoma Research* 28, 73–81.
- Buscà, R., and Ballotti, R. (2000). Cyclic AMP a Key Messenger in the Regulation of Skin Pigmentation. *Pigment Cell Research* 13, 60–69.
- Campbell, A.P., and Smrcka, A.V. (2018). Targeting G protein-coupled receptor signalling by blocking G proteins. *Nat Rev Drug Discov* 17, 789–803.
- Carlino, M.S., Larkin, J., and Long, G.V. (2021). Immune checkpoint inhibitors in melanoma. *The Lancet* 398, 1002–1014.
- Ceraudo, E., Horioka, M., Mattheisen, J.M., Hitchman, T.D., Moore, A.R., Kazmi, M.A., Chi, P., Chen, Y., Sakmar, T.P., and Huber, T. (2021). Direct evidence that the GPCR CysLTR2 mutant causative of uveal melanoma is constitutively active with highly biased signaling. *J Biol Chem* 296, 100163.
- Chen, J., Wu, F., Shi, Y., Yang, D., Xu, M., Lai, Y., and Liu, Y. (2019). Identification of key candidate genes involved in melanoma metastasis. *Mol Med Rep* 20, 903–914.
- Chen, J., Zhou, X., Yang, J., Sun, Q., Liu, Y., Li, N., Zhang, Z., and Xu, H. (2020). Circ-GLI1 promotes metastasis in melanoma through interacting with p70S6K2 to activate

Hedgehog/GLI1 and Wnt/ β -catenin pathways and upregulate Cyr61. *Cell Death Dis* 11, 1–16.

Chen, W., Hoffmann, A.D., Liu, H., and Liu, X. (2018). Organotropism: new insights into molecular mechanisms of breast cancer metastasis. *Npj Precision Onc* 2, 1–12.

Chen, X., Wu, Q., Depeille, P., Chen, P., Thornton, S., Kalirai, H., Coupland, S.E., Roose, J.P., and Bastian, B.C. (2017). RasGRP3 Mediates MAPK Pathway Activation in GNAQ Mutant Uveal Melanoma. *Cancer Cell* 31, 685–696.e6.

Chen, Z., Singer, W.D., Sternweis, P.C., and Sprang, S.R. (2005). Structure of the p115RhoGEF rgRGS domain-Galpha13/i1 chimera complex suggests convergent evolution of a GTPase activator. *Nat Struct Mol Biol* 12, 191–197.

Chidiac, P., Hebert, T.E., Valiquette, M., Dennis, M., and Bouvier, M. (1994). Inverse agonist activity of beta-adrenergic antagonists. *Mol Pharmacol* 45, 490–499.

Chua, V., Lapadula, D., Randolph, C., Benovic, J.L., Wedegaertner, P.B., and Aplin, A.E. (2017). Dysregulated GPCR Signaling and Therapeutic Options in Uveal Melanoma. *Mol Cancer Res* 15, 501–506.

Chung, T.D.Y., Terry, D.B., and Smith, L.H. (2004). In Vitro and In Vivo Assessment of ADME and PK Properties During Lead Selection and Lead Optimization – Guidelines, Benchmarks and Rules of Thumb. In *Assay Guidance Manual*, S. Markossian, A. Grossman, K. Brimacombe, M. Arkin, D. Auld, C.P. Austin, J. Baell, T.D.Y. Chung, N.P. Coussens, J.L. Dahlin, et al., eds. (Bethesda (MD): Eli Lilly & Company and the National Center for Advancing Translational Sciences), p.

Cohen, J.N., Yeh, I., Mully, T.W., LeBoit, P.E., and McCalmont, T.H. (2020). Genomic and Clinicopathologic Characteristics of PRKAR1A-inactivated Melanomas: Toward Genetic Distinctions of Animal-type Melanoma/Pigment Synthesizing Melanoma. *Am J Surg Pathol* 44, 805–816.

Congreve, M., Graaf, C. de, Swain, N.A., and Tate, C.G. (2020). Impact of GPCR Structures on Drug Discovery. *Cell* 181, 81–91.

Cooper, D.M.F. (2003). Regulation and organization of adenylyl cyclases and cAMP. *Biochem J* 375, 517–529.

Cox, J.L., Lancaster, T., and Carlson, C.G. (2002). Changes in the motility of B16F10 melanoma cells induced by alterations in resting calcium influx. *Melanoma Research* 12, 211–219.

Cozzi, S.-J., Parsons, P.G., Ogbourne, S.M., Pedley, J., and Boyle, G.M. (2006). Induction of senescence in diterpene ester-treated melanoma cells via protein kinase C-dependent hyperactivation of the mitogen-activated protein kinase pathway. *Cancer Res* 66, 10083–10091.

Crotty, S., and Pipkin, M.E. (2015). In vivo RNAi screens: concepts and applications. *Trends Immunol* 36, 315–322.

Danev, R., Belousoff, M., Liang, Y.-L., Zhang, X., Eisenstein, F., Wootten, D., and Sexton, P.M. (2021). Routine sub-2.5 Å cryo-EM structure determination of GPCRs. *Nat Commun* 12, 4333.

Delyon, J., Servy, A., Laugier, F., André, J., Ortonne, N., Battistella, M., Mourah, S., Bensussan, A., Lebbé, C., and Dumaz, N. (2017). PDE4D promotes FAK-mediated cell invasion in BRAF-mutated melanoma. *Oncogene* 36, 3252–3262.

- Denning, M.F. (2012). Specifying protein kinase C functions in melanoma. *Pigment Cell & Melanoma Research* 25, 466–476.
- Dessauer, C.W., Scully, T.T., and Gilman, A.G. (1997). Interactions of Forskolin and ATP with the Cytosolic Domains of Mammalian Adenylyl Cyclase *. *Journal of Biological Chemistry* 272, 22272–22277.
- Di Roberto, R.B., Chang, B., and Peisajovich, S.G. (2017). The directed evolution of ligand specificity in a GPCR and the unequal contributions of efficacy and affinity. *Sci Rep* 7, 16012.
- Dissanayake, S.K., Wade, M., Johnson, C.E., O’Connell, M.P., Leotlela, P.D., French, A.D., Shah, K.V., Hewitt, K.J., Rosenthal, D.T., Indig, F.E., et al. (2007). The Wnt5A/Protein Kinase C Pathway Mediates Motility in Melanoma Cells via the Inhibition of Metastasis Suppressors and Initiation of an Epithelial to Mesenchymal Transition *. *Journal of Biological Chemistry* 282, 17259–17271.
- Dobroff, A.S., Wang, H., Melnikova, V.O., Villares, G.J., Zigler, M., Huang, L., and Bar-Eli, M. (2009). Silencing cAMP-response Element-binding Protein (CREB) Identifies CYR61 as a Tumor Suppressor Gene in Melanoma. *Journal of Biological Chemistry* 284, 26194–26206.
- Driever, W., Solnica-Krezel, L., Schier, A.F., Neuhauss, S.C., Malicki, J., Stemple, D.L., Stainier, D.Y., Zwartkuis, F., Abdelilah, S., Rangini, Z., et al. (1996). A genetic screen for mutations affecting embryogenesis in zebrafish. *Development* 123, 37–46.
- Du, L., Anderson, A., Nguyen, K., Ojeda, S.S., Ortiz-Rivera, I., Nguyen, T.N., Zhang, T., Kaoud, T.S., Gray, N.S., Dalby, K.N., et al. (2019). JNK2 Is Required for the Tumorigenic Properties of Melanoma Cells. *ACS Chem Biol* 14, 1426–1435.
- Ebalunode, J.O., Zheng, W., and Tropsha, A. (2011). Application of QSAR and Shape Pharmacophore Modeling Approaches for Targeted Chemical Library Design. In *Chemical Library Design*, J.Z. Zhou, ed. (Totowa, NJ: Humana Press), pp. 111–133.
- Eddy, K., and Chen, S. (2021). Glutamatergic Signaling a Therapeutic Vulnerability in Melanoma. *Cancers (Basel)* 13, 3874.
- Elste, A.P., and Petersen, I. (2010). Expression of proteinase-activated receptor 1-4 (PAR 1-4) in human cancer. *J Mol Histol* 41, 89–99.
- Esguerra, M., Siretskiy, A., Bello, X., Sallander, J., and Gutiérrez-de-Terán, H. (2016). GPCR-ModSim: A comprehensive web based solution for modeling G-protein coupled receptors. *Nucleic Acids Res* 44, W455-462.
- Estrada, Y., Dong, J., and Ossowski, L. (2009). Positive crosstalk between ERK and p38 in melanoma stimulates migration and in vivo proliferation. *Pigment Cell Melanoma Res* 22, 66–76.
- Fagerberg, L., Hallström, B.M., Oksvold, P., Kampf, C., Djureinovic, D., Odeberg, J., Habuka, M., Tahmasebpoor, S., Danielsson, A., Edlund, K., et al. (2014). Analysis of the Human Tissue-specific Expression by Genome-wide Integration of Transcriptomics and Antibody-based Proteomics *. *Molecular & Cellular Proteomics* 13, 397–406.
- Fajardo, A.M., Piazza, G.A., and Tinsley, H.N. (2014). The Role of Cyclic Nucleotide Signaling Pathways in Cancer: Targets for Prevention and Treatment. *Cancers (Basel)* 6, 436–458.
- Feng, X., Degese, M.S., Iglesias-Bartolome, R., Vaque, J.P., Molinolo, A.A.,

- Rodrigues, M., Zaidi, M.R., Ksander, B.R., Merlino, G., Sodhi, A., et al. (2014). Hippo-Independent Activation of YAP by the GNAQ Uveal Melanoma Oncogene through a Trio-Regulated Rho GTPase Signaling Circuitry. *Cancer Cell* 25, 831–845.
- Flem-Karlsen, K., McFadden, E., Omar, N., Haugen, M.H., Øy, G.F., Ryder, T., Gullestad, H.P., Hermann, R., Mælandsmo, G.M., and Flørenes, V.A. (2020). Targeting AXL and the DNA Damage Response Pathway as a Novel Therapeutic Strategy in Melanoma. *Mol Cancer Ther* 19, 895–905.
- Forrest, A.R.R., Kawaji, H., Rehli, M., Kenneth Baillie, J., de Hoon, M.J.L., Haberle, V., Lassmann, T., Kulakovskiy, I.V., Lizio, M., Itoh, M., et al. (2014). A promoter-level mammalian expression atlas. *Nature* 507, 462–470.
- Foskett, J.K., White, C., Cheung, K.-H., and Mak, D.-O.D. (2007). Inositol trisphosphate receptor Ca²⁺ release channels. *Physiol Rev* 87, 593–658.
- Frantz, W.T., and Ceol, C.J. (2020). From Tank to Treatment: Modeling Melanoma in Zebrafish. *Cells* 9, 1289.
- Frey, U., Fritz, A., Rotterdam, S., Schmid, K., Potthoff, A., Altmeyer, P., Siffert, W., and Brockmeyer, N. (2010). GNAS1 T393C polymorphism and disease progression in patients with malignant melanoma. *Eur J Med Res* 15, 422–427.
- Frey, U.H., Alakus, H., Wohlschlaeger, J., Schmitz, K.J., Winde, G., van Calker, H.G., Jöckel, K.-H., Siffert, W., and Schmid, K.W. (2005a). GNAS1 T393C polymorphism and survival in patients with sporadic colorectal cancer. *Clin Cancer Res* 11, 5071–5077.
- Frey, U.H., Eisenhardt, A., Lümmer, G., Rübber, H., Jöckel, K.-H., Schmid, K.W., and Siffert, W. (2005b). The T393C polymorphism of the G alpha s gene (GNAS1) is a novel prognostic marker in bladder cancer. *Cancer Epidemiol Biomarkers Prev* 14, 871–877.
- Fu, Y., Rathod, D., and Patel, K. (2020). Protein kinase C inhibitor anchored BRD4 PROTAC PEGylated nanoliposomes for the treatment of vemurafenib-resistant melanoma. *Experimental Cell Research* 396, 112275.
- Fukuhara, S., Murga, C., Zohar, M., Igishi, T., and Gutkind, J.S. (1999). A novel PDZ domain containing guanine nucleotide exchange factor links heterotrimeric G proteins to Rho. *J Biol Chem* 274, 5868–5879.
- García-Nafria, J., and Tate, C.G. (2020). Cryo-Electron Microscopy: Moving Beyond X-Ray Crystal Structures for Drug Receptors and Drug Development. *Annu Rev Pharmacol Toxicol* 60, 51–71.
- Goding, C.R., and Arnheiter, H. (2019). MITF—the first 25 years. *Genes Dev* 33, 983–1007.
- González, N., Mantey, S.A., Pradhan, T.K., Sancho, V., Moody, T.W., Coy, D.H., and Jensen, R.T. (2009). Characterization of putative GRP- and NMB-receptor antagonist's interaction with human receptors. *Peptides* 30, 1473–1486.
- Green, H., Koes, D.R., and Durrant, J.D. (2021). DeepFrag: a deep convolutional neural network for fragment-based lead optimization. *Chem. Sci.* 12, 8036–8047.
- Guan, L., Yang, H., Cai, Y., Sun, L., Di, P., Li, W., Liu, G., and Tang, Y. (2018). ADMET-score – a comprehensive scoring function for evaluation of chemical drug-likeness †Electronic supplementary information (ESI) available. See DOI:

10.1039/c8md00472b. *Medchemcomm* 10, 148–157.

Gurevich, V.V., and Gurevich, E.V. (2015). Arrestins: Critical Players in Trafficking of Many GPCRs. *Prog Mol Biol Transl Sci* 132, 1–14.

Haffter, P., Granato, M., Brand, M., Mullins, M.C., Hammerschmidt, M., Kane, D.A., Odenthal, J., van Eeden, F.J., Jiang, Y.J., Heisenberg, C.P., et al. (1996). The identification of genes with unique and essential functions in the development of the zebrafish, *Danio rerio*. *Development* 123, 1–36.

Hamm, H.E. (1998). The Many Faces of G Protein Signaling *. *Journal of Biological Chemistry* 273, 669–672.

Hanoune, J., and Defer, N. (2001). Regulation and role of adenylyl cyclase isoforms. *Annu Rev Pharmacol Toxicol* 41, 145–174.

Harding, R.M., Healy, E., Ray, A.J., Ellis, N.S., Flanagan, N., Todd, C., Dixon, C., Sajantila, A., Jackson, I.J., Birch-Machin, M.A., et al. (2000). Evidence for variable selective pressures at MC1R. *Am J Hum Genet* 66, 1351–1361.

Hart, M.J., Jiang, X., Kozasa, T., Roscoe, W., Singer, W.D., Gilman, A.G., Sternweis, P.C., and Bollag, G. (1998). Direct stimulation of the guanine nucleotide exchange activity of p115 RhoGEF by Gα13. *Science* 280, 2112–2114.

Hauser, A.S., Attwood, M.M., Rask-Andersen, M., Schiöth, H.B., and Gloriam, D.E. (2017). Trends in GPCR drug discovery: new agents, targets and indications. *Nat Rev Drug Discov* 16, 829–842.

Hiramoto, K., Murata, T., Shimizu, K., Morita, H., Inui, M., Manganiello, V.C., Tagawa, T., and Arai, N. (2014). Role of phosphodiesterase 2 in growth and invasion of human malignant melanoma cells. *Cell Signal* 26, 1807–1817.

Hoshi, N., Langeberg, L.K., Gould, C.M., Newton, A.C., and Scott, J.D. (2010). Interaction with AKAP79 modifies the cellular pharmacology of PKC. *Mol Cell* 37, 541–550.

Howe, K., Clark, M.D., Torroja, C.F., Tarrant, J., Berthelot, C., Muffato, M., Collins, J.E., Humphray, S., McLaren, K., Matthews, L., et al. (2013). The zebrafish reference genome sequence and its relationship to the human genome. *Nature* 496, 498–503.

Hu, G.-M., Mai, T.-L., and Chen, C.-M. (2017). Visualizing the GPCR Network: Classification and Evolution. *Sci Rep* 7, 15495.

Hu, W., Jin, L., Jiang, C.C., Long, G.V., Scolyer, R.A., Wu, Q., Zhang, X.D., Mei, Y., and Wu, M. (2013). AEBP1 upregulation confers acquired resistance to BRAF (V600E) inhibition in melanoma. *Cell Death Dis* 4, e914–e914.

Huang, J.L.-Y., Urtatiz, O., and Van Raamsdonk, C.D. (2015). Oncogenic G Protein GNAQ Induces Uveal Melanoma and Intravasation in Mice. *Cancer Res* 75, 3384–3397.

Hughes, J., Rees, S., Kalindjian, S., and Philpott, K. (2011). Principles of early drug discovery. *Br J Pharmacol* 162, 1239–1249.

Inoue, A., Raimondi, F., Kadji, F.M.N., Singh, G., Kishi, T., Uwamizu, A., Ono, Y., Shinjo, Y., Ishida, S., Arang, N., et al. (2019). Illuminating G-Protein-Coupling Selectivity of GPCRs. *Cell* 177, 1933–1947.e25.

Ishchenko, A., Stauch, B., Han, G.W., Batyuk, A., Shiriaeva, A., Li, C., Zatspein, N.,

Weierstall, U., Liu, W., Nango, E., et al. (2019). Toward G protein-coupled receptor structure-based drug design using X-ray lasers. *IUCrJ* 6, 1106–1119.

Iwasaki, T., Yamauchi, M., Liang, Z., Itai, A., Sakaguchi, M., Nagano, T., Kamada, S., and Oka, M. (2017). TPA inhibits melanoma growth through inactivation of STAT3 through protein tyrosine phosphatases. *Journal of Dermatological Science* 86, e94.

Jayachandran, A., Anaka, M., Prithviraj, P., Hudson, C., McKeown, S.J., Lo, P.-H., Vella, L.J., Goding, C.R., Cebon, J., and Behren, A. (2014). Thrombospondin 1 promotes an aggressive phenotype through epithelial-to-mesenchymal transition in human melanoma. *Oncotarget* 5, 5782–5797.

Jo, M., and Jung, S.T. (2016). Engineering therapeutic antibodies targeting G-protein-coupled receptors. *Exp Mol Med* 48, e207–e207.

Johannessen, C.M., Boehm, J.S., Kim, S.Y., Thomas, S.R., Wardwell, L., Johnson, L.A., Emery, C.M., Stransky, N., Cogdill, A.P., Barretina, J., et al. (2010). COT drives resistance to RAF inhibition through MAP kinase pathway reactivation. *Nature* 468, 968–972.

Johannessen, C.M., Johnson, L.A., Piccioni, F., Townes, A., Frederick, D.T., Donahue, M.K., Narayan, R., Flaherty, K.T., Wargo, J.A., Root, D.E., et al. (2013). A melanocyte lineage program confers resistance to MAP kinase pathway inhibition. *Nature* 504, 138–142.

Johansson, P., Aoude, L.G., Wadt, K., Glasson, W.J., Warriar, S.K., Hewitt, A.W., Kiilgaard, J.F., Heegaard, S., Isaacs, T., Franchina, M., et al. (2016). Deep sequencing of uveal melanoma identifies a recurrent mutation in PLCB4. *Oncotarget* 7, 4624–4631.

Johnson, J.E., Goulding, R.E., Ding, Z., Partovi, A., Anthony, K.V., Beaulieu, N., Tazmini, G., Cornell, R.B., and Kay, R.J. (2007). Differential membrane binding and diacylglycerol recognition by C1 domains of RasGRPs. *Biochem J* 406, 223–236.

Jones, A.J.Y., Gabriel, F., Tandale, A., and Nietlispach, D. (2020). Structure and Dynamics of GPCRs in Lipid Membranes: Physical Principles and Experimental Approaches. *Molecules* 25, 4729.

Jørgensen, K., Skrede, M., Cruciani, V., Mikalsen, S.-O., Slipicevic, A., and Flørenes, V.A. (2005). Phorbol ester phorbol-12-myristate-13-acetate promotes anchorage-independent growth and survival of melanomas through MEK-independent activation of ERK1/2. *Biochem Biophys Res Commun* 329, 266–274.

Jumper, J., Evans, R., Pritzel, A., Green, T., Figurnov, M., Ronneberger, O., Tunyasuvunakool, K., Bates, R., Žídek, A., Potapenko, A., et al. (2021). Highly accurate protein structure prediction with AlphaFold. *Nature* 596, 583–589.

Katsuya, K., Hori, Y., Oikawa, D., Yamamoto, T., Umetani, K., Urashima, T., Kinoshita, T., Ayukawa, K., Tokunaga, F., and Tamaru, M. (2018). High-Throughput Screening for Linear Ubiquitin Chain Assembly Complex (LUBAC) Selective Inhibitors Using Homogenous Time-Resolved Fluorescence (HTRF)-Based Assay System. *SLAS DISCOVERY: Advancing the Science of Drug Discovery* 23, 1018–1029.

Keatinge, M., Tsarouchas, T.M., Munir, T., Porter, N.J., Larraz, J., Gianni, D., Tsai, H.-H., Becker, C.G., Lyons, D.A., and Becker, T. (2021). CRISPR gRNA phenotypic screening in zebrafish reveals pro-regenerative genes in spinal cord injury. *PLOS Genetics* 17, e1009515.

- Kelly, P., Stemmler, L.N., Madden, J.F., Fields, T.A., Daaka, Y., and Casey, P.J. (2006a). A role for the G12 family of heterotrimeric G proteins in prostate cancer invasion. *J Biol Chem* 281, 26483–26490.
- Kelly, P., Moeller, B.J., Juneja, J., Booden, M.A., Der, C.J., Daaka, Y., Dewhirst, M.W., Fields, T.A., and Casey, P.J. (2006b). The G12 family of heterotrimeric G proteins promotes breast cancer invasion and metastasis. *Proc Natl Acad Sci U S A* 103, 8173–8178.
- Kirschner, L.S., Carney, J.A., Pack, S.D., Taymans, S.E., Giatzakis, C., Cho, Y.S., Cho-Chung, Y.S., and Stratakis, C.A. (2000). Mutations of the gene encoding the protein kinase A type I-alpha regulatory subunit in patients with the Carney complex. *Nat Genet* 26, 89–92.
- Kitaeva, K.V., Rutland, C.S., Rizvanov, A.A., and Solovyeva, V.V. (2020). Cell Culture Based in vitro Test Systems for Anticancer Drug Screening. *Frontiers in Bioengineering and Biotechnology* 8, 322.
- Kleinboelting, S., Diaz, A., Moniot, S., van den Heuvel, J., Weyand, M., Levin, L.R., Buck, J., and Steegborn, C. (2014). Crystal structures of human soluble adenylyl cyclase reveal mechanisms of catalysis and of its activation through bicarbonate. *Proc Natl Acad Sci U S A* 111, 3727–3732.
- Krupnick, J.G., Goodman, O.B., Keen, J.H., and Benovic, J.L. (1997). Arrestin/clathrin interaction. Localization of the clathrin binding domain of nonvisual arrestins to the carboxy terminus. *J Biol Chem* 272, 15011–15016.
- Kuhlmann, L., Cummins, E., Samudio, I., and Kislinger, T. (2018). Cell-surface proteomics for the identification of novel therapeutic targets in cancer. *Expert Rev Proteomics* 15, 259–275.
- Kunz, M., Moeller, S., Koczan, D., Lorenz, P., Wenger, R.H., Glocker, M.O., Thiesen, H.-J., Gross, G., and Ibrahim, S.M. (2003). Mechanisms of Hypoxic Gene Regulation of Angiogenesis Factor Cyr61 in Melanoma Cells *. *Journal of Biological Chemistry* 278, 45651–45660.
- Kwon, H., Kim, J., and Jho, E.-H. (2021). Role of the Hippo pathway and mechanisms for controlling cellular localization of YAP/TAZ. *FEBS J*.
- La Porta, C.A., Porro, D., and Comolli, R. (1998). Opposite effects of TPA on G1/S transition and on cell size in the low metastatic B16F1 with respect to high metastatic BL6 murine melanoma cells. *Cancer Lett* 132, 159–164.
- Langenhan, T., Barr, M.M., Bruchas, M.R., Ewer, J., Griffith, L.C., Maiellaro, I., Taghert, P.H., White, B.H., and Monk, K.R. (2015). Model Organisms in G Protein-Coupled Receptor Research. *Mol Pharmacol* 88, 596–603.
- Latorraca, N.R., Venkatakrisnan, A.J., and Dror, R.O. (2017). GPCR Dynamics: Structures in Motion. *Chem Rev* 117, 139–155.
- Lebon, G., Bennett, K., Jazayeri, A., and Tate, C.G. (2011). Thermostabilisation of an agonist-bound conformation of the human adenosine A(2A) receptor. *J Mol Biol* 409, 298–310.
- Lee, Y., Basith, S., and Choi, S. (2018). Recent Advances in Structure-Based Drug Design Targeting Class A G Protein-Coupled Receptors Utilizing Crystal Structures and Computational Simulations. *J Med Chem* 61, 1–46.

- Leopoldt, D., Hanck, T., Exner, T., Maier, U., Wetzker, R., and Nürnberg, B. (1998). Gβγ Stimulates Phosphoinositide 3-Kinase-γ by Direct Interaction with Two Domains of the Catalytic p110 Subunit *. *Journal of Biological Chemistry* 273, 7024–7029.
- Li, C., Tong, H., Yan, Q., Tang, S., Han, X., Xiao, W., and Tan, Z. (2016). L-Theanine Improves Immunity by Altering TH2/TH1 Cytokine Balance, Brain Neurotransmitters, and Expression of Phospholipase C in Rat Hearts. *Med Sci Monit* 22, 662–669.
- de Ligt, R.A.F., Kourounakis, A.P., and IJzerman, A.P. (2000). Inverse agonism at G protein-coupled receptors: (patho)physiological relevance and implications for drug discovery. *Br J Pharmacol* 130, 1–12.
- Liu, H., and Lee, W. (2019). The XFEL Protein Crystallography: Developments and Perspectives. *Int J Mol Sci* 20, 3421.
- Liu, L., and Jockers, R. (2020). Structure-Based Virtual Screening Accelerates GPCR Drug Discovery. *Trends in Pharmacological Sciences* 41, 382–384.
- Liu, D., Schilling, B., Liu, D., Sucker, A., Livingstone, E., Jerby-Arnon, L., Zimmer, L., Gutzmer, R., Satzger, I., Loquai, C., et al. (2019). Integrative molecular and clinical modeling of clinical outcomes to PD1 blockade in patients with metastatic melanoma. *Nat Med* 25, 1916–1927.
- Liu, Q., Tong, D., Liu, G., Yi, Y., Zhang, D., Zhang, J., Zhang, Y., Huang, Z., Li, Y., Chen, R., et al. (2017). Carney complex with PRKAR1A gene mutation. *Medicine (Baltimore)* 96, e8999.
- Lotta, L.A., Mokrosiński, J., Mendes de Oliveira, E., Li, C., Sharp, S.J., Luan, J., Brouwers, B., Ayinampudi, V., Bowker, N., Kerrison, N., et al. (2019). Human Gain-of-Function MC4R Variants Show Signaling Bias and Protect against Obesity. *Cell* 177, 597-607.e9.
- Lui, J.W., Moore, S.P.G., Huang, L., Ogomori, K., Li, Y., and Lang, D. (2021). YAP facilitates melanoma migration through regulation of actin-related protein 2/3 complex subunit 5 (ARPC5). *Pigment Cell Melanoma Res.*
- Luke, J.J., Flaherty, K.T., Ribas, A., and Long, G.V. (2017). Targeted agents and immunotherapies: optimizing outcomes in melanoma. *Nature Reviews Clinical Oncology* 14, 463–482.
- Luttrell, L.M., Ferguson, S.S., Daaka, Y., Miller, W.E., Maudsley, S., Della Rocca, G.J., Lin, F., Kawakatsu, H., Owada, K., Luttrell, D.K., et al. (1999). Beta-arrestin-dependent formation of beta2 adrenergic receptor-Src protein kinase complexes. *Science* 283, 655–661.
- Luttrell, L.M., Roudabush, F.L., Choy, E.W., Miller, W.E., Field, M.E., Pierce, K.L., and Lefkowitz, R.J. (2001). Activation and targeting of extracellular signal-regulated kinases by β-arrestin scaffolds. *PNAS* 98, 2449–2454.
- Lyon, A.M., and Tesmer, J.J.G. (2013). Structural Insights into Phospholipase C-β Function. *Mol Pharmacol* 84, 488–500.
- Lyons, J., Bastian, B.C., and McCormick, F. (2013). MC1R and cAMP signaling inhibit cdc25B activity and delay cell cycle progression in melanoma cells. *Proc Natl Acad Sci U S A* 110, 13845–13850.
- Ma, M., Dai, J., Tang, H., Xu, T., Yu, S., Si, L., Cui, C., Sheng, X., Chi, Z., Mao, L., et al. (2019). MicroRNA-23a-3p Inhibits Mucosal Melanoma Growth and Progression

through Targeting Adenylate Cyclase 1 and Attenuating cAMP and MAPK Pathways. *Theranostics* 9, 945–960.

Ma, Y., Wang, L., He, F., Yang, J., Ding, Y., Ge, S., Fan, X., Zhou, Y., Xu, X., and Jia, R. (2021). LACTB suppresses melanoma progression by attenuating PP1A and YAP interaction. *Cancer Lett* 506, 67–82.

Magro, C.M., Neil Crowson, A., Desman, G., and Zippin, J.H. (2012). Soluble Adenylyl Cyclase Antibody Profile as a Diagnostic Adjunct in the Assessment of Pigmented Lesions. *Arch Dermatol* 148, 335–344.

Marín, Y.E., Namkoong, J., Cohen-Solal, K., Shin, S.-S., Martino, J.J., Oka, M., and Chen, S. (2006). Stimulation of oncogenic metabotropic glutamate receptor 1 in melanoma cells activates ERK1/2 via PKCepsilon. *Cell Signal* 18, 1279–1286.

Marquette, A., André, J., Bagot, M., Bensussan, A., and Dumaz, N. (2011). ERK and PDE4 cooperate to induce RAF isoform switching in melanoma. *Nat Struct Mol Biol* 18, 584–591.

Martin, E.L., Rens-Domiano, S., Schatz, P.J., and Hamm, H.E. (1996). Potent peptide analogues of a G protein receptor-binding region obtained with a combinatorial library. *J Biol Chem* 271, 361–366.

Martínez-Vicente, I., Abrisqueta, M., Herraiz, C., Jiménez-Cervantes, C., García-Borrón, J.C., and Olivares, C. (2020). Functional characterization of a C-terminal splice variant of the human melanocortin 1 receptor. *Exp Dermatol* 29, 610–615.

Matsuoka, H., Tsubaki, M., Yamazoe, Y., Ogaki, M., Satou, T., Itoh, T., Kusunoki, T., and Nishida, S. (2009). Tamoxifen inhibits tumor cell invasion and metastasis in mouse melanoma through suppression of PKC/MEK/ERK and PKC/PI3K/Akt pathways. *Experimental Cell Research* 315, 2022–2032.

Maurel, D., Comps-Agrar, L., Brock, C., Rives, M.-L., Bourrier, E., Ayoub, M.A., Bazin, H., Tinel, N., Durroux, T., Prézeau, L., et al. (2008). Cell-surface protein-protein interaction analysis with time-resolved FRET and snap-tag technologies: application to GPCR oligomerization. *Nat Methods* 5, 561–567.

Maziarz, M., Leyme, A., Marivin, A., Luebbbers, A., Patel, P.P., Chen, Z., Sprang, S.R., and Garcia-Marcos, M. (2018). Atypical activation of the G protein Gαq by the oncogenic mutation Q209P. *J Biol Chem* 293, 19586–19599.

McDonald, P.H., Chow, C.-W., Miller, W.E., Laporte, S.A., Field, M.E., Lin, F.-T., Davis, R.J., and Lefkowitz, R.J. (2000). β-Arrestin 2: A Receptor-Regulated MAPK Scaffold for the Activation of JNK3. *Science* 290, 1574–1577.

McMullan, G., Faruqi, A.R., and Henderson, R. (2016). Direct Electron Detectors. *Methods Enzymol* 579, 1–17.

Melé, M., Ferreira, P.G., Reverter, F., DeLuca, D.S., Monlong, J., Sammeth, M., Young, T.R., Goldmann, J.M., Pervouchine, D.D., Sullivan, T.J., et al. (2015). Human genomics. The human transcriptome across tissues and individuals. *Science* 348, 660–665.

Miller, W.E., Maudsley, S., Ahn, S., Khan, K.D., Luttrell, L.M., and Lefkowitz, R.J. (2000). beta-arrestin1 interacts with the catalytic domain of the tyrosine kinase c-SRC. Role of beta-arrestin1-dependent targeting of c-SRC in receptor endocytosis. *J Biol Chem* 275, 11312–11319.

- Minami, K., Ueda, N., Ishimoto, K., and Tsujiuchi, T. (2020). Lysophosphatidic acid receptor-2 (LPA2)-mediated signaling enhances chemoresistance in melanoma cells treated with anticancer drugs. *Mol Cell Biochem* 469, 89–95.
- Mo, J.-S., Yu, F.-X., Gong, R., Brown, J.H., and Guan, K.-L. (2012). Regulation of the Hippo–YAP pathway by protease-activated receptors (PARs). *Genes Dev.* 26, 2138–2143.
- Moore, A.R., Ran, L., Guan, Y., Sher, J.J., Hitchman, T.D., Zhang, J.Q., Hwang, C., Walzak, E.G., Shoushtari, A.N., Monette, S., et al. (2018). GNA11 Q209L Mouse Model Reveals RasGRP3 as an Essential Signaling Node in Uveal Melanoma. *Cell Rep* 22, 2455–2468.
- Mullard, A. (2021). What does AlphaFold mean for drug discovery? *Nat Rev Drug Discov* 20, 725–727.
- Müller, J., Krijgsman, O., Tsoi, J., Robert, L., Hugo, W., Song, C., Kong, X., Possik, P.A., Cornelissen-Steijger, P.D.M., Geukes Foppen, M.H., et al. (2014). Low MITF/AXL ratio predicts early resistance to multiple targeted drugs in melanoma. *Nat Commun* 5, 5712.
- Nallet-Staub, F., Marsaud, V., Li, L., Gilbert, C., Dodier, S., Bataille, V., Sudol, M., Herlyn, M., and Mauviel, A. (2014). Pro-invasive activity of the Hippo pathway effectors YAP and TAZ in cutaneous melanoma. *J Invest Dermatol* 134, 123–132.
- Narita, M., Murata, T., Shimizu, K., Nakagawa, T., Sugiyama, T., Inui, M., Hiramoto, K., and Tagawa, T. (2007). A role for cyclic nucleotide phosphodiesterase 4 in regulation of the growth of human malignant melanoma cells. *Oncology Reports* 17, 1133–1139.
- Neves, B.J., Braga, R.C., Melo-Filho, C.C., Moreira-Filho, J.T., Muratov, E.N., and Andrade, C.H. (2018). QSAR-Based Virtual Screening: Advances and Applications in Drug Discovery. *Front Pharmacol* 9, 1275.
- Nishina, H., Nimota, K., Kukimoto, I., Maehama, T., Takahashi, K., Hoshino, S., Kanaho, Y., and Katada, T. (1995). Significance of Thr182 in the nucleotide-exchange and GTP-hydrolysis reactions of the alpha subunit of GTP-binding protein Gi2. *J Biochem* 118, 1083–1089.
- Oakley, R.H., Laporte, S.A., Holt, J.A., Caron, M.G., and Barak, L.S. (2000). Differential Affinities of Visual Arrestin, β Arrestin1, and β Arrestin2 for G Protein-coupled Receptors Delineate Two Major Classes of Receptors*. *Journal of Biological Chemistry* 275, 17201–17210.
- O’Hayre, M., Vázquez-Prado, J., Kufareva, I., Stawiski, E.W., Handel, T.M., Seshagiri, S., and Gutkind, J.S. (2013). The Emerging Mutational Landscape of G-proteins and G-protein Coupled Receptors in Cancer. *Nat Rev Cancer* 13, 412–424.
- Oka, M., Kikkawa, U., and Nishigori, C. (2008). Protein kinase C- β 1 represses hepatocyte growth factor-induced invasion by preventing the association of adapter protein Gab1 and phosphatidylinositol 3-kinase in melanoma cells. *J Invest Dermatol* 128, 188–195.
- Okada, T., Le Trong, I., Fox, B.A., Behnke, C.A., Stenkamp, R.E., and Palczewski, K. (2000). X-Ray Diffraction Analysis of Three-Dimensional Crystals of Bovine Rhodopsin Obtained from Mixed Micelles. *Journal of Structural Biology* 130, 73–80.
- Omori, K., and Kotera, J. (2007). Overview of PDEs and Their Regulation. *Circulation*

Research.

Ostojić, J., Yoon, Y.-S., Sonntag, T., Nguyen, B., Vaughan, J.M., Shokhirev, M., and Montminy, M. (2021). Transcriptional co-activator regulates melanocyte differentiation and oncogenesis by integrating cAMP and MAPK/ERK pathways. *Cell Reports* 35, 109136.

Pace, A.M., Wong, Y.H., and Bourne, H.R. (1991). A mutant alpha subunit of Gi2 induces neoplastic transformation of Rat-1 cells. *Proc Natl Acad Sci U S A* 88, 7031–7035.

Paradis, J.S., Acosta, M., Saddawi-Konefka, R., Kishore, A., Lubrano, S., Gomes, F., Arang, N., Tiago, M., Coma, S., Wu, X., et al. (2021). Synthetic Lethal Screens Reveal Cotargeting FAK and MEK as a Multimodal Precision Therapy for GNAQ-Driven Uveal Melanoma. *Clin Cancer Res* 27, 3190–3200.

Park, H.Y., Russakovsky, V., Ohno, S., and Gilchrist, B.A. (1993). The beta isoform of protein kinase C stimulates human melanogenesis by activating tyrosinase in pigment cells. *J Biol Chem* 268, 11742–11749.

Park, H.-Y., Wu, H., Killoran, C.E., and Gilchrist, B.A. (2004). The receptor for activated C-kinase-I (RACK-I) anchors activated PKC-beta on melanosomes. *J Cell Sci* 117, 3659–3668.

Pathria, G., Garg, B., Garg, K., Wagner, C., and Wagner, S.N. (2016). Dual c-Jun N-terminal kinase-cyclin D1 and extracellular signal-related kinase-c-Jun disjunction in human melanoma. *Br J Dermatol* 175, 1221–1231.

Patton, E.E., Widlund, H.R., Kutok, J.L., Kopani, K.R., Amatruda, J.F., Murphey, R.D., Berghmans, S., Mayhall, E.A., Traver, D., Fletcher, C.D.M., et al. (2005). BRAF mutations are sufficient to promote nevi formation and cooperate with p53 in the genesis of melanoma. *Curr Biol* 15, 249–254.

Patton, E.E., Mueller, K.L., Adams, D.J., Anandasabapathy, N., Aplin, A.E., Bertolotto, C., Bosenberg, M., Ceol, C.J., Burd, C.E., Chi, P., et al. (2021). Melanoma models for the next generation of therapies. *Cancer Cell* 39, 610–631.

Pauwels, J., Fijałkowska, D., Eyckerman, S., and Gevaert, K. (2021). Mass spectrometry and the cellular surfaceome. *Mass Spectrometry Reviews* *n/a*.

Perry, S.J., Baillie, G.S., Kohout, T.A., McPhee, I., Magiera, M.M., Ang, K.L., Miller, W.E., McLean, A.J., Conti, M., Houslay, M.D., et al. (2002). Targeting of Cyclic AMP Degradation to β 2-Adrenergic Receptors by β -Arrestins. *Science* 298, 834–836.

Petit, V., Raymond, J., Alberti, C., Pouteaux, M., Gallagher, S.J., Nguyen, M.Q., Aplin, A.E., Delmas, V., and Larue, L. (2019). C57BL/6 congenic mouse NRASQ61K melanoma cell lines are highly sensitive to the combination of Mek and Akt inhibitors in vitro and in vivo. *Pigment Cell & Melanoma Research* 32, 829–841.

Pfeil, E.M., Brands, J., Merten, N., Vögtle, T., Vescovo, M., Rick, U., Albrecht, I.-M., Heycke, N., Kawakami, K., Ono, Y., et al. (2020). Heterotrimeric G Protein Subunit G α q Is a Master Switch for G β γ -Mediated Calcium Mobilization by Gi-Coupled GPCRs. *Mol Cell* 80, 940-954.e6.

Pierson, E., Consortium, the Gte., Koller, D., Battle, A., and Mostafavi, S. (2015). Sharing and Specificity of Co-expression Networks across 35 Human Tissues. *PLOS Computational Biology* 11, e1004220.

- Plagge, A., Kelsey, G., and Germain-Lee, E.L. (2008). Physiological functions of the imprinted *Gnas* locus and its protein variants *Gas* and *XLas* in human and mouse. *Journal of Endocrinology* *196*, 193–214.
- Potterton, A., Heifetz, A., and Townsend-Nicholson, A. (2018). Synergistic Use of GPCR Modeling and SDM Experiments to Understand Ligand Binding. In *Computational Methods for GPCR Drug Discovery*, A. Heifetz, ed. (New York, NY: Springer), pp. 335–343.
- Pozvek, G., Hilton, J.M., Quiza, M., Houssami, S., and Sexton, P.M. (1997). Structure/function relationships of calcitonin analogues as agonists, antagonists, or inverse agonists in a constitutively activated receptor cell system. *Mol Pharmacol* *51*, 658–665.
- Qin, S., Meng, M., Yang, D., Bai, W., Lu, Y., Peng, Y., Song, G., Wu, Y., Zhou, Q., Zhao, S., et al. (2018). High-throughput identification of G protein-coupled receptor modulators through affinity mass spectrometry screening. *Chem. Sci.* *9*, 3192–3199.
- Robertson, A.G., Shih, J., Yau, C., Gibb, E.A., Oba, J., Mungall, K.L., Hess, J.M., Uzunangelov, V., Walter, V., Danilova, L., et al. (2017). Integrative Analysis Identifies Four Molecular and Clinical Subsets in Uveal Melanoma. *Cancer Cell* *32*, 204–220.e15.
- Rodríguez, C.I., and Setaluri, V. (2018). EPAC mediates the dual role of cAMP signaling in melanoma. *Oncoscience* *6*, 283–284.
- Rodríguez, C.I., Castro-Pérez, E., Prabhakar, K., Block, L., Longley, B.J., Wisinski, J.A., Kimple, M.E., and Setaluri, V. (2017). EPAC–RAP1 Axis-Mediated Switch in the Response of Primary and Metastatic Melanoma to Cyclic AMP. *Mol Cancer Res* *15*, 1792–1802.
- Rodríguez, C.I., Castro-Pérez, E., Longley, B.J., and Setaluri, V. (2018). Elevated cyclic AMP levels promote BRAFCA/Pten-/- mouse melanoma growth but pCREB is negatively correlated with human melanoma progression. *Cancer Lett* *414*, 268–277.
- Rosenbaum, D.M., Cherezov, V., Hanson, M.A., Rasmussen, S.G.F., Thian, F.S., Kobilka, T.S., Choi, H.-J., Yao, X.-J., Weis, W.I., Stevens, R.C., et al. (2007). GPCR engineering yields high-resolution structural insights into beta2-adrenergic receptor function. *Science* *318*, 1266–1273.
- Sánchez-Más, J., Guillo, L.A., Zanna, P., Jiménez-Cervantes, C., and García-Borrón, J.C. (2005). Role of G protein-coupled receptor kinases in the homologous desensitization of the human and mouse melanocortin 1 receptors. *Mol Endocrinol* *19*, 1035–1048.
- Sassone-Corsi, P. (2012). The Cyclic AMP Pathway. *Cold Spring Harb Perspect Biol* *4*, a011148.
- Schechtman, D., and Mochly-Rosen, D. (2001). Adaptor proteins in protein kinase C-mediated signal transduction. *Oncogene* *20*, 6339–6347.
- Schönwasser, D.C., Marais, R.M., Marshall, C.J., and Parker, P.J. (1998). Activation of the mitogen-activated protein kinase/extracellular signal-regulated kinase pathway by conventional, novel, and atypical protein kinase C isoforms. *Mol Cell Biol* *18*, 790–798.
- Scott, M.C., Wakamatsu, K., Ito, S., Kadokaro, A.L., Kobayashi, N., Groden, J., Kavanagh, R., Takakuwa, T., Virador, V., Hearing, V.J., et al. (2002). Human melanocortin 1 receptor variants, receptor function and melanocyte response to UV

radiation. *J Cell Sci* 115, 2349–2355.

Sellers, L.A., Alderton, F., Carruthers, A.M., Schindler, M., and Humphrey, P.P.A. (2000). Receptor Isoforms Mediate Opposing Proliferative Effects through G $\beta\gamma$ -Activated p38 or Akt Pathways. *Mol Cell Biol* 20, 5974–5985.

Sengelaub, C.A., Navrazhina, K., Ross, J.B., Halberg, N., and Tavazoie, S.F. (2016). PTPRN2 and PLC β 1 promote metastatic breast cancer cell migration through PI(4,5)P2-dependent actin remodeling. *EMBO J* 35, 62–76.

Shaulian, E., and Karin, M. (2001). AP-1 in cell proliferation and survival. *Oncogene* 20, 2390–2400.

Shenoy, S.K., and Lefkowitz, R.J. (2003). Multifaceted roles of beta-arrestins in the regulation of seven-membrane-spanning receptor trafficking and signalling. *Biochem J* 375, 503–515.

Shimada, I., Ueda, T., Kofuku, Y., Eddy, M.T., and Wüthrich, K. (2019). GPCR drug discovery: integrating solution NMR data with crystal and cryo-EM structures. *Nat Rev Drug Discov* 18, 59–82.

Shoichet, B.K., and Kobilka, B.K. (2012). Structure-based drug screening for G protein-coupled receptors. *Trends Pharmacol Sci* 33, 268–272.

Skalhegg, B.S., and Tasken, K. (2000). Specificity in the cAMP/PKA signaling pathway. Differential expression, regulation, and subcellular localization of subunits of PKA. *Front Biosci* 5, D678-693.

Smith, M.P., Rowling, E.J., Miskolczi, Z., Ferguson, J., Spoerri, L., Haass, N.K., Sloss, O., McEntegart, S., Arozarena, I., von Kriegsheim, A., et al. (2017). Targeting endothelin receptor signalling overcomes heterogeneity driven therapy failure. *EMBO Mol Med* 9, 1011–1029.

Smith, R., Healy, E., Siddiqui, S., Flanagan, N., Steijlen, P.M., Rosdahl, I., Jacques, J.P., Rogers, S., Turner, R., Jackson, I.J., et al. (1998). Melanocortin 1 receptor variants in an Irish population. *J Invest Dermatol* 111, 119–122.

Smrcka, A.V., Hepler, J.R., Brown, K.O., and Sternweis, P.C. (1991). Regulation of polyphosphoinositide-specific phospholipase C activity by purified Gq. *Science* 251, 804–807.

Stein, R.M., Kang, H.J., McCorvy, J.D., Glatfelter, G.C., Jones, A.J., Che, T., Slocum, S., Huang, X.-P., Savych, O., Moroz, Y.S., et al. (2020). Virtual discovery of melatonin receptor ligands to modulate circadian rhythms. *Nature* 579, 609–614.

Sun, F., Suttapitugsakul, S., and Wu, R. (2021). Unraveling the surface glycoprotein interaction network by integrating chemical crosslinking with MS-based proteomics. *Chem Sci* 12, 2146–2155.

Sun, J., Lu, F., He, H., Shen, J., Messina, J., Mathew, R., Wang, D., Sarnaik, A.A., Chang, W.-C., Kim, M., et al. (2014). STIM1- and Orai1-mediated Ca²⁺ oscillation orchestrates invadopodium formation and melanoma invasion. *J Cell Biol* 207, 535–548.

Sung, H., Ferlay, J., Siegel, R.L., Laversanne, M., Soerjomataram, I., Jemal, A., and Bray, F. (2021). Global Cancer Statistics 2020: GLOBOCAN Estimates of Incidence and Mortality Worldwide for 36 Cancers in 185 Countries. *CA: A Cancer Journal for Clinicians* 71, 209–249.

- Sutherland, E.W., and Rall, T.W. (1958). Fractionation and characterization of a cyclic adenine ribonucleotide formed by tissue particles. *J Biol Chem* 232, 1077–1091.
- Suzuki, I., Cone, R.D., Im, S., Nordlund, J., and Abdel-Malek, Z.A. (1996). Binding of melanotropic hormones to the melanocortin receptor MC1R on human melanocytes stimulates proliferation and melanogenesis. *Endocrinology* 137, 1627–1633.
- Suzuki, N., Nakamura, S., Mano, H., and Kozasa, T. (2003). Galpha 12 activates Rho GTPase through tyrosine-phosphorylated leukemia-associated RhoGEF. *Proc Natl Acad Sci U S A* 100, 733–738.
- Takahashi, M., Li, Y., Dillon, T.J., and Stork, P.J.S. (2017). Phosphorylation of Rap1 by cAMP-dependent Protein Kinase (PKA) Creates a Binding Site for KSR to Sustain ERK Activation by cAMP. *Journal of Biological Chemistry* 292, 1449–1461.
- Tamura, A., Halaban, R., Moellmann, G., Cowan, J.M., Lerner, M.R., and Lerner, A.B. (1987). Normal murine melanocytes in culture. *In Vitro Cell Dev Biol* 23, 519–522.
- Tan, S., Zhao, Z., Qiao, Y., Zhang, B., Zhang, T., Zhang, M., Qi, J., Wang, X., Meng, M., and Zhou, Q. (2021). Activation of the tumor suppressive Hippo pathway by triptonide as a new strategy to potently inhibit aggressive melanoma cell metastasis. *Biochemical Pharmacology* 185, 114423.
- Taskén, K., Skålhegg, B.S., Taskén, K.A., Solberg, R., Knutsen, H.K., Levy, F.O., Sandberg, M., Orstavik, S., Larsen, T., Johansen, A.K., et al. (1997). Structure, function, and regulation of human cAMP-dependent protein kinases. *Adv Second Messenger Phosphoprotein Res* 31, 191–204.
- Tate, C.G. (2010). Practical considerations of membrane protein instability during purification and crystallisation. *Methods Mol Biol* 601, 187–203.
- Tate, C.G., and Schertler, G.F.X. (2009). Engineering G protein-coupled receptors to facilitate their structure determination. *Curr Opin Struct Biol* 19, 386–395.
- Taylor, S.J., Chae, H.Z., Rhee, S.G., and Exton, J.H. (1991). Activation of the beta 1 isozyme of phospholipase C by alpha subunits of the Gq class of G proteins. *Nature* 350, 516–518.
- Teixeira, C., Stang, S.L., Zheng, Y., Beswick, N.S., and Stone, J.C. (2003). Integration of DAG signaling systems mediated by PKC-dependent phosphorylation of RasGRP3. *Blood* 102, 1414–1420.
- The Cancer Genome Atlas Network (2015). Genomic Classification of Cutaneous Melanoma. *Cell* 161, 1681–1696.
- Thul, P.J., Åkesson, L., Wiking, M., Mahdessian, D., Geladaki, A., Ait Blal, H., Alm, T., Asplund, A., Björk, L., Breckels, L.M., et al. (2017). A subcellular map of the human proteome. *Science* 356, eaal3321.
- Titus, S., Neumann, S., Zheng, W., Southall, N., Michael, S., Klumpp, C., Yasgar, A., Shinn, P., Thomas, C.J., Inglese, J., et al. (2008). Quantitative High-Throughput Screening Using a **Live-Cell cAMP Assay Identifies Small-Molecule Agonists of the TSH Receptor**. *J Biomol Screen* 13, 120–127.
- Tizpa, E., Young, H.J., Bonjoc, K.-J.C., Chang, C.-W., Liu, Y., Foulks, J.M., and Chaudhry, A. (2020). Role of AXL in metastatic melanoma and impact of TP-0903 as a novel therapeutic option for melanoma brain metastasis. *JCO* 38, e22021–e22021.
- Trinquet, E., Bouhelal, R., and Dietz, M. (2011). Monitoring Gq-coupled receptor

response through inositol phosphate quantification with the IP-One assay. *Expert Opinion on Drug Discovery* 6, 981–994.

Trubiroha, A., Gillotay, P., Giusti, N., Gacquer, D., Libert, F., Lefort, A., Haerlingen, B., De Deken, X., Opitz, R., and Costagliola, S. (2018). A Rapid CRISPR/Cas-based Mutagenesis Assay in Zebrafish for Identification of Genes Involved in Thyroid Morphogenesis and Function. *Sci Rep* 8, 5647.

Tsubaki, M., Matsuoka, H., Yamamoto, C., Kato, C., Ogaki, M., Satou, T., Itoh, T., Kusunoki, T., Tanimori, Y., and Nishida, S. (2007). The protein kinase C inhibitor, H7, inhibits tumor cell invasion and metastasis in mouse melanoma via suppression of ERK1/2. *Clin Exp Metastasis* 24, 431–438.

Tunyasuvunakool, K., Adler, J., Wu, Z., Green, T., Zielinski, M., Židek, A., Bridgland, A., Cowie, A., Meyer, C., Laydon, A., et al. (2021). Highly accurate protein structure prediction for the human proteome. *Nature* 596, 590–596.

Uehara, H., González, N., Sancho, V., Mantey, S.A., Nuche-Berenguer, B., Pradhan, T., Coy, D.H., and Jensen, R.T. (2011). Pharmacology and selectivity of various natural and synthetic Bombesin related peptide agonists for human and rat bombesin receptors differs. *Peptides* 32, 1685–1699.

Uhlen, M., Zhang, C., Lee, S., Sjöstedt, E., Fagerberg, L., Bidkhori, G., Benfeitas, R., Arif, M., Liu, Z., Edfors, F., et al. (2017). A pathology atlas of the human cancer transcriptome. *Science* 357, eaan2507.

Umemura, M., Baljinnayam, E., Feske, S., De Lorenzo, M.S., Xie, L.-H., Feng, X., Oda, K., Makino, A., Fujita, T., Yokoyama, U., et al. (2014). Store-operated Ca²⁺ entry (SOCE) regulates melanoma proliferation and cell migration. *PLoS One* 9, e89292.

Urtatiz, O., Cook, C., Huang, J.L.-Y., Yeh, I., and Van Raamsdonk, C.D. (2020). GNAQQ209L expression initiated in multipotent neural crest cells drives aggressive melanoma of the central nervous system. *Pigment Cell & Melanoma Research* 33, 96–111.

Usman, S., Khawer, M., Rafique, S., Naz, Z., and Saleem, K. (2020). The current status of anti-GPCR drugs against different cancers. *Journal of Pharmaceutical Analysis* 10, 517–521.

Valencia, C., Dujet, C., Margathe, J.-F., Iturrioz, X., Roux, T., Trinquet, E., Villa, P., Hibert, M., Dupuis, E., Llorens-Cortes, C., et al. (2017). A Time-Resolved FRET Cell-Based Binding Assay for the Apelin Receptor. *ChemMedChem* 12, 925–931.

Van Raamsdonk, C.D., Bezrookove, V., Green, G., Bauer, J., Gaugler, L., O'Brien, J.M., Simpson, E.M., Barsh, G.S., and Bastian, B.C. (2009). Frequent somatic mutations of GNAQ in uveal melanoma and blue naevi. *Nature* 457, 599–602.

Van Raamsdonk, C.D., Griewank, K.G., Crosby, M.B., Garrido, M.C., Vemula, S., Wiesner, T., Obenaus, A.C., Wackernagel, W., Green, G., Bouvier, N., et al. (2010). Mutations in GNA11 in uveal melanoma. *N Engl J Med* 363, 2191–2199.

Vaqué, J.P., Dorsam, R.T., Feng, X., Iglesias-Bartolome, R., Forsthoefel, D.J., Chen, Q., Debant, A., Seeger, M.A., Ksander, B.R., Teramoto, H., et al. (2013). A genome-wide RNAi screen reveals a Trio-regulated Rho GTPase circuitry transducing mitogenic signals initiated by G protein-coupled receptors. *Mol Cell* 49, 94–108.

Verfaillie, A., Imrichova, H., Atak, Z.K., Dewaele, M., Rambow, F., Hulselmans, G., Christiaens, V., Svetlichnyy, D., Luciani, F., Van den Mooter, L., et al. (2015). Decoding

the regulatory landscape of melanoma reveals TEADS as regulators of the invasive cell state. *Nat Commun* 6, 6683.

Vinothkumar, K.R., and Henderson, R. (2016). Single particle electron cryomicroscopy: trends, issues and future perspective. *Q Rev Biophys* 49, e13.

Vogt, S., Grosse, R., Schultz, G., and Offermanns, S. (2003). Receptor-dependent RhoA activation in G12/G13-deficient cells: genetic evidence for an involvement of Gq/G11. *J Biol Chem* 278, 28743–28749.

Voris, J.P., Sitailo, L.A., Rahn, H.R., Defnet, A., Gerds, A.T., Sprague, R., Yadav, V., Caroline Le Poole, I., and Denning, M.F. (2010). Functional alterations in protein kinase C beta II expression in melanoma. *Pigment Cell Melanoma Res* 23, 216–224.

Waldo, G.L., Boyer, J.L., Morris, A.J., and Harden, T.K. (1991). Purification of an AIF4- and G-protein beta gamma-subunit-regulated phospholipase C-activating protein. *J Biol Chem* 266, 14217–14225.

Walsh, D.A., Perkins, J.P., and Krebs, E.G. (1968). An Adenosine 3',5'-Monophosphate-dependant Protein Kinase from Rabbit Skeletal Muscle. *Journal of Biological Chemistry* 243, 3763–3765.

Wells, C.D., Liu, M.-Y., Jackson, M., Gutowski, S., Sternweis, P.M., Rothstein, J.D., Kozasa, T., and Sternweis, P.C. (2002). Mechanisms for reversible regulation between G13 and Rho exchange factors. *J Biol Chem* 277, 1174–1181.

Wettschureck, N., and Offermanns, S. (2005). Mammalian G proteins and their cell type specific functions. *Physiol Rev* 85, 1159–1204.

Worth, C.L., Kreuchwig, F., Tiemann, J.K.S., Kreuchwig, A., Ritschel, M., Kleinau, G., Hildebrand, P.W., and Krause, G. (2017). GPCR-SSFE 2.0-a fragment-based molecular modeling web tool for Class A G-protein coupled receptors. *Nucleic Acids Res* 45, W408–W415.

Wu, V., Yeerna, H., Nohata, N., Chiou, J., Harismendy, O., Raimondi, F., Inoue, A., Russell, R.B., Tamayo, P., and Gutkind, J.S. (2019). Illuminating the Onco-GPCRome: Novel G protein-coupled receptor-driven oncocrine networks and targets for cancer immunotherapy. *J Biol Chem* 294, 11062–11086.

Yu, F.-X., Zhao, B., Panupinthu, N., Jewell, J.L., Lian, I., Wang, L.H., Zhao, J., Yuan, H., Tumaneng, K., Li, H., et al. (2012a). Regulation of the Hippo-YAP pathway by G-protein-coupled receptor signaling. *Cell* 150, 780–791.

Yu, F.-X., Zhao, B., Panupinthu, N., Jewell, J.L., Lian, I., Wang, L.H., Zhao, J., Yuan, H., Tumaneng, K., Li, H., et al. (2012b). Regulation of the Hippo-YAP pathway by G-protein coupled receptor signaling. *Cell* 150, 780–791.

Yu, F.-X., Luo, J., Mo, J.-S., Liu, G., Kim, Y.C., Meng, Z., Zhao, L., Peyman, G., Ouyang, H., Jiang, W., et al. (2014). Mutant Gq/11 promote uveal melanoma tumorigenesis by activating YAP. *Cancer Cell* 25, 822–830.

Zaccolo, M., Zerio, A., and Lobo, M.J. (2021). Subcellular Organization of the cAMP Signaling Pathway. *Pharmacol Rev* 73, 278–309.

Zhai, P., Yamamoto, M., Galeotti, J., Liu, J., Masurekar, M., Thaisz, J., Irie, K., Holle, E., Yu, X., Kupersmidt, S., et al. (2005). Cardiac-specific overexpression of AT1 receptor mutant lacking G α_q /Gai causes hypertrophy and bradycardia in transgenic mice. *The Journal of Clinical Investigation* 115, 3045–3056.

- Zhang, R., and Xie, X. (2012). Tools for GPCR drug discovery. *Acta Pharmacol Sin* 33, 372–384.
- Zhang, H., Kong, Q., Wang, J., Jiang, Y., and Hua, H. (2020a). Complex roles of cAMP–PKA–CREB signaling in cancer. *Experimental Hematology & Oncology* 9, 32.
- Zhang, J., Yang, J., Jang, R., and Zhang, Y. (2015). GPCR-I-TASSER: A hybrid approach to G protein-coupled receptor structure modeling and the application to the human genome. *Structure* 23, 1538–1549.
- Zhang, M., Gui, M., Wang, Z.-F., Gorgulla, C., Yu, J.J., Wu, H., Sun, Z.J., Klenk, C., Merklinger, L., Morstein, L., et al. (2021). Cryo-EM structure of an activated GPCR–G protein complex in lipid nanodiscs. *Nat Struct Mol Biol* 28, 258–267.
- Zhang, X., Yang, L., Szeto, P., Abali, G.K., Zhang, Y., Kulkarni, A., Amarasinghe, K., Li, J., Vergara, I.A., Molania, R., et al. (2020b). The Hippo pathway oncoprotein YAP promotes melanoma cell invasion and spontaneous metastasis. *Oncogene* 39, 5267–5281.
- Zhao, B., Xie, J., Zhou, X., Zhang, L., Cheng, X., and Liang, C. (2021). YAP activation in melanoma contributes to anoikis resistance and metastasis. *Exp Biol Med (Maywood)* 246, 888–896.
- Zhao, X., Geltinger, C., Kishikawa, S., Ohshima, K., Murata, T., Nomura, N., Nakahara, T., and Yokoyama, K.K. (2000). Treatment of mouse melanoma cells with phorbol 12-myristate 13-acetate counteracts mannosylerythritol lipid-induced growth arrest and apoptosis. *Cytotechnology* 33, 123–130.
- Zhou, Q., Yang, D., Wu, M., Guo, Y., Guo, W., Zhong, L., Cai, X., Dai, A., Jang, W., Shakhnovich, E.I., et al. (2019). Common activation mechanism of class A GPCRs. *ELife* 8, e50279.
- Zindel, D., Vol, C., Lecha, O., Bequignon, I., Bilgic, M., Vereecke, M., Charrier-Savournin, F., Romier, M., Trinquet, E., Pin, J.-P., et al. (2019). HTRF® Total and Phospho-YAP (Ser127) Cellular Assays. In *The Hippo Pathway: Methods and Protocols*, A. Hergovich, ed. (New York, NY: Springer), pp. 153–166.
- Zivanov, J., Nakane, T., Forsberg, B.O., Kimanius, D., Hagen, W.J., Lindahl, E., and Scheres, S.H. (2018). New tools for automated high-resolution cryo-EM structure determination in RELION-3. *Elife* 7, e42166.

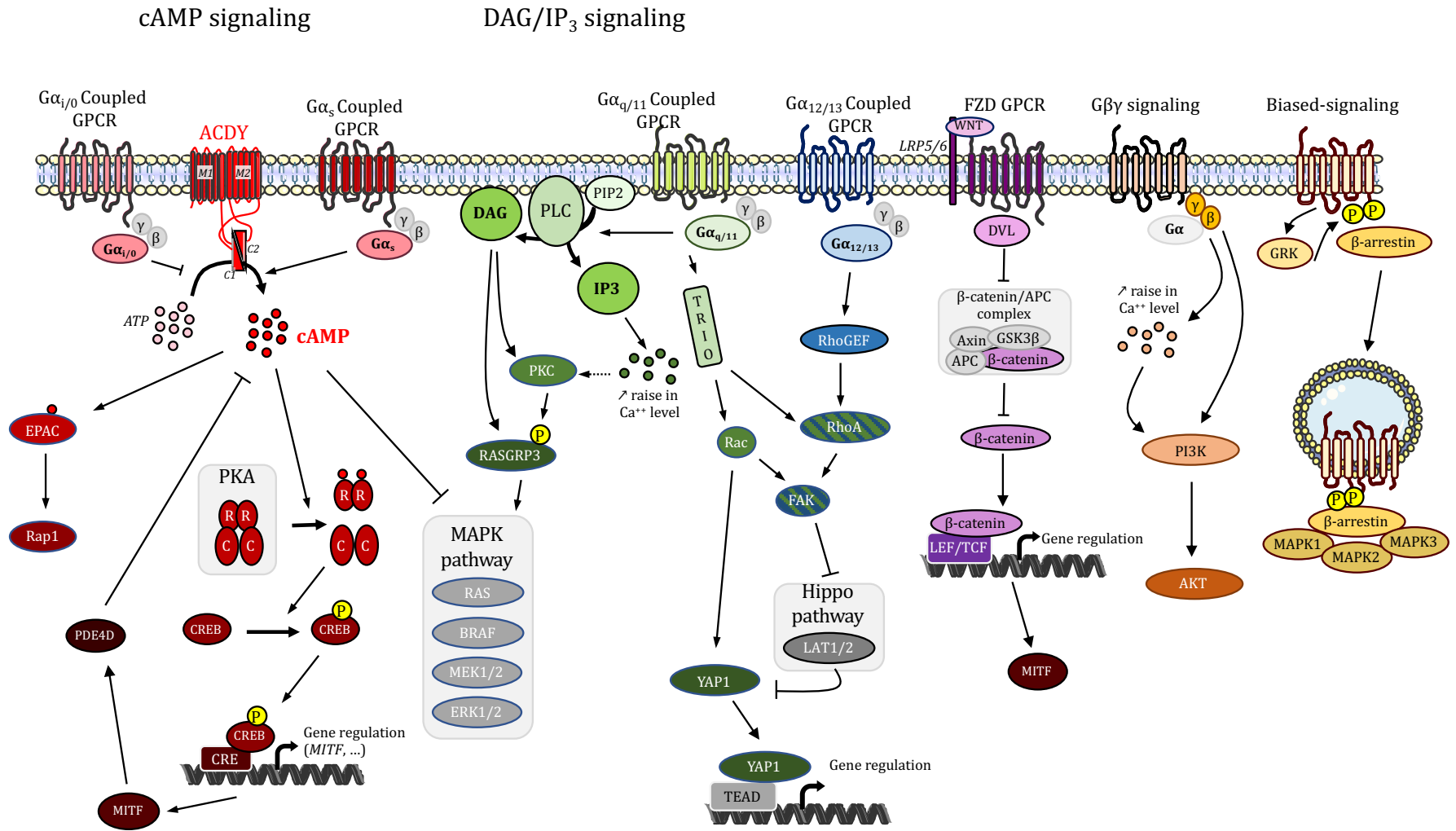


Figure 1: GPCR signaling pathways

C. Scripts R

I. Analyse différentielle de donnée transcriptomiques

```
#chargement des packages nécessaires
library(dplyr)
library(DESeq2)
library(limma)
library(edgeR)
library(ggplot2)
library(readr)

#####
#####          PREPARATION DES DONNEES          #
#####
#####

#définir le dossier où sont les données transcriptomiques
setwd("~/Documents/link to files")

#Télécharger des annotations des gènes
Annotation_Gene <- as.data.frame(read_csv("Fichier d'annotation des gènes.csv"))

#définir comme noms de ligne les identifiants des gènes
#choisir l'ID en cohérence avec les identifiants des tables d'expressions
#Supprimer la lignes devenue inutile
rownames(Annotation_Gene) <- Annotation_Gene$gene_id
Annotation_Gene <- Annotation_Gene[,-which(colnames(Annotation_Gene)=="gene_id")]

#télécharger la table d'expression des comptes bruts
tablecounts_raw <- read_csv("table d'expression des comptes bruts.csv")

#définir comme noms de ligne les identifiants des gènes
#Supprimer la lignes devenue inutile
rownames(tablecounts_raw) <- tablecounts_raw$gene_id
tablecounts_raw <- tablecounts_raw[,-which(colnames(tablecounts_raw)=="gene_id")]

#télécharger la liste des annotations d'échantillons
SampleDescription <- read_csv("table de description des échantillons.csv")

#définir comme noms de ligne les noms d'échantillons,
#être cohérent avec les noms d'échantillons de la matrice d'expression.
rownames(SampleDescription) <- tablecounts_raw$sample_name

#s'assurer que les échantillons de la matrice d'expression
#et de la table d'annotation sont dans le même ordre
tablecounts_raw <- tablecounts_raw[,rownames(SampleDescription)]
```

```

#sauvegarder pour les fois suivantes
save(SampleDescription, file="SampleDescription.Rda")
save(tablecounts_raw, file="tablecounts_raw.Rda")
save(Annotation_Gene, file="Annotation_Gene.Rda")

#####
#####          ANALYSES DIFFERENTIELLES          #
#####
#####

#définir un dossier différent pour enregistrer les analyses
setwd("~/Documents/link to files")

#créer un vecteur détaillant à quel groupe appartient chaque échantillon
conds <- factor(SampleDescription$Group)

#supprimer les gènes non à très peu exprimés exprimés, car ils ont des
#coefficients de variation très élevés et biaisent les analyses transcriptomiques
#Supprime les gènes selon la méthode décrite par Chen et al (2016)
#on besoin d'une expression minimale de k reads dans n échantillons d'au moins 1 groupe
keep.exprs <- filterByExpr(tablecounts_raw, group=conds)
tablecounts_raw <- tablecounts_raw[keep.exprs1057,]

#Créer un objet DGE pour normaliser grâce à edgeR::calcNormFactors
#Va normaliser les librairies en CPM (counts par millions)
#divise l'expression par la taille de la librairie
y <- DGEList(counts=Reads1057, genes=rownames(Reads1057))
y <- calcNormFactors(y1057)

#Créer une matrice représentant l'appartenance de chaque échantillon à chaque groupe
designLimma <- model.matrix(~0+conds1057)

#Application de la normalisation voom aux données
# le but est de les préparer pour appliquer un modèle linéaire
# Pour éviter les variations de variances liées aux fortes expressions.
# les données sont successivement
# *Log Transformée
# *Estime la relation variance/moyenne
# *Calcul des coefficients pondérants les valeurs observées
v <- voom(y,designLimma,plot=TRUE)

#Application du modèle linéaire Limma
fitlimmaVoom <- lmFit(v,designLimma)

#Fait le contrast, un petite matrice indiquant les deux groupes à comparer
#puis applique ce contraste au modèle linéaire
contrast <- makeContrasts(Group_Fem_delEcad - Group_Fem_Ecad, levels =
colnames(coef(fitlimmaVoom)))

```

```

fitlimmaVoom.contrasted <- contrasts.fit(fitlimmaVoom, contrast)

#Appliquer un modèle Bayésien pour évaluer la statistique
fitlimmaVoom.contrasted <- eBayes(fitlimmaVoom.contrasted)

#Récupérer la liste des gènes différentiellement régulés
#rajouter les noms de gènes (surtout utile si gene_id = Ensembl ID / Entrez ID)
ResDA = topTable(fitlimmaVoom.contrasted, number =
nrow(tablecounts_raw))[row.names(tablecounts_raw),]
ResDA <- merge(ResDA, Annotation_Gene, by="row.names")

#enregistrer en txt pour pouvoir travailler hors de R
#sauvegarder pour des utilisations ultérieures
write.table(ResDA, "ResDA_nom du fichier.txt")
save(ResDA, "ResDA_nom du fichier.Rda")

```

II. Visualisation par volcano plot

```

#####
##### VISUALISATION #####
#####
#####
library(ggrepel)
library(ggplot2)
library(dplyr)

res=ResDA
res<-res%>%mutate(threshold = ifelse(logFC >= 1 & adj.P.Val<0.05 ,"A",
  ifelse(logFC<=-1 & adj.P.Val<0.05, "B", "C")))

MaxY <- max(-log10(res$adj.P.Val))
MinX <- min(res$logFC)
MaxX <- max(res$logFC)

g = ggplot(data=res%>%
  arrange(threshold), aes(x=logFC, y=-log10(adj.P.Val))) +
  theme_bw()+
  theme(legend.position = "none") +
  xlim(c(MinX, MaxX)) + ylim(c(0, MaxY)) +
  xlab("") + ylab("")+
  geom_point(aes(colour = threshold), size=1.5, alpha=0.6) +
  scale_colour_manual(values = c("A"= "red", "B"="green", "C"= "black"))

g

ggsave(filename = "Volcano plot.pdf", plot = last_plot(), device = ".pdf",
  dpi = "retina", limitsize = F)

```

III. Téléchargement des données du TCGA

```
library(TCGAbiolinks)
```

```
#Le package TCGAbiolinks va d'abord créer un requête (query). c'est une sorte de token qui sera
```

```
#envoyée au site hébergeant les archives du TCGA.
```

```
query <- GDCquery(project = "TCGA-SKCM", #SKCM = mélanome, tu trouveras la liste des  
abréviations ici https://gdc.cancer.gov/resources-tcga-users/tcga-code-tables/tcga-study-abbreviations
```

```
data.category = "Gene expression", #sur la vignette les différentes catégories et les  
différents types sont listés
```

```
data.type = "Gene expression quantification",
```

```
platform = "Illumina HiSeq",
```

```
file.type = "results", # tu peux aussi mettre 'normalized results', mais tu n'auras pas la  
bonne normalisation pour faire des corrélations
```

```
experimental.strategy = "RNA-Seq", #il existe aussi des vieilles data de microarray que je  
te conseille d'éviter
```

```
legacy = TRUE)
```

```
#cette fonction va télécharger les données que tu veux depuis le site du TCGA. Dans ton dossier  
de travail
```

```
#tu trouveras un fichier nommé GDCdata comportant les données téléchargées.
```

```
#avec la fonction GDCdownload rien ne se passe dans R une fois tout téléchargé.
```

```
GDCdownload(query, method = "api", files.per.chunk = 50)
```

```
#GDCprepare va rassembler tes données téléchargées en un objet R appelé data
```

```
#qui est de classe SummertimeExperiment
```

```
#la classe SummertimeExperiment est un assemblage de tableau.
```

```
data <- GDCprepare(query)
```

```
library(SummertimeExperiment)#package pour jouer avec les SummertimeExperiment
```

```
PatientsInfo <- as.data.frame(colData(data)) #colData récupère les données d'annotation des  
colonnes, donc ici des patients/des échantillons
```

```
geneInfo <- as.data.frame(rowRanges(data)) # récupère les données d'annotation des lignes,  
donc ici des gènes
```

```
#et de façon plus anecdotique
```

```
metadata(data) # date de la realease téléchargée
```

```
### FORMAT DATA TO BE STANDARD
```

```
#le nom des gènes est "symbol HGNC|ENTREZID" on va le simplifier en "symbol HGNC"
```

```
#le nom des colonnes est le nom du patient pour les 12 premiers caractères, trois caractères  
qui définissent
```

```
#si l'échantillon est métastatique (-06) ou d'un primaire (-01) et suivi de caractères définissant  
le type d'échantillon, le lieu du séquençages etc.
```

```
#On va chercher à se débarrasser de ces derniers caractères et se limiter aux 15ers
```

```

#la fonction "assay" va permettre d'accéder aux tableaux d'expression par l'ajout de ",X" à la
fonction
# assay(data,1) <- RSEM (= read counts)
# assay(data,2) <- "Transcript per one" à multiplier par 1.10^6 pour avoir les TPM

TPM <- assay(data,2)*1e6
rownames(TPM) <- sub("\\|.*", "\\|", rownames(TPM)) #remplace le Gene|Entrezid par Gene|
en supprimant tout ce qui se trouve après le "|"
rownames(TPM) <- strsplit(rownames(TPM), "\\|", perl=TRUE) #coupe avant le "|", donc
rowname = Gene
colnames(TPM) <- substr(colnames(TPM),1,15) # simplifie le nom des colonnes : 15 caractères
uniquement
save(TPM, file = "TPM.Rda")#sauvegarde les données TPM

RSEM <- assay(data,1)
rownames(RSEM) <- sub("\\|.*", "\\|", rownames(RSEM)) #remplace le gene|Entrezid par
Gene.
rownames(RSEM) <- strsplit(rownames(RSEM), "\\|", perl=TRUE) #coupe avant le point donc
rowname = Gene
colnames(RSEM) <- substr(colnames(RSEM),1,15) #garde les 15 premiers caractères
uniquement : patients/type d'échantillon
save(RSEM, file = "RSEM.Rda") #sauvegarde les données TPM

```

I. Analyse des scores des signatures phénotypiques et de YAP1

```

#créer les genes set souhaités
Pigmented <-c("MITF", "MLANA", "TRPM1", "DCT", "TYR")
SMC <- c("CD36", "DLX5", "IP6K3", "PAX3", "TRIM67")
Invasive <- c("AXL", "CYR61", "TCF4", "LOXL2", "TNC", "WNT5A")
NCSC_like <- c("AQP1", "GFRA2", "L1XAM", "NGFR", "SLC22A17", "TMEM176B")
YAP1_score <- c("CYR61", "CTGF", "TEAD4", "LATS2", "CRIM1").

#récupérer les données d'expression pour chaque gènes
TPM_Pigmented <- TPM[Pigmented, ]
TPM_SMC <- TPM[SMC, ]
TPM_Invasive <- TPM[Invasive, ]
TPM_NCSC_like <- TPM[NCSC_like, ]
TPM_YAP1_score <- TPM[YAP1_score, ]

#calculer le score en moyennant l'expression de chaque gènes
TPM_Pigmented$mean <- colMeans(TPM_Pigmented)
TPM_SMC$mean <- colMeans(TPM_SMC)
TPM_Invasive$mean <- colMeans(TPM_Invasive)
TPM_NCSC_like$mean <- colMeans(TPM_NCSC_like)
TPM_YAP1_score$mean <- colMeans(TPM_YAP1_score)

#regrouper les score, on transpose par praticité

```

```
Scores <- as.data.frame(cbind(TPM_Pigmented$mean,TPM_SMC$mean, TPM_Invasive$mean,  
    TPM_NCSC_like$mean, TPM_YAP1_score$mean))  
  
#récupérer les donnée d'expression de GRPR et de CDH1  
Exp <- as.data.frame(t(TPM[c("CDH1", "GRPR"),]))  
  
#Merge des deux tableaux  
Score_Exp <- merge(Scores, Exp, by = "row.names")  
  
#sauvegarder  
Write.table(Score_Exp, "Scores et Expressions.txt")
```

D. Curriculum vitae

Doctorant

*Équipe « Développement normal et pathologique des mélanocytes » dirigée par L. LARUE
INSERM U1021 / CRNR UMR3347 / Institut Curie, Orsay, France*

-----EDUCATION-----

- Sept.2017- **Doctorat en Biologie**, Université Paris Sciences & Lettre (PSL),
Financement MESRI et de la ligue contre le cancer
- 2016-2017 **Master 2 BCCP**, Université Paris Descartes & Paris Diderot, mention très bien (5th)
- 2011-2018 **Pharmacie, Filière industrie, spécialité recherche**, Université de Nantes, major
- 2010 **Baccalauréat scientifique**, Rezé - France, mention

-----EXPERIENCES PROFESSIONNELLES-----

- Sept. 2017 - **Étudiant en thèse : Institut Curie CNRS UMR3347/Inserm U1021**, Orsay - France
Étude du rôle de GRPR dans la progression du mélanome
- Jan. -Juil. 2017 **Stage de M2 : Institut Curie CNRS UMR3347/Inserm U1021**, Orsay - France
Étude in vitro du rôle d'E-Cadhérine dans la progression du mélanome
- Feb.-Mai 2016 **Stage 5^e année de pharmacie: CEPR-Inserm U1100**, Tours - France
Rôle de métabolites du glucose lors de l'infection grippale
- Juin-Juil. 2015 **Stage M1 biologie santé : INSERM U791 (LIOAD)**, Nantes - France
Étude de cytotoxicité d'une biocéramique innovante

-----FORMATIONS-----

- Nov.2020 **Analyses RNA-seq**, équivalent 3 jours, Cancéropole - Paris, France
- Sept.2019 **Expérimentation animale**, 2 semaines, Faculté de Pharmacie – Paris Descartes, France
- May 2019 **Analyses DNA-seq**, 3 jours, Cancéropole - Paris, France
- Sept.2018 **Biologie systémique et computationnelle des cancers**, 1 semaine, Institut Curie - Paris, France

-----LANGUES-----

Anglais : TOEIC 955/990

Allemand : bases

-----COMPETENCES & LOGICIELS MAITRISES-----

Compétences:

Biologie cellulaire : Culture cellulaire, analyse d'ARN et de protéine, tests d'activation de GPCR, tests de prolifération/invasion/migration. Incucyte.

Expérimentation animale : Modèles murins : injection de cellules ou de substances, suivis de tumeurs, imagerie non-invasive IVIS, gestion d'élevage.

Bio-informatique: Analyses DNaseq/ChIPseq/RNAseq analysis, data mining.

Logiciels :

Suite Microsoft office (*Word, Excel, Powerpoint*)

Suite Adobe (*Photoshop, Illustrator, Acrobat*)

Graphpad-Prism

Langage de programmation R– R studio (*packages Bioconductor, ggplot2, dplyr*)

-----COMMUNICATIONS-----

- 2020:** Janvier : Réunion d'unité– Institut Curie, Orsay – Talk
- 2019:** Novembre : Cours sur les Crêtes neurales – Institut Curie, Orsay – poster
Septembre : ESDR 2019 – Bordeaux – présentation orale & poster. Travel grant
Mai : retraite de l'École doctorale cancérologie – Roscoff – poster
- 2018:** Novembre : Cours sur les Crêtes neurales – Institut Curie, Orsay – poster. Premier prix.
Septembre : Cours de biologie Computationnelle – Institut Curie, Paris – poster

-----PUBLICATIONS-----

Hamm M*, Sohier P*, Petit V*, **Raymond JH**, Delmas V, Le Coz M, Gesbert F, Kenny C, Aktary Z, Pouteaux M, Rambow F, Sarasin A, Charoenchon N, Bellacosa A, Sanchez-Del-Campo L, Mosteo L, Lauss M, Meijer D, Steingrimsson E, Jönsson GB, Cornell RA, Davidson I, Goding CR, Larue L. BRN2 is a non-canonical melanoma tumor-suppressor. *Nat Commun.* 2021 Jun 17;12(1):3707.

Akil H, Quintana M*, **Raymond JH***, Billoux T, Benboubker V, Besse S, Auzeloux P, Delmas V, Petit V, Larue L, D'Incan M, Degoul F, Rouanet J. Efficacy of Targeted Radionuclide Therapy Using [131I]ICF01012 in 3D Pigmented BRAF- and NRAS-Mutant Melanoma Models and In Vivo NRAS-Mutant Melanoma. *Cancers (Basel).* 2021 Mar 20;13(6):1421.

Petit V, **Raymond JH**, Alberti C, Pouteaux M, Gallagher SJ, Nguyen MQ, Aplin AE, Delmas V, Larue L. C57BL/6 congenic mouse NRAS(Q61K) melanoma cell lines are highly sensitive to the combination of Mek and Akt inhibitors in vitro and in vivo. *Pigment Cell Melanoma Res.* 2019 Nov;32(6):829-841.

**Ces auteurs ont contribué de manière égale*

-----ASSOCIATIONS-----

Membre de la société européenne de dermatologie (ESDR)

Membre la société pour la recherche sur le mélanome (SMR)

Membre de l'Association des Doctorants et post-doctorants de l'Institut Curie (ADIC):

Responsable & chairman de ReSiPi (déjeuners scientifiques mensuels)

RÉSUMÉ

Des progrès considérables ont été réalisés dans la compréhension des mécanismes conduisant aux cancers, malheureusement ceux responsables de l'évolution métastatique reste mal connus. La E-cadhérine (Ecad) est une protéine d'adhésion cellulaire essentielle à l'homéostasie des cellules épithéliales et des mélanocytes dans la peau. De nombreuses études ont montré que le gène codant pour la E-cadhérine, *CDH1*, est un gène suppresseur de tumeurs dans de nombreux carcinomes. Le rôle de *CDH1* dans la mélanomagenèse n'a jamais été formellement établi, seules des corrélations entre la diminution de son expression et un potentiel métastatique accru ont été mises en évidence. Lors de cette thèse, nous avons adressé les conséquences de la perte de *Cdh1* dans la mélanomagenèse à l'aide de souris génétiquement recombinaées exprimant une forme oncogénique de *NRAS*^{Q61K} dans les mélanocytes. Nous avons montré que la délétion conditionnelle de *Cdh1* n'influence pas l'initiation du mélanome, mais favorise efficacement le développement des métastases. De manière intéressante, la perte de *Cdh1* induit fortement l'expression du récepteur au peptide relarguant la gastrine (*Grpr*). GRPR, qui appartient à la famille des récepteurs couplés aux protéines G, est surexprimé dans plusieurs types de cancers, dont les carcinomes. Chez l'homme, nous avons montré une anti-corrélation de l'expression entre *CDH1* et GRPR dans plusieurs carcinomes et dans les mélanomes. D'un point de vue fonctionnel, nous avons montré *in vitro* que l'expression de *Grpr* favorise les processus cellulaires essentiels pour le processus métastatique, tels que la croissance cellulaire, la clonogénicité, la migration et l'invasion. *In vivo*, la surexpression de *Grpr* dans des cellules de mélanome humain ou de souris induit de la formation de foyers métastatiques après allogreffe et xélogreffe, respectivement. Les métastases des cellules surexprimant GRPR sont fortement réduites en présence de l'antagoniste du GRPR, RC-3095. Le GRPR signale via $G\alpha_q$ conduisant à l'activation de la signalisation YAP1, expliquant les caractéristiques moléculaires et cellulaires induits lors de la cascade métastatique. Cette étude souligne l'importance de l'axe Ecad-GRPR dans les métastases de mélanome et apporte la preuve de concept que le GRPR est une cible thérapeutique pour le mélanome métastatique.

MOTS CLÉS

Modèle préclinique, Mélanome, RCPGs, Métastases, Cadhérines

ABSTRACT

While tremendous progress has been made in the understanding of the mechanisms leading to cancers, the understanding of the mechanisms governing the formation of metastases remains poorly understood. E-cadherin (Ecad) is a cell-cell adhesion molecule essential for the homeostasis of epithelial cells and melanocytes in the skin. A large number of studies have established that *CDH1* (encoding for Ecad) is a tumor suppressor gene in carcinomas. However, in melanoma, only correlative studies link its reduced expression to metastatic potential. In this thesis, we addressed the consequences of *Cdh1* loss in melanomagenesis using genetically recombinant mice expressing an oncogenic form of *NRAS*^{Q61K} in melanocytes. We showed that the conditional deletion of *Cdh1* does not influence melanoma initiation but dramatically promotes metastasis. Interestingly, loss of *Cdh1* intensely induces the expression of the Gastrin-releasing peptide receptor (*Grpr*). GRPR, which belongs to the G protein-coupled receptor family, is overexpressed in several types of cancers, including carcinomas. In humans, we have shown anti-correlation of expression between *CDH1* and GRPR in several carcinomas and in melanomas. From a functional point of view, we have shown *in vitro* that *Grpr* expression promotes crucial cellular processes required for metastasis, such as cell growth, clonogenicity, migration and invasion. *In vivo*, overexpression of GRPR in mouse or human melanoma cells induces metastasis after allograft and xenograft, respectively. Metastasis of cells overexpressing GRPR is strongly affected in the presence of the GRPR antagonist RC-3095. GRPR signals through $G\alpha_q$ leading to activation of YAP1 signaling, which explains the molecular and cellular characteristics induced during the metastatic cascade. This study highlights the importance of the Ecad-GRPR axis in melanoma metastases and provides proof-of-concept that GRPR is a therapeutic target for metastatic melanoma.

KEYWORDS

Preclinical models, melanoma, GPCRs, Metastasis, Cadherins